



**The Design, Synthesis and *in vitro* Evaluation of
Proteolysis Targeting Chimeras (PROTACs) for the
Degradation of Protein Arginine Methyltransferase 1**

Poppy Louise Martin

Pembroke College

University of Cambridge

January 2024

Supervised by Professor David R. Spring

This Thesis is Submitted for the Degree of Doctor of Philosophy

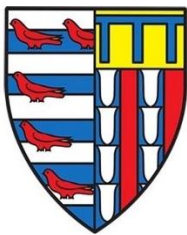
Declaration

This thesis is the result of my own work and includes nothing which is the outcome of work done in collaboration except as declared in the preface and specified in the text. It is not substantially the same as any work that has already been submitted before for any degree or other qualification. It does not exceed the prescribed word limit for the Physics and Chemistry Degree Committee.

Poppy Martin

January 2024

Pembroke College, University of Cambridge



Abstract

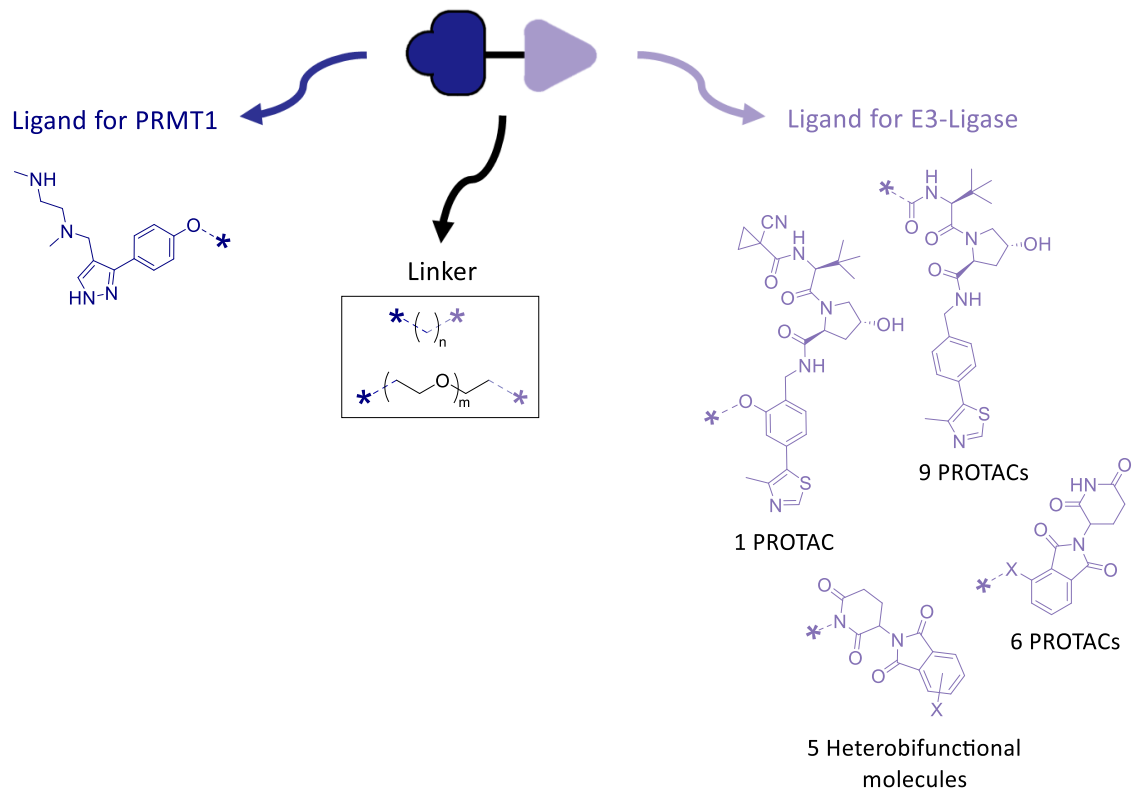
Protein arginine methyltransferase 1 (PRMT1) is a protein responsible for the asymmetric dimethylation of arginine. PRMT1 is upregulated in a wide range of cancers and the reduction of PRMT1 activity reduces cell proliferation and tumour growth in cell and animal models of cancer. A reduction in PRMT1 can also sensitise cancer cells to other treatments. Therefore, targeting PRMT1 is a promising therapeutic strategy in cancer treatment. Published inhibitors for PRMT1 show poor selectivity and dose-limiting toxicities that have precluded their translation to the clinic. The degradation of PRMT1 using a PROTAC may be superior to inhibition as PROTACs can act catalytically at a low dose. PROTACs can also exhibit high selectivity and cause a more pronounced functional outcome compared to inhibition.

In this thesis, PRMT1 is explored as a target protein for PROTAC-induced degradation. The endogenous properties of PRMT1 were evaluated and PRMT1 was determined to be amenable to degradation by a PROTAC. PROTACs were designed that comprised a PRMT1 ligand, a linker and an E3-ligase ligand. Ten PROTACs that recruit the VHL E3-ligase and six PROTACs that recruit the CRBN E3-ligase were synthesised. The degradation of PRMT1 was assessed by Western blot and degradation was not observed for the PROTACs synthesised. Suitable pharmacokinetic properties and target engagement have been shown for selected candidates by the detection of the downstream effects of PRMT1 inhibition and by a NanoBRET assay for E3-ligase binding.

Regioselectivity challenges in the synthesis of the CRBN-recruiting PROTACs led to the isolation of a heterobifunctional molecule with the linker attached to the binding pharmacophore of the CRBN ligand. This molecule was found to degrade PRMT1 and is proposed to be a monomeric degrader that destabilises the structure of PRMT1 upon binding.

This thesis details a novel approach to degrade PRMT1 using a PROTAC and provides insights that may assist the rational design of PROTACs that target PRMT1 in the future.

PROTACs that Target PRMT1



Acknowledgements

I would like to thank Professor David Spring for the opportunity to complete this PhD. He has been a supportive and encouraging supervisor throughout and I have found his group to be a motivational and stimulating research environment where I have been able to develop as an independent scientist.

I am also grateful to Professor Jason Carroll for all his support of this project. I have been fortunate to undertake biological assays in his laboratory and participate in group meetings and group lunches. I always enjoyed working in his lab and learning about transcription factors and cancer biology.

I have been guided and encouraged by Dr Francisco Javier Pérez-Areales and Dr Raoul Walther throughout this project. I want to thank them for their generosity in taking the time to share their knowledge.

Thank you to Dr Shalini Rao for being an inspiring mentor. I feel lucky to have had the opportunity to work with her and her expertise has been invaluable in shaping this project's direction.

I would like to thank the UKRI Medical Research Council for supporting this PhD. For all the training and assistance throughout this project, I would like to thank the NMR team (Peter Gierth, Andrew Mason and Duncan Howe) and the mass spectrometry team (including Roberto Canales) at the Department of Chemistry, as well as the RICS core facility at Cancer Research UK Cambridge Institute.

Thank you to Mahri, Jack and Tomas for their companionship during the long synthesis days and to all the Spring group and Carroll lab members for their friendship, for sharing their research and for the lunchtime chats. It has been a wonderful experience living in Cambridge and this has been due to the friends I have made, the communities at Corpus Christi College and Pembroke College, and the kayakers and rowers with whom I have spent many enjoyable hours on the Cam.

Thank you to Alex for his constant positivity and to Mum and Dad for their support and encouragement.

Abbreviations

Ac	acetyl
AcOH	acetic acid
ADMA	asymmetric dimethylation of arginine
aq	aqueous
ATP	adenosine triphosphate
AMP	adenosine monophosphate
Bcl-xL	B-cell lymphoma-extra large protein
Boc	<i>tert</i> -butylcarbonate
BPin	pinacol boronate
BRCA1	breast cancer type 1 susceptibility protein
BRD	bromodomain-containing protein
BRET	bioluminescence resonance energy transfer
BTK	Bruton's tyrosine kinase
calcd	calculated
CETSA	cellular thermal shift assay
CHX	cycloheximide
CIDE	chemical inducers of degradation
cm	centimeter
CRBN	cereblon
Cryo-EM	cryogenic electron microscopy
CV	column volume(s)
DBU	1,8-diazabicyclo[5.4.0]undec-7-ene
DC ₅₀	concentration required to degrade half the protein
DCM	dichloromethane
DIBALH	diisobutylaluminium hydride
DIPEA	<i>N,N</i> -Diisopropylethylamine
DMA	dimethylacetamide
D _{max}	maximum degradation efficacy
DMEM	Dulbecco's modified eagle medium
DMF	dimethylformamide
DMSO	dimethylsulfoxide
DNA	deoxyribonucleic acid
dppf	1,1'- <i>bis</i> (diphenylphosphino)ferrocene

DTBAD	di- <i>tert</i> -butyl azodicarboxylate
E1-enzyme	ubiquitin-activating enzyme
E2-enzyme	ubiquitin-conjugating enzyme
E3-ligase	ubiquitin-protein ligase
EGFR	epidermal growth factor receptor
eq	equivalent(s)
ER	oestrogen receptor
ESI	electrospray ionisation
EtOAc	ethyl acetate
EtOH	ethanol
FBS	fetal bovine serum
FG	functional group
FOXA1	forkhead box A1
g	gram(s)
g	gravitational force
gRNA	guide RNA
HATU	hexafluorophosphate azabenzotriazole tetramethyl uronium
HBM	heterobifunctional molecule
HER2	human epidermal growth factor receptor 2
HMBC	heteronuclear multiple bond correlation
HNF4G	hepatocyte nuclear factor 4 gamma
HPLC	high pressure liquid chromatography
hr	hour(s)
HRMS	high resolution mass spectrometry
HSQC	heteronuclear single quantum coherence
Hz	hertz
IC ₅₀	concentration required to exert half its maximal inhibitory effect
IR	infrared
<i>J</i>	coupling constant in NMR spectrometry
JMJD6	jumonji domain containing protein 6
K _d	equilibrium dissociation constant
L	litre(s)
LC/MS	liquid chromatography mass spectrometry
m	metre

m	milli ($\times 10^{-3}$)
M	molar (moles per litre)
M	mega ($\times 10^3$)
<i>m/z</i>	mass-to-charge ratio
MDM2	mouse double minute 2 homologue
MeCN	acetonitrile
MEM	minimum essential medium
MeOH	methanol
MetAP-2	protein methionine aminopeptidase-2
min	minute(s)
MMA	monomethylation of arginine
mRNA	messenger RNA
Ms	methylsulfonyl (mesyl)
M_w	molecular weight
n	nano ($\times 10^{-9}$)
N.D.	not detected or not determined
<i>N</i> -Boc	<i>tert</i> -butoxycarbonyl bound to a nitrogen
NCT	national clinical trial
NLuc	NanoLuc luciferase
NLuc-CRBN	fusion protein comprising NanoLuc luciferase and CRBN
NMR	nuclear magnetic resonance
nt	non-targeting control
o/n	overnight
PDAC	pancreatic ductal adenocarcinoma
PDB	protein data bank
PE	petroleum ether
PEG	polyethylene glycol units
pKa	negative log of the acid dissociation constant
PPi	inorganic pyrophosphate
ppm	parts per million
PR	progesterone receptor
PRMT	protein arginine methyltransferase
PROTAC	proteolysis targeting chimera
PVDF	polyvinylidene fluoride

QC	quality control
RING	really interesting new gene
RNA	ribonucleic acid
RNA Pol II	RNA polymerase II transcription machinery
rt	room temperature
R _t	retention time
SAM	S-adenosyl methionine
SCF	Skp1-Cullin-F box complex containing Hrt1
SDMA	symmetric dimethylation of arginine
SDS	sodium dodecyl sulfate
SDS-PAGE	sodium dodecyl-sulfate polyacrylamide gel electrophoresis
SE	standard error
SEM	2-(trimethylsilyl)ethoxymethyl
SEMCI	2-(trimethylsilyl)ethoxymethyl chloride
SERD	selective estrogen receptor degrader
shRNA	short hairpin RNA
SILAC	stable isotope labelling by amino acids in cell culture
siRNA	short interfering RNA
S _N 2	bimolecular nucleophilic substitution
S _N Ar	nucleophilic aromatic substitution
SNR	signal-to-noise ratio
t _{1/2}	half-life
TBAF	tetrabutylammonium fluoride
^t Bu	<i>tert</i> -butyl ester
TE	target engagement
TFA	trifluoroacetic acid
THF	tetrahydrofuran
THP	tetrahydropyranyl ether
TLC	thin layer chromatography
tRNA	transfer RNA
Ts	<i>p</i> -toluenesulfonyl (tosyl)
Ub	ubiquitin
UPS	ubiquitin proteasome system
UV	ultraviolet

VHL	Von-Hippel Lindau
ZEB1	zinc-finger E-box-binding homeobox 1
[M+H] ⁺	the proton-adduct molecular ion of a molecule with a monoisotopic mass of M
°C	degrees Celsius
δ	chemical shift in parts per million from tetramethylsilane
μ	micro (x 10 ⁻⁶)
ν _{max}	maximum absorption wavenumber

Table of Contents

Declaration	i
Abstract	ii
Acknowledgements	iv
Abbreviations	v
Table of Contents	x
1 Introduction	1
1.1 The Protein Arginine Methyltransferases	1
1.1.1 PRMT1 and its role in regulating transcription	3
1.1.2 PRMT1 in cancer	4
1.2 Current Therapeutic Approaches for Targeting PRMT1	6
1.3 The Ubiquitin Proteasome System.....	8
1.4 Targeted Protein Degradation with a PROTAC	10
1.4.1 Introducing literature PROTACs.....	10
1.4.2 Advantages of PROTACs	12
1.4.3 Targeting PRMT1 with a PROTAC.....	15
2 Project Aims	17
3 The Suitability of PRMT1 for PROTAC-Induced Degradation	18
3.1 Development of an Assay to Measure a Change in PRMT1	18
3.1.1 Selecting the tumour-derived cell line	18
3.1.2 The Western blot assay	19
3.1.3 Investigation of the effect of PRMT1 knockdown on arginine methylation.....	23
3.2 The PROTACability of PRMT1	26
3.2.1 Criterion 1: The cellular location of the target protein	27
3.2.2 Criterion 2: Evidence that the target protein has ubiquitylation sites.....	27
3.2.3 Criterion 3: Information about the target protein’s half-life.....	28
3.2.4 Criterion 4: The availability of a small-molecule ligand for the target protein	33
3.3 Conclusions	33
4 PROTAC Design and Ligand Synthesis	34
4.1 The E3-Ligase Ligands.....	34

4.1.1	Ligands for VHL.....	34
4.1.2	Ligands for CRBN.....	37
4.2	The PRMT1 Ligand.....	37
4.2.1	The synthesis of the ligand.....	41
4.2.2	Evaluation of the deprotected PRMT1 ligand	45
4.3	Linker Design.....	50
4.3.1	The linker and ternary complex formation	50
4.3.2	The linker and pharmacokinetic properties.....	51
4.3.3	The linkers for this project	53
4.4	PROTAC Design for PRMT1 Degradation	54
4.5	Controls Experiments to show PROTAC-Induced Degradation	54
5	VHL-Recruiting PROTACs	56
5.1	PROTACs with VHL Ligand 1	56
5.1.1	Synthesis with an alkyl linker	57
5.1.2	Synthesis with a PEG Linker.....	61
5.1.3	The chemical library of VHL-recruiting PROTACs	65
5.1.4	Stability in cell culture media.....	67
5.2	Degradation Efficacy by Western Blot.....	68
5.3	PROTACs with VHL Ligand 2	71
5.4	The HaloPROTAC Assay	72
5.5	Discussion and Conclusions	75
6	CRBN-Recruiting PROTACs.....	78
6.1	Ether bond between linker and CRBN ligand.....	78
6.1.1	Synthesis	78
6.1.2	Stability in cell culture media.....	88
6.2	Amide bond between linker and CRBN ligand	90
6.3	Amine bond between linker and CRBN ligand	91
6.3.1	Synthesis	91
6.3.2	Stability in cell culture media.....	93
6.4	Library of CRBN-Recruiting PROTAC.....	94
6.5	Degradation Efficacy by Western Blot.....	95
6.6	NanoBRET Target Engagement Assay.....	97
6.7	Discussion and Conclusions	100

7	Heterobifunctional Molecules with <i>N</i>-Glutarimide Ring Alkylation	102
7.1	Degradation Efficacy by Western Blot.....	102
7.2	Mechanism for HBM1-Induced PRMT1 Degradation.....	106
7.3	Analogues of HBM1	107
7.4	Discussion and Conclusions	108
8	Conclusion and Future Work	114
8.1	Conclusions	114
8.2	Future Direction for PROTAC Development	114
8.3	Future Direction for PRMT1 Degradation	116
9	Experimental	119
9.1	General Experimental	119
9.2	Synthetic Procedures	121
9.2.1	General Methods	121
9.2.2	Compound 1-47	123
9.2.3	PROTAC A-Q and HBM1-5	159
9.3	Stability Studies.....	179
9.4	Cell Culture.....	179
9.5	SDS-PAGE followed by Western Blot.....	180
9.6	<i>in vitro</i> Assays.....	182
	References	184
	Appendix 1 Supplementary Figures.....	202
	Appendix 2 UV-HPLC Chromatograms of PROTAC A-Q and HBM1-5.....	214
	Appendix 3 NMR Spectra	219

1 Introduction

1.1 The Protein Arginine Methyltransferases

Post-translational modifications are chemical changes to a protein's structure that occur after protein synthesis and allow cells to rapidly react to their environment without the need to synthesise new proteins¹. One such post-translational modification is the methylation of the amino acid arginine in protein substrates. The protein arginine methyltransferases (PRMTs) are the family of proteins responsible for arginine methylation. These proteins are enzymes that catalyse the transfer of a methyl group (CH₃) from the compound S-adenosyl methionine (SAM) to an arginine of the protein substrate (Figure 1.1).

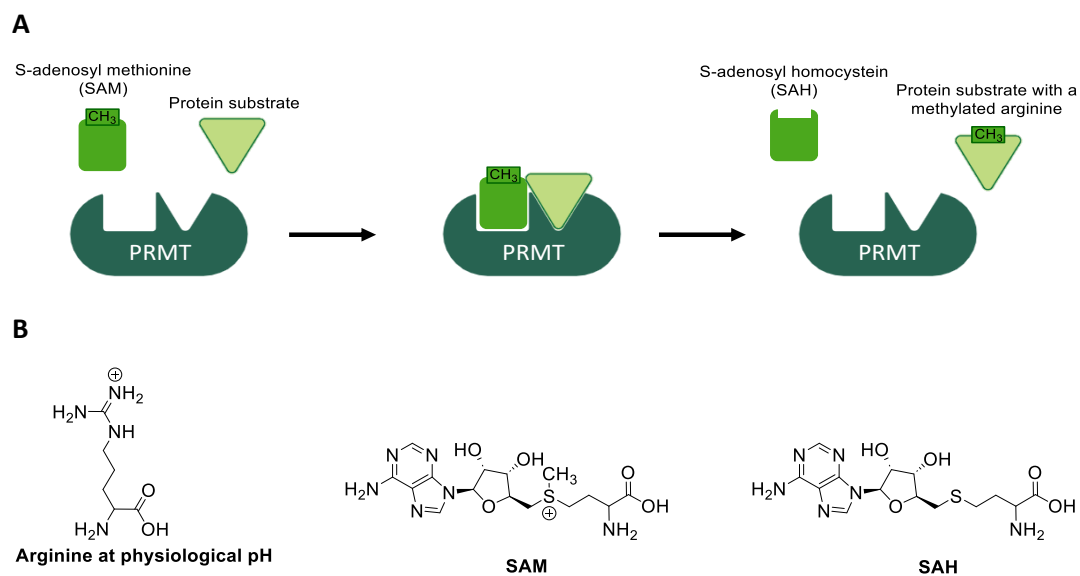


Figure 1.1 PRMT-catalysed arginine methylation. A) Schematic of the PRMT-catalysed methylation of protein substrates. B) Structure of the three key components.

There are nine different PRMT proteins and each PRMT protein has a different protein substrate specificity and a distinct and non-redundant role in the cell¹. The PRMTs are categorised into three 'Types' depending on the arginine methylated product that they form (Figure 1.2).

Type I PRMT catalyses the formation of the asymmetric dimethylation of arginine (ADMA) where two methyl groups are placed upon the same terminal nitrogen atom of the arginine. Type I PRMT includes the proteins PRMT1, PRMT2, PRMT3, PRMT4, PRMT6 and PRMT8.

Type II PRMT catalyses the symmetric dimethylation of arginine (SDMA) where a total of two methyl groups are transferred but one is added to each terminal nitrogen of the arginine. Type II PRMT includes PRMT5 and PRMT9.

Type III PRMT catalyses the monomethylation of arginine (MMA) where a single methyl group is added. Type III includes PRMT7. MMA is also an intermediate for the Type I and Type II PRMTs.

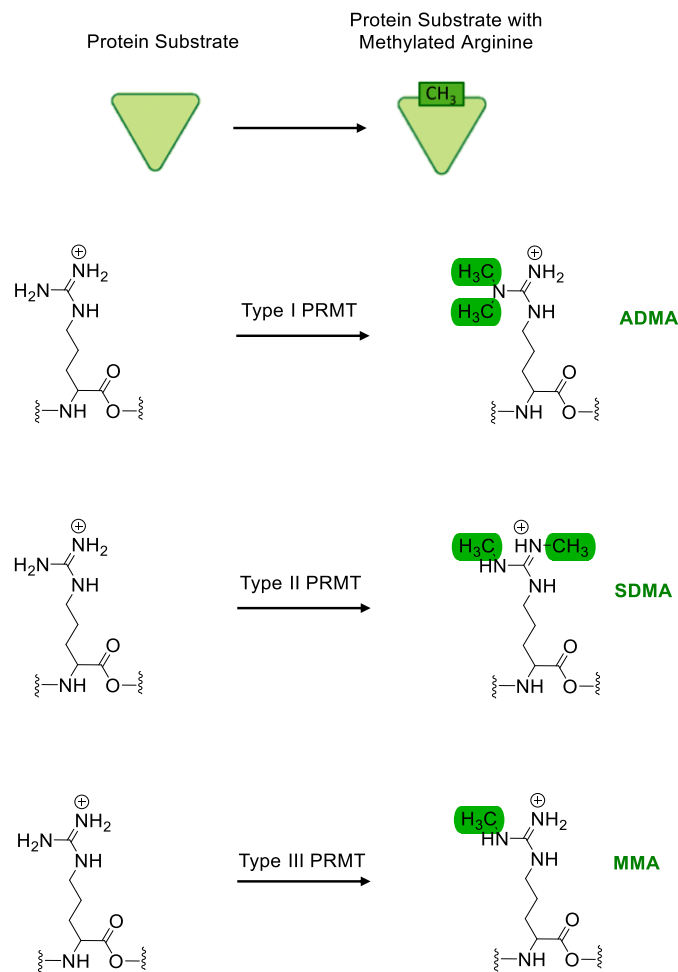


Figure 1.2 Arginine methylation products catalysed by the PRMTs. The protein substrate is made up of a linear chain of amino acids and contains an arginine amino acid. The products following the methylation of arginine by the three Types of PRMT are shown. ADMA is the asymmetric dimethylation of arginine. SDMA is the symmetric dimethylation of arginine. MMA is the monomethylation of arginine.

The methylation of an arginine amino acid in a protein' structure alters the properties of the amino acid. First, the positive charge is retained but distributed over more atoms, thus increasing the hydrophobicity of the amino acid. Second, methylation reduces the hydrogen bonding capacity of the amino acid and changes the relative position of the hydrogen bonding atoms². Finally, methylation changes the steric properties of the amino acid³. An MMA, ADMA or SDMA modification can result in a change of a protein substrate's localisation, its enzymatic ability and its interactions with other proteins. Therefore, arginine methylation regulates many processes in the cell⁴.

Despite the clear regulatory role of arginine methylation in the cell, the mechanism for arginine demethylation is unclear. Arginine methylation was at first considered to be a very stable post-

translational modification where methylation was lost due to protein turnover rather than an enzymatic pathway⁵. However, recent studies now suggest the modification is dynamic as arginine amino acids have been identified that can be cyclically methylated/demethylated in the cell^{6,7}. A protein that uniquely demethylates arginine is yet to be identified. The lysine demethylase jumonji domain containing protein 6 (JMJD6) was reported as an arginine demethylase however a consensus on whether JMJD6 can demethylate arginine amino acids has not been reached⁸⁻¹¹. Future studies are required to clarify whether the demethylation of arginine has an important regulatory role in the cell and identify proteins that can demethylate arginine.

1.1.1 PRMT1 and its role in regulating transcription

PRMT1 is the predominant Type I PRMT and accounts for 85% of cellular ADMA levels¹². PRMT1 regulates many cellular processes to maintain homeostasis which includes gene transcription, RNA processing, signal transduction and the DNA damage response¹³. This project focuses on the role of PRMT1 as a regulator of transcription.

Transcription is the process of making an RNA copy of a gene's DNA sequence. To achieve this, RNA Polymerase II transcription machinery (RNA Pol II) is recruited to the promoter of a gene where it transcribes a gene into its complementary mRNA sequence¹⁴. The spatial and temporal control of RNA Pol II recruitment is highly controlled and is affected by a range of factors, including the structure of chromatin and the activity of regulatory proteins such as transcription factors and cofactors¹⁵. Transcription factors are proteins that bind to specific DNA sequences and, in combination with cofactors, can modify the conformation of chromatin, or affect the ability of RNA Pol II to be recruited to a specific gene promoter¹⁶ (Figure 1.3).

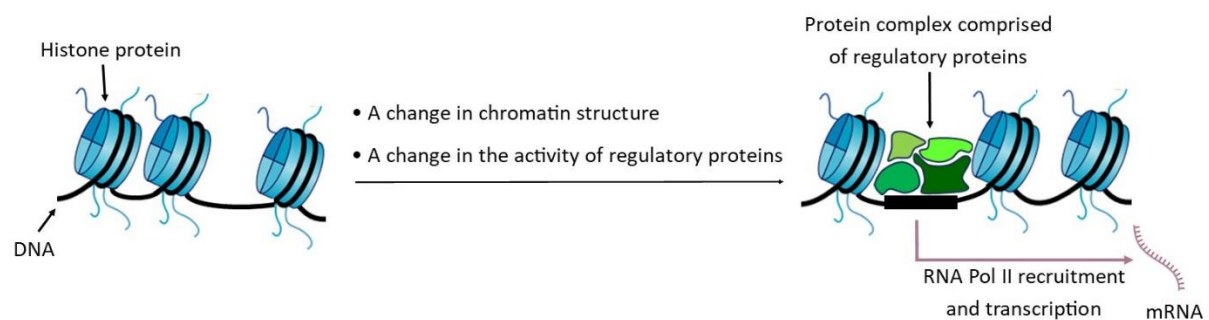


Figure 1.3 Schematic of chromatin and factors that affect transcription. In the cell DNA exists as chromatin where it is highly condensed and in complex with histone proteins. The structure of chromatin is dynamic and for a gene to be transcribed, the required regulatory proteins and RNA Pol II must be recruited. Alternatively, transcription can be prevented by the structure of chromatin and the presence of protein complexes.

PRMT1 has a key role in the regulation of transcription. First, PRMT1 can methylate arginine amino acids on histone proteins. This alters the ability of the histone to form hydrogen bonds and changes the histone's hydrophobicity which can affect the intermolecular interactions between histone proteins as well as the histone-DNA interaction. This can lead to a change in the structure of chromatin which can affect the accessibility of the chromatin to regulatory proteins and RNA Pol II¹⁵.

Second, PRMT1 can modulate the activity of transcription factors and cofactors through methylation. The PRMT1-catalysed methylation of transcription factors can have a significant effect on their activity, their DNA binding ability and their interactions with other regulatory proteins¹⁷. For example, the transcription factor breast cancer type 1 susceptibility protein (BRCA1) is a substrate for PRMT1, and the ADMA post-translational modification on BRCA1 affects the ability of this transcription factor to bind to particular promoters¹⁸. The ADMA modification also alters the cellular localisation of BRCA1, reducing its presence in the nucleus which further impacts its ability to bind to chromatin and initiate transcription¹⁹. A review of the substrates of PRMT1 that are implicated in the regulation of transcription can be found in Pham *et al.*¹⁷.

Finally, the PRMT1 protein itself can form protein-protein interactions with other regulatory proteins and be a part of protein complexes on the chromatin. One example is a chromatin-bound complex containing PRMT1 and the regulatory proteins, forkhead box protein A1 (FOXA1) and hepatocyte nuclear factor 4 gamma (HNF4G)²⁰.

1.1.2 PRMT1 in cancer

Aberrant PRMT1 expression leads to the dysregulation of transcription which affects cellular processes that affect cell growth, proliferation and differentiation²¹. Upregulated PRMT1 expression has been identified in a range of cancers (reviewed in Yang *et al.*²¹) and this project focuses on PRMT1 in breast cancer and pancreatic ductal adenocarcinoma (PDAC).

Breast cancer is the most common cancer in the UK and was diagnosed over 46,000 times in 2017²². Heterogeneity in breast cancer has led to its classification into molecular subtypes based on the expression of three hormone receptors: the oestrogen receptor (ER), the progesterone receptor (PR) and the human epidermal growth factor receptor 2 (HER2)²³. The subtype is indicative of prognosis and is used to inform treatment plans for patients with breast cancer²⁴.

PDAC has the lowest survival rate of all common cancers and is the fourth most frequent cause of cancer-related deaths worldwide with a five-year survival rate of less than 8%²⁵. It is particularly challenging to treat due to profound heterogeneity in gene mutations, metastasis occurring early in

the disease and a dense, desmoplastic microenvironment around the cancer cells that limits drug delivery²⁶. These are cancers where a novel therapeutic strategy could make a significant impact.

In clinical samples of breast cancer and PDAC, upregulated PRMT1 presence has been associated with poor prognosis (breast cancer²⁷⁻²⁹, PDAC^{30,31}). Knockdown studies in cell and animal models of these cancer types have shown that the PRMT1 overexpression is strongly associated with a proliferative phenotype (breast cancer^{27,32,33}, PDAC^{31,34}). These knockdown studies have facilitated substantial work that uncovered specific protein substrates of PRMT1 whose aberrant methylation dysregulates transcription and promotes tumourigenesis. A full summary is available in Hwang *et al.*³⁵.

One notable protein substrate of PRMT1 is the histone H4R3. In homeostasis, there is a sophisticated and competitive mechanism between PRMT1 (Type I PRMT) and PRMT5 (Type II PRMT) to modulate transcription at this site. The ADMA modification catalysed by PRMT1 leads to gene activation whereas the SDMA by PRMT5 leads to gene repression³⁵. Histone H4R3 is located at the promotor for the gene that encodes the zinc-finger E-box-binding homeobox 1 (ZEB1). In breast cancer, the upregulation of PRMT1 leads to the increased transcription of ZEB1 which increases the capability of breast cancer cells for invasion and migration and inhibits senescence (irreversible cell-cycle arrest)³³.

PRMT1 has also been found to be responsible for modulating the activity of the transcription factor, the Progesterone receptor (PR). The PRMT1-catalysed methylation of PR leads to a reduction in PR stability, increasing its rate of degradation. This modulates the transcriptional activity of PR and dysregulates the expression of several genes that control breast cancer cell proliferation and migration²⁷. Hence, there is strong evidence that targeting PRMT1 to reduce its activity is a promising strategy in cancer treatment.

In vitro studies have also highlighted PRMT1 as a promising target in combinatory treatments where a reduction in PRMT1 activity has been shown to make cancer cells more sensitive to existing therapies that target the inhibition of alternative proteins. Synergistic interactions have been identified between PRMT1 and various chemotherapeutics³², immunotherapies³⁶, as well as in combination with inhibitors of the epidermal growth factor receptor (EGFR)^{4,32,37} or the Type II PRMT, PRMT5^{13,38}.

Synergy can be exemplified by Suresh *et al.* where the inhibition of PRMT1 in combination with an inhibitor of EGFR has a greater effect on cell viability than the expected additive effects of the two individual inhibitors³² (Figure 1.4). The overexpression of EGFR is associated with a metastatic phenotype³⁹, and the synergy between PRMT1 and EGFR inhibition can be rationalised biologically by

the effect of PRMT1 on regulating EGFR transcription. PRMT1 binds directly to the promoter region of the gene that encodes EGFR and activates its transcription, shown by a reduction in *EGFR* mRNA and decreased EGFR protein expression with PRMT1 knockdown³². Thus, a reduction in PRMT1 activity will reduce the protein expression of EGFR, and in a cell with lower EGFR expression, an inhibitor for EGFR will have greater potency as a greater fractional occupancy of active sites will be achieved at a given dose.

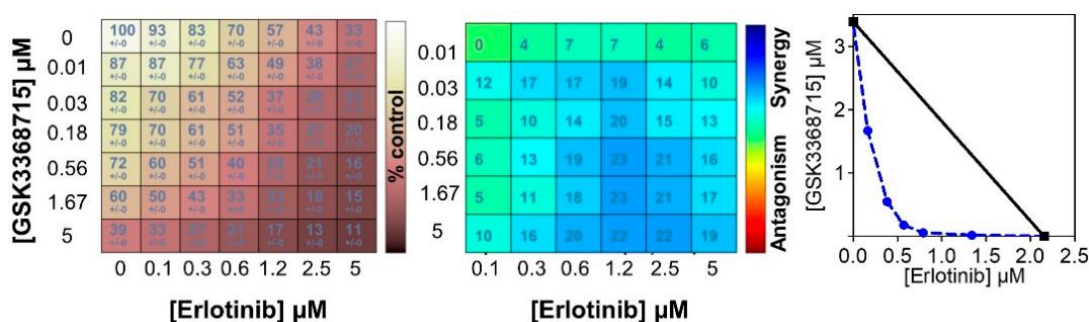


Figure 1.4 PRMT1 inhibition sensitises breast cancer cells to EGFR inhibition. The effect on cell viability of the PRMT1 inhibitor, GSK3368715 in combination with EGFR inhibitor Erlotinib was assessed at various concentrations. The plot on the left shows percentage cell viability compared to a DMSO control. The drug interactions were calculated using the Loewe model and the resulting synergy matrix and isobologram are shown in the middle and on the right. Experiment in the triple-negative breast cancer cell line MBA-MB-468. Figure reprinted from Suresh et al.³².

1.2 Current Therapeutic Approaches for Targeting PRMT1

The identified role that PRMT1 plays in tumourigenesis has led to the development of multiple chemical inhibitors for this protein. These have been used as tools to investigate the physiological role of PRMT1 and an inhibitor for PRMT1 has entered clinical trials.

The first inhibitor for PRMT1 was **AMI-1**, published in 2004. This inhibitor has low potency for PRMT1 ($IC_{50} = 8.8 \mu M$)⁴⁰. Since then, several potent PRMT1 inhibitors have been published. The two most frequently used in epigenetic studies are **MS023** and **GSK3368715**^{13,41}. Both inhibitors bind in the protein substrate binding pocket of PRMT1 and are competitive with the protein substrates.

GSK3368715 is uncompetitive with the methyl-donor SAM so SAM needs to be bound to PRMT1 for the inhibitor to be able to bind. SAM may stabilise the protein substrate binding pocket allosterically or form direct interactions with the inhibitor^{13,42,43}. **MS023** is non-competitive with SAM⁴².

Despite being potent inhibitors of PRMT1, neither **MS023** nor **GSK3368715** exhibit selectivity for PRMT1 over other Type I PRMTs and are pan-Type I inhibitors^{13,41} (Figure 1.5). The development of a selective PRMT1 ligand has been challenging due to the high sequence similarity within the active sites of the Type I PRMTs³⁵, and a specific and potent PRMT1 inhibitor has yet to be discovered.

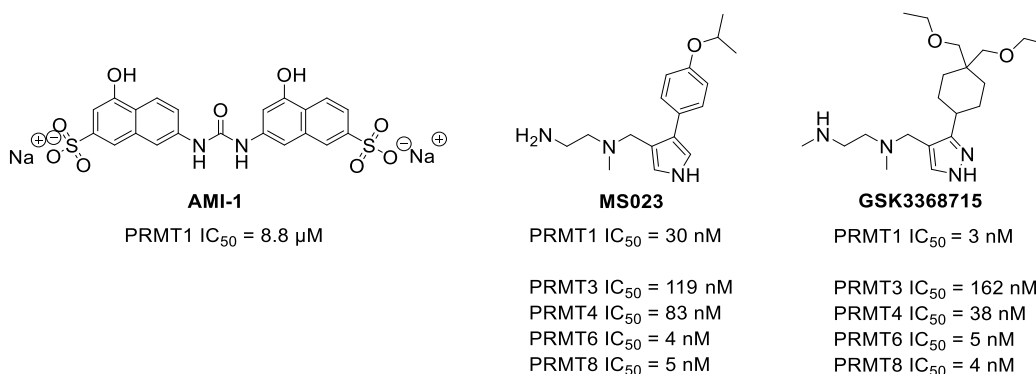


Figure 1.5 **Published PRMT1 inhibitors do not exhibit selectivity to PRMT1 over other Type I PRMTs.** IC₅₀ is the concentration required to exert half its maximal inhibitory effect. The IC₅₀ values were determined by a biochemical assay measuring the incorporation of [³H]SAM into protein substrates following incubation with recombinant protein. IC₅₀ values published in Eram et al.⁴¹ and Fedoriw et al.¹³.

MS023 and **GSK3368715** have been studied extensively in *in vitro* and *in vivo* cancer models and the dose-dependent reduction in tumour volume in mouse xenograft models has been observed. For **MS023** this includes models of ER-positive breast cancer^{38,41} and triple-negative breast cancer⁴⁴, and for **GSK3368715** this includes models of triple-negative breast cancer¹³ and PDAC^{13,34}.

GSK3368715 entered a phase one clinical trial to treat participants with solid tumours and diffuse large B-cell lymphoma [NCT03666988]. The results were published in May 2023 following the early termination of the trial⁴⁵. Several factors led to its termination. First, **GSK3368715** treatment did not cause a reduction in tumour burden in any of the participants. The best response observed was stable disease in 28% of participants, and the remainder saw disease progression. Furthermore, the safety profile of **GSK3368715** was poor; 97% of participants experienced treatment-emergent adverse effects and 52% were severe. Dose-limiting toxicity also led to dose reduction.

Target engagement for **GSK3368715** was moderate and variable. For patients treated with 100 mg of **GSK3368715**, on day 15 there was a 43.1 ± 5.81% (SE) reduction in a specific ADMA modification (ADMA-hnRNP-A1) in the blood. In contrast, in the tumour the same modification was only reduced by 18.5 ± 9.6% levels.

This trial raises the critical question of whether the lack of clinical efficacy and poor safety profile associated with **GSK3368715** results from pan-Type I PRMT inhibition or it is associated with off-target effects and poor pharmacokinetic properties of the inhibitor. An alternative tool to investigate the clinical utility of targeting PRMT1 is needed, and a proteolysis targeting chimera (PROTAC) to degrade PRMT1 may be the answer. The following section will introduce the pharmacology behind PROTAC-induced degradation and will show why a PROTAC that degrades PRMT1 may have a greater

efficacy and a better safety profile compared to **GSK3368715** or any future small-molecule inhibitors for PRMT1.

1.3 The Ubiquitin Proteasome System

The degradation of proteins is an important way in which a cell removes unneeded or damaged proteins to maintain homeostasis. A key system responsible for this degradation is the Ubiquitin Proteasome System (UPS). Protein degradation is regulated by the covalent modification of the amino acid lysine on the protein's surface with ubiquitin, a 76 amino-acid protein. The proteasome is a multicomplex enzyme that recognises covalently attached ubiquitin chains and subsequently degrades proteins tagged with a ubiquitin chain into short peptide fragments⁴⁶ (Figure 1.6).

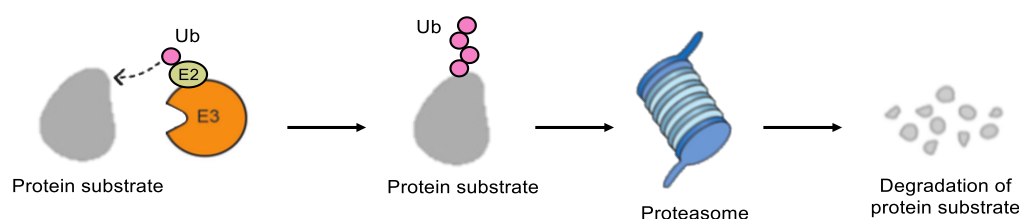


Figure 1.6 Schematic of the degradation pathway of an endogenous protein substrate. A polyubiquitin chain is transferred to a lysine on the surface of a protein substrate which tags a protein for degradation by the proteasome.

The ubiquitination of protein substrates is a highly regulated process that is mediated by three classes of ubiquitination enzymes: the ubiquitin-activating enzyme (E1-enzyme), the ubiquitin-conjugating enzyme (E2-enzyme) and ubiquitin-protein ligase (E3-ligase). These three enzymes work catalytically and in a sequential process to mediate the ubiquitination of a protein substrate (Figure 1.7). First, ubiquitin is adenylated at its C-terminal glycine to form ubiquitin adenylate. A cysteine amino acid of the E1-enzyme then undergoes a nucleophilic substitution reaction with ubiquitin adenylate to form a thioester bond to ubiquitin. Ubiquitin is then transferred via a trans-thioesterification reaction to a cysteine on the E2-enzyme. This E2-ubiquitin complex is recognised by the E3-ligase which mediates the transfer of ubiquitin from the E2-enzyme to a surface lysine of a protein substrate. An isopeptide bond is formed between the C-terminal glycine on ubiquitin and a lysine of the protein substrate⁴⁷. The Really Interesting New Gene (RING) family of E3-ligases act as scaffolding molecules to bring the ubiquitin-charged E2-enzyme into close contact with a protein substrate⁴⁸. There are more than 600 RING E3-ligases and each can recognise different protein substrates for ubiquitination⁴⁹.

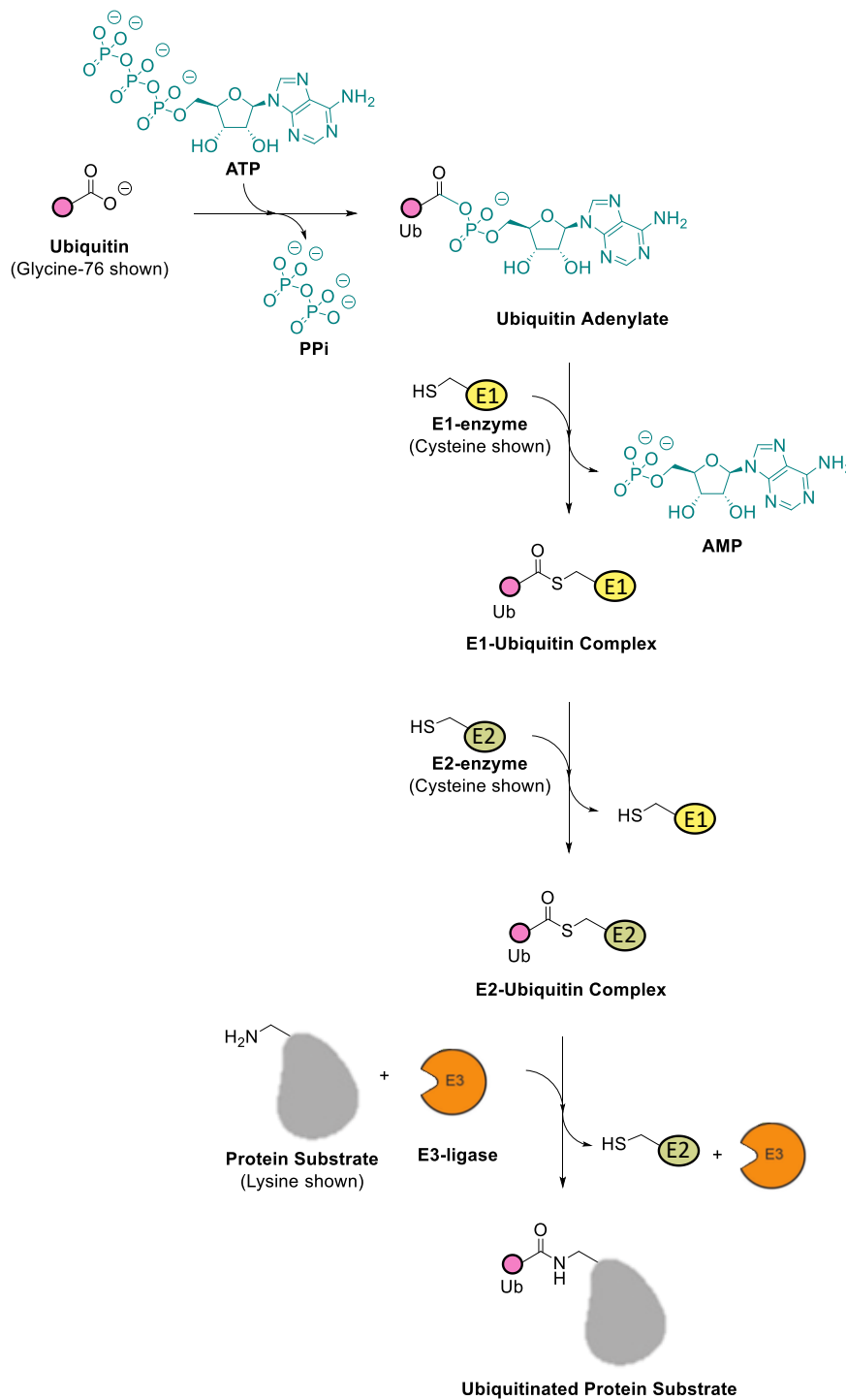


Figure 1.7 **The ubiquitin cascade.** The production of a ubiquitin-charged E2-enzyme that forms a complex with E3-ligase to mediate ubiquitin transfer to protein substrates. The E1-enzyme, E2-enzyme and E3-ligase are catalytic in this cascade. ATP = adenosine triphosphate. PPi = inorganic pyrophosphate. AMP = adenosine monophosphate.

However, ubiquitination of a protein substrate does not always lead to its recognition and degradation by the proteasome. Ubiquitin contains seven lysine amino acids and an *N*-terminal amino group that can form isopeptide bonds to the *C*-terminal glycine amino acid on a subsequent

unit of ubiquitin to generate polyubiquitination chains on the surface of a protein substrate⁵⁰. Depending on the topology of the polyubiquitin chain, ubiquitination can lead to different biological outcomes in the cell⁵¹. For recognition by the proteasome, it has been deciphered that polyubiquitin chains linked at the Lysine-48/ Lysine-11 of ubiquitin are required⁵². This requirement for the correct topology of polyubiquitin chain on a protein substrate adds additional complexity to the regulation of protein degradation.

1.4 Targeted Protein Degradation with a PROTAC

A PROTAC hijacks the UPS by modifying which cellular proteins are ubiquitinated. A PROTAC is a heterobifunctional small molecule; one end binds to a target protein, and one end binds to an E3-ligase. This induces proximity between an E3-ligase and a target protein through a ternary complex and increases the likelihood of ubiquitin transfer which leads to the proteasomal degradation of the target protein (Figure 1.8). By changing the structure of the PROTAC, different proteins can be recruited to the E3-ligase, and in this system, the selectivity of which proteins are ubiquitinated is no longer regulated by E3-ligase substrate specificity.

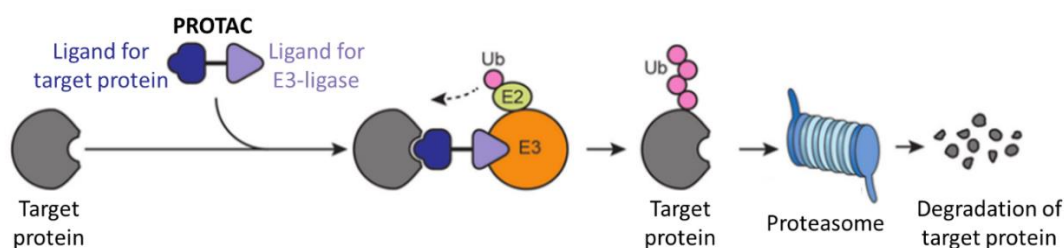


Figure 1.8 Schematic of PROTAC-induced degradation of a target protein. A PROTAC forms a ternary complex with a target protein and E3-ligase which increases proximity between the ubiquitin-charged E2 enzyme and the target protein, facilitating ubiquitin transfer and its recognition by the proteasome. Figure adapted from Huang et al.⁴⁸.

1.4.1 Introducing literature PROTACs

The first PROTAC was published in 2001 by Sakamoto *et al.* and degraded the protein methionine aminopeptidase-2 (MetAP-2). This PROTAC, **protac-1**, consisted of a phosphopeptide joined to a small-molecule ligand by a linker. The phosphopeptide IκBα binds to the E3-ligase Skp1-Cullin-F box complex containing Hrt1 (SCF), and the small-molecule ligand binds to the target protein MetAP-253 (Figure 1.9). It was shown that the degradation of MetAP-2 was **protac-1** dependent that **protac-1** recruited both MetAP-2 and SCF, and that MetAP-2 was ubiquitinated. The biological assays in this publication were undertaken in hen egg extract as the peptidic E3-ligase ligand made the PROTAC impermeable to a cell membrane. This publication demonstrated proof-of-principle that a PROTAC can be used for selective target protein degradation.

Poor cell permeability was a key limitation of PROTACs until 2008 when the first cell-permeable PROTAC was published, **protac-2**. This PROTAC degraded the androgen receptor and used a small-molecule ligand to recruit the mouse double minute 2 homologue (MDM2) E3-ligase⁵⁴. However this PROTAC exhibited low potency with incomplete degradation observed at 10 μ M in a cervical cancer cell line, precluding its potential for clinical translation.

The identification of small-molecule ligands for two E3-ligases belonging to the Cullin RING family of E3-ligases, Cereblon (CRBN)⁵⁵ and Von-Hippel Lindau (VHL)^{56,57}, has led the field to expand tremendously and the publication of a large number of potent and cell-permeable PROTACs. This includes the PROTACs **MZ1** and **ARV-471** (Figure 1.9).

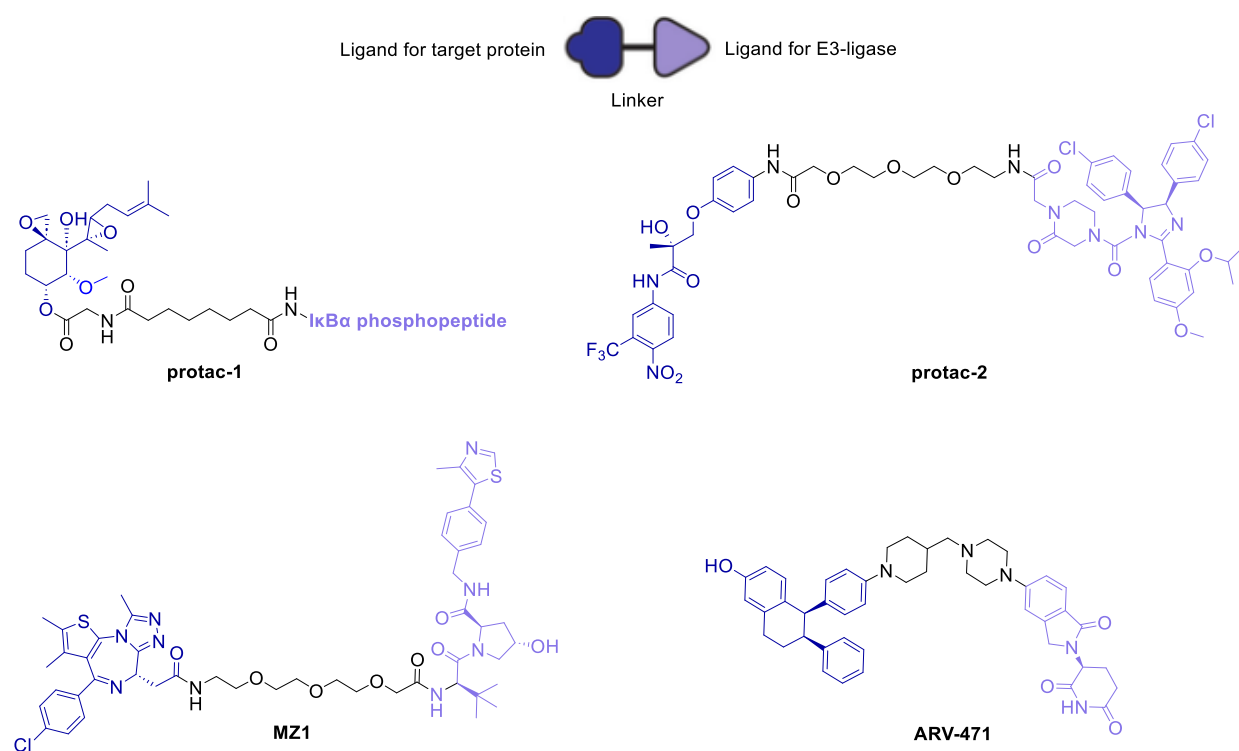


Figure 1.9 Structure of selected PROTACs from the literature. PROTACs follow a general structure of a ligand for the target protein (blue) connected to a linker (black) which is attached to a ligand for a E3-ligase (lilac).

Published in 2017, **MZ1** comprised a small-molecule ligand for the E3-ligase VHL joined via a linker of repeating polyethylene glycol units (PEG) to a small-molecule ligand for the bromodomain-containing proteins BRD2, BRD3 and BRD4⁵⁸. **ARV-471** comprises a small-molecule ligand for the E3-ligase CRBN attached via a linker to a ligand for the target protein, the oestrogen receptor (ER). In 2019, this PROTAC entered a phase 1/2 clinical trial in patients with ER+/HER2- locally advanced or metastatic breast cancer [NCT04072952]. **ARV-471** degraded ER with a median degradation of 69% and clinical

benefit was observed in 38% of participants⁵⁹. Subsequently, **ARV-471** was the first PROTAC to enter a phase 3 trial and the trial is currently underway for patients with advanced ER+/HER2- metastatic breast cancer [NCT05654623].

Using the PROTACs introduced above, the next section will highlight the three major advantages that PROTAC-induced degradation of PRMT1 may have over PRMT1 inhibition. To date there have not been any PROTACs published that target PRMT1 or a Type I PRMT.

1.4.2 Advantages of PROTACs

1.4.2.1 Event-driven

A PROTAC proceeds by an event-driven pharmacological strategy where PROTAC binding and ternary complex formation trigger an event, the transfer of a ubiquitin group. Once the ubiquitination of the target protein has occurred, the PROTAC can be released and can act catalytically to mediate the ubiquitination of multiple copies of a given target protein⁶⁰. This has the advantage that a low dose can elicit a strong biological response.

PROTACs can act at low nanomolar concentrations. For an inhibitor molecule, a cellular IC₅₀ (concentration required to exert half its maximal inhibitory effect) of below 100 nM is generally considered a suitable potency⁶¹. PROTACs can operate below this level; the DC₅₀ (concentration required to degrade half the protein) of **ARV-471** in the MCF-7 breast cancer cell line is 0.9 nM⁶² and between 6-33 nM for **MZ1** in eight breast cancer cell lines⁶³.

This high potency means that a PROTAC could be administered at a lower dose compared to an inhibitor. Off-target effects are frequently associated with inhibition-driven pharmacology. Inhibitors bind to proteins and block their function, and hence the higher the dose the greater the efficacy. Therefore, a high and sustained concentration of the inhibitor molecule is required for therapeutic benefit⁶⁴. However with most drugs there is also a dose-toxicity relationship⁶⁵ and in phase one clinical trials off-target toxicity is the primary basis for halting dose escalation rather than achieving the maximum efficacy from target inhibition^{66,67}. A PROTAC for PRMT1 has the potential to be administered at a lower dose than an inhibitor resulting in less off-target effects.

The speed at which PROTACs have emerged from a proof-of-concept to their translation to the clinic has meant that their safety profile and utility for human patients are still being investigated⁶⁸. However the data emerging from clinical trials is promising. In the phase ½ clinical trials of **ARV-471**, high tolerability was observed at a 200 mg dose with only 6 % of patients experiencing an treatment related adverse effect at stage 3 or 4, and none at stage 5⁵⁹.

1.4.2.2 Ternary complex

One reason why the PROTAC field has expanded so rapidly, and a large range of target proteins have been degraded, is that previously published ligands for a target protein can be readily adapted into a PROTAC through the attachment of the linker and E3-ligase ligand.

MZ1 contains the same pharmacophore as the inhibitor **JQ1**. In this thesis, pharmacophore is defined as the precise arrangement of atoms or functional groups in a small molecule required for the binding interaction with its biological target. Similar to the inhibitor **JQ1**, PROTAC **MZ1** has a similar *in vitro* binding affinity to the proteins BRD2, BRD3 and BRD4 (Figure 1.10). However **MZ1** only degrades BRD4⁵⁷. Selective degradation can be observed with a non-selective target protein ligand and degradation efficacy cannot be rationalised through a difference in binding affinity.



Figure 1.10 Inhibitor **JQ1** and PROTAC **MZ1** contain the same pharmacophore. PROTAC **MZ1** has similar binding affinities to BRD2, BRD3 and BRD4 but selectively degrades BRD4. A) Chemical structure of inhibitor **JQ1**. B) Data for **MZ1** binding to bromodomain 2 of the indicated protein. The higher the K_d value, the lower the affinity. The K_d values were obtained by isotherm titration calorimetry and published in Zengerle et al.⁵⁷.

The selectivity of degradation arises because of the ternary complex formed with the target protein, PROTAC and E3-ligase. Gadd *et al.* investigated the selectivity exhibited with **MZ1** and highlighted a correlation between the stability of the ternary complex and degradation⁵⁸. By elucidating the X-ray crystal structure of the ternary complex and looking at the thermodynamics of its formation, they showed that the ternary complex is affected by protein-protein interactions between the E3-ligase and the target protein. They call this cooperativity. Positive cooperativity is when the PROTAC-induced protein-protein interactions enhance the formation of the ternary complex. Negative cooperativity diminishes ternary complex formation through repulsive interactions or steric hindrance between the two proteins (Figure 1.11). For **MZ1**, they found that BRD4 has greater PROTAC-induced cooperativity than BRD2 or BRD3 and rationalised the observed selective degradation based on this^{58,69}.

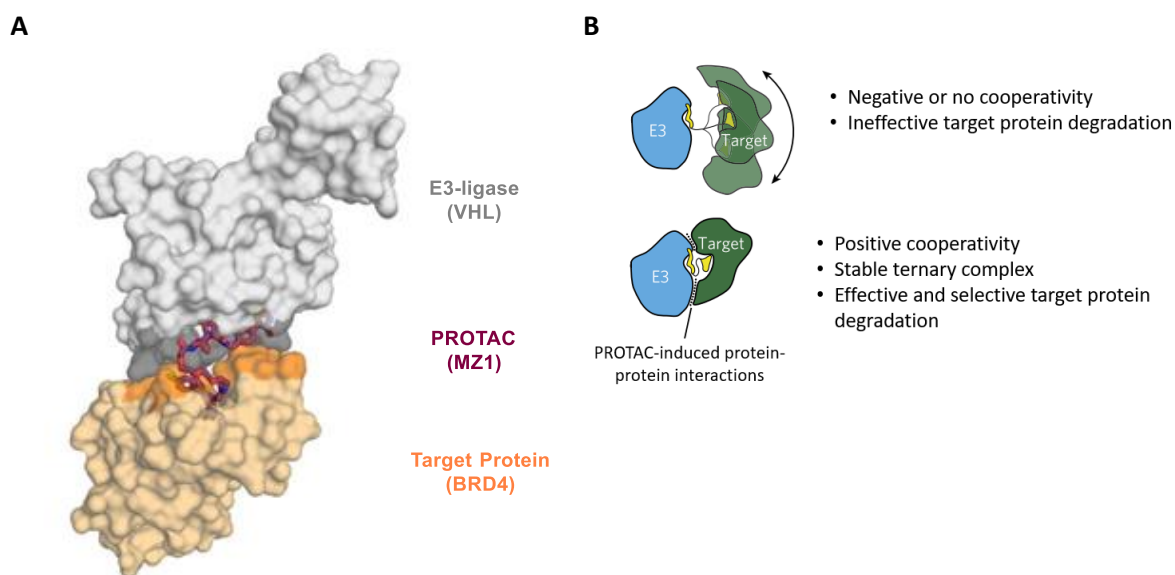


Figure 1.11 Protein-protein interaction between the E3-ligase and target protein can occur in the ternary complex. A) Crystal structure of ternary complex of PROTAC **MZ1**, BRD4 and the VHL E3-ligase. A folded conformation of PROTAC **MZ1** facilitates extensive protein-protein interactions between BRD4^{BRD2} and VHL. Crystal structure first reported by Gadd *et al.*⁵⁸ and figure reprinted from ⁷⁰. B) Schematic of how PROTAC-induced protein-protein interactions can affect the stability of a ternary complex. Figure adapted from Gadd *et al.*⁵⁸.

However Bondeson *et al.* show that ternary complex stability is not the only factor. They synthesised a PROTAC with the same pharmacophore as the promiscuous kinase ligand **Foretinib** and produced **protac-3** that has a high affinity to 54 kinases but only degrades 9 kinases (Figure 1.12). To determine which kinases form a ternary complex with this PROTAC, they undertook a pull-down experiment with GST-tagged VHL followed by Western blot. The 9 kinases **protac-3** degraded were identified however it also revealed additional kinases that form a stable ternary complex but are not degraded. They propose that despite stable ternary complexes forming, the orientation of a lysine on the target protein is not suitable and cannot accept a ubiquitin group from the E2-enzyme⁷¹.

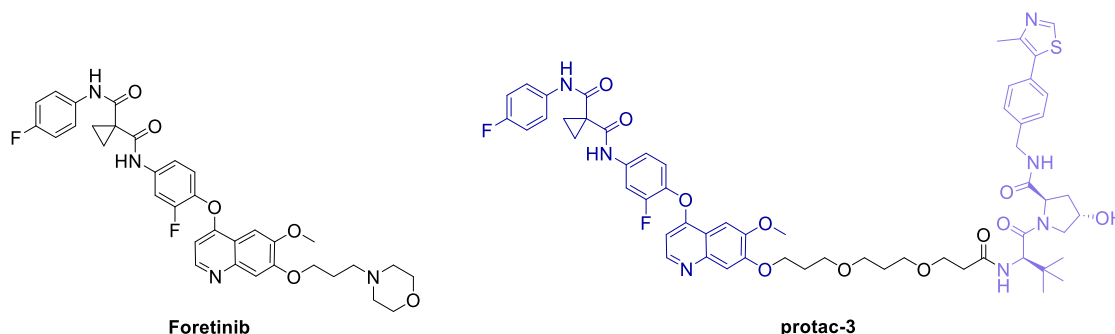


Figure 1.12 Structure of the promiscuous kinase inhibitor Foretinib and protac-3 that has the same binding pharmacophore. The PROTAC is comprised of the target protein ligand (blue), a PEG linker (black) and the VHL E3-ligase ligand (lilac).

No PRMT1-selective inhibitors have been published however a PROTAC containing the same pharmacophore as a pan-Type I inhibitor such as **MS023** or **GSK3368715** could show selectivity for PRMT1 degradation because of ternary complex formation. Specifically targeting PRMT1 over the other Type I PRMTs may result in a different (and superior) physiological effect.

1.4.2.3 Protein degradation

The final advantage of a PROTAC over an inhibitor is that PROTAC-induced degradation removes the entire protein unlike an inhibitor which blocks the active site. This can lead to a difference in physiological effect as non-enzymatic functions of the protein are also removed. **MZ1** exemplifies this as the mRNA expression profile obtained by the **MZ1**-induced degradation of BRD4 is more similar to that from the knockdown of BRD4 using siRNA than the inhibition of BRD4 with the parent inhibitor **JQ1**⁵⁷.

PRMT1 may have non-enzymatic regulatory roles that promote cancer progression. It has been identified that binding between PRMT1 and the orphan nuclear receptor TR3 does not lead to methylation but stabilises TR3 and modulates its DNA binding and transcriptional activity⁷². PRMT1 may also have a role as a cofactor where it may have scaffold-like properties that facilitate protein-protein interactions on the DNA, such as those between transcription factors and cofactors²⁰. PRMT1 degradation could lead to a different physiological effect compared to inhibition.

1.4.3 Targeting PRMT1 with a PROTAC

As with any compound that aims to change cellular function in a new way, there are challenges and limitations that may need circumventing when using a PROTAC for PRMT1.

First, it has been postulated that a drug targeting PRMT1 in cancer should aim to restore PRMT1 to normal levels rather than completely eliminating its activity⁷³⁻⁷⁵. This is because PRMT1 is ubiquitously expressed in all cell types and tissues in the human body, it is required for distinct cellular differentiation processes and the genetic knockout in mice is embryonically lethal. However PRMT1 is not required for viability¹². If a PROTAC that degrades PRMT1 is produced, an investigation will be required to see if the PROTAC-induced degradation of PRMT1 leads to cytotoxicity or if it reduces the cell's capability to contribute to tumourigenesis and whether the balance between these two outcomes can be modulated by the efficacy of PRMT1 degradation.

Second, Patient stratification may be required with a PROTAC for PRMT1 to maximise therapeutic effect. In renal cancer, there is evidence that the clinical utility of reducing PRMT1 activity can vary depending on the grade and stage of the disease⁷⁶. Furthermore, it has been identified that in PDAC patients following tumour resection or chemotherapy, upregulated PRMT1 expression correlates

with an extended survival rate suggesting that PRMT1 may contribute to a tumour-suppressive response under certain circumstances⁷⁷.

Finally, no PROTACs have yet been approved for clinical use and a complete understanding of the safety and utility of this event-driven pharmacological strategy is still being investigated⁶⁸. Only further research and time will enable a conclusion on whether PROTACs can be a safe and efficacious therapy in the clinic.

2 Project Aims

The degradation of PRMT1 by a PROTAC is a promising therapeutic strategy. In clinical samples of breast cancer and PDAC PRMT1 upregulation is associated with poor prognosis and the genetic knockdown of PRMT1 and the inhibition of PRMT1 in models of cancer have shown strong antiproliferative effects. The PROTAC-induced degradation of PRMT1 may lead to a superior safety profile and functional outcome compared to PRMT1 (and pan-Type I PRMT) inhibition as a PROTAC may be more potent, may lead to the selective degradation of PRMT1 and may remove non-enzymatic functions of PRMT1.

The project aims to:

- Determine if endogenous PRMT1 has suitable properties for PROTAC-induced degradation.
- Design and synthesise PROTACs for PRMT1 (Figure 2.1).

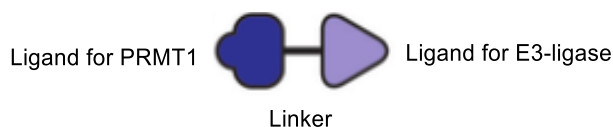


Figure 2.1 Structure of a PROTAC for PRMT1.

- Assess the synthesised PROTACs for their ability to degrade PRMT1 in models of breast cancer and PDAC.

If PRMT1 degradation is observed this project should:

- Confirm that the PRMT1 degradation occurs by the ternary complex-mediated ubiquitination of PRMT1.
- Investigate the PROTAC-induced degradation of PRMT1 for selectivity to PRMT1 over other Type I PRMTs.

3 The Suitability of PRMT1 for PROTAC-Induced Degradation

In this chapter, the endogenous properties of PRMT1 are assessed to determine if it is a suitable target for PROTAC-induced degradation. The ability to measure changes in PRMT1 protein levels was confirmed and a sensitive and selective Western blot assay for this purpose was validated. This included the knockdown of PRMT1 and an investigation into the associated downstream effects. The validated assay was then used, alongside available literature data, to assess what properties of a target protein make it amenable to PROTAC-induced degradation and whether PRMT1 has these properties.

3.1 Development of an Assay to Measure a Change in PRMT1

Human tumour-derived cell lines are an *in vitro* model system that have been used for many years in anti-cancer drug discovery. The cell line retains the genomic features of the primary tumour from which it was derived and can be used to predict the clinical efficacy of new therapeutic compounds⁷⁸. This makes it a suitable model system to investigate the effect of PRMT1 degradation on tumourigenesis.

3.1.1 Selecting the tumour-derived cell line

The most diagnosed subtype of breast cancer, accounting for over 70% of cases, is the luminal A subtype which is characterised by the expression of the ER and PR hormone receptors but not HER2⁷⁹. PRMT1 has been shown to be upregulated in this breast cancer subtype, and this upregulation correlates with a reduction in relapse-free survival for patients^{27,80}. The MCF-7 cell line is derived from metastatic breast adenocarcinoma of the luminal A subtype, and it is the most studied breast cancer cell line in the world⁸¹. Anti-proliferative effects have been observed in MCF-7 cells with the pan-Type I inhibition **MS023**^{38,41}, and the genetic knockdown of PRMT1 leads to a decrease in ADMA levels on histone H4R3⁴¹. This cell line is sensitive to a reduction in PRMT1 activity and has been used in this project.

PDAC is a disease characterised by vast heterogeneity, but specific genes are frequently mutated and drive disease progression. The most frequently mutated genes in PDAC are the oncogene *KRAS* and the tumour suppressive gene *p53*⁸². The HPAF-II and KP-3 cell lines have been selected for this project as they have mutations in the *KRAS* and *p53* genes that differ from each other⁸³. These cell lines also have different sensitivity to pan-Type I PRMT inhibition³⁴ (Figure 3.1).

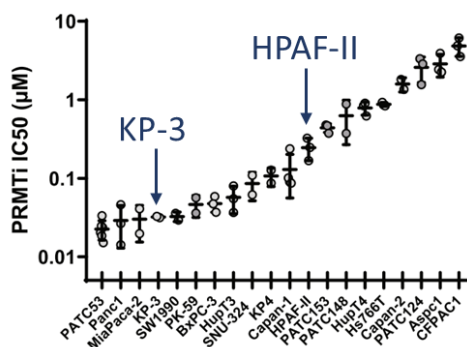


Figure 3.1 The potency of pan-Type I PRMT inhibition varies between different PDAC-derived cell lines. The Y-axis is the IC₅₀ values of the pan-Type I PRMT inhibitor GSK3368715 (PRMTi) as calculated by a dose-response curve in a colony formation assay. The X-axis is the different PDAC-derived cell lines. Figure adapted from Giuliani et al.³⁴.

3.1.2 The Western blot assay

Following the treatment of a cell line with a PROTAC or other probe compound, the Western blot assay was proposed as a suitable method to measure the level of PRMT1 protein. Western Blot is a fixed endpoint method where the amount of a target protein is measured after a defined incubation time following treatment and a change in protein level is inferred by comparing the protein level to a control (untreated) sample⁸⁴. The semi-quantitative measurement of protein levels is achieved using a primary antibody that specifically recognises the target protein. A fluorescent secondary antibody selectively binds to the primary antibody and the fluorescent signal intensity is proportional to the amount of target protein. The key stages of the assay are shown in Figure 3.2.

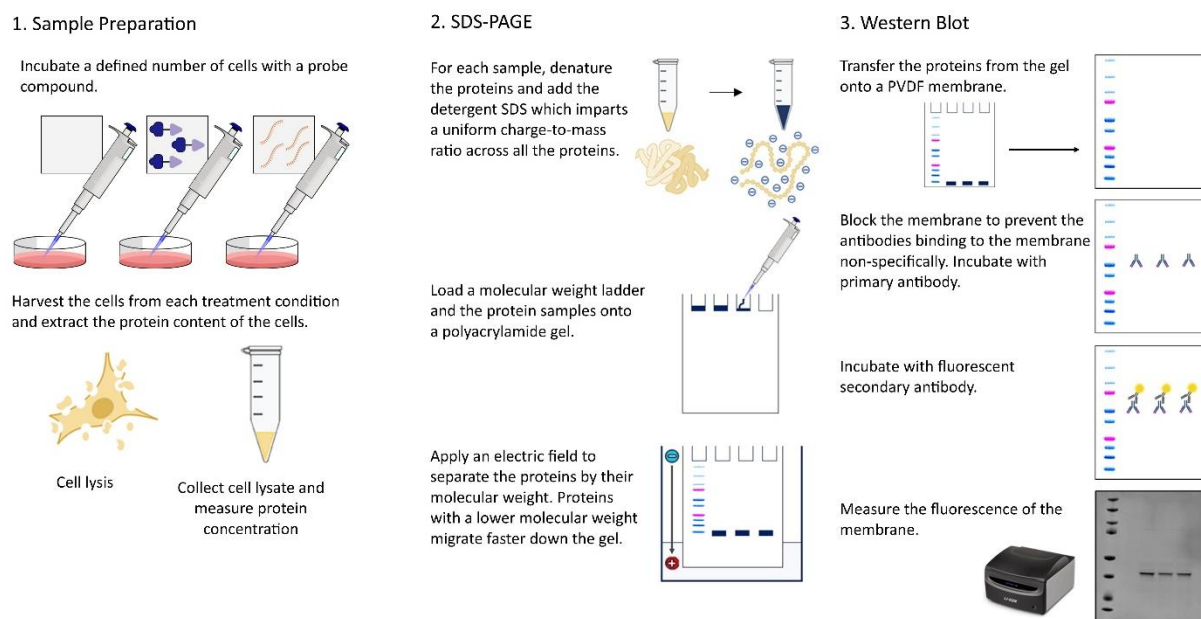


Figure 3.2 *The key steps in the Western blot protocol used for the assessment of PRMT1 levels. The protein concentration of each cell lysate is determined by spectrophotometer and a defined amount of total protein is denatured and treated with the detergent SDS. SDS anions coat the linear polypeptide chain at approximately 1.4 g of SDS per 1 g of protein and ensure all proteins in the sample have the same charge-to-mass ratio. This leads to their separation by their molecular weight once the electrical current is applied. Protein transfer is achieved by a dry transfer method with the iBlot 2 gel transfer device. Wash steps after incubation with primary and secondary antibodies remove any unbound or weakly-bound antibodies.*

To account for variation in the amount of protein loaded per lane of the gel and to allow cross-lane comparisons, the fluorescent signal intensity from the target protein must be normalised to that of a housekeeping protein. A housekeeping protein is a cellular protein whose concentration will not change with treatment as the gene is transcribed at a constant level regardless of the cell environment conditions⁸⁵.

However there are limitations of the Western blot method. First, it is a low throughput method that relies heavily on manual steps. Furthermore, it was initially designed as a qualitative method and only with appropriate validation can it be used to assess protein levels semi-quantitatively⁸⁵. Mass spectrometry-based proteomic experiments can allow for the quantitative analysis of cellular protein levels however this method requires specialist equipment, extensive method development and technical expertise in data analysis and has not been used in this project⁸⁶. A good relationship however has been shown between the quantitative values obtained by proteomic experiments and Western blot when measuring the degradation efficacy of the promiscuous kinase degrader **protac-3**⁷¹ (Figure 3.3). Therefore a validated Western blot method will provide sufficient accuracy and precision for measuring PROTAC-induced changes in PRMT1 levels.

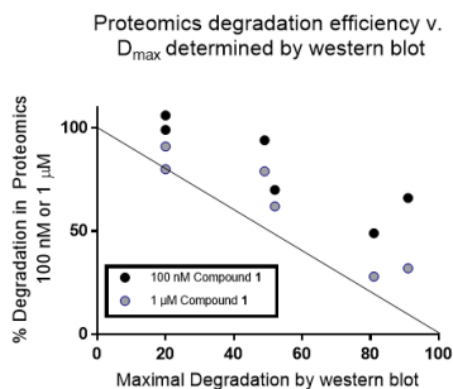


Figure 3.3 For the protac-3-induced degradation of selected kinases, there is good agreement between the quantitative values for the efficacy of degradation determined by mass-spectrometry based proteomics and Western blot. protac-3 degrades six kinases as it contains a promiscuous pharmacophore with high affinity to multiple kinases (protac-3 was introduced in Section 1.4.2.2). The identities of the six kinases shown in the figure were not published. The X-axis is the maximal percent decrease in protein levels determined by Western blot. The Y-axis shows the percent degradation in the whole cell proteomics dataset for the treatment of protac-3 at 100 nM (black dots) or 1 μM (gray dots). Figure reprinted from Bondeson et al.⁷¹.

The following sections detail the validation of a Western blot protocol previously developed in-house by Dr Shalini Rao to ensure it is sensitive to changing PRMT1 levels and detects PRMT1 specifically.

3.1.2.1 Sensitivity

Western blot can be used for the semi-quantitative analysis of protein levels if the signal intensity of the band is proportional to the abundance of the protein⁸⁵. The band must also have an acceptable signal-to-noise ratio (SNR). The cell lysate of untreated MCF-7 was loaded onto a gel for SDS-PAGE. To assess the linearity between the signal intensity and PRMT1 concentration, a two-fold dilution series of the lysate was prepared and loaded onto a gel. To assess the cross-gel variation and the accuracy of the dilution series, additional QC samples were also loaded at the start and end of the gel at the recommended loading amount of total protein (14.4 μg), and one-fifth of this value.

Analysis by Western blot showed that the band intensity for PRMT1 had a linear relationship with the amount of total protein loaded in the range assessed. The SNR was acceptable by visual inspection for total protein loadings greater than 1.5 μg and cross-gel variation was found to be minimal (determined by QC1 and QC2) (Figure 3.4). The membrane was also probed with a different commercially available antibody for PRMT1 but did not show an improved SNR at the low protein loading (Appendix 1A). The housekeeping protein vinculin however did not show linearity in the range investigated as the band intensity plateaued at high protein loading. The membrane was probed for an alternative housekeeping protein β-tubulin but this also showed non-linearity at high protein loadings (Figure 3.4).

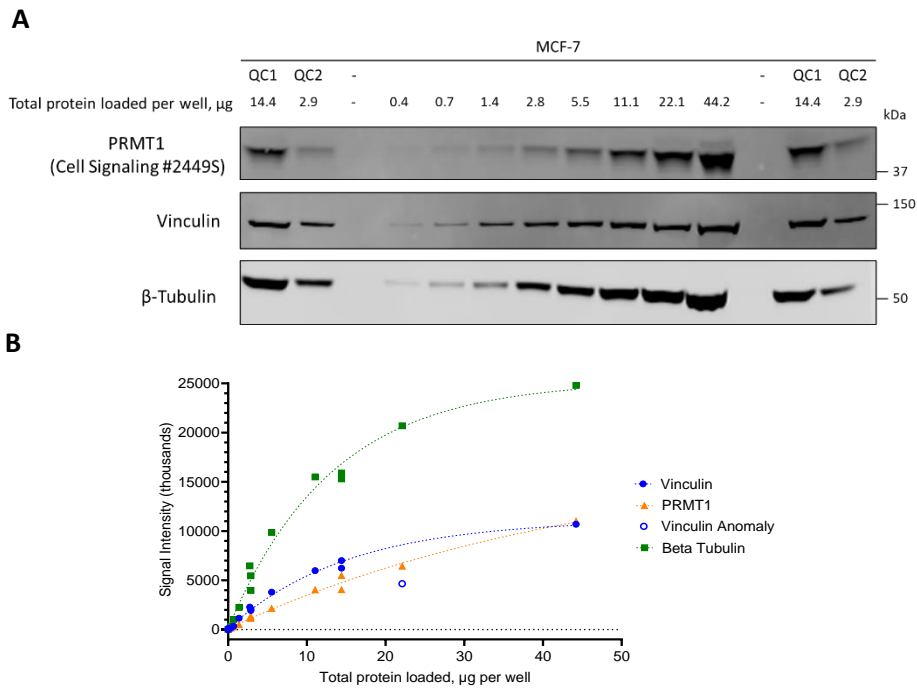


Figure 3.4 Linear relationship between PRMT1 and total protein. The housekeeping protein shows non-linearity. A) A dilution series of the cell-lysate derived from MCF-7 cells was analysed by Western blot. B) The protein bands were quantified with Image Studio analysis software and plotted against the amount of total protein loaded to the well.

To use Western blot to assess PRMT1 levels semi-quantitatively, the intensity of the band from the target protein and the housekeeping must both be linear with the total protein loaded. From this point forward, the amount of total protein was lowered from 14.4 μg per well to 11 μg per well. This provided a suitable SNR for PRMT1 and an improved linear relationship between the vinculin signal intensity and the total protein loaded (Figure 3.5). The visual inspection of the blot was deemed sufficient to assess PRMT1 degradation and the quantification of PRMT1 has only been used in Chapter 7.

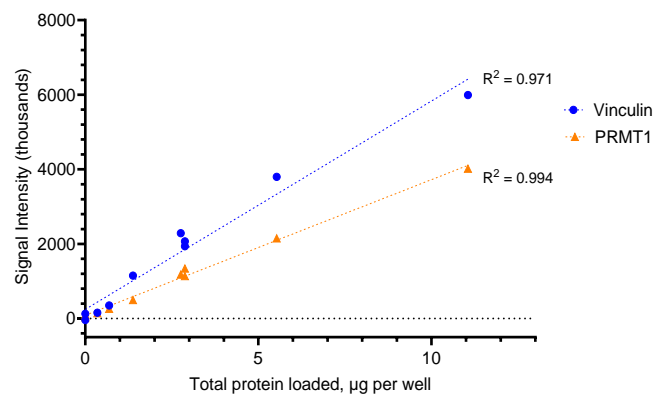


Figure 3.5 The determined linear range for the semi-quantitative measurement of PRMT1 and vinculin levels by Western blot. A total protein loading of 11 μg per well was chosen for future assays. Data from Figure 3.4.

3.1.2.2 Specificity

To show that the available PRMT1 primary antibody binds only to PRMT1, the knockdown of PRMT1 by RNA interference was undertaken and the level of PRMT1 was measured. A siRNA (short interfering RNA) for PRMT1 leads to the selective degradation of the mRNA that encodes PRMT1. This prevents the translation of mRNA into the amino acid sequence for PRMT1 and thus inhibits *de novo* PRMT1 synthesis⁸⁷. Compared to untreated cells, the cells treated with PRMT1 siRNA should have a significantly reduced PRMT1 signal intensity when analysed by Western blot.

MCF-7 cells were treated with PRMT1 siRNA, following a 48- and 72-hour incubation, the level of PRMT1 was analysed by Western blot. PRMT1 has a molecular weight of 41 kDa, and a single band at this molecular weight was observed in the untreated cells but absent in the PRMT1 siRNA-treated cells (Figure 3.6). When the membrane was probed for the housekeeping protein vinculin, a persistent band with constant intensity was visible, which shows that the loss of signal is not due to variation in the amount of total protein loaded into each well. The antibody is specific to PRMT1.

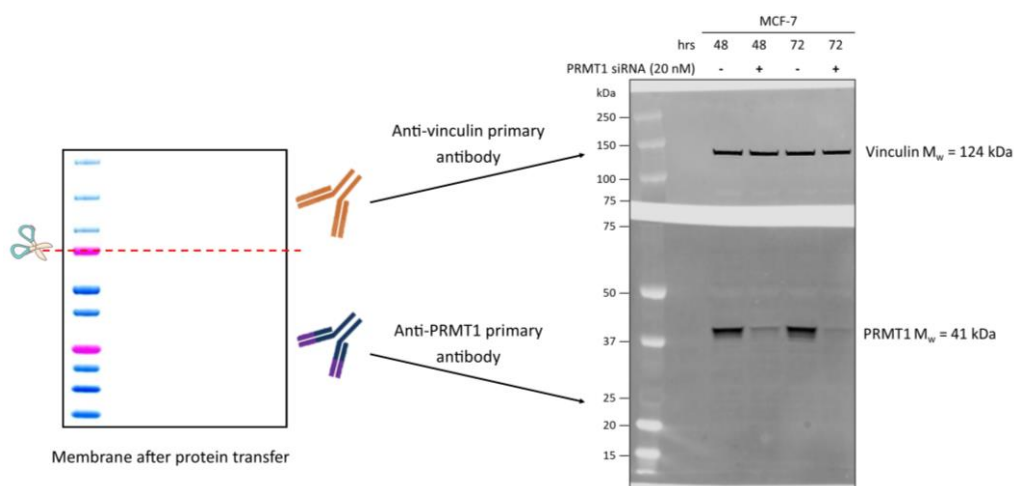


Figure 3.6 The PRMT1 primary antibody is specific to PRMT1. MCF-7 cells were treated with PRMT1 siRNA or non-targeting control siRNA (nt siRNA) for 48 or 72 hr and then the cells were harvested for SDS-PAGE. Before membrane blocking, the membrane was cut and the top section was analysed by Western blot for vinculin and the bottom section was analysed for PRMT1 using the Cell Signaling #2449 primary antibody. M_w refers to the molecular weight of the protein. Image representative of two independent experiments.

3.1.3 Investigation of the effect of PRMT1 knockdown on arginine methylation

The effect of PRMT1 knockdown was probed further to glean information of the downstream effects of the loss of PRMT1 activity in the MCF-7 cell line. A PRMT1 PROTAC that degrades PRMT1 should cause a similar biological effect to PRMT1 knockdown⁵⁷, and thus the effect of PRMT1 knockdown on arginine methylation and cell viability can be used as a guide for the predicted effect of PROTAC-induced PRMT1 degradation.

The siRNA was first shown to selectively knockdown PRMT1 as a change in the protein level of two other PRMTs, PRMT5 (Type II) and PRMT6 (Type I), was not observed. The effect of PRMT1 knockdown on the arginine methylation products MMA and ADMA was then investigated. Upon PRMT1 knockdown, a significant increase in monomethylated arginine (MMA) was observed and a modest reduction in the asymmetric dimethylation of arginine (ADMA) (Figure 3.7).

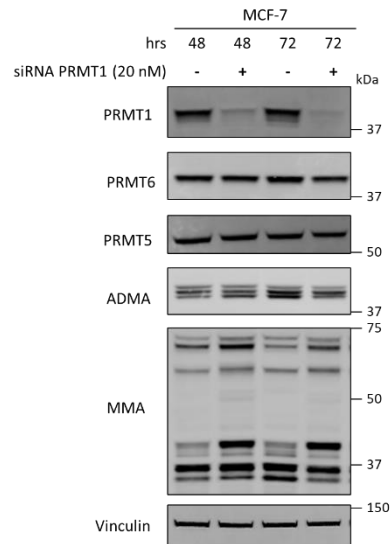


Figure 3.7 The effect of siRNA for PRMT1 on global arginine methylation levels and PRMT proteins. The experiment shown in Figure 3.6 was analysed by Western blot for PRMT5 (Mw=72 kDa), PRMT6 (Mw=42 kDa) and the arginine methylation products ADMA and MMA. Data representative of two independent experiments.

The significant increase in MMA can be attributed to a reduction in PRMT1 activity. There is literature precedence that the loss of PRMT1 activity specifically causes an increase in MMA and this increase is not observed with the loss of activity of any of the other Type I PRMTs. Giuliani *et al.* use CRISPR/cas9-mediated knockdown of PRMT1, PRMT4 and PRMT6 in a PDAC-derived cell line and show that a large increase in MMA is only observed with PRMT1 knockout³⁴ (Figure 3.8 A). The same trend was observed by Dhar *et al.* in mouse embryonic fibroblasts where PRMT1, PRMT3, PRMT4 and PRMT6 were knocked down and only PRMT1 knockdown caused a large increase in MMA⁸⁸.

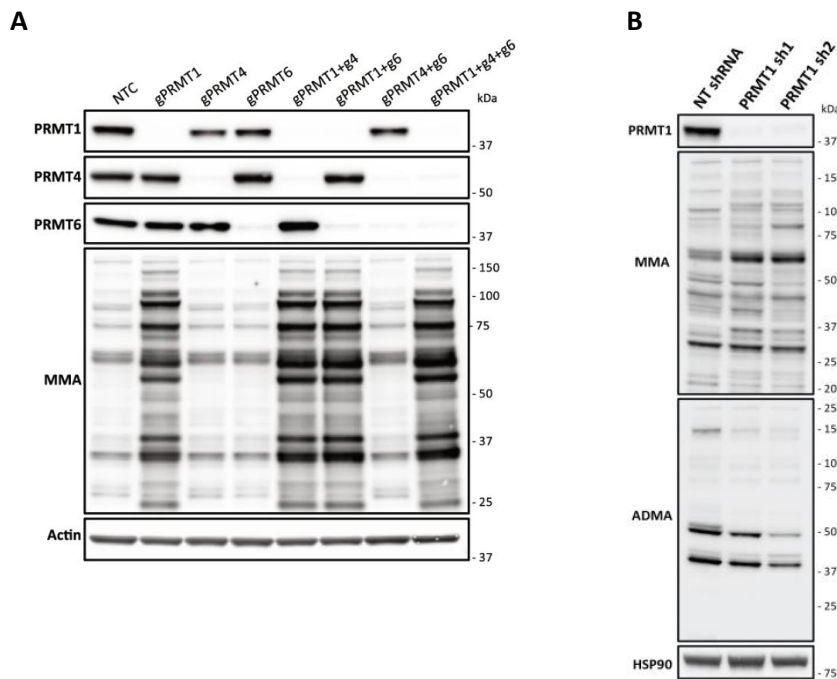


Figure 3.8 Literature example of the effect of PRMT1 knockdown on arginine methylation. A) The effect of CRISPR/Cas9-mediated knockdown of PRMT1, PRMT4 and PRMT6 individually, or in combination, on arginine methylation status. PATC153 cells were treated with guide RNA (gRNA) that induce efficient depletion of target protein levels. gPRMT1 indicates a gRNA specific to PRMT1. NTC = non-targeting control gRNA. B) PRMT1 genetic knock-down in the PATC153 cell line engineered with two independent PRMT1-targeting or non-targeting (NT) short hairpin RNA (shRNA). Figures reprinted from Giuliani *et al.*³⁴.

The activity of PRMT1 accounts for approximately 85% of cellular ADMA levels, and therefore a significant loss of ADMA levels was expected upon PRMT1 knockdown¹². However only a modest reduction in ADMA was observed. A similar result was obtained by Giuliani *et al.* upon PRMT1 knockdown (Figure 3.8 B) which they attribute to substrate scavenging; substrates that were previously methylated by PRMT1 are now methylated by a different Type I PRMT⁸⁸ and thus the level of ADMA does not change significantly as all Type I PRMTs deposit the ADMA post-translational modification. The ability of a protein substrate to be methylated by multiple Type I PRMTs has been shown^{89,90}. This hypothesis is further supported by Dhar *et al.* who observe an increase in the protein levels of PRMT4 and PRMT6 following PRMT1 knockdown⁸⁸. This suggests that the absence of PRMT1 alters the activity of other Type I PRMTs, potentially to compensate for the loss of PRMT1. Alternatively, as the ADMA modification is considered a stable modification, and the processes that regulate arginine demethylation are not understood, the persistent presence of ADMA signal may be a protein substrate that was methylated prior to siRNA treatment. The level of ADMA over a greater time following PRMT1 knockdown should be monitored.

Finally, PRMT1 knockdown was accompanied by a reduction in cell viability which supports the hypothesis that PRMT1 degradation will have anti-tumourigenic effects (Figure 3.9).

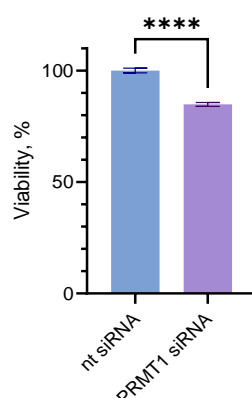


Figure 3.9 Viability loss was observed with PRMT1 knockdown. A) MCF-7 cells were treated with PRMT1 siRNA or nt siRNA for 72 hr and viability was assessed using the Promega Cell Titre-Glo assay. In this assay, the generation of a luminescent signal is proportional to the amount of ATP present. The amount of ATP is directly proportional to the number of viable cells present in the culture. Data from two independent experiments with three technical replicates. Mean and standard error plotted. Statistical analysis by an unpaired t-test, **** $p \leq 0.0001$.

3.2 The PROTACability of PRMT1

Schneider *et al.* coined the term ‘PROTACability’, a contraction of the words PROTAC and tractability, and use it to describe a systematic approach to assess whether the properties of a protein make it an amenable target for PROTAC-induced degradation⁹¹. They used the following criteria to evaluate a target protein’s PROTACability:

- 1) The cellular location of the target protein
- 2) Evidence that the target protein has ubiquitylation sites
- 3) Information about the target protein’s half-life
- 4) The availability of a small-molecule ligand for the target protein

Using a diverse range of publicly available resources, they analysed over 19,000 targets and identified 1,067 proteins where the criteria were met. They labelled these proteins as a ‘discovery opportunity’. PRMT1 is identified as a discovery opportunity and in the following sections the data used by Schneider *et al.* to come to this conclusion is evaluated. Their analysis however did not specifically look at the target protein in cancer and therefore additional published data is presented, as well as

results from experiments undertaken as part of this project, to assess the PROTACability of PRMT1 in cancer.

3.2.1 Criterion 1: The cellular location of the target protein

It is well documented that PRMT1 is highly mobile and shuttles between the cytoplasm and nucleus depending on the methylation status of its protein substrates^{28,92}. In the PROTACability criteria, a target protein located in the cytoplasm and/or nucleus is given the score of 'good'. The rationale behind this score is not given however the work of Simpson *et al.* can validate this assessment. They interrogated how the subcellular location of a protein affects its ability to be degraded by a PROTAC that recruits the CRBN or VHL E3-ligase. Fusion proteins that localise to specific compartments in the cell were generated and high degradation efficacy was observed with proteins localised to the nucleus and cytoplasm⁹³.

3.2.2 Criterion 2: Evidence that the target protein has ubiquitylation sites

As described in the introduction, the key step for PROTAC-induced degradation is the E3-ligase mediated transfer of a ubiquitin group onto a target protein. Schnieder *et al.* surveyed the available data from three genomic databases of proteins and assessed target proteins based on the presence of reported ubiquitination sites⁹⁴⁻⁹⁶. PRMT1 was identified in all three databases as a protein that can be ubiquitinated and thus met criterion 2.

It can also be inferred that PRMT1 can be ubiquitinated as the degradation of endogenous PRMT1 is E3-ligase dependent and proteasome dependent. PRMT1 is a substrate of the E3-ligase E4B, and PRMT1 degradation is accelerated with the overexpression of this E3-ligase⁹⁷. Furthermore, PRMT1 degradation does not occur when the activity of proteasome is inhibited with the small-molecule inhibitor **MG132**. This inhibitor binds to the 20S subunit of the proteasome and blocks its peptidase function which prevents the cleavage of peptide bonds and hence the degradation of proteins⁸⁴. Published data has shown that PRMT1 degradation is proteasome dependent as in a Western blot assay an increase in signal intensity for PRMT1 was observed in **MG132**-treated cells compared to untreated cells in mouse lung epithelial cells⁹⁸ and in mouse primary hepatocytes⁹⁹.

As part of this project the effect of **MG132** on PRMT1 levels in the MCF-7 cell line was investigated and a time-dependent increase in PRMT1 signal was observed when the activity of the proteasome was inhibited (Figure 3.10). The degradation of endogenous PRMT1 is proteasome dependent.

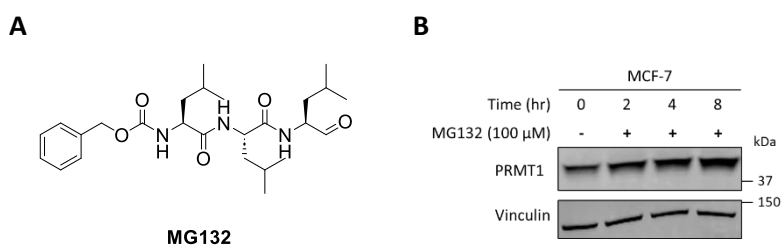


Figure 3.10 PRMT1 degradation in MCF-7 cells can be inhibited by the proteasome inhibitor MG132. A) Structure of MG132. B) MCF-7 cells were treated with the proteasome inhibitor MG132 (100 μM) for the indicated time and PRMT1 levels were analysed by Western blot. Results are representative of two independent experiments.

3.2.3 Criterion 3: Information about the target protein's half-life

The third criterion focuses on the half-life of the target protein. A protein's half-life tells us about the propensity of a protein to be degraded by the UPS and it is defined as the time required for the amount or concentration of a protein to be reduced by 50% under physiological conditions¹⁰⁰. A short half-life indicates rapid protein turnover in homeostasis and therefore that the protein has a rapid resynthesis rate¹⁰¹.

Schneider *et al.*'s criterion is that 'information about the protein's half-life' is available. It is striking that they only require 'information'. They state that 'a very short protein half-life may limit the effective utility of a PROTAC'⁹¹ however they do not state what constitutes a short half-life nor provide any suitable quantitative values. A search of the literature has highlighted that the half-life of a target protein is often discussed as a critical parameter for the efficacy of PROTAC-induced degradation however quantitative values for a suitable half-life are never given^{91,100-102}. This may be because, rather than the half-life having a defined value, it is more important that the PROTAC-induced rate of degradation is significantly faster than the resynthesis rate of the endogenous protein; it is the balance between these two processes that affects the efficacy, selectivity and duration of PROTAC-induced degradation¹⁰³. The half-life of a protein should not be included in the PROTACability criteria as it has no discriminatory value as suitable values are not known. A systematic investigation into published PROTACs and the half-life of their respective target protein could yield valuable information that could enhance the PROTACability criteria going forward.

It should also be highlighted that Schneider *et al.* used a single database to source the protein half-lives. This database lists the half-life of >4000 proteins in four non-dividing cell types: human B-cells, mouse neurons, primary human monocytes and primary human hepatocytes¹⁰⁴. The half-life of a protein in a non-dividing cell can be very different from a dividing cell¹⁰⁵. As cancer cells divide, only a half-life determined in a dividing cell type would be informative.

There is however value in determining the half-life of a target protein as it can provide information that helps determine the time point after PROTAC treatment that protein levels should be evaluated and what dosing interval/frequency may result in maximal degradation^{103,106}. The following sections look at the evidence for the half-life of PRMT1 in dividing cells.

3.2.3.1 Reported half-life values for PRMT1

There are two methods frequently used to determine the half-life of PRMT1. The first is to inhibit protein synthesis in the cell using the translational inhibitor cycloheximide (**CHX**). This small-molecule inhibitor prevents the relocation of tRNA and mRNA to the ribosome and inhibits translation⁸⁴ (Figure 3.11).

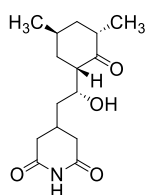


Figure 3.11 **Structure of cycloheximide (CHX).**

A more rigorous assay to determine a protein's half-life is stable isotope labelling by amino acids in cell culture (SILAC) coupled to mass spectrometry. This method involves incubating cells in cell media containing isotopically labelled amino acids for a defined duration. New proteins synthesised during this time will incorporate the labelled amino acids and can be distinguished from their non-labelled protein counterpart by mass spectrometry. This method can be used to determine protein half-life (by measuring the reduction in nonlabelled protein) and the rate of *de novo* synthesis (by measuring the increase in labelled protein)¹⁰².

The half-lives for PRMT1 in a range of dividing mammalian cell lines have been published and are shown in Table 3.1. There is vast variation in the values, even between the same cell line, and no conclusions can be made. An attempt was therefore made to empirically determine the half-life of PRMT1 in the MCF-7 cell line.

Table 3.1 *Published half-life data for PRMT1 in dividing mammalian cells.*

Cell line	Origin of cell line	Half-life, hr	Method	Ref
MLE12	Mouse lung epithelial	4	Western Blot with CHX	98
HEK293 transfected with empty pLenti	Human embryonic kidney	5	Western blot with CHX	97
U2OS	Human osteosarcoma	>8*	Proteomics with CHX	107
HEK293	Human embryonic kidney	>8*	Proteomics with CHX	107
HCT116	Human colorectal carcinoma	>8*	Proteomics with CHX	107
RPE1	Human retinal pigment epithelial	>8*	Proteomics with CHX	107
HEK293	Human embryonic kidney	>10**	Western blot with CHX	108
HeLa	Human uterus/cervical epithelial adenocarcinoma	44.7	SILAC-Proteomics	109
C2C12	Mouse myoblast	69.7	SILAC-Proteomics	109

*No significant change in protein level at 8 hr compared to 0 hr. ** persistent band, equal intensity at indicated time to the untreated control.

3.2.3.2 Experimental investigation of the half-life of PRMT1

A cycloheximide chase experiment was undertaken and endogenous PRMT1 in MCF-7 cells was monitored by Western blot. A time-dependent reduction in PRMT1 signal would be expected as **CHX** inhibits *de novo* synthesis of PRMT1 but does not affect PRMT1 degradation.

MCF-7 cells were treated with **CHX** at 50, 100, 150 and 200 $\mu\text{g mL}^{-1}$ and a reduction in PRMT1 signal was not observed (Figure 3.12). A visual inspection of the cells showed that cytotoxicity increased with CHX concentration and time, and longer time points were precluded because of high levels of cytotoxicity. The results from these cycloheximide chase experiments suggest that PRMT1 is long-lived with a half-life greater than 8 hours.

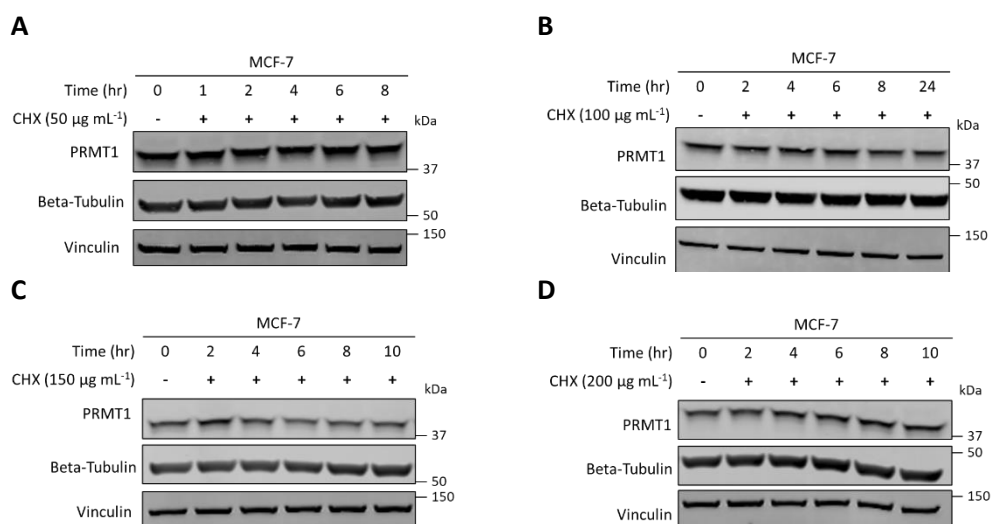


Figure 3.12 Cycloheximide treatment did not affect the level of PRMT1. MCF-7 cells were treated with the translational inhibitor cycloheximide for the indicated time and PRMT1 levels were analysed by Western blot. The level of the housekeeping proteins vinculin and beta-tubulin were also determined. The dose of CHX was escalated from 50 µg mL⁻¹ (A) to 100, 150 and 200 µg mL⁻¹ (B, C and D).

There is evidence that the potency of **CHX** in the MCF-7 cell line is reduced when serum is present in the cell media as ‘factors present in the serum may stabilise some crucial cell proteins such as key enzymes, cytoskeletal, or membrane components, which are vital for cell life’¹¹⁰. To eliminate the possibility that the serum may stabilise PRMT1, further studies were undertaken using serum free cell media. The change to serum free media however had no effect on PRMT1 levels as persistent bands of unchanging intensity were observed by Western blot. To confirm that **CHX** was inhibiting translation, the protein level of the FOXA1 protein was also investigated. This protein has a published half-life of 4-6 hours in MCF-7 cells^{111,112} and hence a loss of signal should be observed upon CHX treatment. However a change in FOXA1 was not observed. The assay was repeated in the KP-3 cell line to confirm that the observed results were dependent on the cell line. The levels of FOXA1 and PRMT1 also remained unchanged in this cell line (Figure 3.13).

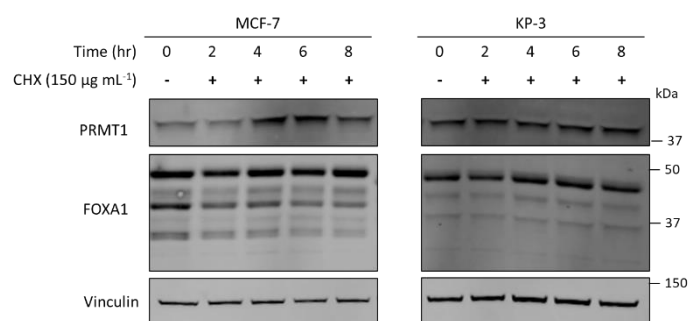


Figure 3.13 Cycloheximide treatment with serum free media did not affect the level of PRMT1 or FOXA1 in MCF-7 and KP-3 cells. MCF-7 and KP-3 cells were seeded for the experiment in DMEM supplemented with 10% FBS and left for 24 hr. The media was then replaced with serum free media and the cells incubated for a further 24 hr. The media was then removed and replaced with serum free media containing 150 $\mu\text{g mL}^{-1}$ CHX. The cells were incubated for the indicated time and PRMT1 and FOXA1 levels were analysed by Western blot. The top band in the FOXA1 blot correlates with the molecular weight of this protein (49 kDa).

Due to the persistence of the FOXA1 band it was questioned if the **CHX** stock was inhibiting translation. **CHX** was purchased from a commercial supplier and obtained as a lyophilised powder. The identity of this compound was characterised in-house and NMR analysis matched previously reported spectra. Analysis by LC/MS showed the presence of a compound with the correct mass-to-charge ratio (m/z) for **CHX** but at a purity of 61% (Appendix 1B). It was not possible to confirm the diastereomeric purity of the sample. The cycloheximide chase assay was repeated with MCF-7 and KP-3 cells with this new CHX supply, and the lyophilised powder was dissolved in DMSO immediately before addition to the cells. No reduction in PRMT1 nor FOXA1 was observed in this assay (Figure 3.14).

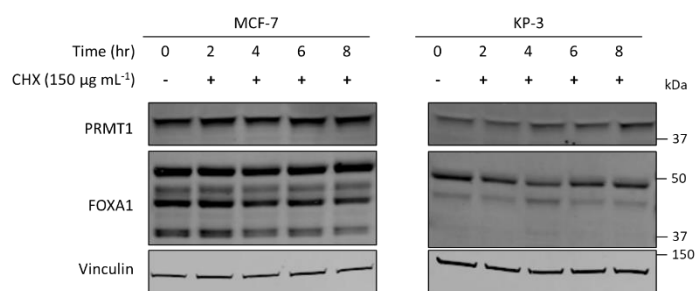


Figure 3.14 A fresh stock of cycloheximide and treatment in serum free media did affect the level of PRMT1 or FOXA1 in MCF-7 and KP-3 cells. MCF-7 and KP-3 cells were seeded for the experiment in DMEM supplemented with 10% FBS and left for 24 hr. The media was then replaced with serum free media and the cells incubated for a further 24 hr. The media was then removed and replaced with serum free media containing 150 $\mu\text{g mL}^{-1}$ CHX. The cells were incubated for the indicated time and PRMT1 and FOXA1 levels were analysed by Western blot.

It was not determined whether translation was being inhibited in the **CHX** chase. Future work should validate that the correct diastereomer of **CHX** is present as the inversion of a single stereogenic centre in cycloheximide can significantly reduce its ability to inhibit translation¹¹³ (Figure 3.15).

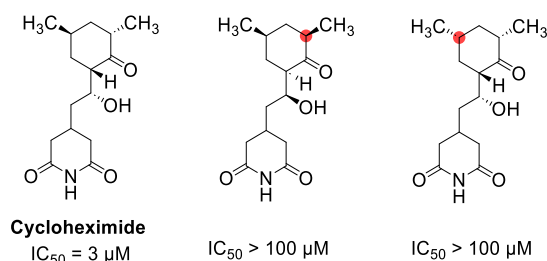


Figure 3.15 Changing the configuration of stereogenic centre in cycloheximide changes its potency to translational inhibition. Analogues differ from cycloheximide by inversion at the stereogenic centre shown in red. IC_{50} values determined by a *O*-propargyl puromycin translation inhibition assay in K562 cells and published in Park *et al.*¹¹³.

Further work to determine the half-life of PRMT1 in MCF-7 cells should use an alternative protein synthesis inhibitor in a chase assay¹¹⁴ or a SILAC experiment should be undertaken. However, as discussed previously, knowledge of the target protein half-life is not a discriminative factor when assessing the suitability of a target protein for PROTAC-induced degradation.

3.2.4 Criterion 4: The availability of a small-molecule ligand for the target protein

Small-molecule pan-Type I inhibitors that bind to PRMT1 were highlighted in the introduction. This enables the design of a PROTAC for PRMT1 and this is discussed in depth in section 4.2.

3.3 Conclusions

Considering the PROTACability criteria laid out by Schneider *et al.*, three out of the four criteria are met for targeting PRMT1 in cancer. There is strong evidence that PRMT1 is localised to the nucleus and cytoplasm (Criterion 1), PRMT1 can be ubiquitinated and its degradation is proteasome dependent (Criterion 2) and there are published small-molecule ligands for PRMT1 (Criterion 4). The knowledge of a reproducible half-life for PRMT1 is lacking however this does not impact the assessment of PRMT1 as a protein that is amenable to degradation by a PROTAC.

PRMT1 is a promising target protein for PROTAC-induced degradation and focus should turn to synthesising PROTACs that target PRMT1. A Western blot assay has been validated for the semi-quantitative assessment of PRMT1 levels in the MCF-7 cell line and this will provide a screening tool to evaluate the efficacy of synthesised PROTACs.

4 PROTAC Design and Ligand Synthesis

PRMT1 is a promising target for PROTAC-induced degradation due to its therapeutic potential and the properties of endogenous PRMT1. This chapter outlines the design of each part of a PROTAC for PRMT1: the E3-ligase ligand, the PRMT1 ligand and the linker that joins these two ligands into a PROTAC. A modular synthetic strategy was chosen so the design and synthesis of the three parts are discussed independently (Figure 4.1).

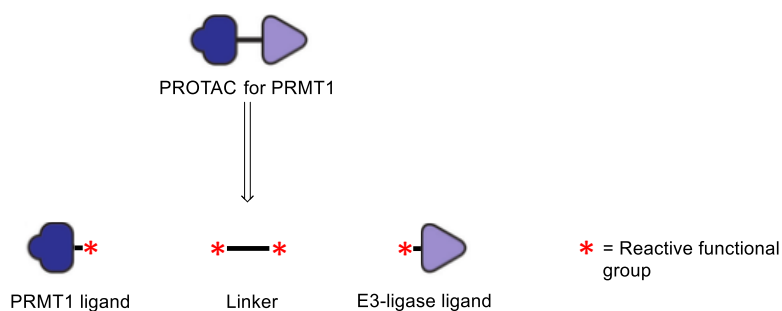


Figure 4.1 Retrosynthesis of PROTACs for PRMT1.

4.1 The E3-Ligase Ligands

For the design of the E3-ligase ligand, literature precedence was used. The majority of published PROTACs recruit either the VHL or CRBN E3-ligase and these E3-ligases have been used successfully to degrade a wide range of target proteins with high potency¹¹⁵, including in the MCF-7 cell line^{116,117}. As previously discussed, the subcellular location of PRMT1 makes it suitable for degradation by the VHL and CRBN E3-ligases (Section 3.2.1). It has however been observed that the identity of the E3-ligase recruited can be critical to whether degradation occurs¹¹⁸ and therefore to maximise the likelihood of synthesising a PROTAC that can degrade PRMT1, PROTACs that recruit both the VHL and CRBN E3-ligases will be synthesised.

4.1.1 Ligands for VHL

In addition to the identity of the E3-ligase recruited, the position of linker attachment on the VHL ligand can affect degradation efficacy^{119,120}. Two different positions of linker attachment on the high-affinity VHL ligand **VH032** will be investigated, both of which have strong literature evidence to show that binding affinity is not lost upon linker attachment^{56,115}. Following *N*-Boc deprotection, VHL ligand **1** will attach to the linker by an amide bond at the nitrogen following the *tert*-leucine amino acid. VHL ligand **2** will be attached to the linker at the phenol functional group on the benzene ring (Figure 4.2).

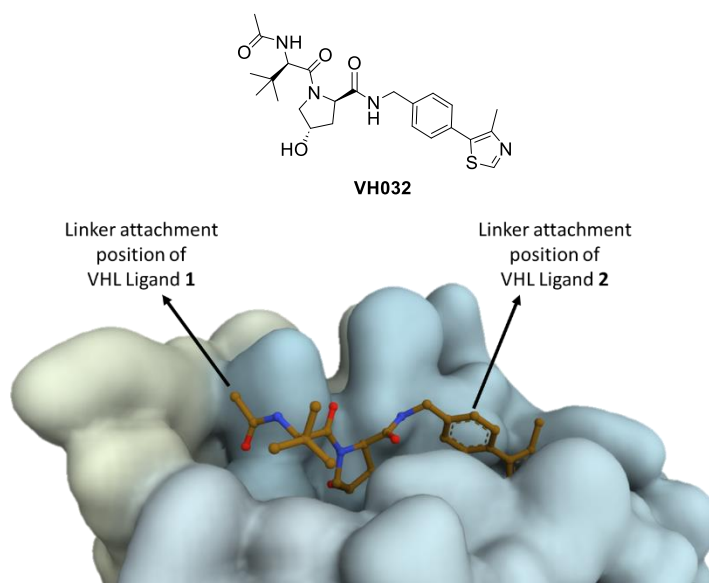
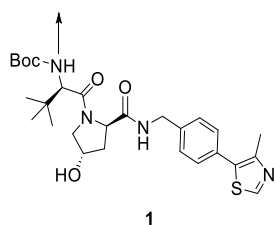
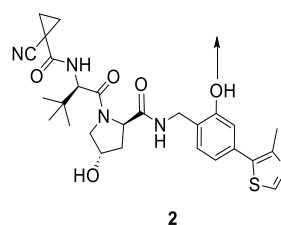
A**B****C**

Figure 4.2 Published small-molecule ligand for VHL and positions on the molecule suitable for linker attachment. A) Crystal structure of VH032 bound to VHL (PDB: 4W9H). Two published linker attachment positions are indicated by the black arrows. Molecular surface representation of VHL (blue) and a ball and stick model of VH032 (brown) generated with Mol*¹²¹. Crystal structure first published in Galdeano et al.⁵⁶. B and C) The two VHL ligands to be used in this project. The site for linker attachment is shown by the black arrow. VHL ligand 1 will require N-Boc deprotection prior to linker attachment.

VHL ligands **1** and **2** were synthesised using published procedures. Aryl-bromide **3** (**3a** for the synthesis of VHL ligand **1** and **3b** for VHL ligand **2**) was coupled to 4-methyl triazole by the Heck reaction to give **4**. The nitrile group of **4** was then reduced to produce **5** that contained a free benzylic amine (Figure 4.3).

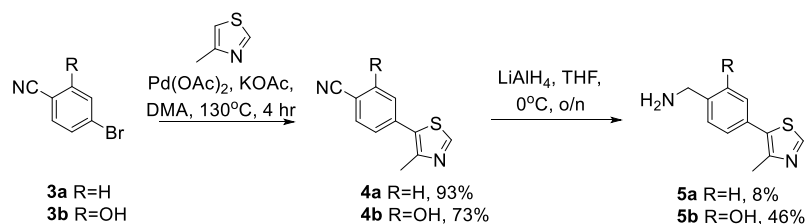


Figure 4.3 Synthesis of amine 5. Synthetic route from Buckley et al.¹²².

5b was produced in moderate yield and taken forward for subsequent amide couplings and *N*-Boc deprotection to produce VHL ligand **2** (Figure 4.4).

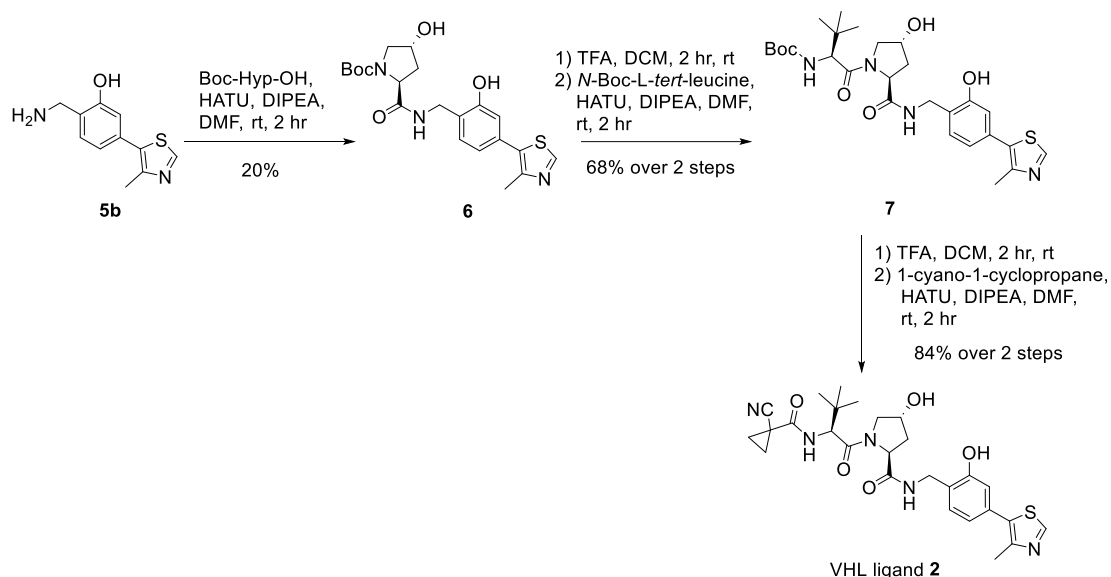


Figure 4.4 Synthesis of VHL ligand **2**.

The reduction of the nitrile **4a** was low yielding, with multiple products produced. The reduction was attempted twice (6% and 8% yield of **5a**), and then a different synthesis route was followed¹²³. A reductive amination with commercially available 4-bromobenzaldehyde and *tert*-butyl carbonate produced amine **8** which was then coupled to 4-methyl triazole by a Heck coupling to give **9**. **9** was then deprotected and subjected to successive amide couplings and deprotections to produce VHL ligand **1** (Figure 4.5).

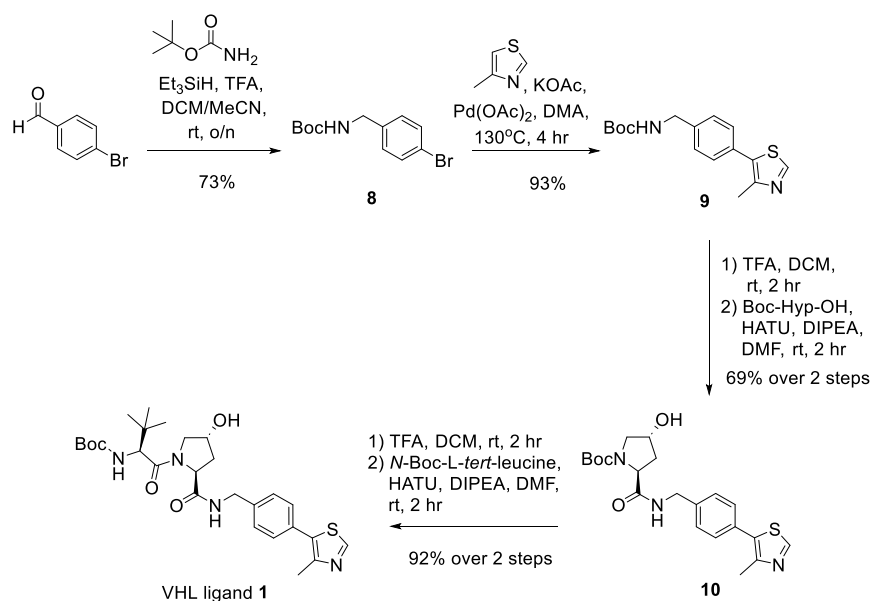


Figure 4.5 Synthesis of VHL ligand **1**. Synthetic route from Steinebach et al.¹²³.

4.1.2 Ligands for CRBN

The most frequently used ligands for the CRBN E3-ligase contain the pharmacophore of a phthalimide group coupled to a glutamine ring. The attachment of the linker to the phthalimide ring at the 4-position and 5-position is tolerated with various functional groups¹¹⁵ (Figure 4.6). CRBN ligands that contain a reactive functional group at the position for linker attachment are commercially available.

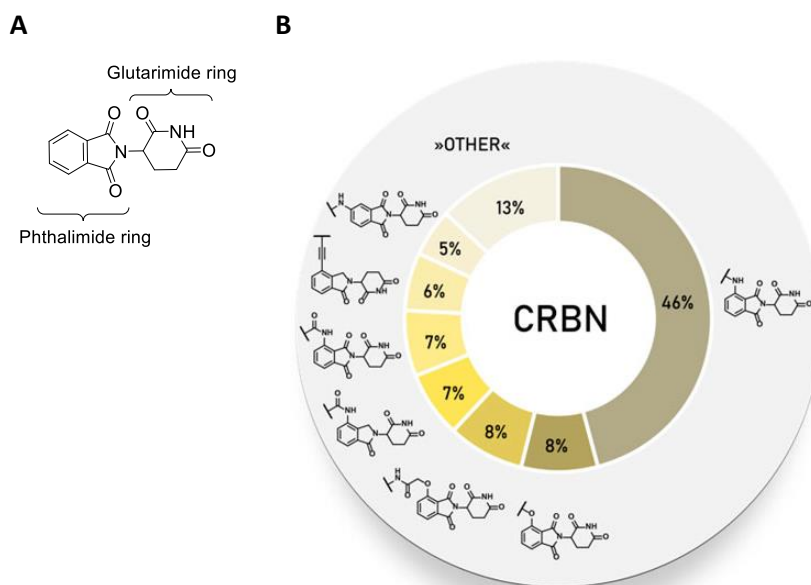


Figure 4.6 **Frequently used small-molecule ligands for the Cereblon (CRBN) E3-ligase.** A) Pharmacophore for CRBN binding. B) Frequency of CRBN ligands used in PROTAC compounds. Figure reprinted from Bricelj et al.¹¹⁵.

4.2 The PRMT1 Ligand

A pharmacophore for PRMT1 binding can be taken from published high-affinity ligands for PRMT1. The two frequently used pan-Type I inhibitors **GSK3368715** and **MS023** were introduced in the introduction, and both inhibitors cause potent inhibition of PRMT1, bind reversibly to PRMT1 and occupy the protein substrate binding pocket of PRMT1. Despite the termination of the phase one trial with **GSK3368715**, the pharmacophore of **GSK3368715** is suitable for use in a PROTAC; target engagement was observed in the blood and the low target engagement in the tumours may be explained by pharmacokinetic factors¹²⁴. In addition, the poor safety profile of **GSK3368715** may be associated with inhibition-driven pharmacology and may not be observed with a PROTAC that targets PRMT1.

The pharmacophore essential for PRMT1 binding in **GSK3368715** and **MS023** is an ethylenediamino group attached to a pyrrole or pyrazole heterocycle. The crystal structure of **GSK3368715** bound to PRMT1 shows that the ethylenediamino group and pyrazole interact with histidine and glutamic acid

amino acids in the protein substrate binding pocket of PRMT1¹³. In addition, chemical modifications to the ethylenediamino group in **MS023** result in a loss of potency for PRMT1 inhibition⁴¹ (Figure 4.7). The linker must not be attached to this pharmacophore.

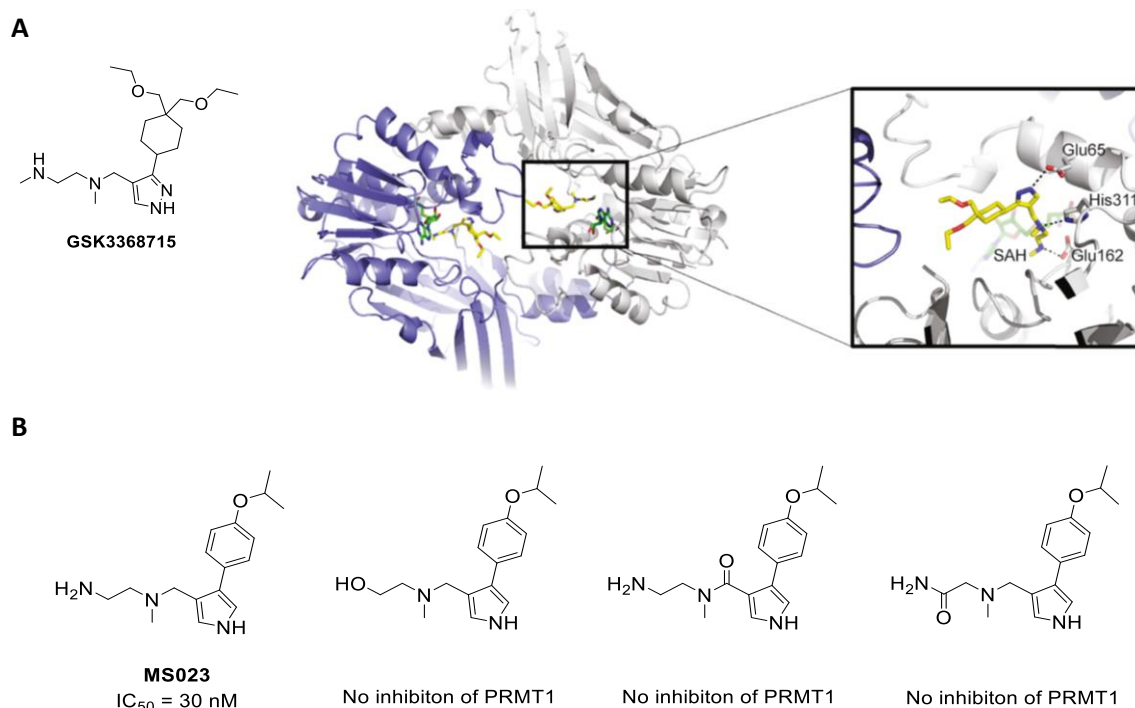


Figure 4.7 The ethylenediamino functional group is required for PRMT1 binding. A) Crystal structure of **GSK3368715** bound to PRMT1 (PDB: 6NT2). Crystal structure first published by Fedoriw *et al.*¹³ and figure reprinted from this publication. B) Structure activity-relationship of the ethylenediamino group and potency for PRMT1. Replacing the terminal primary amino group with a hydroxyl group or replacing the either of the two basic amino groups with an amide group reduces potency for PRMT1. IC₅₀ was determined by a scintillation proximity assay using [³H]SAM and published in Eram *et al.*⁴¹.

Linker attachment to the 6-membered ring will likely be tolerated without a significant loss in PRMT1 binding affinity. The crystal structure of **GSK3368715** bound to PRMT1 shows that the cyclohexane ring and the diethylene chains on this ring do not interact with amino acids in PRMT1. In addition, PRMT1 is active as a homodimer where a toroidal structure is formed from two PRMT1 protein molecules, and the binding pocket of each PRMT1 molecule faces inwards and into a solvent-filled channel⁴³. When **GSK3368715** is bound to this dimer, the substituted cyclohexane ring projects into the centre of this toroidal structure (Figure 4.7 A). Substantial structure modification can often be tolerated at a position on a drug molecule when it is solvent exposed without serious loss of activity¹²⁵. Finally, structure-activity experiments undertaken by Mitchell *et al.* in their search for a selective PRMT6 inhibitor show that a wide range of substituents can be tolerated at the para-position and meta-position of an aryl ring that is attached to the pharmacophore of **GSK3368715**

without a significant loss of binding affinity¹²⁶ (Figure 4.8). The attachment of the linker to the aryl or cyclohexane ring should result in a molecule that retains high PRMT1 binding affinity.

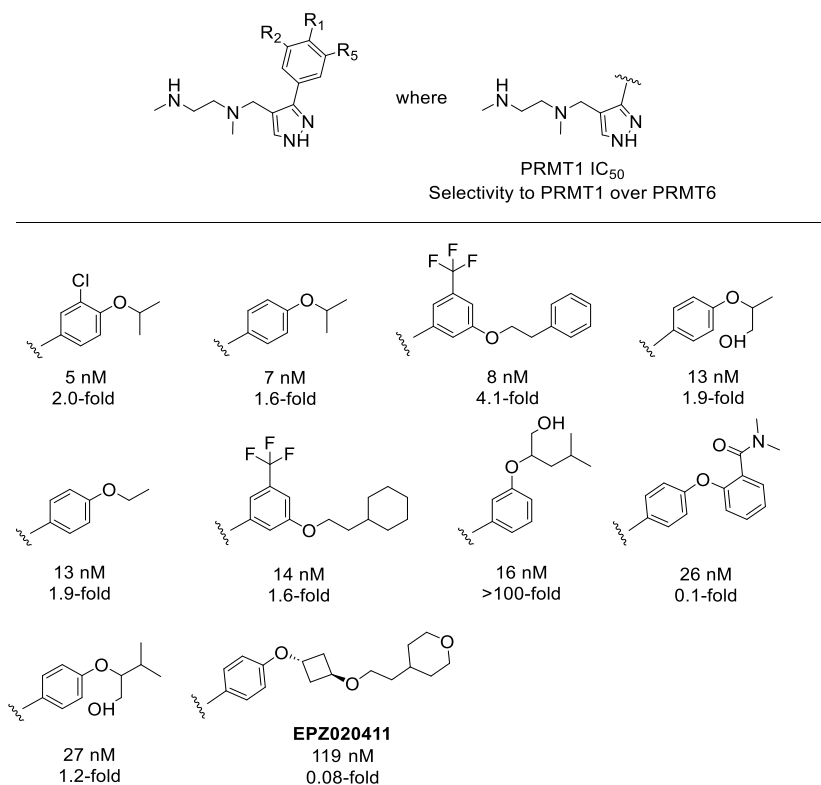


Figure 4.8 A range of substituents can be tolerated on the aryl ring without a significant loss of PRMT1 affinity. The substituent can also affect the selectivity of PRMT1 inhibition over PRMT6. IC₅₀ determined by a [³H]SAM methylation assay and published in Mitchell et al.¹²⁶.

Two options for the structure of the PRMT1 ligand have been proposed and are shown in Figure 4.9. Structure A and B both contain the PRMT1 binding pharmacophore of **GSK3368715** and **MS023** and have the linker attached at the para-position of either a cyclohexane ring or an aryl ring. The attachment of a linker to an unsaturated 6-membered ring will introduce stereogenic centres on the ring (Structure A in Figure 4.9). This is undesirable synthetically and biologically as each isomer would require isolation and evaluation *in vitro* as they can possess different activity¹²⁷. Hence, an aryl ring was chosen (Structure B).

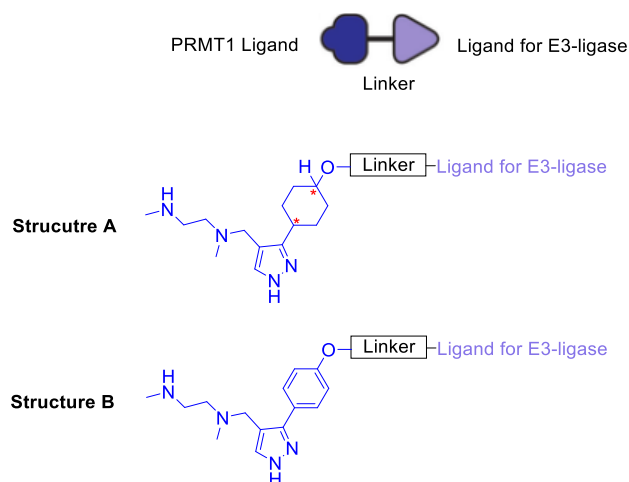


Figure 4.9 Proposed structures for the PRMT1 ligand. A red asterisk indicates a stereogenic centre.

In the design of the PRMT1 ligand, the focus has been on PRMT1 affinity rather than the selectivity of the ligand to PRMT1 over other Type I PRMTs. Mitchell *et al.* show that selectivity to PRMT1 over PRMT6 varies significantly with changing aryl ring substituent (Figure 4.8) and therefore each PROTAC with a different structure may have a different selectivity profile to the Type I PRMTs. In addition, the selectivity of a PROTAC to the different members of the Type I PRMTs will be affected by cooperativity in the ternary complex (as discussed with PROTAC **MZ1** in section 1.3.2.2) and this cooperativity may be significantly affected by the linker used and the E3-ligase recruited.

Finally, the pharmacophore chosen was found to be suitable as a cursory look at the distribution of lysine amino acids in PRMT1 highlighted that there are lysine amino acids on the same surface as the protein substrate binding pocket in which **GSK3368715** binds (Figure 4.10). As the PROTACs synthesised contain the same pharmacophore as **GSK3368715**, PROTAC binding will induce proximity between this surface on PRMT1 and the ubiquitin-charged E2-enzyme in complex with the E3-ligase.

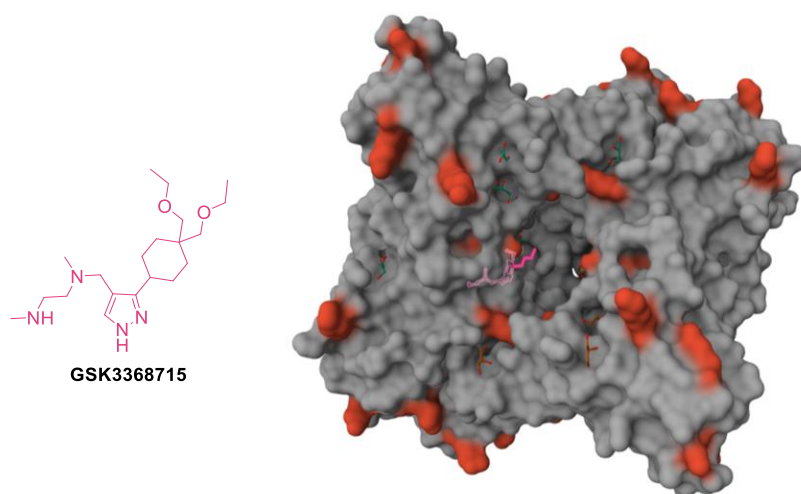


Figure 4.10 Lysine amino acids (red) are present on the same surface of PRMT1 as GSK3368715 (pink) binds. Crystal structure of GSK3368715 bound to PRMT1 (PDB: 6NT2) where the lysine amino acids are shown in red and all other amino acids are shown in grey. GSK3368715 is shown in pink. Molecular surface representation of dimerised PRMT1 and ball and stick model of GSK3368715 generated with Mol*¹²¹. Crystal structure first published in Fedoriw et al.¹³.

4.2.1 The synthesis of the ligand

To allow for linker attachment, a phenol was chosen as a reactive-functional group at the para-position of the phenyl ring. To ensure the regioselective attachment of the linker, protecting groups were employed for the pyrazole and the secondary amine. The protecting groups were taken from the synthesis of **GSK3368715** and both are acid labile so they can be readily removed in a single step following regioselective linker attachment. The structure for the PRMT1 ligand to be used in PROTAC synthesis is shown in Figure 4.11.

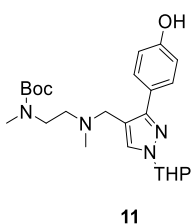


Figure 4.11 PRMT1 ligand for PROTAC synthesis. The pyrazole and secondary amine are protected to enable regioselective linker attachment to the phenol.

A retrosynthetic scheme for PRMT1 ligand **11** was produced by adapting the published synthesis of **GSK3368715**¹³. The synthesis is split into three key stages (Figure 4.12).

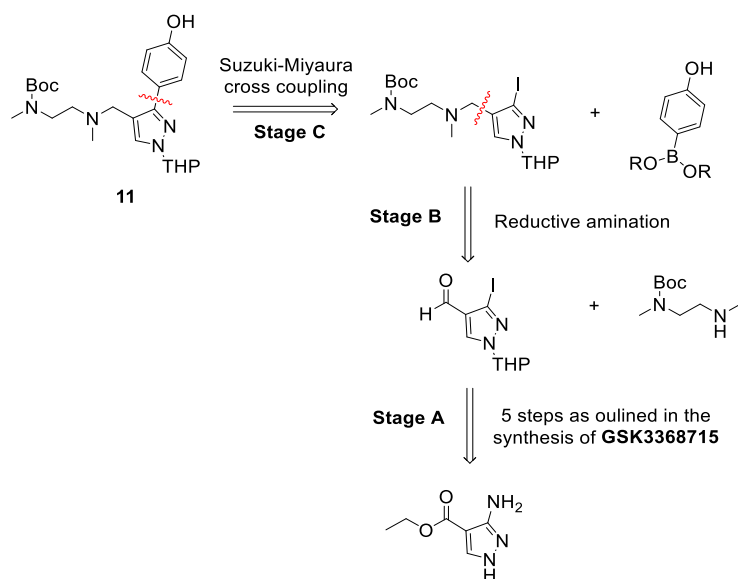


Figure 4.12 Retrosynthesis of **11**.

4.2.1.1 Stage A

Stage A followed the literature procedure for **GSK3368715** directly¹³. Ethyl 3-amino-1*H*-pyrazole-4-carboxylate was iodinated to give the pyrazole **12** which was then protected with 3,4-dihydropyran to give **13**. The ester was then hydrolysed to give carboxylic acid **14** which was reduced to alcohol **15** and then oxidised to aldehyde **16** (Figure 4.13).

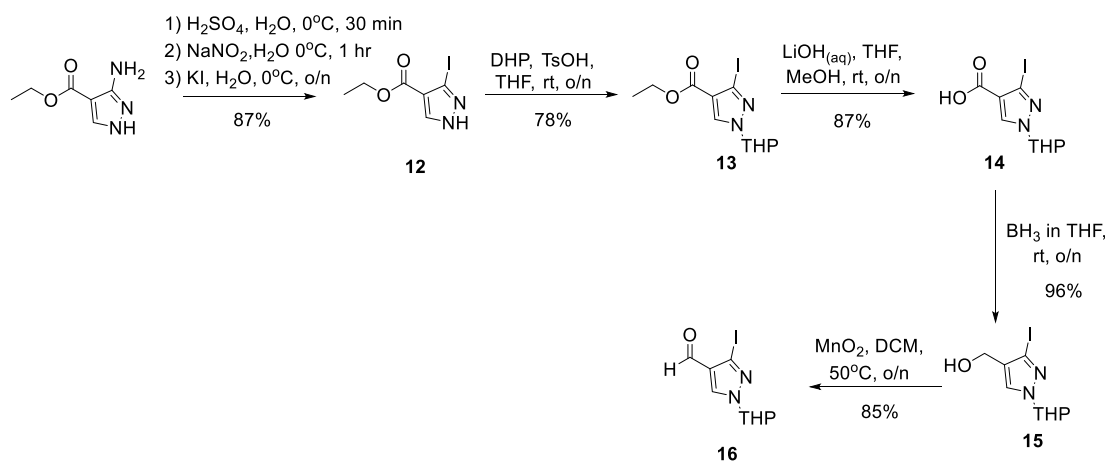
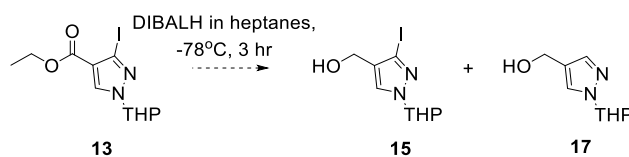


Figure 4.13 Stage A in the synthesis of **PRMT1** ligand **11**.

To reduce the number of steps, the reduction of **13** was attempted with diisobutylaluminium hydride (DIBALH) however due to poor control over deiodination and low conversion, this route was abandoned (Table 4.1).

Table 4.1 **Attempted reduction of 13**. 1 equivalent of DIBALH led to incomplete reduction. 3 equivalents formed the deiodinated alcohol **17**. Other species indicated by LC/MS or crude ¹H NMR.



Entry	Equivalents of DIBALH	Isolated product	Other species present
1	1	32% 15	Starting material 13
2	3	41% 17	Alcohol 15 and starting material 13

4.2.1.2 Stage B

Stage B is the addition of the ethylenediamino group. A single nitrogen in methyl[2-(methylamino)ethyl]amine was protected with the *N*-Boc protecting group to give **18** at quantitative yield (Figure 4.14).

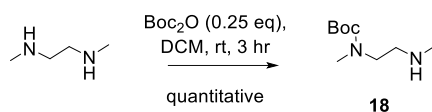
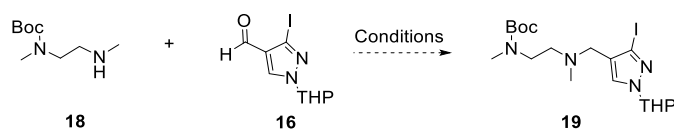


Figure 4.14 **Synthesis of 18**.

Using reductive amination conditions published in the literature, **18** was reacted with aldehyde **16** but none of the conditions yielded the desired product (Table 4.2).

Table 4.2 Attempted reductive amination with amine **18** and aldehyde **16**.



Entry	Conditions	Reference	Product 19 ,	Starting material 16
			%	recovered, %
1	NaH(OAc) ₃ , DCM, rt, 12 hr	13	0	quantitative
2	NaH(OAc) ₃ , AcOH, DCE, rt, o/n*	128	0	84
3	Et ₃ SiH, TFA, rt, 12 hr	123	0	60
4	NaBH ₃ CN in EtOH, MeOH, 64°C, o/n	129	0	87

*The reaction conditions were modified but no reaction occurred: 1) Temperature increased to 80°C. 2) Addition of molecular sieves. 3) Aldehyde **16** and AcOH were mixed in DCE for 1 hr. Amine **18** was then added and the mixture stirred for a further 1 hr. NaH(OAc)₃ was then added. 4) The reaction underwent microwave irradiation at 100°C for 30 min.

Since the reductive amination to synthesise **19** was unsuccessful with a range of reducing agents, alkylation was considered as an alternative strategy. Alcohol **15** was resynthesised through the reduction of aldehyde **16** with borane-tetrahydrofuran and the alcohol was then converted to a good leaving group and alkylated with amine **18**. Both proceeding via a bromide and tosylate intermediate product yielded the desired product **19** (Figure 4.15).

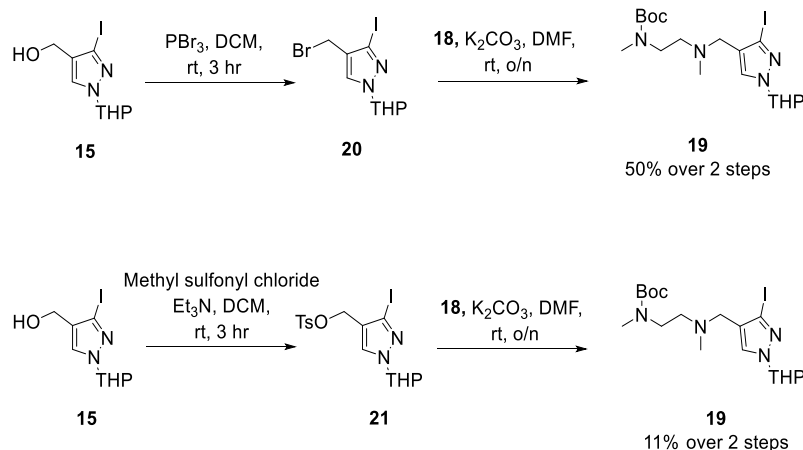
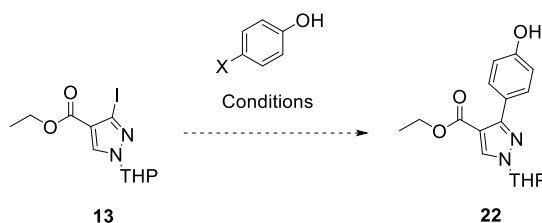


Figure 4.15 Two routes for the synthesis of **19**.

4.2.1.3 Stage C

The final stage in the synthesis of PRMT1 ligand **11** was the addition of the phenol ring. To ensure the proposed Suzuki-Miyaura cross-coupling can tolerate a phenol group, the reaction was first undertaken on the model substrate ester **13** using a range of conditions (Table 4.3).

Table 4.3 *Optimisation of the Suzuki-Miyaura cross coupling on model substrate 13.*



Entry	X	Conditions	Reference	Yield of 22 , %
1	B(OH) ₂	Pd(OAc) ₂ , Na ₂ CO ₃ , acetone/H ₂ O, 35°C, o/n	130	34
2	B(OH) ₂	Pd(dppf)Cl ₂ , Cs ₂ CO ₃ , 1,4-dioxane/H ₂ O, 100°C, o/n	13	12
3	BPin	Pd(dppf)Cl ₂ , Cs ₂ CO ₃ , 1,4-dioxane/H ₂ O, 100°C, o/n	13	78

Entry 3 gave the highest yield, and the conditions were used to produce **11**. Following failed attempts to isolate the product using silica gel flash column chromatography, PRMT1 ligand **11** was isolated in high yield by automated reverse-phase chromatography with ammonium hydroxide as an additive in the mobile phase (Figure 4.16).

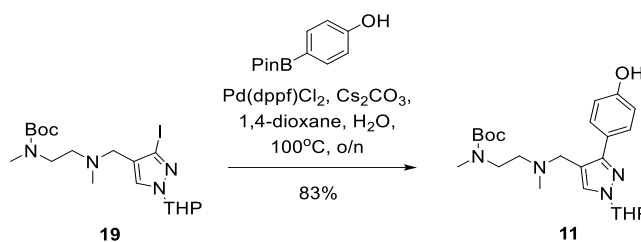
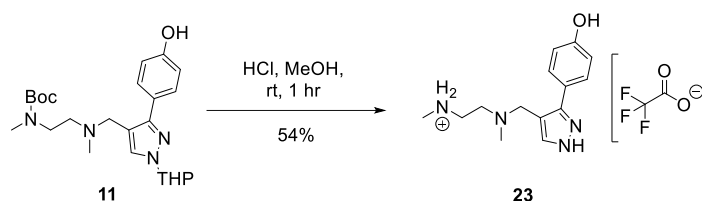


Figure 4.16 *Synthesis of PRMT1 ligand 11. Purification by reverse phase automated chromatography under basic conditions.*

4.2.2 Evaluation of the deprotected PRMT1 ligand

Before synthesising a library of PROTACs, it was confirmed that **11** can be deprotected to produce a ligand with affinity to PRMT1. The *N*-Boc and THP protecting groups on **11** were removed under acidic conditions to give deprotected PRMT1 ligand **23**. Due to the high polarity of **23**, purification was undertaken using reverse-phase chromatography on a preparative HPLC instrument with 0.05-

0.1% trifluoroacetic acid (TFA) as an additive in the mobile phase. This was followed by lyophilisation and the resulting product was characterised as the trifluoroacetate salt of **23** (Figure 4.17).



*Figure 4.17 Deprotection of **11** to give the active pharmacophore for PRMT1 binding. Purification using preparative HPLC with TFA in the mobile phase yielded the trifluoroacetate salt of **23**. The 2D-NMR spectra of **23** and the NMR spectra of silver trifluoroacetate used for characterisation are shown in Appendix 1C.*

Characterisation of **23** as the trifluoroacetate salt shown in Figure 4.17 was confirmed by NMR (Appendix 1C). The ^{13}C NMR spectra contains two quartets that can be attributed to the two carbons atoms in a trifluoroacetate anion through comparison to the ^{13}C spectra for silver trifluoroacetate which contains the trifluoroacetate anion. In addition, in the ^1H NMR spectra for **23**, the peak at ~ 8.9 ppm has an integral of two protons. This peak has been assigned as the protonated terminal secondary amine on the ethylenediamino chain of **23**.

The ^{13}C and ^1H NMR spectra also exhibit broad peaks which can be attributed to the presence of isomers that co-exist in solution. These isomers can constantly interconvert in solution and this leads the nuclei of the molecule to experience a constantly changing local magnetic field. When the interconversion of the isomers is slow with respect to the NMR timescale, the peaks in the spectra appear broad¹³¹. The presence of tautomers and conformational isomers of **23** is likely the cause of the observed peak broadening. Tautomerism is the existence of two or more structural isomers that interconvert by an intramolecular proton transfer, and in **23** it is the pyrazole group that can tautomerise^{132,133} (Figure 4.18). Conformational isomers (rotamers) are produced by rotation around a single bond. The broad peaks in the ^1H NMR and ^{13}C NMR spectra have been assigned to the pyrazole and the ethylenediamino chain, and it is inferred that there is restricted rotation around the bond highlighted in Figure 4.18¹³⁴.

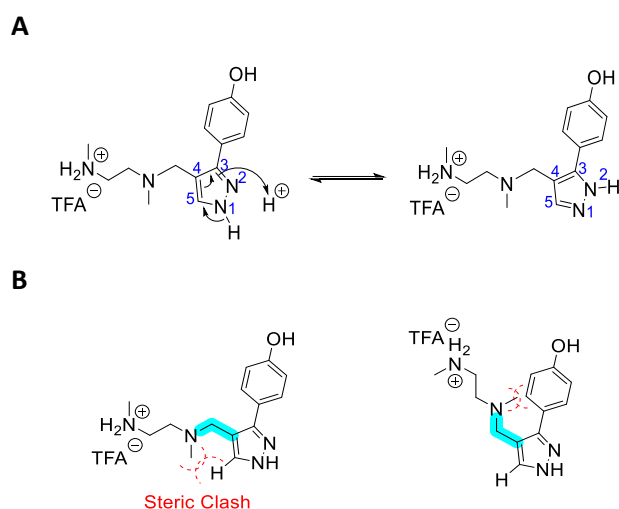
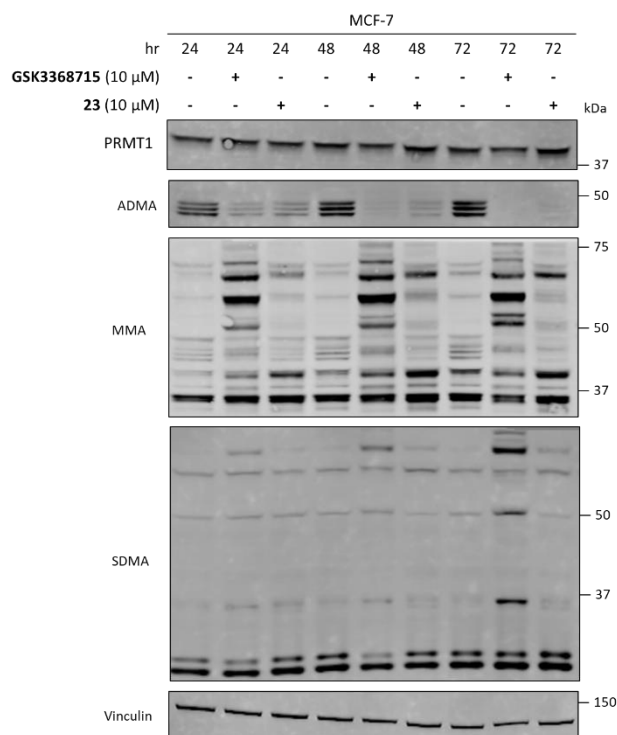


Figure 4.18 **Proposed isomers of deprotected ligand 23.** A) Tautomers of **23** that interconvert in solution by an intramolecular proton transfer. B) Proposed rotational isomers that are energetically unfavourable and lead to restricted rotation around the highlighted bonds.

The ability of **23** to bind to PRMT1 was investigated by Western blot. For this assay, cells were treated with **23** at a concentration (10 μM) that is significantly greater than the published IC_{50} for **GSK3368715** (3 nM)¹³. A similar approach was taken by Fedoriw *et al.* where they published an IC_{50} of 3 nM for **GSK3368715** yet used a concentration of 2 μM in cellular assays to investigate the effect of **GSK3368715** on arginine methylation by Western blot¹³.

Potency in biochemical assays can vary significantly from potency in a cellular assay. The IC_{50} of **GSK3368715** was determined in a biochemical assay where a mixture of recombinant PRMT1 protein, [³H]SAM, **GSK3368715** and a solution of peptide substrates were incubated for 60 minutes and the incorporation of tritium-labelled methyl groups into peptide substrates was measured¹³. The potency of a compound is often reduced in a cellular assay compared to a biochemical assay because of several factors. First, the effective concentration of the compound in the cell can be affected by the permeability of the compound across the cell membrane, the binding of the compound to serum in the cell culture media, as well as the hydrolytic and metabolic stability of the compound¹³⁵. Second, for a compound that binds to (and inhibits) PRMT1, potency may also be affected by competition with endogenous protein substrates for binding in the active site. Furthermore, PRMT1 is predominantly present as a component of multi-protein complexes¹³⁶. This may alter the binding affinity of the compound (compared to recombinant protein); the presence of PRMT1 in a complex may hinder the accessibility of the binding site to a compound or may alter the conformation of the protein¹³⁷. A change in binding affinity may also occur due to post-translational modifications on PRMT1 iteslf^{138,139}.

To account for a reduction in potency in the cellular assay compared to a biochemical assay, MCF-7 cells were treated with 10 μ M **23** and the change in PRMT1 protein level, and the level of the MMA and ADMA modification, were compared to that of untreated cells by Western blot. **GSK3368715** was also tested as a positive control. Cytotoxicity was not observed with either compound (Figure 4.19).



*Figure 4.19 **23** and GSK3368715 inhibit the activity of PRMT1 and Type I PRMTs. MCF-7 cells were treated with the indicated compound for 24, 48 or 72 hr and then protein levels were analysed by Western blot. The level of the post-translational modifications ADMA, MMA and SDMA were analysed in addition to the protein levels of PRMT1 and vinculin. Full uncropped blots are shown in Appendix 1D.*

First, as expected for an inhibitor of PRMT1, **23** does not affect the level of PRMT1.

As the chosen pharmacophore for PRMT1 binds in the protein-substrate binding pocket and is competitive with the protein substrates of PRMT1¹³, the ability of **23** to bind to PRMT1 can be inferred from whether **23** inhibits arginine methylation.

The ability of **23** and **GSK3368715** to bind to PRMT1 is shown by the large increase in MMA upon treatment with **23** and **GSK3368715**. An increase in MMA was observed with the knockdown of PRMT1 by siRNA shown previously in Figure 3.7 which is indicative of the specific inhibition of PRMT1 activity^{34,88}.

However, in contrast to PRMT1 knockdown where a modest reduction in ADMA was observed, both **23** and **GSK3368715** resulted in the complete loss of ADMA signal. The modest loss of ADMA with PRMT1 knockdown by siRNA was rationalised by shared protein substrates within the Type I PRMT

family and substrates that were previously methylated by PRMT1 are methylated by a different Type I PRMT upon PRMT1 knockdown (Section 3.1.3). However in contrast to the selective knockdown of PRMT1 by siRNA, **23** and **GSK3368715** contain a pharmacophore that is pan-selective for the Type I PRMTs and inhibits the activity of multiple Type I PRMT proteins¹³. Thus substrate scavenging does not occur and the ability of the cell to deposit the ADMA modification is significantly diminished. The complete inhibition of ADMA can be attributed to **23** and **GSK3368715** binding (and inhibiting) multiple Type I PRMTs.

SDMA is the unique post-translation modification catalysed by the Type II PRMTs and a time-dependent increase in SDMA was observed following treatment with **23** and **GSK3368715**. A similar increase in SDMA following PRMT1 knockdown was observed by Dhar *et al.*⁸⁸. They rationalise the observation by “with the loss of PRMT1, a large number of substrates become targets for Type II and Type III PRMTs, because these substrates are presumably no longer blocked by an ADMA modification”⁸⁸.

23 is suitable for use in a PROTAC for PRMT1 as it inhibits PRMT1 activity and therefore must bind to PRMT1. A summary of the change in arginine methylation status with inhibition is shown in Figure 4.20.

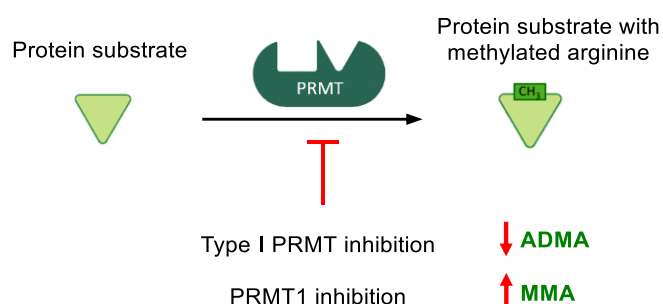


Figure 4.20 The effect of inhibition on Type I-catalysed arginine methylation.

Following the evaluation of the effect of **23** on arginine methylation, the biochemical potency of this molecule was published and corroborated that **23** is a potent PRMT1 ligand and a pan-Type I inhibitor. It also identified that **23** has the greatest potency to PRMT6¹⁴⁰ (Table 4.4). Consequently, all PROTACs synthesised in this project that contain the same pharmacophore of **23** were investigated for PRMT6 degradation in addition to PRMT1 degradation. It is however likely that the selectivity profile of the PRMT1 ligand to the Type I PRMTs will change on linker attachment.

Table 4.4 **23 is potent for both PRMT1 and PRMT6 inhibition.** All the proteins listed are Type I PRMTs. Values determined by a biochemical assay measuring the incorporation of [³H]SAM into peptide substrates. IC₅₀ values published in patent¹⁴⁰.

	IC ₅₀ , nM
PRMT1	98
PRMT3	>10,000
PRMT4	1710
PRMT6	19
PRMT8	712

4.3 Linker Design

The following sections discuss the challenges in designing a linker for a PROTAC and highlight how rational design is hindered by two factors: ternary complex formation and pharmacokinetics.

4.3.1 The linker and ternary complex formation

As discussed in the introduction, a PROTAC brings two proteins into close proximity and protein-protein interactions affect the stability of a ternary complex. The length of the linker is important as, if the linker is too short, the ternary complex may not form due to a steric clash between the target protein and E3-ligase, and if too long, entropic effects can prevent favourable protein-protein interactions occurring between the E3-ligase and target protein¹⁴¹. However ternary complex formation alone does not cause degradation as ubiquitin transfer must occur for the target protein to be recognised by the proteasome¹⁴². This ubiquitin transfer will be dependent on the distance between, as well as the relative orientation of, the ubiquitin-charged E2-enzyme (which is in a complex with the E3-ligase) and a lysine that can be ubiquitinated on the surface of the target protein. It is this required conformation that makes rational linker design challenging.

With PROTACs that degrade their target protein, X-ray crystallographic data of binary and ternary complexes has led to the development of reliable computational models that look at the energy landscapes of the protein-protein interfaces in the ternary complex. These models have successfully guided structure optimisation and have been used to rationalise the potency and selectivity of degradation in pre-existing, bioactive PROTACs (summarised in Bemis *et al.*¹⁴¹).

It is challenging to design a PROTAC for a novel target protein such as PRMT1 as the required relationship between a lysine on the target protein and the ubiquitin-charged E2-enzyme is not fully understood^{142,143}. The elucidation of the relationship required has been hindered by the inability to

characterise ternary complex structure routinely¹⁴⁴. Ternary complexes are difficult to study as they can be short-lived and exhibit multiple stable conformations *in situ*¹⁴⁵. Furthermore, for the most frequently used assays, X-ray crystallography and cryogenic electron microscopy (cryo-EM), sample preparation and purification conditions can influence which ternary complexes are observed, and it is not guaranteed that the *in vivo* functional conformation will be captured¹⁴⁵. Multiple ternary complexes with differing conformations may also exist *in situ* and it is difficult to ascertain which ternary complexes induce ubiquitin transfer and which do not¹⁴⁶.

4.3.2 The linker and pharmacokinetic properties

The linker is also decisive for the pharmacokinetic properties of the PROTAC. Pharmacokinetics describes the movement and fate of the PROTAC molecule in the body and generally examines four key processes of the molecule: absorption, distribution, metabolism and excretion.

Lipinski's 'rule of 5' and Veber's rules are guidelines for medicinal chemists in designing molecules with suitable pharmacological properties for oral administration and focus on solubility and permeability^{147,148}. Solubility refers to how effectively the molecule will be absorbed into the bloodstream across the intestinal membrane, whereas permeability is concerned with the passage of the molecules across a lipid bilayer, for example entry into a cancer cell. PROTACs frequently exhibit high molecular weight, high polarity and many rotatable bonds, and these properties fall outside the guidelines¹⁴⁹ (Figure 4.21 A-B). Focussing on permeability (as poor solubility can be overcome through administration through intravenous infusion¹⁵⁰), the use of a suitable linker can allow a PROTAC to be cell permeable even if its properties fall outside Lipinski's rule of 5 and Veber's rules. For example, a flexible linker can allow a PROTAC to adopt a conformation that sufficiently minimises its size and polarity to allow it to pass through the cell membrane (Figure 4.21 C-D)^{151,152}. The screening of flexible linkers should be undertaken.

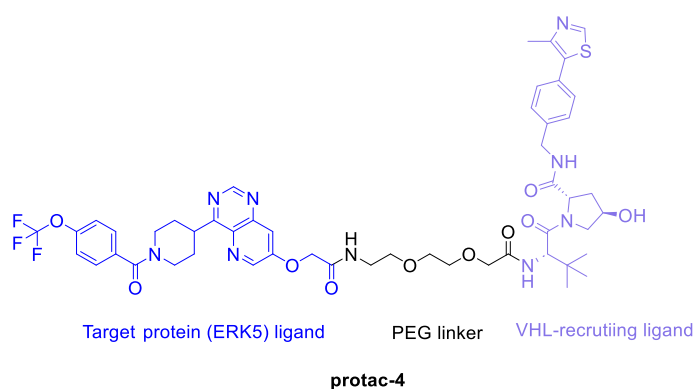
A

Lipinski's rule of 5:

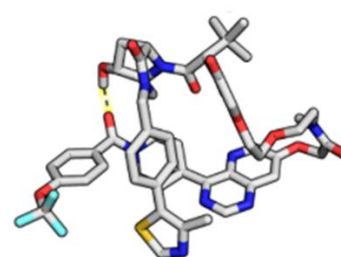
- Molecular weight (M_w) \leq 500 Da
- Partition coefficient (cLogP) \leq 5 (measure of lipophilicity)
- Number of hydrogen bond acceptors (HBA) \leq 10
- Number of hydrogen bond donor (HBD) \leq 5

Veber's rule:

- Polar surface area (TPSA) \leq 140 Å²
- Number of rotatable bonds (NRotB) \leq 10

C**B**

	ARV-471	MZ1
M_w , Da	723.9	1001.4
cLogP	6.8	4.9
HBA	8	17
HBD	2	4
TPSA, Å ²	96.4	210
NRotB	7	25

D

- Intramolecular hydrogen bond reduces polarity
- Shielding of NH amide groups reduces polarity
- π - π interaction reduced size

Figure 4.21 **PROTACs sit outside the 'Rule-of-5' chemical space but can be cell permeable** A) Lipinski rules and the expanded rules by Veber. B) Pharmacochemical properties of the PROTACs ARV-471 and MZ1^{100,149}. Values in red indicate they break Vebers and Lipinski's rules. ARV-471 in in phase 3 clinical trials with oral-delivery. C) Chemical structure of protac-4. D) The major conformation adopted by protac-4 in chloroform. Chloroform has a similar dielectric constant to the cell membrane and was chosen to mimic this environment. The intermolecular bond between the hydroxyl group of the VHL ligand and the tertiary amide of the ERK5 ligand is shown in yellow. Figure reprinted from Atilaw *et al.*¹⁵².

Furthermore, the linker has been found to impact PROTAC metabolism. One striking result, published by Goracci *et al.*, is that linker length and composition can significantly affect the metabolic stability of a PROTAC¹⁵³ (Figure 4.22). The linker identity is hypothesised to affect the ability of the PROTAC to enter the catalytic site of metabolic enzymes however general trends that lead to the increased metabolic stability of a PROTAC could not be identified which highlights how an empirical approach for linker design is required.

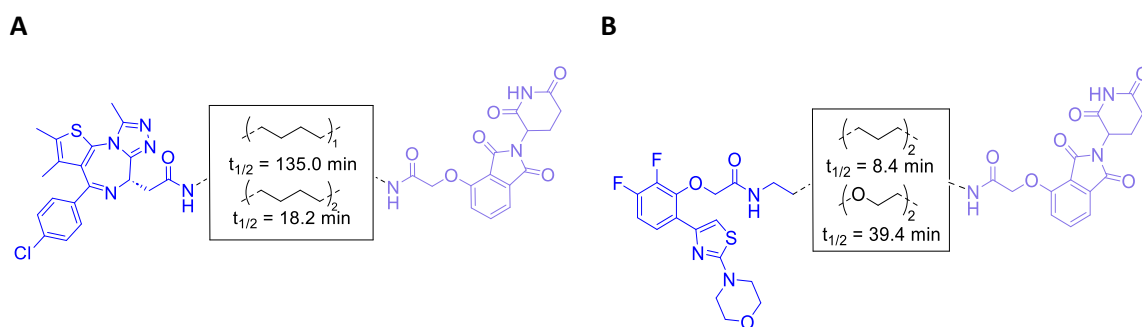


Figure 4.22 **Linker identity can affect the metabolic stability of a PROTAC.** $t_{1/2}$ is the half-life of the indicated PROTAC in cryopreserved human hepatocytes in Williams E medium at 37°C. A) Changing the linker length affects $t_{1/2}$. B) Changing the linker composition affects $t_{1/2}$. Target protein ligand shown in blue and E3-ligase ligand shown in lilac. Half-life values published in Goracci *et al.*¹⁵³.

4.3.3 The linkers for this project

The approach frequently adopted when developing a PROTAC for a novel target protein such as PRMT1 is an iterative trial and error approach where a library of PROTACs with varying length and polarity linkers are synthesised and screened for degradation efficacy. The most promising candidates are structurally optimised through alterations in their linker design and retested. This continues until degradation efficacy is maximised¹⁴³.

This project will synthesise a library of PROTACs with linkers containing PEG and alkyl chains; 64% of published PROTACs contain PEG or alkyl linkers¹⁵⁴ and these linkers allow the exploration of the effect of linker length on ternary complex formation and their high flexibility allows for multiple spatial orientations between the E3-ligase and the target protein. The PEG and alkyl chains also have a different hydrophobicity, and by synthesising PROTACs using both linkers, a range of pharmacokinetic properties are also screened¹¹⁸. The use of both PEG and alkyl linkers maximises the likelihood of forming an intracellular stable ternary complex with positive cooperativity between the E3-ligase and target protein¹⁵⁵.

If degradation is observed, structure-activity optimisation would be undertaken where linkers with a more rigid backbone or that can be protonated to improve solubility would be investigated, for example a piperazine-containing linker¹⁵⁶. A literature example of this is Han *et al.* where 41 PROTACs were screened and structure-activity guided optimisation culminated in a PROTAC for the oestrogen receptor that has a DC₅₀ < 1 nM and a maximum degradation efficacy (D_{max}) of > 95% in a prostate cancer cell line¹⁵⁷.

Linkers with suitable reactive functional groups on either end are commercially available, and this will allow for a modular approach to be followed when synthesising PROTACs for PRMT1.

4.4 PROTAC Design for PRMT1 Degradation

The chosen structures for the initial library of PROTACs that target PRMT1 is shown in Figure 4.23.

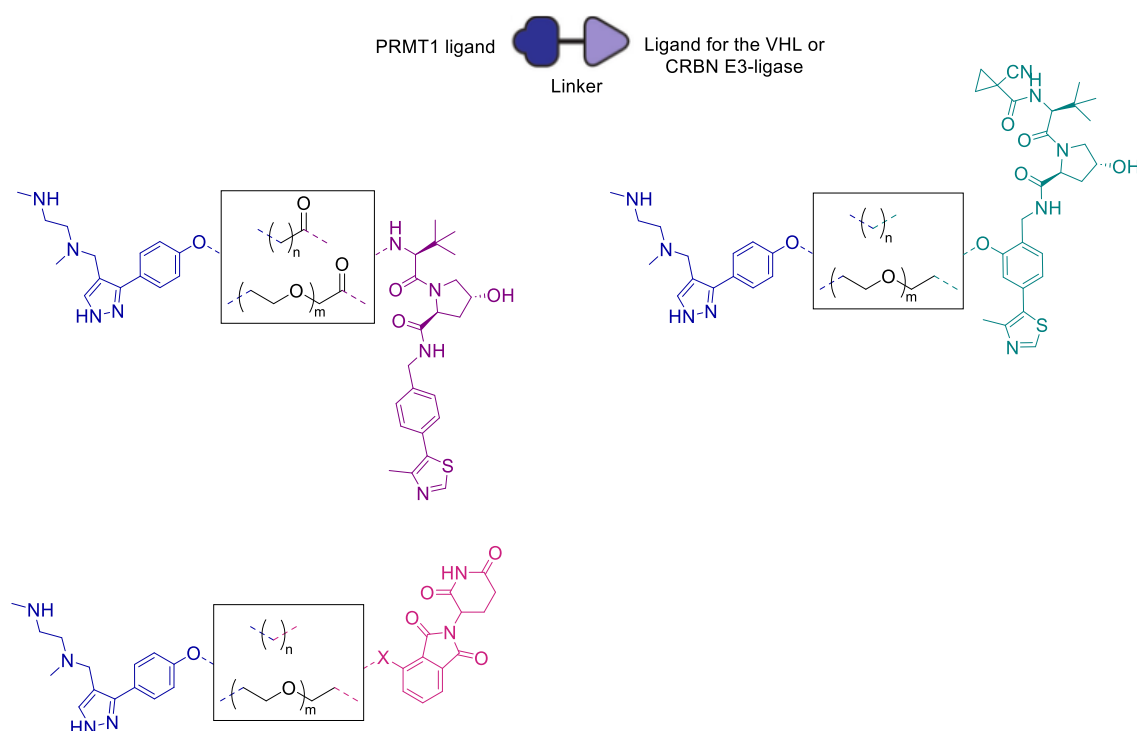


Figure 4.23 Design of PROTACs for PRMT1.

4.5 Controls Experiments to show PROTAC-Induced Degradation

If PRMT1 degradation is observed upon PROTAC treatment, it should be confirmed that the degradation is PROTAC-induced and UPS-dependent. This can be achieved by blocking distinct steps in the proposed mechanism of action and monitoring the effect on PRMT1 degradation.

First, the dependence of degradation on PROTAC binding to the E3-ligase and PRMT1 must be shown. Inactive negative control heterobifunctional molecules, where the PRMT1 ligand or the E3-ligase ligand is replaced with its inactive non-binding control ligand, should be synthesised (Figure 4.24). Heterobifunctional molecules that contain these ligands will be unable to form a ternary complex but will retain a close structural similarity to the active PROTAC and therefore retain off-target activity¹⁵⁸. PRMT1 degradation would not be observed if degradation is PRMT1/E3-ligase binding dependent. Alternatively, incubating the PROTAC with a saturating concentration of the PRMT1 ligand or E3-ligase ligand would reduce PROTAC binding and ternary complex formation. The absence of degradation in this experiment would confirm the necessity of PROTAC binding to both the E3-ligase and the target protein.

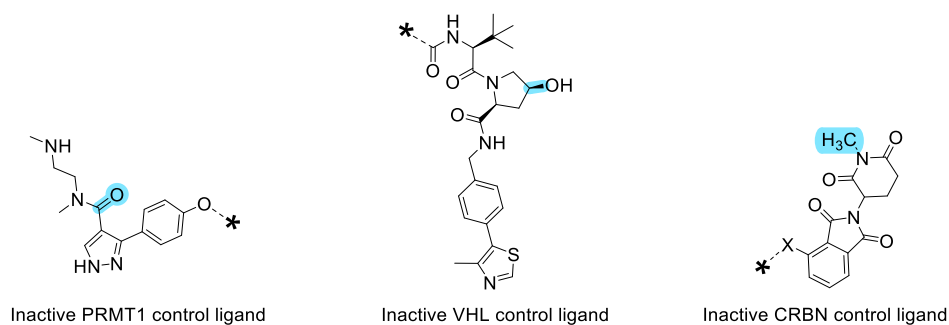


Figure 4.24 Inactive control ligands for the synthesis of inactive control heterobifunctional molecules. The position where the ligand differs from its active ligand is highlighted in blue. For the PRMT1 ligand an amide functional group has been introduced adjacent to the pyrazole ring. In the structure-activity relationship studies for MS023, this change in structure resulted in a total loss of potency for PRMT1 inhibition⁴¹ (previously shown in Figure 4.7). For the VHL ligand, the stereochemistry of the hydroxyproline has been changed from R (active) to S (inactive), and for the CRBN ligand, the nitrogen of the glutarimide ring is methylated. Literature precedence for these inactive control molecules includes Bondeson et al.⁷¹.

The dependence of degradation on the UPS can be shown by an absence of degradation when cells are co-treated with the PROTAC and the proteasome inhibitor **MG132**⁸⁴. In addition, for PROTACs that recruit Cullin-RING E3-ligases such as VHL and CRBN, the active complex required for the ubiquitination of the target protein (which contains the E3-ligase and ubiquitin-charged E2-enzyme) can be inactivated by the neddylation inhibitor **MLN4924**¹⁵⁹ (Figure 4.25); an absence of degradation upon co-treatment with PROTAC and **MLN4924** would show that the degradation is dependent on the ubiquitinating enzymes. E3-ligase dependence can also be shown by the absence of degradation in a cell line with E3-ligase knockdown¹⁶⁰.

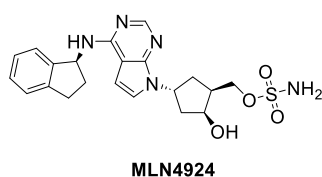


Figure 4.25 Structure of MLN4924. This molecule blocks Cullin neddylation (a post-translational modification) which deactivates Cullin-RING ligases and prevents the ubiquitination of protein substrates as part of the UPS.

5 VHL-Recruiting PROTACs

This chapter details the synthesis and *in vitro* evaluation of PROTACs that recruit the VHL E3-ligase (Figure 5.1).

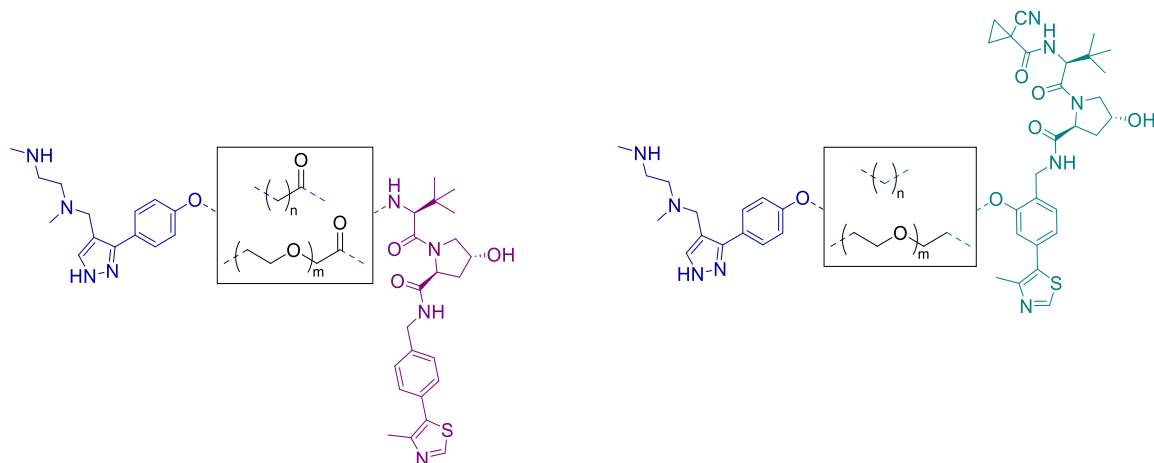


Figure 5.1 **Design of the VHL-recruiting PROTACs.** The structure of the left is synthesised from VHL ligand **1** and on the right from VHL ligand **2**.

5.1 PROTACs with VHL Ligand **1**

A retrosynthesis for PROTACs from VHL ligand **1** was devised. An amide bond connects the VHL ligand to an alkyl or PEG linker. A leaving group on the other end of a linker can then be *O*-alkylated by **11** and the subsequent deprotection of the *N*-Boc and THP group on the PRMT1 ligand gives the pharmacophore for PRMT1 binding (Figure 5.2).

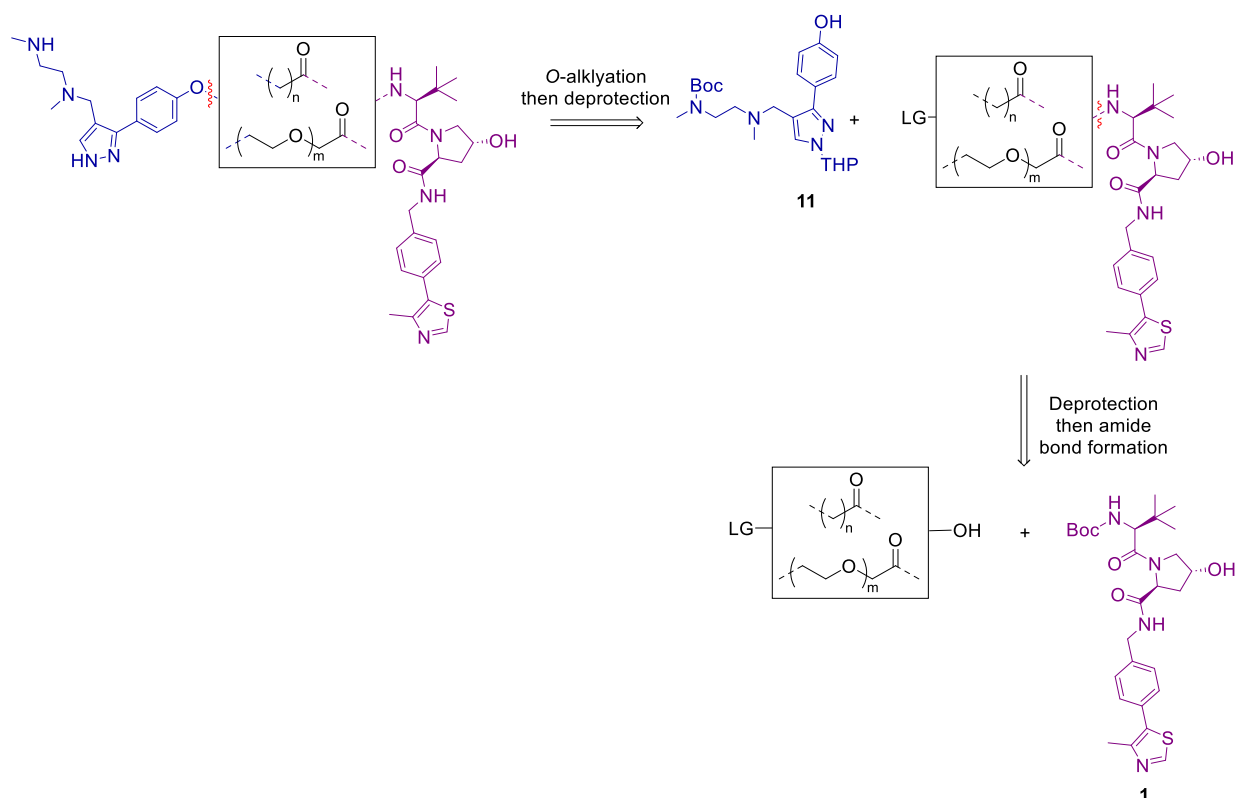


Figure 5.2 Retrosynthesis of PROTACs with VHL ligand 1. LG = leaving group.

5.1.1 Synthesis with an alkyl linker

The first PROTAC was synthesised. VHL ligand **1** was deprotected to give a primary amine which underwent an amide coupling reaction with commercially available 6-chlorohexanoic acid to give **24** (Figure 5.3). Purification by column chromatography resulted in a mixture of **24** with unreacted 6-chlorohexanoic acid. The acid was removed by washing with aqueous sodium hydrogen carbonate and this wash step was incorporated into the initial work-up after the reaction in future amide coupling reactions.

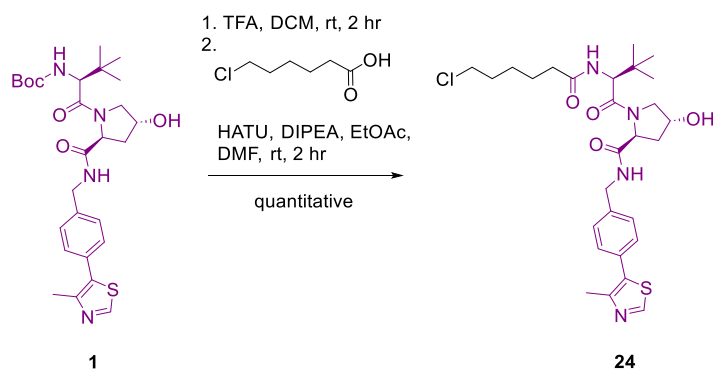


Figure 5.3 Synthesis of alkyl chloride **24**.

The alkyl chloride of **24** was *O*-alkylated by PRMT1 ligand **11** to give **25**. This reaction proceeds by a bimolecular nucleophilic substitution (S_N2) and a catalytic amount of potassium iodide was added to enable halogen exchange *in situ* and convert the alkyl chloride into a better leaving group. However the *O*-alkylation with **11** was slow and **11** was only completely consumed after five days of heating. After purification, **25** was deprotected using acidic conditions to give **PROTAC B** (Figure 5.4).

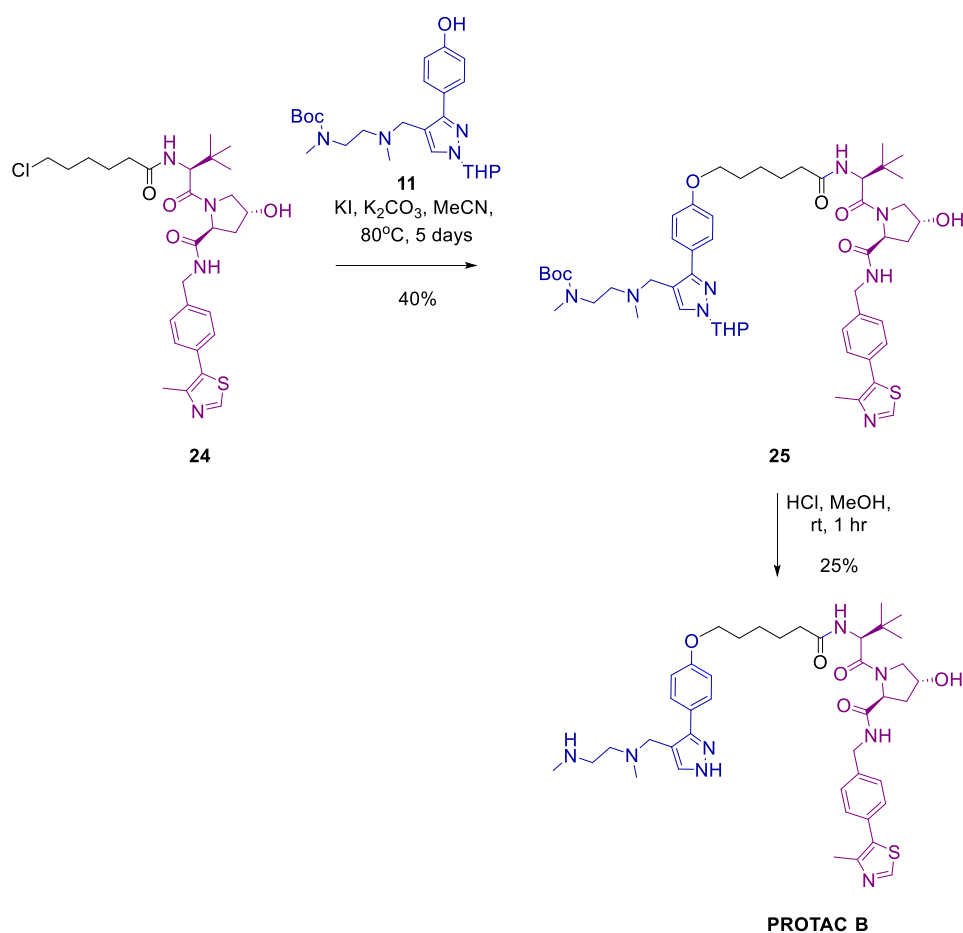
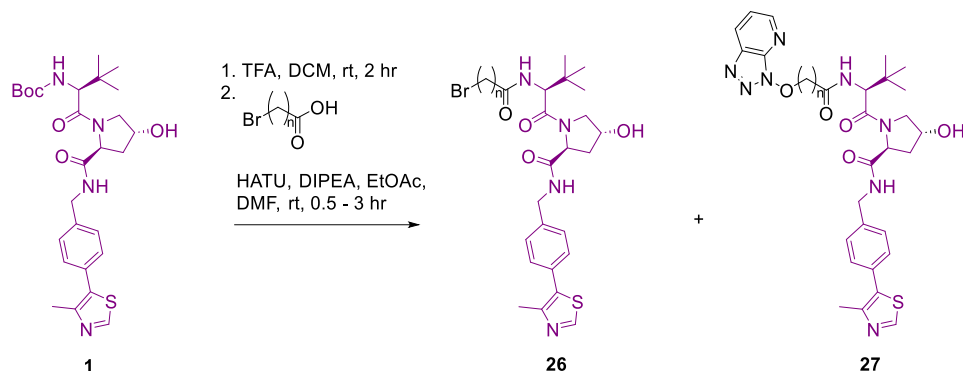


Figure 5.4 Synthesis of PROTAC B.

To reduce the reaction time for *O*-alkylation, the same reaction conditions were used with an alkyl bromide. The bromide anion is more stable than chloride and therefore the *in situ* iodination and *O*-alkylation should occur more readily. VHL ligand **1** was deprotected and underwent an amide coupling reaction with 8-bromooctanoic acid (entry c, Table 5.1). **26c** was isolated at a 30% yield and taken forward for *O*-alkylation. The major product of the amide coupling was not the alkyl bromide **26c**, but **27c** which forms from a substitution of the alkyl bromide with a by-product from the HATU coupling reagent (proposed mechanism in Figure 5.5). When the reaction was repeated with linkers of different lengths, shortening the reaction time to 30 minutes reduced the yield of undesired product **27** (entry d-f, Table 5.1).

Table 5.1 Amide coupling of **1** with various alkyl bromide linkers to give **26**. Product **27** forms from the substitution of the alkyl bromide by the anion of 1-hydroxy-7-azabenzotriazol. N.D. = not determined.



Entry	n=	Reaction Time	Product 26 , %	Product 27 , %
c	7	3 hr	30	33
d	9	0.5 hr	78	14
e	11	0.5 hr	81	N.D.
f	15	0.5 hr	84	N.D.

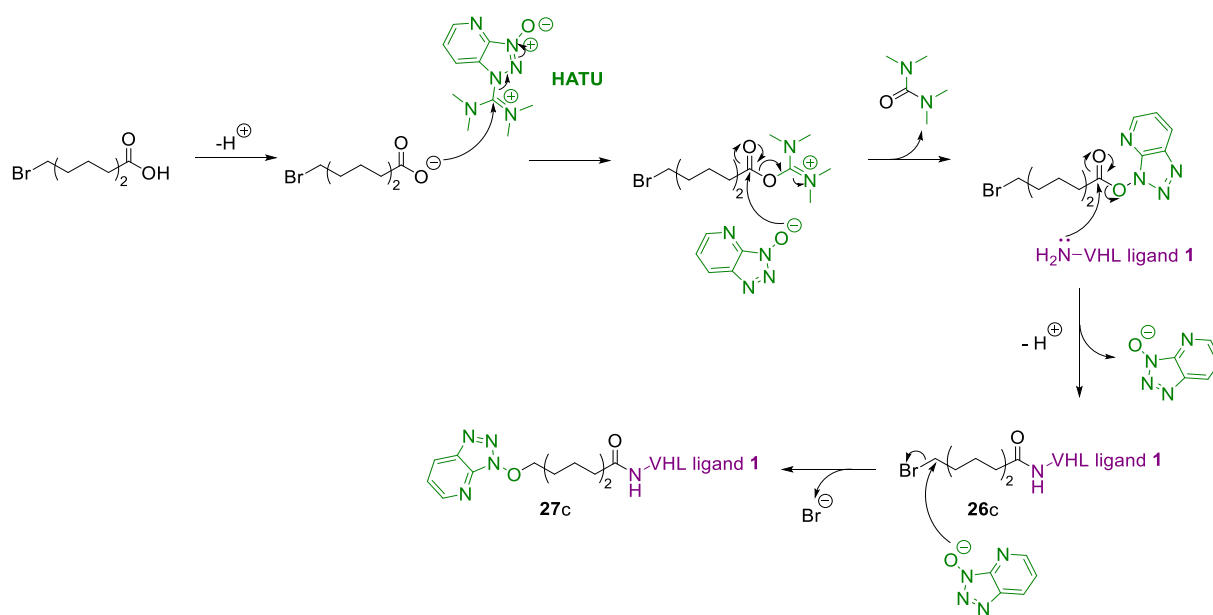
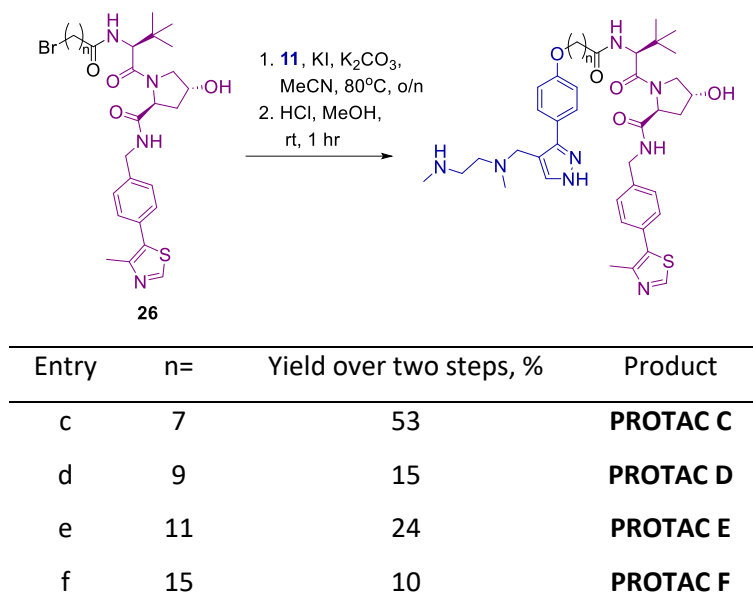


Figure 5.5 Mechanism for formation of product **26c** and one possible mechanism for product **27c** formation. An amide coupling reaction with the HATU coupling reagent. Anion of 1-hydroxy-7-azabenzotriazol is produced from the HATU reagent and can undergo a S_N2 reaction at the alkyl bromide of product **26c** to give product **27c**. **27c** may also form if the anion substitutes the alkyl bromide prior to the linker undergoing the amide coupling (not shown for simplicity).

With alkyl bromide **26** in hand, the *O*-alkylation reaction with PRMT1 ligand **11** was undertaken and the reaction went to full completion overnight. This was significantly faster than the alkyl chloride analogue which took 5 days. The solvent was removed from the *O*-alkylation reaction and the product taken forward without purification for deprotection to give **PROTAC C-F** (Table 5.2).

Table 5.2 *Synthesis of PROTAC C-F.*



To avoid the side reaction observed with HATU, amide bond formation was attempted using an electrophilic derivative of a carboxylic acid, an acyl chloride. With chloroacetyl chloride, the desired product **28** formed at a moderate yield, with the major side product being the di-acetylated product **29**. With the alkyl bromide linker 4-bromobutyryl chloride, the desired product was not formed and the isotope pattern for bromine was not present in any of the products in the crude LC/MS following the reaction. The route was abandoned (Figure 5.6).

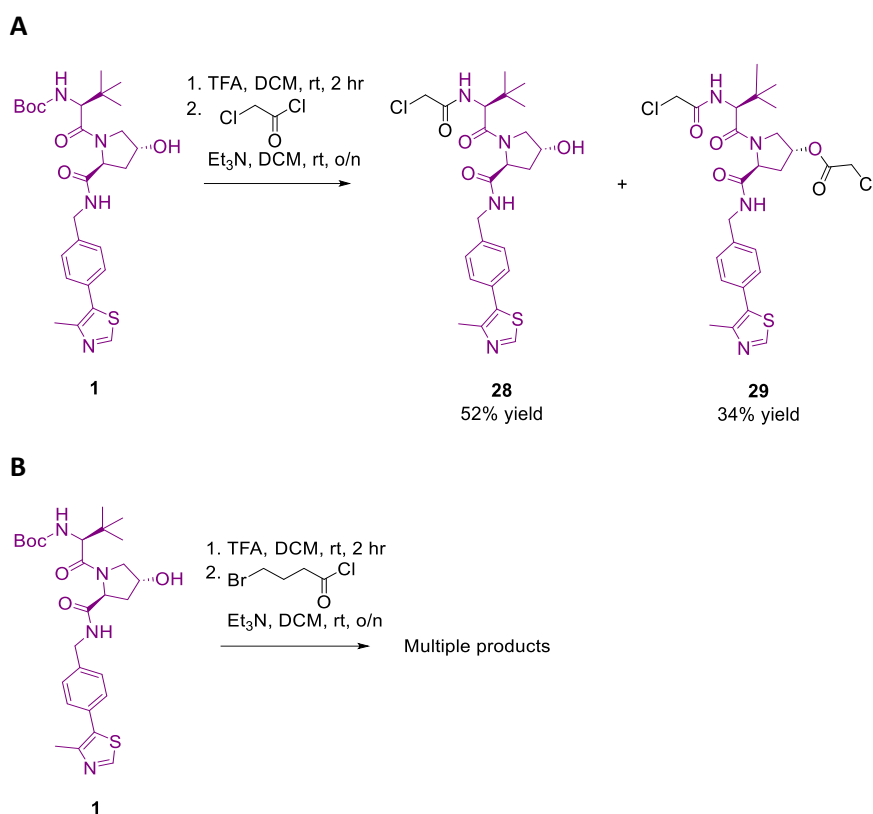


Figure 5.6 Amide bond synthesis using an acyl chloride.

28 was taken forward for *O*-alkylation with **11** and deprotected to give **PROTAC A** (Figure 5.7).

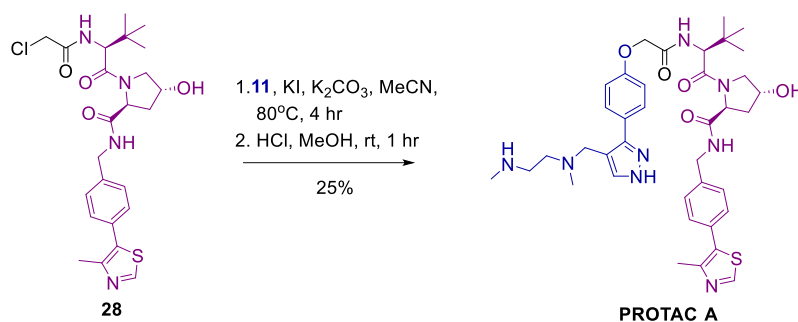


Figure 5.7 Synthesis of **PROTAC A**.

5.1.2 Synthesis with a PEG Linker

The synthetic route optimised with the alkyl linkers was then used PEG linkers. The required linkers were not commercially available so a route was devised for their synthesis. For synthetic accessibility, alkyl chlorides were chosen despite the longer reaction time for *O*-alkylation compared to an alkyl bromide (Figure 5.8).

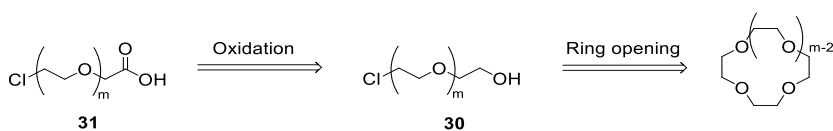


Figure 5.8 Retrosynthesis of PEG linker **31**.

Analogue of **30** with $m=1$ and $m=2$ are commercially available. For the longer PEG linkers, $m=3$ and $m=5$, **30** was synthesised by a ring opening reaction with Zirconium (IV) chloride in good yield. This reaction was first described in 1986 and the conditions optimised by Abronina *et al.*^{161,162} (Figure 5.9).

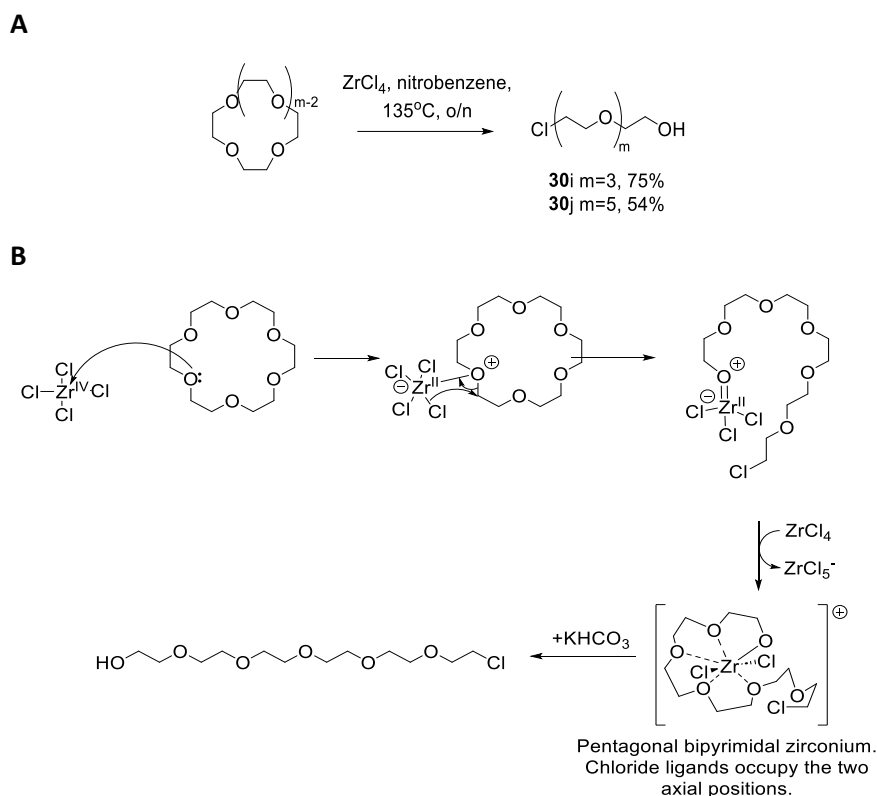


Figure 5.9 Ring opening of a crown ether to give alcohol **30** A) Synthesis of **30**. B) Mechanism for the ring opening reaction. An oxygen atom in the crown ether adds to the zirconium atom. A chloride is then transferred from the zirconium to the carbon atom adjacent to the now-positively charged oxygen atom. A chloride is then abstracted from the zirconium ion to give the pentagonal-bipyramidal cation. X-ray crystallography structure first published in Prinz *et al.*¹⁶¹. The addition of potassium hydrogen carbonate cleaves the zirconium oxygen bond to give the ring-opened product. The geometry around the zirconium ion is unspecified except where labelled. Solvent molecules are not shown.

With alcohol **30** in hand, oxidation was performed by Jones oxidation where chromic acid is produced *in situ* from chromium (VI) oxide and sulfuric acid¹⁶³. Carboxylic acid **31** was taken forward without purification (Figure 5.10).

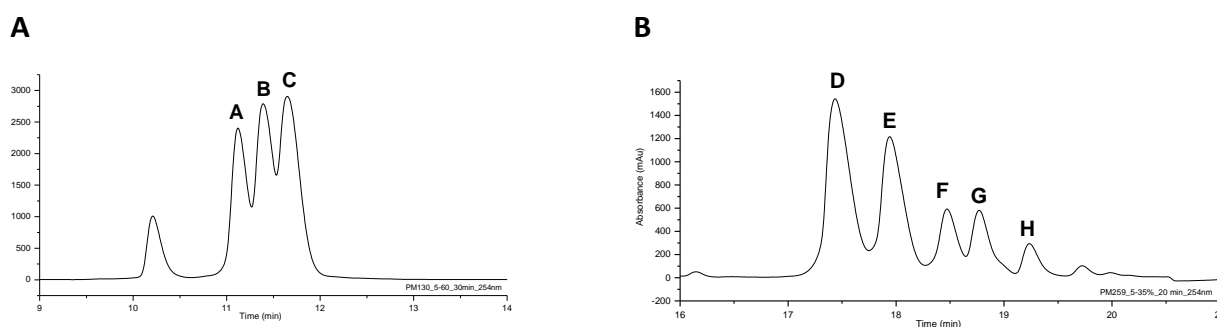


Figure 5.11 The preparative UV-HPLC chromatogram following the final step of entry *i* and entry *j* in Table 5.3. A) Chromatogram for entry *i* where $m=3$. B) Chromatogram for entry *j* where $m=5$. The number of peaks is equal to the value of m in the linker used. Absorbance recorded at $\lambda = 254 \text{ nm}$.

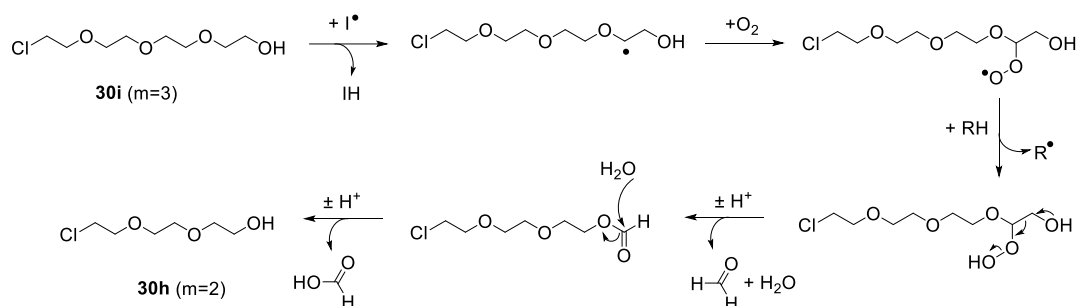
Table 5.4 Characterisation of the peaks of the UV-HPLC chromatogram shown in Figure 5.11. $[M+H]^+$ is the proton adduct molecular ion that is generated upon ionisation in LC/MS, where $[M+H]^+$ is equal to the sum of the monoisotopic mass of the molecule, M , and the mass of a proton.

Peak	m/z	m/z equal to $[M+H]^+$ of	NMR characterisation
A	775	PROTAC G (m=1)	-
B	819	PROTAC H (m=2)	PROTAC H (m=2)
C	863	PROTAC I (m=3)	PROTAC I (m=3)
D	775	PROTAC G (m=1)	PROTAC G (m=1)
E	819	PROTAC H (m=2)	-
F	863	PROTAC I (m=3)	-
G	847	-	-
H	951	PROTAC J (m=5)	-

It is probable that PEG chain cleavage was a side reaction during the synthesis of linker **31**, and by size exclusion chromatography, it should be determined whether it was the conditions of the ring opening reaction and/or Jones oxidation reaction that led to a mixture of products of varying length PEG chains. Substantial PEG chain cleavage has been previously reported with the direct oxidation of a PEG alcohol using the Jones conditions¹⁶⁴ however the conditions of both the ring-opening reaction and the Jones oxidation may lead to PEG chain cleavage by a free-radical process^{165,166}. A transition metal or an impurity such as peroxide may act as an initiator in a radical mechanism¹⁶⁷. Alternatively, the hydrolysis or nucleophilic substitution at an ether bond of the PEG chain may occur in the

presence of a Lewis acid^{168,169} (Figure 5.12). Both mechanisms would generate an alcohol functional group on a shorter PEG chain that may be oxidised to give a shorter analogue of linker **31**.

A



B

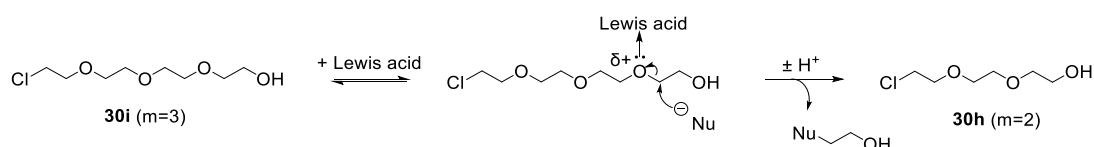


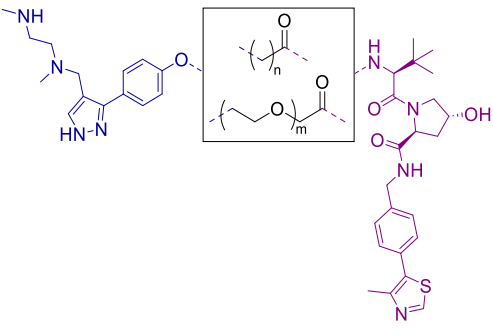
Figure 5.12 Possible mechanisms for PEG chain cleavage. A) A free-radical mechanism where hydrogen-atom abstraction is followed by a reaction with oxygen and subsequent hydrolysis to give formaldehyde, formic acid, and a PEG chain with a chain of less repeating PEG units. I^\bullet is a radical initiator and may be a metal (such as the zirconium used in the ring opening or the chromium in the Jones oxidation) or an impurity. B) A S_N2 where the nucleophilic attack is catalysed by a Lewis acid (such as zirconium or chromium). The nucleophile in this reaction may be water or a neighbouring oxygen of the PEG chain.

An alternative route should be used to introduce a carboxylic acid onto a PEG chain to produce linker **31** however the biological properties of **PROTACs G-I** meant that this was not required (shown in Section 5.2).

5.1.3 The chemical library of VHL-recruiting PROTACs

In total, 9 PROTACs were synthesised using VHL ligand **1** (Table 5.5).

Table 5.5 VHL-recruiting PROTACs synthesised.



Linker	
n=1	PROTAC A
n=5	PROTAC B
n=7	PROTAC C
n=9	PROTAC D
n=11	PROTAC E
n=15	PROTAC F
m=1	PROTAC G
m=2	PROTAC H
m=3	PROTAC I

Each PROTAC was purified by preparative HPLC with 0.05-0.1% trifluoroacetic in the mobile phase to afford high-purity PROTAC. Purity was determined by analytical HPLC and the UV-HPLC chromatograms of the PROTACs synthesised in this project are shown in Appendix 2. Similar to deprotected ligand **23**, characterisation by NMR indicates that each PROTAC exists as a salt with the trifluoroacetate anion and that the secondary amine on the PRMT1 ligand is protonated.

GSK3368715 is characterised as the di-hydrochloride salt by elemental analysis¹³ and therefore in an attempt to make accurate stock solutions of the PROTAC, the molecular weight of $[\text{PROTAC}+2\text{H}^+][2\text{TFA}^-]$ was used throughout this project (Figure 5.13). However future work should empirically quantify the number of trifluoroacetate anions per PROTAC molecule to increase the accuracy of the stock solution's concentration. This could be achieved by a quantitative NMR experiment where, by reference to external reference samples, the relative concentration of the trifluoroacetate anion, determined by ¹⁹F NMR, is compared to the relative concentration of the PROTAC molecule, determined by ¹H NMR^{170,171}.

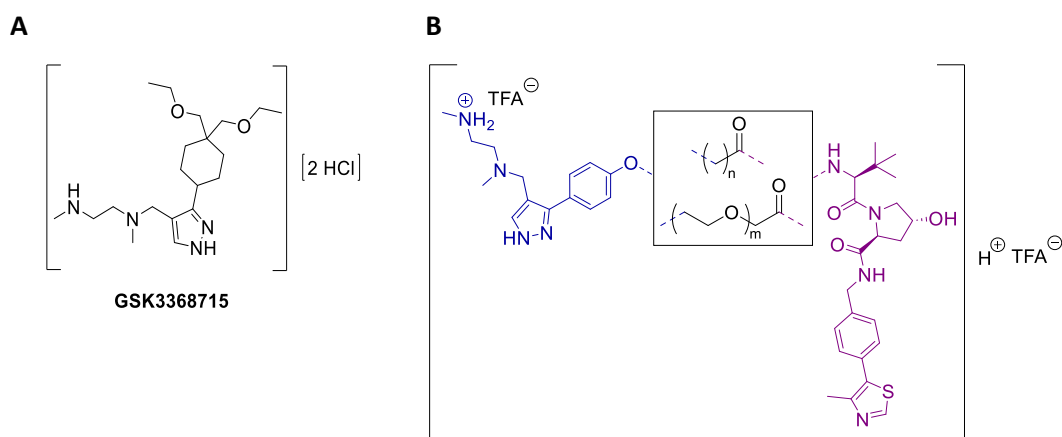


Figure 5.13 Each PROTAC has been assumed to exist as a di-trifluoroacetate salt. A) The species of GSK3368715 isolated following a deprotection step with HCl followed by filtration. Synthetic route published in Fedoriw et al.¹³. B) The molecular weight of $[\text{PROTAC}+2\text{H}^+][2\text{TFA}^-]$ was used to make precise stock solutions. TFA is the trifluoroacetate anion (CF_3COO^-). The protonation of the terminal secondary nitrogen is seen in the ^1H NMR spectra.

A ≥ 10 mM stock of each PROTAC was produced in sterile d_6 -DMSO and this stock solution was analysed by NMR prior to use in cell culture. The presence of a high concentration of TFA in cell culture can affect cell viability and proliferation¹⁷² however for the initial screen of PROTAC activity by Western blot, this should not affect whether the degradation of PRMT1 is observed. If a PROTAC is taken forward for more rigorous *in vitro* investigation, the PROTAC would be synthesised as a hydrochloride salt and an accurate molecular weight would be determined¹⁷³.

5.1.4 Stability in cell culture media

Prior to *in vitro* studies, the stability of the PROTACs in cell culture media was measured as the stability of a PROTAC will affect its therapeutic efficacy as well as its pharmacokinetic properties and toxicology¹⁷⁴. The PROTAC should be stable so that the PROTAC enters the cell intact and can bind to PRMT1 and the E3-ligase.

The stability of **PROTAC C** (alkyl linker $n=7$) and **PROTAC G** (PEG linker $m=1$) was investigated. Cell culture media was incubated at 37°C with $400\ \mu\text{M}$ of the chosen PROTAC and $400\ \mu\text{M}$ of caffeine. At frequent intervals, an aliquot was taken and analysed by HPLC. The respective peak areas of the PROTAC and caffeine in the UV-HPLC chromatogram were compared as the peak area is proportional to the concentration of the compound. As caffeine is stable under the conditions of this experiment and its concentration will not change over time it can be used as an internal standard. Any change in the PROTAC peak area and the caffeine peak area ratio can be attributed to PROTAC instability. PROTAC C and PROTAC G were found to be stable with $>85\%$ of the PROTAC remaining following a 94 hour incubation (Figure 5.14).

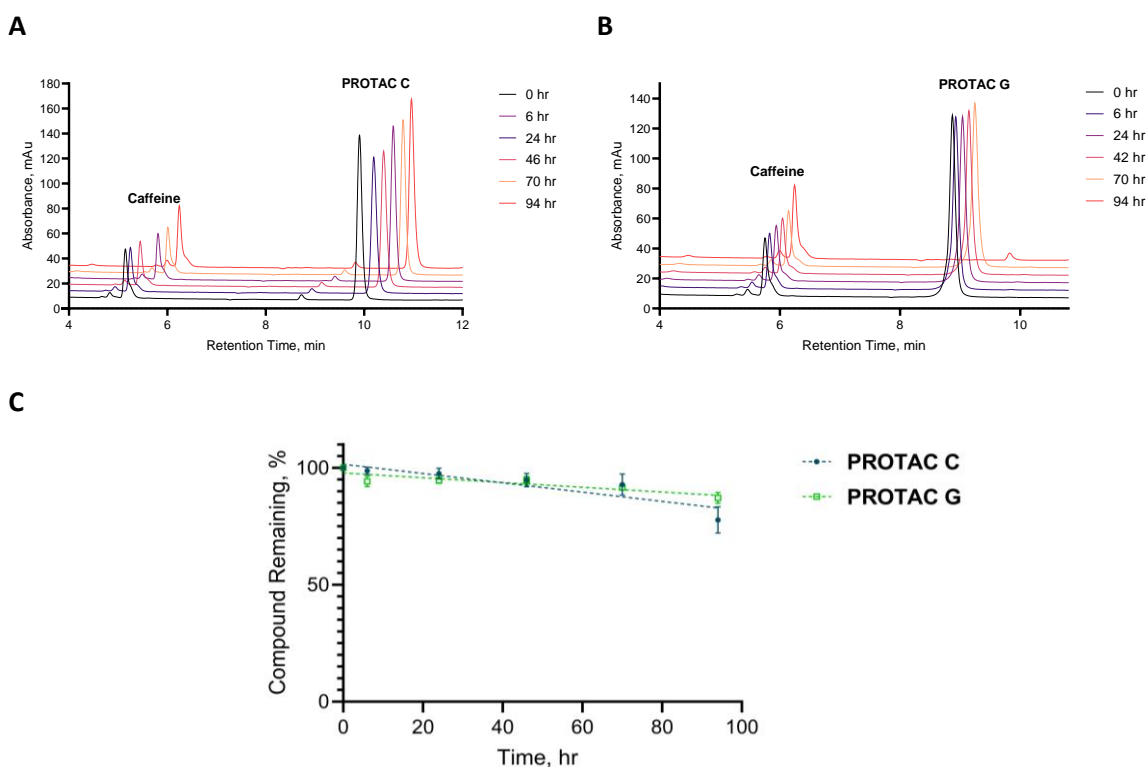


Figure 5.14 Stability of PROTAC C and PROTAC G in cell culture media. 400 μ M PROTAC and 400 μ M caffeine were incubated in DMEM supplemented with 10% FBS at 37°C in an ambient atmosphere for 94 hr. A) Representative UV-HPLC chromatograms for PROTAC C at various time intervals. Absorbance recorded at $\lambda = 254$ nm. B) Same as A with PROTAC G. C) The Y-axis is the percentage of PROTAC remaining compared to the peak area ratio of PROTAC-to-caffeine at 0 hr. Data from three independent experiments. Mean and standard error plotted.

5.2 Degradation Efficacy by Western Blot

The ability of the synthesised PROTACs to degrade PRMT1 *in vitro* was investigated by Western blot. MCF-7 cells were incubated with 10 μ M of each PROTAC for 24 hours and analysed by Western blot. Neither PRMT1 nor PRMT6 degradation was observed with any of the PROTACs. Type I PRMT inhibition was observed with **PROTAC B**, **PROTAC C** and **PROTAC D** (shown by a reduction in the signal intensity for ADMA), and **PROTAC C** and **PROTAC D** were also shown to inhibit PRMT1 (shown by an increase in the signal intensity for MMA) (Figure 5.15). **PROTAC E** and **PROTAC F** were cytotoxic at this concentration and not analysed.

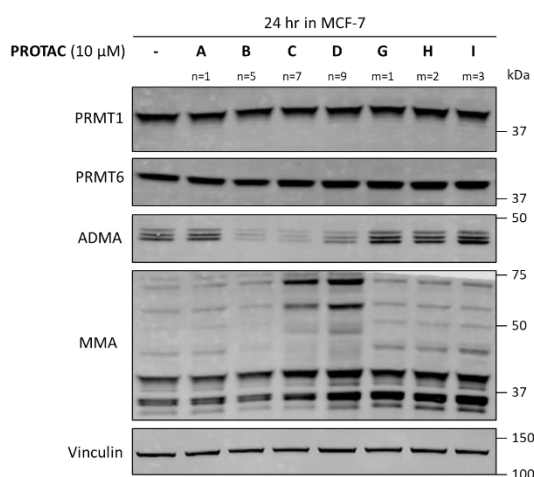


Figure 5.15 Western blot of PROTAC A-I in the MCF-7 cell line at 10 μM . MCF-7 cells were treated with the indicated compounds at 10 μM for 24 hr and then harvested for analysis by Western blot. PROTAC E and F were cytotoxic and not analysed. 'n=' and 'm=' refer to the length of the linker in the PROTAC. Image representative of two independent experiments.

PROTAC-induced degradation of a target protein is dependent on ternary complex formation and PROTACs exhibit a 'hook effect' where increasing the PROTAC concentration above an optimal level reduces degradation efficacy. At high PROTAC concentrations, binary complexes predominate and there is a reduction in the number of ternary complexes. This reduces the likelihood of the ubiquitination of the target protein and its subsequent degradation⁴⁶ (Figure 5.16).

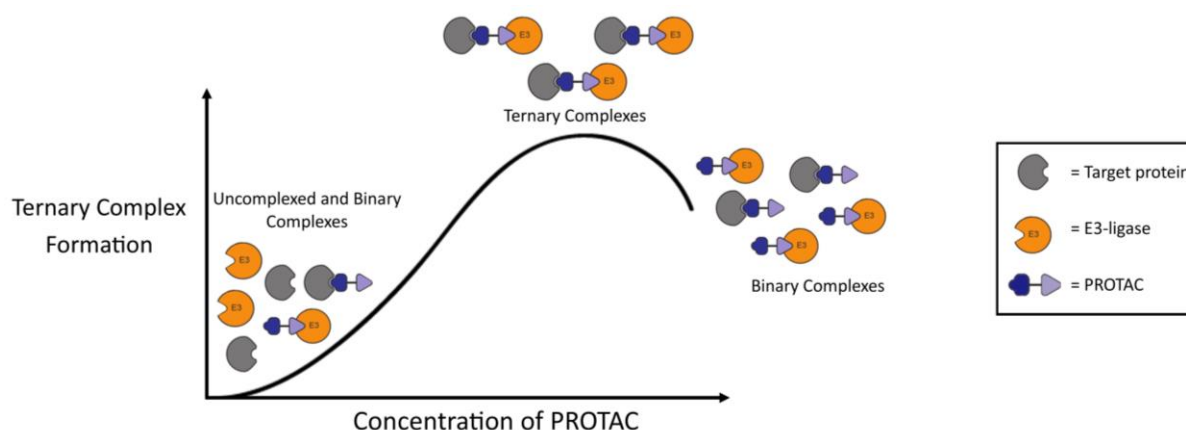


Figure 5.16 Schematic of the Hook effect. The E3-ligase would be in a complex with a ubiquitin-charged E2-enzyme (not shown).

The hook effect can be exemplified with the published PROTAC **protac-5** which recruits the VHL E3-ligase to degrade the B-cell lymphoma-extra large protein (Bcl-xL)¹⁷⁵. Degradation is dose-dependent until an optimal concentration of 0.3 μM is reached and above this concentration, Bcl-xL degradation is reduced (Figure 5.17).

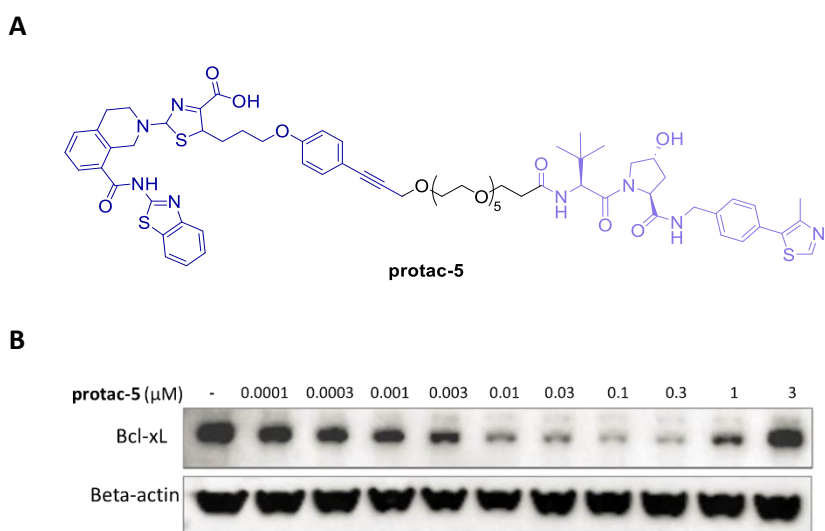


Figure 5.17 Bcl-xL degradation with protac-5 exhibits the hook effect. A) Structure of protac-5. A ligand for Bcl-xL (blue) is connected to a ligand for the VHL E3-ligase (lilac) by a PEG linker (black). B) THP-1 cells were treated with protac-5 at various concentrations for 24 hr and then harvested for analysis by Western blot. Beta-actin is a housekeeping protein. Figure adapted from Chung et al.¹⁷⁵.

The optimal concentration for degradation varies with PROTAC and target protein^{176,177} however if **PROTAC A-I** have a similar potency as **protac-5**, degradation would not be seen with a 10 μM treatment because of the hook effect. Therefore the PROTACs that inhibited at 10 μM , **PROTAC B**, **PROTAC C** and **PROTAC D**, were tested at 1 and 0.1 μM in MCF-7 cells. **PROTAC E** and **PROTAC F**, which were cytotoxic at 10 μM were also tested at the lower concentrations. PRMT1 degradation was not observed with any of the PROTACs (Figure 5.18).

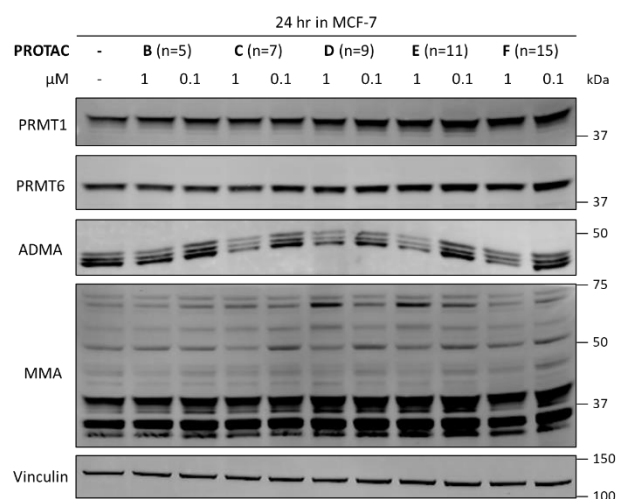


Figure 5.18 Western blot of PROTAC B-F in the MCF-7 cell line at 1 and 0.1 μM . MCF-7 cells were treated with the indicated compounds at 1 or 0.1 μM for 24 hr and then harvested for analysis by Western blot. Image representative of two independent experiments.

Finally, reproducibility was assessed in two PDAC cell lines. HPAF-II and KP-3 cells were treated with 10 μ M **PROTAC A-I** and incubated for 24 hours. The HPAF-II line was less sensitive to treatment and **PROTAC E** and **PROTAC F** were not cytotoxic at this concentration. PRMT1 degradation was not observed and the trends in target engagement were the same as observed in the MCF-7 cell line (Figure 5.19).

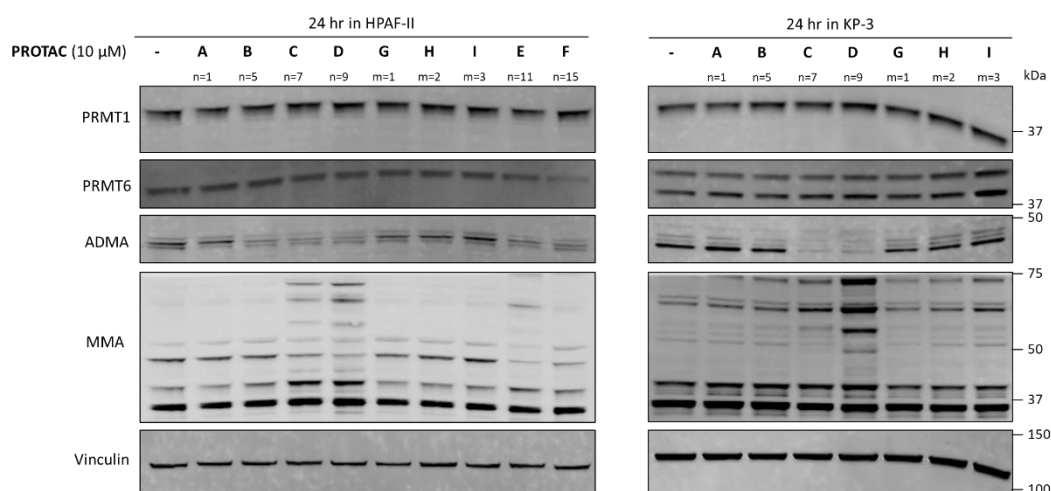


Figure 5.19 Western blot of **PROTAC A-F** in two PDAC-derived cell lines at 10 μ M. HPAF-II and KP-3 cells were treated with the indicated compounds at 10 μ M for 24 hr and then harvested for analysis by Western blot. **PROTAC E** and **PROTAC F** were cytotoxic in the KP-3 line.

5.3 PROTACs with VHL Ligand 2

A single PROTAC with VHL ligand **2** was synthesised. The *O*-alkylation of the phenol ring of VHL ligand **2** with commercially available 1,10-diiododecane gave **33**. This was then *O*-alkylated by PRMT1 ligand **11** and subsequently deprotected to give **PROTAC K** (Figure 5.20).

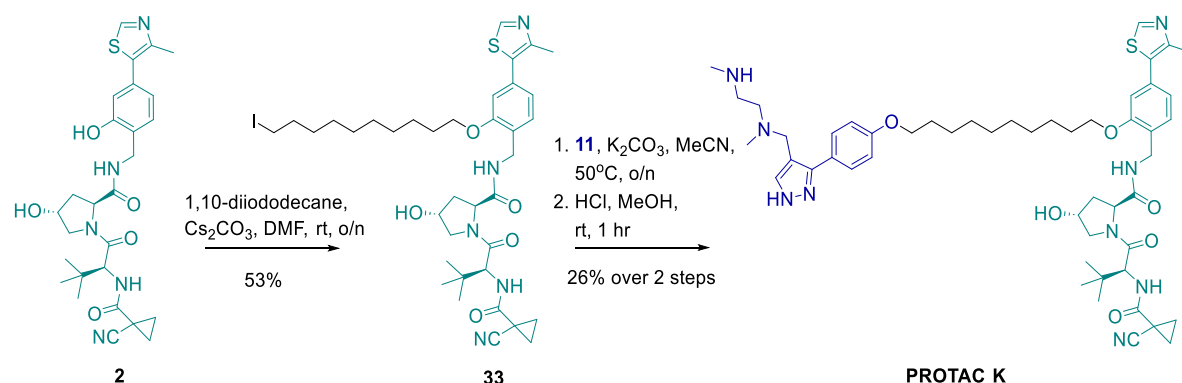


Figure 5.20 Synthesis of **PROTAC K**.

The degradation efficacy of **PROTAC K** was then investigated. **PROTAC K** was cytotoxic at 10 μ M in the MCF-7, HPAF-II and KP-3 cell line following treatment for 24 hours. At a reduced concentration in the

MCF-7 cell line, PRMT1 and PRMT6 degradation was not observed and Type I PRMT activity was inhibited (Figure 5.21).

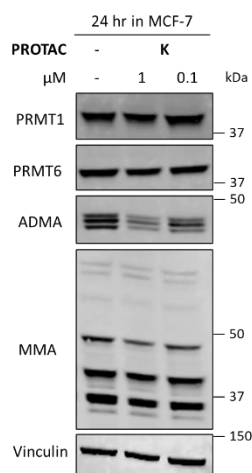


Figure 5.21 Western blot of PROTAC K in the MCF-7 cell line at 1 and 0.1 μM . MCF-7 cells were treated with PROTAC K at 1 and 0.1 μM for 24 hr and then harvested for analysis by Western blot.

5.4 The HaloPROTAC Assay

As PRMT1 degradation was not observed with the PROTACs synthesised it was investigated whether PRMT1 can be degraded by the VHL E3-ligase using the HaloPROTAC assay¹⁷⁸. In this *in vitro* assay, proximity is induced between the VHL E3-ligase and a fusion protein comprising the target protein fused to the HaloTag protein. The HaloTag protein is a 33 kDa protein that covalently binds to a hexyl chloride tag in a highly specific, rapid and biorthogonal reaction¹⁷⁹. The heterobifunctional small-molecule **HaloPROTAC3** can simultaneously bind the HaloTag fusion protein by a covalent bond and the VHL E3-ligase through high-affinity interactions. This HaloPROTAC3-induced ternary complex facilitates ubiquitin transfer and the subsequent proteasomal degradation of the fusion protein (Figure 5.22). This assay can confirm whether PRMT1 is present in the same subcellular location as VHL, and **HaloPROTAC3**-induced degradation can be used to assess the effect of PRMT1 degradation on tumourigenesis. It must be highlighted that this assay does not provide evidence that PRMT1 can be ubiquitinated by VHL as the HaloTag protein is predominantly ubiquitinated in this assay¹⁸⁰.

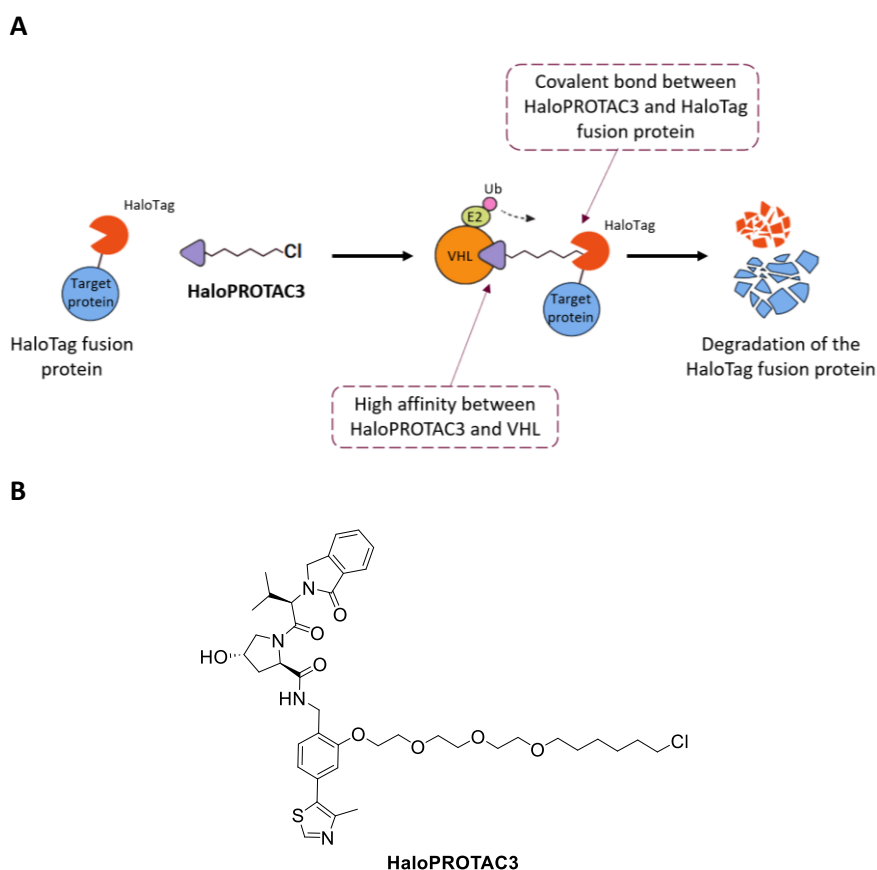


Figure 5.22 The HaloPROTAC assay. A) Schematic of the degradation pathway induced by HaloPROTAC3. Figure adapted from the HaloPROTAC3 Technical Manual (Promega, #GA3110). B) The structure of HaloPROTAC3. The hexylchloride motif is attached to an analogue of the VHL ligand VH032.

The first step towards this assay was the expression of a fusion protein of PRMT1 and the HaloTag protein. A plasmid that encodes the 'PRMT1-HaloTag-6xHis' fusion protein was obtained in a bacteria stab from addgene.org. The bacteria stab was streaked onto an agar plate and a single colony was picked and inoculated to form a bacteria culture. The DNA plasmid was isolated using a plasmid purification kit, transiently transfected into MCF-7 cells and the protein levels of the cells analysed by Western blot.

An antibody for PRMT1 would be expected to give two bands; a band for endogenous PRMT1 at 41 kDa, and if the transfection was successful and the fusion protein was transcribed, an additional band for the PRMT1-HaloTag-6xHis fusion protein at 75 kDa {the sum of the molecular weights of PRMT1 (41 kDa) + HaloTag (33 kDa) + 6xHis (0.8 kDa)}. However when the plasmid was transfected into MCF-7 cells at the recommended concentration for use with **HaloPROTAC3**, a single band that correlated with the molecular weight of endogenous PRMT1 was observed. A band for the fusion protein was not observed (Figure 5.23).

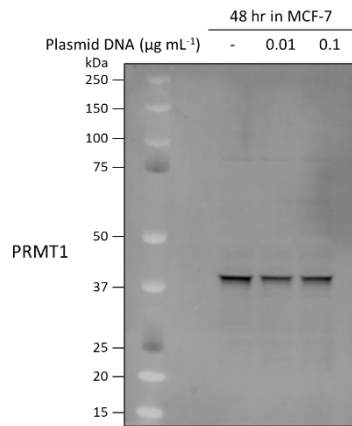


Figure 5.23 Western blot following the transfection of MCF-7 cells with the 'PRMT1-HaloTag-6xHis' plasmid. The fusion protein is not observed. The single band is for endogenous PRMT1. A band that at 75 kDa would correlate to the fusion protein. MCF-7 cells harvested 48 hr after transfection.

The experiment was repeated with an increased concentration of the DNA plasmid but again only a single band for endogenous PRMT1 was observed (Figure 5.24). Considering the possibility that the PRMT1 antibody does not bind to the fusion protein, the membrane was reprobed with an antibody for the 6xHis protein. Again, no band at the expected molecular weight for the fusion protein was observed. It was concluded that the fusion protein was not expressed.

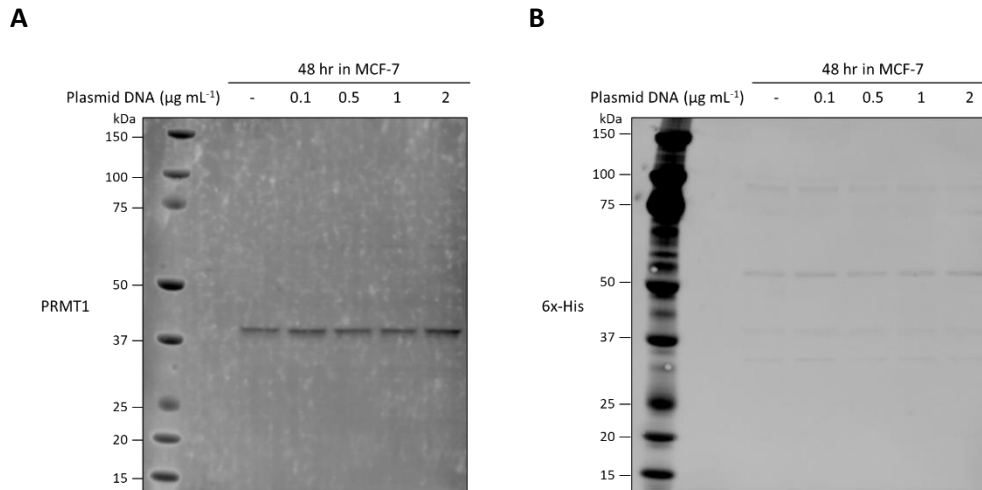


Figure 5.24 Western blot following the transfection of MCF-7 cells with the 'PRMT1-HaloTag-6xHis' plasmid at an increased concentration of the DNA plasmid. The fusion protein was not observed. A band that at 75 kDa would correlate to the fusion protein. MCF-7 cells harvested 48 hr after transfection. A) Antibody for PRMT1. B) Antibody for 6x-His. Non-specific binding is observed.

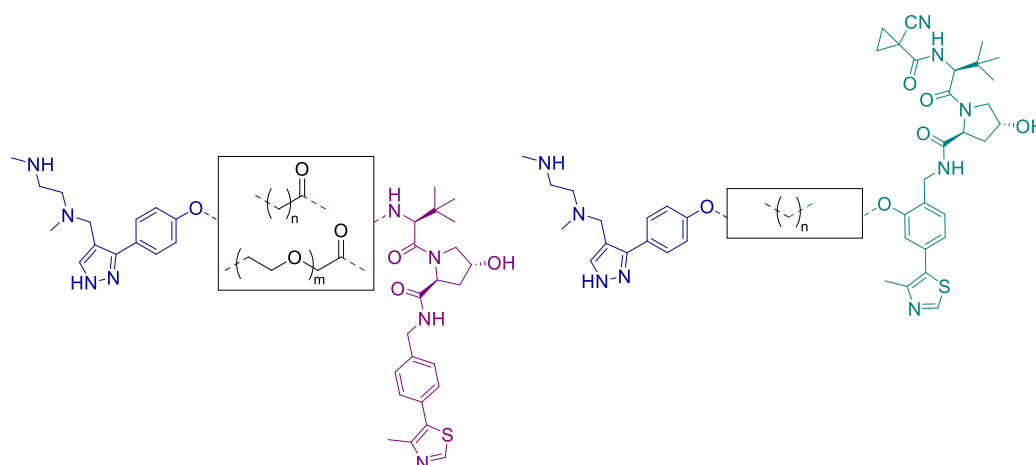
Examination of the sequence of the plasmid revealed why the fusion protein was not expressed (Appendix 1E). The promoter of a gene is a region of DNA where the RNA polymerase machinery binds to initiate transcription, and in the PRMT1-HaloTag-6xHis plasmid, the promoter is T7. This

promotor is recognised by the T7 RNA polymerase which is only present in prokaryotic (bacteria) cells¹⁸¹. The plasmid was not transcribed in the MCF-7 cells as the promotor was not recognised by the mammalian RNA polymerase machinery. The assay was abandoned.

5.5 Discussion and Conclusions

Neither PRMT1 nor PRMT6 degradation was observed with the VHL-recruiting PROTACs synthesised. The binary interaction between the PROTAC and PRMT1 was observed with selected PROTACs (Table 5.6).

Table 5.6 **A summary of the biological activity of the VHL-recruiting PROTACs in the MCF-7 cell line.** Inhibition and degradation were determined by Western blot with 24 hr treatment of $\leq 10 \mu\text{M}$ of the PROTAC in the MCF-7 cell line. Type I PRMT inhibition was characterised by a reduction in ADMA and PRMT1 inhibition was characterised by an increase in MMA.



	VHL Ligand	Linker	Degradation		Inhibition	
			PRMT1	PRMT6	Type I PRMT	PRMT1
PROTAC A	1	n=1	x	x	x	x
PROTAC B	1	n=5	x	x	✓	x
PROTAC C	1	n=7	x	x	✓	✓
PROTAC D	1	n=9	x	x	✓	✓
PROTAC E	1	n=11	x	x	✓	✓
PROTAC F	1	n=15	x	x	✓	x
PROTAC G	1	m=1	x	x	x	x
PROTAC H	1	m=2	x	x	x	x
PROTAC I	1	m=3	x	x	x	x
PROTAC K	2	n=10	x	x	✓	x

Except for **PROTAC A** (which has the shortest alkyl chain), Type I PRMT inhibition was observed with all the PROTACs containing an alkyl linker. **PROTAC D** (n=9) showed the highest potency for PRMT1 inhibition. None of the PROTACs with a PEG linker inhibited the activity of the Type I PRMTs.

Since **PROTAC D** and **PROTAC H** have the same number of atoms in their linker, the difference in inhibitory activity must be due to linker composition (Figure 5.25).

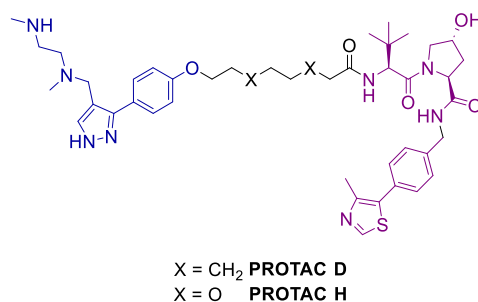
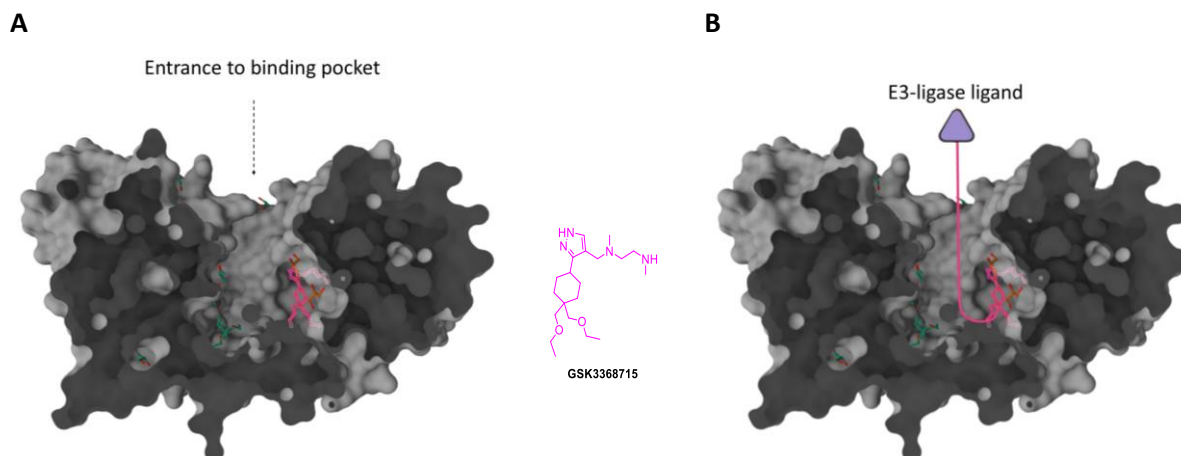


Figure 5.25 Structure of **PROTAC D** and **PROTAC H**.

Linker composition may alter the PROTAC's activity in two ways: by affecting pharmacokinetic properties or by affecting binding affinity. Regarding pharmacokinetics, the PEG linker may limit the cell permeability of the PROTAC. A PEG linker is more polar and less flexible than an alkyl linker of the same length, and this may affect the diffusion of the PROTAC across the hydrophobic cell membrane^{151,182}. Alternatively, the PEG chain may reduce the binary affinity of the PROTAC to PRMT1. A cell permeability assay and an assay that measures affinity (such as isothermal titration calorimetry¹⁸³) should be undertaken with **PROTAC D** and **PROTAC H** to rationalise the observed differences in their inhibitory properties.

Prior to the synthesis of any further PROTACs that recruit VHL, it be determined if any of the PROTACs form a ternary complex with VHL and PRMT1. A number of *in vitro* biophysical techniques have been developed to measure ternary complex formation and are summarised in Ward *et al.*¹⁴⁴.

If a ternary complex is not observed, the effect of changing linker composition should be explored further. This should focus on PROTACs with long linkers because, on a more careful analysis of the binding mode of **GSK3368715**, it is observed that it binds at the bottom of a deep pocket in PRMT1. As the PROTACs synthesised contain the same binding pharmacophore, it is likely that a long linker will be required to enable the VHL ligand of the PROTAC to enter the intracellular fluid and bind to VHL (Figure 5.26). However longer alkyl chain linkers cannot be used as they tend to collapse in on themselves in the polar intracellular environment. Rigid hydrophobic linkers, for example, a cyclic or alkyne group, should be investigated so that the longer lengths can be accessed¹⁵⁵.



*Figure 5.26 GSK3368715 binds in a deep binding pocket of PRMT1 and a PROTAC with a long linker is envisaged to be required to allow the E3-ligase ligand to enter the intracellular environment. A) Crystal structure of GSK3368715 bound to PRMT1 (PDB: 6NT2). A molecular surface representation of PRMT1 (grey) and the dark grey indicates where the protein is cut to enable visualisation of the protein substrate binding pocket. GSK3368715 as a ball and stick model (pink) and with the chemical structure is shown at the correct orientation. Crystal structure published in Fedoriw et al.¹³ and visualised using Mol*¹²¹ B) The predicted required trajectory for the linker that will enable the E3-ligase ligand to recruit VHL.*

If a ternary complex is observed, optimisation of linker length is not required as it is likely that the conformation of the ternary complex does not induce the ubiquitination of the target protein in a way that leads to its recognition by the proteasome. Therefore focus should turn to synthesising PROTACs that promote the ubiquitination of a different lysine of PRMT1, or a different topology of polyubiquitin chain. This may be achieved by using a ligand that binds to a different surface on VHL or PRMT1 or by recruiting a different E3-ligase.

6 CRBN-Recruiting PROTACs

This chapter details the synthesis and *in vitro* evaluation of PROTACs that recruit the CRBN E3-ligase (Figure 6.1).

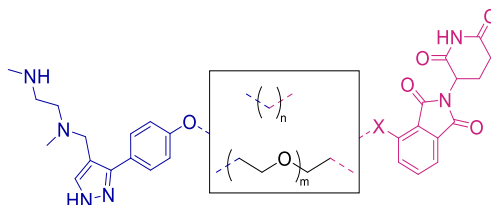


Figure 6.1 General design of CRBN-recruiting PROTACs.

6.1 Ether bond between linker and CRBN ligand

6.1.1 Synthesis

A retrosynthesis was devised for CRBN-recruiting PROTACs that have an ether bond between the CRBN ligand and the linker. This route will allow the use of the same linkers as the previous chapter and proceeds by a Mitsunobu reaction with the PRMT1 ligand followed by an *O*-alkylation of commercially available 4-hydroxythalidomide (Figure 6.2).

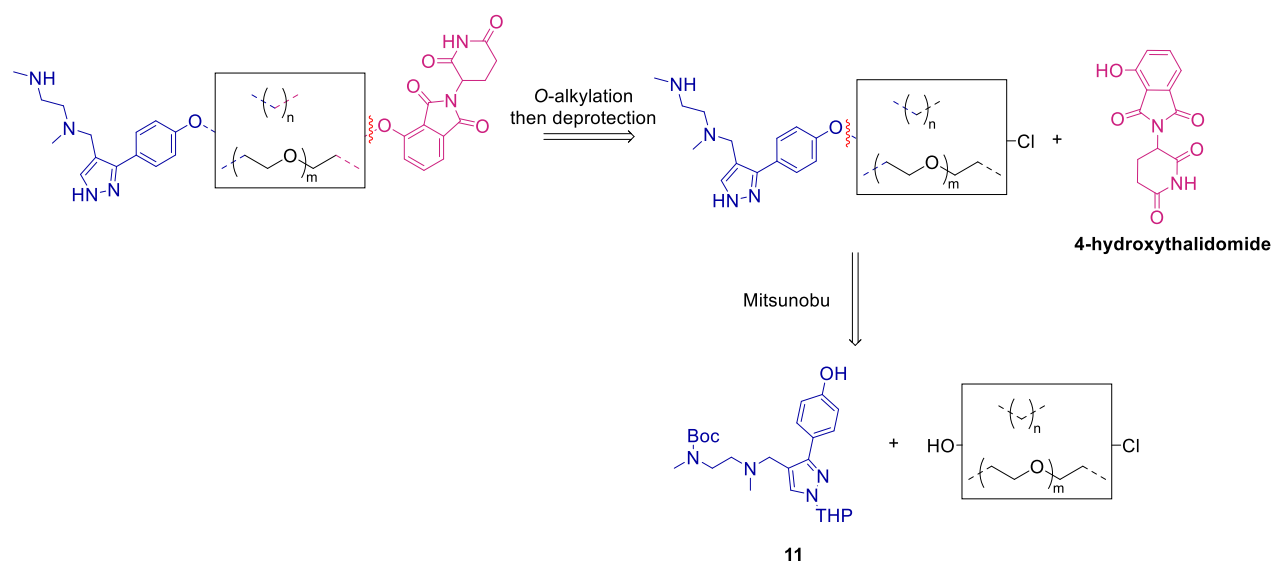


Figure 6.2 Retrosynthesis of CRBN-recruiting PROTACs with an ether bond between the linker and CRBN ligand.

6.1.1.1 Synthesis attempt

A Mitsunobu reaction between PRMT1 ligand **11** and 2-(2-chloroethoxy)ethanol gave the desired product **34** in moderate yield (Figure 6.3).

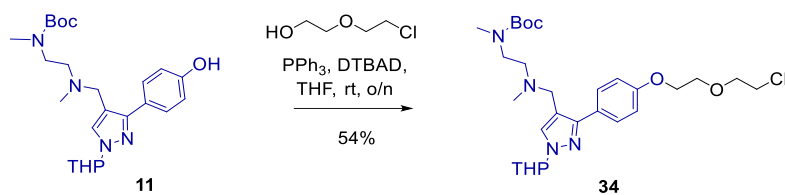


Figure 6.3 **Synthesis of 34.**

A single product was isolated from the *O*-alkylation of **34** with 4-hydroxythalidomide with a m/z of 605.3. This m/z matches the $[M+H]^+$ for the desired PROTAC however in 4-hydroxythalidomide, both the proton of the hydroxyl group and the amide proton of the glutarimide ring are acidic and have similar pK_a values. Therefore, both are likely to be nucleophilic during the alkylation reaction and alkylation at either position would give a product with the molecular weight of 604.3 Da (Figure 6.4).

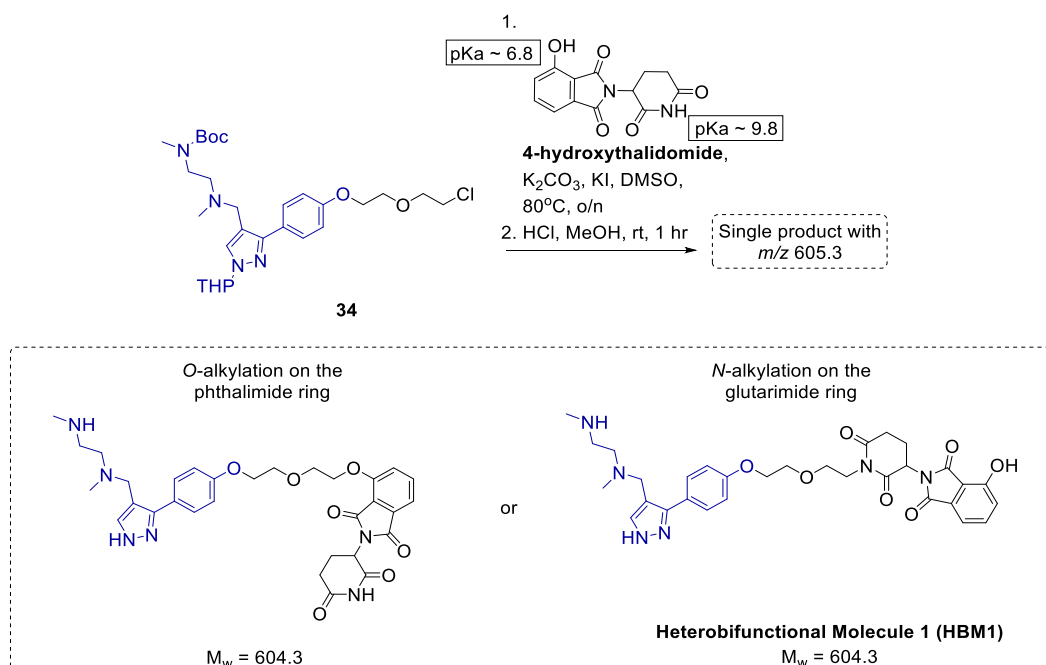


Figure 6.4 **Alkylation of 34 with 4-hydroxythalidomide.** The structures in the dashed box are possible products that result from the alkylation of 4-hydroxythalidomide. m/z determined by LC/MS. M_w is the molecular weight in Da. pK_a predicted by MolGpka¹⁸⁴.

By two-dimensional NMR spectroscopy, the isolated product has been characterised as heterobifunctional molecule 1 (**HBM1**) resulting from the *N*-alkylation of the glutarimide ring. The HSQC spectrum shows that a single carbon of the linker has a chemical shift much lower than that of the other three. This can be attributed to increased shielding upon binding to the nitrogen of the glutarimide ring (Figure 6.5 A-B). The HMBC spectrum shows 1H - ^{13}C correlations from the protons on the linker to the carbonyl groups of the glutarimide ring (Figure 6.5 C-D). The full 2D NMR spectra are shown in Appendix 1F and **HBM1** is investigated *in vitro* in Chapter 7.

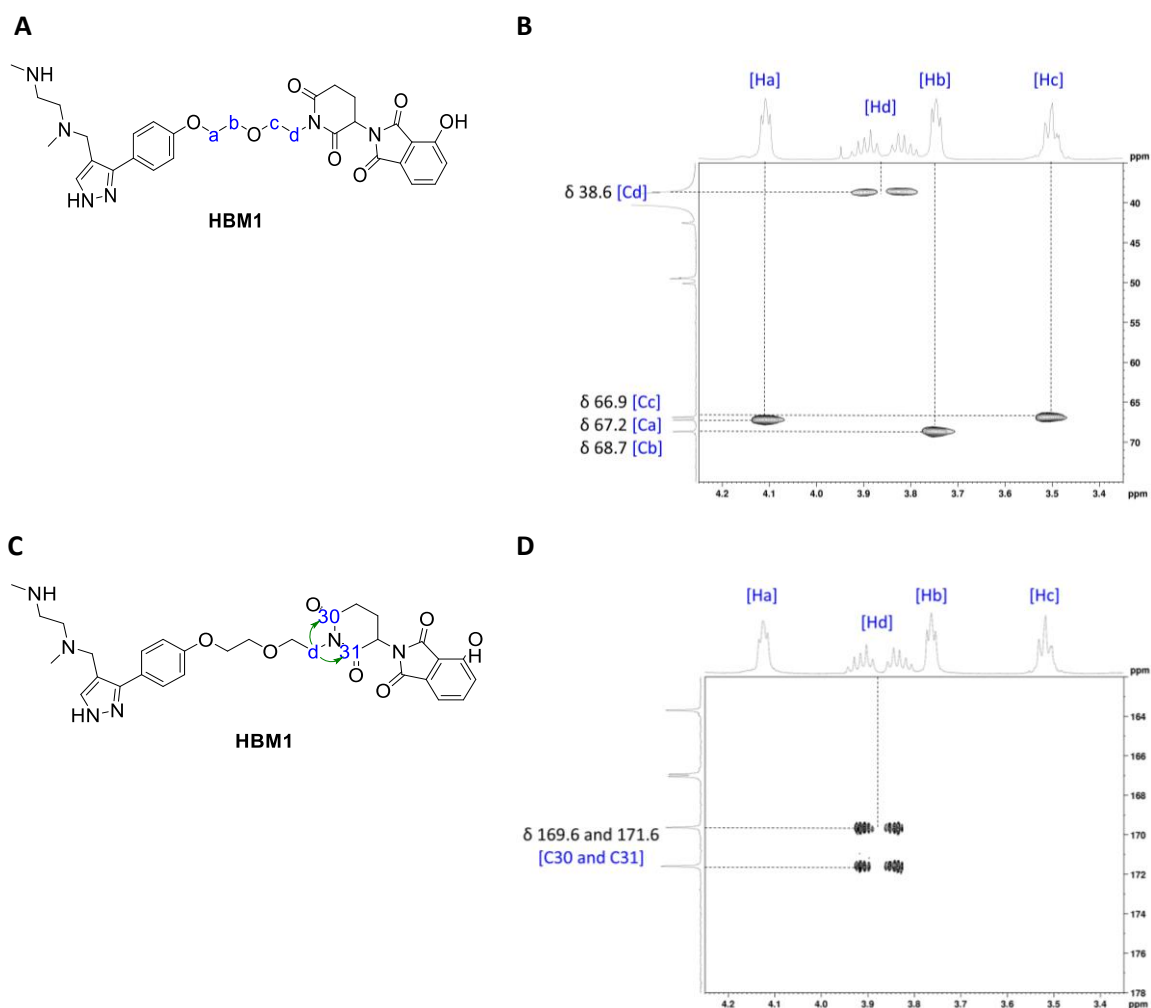


Figure 6.5 The two-dimensional NMR spectra of HBM1 support that N-alkylation of the glutarimide ring occurred. A) Structure of HBM1. B) ^1H - ^{13}C HSQC correlations of the PEG linker. The peak for the carbon [Cd] appears at a low chemical shift. C) Structure of HBM1 with selected ^3J couplings shown by green arrow. D) HMBC correlations from protons [Hd] of the PEG linker to the carbonyls of the glutarimide ring [C30 and C31]. Full 2D spectra in Appendix 1F.

An examination of the binding interactions of thalidomide shows that the glutarimide ring is crucial for CRBN binding; hydrogen bonds between the carbonyl groups and amide proton of the glutarimide ring, as well as hydrophobic interactions, lead to a ‘tight-fit’ of the glutarimide ring in the binding pocket on CRBN¹⁸⁵(Figure 6.6). **HBM1** does not contain the unmodified glutarimide ring and will therefore have a reduced binding affinity to CRBN.

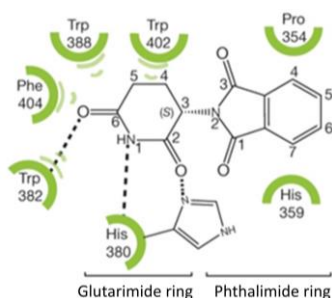


Figure 6.6 The glutarimide ring of the CRBN ligand is essential for CRBN binding. Binding interactions of thalidomide when bound to CRBN (PDB: 4CI1). Hydrogen bonds are shown as dashed lines and hydrophobic interactions as green semi-circles. Crystal structure first published in Fischer et al.¹⁸⁵ and figure reprinted from this publication.

An alternative synthetic route was required to synthesise CRBN-recruiting PROTACs. Poor control over regioselectivity will likely be a persistent problem with 4-hydroxythalidomide because of the similarity in pKa values for the two acidic hydrogens, however the use of a protecting group on the nitrogen of the glutarimide ring may circumvent this problem (Figure 6.7).

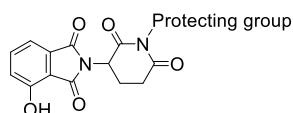


Figure 6.7 A protecting group on the glutarimide ring would prevent N-alkylation.

6.1.1.2 Synthesis of a protected CRBN Ligand

There is literature precedence for the use of the 2-(trimethylsilyl)ethoxymethyl group (SEM) to protect the amide of the glutarimide ring of a CRBN ligand. This protecting group is used in the synthesis of PROTAC **SJF608**, a degrader of Bruton's tyrosine kinase (BTK)¹⁸⁶, and the SEM group is removed in the final step following selective *O*-alkylation of the phthalimide ring (Figure 6.8).

To produce the *N*-SEM-protected CRBN ligand **35**, 4-hydroxythalidomide was reacted with 2-(trimethylsilyl)ethoxymethyl chloride (SEMCl) using a range of conditions. However in each case, the nitrogen of the glutarimide ring was not protected and the only product isolated was **36** where the hydroxyl group on the phthalimide ring is protected by SEM (Table 6.1).

Table 6.1 Attempted protection of the glutarimide ring with SEMCl. Product **35** is the desired product with the amide of the glutarimide ring protected. **36** results from the protection of the hydroxyl group attached to the phthalimide ring. In entry 1, the low yield is likely due to the hydrolysis of the glutarimide ring (discussed in more detail later).

Entry	Conditions	Yield of 35 , %	Yield of 36 , %
1	SEMCl, KI, K ₂ CO ₃ , DMSO, 80°C, o/n	0	11
2	SEMCl, DBU, DMF, rt, 2 hr	0	58

To confirm that the glutarimide ring can be protected, 4-fluorothalidomide was reacted with SEMCl and the protection of the glutarimide ring was observed at quantitative yield (Figure 6.10).

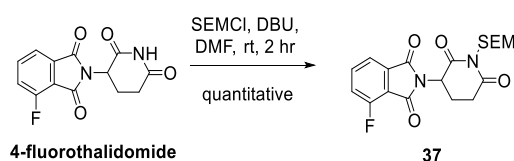


Figure 6.10 SEM protection of 4-fluorothalidomide.

Attempts at the regioselective protection of 4-hydroxythalidomide were abandoned and **35** was synthesised using a literature procedure where the glutarimide ring is protected prior to the presence of other acidic groups¹⁸⁷. *tert*-Butyl(2,6-dioxopiperidin-3-yl)carbamate was protected with SEMCl to give **38**, which subsequently underwent a deprotection/condensation reaction with 4-hydroxyisoindole-1,3-dione to give **35** (Figure 6.11). The reaction time for this step was optimised to 2 hours. After 4 hours of heating, the only product identified in the reaction mixture was 4-hydroxythalidomide, likely occurring due to deprotection of the SEM group of product **35** with extended heating in trifluoroethanol¹⁸⁸.

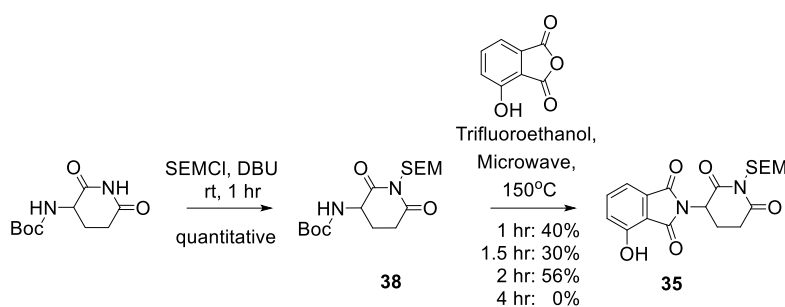
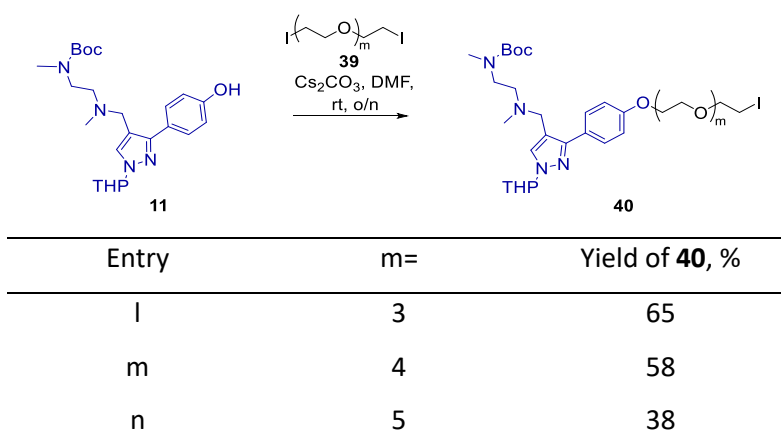


Figure 6.11 *Synthesis of SEM-protected 4-hydroxythalidomide. Conditions adapted from Burslem et al.*¹⁸⁷.

6.1.1.3 PROTAC synthesis

With SEM-protected CRBN ligand **35** in hand, PROTAC synthesis commenced. An *O*-alkylation reaction with PRMT1 ligand **11** and linker **39** produced **40** in moderate yield (Table 6.2). The over-alkylated product, where both iodine atoms of the linker are substituted with the PRMT1 ligand, was identified in the reaction mixture by LC/MS, however its formation was minimised by the slow addition of four equivalents of linker **39** to PRMT1 ligand **11** at 0°C.

Table 6.2 *Synthesis of 40. Linker 39 was synthesised Dr F. Javier Pérez-Areales.*



40n was taken forward for *O*-alkylation with CRBN ligand **35** and then deprotected under acidic conditions. The THP, *N*-Boc and SEM protecting group would be expected to be removed as they are all acid labile¹⁸⁹ however in the deprotection of **41n**, the SEM group was only partially removed to give the hemiaminal **42n** with a *N*-hydroxymethyl group (Figure 6.12). This compound has a distinctive singlet in the ¹H NMR spectrum at δ 5.05 which is characteristic of the methylene protons (*N*-CH₂OH).

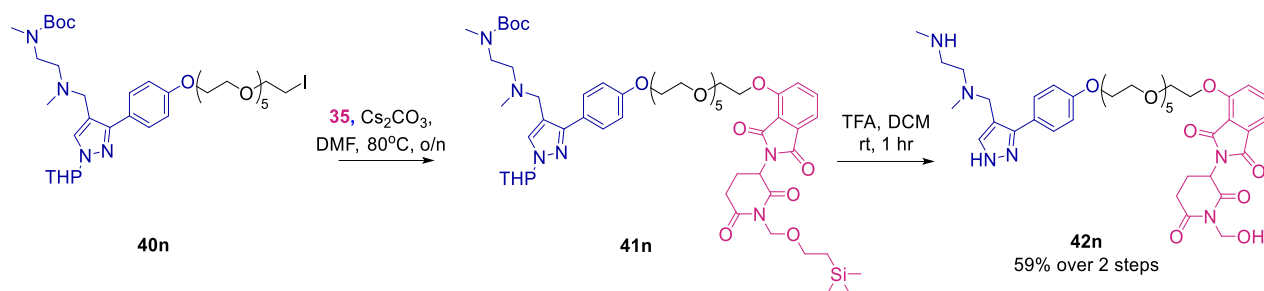


Figure 6.12 Synthesis of 42n. The incomplete removal of the SEM protecting group was observed with the same acidic deprotection conditions (1:1 TFA:DCM) used in the synthesis of SJF608 (Figure 6.8). **41n** was taken forward to the deprotection step without purification.

With the intention to obtain a model substrate on which conditions for the removal of the *N*-hydroxymethyl group could be optimised, SEM-protected 4-fluorothalidomide **37** was deprotected using the acidic conditions used in Figure 6.12 but complete SEM deprotection was observed (Figure 6.13).

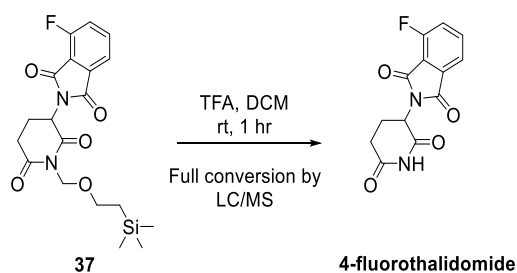


Figure 6.13 Complete SEM deprotection when 37 was subjected to the deprotection conditions used in Figure 6.12.

The removal of the SEM protecting group on a nitrogen has been reported to be more problematic than an oxygen and the ease of deprotection varies with the substrate^{190,191}. In the deprotection of **41n**, the *N*-hydroxymethyl product **42n** may form because the nitrogen of the glutarimide ring is not protonated due to resonance stabilisation (Figure 6.14). The *N*-hydroxymethyl group of **42n** may be stable to further deprotection because of intramolecular hydrogen bonding interactions¹⁹².

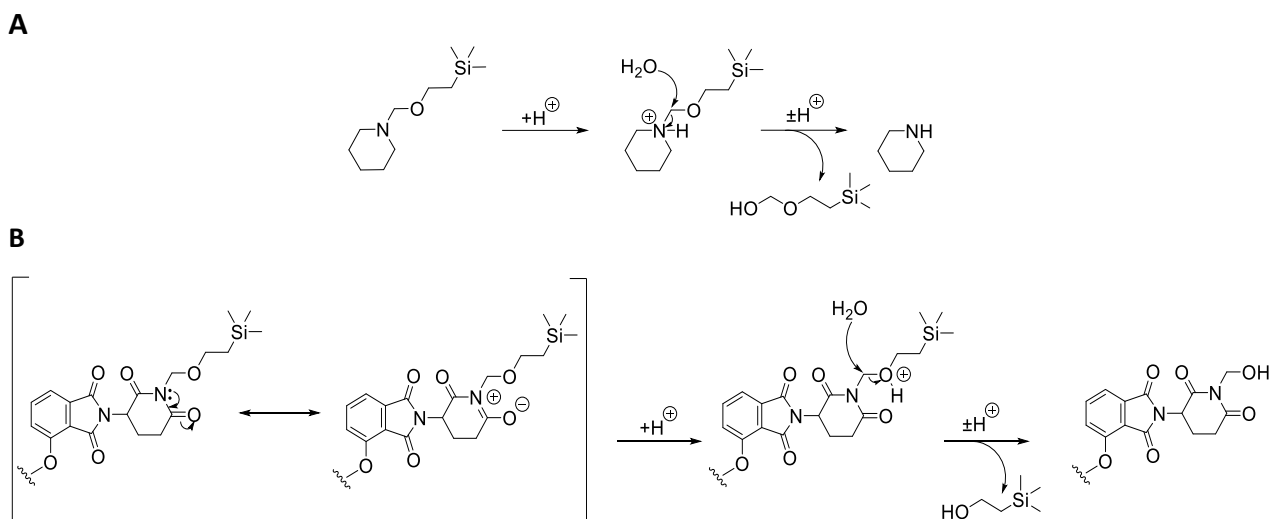
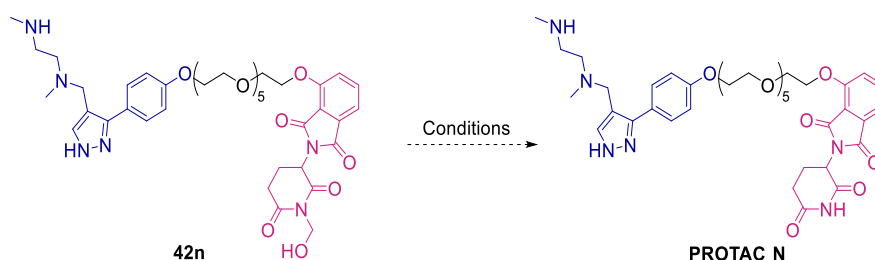


Figure 6.14 Proposed mechanism for complete (A) and partial (B) N-SEM deprotection. A) In a molecule that contains a nitrogen that can readily act as a Lewis base, full deprotection of the SEM group occurs under acidic conditions. B) With a SEM-protected CRBN ligand, the nitrogen is not protonated under the acidic conditions due to resonance stabilisation (a single resonance structure is shown) and the N-hydroxymethyl product forms.

To remove the N-hydroxymethyl group, a range of conditions were attempted in small-scale reactions of **42n** with reaction monitoring by LC/MS. The hemiaminal was found to be stable to acidic conditions (entry 1-5) but was successfully removed under basic conditions (entry 7) (Table 6.3).

Table 6.3 Attempted deprotection of 42n. Analysis by LC/MS must use the spectra obtained from ionisation in the ESI⁺ mode as fragmentation in the ESI⁻ mode results in the same m/z value for both the products from partial and complete SEM deprotection.



Entry	Conditions	Ref	Result indicated by LC/MS
1	HCl, MeOH, rt, 1 hr	-	No change
2	1:1 TFA/EtOAc, rt, 1 hr	-	No change
3	100% TFA, rt, 5 hr	193	No change
4	Methane sulfonic acid, MeCN, rt, o/n	194	No change
5	MgBr ₂ , Et ₂ O, MeNO ₂ , rt, 2 hr	195	No change
6	TBAF, THF, rt, 1 hr	195	Multiple UV active products formed.
7	NH ₄ OH, MeCN, rt, 1 hr	196	Full conversion to desired product

The requirement of a two-step deprotection of an *N*-SEM group with acidic conditions followed by basic conditions is reported in the literature^{194,196–198}. Furthermore, in the synthesis of **SJF608**, although complete *N*-SEM deprotection was reported with a single acidic deprotection step, purification was then undertaken by preparative TLC using a basic mobile phase¹⁸⁶. It is unclear at which stage complete deprotection to the glutarimide occurred.

Caution was taken as the hydrolysis of thalidomide, which has the same pharmacophore as the CRBN ligands used in this project, is base-catalysed^{199,200}. The hydrolysis of thalidomide results in the opening of the glutarimide ring, or the 5-membered ring of the phthalimide group (Figure 6.15) which affects the binding affinity of the ligand to CRBN and the ligand's pharmacokinetic properties²⁰¹.

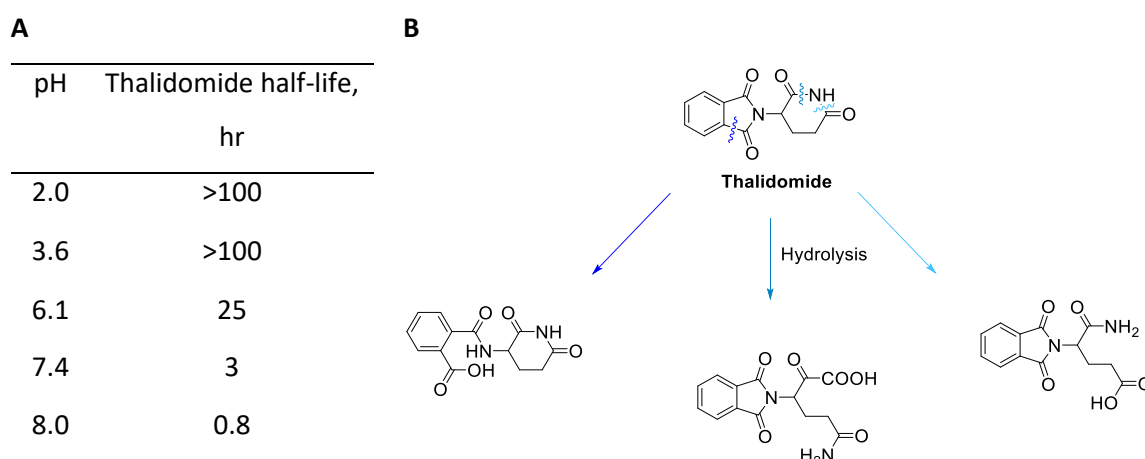
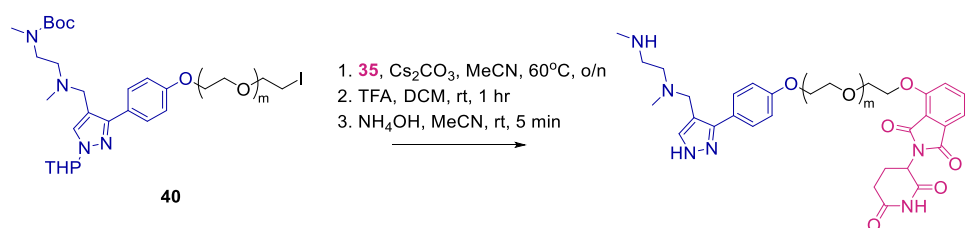


Figure 6.15 Thalidomide is hydrolysed under basic conditions. A) pH has a significant effect of the half-life of thalidomide at 37°C in 0.1 M phosphate buffer with an ionic strength of 0.3. Half-life values published in Reist et al.²⁰⁰. B) Structure of the three major products of thalidomide hydrolysis¹⁹⁹.

Reaction monitoring by LC/MS identified that complete deprotection of the *N*-hydroxymethyl group in **42n** occurred within 5 minutes. The reaction was then acidified to pH 1 to minimise hydrolysis. This optimised route was used to afford three CRBN-recruiting PROTACs, **PROTAC L-N** (Table 6.4).

Table 6.4 **Synthesis of PROTAC L-N.**



Entry	m=	Yield over 3 steps, %	Product
l	3	7	PROTAC L
m	4	4	PROTAC M
n	5	25	PROTAC N

6.1.2 Stability in cell culture media

The stability of **PROTAC L** and **PROTAC N** was tested in cell culture media and the PROTACs were found to have low stability and were converted to compounds with higher polarity. The low stability is likely due to the hydrolysis of the glutarimide ring which, under the conditions of this experiment, is expected to follow pseudo first-order kinetics^{200,202}. An exponential decay curve was fitted and the half-life of **PROTAC L** and **PROTAC N** was determined as 0.9 hours and 1.0 hour respectively (Figure 6.16).

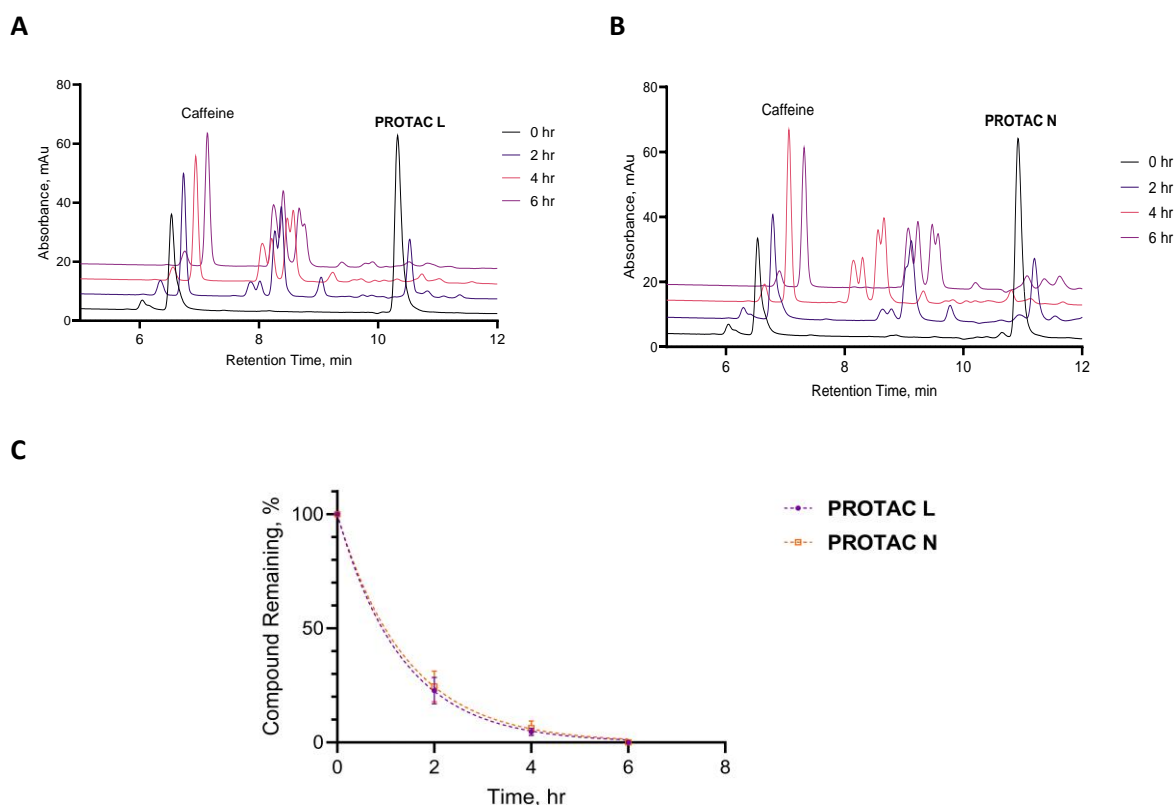
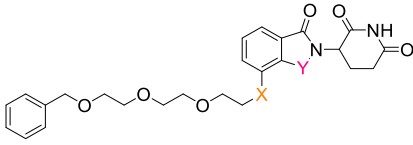


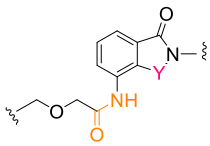
Figure 6.16 Stability of PROTAC L and PROTAC N in cell culture media. 400 μM PROTAC and 400 μM caffeine were incubated in DMEM supplemented with 10% FBS at 37°C in an ambient atmosphere. A). Representative UV-HPLC chromatograms for PROTAC L at various time intervals. Absorbance recorded at $\lambda = 254 \text{ nm}$. B) Same as A with PROTAC N. C) The Y-axis is the percentage of PROTAC remaining compared to the peak area ratio of PROTAC-to-caffeine at 0 hr. Data from three independent experiments. Mean and standard error plotted. The data was fitted with an exponential decay function with the plateau constrained to zero.

This assay is sufficient to show that the half-lives are short. To calculate a more accurate half-life, analysis should be undertaken at more frequent time intervals. In addition, an analytical method with a shorter analysis time should be used as the run time of the HPLC method in this experiment was 15 minutes and on-column hydrolysis may have affected the accuracy of the observed half-life²⁰³.

Bricelj *et al.* show that changing the functional group between the CRBN ligand and the linker can have a large effect on PROTAC stability in aqueous buffer. They show that an amide and a secondary amine have significantly greater stability than an ether functional group²⁰⁴ (Table 6.5). Thus, focus turned to synthesising PROTACs that contain these functional groups.

Table 6.5 **Published stability of different functional groups between a ligand and CRBN ligand.** Stability refers to the remaining starting material as determined by HPLC. The PEG linker and benzyl ether group were shown to be stable under the conditions of the experiment. Stability data published in Bricelj et al.²⁰⁴.



Entry	X	Y	Stability after 24 hr in PBS (pH 7.4) at 37°C, % ²⁰⁴
1	O	CO	46
2		CH ₂	79
3	NH	CO	80

6.2 Amide bond between linker and CRBN ligand

A retrosynthetic scheme was devised to synthesise PROTACs with an amide bond between the CRBN ligand and the linker. The PRMT1 ligand must be alkylated first to avoid *N*-alkylation of the CRBN ligand's glutarimide ring. In the first step, a protecting group must be employed to protect the carboxylic acid on the linker. It should then be removed selectively prior to the amide coupling reaction (Figure 6.17).

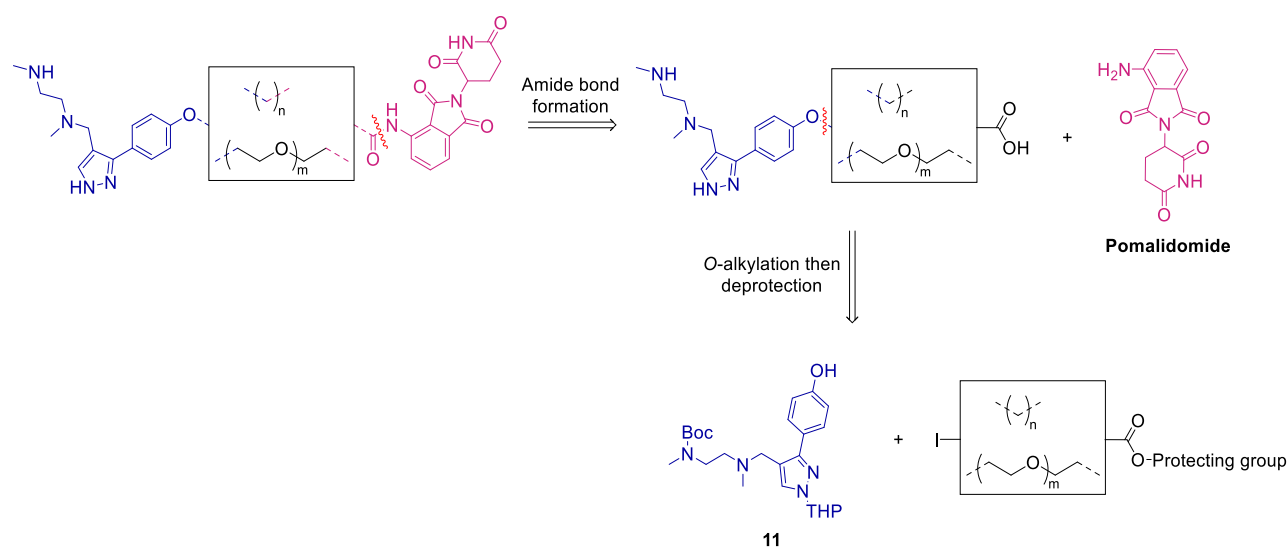
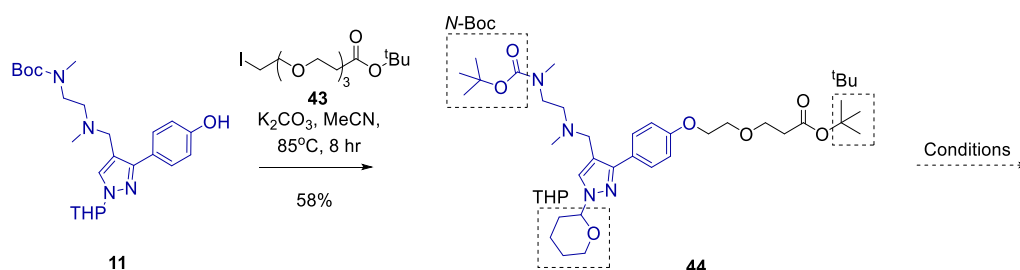


Figure 6.17 **Retrosynthesis of CRBN-recruiting PROTACs with an amide bond between the linker and CRBN ligand.**

The *tert*-butyl ester (^tBu) protecting group was chosen as there are reports of the selective removal of the ^tBu group in the presence of a *N*-Boc protecting group^{205,206}. The ^tBu-protected linker **43** was reacted with PRMT1 ligand **11** to give **44**. **44** was subjected to the published literature conditions for selective ^tBu deprotection however non-selective deprotection was observed and the route was abandoned (Table 6.6).

Table 6.6 Attempts to remove the ^tBu protecting group selectively in the presence of the *N*-Boc and THP protecting groups. The acid labile protecting groups are shown in a black dashed box. Linker 43 was synthesised by Dr F. Javier Pérez-Areales.



Entry	Conditions	Reference	Result indicated by LC/MS analysis
1	ZnBr ₂ , DCM, rt, o/n	205	<i>N</i> -Boc and ^t Bu deprotection
2	1. CeCl ₃ ·7H ₂ O-NaI, MeCN, 85°C, o/n 2. Reaction quenched with large excess of acid	206	<i>N</i> -Boc, ^t Bu and THP deprotection
3	1. CeCl ₃ ·7H ₂ O-NaI, MeCN, 85°C, o/n 2. Reaction quenched with acid to give a 0.1 mM solution	206	Large number of products. None with correct mass for selective ^t Bu deprotection.

Future work should repeat the proposed route with a protecting group for the carboxylic acid that can be selectively removed, for example the methyl ester²⁰⁷. Alternatively, the product from entry 1 of Table 6.6 should be re-protected with di-*tert*-butyl dicarbonate (Boc₂O) to give the desired product²⁰⁸.

6.3 Amine bond between linker and CRBN ligand

6.3.1 Synthesis

The nitrogen of a primary amine is a better nucleophile than the oxygen of a primary alcohol and can undergo nucleophilic aromatic substitution reactions (S_NAr)²⁰⁹. 6-amino-1-hexanol was reacted with PRMT1 ligand **11** in a Mitsunobu reaction to give **45** which contains a nucleophilic primary amine. A S_NAr was then undertaken with 4-fluorothalidomide and the product deprotected to give the

PROTAC P at low yield (Figure 6.18). Each step in this synthesis saw conversion to multiple products and careful, time-intensive purification was required. The route required optimisation.

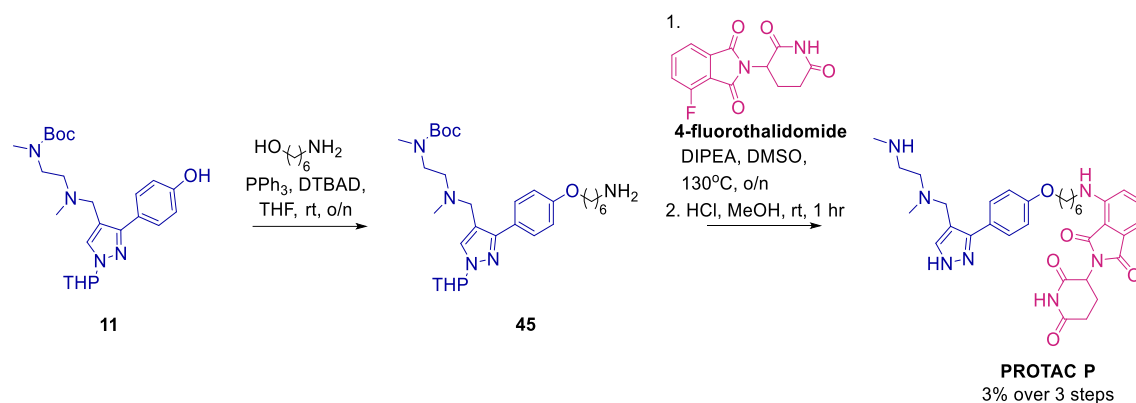


Figure 6.18 **Synthesis of PROTAC P**. Despite multiple rounds of purification, **45** was taken forward to the S_NAr reaction impure. The S_NAr reaction produced many products and purification was undertaken before and after the deprotection step.

The order of the first two steps was reversed so the S_NAr occurred first to give **46** which contains a hydroxyl group. A Mitsunobu reaction with PRMT1 ligand **11** was then attempted but produced many products, none of which had the desired m/z in the LC/MS spectrum (Figure 6.19).

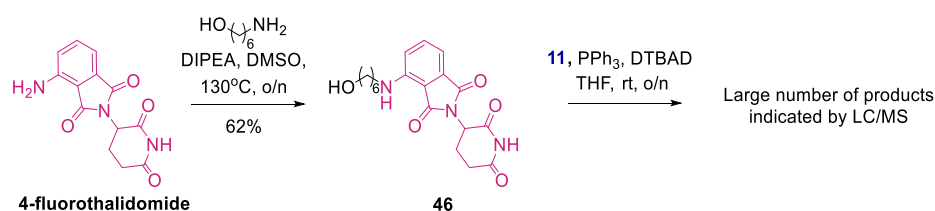
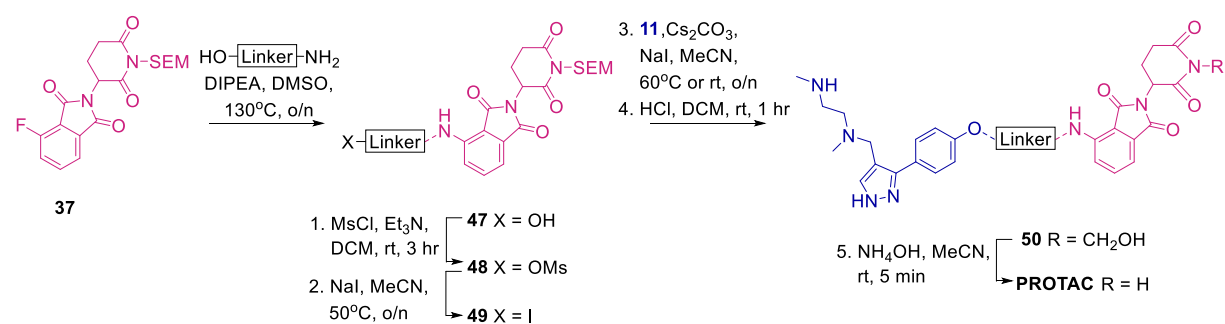


Figure 6.19 **Attempted alternative synthetic route for PROTAC P**. The order of Mitsunobu reaction and S_NAr was reversed compared to the route shown in Figure 6.18.

The Mitsunobu reaction appeared to be the yield-limiting step and therefore it was abandoned and replaced with an alkylation reaction. To prevent a competing alkylation reaction on the glutarimide ring of the CRBN ligand, the S_NAr reaction was repeated with SEM-protected 4-fluorothalidomide **37**. **37** underwent a S_NAr with the primary amine of the linker to give **47**. The hydroxyl group on **47** was converted to a good leaving group by mesylation followed by iodination to give **49**. This underwent an alkylation reaction with PRMT1 ligand **11** and then deprotection using acidic conditions to afford **50**. The *N*-hydroxymethyl group from the partial deprotection of the SEM group was then removed using basic conditions to give **PROTAC O**, **PROTAC P** and **PROTAC Q** (Table 6.7).

The yield of **PROTAC P** achieved via this route (13%) was higher yielding than the first route attempted (3% in Figure 6.18).

Table 6.7 **Synthesis of PROTAC O-Q.**



Entry	Linker =	Yield of 47 , %	Yield over 5 steps, %	Product
o	m=5	51	35	PROTAC O
p	n=6	47	27	PROTAC P
q	n=10	65	5	PROTAC Q

6.3.2 Stability in cell culture media

The stability of **PROTAC O-Q** in cell media was greater than that for the PROTACs with an ether bond between the linker and CRBN ligand. The half-life of **PROTAC O** and **PROTAC P** were determined as 2.1 and 2.2 hours respectively and **PROTAC Q** had a longer half-life of 6.2 hours (Figure 6.20).

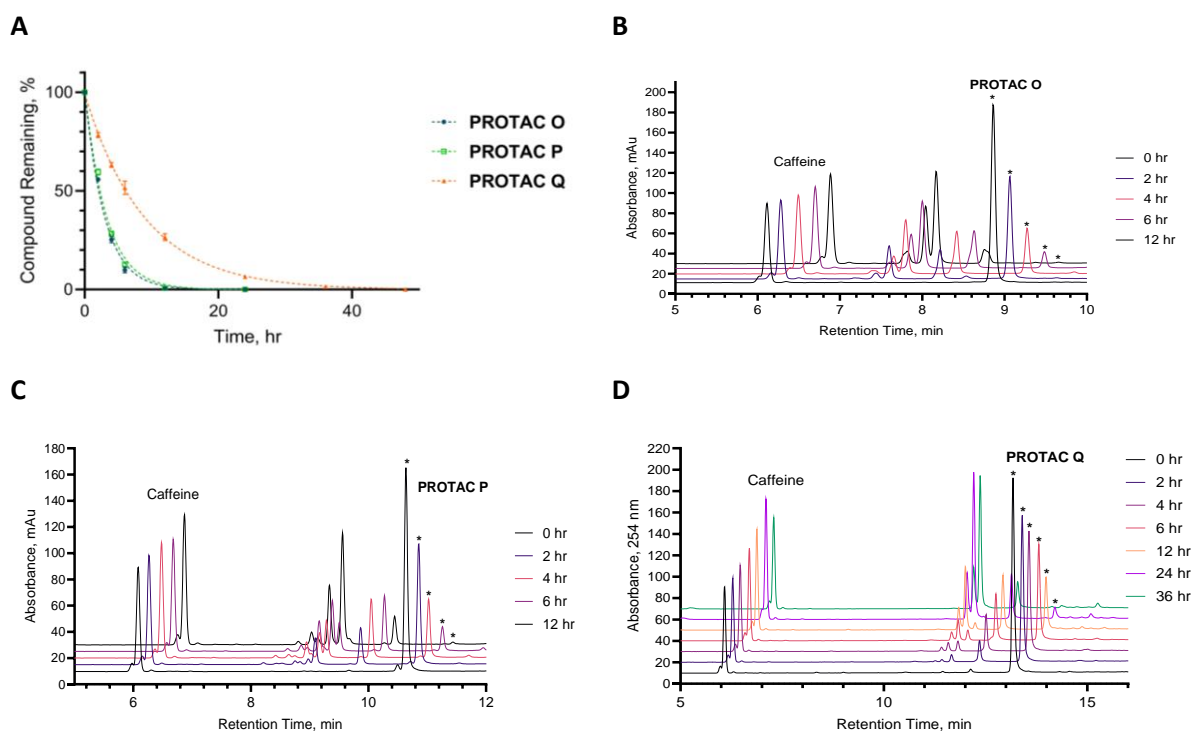


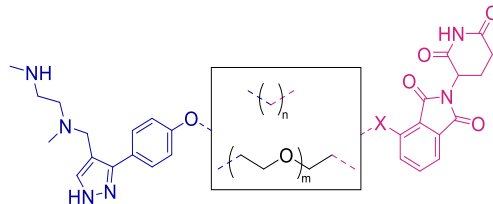
Figure 6.20 Stability of PROTAC O-Q in cell culture media. 400 μM PROTAC and 400 μM caffeine were incubated in DMEM supplemented with 10% FBS at 37°C in an ambient atmosphere for 48 hr. A) The Y-axis is the percentage of PROTAC remaining compared to the peak area ratio of PROTAC-to-caffeine at 0 hr. Data from three independent experiments. Mean and standard error plotted. The data was fitted with an exponential decay function with the plateau constrained to zero. B-D) Representative UV-HPLC chromatograms for PROTAC O-Q at various time intervals. Absorbance recorded at $\lambda = 254 \text{ nm}$. * indicates the peak integrated for the respective PROTAC.

To validate the precision and accuracy of the determined half-lives for the PROTACs, a comparison of the half-life of pomalidomide using this assay to literature values was attempted. However the absence of reported values for pomalidomide prevented any conclusions on the validity of the assay to be made (Appendix 1G).

6.4 Library of CRBN-Recruiting PROTAC

The six CRBN-recruiting PROTACs synthesised were taken forward for *in vitro* testing (Table 6.8).

Table 6.8 *CRBN-recruiting PROTACs synthesised.*



Linker	X	PROTAC
m=3	O	PROTAC L
m=4	O	PROTAC M
m=5	O	PROTAC N
m=5	NH	PROTAC O
n=6	NH	PROTAC P
n=10	NH	PROTAC Q

6.5 Degradation Efficacy by Western Blot

The six PROTACs were tested in MCF-7 cells at 10 μ M. Neither PRMT1 nor PRMT6 degradation was observed. **PROTAC P** inhibited PRMT1 and Type I PRMT as shown by an increase in the level of MMA and a decrease in ADMA. A small decrease in ADMA was observed with **PROTAC Q** suggesting Type I PRMT inhibition (Figure 6.21).

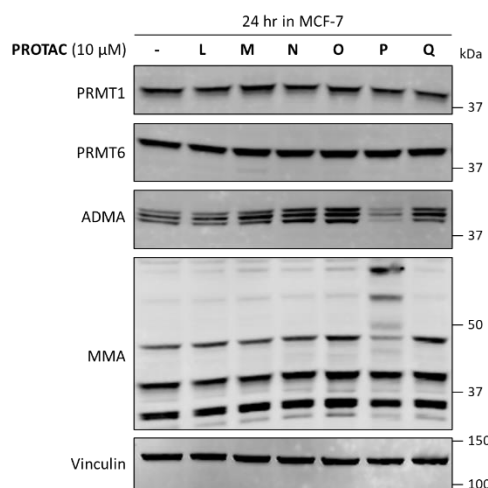


Figure 6.21 *Western blot of PROTAC L-Q in the MCF-7 cell line at 10 μ M. MCF-7 cells were treated with the indicated compounds at 10 μ M for 24 hr and then harvested for analysis by Western blot. Image representative of two independent experiments.*

To account for the hook effect, the PROTACs that showed inhibitory activity at 10 μM were tested at lower concentrations in the MCF-7 cells. PRMT1 and PRMT6 degradation was not observed (Figure 6.22).

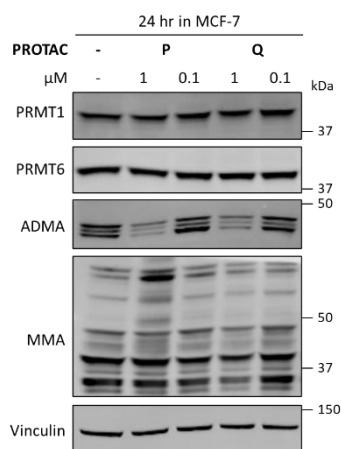


Figure 6.22 Western blot of PROTAC P and PROTAC Q in the MCF-7 cell line at 1 and 0.1 μM . MCF-7 cells were treated with the indicated compounds for 24 hr and then harvested for analysis by Western blot. Image representative of two independent experiments.

The empirically determined half-lives for PROTAC L-Q were between 0.9 and 6.2 hours. To maintain a concentration of at least 50% of the initial concentration of PROTAC, an experiment was undertaken where MCF-7 cells were treated hourly with 1 μM of the PROTAC for six hours. PRMT1 and PRMT6 degradation was not observed with any of the PROTACs (Figure 6.23).

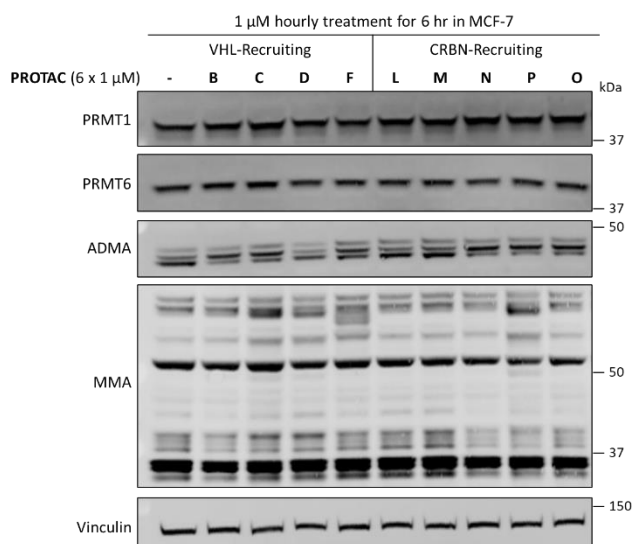


Figure 6.23 Western blot of selected VHL-recruiting PROTACs and CRBN-recruiting PROTACs in the MCF-7 cell line. 1 μM of PROTAC was added hourly for six hours. MCF-7 cells were treated with 1 μM of the indicated PROTAC and one-hour later an additional 1 μM of PROTAC was added. This was repeated 4 further times (the total concentration of PROTAC added was 6 μM and the total incubation time was 6 hr). The cells were then harvested for analysis by Western blot.

Finally, the PROTACs were tested at 10 μM in the PDAC cell lines. PRMT1 and PRMT6 degradation was not observed. Type I PRMT and PRMT1 inhibition was observed with **PROTAC P** and **PROTAC Q** (Figure 6.24).

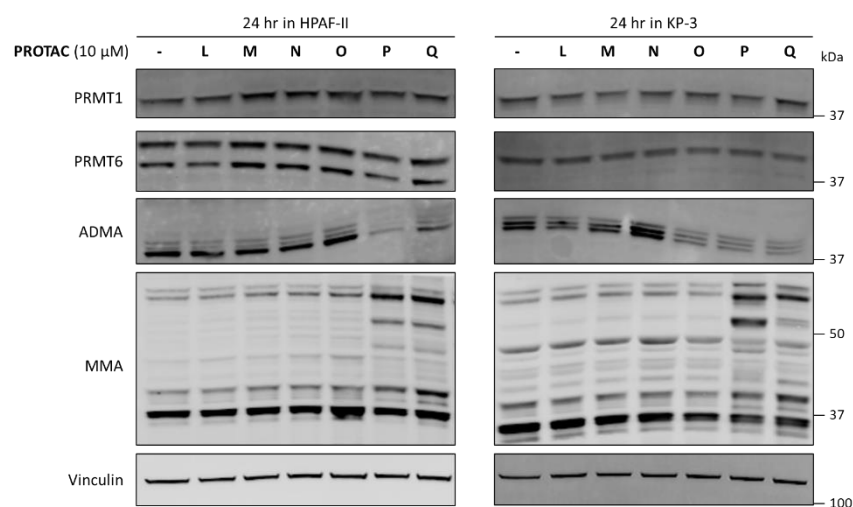
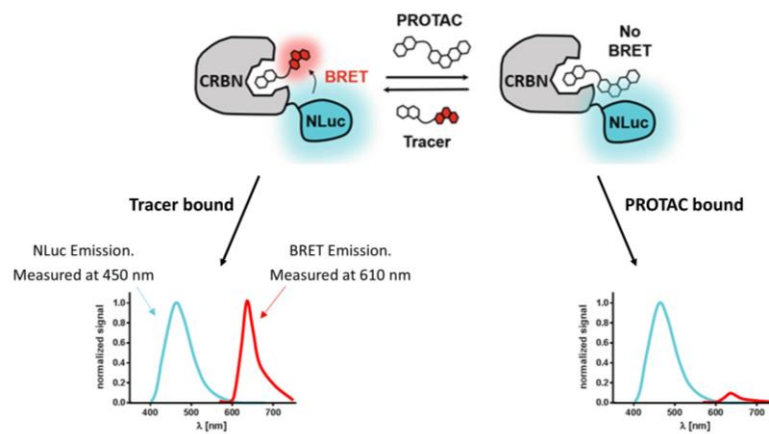


Figure 6.24 Western blot of PROTAC L-Q in two PDAC-derived cell lines at 10 μM . HPAF-II and KP-3 cells were treated with the indicated compounds at 10 μM for 24 hr and then harvested for analysis by Western blot.

6.6 NanoBRET Target Engagement Assay

To gain mechanistic insight into whether the PROTACs bind to CRBN, a NanoBRET target engagement assay was undertaken. Bioluminescence resonance energy transfer (BRET) is measured in this assay. BRET is achieved by the transfer of luminescent energy from a fusion protein comprising NanoLuc luciferase and CRBN (NLuc-CRBN) to a fluorescent tracer. When the tracer is bound to NLuc-CRBN, BRET occurs. When the tracer is incubated with a PROTAC that also binds to the CRBN-NLuc fusion protein, there is competition for binding and a decrease in BRET (Figure 6.25). The decrease in BRET is proportional to ‘target engagement’ which refers to the ability of the PROTAC to bind to the NLuc-CRBN fusion protein. Target engagement will reflect the PROTAC’s binding affinity to CRBN and the PROTAC’s pharmacokinetic properties such as cell permeability and PROTAC stability.

A



B

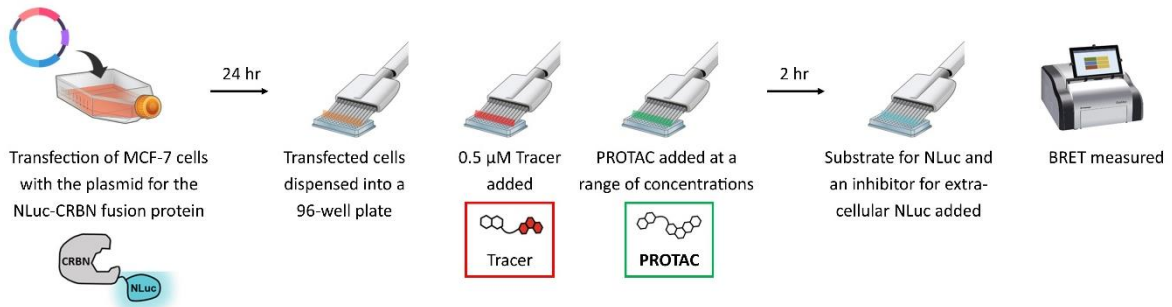


Figure 6.25 **Schematic of the NanoBRET assay to measure the ability of a PROTAC to bind to CRBN in live cells.** A) The effect of PROTAC binding on BRET. B) Summary of key steps in the protocol. A NanoBRET assay was first described by Machleidt et al.²¹⁰. Figure adapted from the ‘NanoBRET TE Intracellular E3 Ligase Assay’ technical manual (Promega, #N2910).

The assay was undertaken with selected PROTACs and pomalidomide was used as a positive control. It can be assumed that binding to the NLuc-CRBN fusion protein is representative of binding to endogenous CRBN²¹¹. BRET was measured after a two hour incubation so the data is representative of this timepoint and the IC₅₀ is defined as the concentration of the PROTAC that results in half-maximal inhibition of tracer binding to NLuc-CRBN fusion protein. The results are shown in Figure 6.26 and Table 6.9.

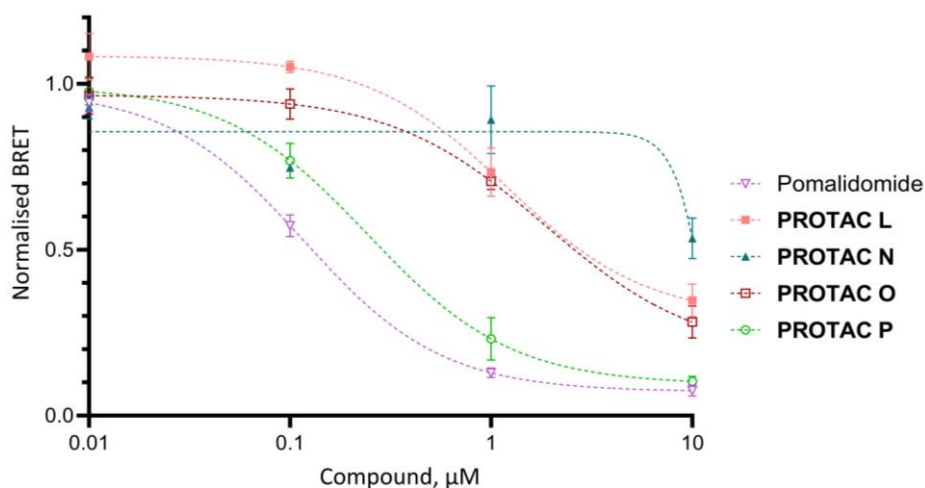
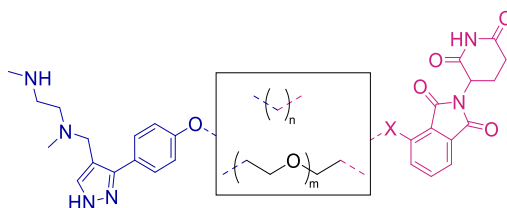


Figure 6.26 Target engagement of selected PROTACs to NLuc-CRBN in the MCF-7 cell line. Data is normalised to untreated cells and BRET calculated by BRET emission intensity / NLuc emission intensity. The mean and standard error of two independent experiments, with multiple biological replicates, are shown.

Table 6.9 IC_{50} for PROTAC binding to NLuc-CRBN in the MCF-7 cell line. The lower the IC_{50} the greater the target engagement of the PROTAC. IC_{50} values calculated using the [inhibitor] vs. response curve fit with variable slope in GraphPad Prism.



	X	Linker	IC_{50} , μM
Pomalidomide	NH ₂	-	0.1
PROTAC L	O	m=3	1.2
PROTAC N	O	m=5	>10
PROTAC O	NH	m=5	1.9
PROTAC P	NH	n=6	0.2

PROTAC P showed a similar target engagement to CRBN as pomalidomide. A dose-dependent reduction in BRET was observed at 1 and 10 μM with **PROTAC L** and **PROTAC O**, whereas **PROTAC M** saw only a reduction in BRET at 10 μM . These results show that all the PROTACs tested are cell permeable and bind to CRBN, albeit at differing potencies.

PROTAC N and **PROTAC O** differ only in the functional group between the CRBN ligand and the linker, and therefore target engagement for CRBN appears greater with an amine bond between the linker and CRBN ligand compared to an ether bond (Figure 6.27).

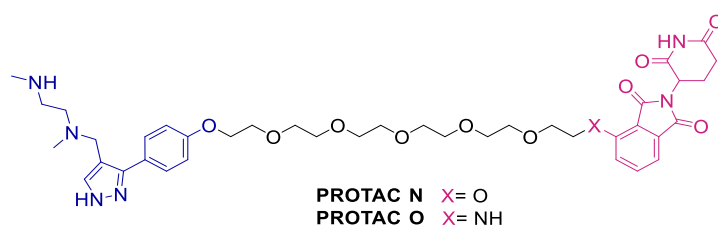


Figure 6.27 Structure of PROTAC N and PROTAC O.

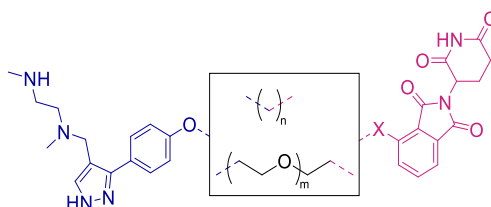
This assay should be repeated with a greater range of PROTACs to gain insight into the effect of varying linker identity and the functional group that connects the linker on CRBN target engagement.

6.7 Discussion and Conclusions

PRMT1 degradation was not observed with any of the six CRBN-recruiting PROTACs synthesised. PROTAC stability and CRBN target engagement were greater with an amine functional group between the linker and CRBN ligand than an ether functional group. The two PROTACs that contain an alkyl linker inhibited PRMT1 (Table 6.10).

Table 6.10 A summary of the biological activity of the CRBN-recruiting PROTACs in the MCF-7 cell line.

Inhibition and degradation were determined by Western blot with 24 hr treatment of $\leq 10 \mu\text{M}$ of the PROTAC in the MCF-7 cell line. CRBN target engagement was determined by the NanoBRET assay and scored depending on the fold-change in IC_{50} compared to pomalidomide. High is < 5-fold less potent. Medium is < 20-fold less potent. Low is > 20-fold less potent but potency is observed. N.D. = not determined.



	Linker	X	$t_{1/2}$, hr	Degradation		Inhibition		CRBN target engagement
				PRMT1	PRMT6	Type I	PRMT1	
PROTAC L	m=3	O	0.9	✗	✗	✗	✗	Medium
PROTAC M	m=4	O	N.D.	✗	✗	✗	✗	N.D.
PROTAC N	m=5	O	1.0	✗	✗	✗	✗	Low
PROTAC O	m=5	NH	2.1	✗	✗	✗	✗	Medium
PROTAC P	n=6	NH	2.2	✗	✗	✓	✓	High
PROTAC Q	n=10	NH	6.2	✗	✗	✓	✓	N.D.

The CRBN-recruiting PROTACs with a PEG linker did not inhibit Type I PRMT activity despite the NanoBRET target engagement assay showing they were cell permeable. The VHL-recruiting PROTACs with a PEG linker also did not inhibit Type I PRMT activity. This leads to the tentative conclusion that the PEG chain prevents PRMT1 binding, and this is likely through unfavourable electrostatic repulsions between the PEG chain oxygens of the PROTAC and amino acid sidechains in the binding pocket on PRMT1. The effect of the linker composition on PRMT1 binding affinity should be determined by measuring the binding affinity of the PROTACs to recombinant PRMT1 protein, and the reason behind any differences could be investigated by computational protein-ligand docking²¹².

Further investigation into **PROTAC P** should be undertaken as it can bind both PRMT1 and CRBN. As degradation was not observed, it can be assumed that the ubiquitination of PRMT1 does not occur with **PROTAC P**. Before the synthesis of further PROTACs, it should be determined if a ternary complex does occur, as this will determine the next stage for PROTAC design (Figure 6.28).

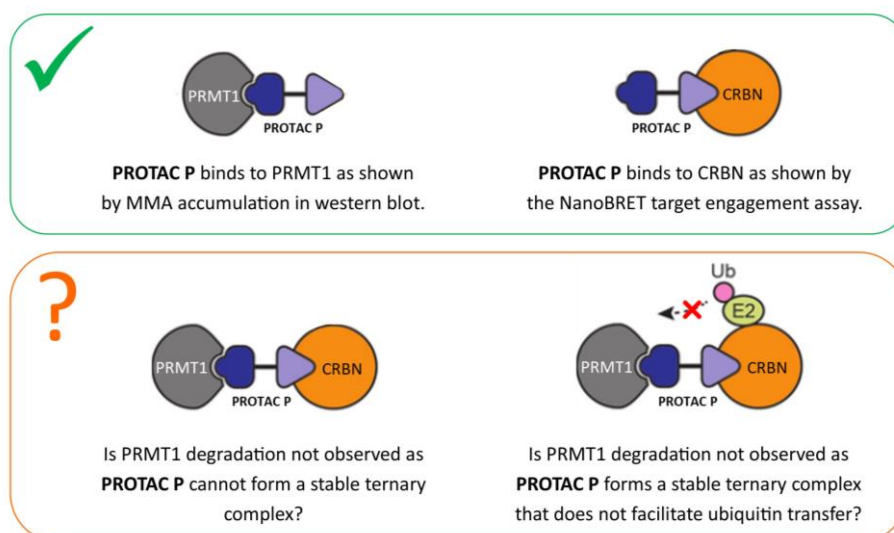


Figure 6.28 Schematic of the binding interactions of **PROTAC P**.

All the CRBN-recruiting PROTACs synthesised in this project were unstable in cell culture media. CRBN ligands that are more stable to hydrolysis have been published which include a phenyl glutarimide²¹³ and two phenyl dihydrouracils^{214,215} (Figure 6.29). These ligands should be used in the future synthesis of CRBN-recruiting PROTACs for PRMT1.

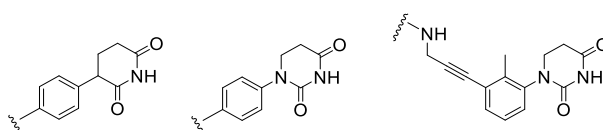


Figure 6.29 Published CRBN ligands that have high stability to hydrolysis. Ligands published by Min et al.²¹³, Jarusiewicz et al.²¹⁴ and Xie et al.²¹⁵.

7 Heterobifunctional Molecules with *N*-Glutarimide Ring Alkylation

During the synthesis of the CRBN-recruiting PROTACs, the undesired *N*-alkylation of the glutarimide ring of the CRBN ligand led to the isolation of product **HBM1** (Figure 7.1).

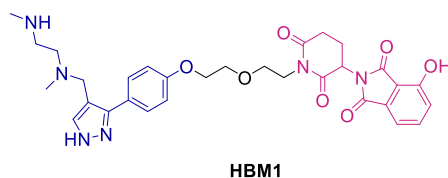


Figure 7.1 **Structure of HBM1**. The synthesis and characterisation of HBM1 were discussed in Section 6.1.1.1.

In MCF-7 cell culture media, the half-life of **HBM1** was determined as 9.5 hours (Figure 7.2). Similar to thalidomide, the hydrolysis of the glutarimide ring and the 5-membered ring of the phthalimide group of the CRBN ligand are considered the reasons for this instability¹⁹⁹.

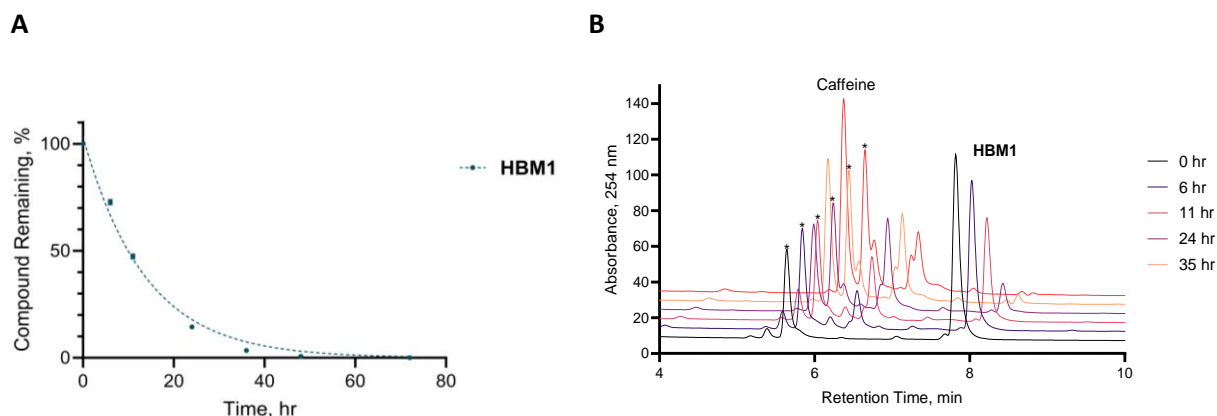


Figure 7.2 **Stability of HBM1 in cell culture media**. 400 μ M HBM1 and 400 μ M caffeine were incubated in DMEM supplemented with 10% FBS at 37°C in an ambient atmosphere for 48 hr. A) The Y-axis is the percentage of HBM1 remaining compared to the peak area ratio of HBM1-to-caffeine at 0 hr. Data from two independent experiments with duplicate technical replicates. Mean and standard error plotted. The data was fitted with an exponential decay function with the plateau constrained to zero. B) Representative UV-HPLC chromatograms for HBM1 at various time intervals. Absorbance recorded at $\lambda = 254$ nm. * indicates the peak integrated for caffeine.

7.1 Degradation Efficacy by Western Blot

HBM1 was investigated in the MCF-7 cell line and a loss of PRMT1 signal was observed at 10 μ M (Figure 7.3).

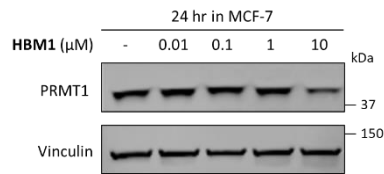


Figure 7.3 Western blot of HBM1 in the MCF-7 cell line. MCF-7 cells were treated with HBM1 at the indicated concentration for 24 hr and then harvested for analysis by Western blot.

The reproducibility of the observed reduction in PRMT1 signal was investigated further with an increased dose of HBM1 and in three cell lines. Quantification of the signal has been undertaken however the values have been rounded to one decimal place to account for the uncertainty in the measurements in the Western blot assay⁸⁵. The dose-dependent degradation of PRMT1 by HBM1 was observed in all three cell lines. For MCF-7 cells treated with 10 μM HBM1 for 24 hours, the mean PRMT1 degradation efficacy is 63 ± 6 % (SE) (n=6), and the degradation appears selective to PRMT1 over PRMT6. In the HPAF-II and KP-3 cell lines, PRMT1 degradation was observed however the effect of HBM1 on the protein level of PRMT6 is inconclusive (Figure 7.4).

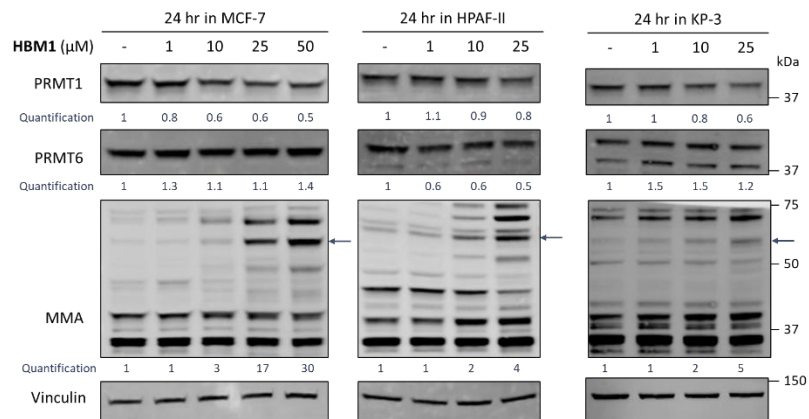


Figure 7.4 Western blot of HBM1 in the MCF-7, HPAF-II and KP-3 cell lines. Cells were treated with HBM1 at the indicated concentration for 24 hr and then harvested for analysis by Western blot. The arrow (\leftarrow) indicates the band quantified for MMA.

Additional time points were also investigated, and PRMT1 degradation was not observed at the shorter time points tested (4 and 8 hours). Degradation was however observed at 48 hours (Figure 7.5).

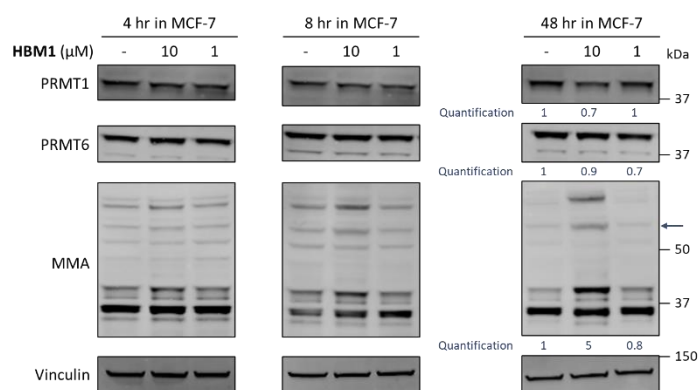


Figure 7.5 Western blot of HBM1 in the MCF-7 cell line at various time points. MCF-7 cells were treated with HBM1 at the concentration and time indicated and then harvested for analysis by Western blot. The arrow (←) indicates the band quantified for MMA.

To assess the effect of **HBM1** on cell proliferation, a colony formation assay was undertaken with MCF-7 cells treated with **HBM1** for 15 days. In this assay, the ability of single cells to survive and reproduce to form colonies is assessed. Cells are seeded at a very low density and after the desired period, cell colonies are fixed and stained with crystal violet. The fewer the number and smaller the size of colonies, the lower the proliferation. The effect of **HBM1** was investigated following a 15-day incubation in MCF-7 cells with treatment on day 0 and day 8. With 10 μM **HBM1** treatment, a reduction in cell proliferation was observed alongside the reduction in the protein level of PRMT1. There was no change in the level of PRMT6. The expected inhibitory effects on Type I PRMT and PRMT1 activity were also observed indicating that **HBM1** binds to Type I PRMT and PRMT1. In this experiment, **GSK3368715** was found to be a more potent inhibitor of PRMT1 but it did not degrade PRMT1 (Figure 7.6).

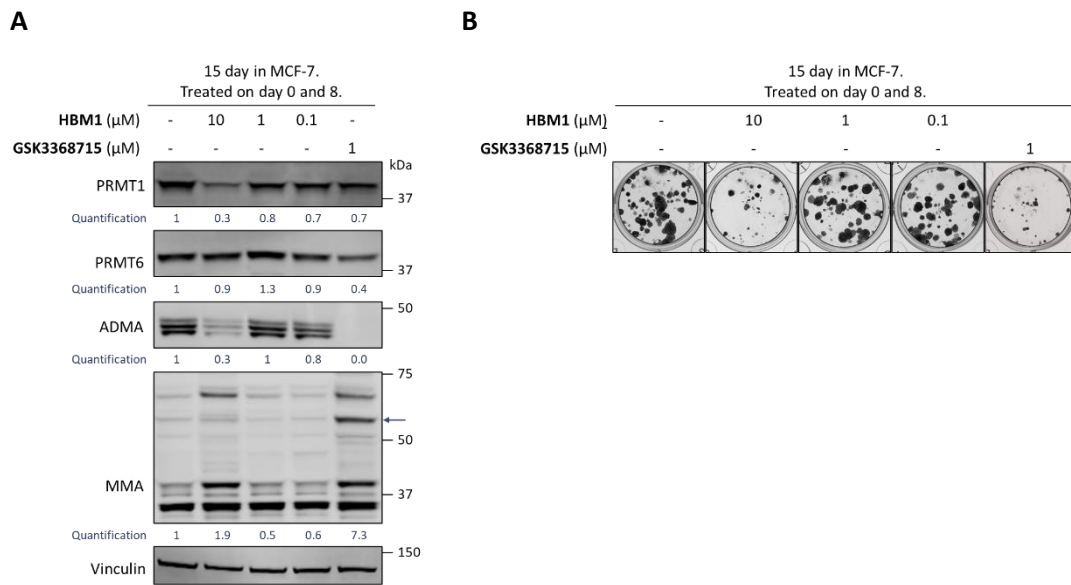


Figure 7.6 Colony formation experiment with HBM1 in the MCF-7 cell line. MCF-7 cells were treated with HBM1 at the indicated concentration. On day 7, the media was replaced, and the cells retreated with HBM1 at the indicated concentration. On day 15, the cells were (A) harvested for analysis by Western blot or (B) stained with crystal violet. The arrow (←) indicates the band quantified for MMA. Image representative of two independent experiments.

Finally, a cell viability assay was undertaken and neither **HBM1** nor **GSK3368715** had a significant effect on cell viability at 48 hours following treatment. At 120 hours, treatment with **HBM1** at 10 μM resulted in a significant loss of cell viability compared to untreated cells (Figure 7.7).

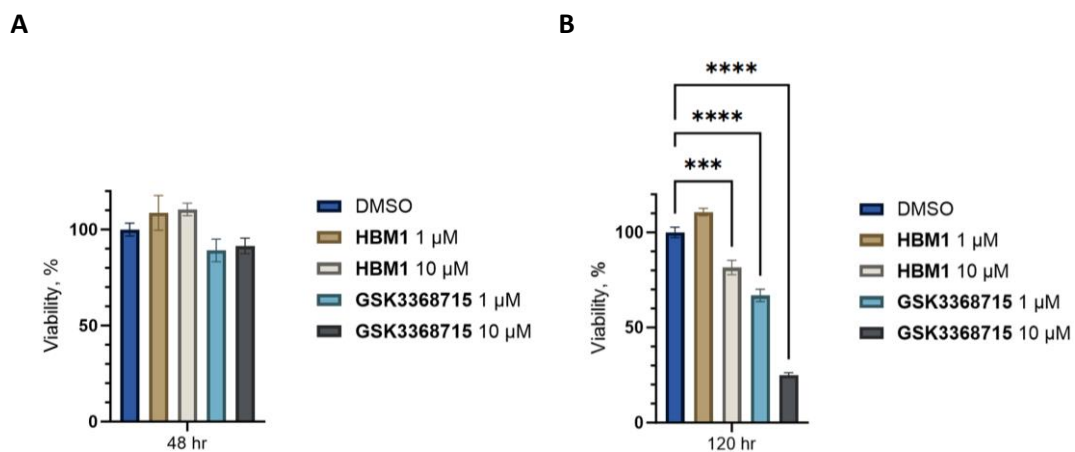


Figure 7.7 A significant loss in cell viability was observed in MCF-7 cells following incubation with HBM1 for 120 hr, but not 48 hr. MCF-7 cells were treated with GSK3368715 or HBM1 for (A) 48 hr or (B) 120 hr, and viability was assessed using the Promega Cell Titre-Glo assay. Mean and standard error plotted. For HBM1, data is from a single experiment with six technical replicates. For GSK3368715, data is representative of two independent experiments. Statistical analysis by a one-way ANOVA, *** $p \leq 0.001$, **** $p \leq 0.0001$, $p > 0.05$ are not significant and are not labelled.

7.2 Mechanism for HBM1-Induced PRMT1 Degradation

The mechanism by which **HBM1** degrades PRMT1 was investigated. First, the assumption that **HBM1** does not bind to CRBN was confirmed using the NanoBRET target engagement assay. In contrast to pomalidomide where a dose-dependent loss of BRET was observed, treatment with **HBM1** does not affect BRET (Figure 7.8).

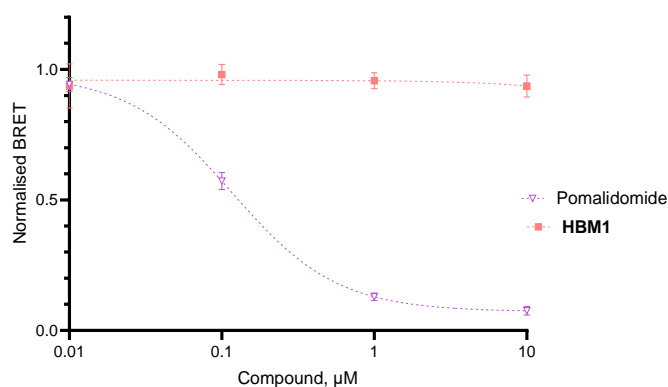


Figure 7.8 HBM1 does not bind to the E3-ligase CRBN. Data is normalised to untreated cells and BRET calculated by BRET emission intensity / NLuc emission intensity. The mean and standard error of two independent experiments with multiple biological replicates are shown.

The degradation of PRMT1 by **HBM1** was also found to be dependent on the proteasome; when MCF-7 cells were treated with both **HBM1** and the proteasome inhibitor **MG132**, PRMT1 degradation was not observed. **MG132** also affected the ability of **HBM1** to inhibit PRMT1 and Type I PRMT activity (Figure 7.9).

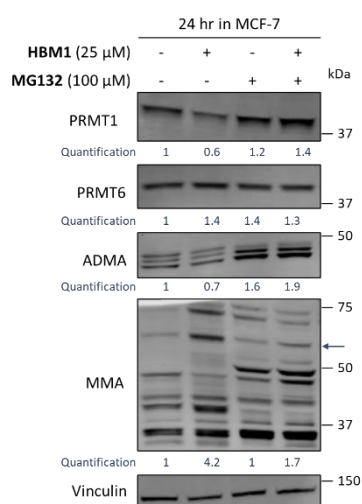
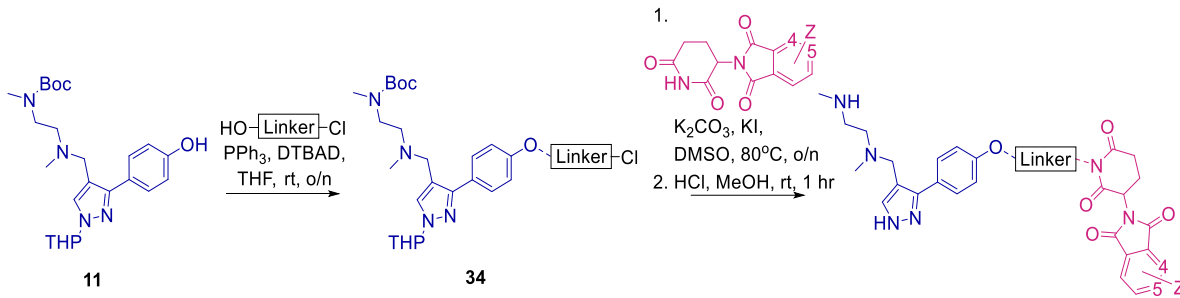


Figure 7.9 The HBM1-induced degradation of PRMT1 is proteasome dependent. MCF-7 cells were treated with MG132 (100 µM), HBM1 (25 µM) or both compounds for 24 hr. The cells were harvested for analysis by Western blot. The arrow (←) indicates the band quantified for MMA. Image representative of two independent experiments.

7.3 Analogues of HBM1

With the aim of increasing the maximum degradation efficacy observed, analogues of **HBM1** were synthesised and evaluated for their ability to induce PRMT1 degradation. These heterobifunctional molecules differed from **HBM1** in their linker composition and/or the substituent on the phthalimide ring of the CRBN ligand. The synthetic route for **HBM1** was followed; a Mitsunobu reaction synthesised analogues of **34** which were *N*-alkylated by a CRBN ligand and deprotected to give **HBM1-5** (Table 7.1).

Table 7.1 *Synthesis of HBM1-5.*



Entry	Linker =	Z	Yield of 34 , %	Yield over two steps, %	Product
1	$(-CH_2-)_m$	4-OH	54	34	HBM1
2	$(-CH_2-)_m$	5-OH	54	14	HBM2
3	$(-CH_2-CH_2-O-)_m$	4-OH	70	75	HBM3
4	$(-CH_2-CH_2-O-)_m$	4-NH ₂	70	39	HBM4
5	$(-CH_2-CH_2-O-)_m$	4-NH ₂	46	7 ^(a)	HBM5

^(a) Alternative conditions used: 1) NaI, Acetone, 80°C, 4 hr. 2) NaHCO₃, NMP, 110°C, 3 days. Step 3) HCl MeOH, rt, 1 hr.

HBM1-5 were tested at 10 μM and 25 μM in the MCF-7 cell line for 24 hours. **HBM1** and **HBM3** degraded PRMT1, and **HBM1** had the greatest potency for degradation out of the molecules tested. **HBM4** had high potency for PRMT1 inhibition but did not degrade PRMT1 (Figure 7.10). From this data, it can be tentatively concluded that a 4-OH substituent on the phthalimide ring of the CRBN ligand is required for the degradation of PRMT1.

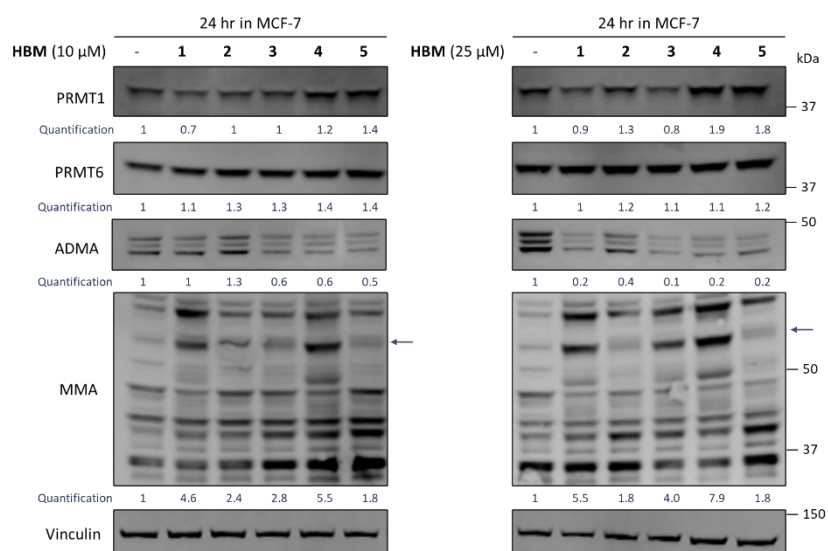


Figure 7.10 Western blot of HBM1-5 in the MCF-7 cell line. MCF-7 cells were treated with HBM1-5 at either 10 μ M (left) or 25 μ M (right) for 24 hr and then harvested for analysis by Western blot. Image representative of two independent experiments.

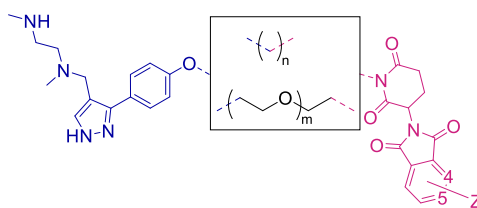
The molecules were further investigated. MCF-7 cells were treated hourly with 1 μ M **HBM1-5** for 6 hours and PRMT1 degradation was not observed with any of the molecules. Upon the treatment of MCF-7 cells with 10 μ M **HBM1-4** for 48 hours, the same trends as shown in Figure 7.10 were observed, and with 1 μ M **HBM1-4** PRMT1 degradation was not observed (Appendix 1H).

7.4 Discussion and Conclusions

Five heterobifunctional molecules were synthesised and evaluated for PRMT1 degradation (Table 7.2).

Table 7.2 A summary of the biological activity of the heterobifunctional molecules in the MCF-7 cell line.

Inhibition and degradation determined by Western blot with 24 hr treatment of $\leq 25 \mu\text{M}$ of the molecule in the MCF-7 cell line. N.D. = not determined (inconclusive data in this instance).



	Linker	Z	Degradation		Inhibition	
			PRMT1	PRMT6	Type I	PRMT1
HBM1	m=1	4-OH	✓	✗	✓	✓
HBM2	m=1	5-OH	✗	✗	N.D.	N.D.
HBM3	n=5	4-OH	✓	✗	✓	✓
HBM4	n=5	4-NH ₂	✗	✗	✓	✓
HBM5	m=2	4-NH ₂	✗	✗	✓	✓

PRMT1 degradation was observed with **HBM1** in the MCF-7, HPAF-II and KP-3 cell lines. In the MCF-7 cell line, the degradation appears selective to PRMT1 over PRMT6 and is proteasome dependent.

HBM1 also inhibited PRMT1 and Type I PRMT activity, and a loss of cell viability and proliferation was observed with the prolonged incubation of MCF-7 cells with **HBM1**.

The degradation and observed selectivity of **HBM1** should be investigated further. Considering the delay between **HBM1** treatment and an observed loss of cell viability, as well as the sustained PRMT1 degradation observed by Western blot in the colony formation experiment, a quantitative assay to measure the time course of PRMT1 degradation should be used to determine at what time point maximal PRMT1 degradation occurs. A fusion protein should be used where PRMT1 is tagged with a fluorescent protein (such as green fluorescent protein) or a luminescent protein (such as the HiBit protein) as this would enable the sensitive and kinetic measurement of PRMT1 protein levels⁸⁶.

The mechanism by which **HBM1** induces the degradation of PRMT1 will now be considered. The degradation of **HBM1** is proteasome dependent and does not require binding to the E3-ligase CRBN. Since the PRMT1 ligand **23** does not cause degradation (Section 4.2.2), nor any of the PROTACs synthesised in this project, it is proposed that the binding of the PRMT1 pharmacophore does not induce degradation, but instead it is the bifunctional nature of **HBM1** with the *N*-alkylated CRBN ligand and a hydroxyl group at the 4-position of the phthalimide ring. The importance of the hydroxyl

functional group in causing PRMT1 degradation should be probed by evaluating the *O*-methylated analogue of **HBM1** *in vitro* (Figure 7.11).

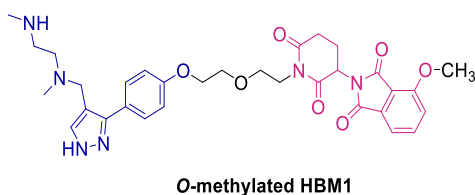


Figure 7.11 A methylated analogue of HBM1 should be investigated to determine if the 4-OH substituent on the CRBN ligand is critical for PRMT1 degradation.

From the literature, two mechanisms for monomeric degradation are highlighted as the potential route by which **HBM1** induces PRMT1 degradation. First, the degradation may occur by a mechanism similar to the FDA-approved selective estrogen receptor degrader (SERD) **fulvestrant**. **Fulvestrant** is a heterobifunctional molecule comprising the endogenous ligand for ER oestradiol attached to a highly lipophilic perfluoroalkyl functional group²¹⁶ (Figure 7.12). **Fulvestrant** induces ER degradation by binding to a monomer of ER. This prevents the dimerisation of ER and its translocation to the nucleus. Monomeric ER cannot translocate which results in the acceleration of ER degradation in the nucleus²¹⁷.

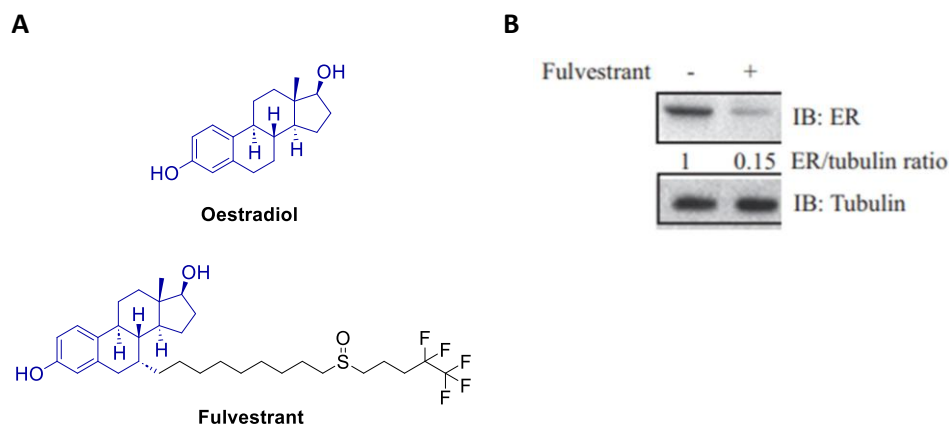


Figure 7.12 Fulvestrant degrades the estrogen receptor (ER). A) Structure of oestradiol and Fulvestrant. B) ER degradation is induced by fulvestrant. T47D cells were treated with 0.1 mmol/L fulvestrant for 2 hr and analysed by Western blot. Figure adapted from Ishii *et al.*²¹⁸.

To proceed by this mechanism, **HBM1** must bind to non-dimerised PRMT1. Ligands frequently have high affinity to a specific conformation of their target protein²¹⁹, and the only available data for the PRMT1 pharmacophore used in **HBM1** is for dimerised PRMT1¹³. Therefore, to validate if **HBM1** induces degradation in an analogous way to **Fulvestrant**, it should be determined whether **HBM1** can bind to non-dimerised PRMT1.

protein folding. The inability to recruit the molecular chaperone can lead to protein misfolding and their recognition for degradation by the ubiquitin-proteasome system^{84,224}.

A Cellular Thermal Shift Assay (CETSA) should be used to determine whether **HBM1** binding destabilises the structure of PRMT1. This assay measures a change in the thermal stability of a protein upon ligand binding. Upon heating to a certain temperature, a protein will unfold and lose its tertiary structure. The temperature when this occurs can be altered if, upon ligand binding, the protein is stabilised or destabilised²²⁵. In a CETSA, cells are exposed to a ligand and heated to a range of defined temperatures. The cells are then lysed and the soluble proteins are separated from insoluble protein aggregates by centrifugation. Denatured (unstable) protein precipitates whereas stable proteins remain solubilised. The amount of solubilised protein is quantified and plotted as a function of the temperature. If **HBM1** destabilises the structure of PRMT1 upon binding, a decreased amount of solubilised protein at a given temperature would be observed compared to untreated cells (Figure 7.14).

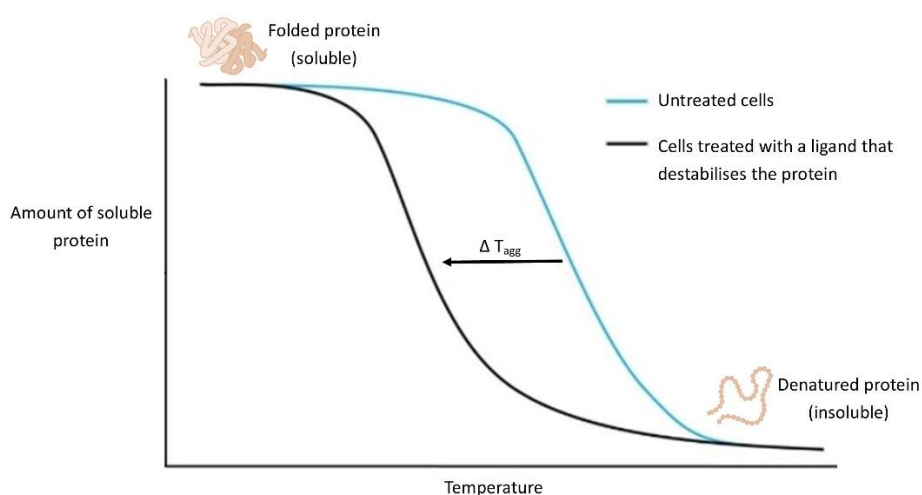


Figure 7.14 Expected results for a cellular thermal shift assay where HBM1 destabilises PRMT1 upon binding.

T_{agg} is the temperature where 50% aggregation (unfolding) is observed. Protein destabilisation upon ligand binding will lead to a decreased T_{agg} .

With the aim of provoking the destabilisation of PRMT1, a small library of hydrophobic tagged molecules should also be synthesised and evaluated for PRMT1 degradation. A range of linker compositions and lengths should be used to increase the likelihood of potent PRMT1 degradation (Figure 7.15). If degradation is observed, the biological effects of PRMT1 degradation should be evaluated as this may provide insight into the clinical utility of PRMT1 degradation. In addition, the selectivity of the molecules to PRMT1 over the other Type I PRMTs should be investigated.

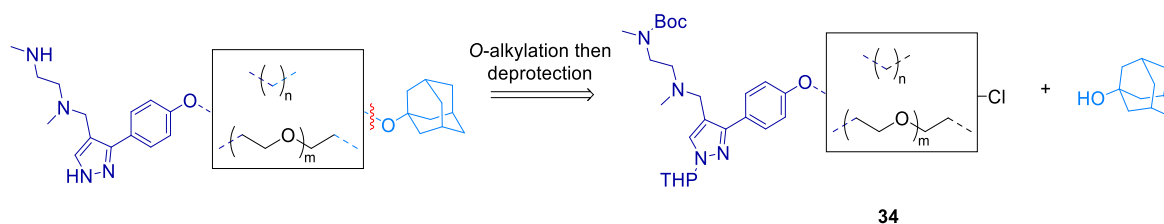


Figure 7.15 *Retrosynthesis of a library of hydrophobic-tagged monomeric degraders for PRMT1.*

Focus should however remain on developing a PROTAC for PRMT1 rather than a monomeric degrader as provoking degradation through protein instability has its disadvantages. One example is that the accumulation of misfolded proteins in the cell can cause stress which can lead to adverse effects, including cytotoxicity by apoptotic cell death²²⁶. Furthermore, it is unclear whether monomeric degraders proceed by event-driven pharmacology and can act catalytically or whether a high and sustained concentration of the molecule is required for effective degradation. The requirement of a high and sustained concentration would be disadvantageous as this often results in off-target binding and adverse effects⁶⁴.

8 Conclusion and Future Work

8.1 Conclusions

This thesis details a novel approach to degrade PRMT1 using a PROTAC. PRMT1 has been highlighted as a protein whose degradation is a promising strategy for the treatment of breast cancer and PDAC. PRMT1 has also been determined to possess properties that make it amenable to PROTAC-induced degradation.

Sixteen PROTACs comprised of a PRMT1 ligand, a linker and an E3-ligase ligand were synthesised. Synthetic routes were optimised for both VHL-recruiting PROTACs and CRBN-recruiting PROTACs and can be readily adapted to synthesise PROTACs with a range of linker lengths and compositions. In the synthesis of CRBN-recruiting PROTACs, regioselectivity challenges were overcome by the employment of a protecting group on the nitrogen of the glutarimide ring. The stability of the PROTACs in cell media was explored and improved for the CRBN-recruiting PROTACs by changing the functional group that attaches the linker to the CRBN ligand.

A selective and sensitive Western blot protocol was used to measure changes in PRMT1 levels. PRMT1 degradation was not observed with any of the PROTACs synthesised. Cell permeability and PRMT1 binding were shown with selective PROTACs by the increased level of mono-methylated arginine upon PROTAC treatment. In addition, despite the short half-life of the CRBN-recruiting PROTACs in cell media, these PROTACs were shown to bind to CRBN.

Five heterobifunctional molecules comprised of the PRMT1 ligand connected via a linker to the pharmacophore of the CRBN ligand were evaluated *in vitro*. The degradation of PRMT1 was observed with **HBM1** in the MCF-7, HPAF-II and KP-3 cell lines. The degradation was proteasome dependent and appeared selective to PRMT1 over PRMT6. **HBM1** does not bind to CRBN and is proposed to induce degradation by preventing PRMT1 dimerisation or destabilising the quaternary protein structure of PRMT1.

8.2 Future Direction for PROTAC Development

The PROTACs synthesised in this project should be assessed for their ability to form a ternary complex with PRMT1 and their respective E3-ligase. A BRET assay should be employed in which BRET occurs when proximity is induced between a fusion protein of PRMT1 and a fusion protein of the E3-ligase²¹¹. In the absence of ternary complex formation, additional PROTACs should be synthesised with different linkers. If a ternary complex is observed, PROTACs that have a different chemical structure should be synthesised to increase the conformational diversity in the induced ternary complexes; this would increase the likelihood that a suitable orientation and distance between a

PRMT1 surface lysine and the ubiquitin of a charged E2-enzyme would occur and enable ubiquitin transfer.

However, it is plausible that properties of the chosen PRMT1 ligand may prevent the PROTAC from simultaneously binding PRMT1 and the E3-ligase. **GSK3368715** binds at the base of the large deep substrate binding pocket of PRMT1¹³, and as the PROTACs synthesised in this project contain the same pharmacophore as **GSK3368715**, they will bind at the same position. Binding at the base of a deep pocket may limit the ability of the E3-ligase ligand to project into the intracellular fluid; the linker may not be of a sufficient length, or the flexible linker may 'collapse' to form favourable intermolecular interactions or interactions with amino acids in the hydrophobic substrate binding pocket of PRMT1. When selecting the PRMT1 ligand, focus was on the selection of a potent PRMT1 ligand that could tolerate linker attachment without a loss in PRMT1 binding affinity. The spatial position of the ligand bound to PRMT1, and the predicted trajectory of the linker and E3-ligase ligand, were not considered and may be unsuitable. A PRMT1 ligand, that binds at a shallower pocket of PRMT1 should be used in the design of future PRMT1 PROTACs.

A further limitation of the PRMT1 ligand used in this project is that the pharmacophore is not selective to PRMT1 over the other Type I PRMTs, and although a pan-selective ligand can be converted into a selective PROTAC, this has generally been a fortuitous occurrence and not through rational design²²⁷⁻²³⁰. The synthesis of additional PROTACs for PRMT1 should use an alternative PRMT1 ligand. However no selective PRMT1 ligands have been published to date; the PRMT1 ligands published are either a protein substrate mimetic or a SAM mimetic and because of the high sequence homology between the Type I PRMTs in the binding pockets for the protein substrate or SAM, they are all pan-Type I PRMT ligands²³¹. A selective, allosteric, high-affinity ligand for PRMT1 that binds in a shallow binding pocket should be developed and incorporated into a PROTAC. Schapira *et al.* have used a computational model to systematically search the PRMT1 structure for potential ligand binding pockets on the protein's surface but do not identify one selective to PRMT1, nor PRMT6²³². However a selective PRMT6 inhibitor was identified by Shen *et al.* by a high-throughput screening assay and subsequent structure-activity relationship studies²³³. This empirical approach will likely be required to identify a suitable ligand for PRMT1.

Regarding the E3-ligase, focus should turn to synthesising PROTACs that recruit a different E3-ligase as it has yet to be elucidated if a single E3-ligase can promote the degradation of every given target protein²³⁴. In particular, it may be beneficial to recruit E4B as PRMT1 is a native substrate of this E3-ligase⁹⁷. Hijacking this existing process may increase the chance of inducing ubiquitin transfer and PRMT1 degradation.

8.3 Future Direction for PRMT1 Degradation

Moving forward from PROTAC-induced degradation, the efficient degradation of PRMT1 may be achieved by a heterobifunctional molecule that recruits a different component of the ubiquitin proteasome system.

There are more than 600 different E3-ligases but only around 40 E2-enzymes²³⁵. A heterobifunctional molecule that recruits an E2-enzyme may induce the degradation of a broader and different scope of target proteins. This heterobifunctional molecule would still proceed via a ternary complex that facilitates the ubiquitination of the target protein and therefore it could act catalytically and have the ability for selective degradation. Forte *et al.* use heterobifunctional molecules containing a covalent ligand for the E2-enzyme UBE2D to degrade the proteins BRD4 and the androgen receptor²³⁶. An analogous heterobifunctional molecule for PRMT1 could lead to effective PRMT1 degradation, and a small library of molecules should be synthesised (Figure 8.1).

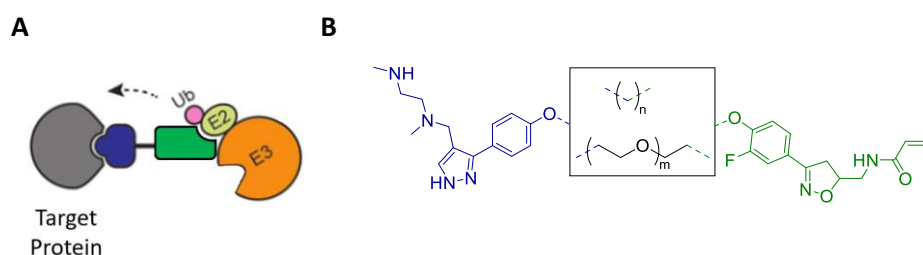


Figure 8.1 Direct E2-enzyme recruitment for PRMT1 degradation. A) Schematic of ternary complex with a heterobifunctional molecule bound to the target protein and the E2-enzyme. Ubiquitination of the target protein would lead to its recognition by the proteasome for degradation. B) Proposed structure of a library of heterobifunctional molecules that recruit the UBE2D E2-enzyme (green) and PRMT1 (blue). A heterobifunctional molecule using the UBE2D ligand is published in Forte *et al.*²³⁶. Similar to the design of PROTACs, a range of linkers would be screened to maximise the likelihood of ternary complex formation and favourable pharmacokinetic properties.

To avoid the necessity of the ubiquitination of PRMT1, a library of heterobifunctional molecules that directly bind to the proteasome should also be investigated. A macrocycle for binding to the proteasome has been published, and heterobifunctional molecules with this ligand have been coined 'chemical inducers of degradation' (CIDE). Proof-of-principle has been shown with the degradation of the target protein BRD4²³⁷. For PRMT1 degradation, a small-molecule library of CIDEs with the PRMT1 ligand used in this project should be investigated (Figure 8.2).

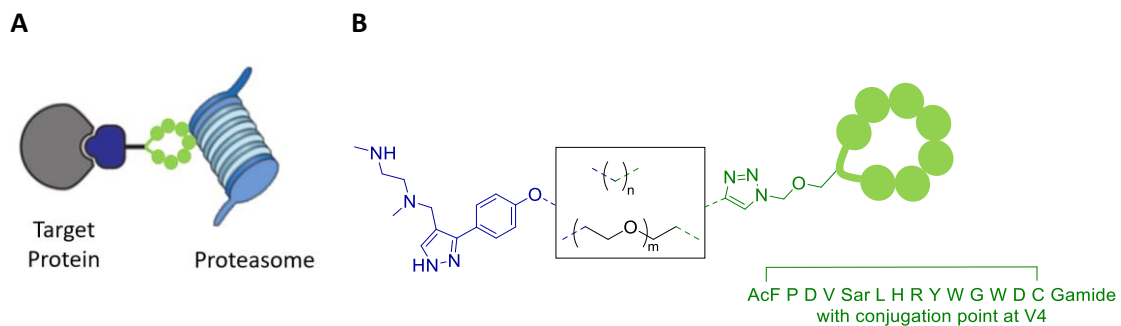


Figure 8.2 Direct 26S recruitment for PRMT1 degradation. A) Schematic of ternary complex with a CIDE bound to the target protein and a subunit of the 26S proteasome. The proximity of the target protein to the proteasome would lead to its degradation. B) Proposed structure of a library of CIDEs comprised of a PRMT1 ligand (blue) and a peptidic macrocycle that binds to the proteasome (green) connected by a linker. The full structure of the macrocycle is published in Bashore et al.²³⁷.

9 Experimental

9.1 General Experimental

All chemistry experiments were undertaken at the Yusuf Hamied Department of Chemistry, University of Cambridge. All non-aqueous reactions were conducted under a stream of dry nitrogen using oven-dried glassware. Temperatures of 0°C were maintained using an ice-water bath. All temperatures below -10°C were maintained using an acetone-cardice bath. Room temperature (rt) refers to ambient temperature. Reactions performed under microwave irradiation were performed in sealed vials using a Biotage Initiator+ microwave synthesiser.

Solvents and Reagents Solvent and reagents were used as received from commercial sources unless otherwise stated. Anhydrous dimethylformamide (DMF), dimethyl sulfoxide (DMSO) and 1,4-dioxane were purchased from commercial sources and used without further purification. Ethyl acetate (EtOAc), methanol (MeOH), dichloromethane (DCM) and acetonitrile were distilled from calcium hydride. Diethyl ether (Et₂O) was distilled from a mixture of lithium aluminium hydride and calcium hydride. Tetrahydrofuran was dried using sodium wire and distilled from a mixture of lithium aluminium hydride and calcium hydride with triphenylmethane as an indicator. Petroleum ether (PE) was distilled before use and refers to the fraction between 40–60 °C. All other solvents and reagents were obtained from commercial suppliers and used without further purification.

Reaction Monitoring Thin layer chromatography (TLC) was performed using pre-coated Merck glass backed silica gel 60 F254 plates and visualised by quenching of UV fluorescence ($\lambda_{\text{max}} = 254 \text{ nm}$) or by staining with potassium permanganate or ninhydrin. LC/MS was also used.

LC/MS Liquid chromatography mass spectroscopy (LC/MS) was carried out using a Waters ACQUITY HClass UPLC with an ESCi Multi-Mode Ionisation Waters SQ Detector 2 spectrometer and a PDA eλ Detector (220–800 nm). The instrument was operated and data analysed using MassLynx 4.1. The instrument was equipped with a ACQUITY UPLC CSH C18 column (2.1 mm × 50 mm, 1.7 μm, PN: 186005296) at 40 °C. A linear gradient system was used of 5-95% mobile phase B in mobile phase A, with constant 5% mobile phase C over 1 minute at flow rate of 0.6 mL/minute. Mobile phase A = 2mM NH₄OAc in H₂O/MeCN (95:5), mobile phase B = MeCN, and mobile phase C = 2% HCOOH_(aq). Low resolution mass spectrometry (LRMS) data was obtained from this instrument.

Purification Flash column chromatography was carried out as detailed in Still *et al.*²³⁸ using Merck 9385 Kieselgel 60 SiO₂ (230–400 mesh) under a positive pressure of air. Automated flash column chromatography was carried out on a Combiflash Rf200 automated chromatography system with Redisep reverse-phase C18-silica flash columns (20–40 μm, 5.5/15/50 g). Preparative HPLC was

carried out using an Agilent 1260 Infinity with a reversed-phase Supelcosil™ ABZ+PLUS column (C18, 250 mm × 21.2 mm, 5 μm, PN:54885) or Agilent Prep Agilent Prep 100Å (C18, 250 x 21.2 mm, 10 μm, PN: 410910-702). A linear gradient system was used (solvent A: 0.1% TFA in H₂O, solvent B: 0.05% TFA in MeCN) at a flow rate of 20 mL min⁻¹. HPLC was monitored by UV absorbance at 220 and 254 nm.

Analytical HPLC High pressure Liquid chromatography (HPLC) retention times (R_t) are reported from an Agilent 120 or 12600 Infinity system with a reversed-phase Agilent ZORBAX Eclipse XDB-C18 (150 x 4.6 mm, 5 μm, PN:993967-902) or a Supelcosil™ ABZ+PLUS column (150 x 4.6mm, 3 μm PN:59194) eluting with a linear gradient system (solvent A: 0.05% TFA in H₂O, solvent B: 0.05% TFA in MeCN) over 15 minutes at a flow rate of 1 mL min⁻¹. HPLC was monitored by UV absorbance at 220 and 254 nm.

NMR Nuclear magnetic resonance spectra were recorded at ambient temperature on a Bruker DPX-400 (400 MHz, 101 MHz), Bruker Advance 400 QNP (400 MHz, 101 MHz), Bruker Avance 500 Cryo Ultrashield (500 MHz, 126 MHz) and Bruker Advance 700 TXO Cryo Ultrashield (700 MHz). For proton NMR, ¹H NMR chemical shifts (δ H) are reported in parts per million (ppm), to the nearest 0.01 ppm, and are referenced to the residual non-deuterated solvent peak (CDCl₃: 7.26, DMSO-d₆: 2.50). Coupling constants (J) are reported in Hertz (Hz) to the nearest 0.1 Hz. Data are reported as follows: chemical shift, multiplicity (s = singlet; d = doublet; t = triplet; q = quartet, m = multiplet, br=broad peak) or as a combination of these), coupling constant(s), integration and assignment. For carbon NMR, ¹³C Chemical shifts (δ C) are quoted in ppm, to the nearest 0.1 ppm, and are referenced to the residual non-deuterated solvent peak (CDCl₃: 77.16, DMSO-d₆: 39.52). ¹H NMR and ¹³C NMR spectra assignments were supported by DEPT-135, COSY (2D, ¹H-¹H correlations), HSQC (2D, one bond ¹H-¹³C correlations), HMBC (2D, multiple bond ¹H-¹³C correlations) and NOESY/ROESY (2D, ¹H-¹H correlations) where appropriate. The numbering of molecules used for ¹³C and ¹H NMR assignments does not conform to IUPAC standards. Spectra were processed using TopSpin v.4.1.3 (Bruker).

HRMS High resolution mass spectrometry (HRMS) measurements were recorded with an Agilent 6230 time-of-flight LC/MS with the Agilent 1260 Infinity II Prime LC system using Electrospray ionisation (ESI) techniques.

IR Infrared (IR) spectra were recorded neat on a Perkin-Elmer Spectrum One or Bruker Alpha II FT-IR spectrometer using an Attenuated Total Reflectance (ATR) sampling accessory either as solids or oils. Selected absorptions (ν_{\max}) are reported in wavenumbers (cm⁻¹) with the following abbreviations: w, weak; m, medium; s, strong; br, broad. Peaks were assigned using Coates *et al.*²³⁹.

9.2 Synthetic Procedures

9.2.1 General Methods

General method A The respective *N*-Boc protected amine (1 eq) was dissolved in DCM (5 mL/mmol) and TFA (5 mL/mmol) was added and the mixture stirred at room temperature for 30 minutes. The solvent was removed *in vacuo*. To remove excess TFA, the residue was coevaporated with MeOH (x2) and toluene (x2). The deprotected amine and alcohol (1 eq) were dissolved in DMF (1 mL/mmol) and EtOAc (5 mL/mmol). DIPEA (2 eq) was added dropwise and the mixture was stirred for 10 minutes at room temperature. HATU (1 eq) was added and the mixture was stirred at room temperature for 2 min. DMF (1 mL/mmol) was then added and the solution stirred for 1 hr at room temperature. DIPEA (1 eq) was then added and the reaction stirred for another 1 hr. The solvent was then removed *in vacuo*.

General method B VHL ligand **1** (1 eq) was dissolved in DCM (5 mL/mmol) and TFA (5 mL/mmol) was added and the mixture stirred at room temperature for 30 minutes. The solvent was removed *in vacuo*. To remove excess TFA, the residue was coevaporated with MeOH (x2) and toluene (x2). The deprotected amine and the respective linker (1.2 eq) were dissolved in DMF (1 mL/mmol) and EtOAc (5 mL/mmol). DIPEA (3.2 eq) was added dropwise and the mixture was stirred for 10 minutes at room temperature. HATU (1.2 eq) was added and the mixture was stirred at room temperature for 2 min. DMF (1 mL/mmol) was then added and the solution stirred for 2 hr (alkyl chloride linker) or 30 min (alkyl bromide linker). The solvent was then removed *in vacuo*.

General method C Crown ether (1 eq) was dissolved in nitrobenzene (1 mL/mmol) and ZrCl₄ (1.5 eq) was added. The reaction was stirred at 135°C overnight. After allowing to cool to reach room temperature, the reaction was quenched with solid KHCO₃ and water and the resulting suspension filtered through Celite and the solids washed with DCM. The filtrate was extracted with DCM (x3) and the combined organic layers dried with Na₂SO₄ and the solvent removed *in vacuo* to give a brown liquid. The nitrobenzene was removed by a short silica plug column (0% followed by 9% MeOH in DCM) to give the title compound.

General method D The alcohol (1 eq) was dissolved in acetone (1 mL/mmol) and chromic acid solution {CrO₃ (1.5 eq), water (100 μL/1 mmol of CrO₃) and concentrated H₂SO₄ (66 μL/1 mmol of CrO₃)} was slowly added at 0°C. The reaction was then stirred overnight at room temperature. The mixture was extracted with diethyl ether (x3). The combined organic layers were washed with brine, washed with water, dried with Na₂SO₄ and the solvent removed *in vacuo* to give the carboxylic acid which was used without further purification.

General method E To a solution of triphenylphosphine (2 eq) and alcohol (2 eq) dissolved in THF (1 mL/mmol) was added DTBAD (2 eq) in THF (1 mL/mmol) at 0°C. Finally, a solution of PRMT1 ligand **11** (1 eq) in THF (1 mL/mmol) was added dropwise at 0°C. The mixture was stirred for 1 hr at 0 °C then allowed to warm to room temperature and stirred overnight. The solvent was removed *in vacuo* and the residue purified by automated column chromatography (C18 Gold, 5-60% MeCN in 1% HCOOH_(aq) over 45 CV).

General method F The glutarimide-containing starting material (1 eq) and DBU (1.5 eq) were dissolved in DMF (5 mL/mmol). SEMCl (1.2 eq) was added dropwise at 0°C and the reaction stirred at room temperature for 2 hr. The reaction was quenched with NH₄Cl_(aq, saturated) and extracted with EtOAc (x3).

General method G PRMT1 ligand **11** (1 eq) and Cs₂CO₃ (2 eq) were dissolved in DMF (10 mL/mmol). The respective diiodo-linker (4 eq) in DMF (5 mL/mmol) was added dropwise at 0°C and the reaction stirred overnight at room temperature. The reaction was then purified by automated column chromatography (C18 Gold, 5-60% MeCN in 1% HCOOH_(aq) over 40 CV).

General method H CRBN ligand **37** (1 eq) and linker (1.1 eq) were dissolved in DMSO (10 mL/mmol). DIPEA (2 eq) was added and the mixture heated at 130°C for 2 hr. The mixture was then diluted with water and extracted with EtOAc. The organic layer was washed with water (x3), washed with brine, dried with Na₂SO₄ and the solvent removed *in vacuo*. The residue was then purified by automated column chromatography (C18 Gold, 5-95% MeCN in 1% HCOOH_(aq) over 40 CV).

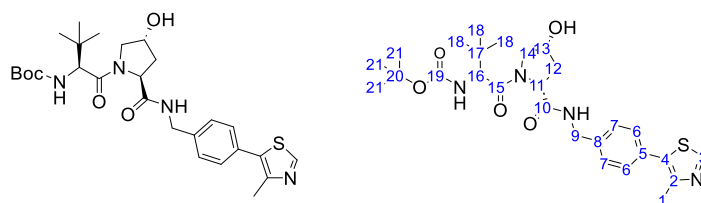
General method I Alkyl halide (1 eq), PRMT1 ligand **11** (1 eq), K₂CO₃ (2 eq) and KI (0.2 eq) were dissolved in MeCN (15 mL/mmol) and heated at 80°C. The solvent was removed *in vacuo* and the residue dissolved in MeOH (20 mL/mmol) and HCl_(aq, 37%) (20 mL/mmol) was added dropwise and the mixture stirred at room temperature for 1 hr. The solvent was then removed *in vacuo*.

General method J The alcohol (1 eq) was dissolved in DCM (5 mL/mmol). At 0°C, Et₃N (1.5 eq) and methanesulfonyl chloride (1.5 eq) were added in succession and the mixture stirred at room temperature for 3 hr. The reaction was quenched by the careful addition of MeOH and the solvent removed *in vacuo*. The residue was dissolved in water and extracted with EtOAc. The organic layer was washed with brine, dried with Na₂SO₄ and the solvent removed *in vacuo*. The residue and NaI (2 eq) were dissolved in MeCN (5 mL/ml) and heated at 50°C overnight. The solvent was removed *in vacuo* and the residue diluted with Na₂S₂O_{3(aq, 10%)} and extracted with DCM (x3). The combine organic layers were washed with water, dried with Na₂SO₄ and the solvent removed *in vacuo*.

General method K The alkyl chloride (1 eq) in DMSO (1.4 mL) was added to the respective CRBN ligand (1.2 eq), K₂CO₃ (2 eq) and KI (1 eq) and heated overnight at 80°C. The mixture was then diluted with water and extracted with DCM (x3). The combined organic layers were washed with water, dried with Na₂SO₄ and the solvent removed *in vacuo*. The residue was dissolved in MeOH (20 mL/mmol) and HCl_(aq, 37%) (20 mL/mmol) was added dropwise and the mixture stirred at room temperature for 1 hr. The solvent was then removed *in vacuo*.

9.2.2 Compound 1-47

***tert*-butyl *N*-[(1*S*)-1-[(2*S*,4*R*)]-4-hydroxy-2-[[4-(4-methylthiazol-5-yl)phenyl]methyl-carbamoyl]pyrrolidine-1-carbonyl]-2,2-dimethyl-propyl]carbamate (1)**

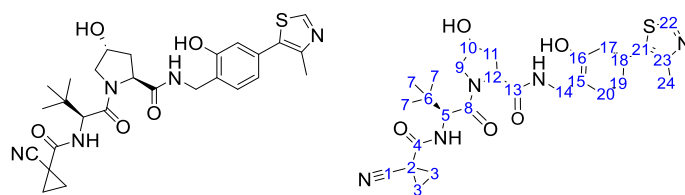


General method A was followed with *N*-Boc protected amine **10** (2.6 g, 6.3 mmol) and *N*-Boc-*L*-*tert*-leucine. The resulting residue was then dissolved in EtOAc, washed with water, washed with brine, dried with Na₂SO₄ and the solvent removed *in vacuo*. The residue was purified by silica gel chromatography (0-5% MeOH in DCM) to give the title compound as a white solid (3.1 g, 92%).

¹H NMR (500 MHz, d₆-DMSO) δ 8.98 (s, 1H, H3), 8.58 (t, *J*=5.9 Hz, 1H, 9-NH), 7.40 (m, 4H, H6 and H7), 6.46 (d, *J*=9.3 Hz, 1H, 16-NH), 5.14 (d, *J*=3.1 Hz, 1H, 13-OH), 4.46-4.36 (m, 3H, H9 and H13), 4.23 (dd, *J*=15.8 and 5.6 Hz, 1H, H11), 4.15 (d, *J*=9.3 Hz, 1H, H16), 3.67-3.60 (m, 2H, H14), 2.44 (s, 3H, H1), 2.07-2.02 and 1.93-1.88 (m, 2H, H12), 1.38 (s, 9H, H21), 0.93 (s, 9H, H18). **¹³C NMR (125 MHz, d₆-DMSO)** δ 171.9 (C10), 169.8 (C19), 155.3 (C15), 151.4 (C3), 147.7 (C2), 139.5 (C5), 131.2 and 129.7 (C4 and C8), 128.7 and 127.4 (C6 and C7), 78.1 (C20), 68.9 (C13), 58.7 (C9), 58.4 (C16), 56.4 (C14), 41.6 (C11), 38.0 (C12), 35.4 (C17), 28.2 (C21), 26.3 (C18), 15.9 (C1). **Lab reference** PM26 and PM27.

Data are in accordance with those reported previously in literature¹²³.

(2*S*,4*R*)-4-hydroxy-*N*-[[2-hydroxy-4-(4-methylthiazol-5-yl)phenyl]methyl]-1-[(2*S*)-2-[(1-isocyanocyclopropanecarbonyl)amino]-3,3-dimethylbutanoyl]pyrrolidine-2-carboxamide (2)

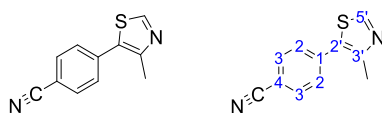


General method A was followed with *N*-Boc protected amine **7** (420 mg, 0.77 mmol) and 1-cyano-1-cyclopropanecarboxylic acid. The resulting residue was purified by silica gel chromatography (0-7% MeOH in DCM with 0.5% NH₄OH_(aq)) to give the title compound as a colourless oil (332 mg, 84%).

¹H NMR (500 MHz, d₆-DMSO) δ 9.81 (s, 1H, 16-OH), 8.94 (s, 1H, H22), 8.52 (t, *J*=5.9 Hz, 1H, 14-NH), 7.36 (d, *J*=8.9 Hz, 1H, 5-NH), 7.31 (d, *J*=7.8, 1H, H20), 6.91 (d, *J*=1.8, 1H, H17) 6.83 (dd, *J*=7.8 and 1.8 Hz, 1H, H19), 5.16 (d, *J*=3.7 Hz, 1H, 10-OH), 4.51 (m, 2H, H12 and H5), 4.34 (m, 1H, H10), 4.22 (m, 2H, H14), 3.64-3.55 (m, 2H, H9), 2.44 (s, 3H, H24), 2.09-1.88 (m, 2H, H11) 1.65-1.7 (m, 4H, H3), 0.94 (s, 9H, H7). **¹³C NMR (125 MHz, d₆-DMSO)** δ 171.9 (C13), 168.7 (C8), 164.5 (C4), 154.8 (C16), 151.3 (C22), 147.5 (C23), 131.3 and 130.7 (C18 and C21), 128.5 (C20), 125.2 (C15), 120.2 (C1), 119.3 (C19), 115.0 (C17), 68.9 (C10), 58.8 and 57.4 (C12 and C5), 56.7 (C9), 37.9 (C14), 37.3 (C11), 36.3 (C6), 26.1 (C7), 16.8 and 16.6 (C3), 16.1 (C24), 13.8 (C2). **Lab reference** PM13 and PM16.

Data are in accordance with those reported previously in literature¹²³.

4-(3-methylthiophen-2-yl)benzonitrile (**4a**)

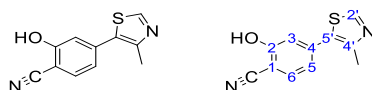


To a solution of 4-bromo-2-hydroxybenzonitrile (2.5 g, 13.7 mmol, 1 eq) and Pd(OAc)₂ (31 mg, 0.1 mmol, 0.1 eq) in dimethylacetamide (40 mL) were added KOAc (2.7 g, 27.5 mmol, 2 eq) and 4-methylthiazole (2.5 mL, 27.5 mmol, 2 eq). The resulting mixture was heated overnight at 150°C and then diluted with water and extracted with DCM (x4). The combined organic layers were dried with MgSO₄ and the solvent removed *in vacuo*. The residue was purified by silica gel chromatography (0-30% EtOAc in PE) to give the title compound as a pale yellow solid (2.5 g, 93%).

¹H NMR (400 MHz, CDCl₃) δ 8.76 (s, 1H, H5'), 7.73 (d, *J*=8.2 Hz, 2H, H2 or H3), 7.56 (d, *J*=8.3 Hz, 2H, H2 or H3), 2.57 (s, 3H, 3'-CH₃). **Lab reference** PM01 (13.7 mmol, 87%), PM08 (13.7 mmol, 93%).

Data are in accordance with those reported previously in literature²⁴⁰.

2-hydroxy-4-(4-methylthiazol-5-yl)benzonitrile (4b)

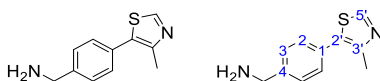


To a solution of 4-bromo-2-hydroxybenzonitrile (2.5 g, 12.6 mmol, 1 eq) and Pd(OAc)₂ (28 mg, 0.1 mmol, 0.1 eq) in dimethylacetamide (50 mL) were added KOAc (2.5 g, 25.3 mmol, 2 eq) and 4-methylthiazole (2.3 mL, 25.3 mmol, 2 eq). The resulting mixture was heated overnight at 150°C and then diluted with water and extracted with DCM (x5). The combined organic layers were dried with MgSO₄ and the solvent removed *in vacuo*. The residue was purified by silica gel chromatography (0-50% EtOAc in PE) to give the title compound as a pale yellow solid (2.0 g, 74%).

¹H NMR (500 MHz, d₆-DMSO) δ 11.44 (br s, 1H, 2-OH), 9.05 (s, 1H, H2'), 7.69 (d, *J*=7.7 Hz, 1H, H6), 7.11 (d, *J*=1.6 Hz, 1H, H3), 7.06 (dd, *J*=8.1 and 1.6 Hz, 1H, H5), 2.48 (s, 3H, 4'-CH₃). **Lab reference** PM02

Data are in accordance with those reported previously in literature¹⁷⁸.

(4-(4-methylthiazol-5-yl)phenyl)methanamine (5a)

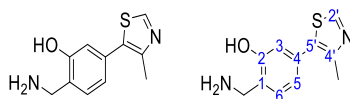


4a (2.4 g, 12 mmol, 1 eq) was dissolved in anhydrous THF (60 mL) and cooled to 0°C. LiAlH₄ (2.4 M in THF, 9.0 mL, 36 mmol, 3 eq) was added dropwise and the resulting mixture was stirred at room temperature overnight. The mixture was cooled to 0°C and quenched sequentially with water (10 mL) and NaOH_(aq) (1M, 10 mL) then stirred for 15 minutes. The solvent was then removed *in vacuo* and the resulting residue purified by silica gel chromatography (0-4% MeOH in DCM with 0.5% NH₄OH) to give an orange oil, which was further purified by automated column chromatography (C18 Gold, 5-95% MeCN in 0.5% CH₃COOH_(aq) over 40 CV) to give the title compound as an orange oil (137 mg, 6%).

¹H NMR (500 MHz, d₆-DMSO) δ 8.98 (s, 1H, H2'), 7.49-7.45 (m, 4H, H2, H3, H5 and H6), 3.88 (s, 2H, 4-CH₂), 2.45 (s, 3H, 3'-CH₃). **NH₂** not identified. **Lab reference** PM03 (12.0 mmol, 6%) and PM10 (12.7 mmol, 8%).

Data are in accordance with those reported previously in literature¹²².

2-hydroxy-4-(4'-methylthiazol-5-yl)benzylamine (5b)

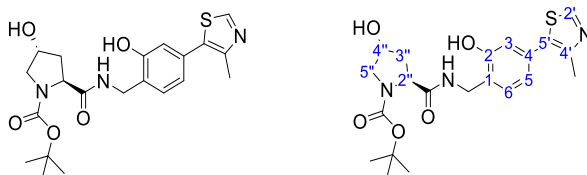


4b (2.0 g, 9.25 mmol, 1 eq) was dissolved in anhydrous THF (40 mL) and cooled to 0°C. LiAlH₄ (2.4 M in THF, 11.3 mL, 3 eq) was added dropwise and the resulting mixture was stirred at room temperature overnight. The mixture was cooled to 0°C and quenched sequentially with water (10 mL) and NaOH_(aq) (1M, 10 mL) and stirred for 15 minutes. The solvent was then removed *in vacuo* and the resulting residue purified by silica gel chromatography (0-10% MeOH in DCM with 0.5% NH₄OH) to give an orange oil, which was further purified by automated column chromatography (C18 Gold, 5-95% MeCN in 0.5% CH₃COOH_(aq) over 40 CV) to give the title compound as an orange oil (987 mg, 46%).

¹H NMR (500 MHz, d₆-DMSO) δ 8.94 (s, 1H, H2'), 7.21 (d, *J*=7.7 Hz, 1H, H6), 6.87 (d, *J*=1.5 Hz, 1H, H3), 6.84 (dd, *J*=7.7 and 1.7 Hz, 1H, H5), 3.89 (s, 2H, 1-CH₂), 2.44 (s, 3H, 4'-CH₃). 2-OH and NH₂ not identified. **Lab reference** PM04.

Data are in accordance with those reported previously in literature¹⁷⁸.

(2*S*,4*R*)-*tert*-butyl 4-hydroxy-2-((2-hydroxy-4-(4-methylthiazol-5-yl)benzyl)carbamoyl)pyrrolidine-1-carboxylate (6)



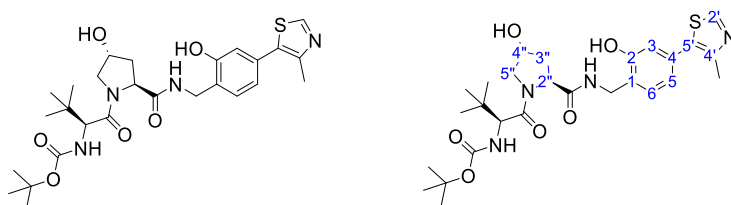
5b (940 mg, 4.3 mmol, 1 eq) and Boc-Hyp-OH (980 mg, 4.3 mmol, 1 eq) were dissolved in DMF (4.3 mL) and EtOAc (21 mL). DIPEA (0.74 mL, 1 eq) was added dropwise and the mixture was stirred for 10 minutes at room temperature. HATU (1.6 g, 4.3 mmol, 1 eq) was added and the mixture was stirred at room temperature for 2 min. DMF (4.3 mL) was added and the solution stirred for 1 hr at room temperature. DIPEA (0.74 mL, 1 eq) was then added and the reaction stirred for another 1 hr. The solvent was then removed *in vacuo* and the residue dissolved in EtOAc, washed with water (x2), washed with brine (x2), dried with MgSO₄ and the solvent removed *in vacuo*. The residue was purified by silica gel chromatography (0-5% MeOH in DCM with 0.5% NH₄OH) to yield the title compound as white crystals (360 mg, 20%).

¹H NMR (500 MHz, d₆-DMSO) δ 9.94 and 9.83 (s, 1H, 2-OH), 8.95 (s, 1H, H2'), 8.48 and 8.33 (t, *J*=6.0 Hz, 1H, NH), 7.24 and 7.19 (d, *J*=7.8 Hz, 1H, H6), 6.91 (d, *J*=1.7 Hz, 1H, H3), 6.87 and 8.83 (dd, *J*=7.8 and 1.7 Hz, 1H, H5), 5.03 (m, 1H, 4''-OH), 4.29-4.14 (m, 4H, H2'' and H4'' and 1-CH₂), 3.29 (m, 2H, H5''), 2.43 (s, 3H, 4'-CH₃), 2.10-1.83 (m, 2H, H3''), 1.40 and 1.23 (s, 9H, C(CH₃)₃). Rotamers present.

Lab reference PM06

Data are in accordance with those reported previously in literature¹⁷⁸.

***tert*-butyl((*S*)-1-((2*R*,4*R*)-4-hydroxy-2-((2-hydroxy-4-(4-methylthiazol-5-yl)benzyl)carbamoyl)pyrrolidin-1-yl)-3,3-dimethyl-1-oxobutan-2-yl)carbamate (7)**

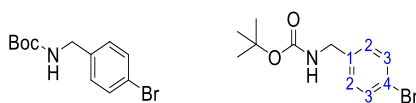


General method A was followed with *N*-Boc protected amine **6** (360 mg, 0.83 mmol) and *N*-Boc-*L*-*tert*-leucine. The resulting residue was dissolved in EtOAc, washed with water (x3), washed with brine (x2), dried with Na₂SO₄ and the solvent removed *in vacuo*. The residue was purified by silica gel chromatography (0-5% MeOH in DCM with 0.5% NH₄OH_(aq)) to give the title compound as a white solid (421 mg, 68%).

¹H NMR (500 MHz, d₆-DMSO) δ 9.83 (s, 1H, 2-OH), 8.93 (s, 1H, H2'), 8.46 (t, *J*=5.9 Hz, 1H, 1-CH₂-NH), 7.34 (d, *J*=7.8 Hz, 1H, H6), 6.89 (d, *J*=1.7 Hz, 1H, H3), 6.81 (dd, *J*=7.8 and 1.6 Hz, 1H, H5), 6.43 (d, *J*=9.0 Hz, 1H, 1''-CO-C-NH), 5.17 (d, *J*=3.1 Hz, 1H, 4''-OH), 4.48-4.12 (m, 5H, H2'' and H4'' and 1-CH₂, and 1''-C(O)-CH), 3.66-3.59 (m, 2H, H5''), 2.43 (s, 3H, 4'-CH₃), 2.06-1.89 (m, 2H, 3''), 1.37 (s, 9H, Boc C(CH₃)₃), 0.91 (s, 9H, C(CH₃)₃). **Lab reference** PM07 and PM09

Data are in accordance with those reported previously in literature²⁴¹.

***tert*-butyl *N*-[(4-bromophenyl)methyl]carbamate (8)**



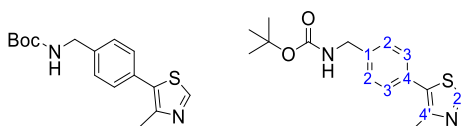
tert-butyl carbamate (4.75 g, 40.5 mmol, 3 eq) and 4-bromobenzaldehyde (2.5 g, 13.5 mmol, 1 eq) were dissolved in DCM (27 mL) and MeCN (81 mL). Et₃SiH (6.5 mL, 40.5 mmol, 3 eq) was added

dropwise, followed by the dropwise addition of trifluoroacetic acid (2.1 mL, 27 mmol, 2 eq). The resulting mixture was stirred overnight at room temperature and then carefully quenched by the addition of $\text{NaHCO}_3(\text{aq})$ (10 mL) and the solvent removed *in vacuo*. The residue was diluted with water and extracted with DCM (x3). The combined organic layers were washed with water, dried with Na_2SO_4 and the solvent removed *in vacuo*. The residue was purified by automated column chromatograph (C18 Gold, 30-100% MeCN in 0.1 M $\text{NH}_4\text{OH}(\text{aq})$ over 15 CV) to give the title compounds as a white solid (2.8 g, 73%).

$^1\text{H NMR}$ (500 MHz, $\text{d}_6\text{-DMSO}$) δ 7.47 (d, $J=8.3$ Hz, 2H, H3), 7.36 (t, $J=6.0$ Hz, 1H, NH), 7.17 (d, $J=8.4$ Hz, 2H, H2), 4.06 (d, $J=6.2$ Hz, 2H, 1- CH_2), 1.36 (s, 9H, C(CH_3) $_3$). **Lab reference** PM15 (2.7 mmol, 65%) and PM19 (40.5 mmol, 73%).

Data are in accordance with those previously reported in the literature¹²³.

***tert*-butyl *N*-{[4-(4-methylthiazol-5-yl)phenyl]methyl}carbamate (9)**

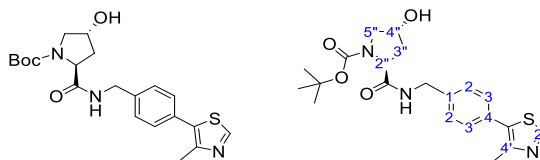


8 (2.8 g, 9.8 mmol, 1 eq), $\text{Pd}(\text{OAc})_2$ (22.1 mg, 0.1 mmol, 0.01 eq) and KOAc (1.93 g, 19.6 mmol, 2 eq) were dissolved in *N,N*-dimethylacetamide (10 mL). 4-Methylthiazole (1.8 mL, 19.6 mmol, 2 eq) was added and the solution was heated to 130°C for 4 hr. The mixture was cooled to room temperature, diluted with water and extracted with DCM (x3). The combined organic layers were washed with water, dried with Na_2SO_4 and the solvent removed *in vacuo*. The residue was purified by silica gel chromatography (0-5% EtOAc in PE) to give the title compound as a pale yellow solid (2.8 g, 93%).

$^1\text{H NMR}$ (500 MHz, $\text{d}_6\text{-DMSO}$) δ 8.98 (s, 1H, H2'), 7.44 (m, 3H, NH and H2 or H3), 7.33 (d, $J=8.1$ Hz, 2H, H2 or H3), 4.17 (d, $J=6.2$ Hz, 2H, 1- CH_2), 2.45 (s, 3H, 4'- CH_3), 1.40 (s, 9H, C(CH_3) $_3$). **Lab reference** PM17 (1.7 mmol, 88%) and PM21 (9.8 mmol, 93%).

Data are in accordance with those reported previously in literature¹²³.

***tert*-butyl (2*S*,4*R*)-4-hydroxy-2-[[4-(4-methylthiazol-5-yl)phenyl]methylcarbamoyl] pyrrolidine-1-carboxylate (10)**

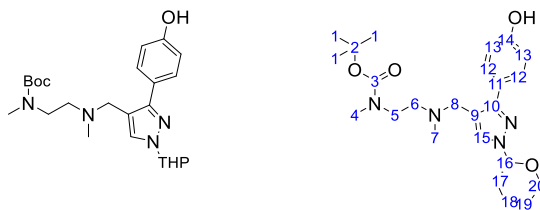


General method A was followed with *N*-Boc protected amine **9** (2.8 g, 9.1 mmol) and *N*-Boc-*trans*-4-hydroxy-L-proline. The resulting residue was then dissolved in EtOAc, washed with water (x2), washed with brine (x2), dried with Na₂SO₄ and the solvent removed *in vacuo*. The residue was purified by silica gel chromatography (0-5% MeOH in DCM with 0.5% NH₄OH_(aq)) to give the title compound as a white solid (2.6 g, 69%).

¹H NMR (500 MHz, d₆-DMSO) δ 8.96 (s, 1H, H2'), 8.51 (m, 1H, NH), 7.37 (m, 4H, H2 and H3), 5.10 (s, 1H, 4''-OH), 4.36-4.19 (m, 4H, H2'', H4'' and 1-CH₂), 3.36 (m, 2H, H5''). 2.43 (s, 3H, 4'-CH₃), 1.95 (m, 2H, H3''), 1.39 and 1.23 (s, 9H, C(CH₃)₃). Rotamers present. **Lab reference** PM23 and PM25.

Data are in accordance with those reported previously in literature¹²³.

***tert*-butyl (2-(((3-(4-hydroxyphenyl)-1-(tetrahydro-2H-pyran-2-yl)-1H-pyrazol-4-yl)methyl)(methyl)amino)ethyl)(methyl)carbamate (**11**)**



19 (2.3 g, 4.8 mmol, 1 eq), 4-hydroxybenzeneboronic acid pinacol ester (2.1 g, 9.5 mmol, 2 eq) and Cs₂CO₃ (4.7 g, 14.3 mmol, 3 eq) were dissolved in dioxane (15 mL) and water (1.5 mL). Pd(dppf)Cl₂ (170 mg, 0.2 mmol, 0.05 eq) was then added and the resulting mixture heated overnight at 100°C. The resulting solution then was cooled to room temperature, diluted with water and extracted with DCM (x3). The combined organic layers were washed with water, dried with Na₂SO₄ and the solvent removed *in vacuo*. The residue was purified by automated column chromatography (C18 Gold, 5-95% MeCN in 0.1 M NH₄OH_(aq) over 40 CV) to give a dark brown solid (1.75 g, 83%).

¹H NMR (400 MHz, d₆-DMSO) δ 9.42 (s, 1H, 14-OH), 7.75 (s, 1H, H15), 7.63 (d, *J*=8.3 Hz, 2H, H12), 6.79 (d, *J*=8.5 Hz, 2H, H13), 5.34 (dd, *J*=9.5 and 2.1 Hz, 1H, H16), 3.92 and 3.62 (m, 2H, H20), 3.32 (s, 2H, H8), 3.28 (m, 2H, H5), 2.74 and 2.72 (s, 3H, H4), 2.46 (t, *J*=6.3 Hz, 2H, H6), 2.16 (s, 3H, H7), 2.10-2.07 (m, 1H, H17), 1.95-1.89 (m, 2H, H17 and H18), 1.69-1.64 (m, 1H, H18), 1.56-1.50 (m, 2H, H19), 1.36 and 1.34 (s, 9H, H1). Rotamers present. **¹³C NMR (100.6 MHz, d₆-DMSO)** δ 156.8 (C14), 154.7

(C3), 149.6 (C10), 130.3 (C15), 128.9 (C12), 124.6 (C11), 115.2 (C9), 115.1 (C13), 86.7 (C16), 78.2 (C2), 66.8 (C20), 54.5 and 54.2 (C6), 52.3 (C8), 45.9 and 45.2 (C5) 41.2 (C7), 33.9 (C4), 29.8 (C17), 28.0 (C1), 24.6 (C19), 22.1 (C18). Rotamers present. **IR** (neat film, ν_{\max} , cm^{-1}) 3292 (br, w, -OH), 3087 (m, C-H aromatic), 2959 (m, C-H alkane), 1661 (s, C=O), 1622 (s, C=O), 1519 (s, C=C), 1083 (m, C-O-C cyclic ether). **HRMS (ESI)** m/z calcd for $\text{C}_{24}\text{H}_{36}\text{N}_4\text{O}_4$ $[\text{M}+\text{H}]^+$: 445.2809; found 445.2822. **Lab reference** PM79 (0.10 mmol, 77%), PM80 (0.78 mmol, 53%), PM96 (2.0 mmol, 37%), PM122 (4.8 mmol, 83%), PM166 (4.5 mmol, 45%), PM243 (1.5 mmol, 33%).

Ethyl 3-iodo-1*H*-pyrazole-4-carboxylate (**12**)

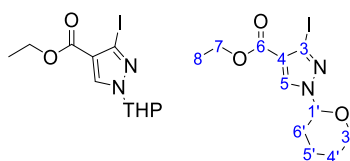


Ethyl 3-amino-1*H*-pyrazole-4-carboxylate (2.5 g, 16.1 mmol, 1 eq) was added portionwise to a solution of $\text{H}_2\text{SO}_{4(\text{aq}, 95-99\%)}$ (5.3 mL) in water (4.4 mL) at 0°C . The mixture was stirred at 0°C for 30 min. A solution of NaNO_2 (1.7 g, 24.2 mmol, 1.5 eq) in water (7.4 mL) was added dropwise at 0°C , and the mixture was stirred at 0°C for an additional hour. Next a solution of KI (5.4 g, 32.3 mmol, 2 eq) in water (7.4 mL) was added dropwise at 0°C . The mixture was stirred at room temperature overnight and then extracted with EtOAc (x3) and the combined organic layers were washed with $\text{Na}_2\text{SO}_{3(\text{aq}, \text{saturated})}$ (x3) and brine. The resulting organic layer was dried with Na_2SO_4 and the solvent removed *in vacuo* to give the title compound as a yellow solid (3.7 g, 87%).

^1H NMR (500 MHz, $\text{d}_6\text{-DMSO}$) δ 13.76 (s, 1H, NH), 8.27 (s, 1H, H5), 4.21 (q, $J=7.1$ Hz, 2H, H7), 1.27 (t, $J=7.0$ Hz, 3H, H8). **Lab reference** PM12 (1.3 mmol, 61%), PM20 (16.1 mmol, 79%), PM49 (16.1 mmol, 87%), PM108 (16.1 mmol, 79%), PM110 (16.1 mmol, 91%), PM182 (16.1 mmol, 82%).

Data are in accordance with those reported previously in literature¹²⁸.

Ethyl 3-iodo-1-(oxan-2-yl)-1*H*-pyrazole-4-carboxylate (**13**)



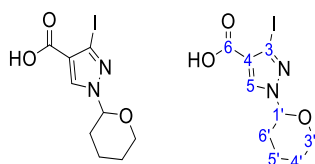
12 (7.2 g, 27.0 mmol, 1 eq) and TsOH (460 mg, 2.7 mmol, 0.1 eq) were dissolved in THF (40 mL). 3,4-dihydro-*H*-pyran (7.4 mL, 81.2 mmol, 3 eq) was added dropwise at 0°C and the resulting solution

stirred overnight at room temperature. The solvent was then removed *in vacuo* and the residue diluted with water and extracted with EtOAc (x2). The combined organic layers were washed with brine (x2), dried with Na₂SO₄ and the solvent removed *in vacuo*. The residue was purified by silica gel chromatography (0-15% EtOAc in PE) to give the title compound as an orange oil (7.4 g, 78%).

¹H NMR (500 MHz, d₆-DMSO) δ 8.40 (s, 1H, H5), 5.45 (dd, *J*=10.0 and 2.4 Hz, 1H, H1'), 4.22 (q, *J*=7.0 Hz, 2H, H7), 3.94-3.90 and 3.63-3.58 (m, 2H, H3'), 2.11-2.03 (m, 1H, H6'), 1.92-1.87 (m, 2H, H6' and H5'), 1.68-1.59 (m, 1H, H5'), 1.55-1.50 (m, 2H, H4'), 1.27 (t, *J*=7.0 Hz, 3H, H8). **Lab reference** PM14 (0.8 mmol, 27%), PM22 (12.7 mmol, 65%), PM53 (27.0 mmol, 78%), PM113 (37.5 mmol, 83%), PM185 (26.3 mmol, 51%).

Data are in accordance with those reported previously in literature¹²⁸.

3-iodo-1-(tetrahydro-2H-pyran-2-yl)-1H-pyrazole-4-carboxylic acid (14)

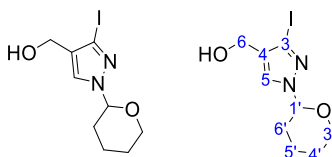


13 (3.0 g, 8.6 mmol, 1 eq) was dissolved in THF (6 mL) and methanol (6 mL). LiOH (600 mg, 25.7 mmol, 3 eq) in water (4.5 mL) was added dropwise with stirring at 0°C and the resulting solution stirred overnight at room temperature. The solvent was removed *in vacuo* and the residue diluted with HCl_(aq, 1M) and extracted with DCM (x3). The combined organic layers were washed with water, dried with Na₂SO₄ and the solvent removed *in vacuo* to give the title compound as a white solid (2.4 g, 87%).

¹H NMR (500 MHz, d₆-DMSO) δ 12.59 (s, 1H, 6-COOH) 8.32 (s, 1H, H5), 5.43 (dd, *J*= 2.4 and 10.0 Hz, 1H, H1'), 3.92 and 3.64-3.58 (m 2H, H3'), 2.12-2.02 (m, 1H, H6'), 1.94-1.86 (m, 2H, H6' and H5'), 1.68-1.58 (m, 1H, H5'), 1.55-1.49 (m, 2H, H4'). **Lab reference** PM28 (0.1 mmol, 82%), PM33 (0.7 mmol, 78%), PM56 (8.6 mmol, 87%), PM67 (12.8 mmol, 93%), PM114 (30.9 mmol, 86%), PM192 (13.4 mmol, 53%).

Data are in accordance with those reported previously in literature¹²⁸.

3-iodo-1-(oxan-2-yl)-1H-pyrazol-4-yl]methanol (15)

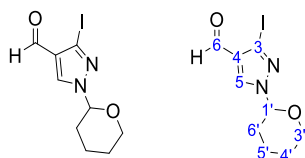


To **14** (2.3 g, 7 mmol, 1 eq) was added a 1M solution of BH_3 in THF (35 mL, 35 mmol, 5 eq) dropwise at 0°C and the resulting solution was stirred overnight at room temperature. The resulting mixture was quenched with $\text{NH}_4\text{Cl}_{(\text{aq, saturated})}$, diluted with water and extracted with EtOAc (x3). The combined organic layers were washed with brine, dried with Na_2SO_4 and the solvent removed *in vacuo* to give the title compound as a pale yellow oil (2.2 g, 96%).

$^1\text{H NMR}$ (500 MHz, $\text{d}_6\text{-DMSO}$) δ 7.73 (s, 1H, H5), 5.35 (dd, $J=10.1$ and 2.5 Hz, 1H, H1'), 4.91 (t, $J=5.2$ Hz, 6-OH), 4.20 (d, $J=5.0$ Hz, 2H, H6), 3.91-3.87 and 3.62-3.57 (m, 2H, H3'), 2.07-2.00 (m, 1H, H6'), 1.93-1.83 (m, 2H, H6' and H5'), 1.68-1.59 (m, 1H, H5'), 1.53-1.46 (m, 2H, H4'). **Lab reference** PM38 (0.3 mmol, 107%), PM44 (1.3 mmol, 200%), PM51 (0.3 mmol, 99%), PM57 (7.0 mmol, 96%), PM68 (11.8 mmol, 92%), PM117 (26.5 mmol, quantitative), PM196 (7.1 mmol, 89%).

Data are in accordance with those reported previously in literature¹²⁸.

3-iodo-1-(oxan-2-yl)-1H-pyrazole-4-carbaldehyde (**16**)

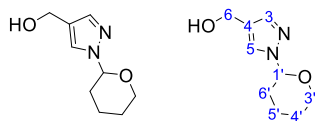


To a solution of **15** (2.1 g, 6.7 mmol, 1 eq) in DCM (15 mL) was added MnO_2 (2.9 g, 33.5 mmol, 5 eq) and the resulting mixture was stirred overnight at 50°C . The solids were filtered off and the filtrate was concentrated *in vacuo*. The resulting solid was resuspended in DCM and the resulting mixture filtered through celite and the filtrate concentrated *in vacuo*. The residue was purified by silica gel chromatography (0-4% MeOH in DCM) to give the title compound as an orange oil (1.7 g, 85%).

$^1\text{H NMR}$ (500 MHz, $\text{d}_6\text{-DMSO}$) δ 9.69 (1H, s, COH), 8.56 (s, 1H, H5), 5.49 (dd, $J=9.7$ and 2.5 Hz, 1H, H1'), 3.95-3.90 and 3.66-3.61 (m, 2H, H3'), 2.09-2.01 (m, 1H, H6'), 1.95-1.89 (m, 2H, H6' and H5'), 1.69-1.60 (m, 1H, H5'), 1.56-1.51 (m, 2H, H4'). **Lab reference** PM46 (1.3 mmol, 45%), PM58 (6.7 mmol, 85%).

Data are in accordance with those reported previously in literature¹²⁸.

1-(oxan-2-yl)-1H-pyrazol-4-yl]methanol (**17**)

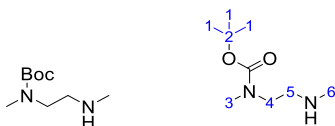


To a solution of **13** (100 mg, 0.3 mmol, 1 eq) in DCM (1.5 mL) was added diisobutylaluminium hydride solution (1M in heptanes, 0.9 mL, 0.9 mmol, 3 eq) dropwise at -78°C . The resulting solution was stirred at -78°C for 3 hr before the reaction was quenched with $\text{HCl}_{(\text{aq}, 1\text{M})}$ (3 mL) and allowed to reach room temperature. The resulting mixture was diluted with $\text{HCl}_{(\text{aq}, 1\text{M})}$ and extracted with DCM (x3). The combined organic layers were washed with water, dried with Na_2SO_4 and the solvent removed *in vacuo* to give the title compound as a colourless oil (22 mg, 41%).

^1H NMR (500 MHz, d_6 -DMSO) δ 7.72 (s, 1H, H5), 7.39 (s, 1H, H3), 5.33 (dd, $J=10.1$ and 2.5 Hz, 1H, H1'), 4.35 (s, 2H, H6), 3.9-3.88 and 3.63-3.57 (m, 2H, H3'), 2.09-2.01 (m, 1H, H6'), 1.94-1.84 (m, 2H, H6' and H5'), 1.69-1.60 (m, 1H, H5'), 1.54-1.49 (m, 2H, H4'). 6-OH not identified. **Lab reference** PM31 (0.3 mmol, 44%), PM32 (0.3 mmol, 41%).

Data are in accordance with those reported previously in literature²⁴².

N-(tert-butoxycarbonyl)-*N*-methyl-2-(methylamino)ethylamine (**18**)



To a solution of methyl[2-(methylamino)ethyl]amine (6 mL, 55.8 mmol, 4 eq) in DCM (20 mL) was added Boc_2O (3.0 g, 13.8 mmol, 1 eq) in DCM (20 mL) dropwise at 0°C . The resulting solution was stirred for 3 hr at room temperature. The solvent was then removed *in vacuo* and the residue diluted with water and subsequently extracted with EtOAc (x3). The combined organic layers were washed with brine (x2), dried with Na_2SO_4 and the solvent removed *in vacuo* to give the title compound as a colourless oil (2.7 g, quantitative yield).

^1H NMR (500 MHz, d_6 -DMSO) δ 3.18 (t, $J=6.7$ Hz, 2H, H4), 2.77 (s, 3H, H3), 2.55 (t, $J=6.7$ Hz, 2H, H5), 2.26 (s, 3H, H6), 1.38 (s, 9H, H1). 6-NH not identified. **Lab reference** PM59 (9.3 mmol, 91%), PM73 (14.0 mmol, quantitative), PM115 (25.6 mmol, 91%), PM160 (34.5 mmol, 93%).

Data are in accordance with those reported previously in literature²⁴³.

tert-butyl (2-((3-iodo-1-(tetrahydro-2H-pyran-2-yl)-1H-pyrazol-4-yl)methyl)(methyl)amino)ethyl (methyl)carbamate (19)

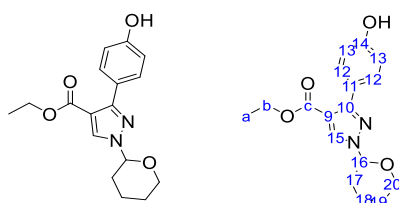


To a solution of **16** (1.0 g, 3.3 mmol, 1 eq) in DCM (20 mL) was added PBr_3 (780 μL , 9.8 mmol, 3 eq) dropwise at 0°C . The solution was stirred at room temperature for 3 hr. The reaction was quenched with $\text{NH}_4\text{Cl}_{(\text{aq, saturated})}$ and extracted with DCM (x5). The combined organic layers were washed with brine, dried with Na_2SO_4 and the solvent removed *in vacuo* to give intermediate product **20** as a pale yellow oil (750 mg). Intermediate product **20** (750 mg), **18** (1.2 g, 6.6 mmol, 2 eq) and K_2CO_3 (450 mg, 3.3 mol, 1 eq) were dissolved in DMF (20 mL) and stirred overnight at room temperature. The resulting mixture was diluted with water and extracted with EtOAc (x2). The combined organic layers were washed with brine, dried with Na_2SO_4 and the solvent removed *in vacuo*. The residue was purified by silica gel chromatography (0-4% MeOH in DCM) to give the title compound as a pale yellow oil (790 mg, 50% over two steps).

^1H NMR (500 MHz, $\text{d}_6\text{-DMSO}$) δ 7.70 and 7.69 (s, 1H, H15), 5.34 (dd, $J=10.3$ and 2.3 Hz, 1H, H16), 3.90-3.57 (m, 2H, H20), 3.25 (m, 4H, H8 and H5), 2.77 and 2.73 (s, 3H, H4), 2.40 (t, $J=6.7$ Hz, 2H, H6), 2.15 and 2.13 (s, 3H, H7), 2.07- 2.00 (m, 1H, H17), 1.91 -1.85 (m, 2H, H17 and H18), 1.65-1.60 (m, 1H, H18), 1.52 -1.48 (m, 2H, H19), 1.38 and 1.35 (s, 9H, H1). Rotamers present. **Lab reference** PM71 (0.7 mmol, 24%), PM74 (3.3 mmol, 50%), PM92 (5.0 mmol, 48%), PM120 (15.4 mmol, 31%), PM161 (9.4 mmol, 49%), PM207 (6.3 mmol, 24%).

Data are in accordance with those reported previously in literature¹²⁸.

Ethyl 3-(4-hydroxyphenyl)-1-(tetrahydro-2H-pyran-2-yl)-1H-pyrazole-4-carboxylate (22)

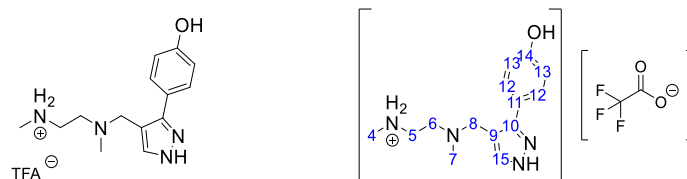


13 (100 mg, 0.3 mmol 1 eq), 4-hydroxybenzeneboronic acid pinacol ester (130 mg, 0.6 mmol, 2 eq), Cs_2CO_3 (280 mg, 0.9 mmol, 3 eq) and $\text{Pd}(\text{dppf})\text{Cl}_2$ (11 mg, 0.02 mmol, 0.05 eq) were dissolved in dioxane (2 mL) and water (0.2 mL) and heated overnight at 100°C . The resulting solution then was

cooled to room temperature, diluted with water and extracted with EtOAc (x3). The combined organic layers were washed with brine, dried with Na₂SO₄ and the solvent removed *in vacuo*. The residue was purified by silica gel chromatography (0-3% MeOH in DCM) to give a brown oil (72 mg, 78%).

¹H NMR (500 MHz, d₆-DMSO) δ 9.59 (s, 1H, 14-OH), 8.42 (s, 1H, H15), 7.56 (d, *J*=8.6 Hz, 2H, H12), 6.78 (d, *J*=8.4 Hz, 2H, H13), 5.46 (d, *J*=2.0 and 10.0 Hz, 1H, H16), 4.17 (q, *J*=7.1 Hz, 2H, Hb), 3.96-3.94 and 3.66-3.61 (m, 2H, H20), 2.15-2.08 (m, 1H, H17), 1.96-1.91 (m, 2H, H17 and H18), 1.68-1.64 (m, 1H, H18), 1.57-1.53 (m, 2H, H19), 1.23 (t, *J*=7.1 Hz, 3H, Ha). **¹³C NMR (125 MHz, d₆-DMSO)** δ 162.5 (Cc), 157.4 (C14), 151.4 (C10), 134.7 (C15), 130.2 (C12), 123.0 (C11), 114.5 (C13), 110.6 (C9), 86.9 (C16), 67.0 (C20), 59.6 (Cb), 29.5 (C17), 24.5 (C19), 21.8 (C18), 14.2 (Ca). **IR** (neat film, *v*_{max}, cm⁻¹) 3336 (br, m, -OH), 2942 (m, C-H aromatic), 2865 (m C-H alkane), 1680 (s, C=O), 1518 (m, C=C). **HRMS** *m/z* calcd for C₁₇H₂₀N₂O₄ [M+H]⁺: 317.1496; found 317.1505. **Lab reference** PM39.

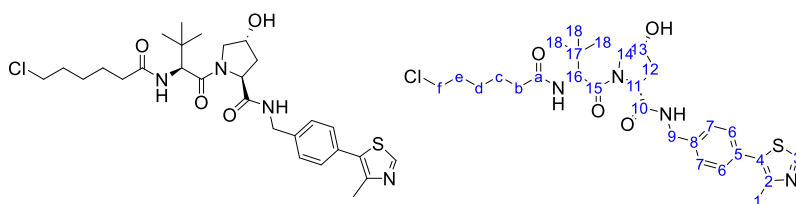
4-(4-((methyl(2-(methylamino)ethyl)amino)methyl)-1H-pyrazol-3-yl)phenol (23)



11 (37 mg, 0.08 mmol, 1 eq) was diluted in MeOH (1 mL) and HCl_(aq, 37%) (1 mL) was added dropwise and the mixture stirred at room temperature for 1 hr. The solvent was then removed *in vacuo* and the residue and purified by preparative HPLC (5-20% MeCN (0.05% TFA) in H₂O (0.1% TFA) over 10 min) and lyophilised to give the title compound as a pale orange solid (11.5 mg, 54%).

¹H NMR (500 MHz, d₆-DMSO) δ 10.30 and 9.82 (two br s, 2H, 13-OH and 15-NH), 8.87 (s, 2H, 4-NH₂⁺), 7.83 (s, 1H, H15), 7.37 (d, *J*=8.6 Hz, 2H, H12), 6.88 (d, *J*=6.8 Hz, 2H, H13), 4.33 (s, 2H, H8), 3.29 (m, 4H, H5 and H6), 2.63 (s, 3H, H4), 2.55 (s, 3H, H7). **¹³C NMR (125 MHz, d₆-DMSO)** δ 158.6 (q, ²*J*_{C-F} = 33.0 Hz, CF₃COO⁻), 157.9 (C14), 129.6 (C12), 116.5 (q, ¹*J*_{C-F} = 295.7 Hz, CF₃COO⁻), 115.7 (C13), 50.1 (C8), 49.3 and 42.5 (C5 and C6), 39.1 (C4), 32.6 (C7). Peaks indicated by HSQC δ 137.2 (C15). Peaks indicated by HMBC δ 147.1 (C10), 121.1 (C11), 105.4 (C9). **IR** (neat film *v*_{max}, cm⁻¹) 3199 (w, -OH), 2978 (w, C-H aromatic), 2687 (m, C-H alkane), 1781 (w), 1669 (s, -N-N- pyrazole), 1171 (s, C-N tertiary amine), 1127 (s, C-N secondary amine). **HRMS (ESI)** *m/z* calcd for C₁₄H₂₀N₄O[M+H]⁺: 261.1710; found 261.1732. **Lab reference** PM111 and PM151.

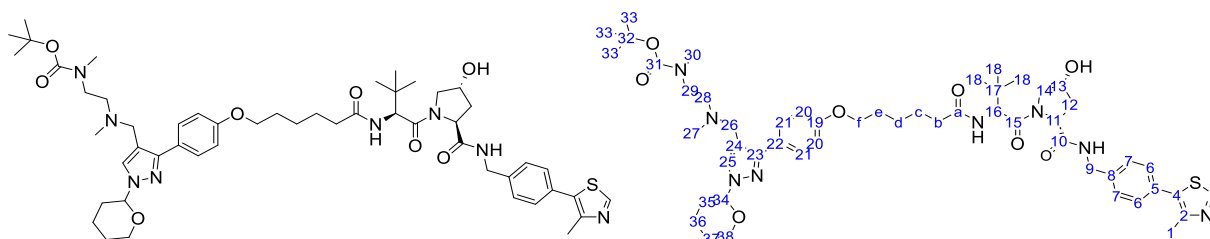
(2*S*,4*R*)-1-(((*S*)-2-(6-chlorohexanamido)-3,3-dimethylbutanoyl)-4-hydroxy-*N*-(4-(4-methylthiazol-5-yl)benzyl)pyrrolidine-2-carboxamide (24)



General method B was followed with VHL ligand **1** (150 mg, 0.28 mmol) and the linker 6-chlorohexanoic acid. The residue was then purified by silica gel chromatography (0-5% MeOH in DCM) and the product dissolved in DCM and washed with saturated Na₂HCO₃(aq), washed with water, dried with Na₂SO₄ and the solvent removed *in vacuo* to give the title compound as a white solid (161 mg, quantitative).

¹H NMR (500 MHz, d₆-DMSO) δ 8.98 (s, 1H, H3), 8.56 (t, *J*=6.0 Hz, 1H, 9-NH), 7.88 (d, *J*=7.9 Hz, 1H, 16-NH), 7.40 (m, 4H, H6 and H7), 5.12 (d, *J*=3.5 Hz, 1H, 13-OH), 4.54 (d, *J*=9.4 Hz, 1H, H16), 4.46-4.34 (m, 3H, H9 and H13), 4.22 (dd, *J*=15.9 and 5.5 Hz, 1H, H11), 3.69-3.64 (m, 2H, H14), 3.61 (m, 2H, Hf), 2.44 (s, 3H, H1), 2.30-2.23 and 2.16-2.09 (m, 2H, Hb), 2.05-2.01 and 1.92-1.87 (m, 2H, H12), 1.74-1.67 (m, 2H, He), 1.56-1.32 (m, 4H, Hc and Hd), 0.93 (s, 9H, H18). **¹³C NMR (125 MHz, CDCl₃)** δ 173.5 (Ca), 172.0 (C15), 170.9 (C10), 150.5 (C3), 148.6 (C2), 138.2 and 131.7 and 131.1 (C4, C5 and C8), 129.7 and 128.2 (C6 and C7), 70.1 (C13 or C16), 58.7 (C9), 57.6 (C13 or C16), 56.8 (C14), 44.9 (Cf), 43.4 (C11), 36.3 and 36.0 (Cb and C12), 35.1 (C17), 32.3 (Ce), 26.5 and 26.5 (C18 and Cd) 24.9 (Cc), 16.2 (C1). **IR** (neat film, ν_{max}, cm⁻¹) 3288 (br, w, OH), 2922 (s, C-H aromatic), 2858 (m, C-H aliphatic), 1623 (C=O). **HRMS (ESI)** *m/z* calcd for C₂₈H₃₉ClN₄O₄S [M+H]⁺: 263.2453; found 263.2453. **Lab reference** PM82 (0.14 mmol, 43%) and PM152 (0.28 mmol, quantitative).

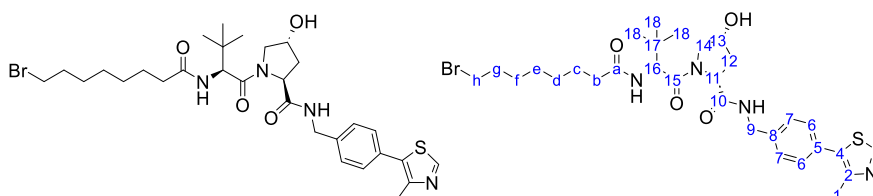
***tert*-butyl (2-(((3-(4-(((*S*)-1-((2*S*,4*R*)-4-hydroxy-2-((4-(4-methylthiazol-5-yl)benzyl)carbamoyl)pyrrolidin-1-yl)-3,3-dimethyl-1-oxobutan-2-yl)amino)-6-oxohexyl)oxy)phenyl)-1-(tetrahydro-2*H*-pyran-2-yl)-1*H*-pyrazol-4-yl)methyl)(methyl)amino)ethyl)(methyl)carbamate (25)**



PRMT1 ligand **11** (16 mg, 0.04 mmol, 1 eq), **24** (36 mg, 0.06 mmol, 1.8 eq), K₂CO₃ (17 mg, 0.13 mmol, 3.5 eq) and KI (2 mg, 0.01 mmol, 0.4 eq) were dissolved in MeCN (1 mL) and heated at 80°C for 5 days. The solvent was removed *in vacuo* and the residue purified by automated column chromatography (C18 Gold, 5-95% MeCN in H₂O over 45 CV) to give the title compound as a white solid (14 mg, 40%).

¹H NMR (500 MHz, d₆-DMSO) δ 8.98 (s, 1H, H3), 8.55 (t, *J*=6.1 Hz, 1H, 9-NH), 7.88 (d, *J*=9.4 Hz, 1H, 16-NH), 7.79 (s, 1H, H25), 7.75 (d, *J*=8.6 Hz, 2H, H21), 7.40 (m, 4H, H6 and H7), 6.94 (d, *J*=8.9 Hz, 2H, H20), 5.36 (dd, *J*=10.1 and 2.1 Hz, 1H, H34), 5.12 (br s, 1H, 13-OH), 4.55 (d, *J*=9.4 Hz, 1H, H16), 4.45-4.41 (m, 2H, H9), 4.35 (m, 1H, H13), 4.21 (dd, *J*=15.9 and 5.7 Hz, 1H, H11), 3.96 (t, *J*=6.5 Hz, 2H, Hf), 3.93 (d, *J*=12.4 Hz, 1H, H38), 3.69-3.60 (m, 3H, H38 and H14), 3.27 (m, 4H, H26 and H29), 2.74 and 2.72 (s, 3H, H30), 2.46 (m, 2H, H28), 2.44 (s, 3H, H1), 2.34-2.28 (m, 1H, Hb), 2.16-2.10 (m, 3H, H27 and Hb), 2.12-2.01 (m, 2H, H12 and H35), 1.96-1.87 (m, 3H, H12 and H35 and H36), 1.72-1.36 (m, 9H, H36, H37 and Hc-e), 1.36 and 1.33 (s, 9H, H33), 0.94 (s, 9H, H18). Rotamers present. **¹³C NMR (125 MHz, d₆-DMSO)** δ 172.0 (Ca), 171.9 (C10), 169.7 (C15), 158.1 (C19), 154.8 (C31), 151.4 (C3), 149.3 (C23), 147.7 (C2), 139.5 (C4 or C5 or C8), 131.2 (C25), 130.5 (C4 or C5 or C8), 129.6 (C4 or C5 or C8), 126.1 (C22), 128.8 (C21), 128.7 and 127.4 (C6 and C7), 115.4 (C24), 114.2 (C20), 86.7 (C34), 78.2 (C32), 68.9 (C13), 67.3 (Cf), 66.8 (C38), 58.7 (C9), 56.4 and 56.3 (C14 and C16), 54.4 (d, C28), 52.2 (d, C26 or C29), 45.6 (d, C26 or C29), 41.6 (C11), 41.0 (C27), 37.9 (C12 or C35), 35.2 (Cb), 34.8 (C17), 34.1 (C30), 29.8 (C12 or C35), 28.4 (C37), 28.0 (C33), 26.4 (C18), 25.2-24.6 (Cc-Ce), 22.1 (C36), 15.9 (C1). Rotamers present. **IR** (neat film, *v*_{max}, cm⁻¹) 3296 (br w, OH), 2961 (m, C-H aromatic), 2865 (m, C-H aliphatic), 1674 (s, C=O), 1630 (s, C=O), 108 (m, C-O-C cyclic ether). **HRMS (ESI)** *m/z* calcd for C₅₁H₇₄N₈O₈S [M+H]⁺: 971.5423; found 971.5425. **Lab reference** PM84 (0.02 mmol, 36%), PM91 (0.06 mmol, 40%), PM153 (0.25 mmol, 27%).

(2*S*,4*R*)-1-((*S*)-2-(8-bromooctanamido)-3,3-dimethylbutanoyl)-4-hydroxy-*N*-(4-(4-methylthiazol-5-yl)benzyl)pyrrolidine-2-carboxamide (26c)

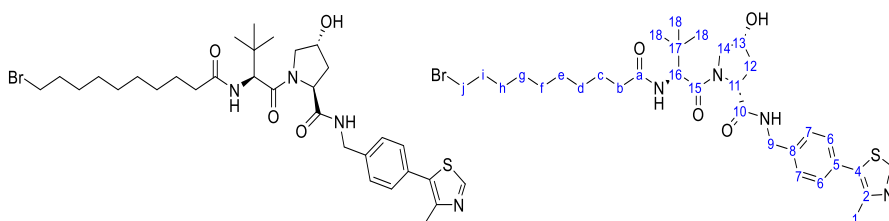


General method B was followed with VHL ligand **1** (150 mg, 0.28 mmol) and the linker 8-bromooctanoic acid. The reaction was stirred for 3 hr. The residue was then purified by silica gel

chromatography (0-5% MeOH in DCM). The product was dissolved in DCM and washed with saturated $\text{Na}_2\text{HCO}_3(\text{aq})$ (x2), washed with water, dried with Na_2SO_4 and the solvent removed *in vacuo* to give a colourless solid (54 mg, 30%).

^1H NMR (500 MHz, d_6 -DMSO) δ 8.98 (s, 1H, H3), 8.55 (t, $J=6.0$ Hz, 1H, 9-NH), 7.84 (d, $J=9.4$ Hz, 1H, 16-NH), 7.40 (dd, $J=9.1$ and 9.0 Hz, 4H, H6 and H7), 5.12 (br s, 1H, 13-OH), 4.54 (d, $J=9.4$ Hz, 1H, H16), 4.46-4.34 (m, 3H, H9 and H13), 4.21 (dd, $J=15.8$ and 5.5 Hz, 1H, H11), 3.69-3.62 (m, 2H, H14), 3.51 (t, $J=6.7$, 2H, Hh), 2.44 (s, 3H, H1), 2.29-2.08 (m, 2H, Hb), 2.05-2.01 and 1.92-1.87 (m, 2H, H12), 1.80-1.74 (m, 2H, Hg), 1.54-1.43 (m, 2H, Hc), 1.39-1.23 (m, 6H, Hd-f), 0.93 (s, 9H, H18). **^{13}C NMR (125 MHz, d_6 -DMSO)** δ 172.0 (Ca), 171.9 (C15), 169.7 (C10), 151.4 (C3), 147.7 (C2), 139.5 and 131.2 and 129.6 (C4, C5 and C8), 128.6 and 127.4 (C6 and C7), 68.8 (C13 or C16), 58.7 (C9), 56.3 and 53.3 (C13 or C16 and C14), 41.6 (C11), 37.9 (C12), 35.20 and 35.17 and 34.8 (Cb, Ch and C17), 32.2 (Cg), 28.4-27.4 (Cd-f), 26.4 (C18), 25.3 (Cc), 15.9 (C1). **IR** (neat film, ν_{max} , cm^{-1}) 3299 (br m, OH), 3071, 2928 (m, C-H aromatic), 2857 (C-H aliphatic), 1659 (m, C=O), 1622 (s, C=O), 1531 (m, C=O). **HRMS (ESI)** m/z calcd for $\text{C}_{30}\text{H}_{43}\text{BrN}_4\text{O}_4\text{S}$ $[\text{M}+\text{H}]^+$: 635.2261; found 635.2269. **Lab reference** PM86.

(2S,4R)-1-((S)-2-(10-bromodecanamido)-3,3-dimethylbutanoyl)-4-hydroxy-N-(4-(4-methylthiazol-5-yl)benzyl)pyrrolidine-2-carboxamide (26d)

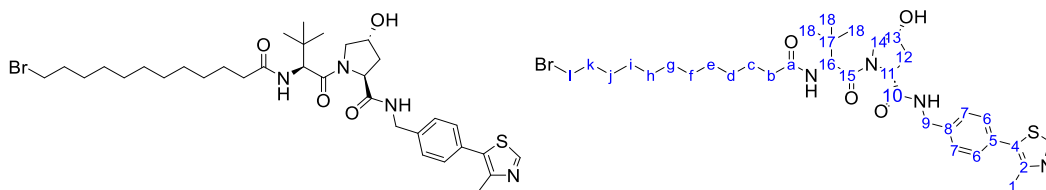


General method B was followed with VHL ligand **1** (100 mg, 0.19 mmol) and the linker 10-bromodecanoic acid. The residue was then purified by flash column chromatography (C18 Gold, 5-95% MeCN in 1% $\text{HCOOH}(\text{aq})$ over 40 CV) to give a colourless oil (98 mg, 78%).

^1H NMR (500 MHz, d_6 -DMSO) δ 8.98 (s, 1H, H3), 8.55 (t, $J=6.1$ Hz, 1H, 9-NH), 7.83 (d, $J=9.4$ Hz, 1H, 16-NH), 7.40 (m, 4H, H6 and H7), 5.12 (br s, 1H, 13-OH), 4.54 (d, $J=9.4$ Hz, 1H, H16), 4.43 (m, 2H, H9), 4.35 (m, 1H, H13), 4.21 (dd, $J=15.8$ and 5.5 Hz, 1H, H11), 3.66 (m, 2H, H14), 3.50 (m, 2H, Hj), 2.44 (s, 3H, H1), 2.27-2.23 and 2.13-2.21 (m, 2H, Hb), 2.05-2.00 and 1.92-1.88 (m, 2H, H12), 1.78 (m, 2H, Hi), 1.48 (m, 2H, Hc), 1.38 (m, 2H, Hh), 1.25 (m, 8H, Hd-Hg), 0.93 (s, 9H, H18). **^{13}C NMR (125 MHz, d_6 -DMSO)** δ 172.1 (Ca), 171.9 (C10), 169.7 (C15), 151.4 (C3), 147.7 (C2), 139.5 and 131.2 and 129.6 (C4, C5 and C8), 128.6 and 127.4 (C6 and C7), 68.9 and 58.7 (C9 and C13), 56.3 and 26.3 (C16 and C14), 41.8 (C11), 37.9 (C12), 35.21 and 35.17 (Cb and Cj), 34.9 (C17), 32.2 (Ci), 28.8-28.0 (Cd-Cg), 27.5 (Ch),

26.4 (C18), 25.4 (Cc), 15.9 (C1). IR (neat film, ν_{\max} , cm^{-1}) 3301 (br w, OH), 2925 (m, C-H aromatic), 2854 (w, C-H aliphatic), 1665 (s, C=O), 1621 (s, C=O). HRMS (ESI) m/z calcd for $\text{C}_{32}\text{H}_{47}\text{BrN}_4\text{O}_4\text{S}$ $[\text{M}+\text{H}]^+$: 663.2574; found 223.2564. Lab reference PM228.

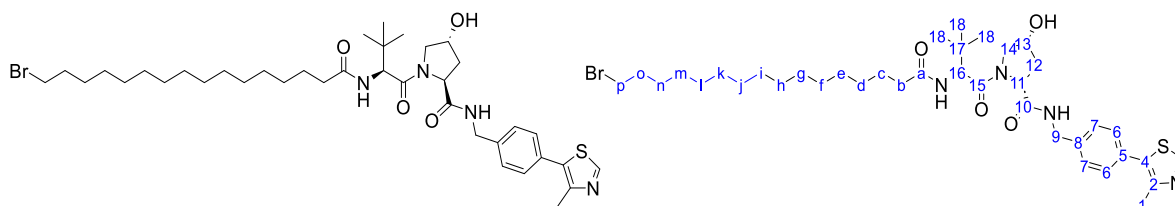
(2S,4R)-1-((S)-2-(12-bromododecanamido)-3,3-dimethylbutanoyl)-4-hydroxy-N-(4-(4-methylthiazol-5-yl)benzyl)pyrrolidine-2-carboxamide (26e)



General method B was followed with VHL ligand **1** (100 mg, 0.19 mmol) and the linker 12-bromododecanoic acid. The residue was then purified by flash column chromatography (C18 Gold, 5-95% MeCN in 1% $\text{HCOOH}_{(\text{aq})}$ over 40 CV) to give a pale yellow oil (106 mg, 81%).

^1H NMR (500 MHz, CDCl_3) δ 8.68 (s, 1H, H3), 7.40 (t, $J=8.0$ Hz, 1H, 9-NH), 7.31 (m, 4H, H6 and H7), 6.56 (d, $J=9.0$ Hz, 1H, 16-NH), 4.63 (t, $J=8.0$ Hz, 1H, H9), 4.56-4.48 (m, 3H, H13 and H16), 4.29 (dd, $J=15.1$ and 5.3 Hz, 1H, H11), 4.02 and 3.63 (m, 2H, H14), 3.36 (m, 2H, H1), 2.47 (s, 3H, H1), 2.37-2.31 (m, 1H, H12), 2.19-2.08 (m, 3H, H12 and Hb), 1.81 (m, 2H, Hk), 1.56-1.52 (m, 2H, Hc), 1.37 (m, 2H, Hj), 1.23 (m, 12H, Hd-Hi), 0.92 (s, 9H, H18). 13-OH not identified. ^{13}C NMR (125 MHz, CDCl_3) δ 174.2 (Ca), 171.8 (C15). 171.2 (C10), 150.6 (C3), 148.2 (C2), 138.3 and 131.8 and 130.8 (C4, C5 and C8), 129.5 and 128.0 (C6 and C7), 70.0 (C13 or C16), 59.0 (C9), 57.5 (C13 or C16), 57.0 (C14), 43.2 (C11), 36.5 and 36.4 (C12 and Cb), 35.3 (Cl), 32.8 and 32.8 (Ck and C17), 29.5-28.8 (Cd-Ci), 28.2 (Cj), 26.4 (C18), 25.7 (Cc), 15.9 (C1). IR (neat film, ν_{\max} , cm^{-1}) 3297 (br m, OH), 3076 (w), 2924 (s, C-H aromatic), 2852 (m, C-H aliphatic), 1619 (C=O). HRMS (ESI) m/z calcd for $\text{C}_{34}\text{H}_{51}\text{BrN}_4\text{O}_4\text{S}$ $[\text{M}+\text{H}]^+$: 691.2887; found 691.2894. Lab reference PM266.

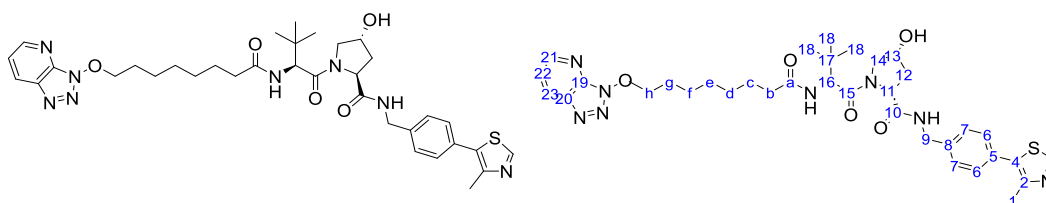
(2S,4R)-1-((S)-2-(16-bromohexadecanamido)-3,3-dimethylbutanoyl)-4-hydroxy-N-(4-(4-methylthiazol-5-yl)benzyl)pyrrolidine-2-carboxamide (26f)



General method B was followed with VHL ligand **1** (100 mg, 0.19 mmol) and the linker 16-bromohexadecanoic acid. The residue was then purified by flash column chromatography (C18 Gold, 5-95% MeCN in 1% HCOOH_(aq) over 40 CV) to give a yellow oil (119 mg, 84%).

¹H NMR (500 MHz, CDCl₃) δ 8.71 (s, 1H, H3), 7.37 (t, *J*=5.9 Hz, 1H, 9-NH), 7.31 (m, 4H, H6 and H7), 6.56 (d, *J*=8.9 Hz, 1H, 16-NH), 4.68 (t, *J*=7.9 Hz, 1H, H9), 4.56-4.51 (m, 3H, H13 and H16), 4.30 (dd, *J*=15.1 and 5.3 Hz, 1H, H11), 4.04 and 3.63 (m, 2H, H14), 3.37 (m, 2H, H_p), 2.47 (s, 3H, H₁), 2.41 (m, 1H, H₁₂), 2.17-2.10 (m, 3H, H₁₂ and H_b), 1.82 (m, 2H, H_o), 1.60-1.52 (m, 2H, H_c), 1.39 (m, 2H, H_n), 1.22 (m, 20H, H_d-H_m), 0.92 (s, 9H, H₁₈). 13-OH not identified. **¹³C NMR (125 MHz, CDCl₃)** δ 174.2 (Ca), 171.9 (C15), 171.1 (C10), 150.7 (C3), 148.2 (C2), 138.3 and 131.9 and 130.7 (C4, C5 and C8), 129.5 and 128.1 (C6 and C7), 70.0 (C13 or C16), 59.0 (C9), 57.5 (C13 or C16), 57.0 (C14), 43.2 (C11), 36.5 and 36.4 (C_b and C12), 35.3 (C_p), 34.1 and 32.9 (C_o and C17), 29.8-28.8 (C_d-C_m) 28.2 (C_n), 26.5 (C18), 25.8 (C_c), 15.9 (C1). **IR** (neat film, *v*_{max}, cm⁻¹) 3295 (br, m, OH), 3071 (w), 2922 (s, C-H aromatic), 2852 (m, C-H aliphatic), 1710 (s, C=O), 1620 (s, C=O), 1534 (m, C=O). **HRMS (ESI)** *m/z* calcd for C₃₈H₅₉BrN₄O₄S [M+H]⁺: 747.3513; found 747.3520. **Lab reference** PM261.

(2*S*,4*R*)-1-((*S*)-2-(8-((3*H*-[1,2,3]triazolo[4,5-*b*]pyridin-3-yl)oxy)octanamido)-3,3-dimethylbutanoyl)-4-hydroxy-*N*-(4-(4-methylthiazol-5-yl)benzyl)pyrrolidine-2-carboxamide (27c)

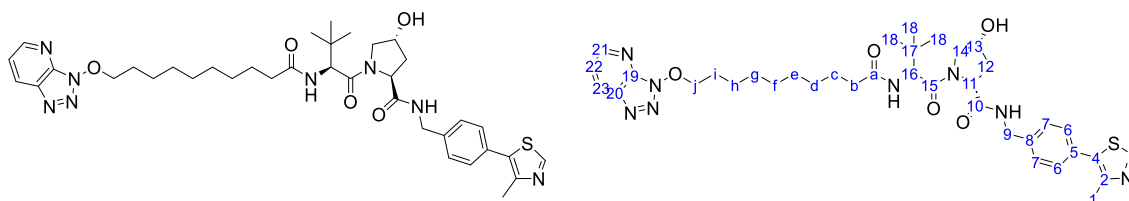


The reaction that yielded product **26c** also produced **27c** (64 mg, 33%).

¹H NMR (500 MHz, d₆-DMSO) δ 8.98 (s, 1H, H3), 8.81 (dd, *J*=1.4 and 4.4 Hz, 1H, H23), 8.61 (dd, *J*=1.4 and 8.4 Hz, 1H, H21), 8.54 (t, *J*=6.1 Hz, 1H, 9-NH), 7.83 (d, *J*=9.3 Hz, 1H, 16-NH), 7.57 (dd, *J*=8.4 and 4.4 Hz, H22), 7.42-7.37 (m, 4H, H6 and H7), 5.11 (d, *J*=3.5 Hz, 1H, 13-OH), 4.60 (t, *J*=6.5 Hz, 2H, H_h), 4.54 (d, *J*=9.4 Hz, 1H, H16), 4.43 (m, 2H, H9), 4.36 (m, 1H, H13), 4.21 (dd, *J*=15.9 and 5.5 Hz, 1H, H11), 3.68-3.65 (m, 2H, H14), 2.44 (s, 3H, H₁), 2.28-2.12 (m, 2H, H_b), 2.05-2.01 and 1.93-1.87 (m, 2H, H₁₂), 1.77-1.74 (m, 2H, H_g), 1.53-1.47 (m, 2H, H_c), 1.36-1.23 (m, 6H, H_d-f), 0.92 (s, 9H, H₁₈). **¹³C NMR (125 MHz, d₆-DMSO)** δ 172.1 (Ca), 171.9 (C15), 169.7 (C10), 151.8 (C23) 151.4 (C3), 147.7 (C2), 139.5 and 139.2 (C19 and C20), 134.5 and 131.1 and 129.6 (C4, C5 and C8), 129.4 (C21), 128.6 and 127.4 (C6 and C7), 121.2 (C22), 81.2 (Ch), 68.8 (C13 or C16), 58.7 (C9), 56.32 and 56.25 (C13 or C16 and C14), 41.6 (C11), 37.9 (C12), 35.2 (C_b), 34.8 (C17), 28.5-28.3 (C_d-f), 27.5 (C_g), 26.4 (C18), 25.3 (C_c), 15.9

(C1). IR (neat film, ν_{\max} , cm^{-1}) 2395 (br m, OH), 2923 (m, C-H aromatic), 2857 (w, C-H aliphatic), 1664 (s, C=O), 1626 (s, C=O), 1531 (s, N-O). HRMS (ESI) m/z calcd for $\text{C}_{35}\text{H}_{46}\text{N}_8\text{O}_5\text{S}$ $[\text{M}+\text{H}]^+$: 691.3385; found 691.3387. Lab reference PM86.

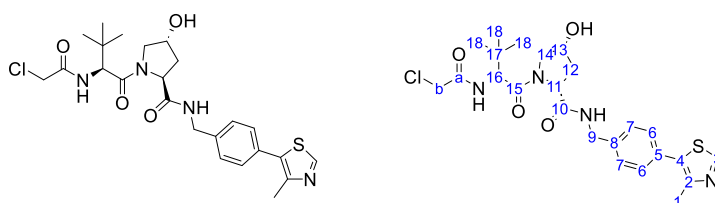
(2S,4R)-1-((S)-2-(10-((3H-[1,2,3]triazolo[4,5-b]pyridin-3-yl)oxy)decanamido)-3,3-dimethylbutanoyl)-4-hydroxy-N-(4-(4-methylthiazol-5-yl)benzyl)pyrrolidine-2-carboxamide (27d)



The reaction that yielded product **26d** also produced **27d** (19 mg, 14%).

^1H NMR (500 MHz, d_6 -DMSO) δ 8.98 (s, 1H, H3), 8.81 (dd, $J=4.4$ and 1.4 Hz, 1H, H23), 8.60 (dd, $J=8.4$ and 1.4 Hz, 1H, H21), 8.56 (t, $J=6.1$ Hz, 1H, 9-NH), 7.83 (d, $J=9.4$ Hz, 1H, 16-NH), 7.57 (dd, $J=8.4$ and 4.4 Hz, 1H, H22), 7.40 (m, 4H, H6 and H7), 5.13 (br s, 1H, 13-OH), 4.60 (t, $J=6.4$ Hz, 2H, Hj), 4.54 (d, $J=9.4$ Hz, 1H, H16), 4.42 (m, 2H, H9), 4.35 (m, 1H, H13), 4.21 (dd, $J=15.9$ and 5.5 Hz, 1H, H11), 3.66 (m, 2H, H14), 2.44 (3H, s, H1), 2.26 and 2.11 (m, 2H, Hb), 2.03 and 1.90 (m, 2H, H12), 1.76 (m, 2H, Hj), 1.53-1.21 (m, 14H, Hc-Hi), 0.93 (s, 9H, H18). LRMS (ESI) m/z calcd for $\text{C}_{37}\text{H}_{50}\text{N}_8\text{O}_5\text{S}$ $[\text{M}+\text{H}]^+$: 719.9; found 719.9. Lab reference PM228.

(2S,4R)-1-((S)-2-(2-chloroacetamido)-3,3-dimethylbutanoyl)-4-hydroxy-N-(4-(4-methylthiazol-5-yl)benzyl)pyrrolidine-2-carboxamide (28)

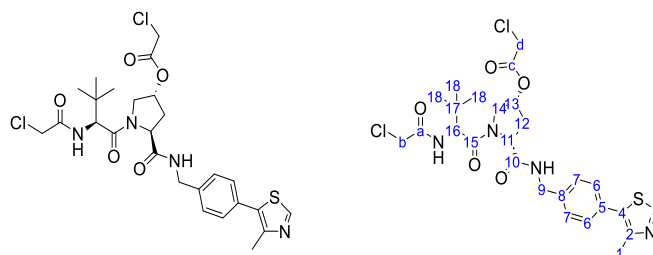


1 (150 mg, 0.28 mmol, 1 eq) was dissolved in DCM (1.4 mL) and TFA (1.4 mL) was added and the resulting mixture stirred at room temperature for 30 minutes. The solvent was removed *in vacuo*. To remove excess TFA, the residue was coevaporated with MeOH (x2) and toluene (x2). The residue was dissolved in DCM (3 mL) and triethyl amine (200 μL , 1.4 mmol, 5 eq) was added. The reaction was cooled to 0°C and chloroacetyl chloride (45 μL , 0.6 mmol, 2 eq) was added and the reaction stirred overnight at room temperature. The reaction was diluted with water and extracted with DCM (x3).

The combined organic layers were washed with water, dried with Na₂SO₄ and the solvent removed *in vacuo*. The residue was purified by silica gel chromatography (0-5% MeOH in DCM) to yield the title compound as an orange oil (75 mg, 52%).

¹H NMR (500 MHz, d₆-DMSO) δ 8.98 (s, 1H, H3), 8.60 (t, *J*=6.0 Hz, 1H, 9-NH), 8.29 (d, *J*=9.3 Hz, 1H, 16-NH), 7.43-7.38 (m, 4H, H6 and H7), 5.16 (d, *J*=3.5 Hz, 1H, 13-OH), 4.54 (d, *J*=9.4 Hz, 1H, H16), 4.43 (m, 2H, H9), 4.36 (m, 1H, H13), 4.23-4.15 (m, 3H, H11 and Hb), 3.68-3.61 (m, 2H, H14), 2.44 (s, 3H, H1), 2.08-2.01 and 1.92-1.88 (m, 2H, H12). 0.95 (s, 9H, H18). **¹³C NMR (125 MHz, d₆-DMSO)** δ 171.8 (C10), 168.9 (C15), 165.7 (Ca), 151.6 (C3), 147.7 (C2), 139.5 and 131.2 and 129.5 (C4, C5 and C8), 128.6 and 127.4 (C6 and C7), 68.9 and 58.7 (C9 and C13), 56.8 and 56.6 (C16 and C14), 42.5 and 41.7 (C11 and Cb), 37.9 (C17) 35.7 (C12), 26.2 (C18), 15.9 (C1). **IR** (neat film, *v*_{max}, cm⁻¹) 3665 (br w, OH), 2395 (br w, NH), 2974 (s, C-H aromatic), 2903 (m, C-H aliphatic), 1751 (m, C=O or C=N), 1660 (s, C=O), 1630 (s, C=O), 799 (m, C-Cl). **HRMS (ESI)** *m/z* calcd for C₂₄H₃₁ClN₄O₄S [M+H]⁺: 507.1827; found 507.1827. **Lab reference** PM98.

(3*R*,5*S*)-1-((*S*)-2-(2-chloroacetamido)-3,3-dimethylbutanoyl)-5-((4-(4-methylthiazol-5-yl)benzyl)carbamoyl)pyrrolidin-3-yl 2-chloroacetate (29)



The reaction that yielded product **28** also produced **29** as an oil (57 mg, 34%).

¹H NMR (500 MHz, d₆-DMSO) δ 8.98 (s, 1H, H3), 8.64 (t, *J*=6.0 Hz, 1H, 9-NH), 8.31 (d, *J*=8.5 Hz, 1H, 16-NH), 7.40 (m, 4H, H6 and H7), 5.38 (m, 1H, H13), 4.50 (t, *J*=8.4 Hz, 1H, H16), 4.56-4.332 (m, 4H, H9 and Hd), 4.25 (m, 1H, H11), 4.17 (dd, *J*=22.6 and 12.7 Hz, 2H, Hb), 4.04 and 3.84 (m, 2H, H14) 2.44 (s, 3H, H1), 2.35-2.22 (m, 2H, H12), 0.96 (s, 9H, H18). **LRMS (ESI)** *m/z* calcd for C₂₆H₃₃Cl₂N₄O₅S [M+H]⁺: 584.5; found 584.6.

2-(2-(2-(2-chloroethoxy)ethoxy)ethoxy)ethan-1-ol (30i)



General method C was followed with 12-crown-4 (200 μ L, 1.2 mmol) to give the title compound as a brown oil (189 mg, 75%).

$^1\text{H NMR}$ (500 MHz, d_6 -DMSO) δ 4.56 (t, $J=5.5$ Hz, 1H, a-OH), 3.72-3.70 (m, 2H, Hh), 3.68-3.66 (m, 2H, Hg), 3.55-3.52 (m, 8H, Hc-f), 3.50-3.47 and 3.42-3.40 (m, 4H, Ha and Hb). **Lab reference** PM119.

Data are in accordance with those reported in literature²⁴⁴.

2-[2-[2-[2-(2-chloroethoxy)ethoxy]ethoxy]ethoxy]ethoxy]ethanol (30j)



General method C was followed with 18-crown-6 (250 mg, 1.0 mmol) to give the title compound as a brown oil (154 mg, 54%).

$^1\text{H NMR}$ (400 MHz, d_6 -DMSO) δ 4.56 (t, $J=5.5$ Hz, 1H, a-OH), 3.73-3.65 (m, 4H, Hk and Hl), 3.58-3.51 (m, 16H, Hc-j), 3.45-3.46 and 3.43-3.40 (m, 4H, Ha and Hb). **Lab reference** PM107.

Data are in accordance with those previously reported in literature¹⁶².

2-(2-chloroethoxy)acetic acid (31g)



General method D was followed with 2-(2-chloroethoxy)ethanol (100 μ L, 0.9 mmol) to give the title compound as an oil (49 mg) which was used without further purification.

$^1\text{H NMR}$ (400 MHz, d_6 -DMSO) δ 12.68 (s, 1H, COOH), 4.07 (s, 2H, Hb), 3.74-3.66 (m, 4H, Hc and Hd).

Lab reference PM101.

Data are in accordance with those previously reported in literature²⁴⁵.

2-(2-(2-chloroethoxy)ethoxy)acetic acid (31h)



General method D was followed with 2-[2-(2-chloroethoxy)ethoxy]ethanol (180 μ L, 1.3 mmol) to give the title compound as a pale yellow oil (178 mg) which was used without further purification.

$^1\text{H NMR}$ (500 MHz, d_6 -DMSO) δ 12.59 (s, 1H, COOH), 4.03 (s, 2H, Hb), 3.73-3.66 (m, 4H, He and Hf), 3.60-3.58 (m, 4H, Hc and Hd). **Lab reference** PM127.

Data are in accordance with those previously reported in literature²⁴⁶.

2-(2-(2-(2-chloroethoxy)ethoxy)ethoxy)ethoxy)acetic acid (31i)



General method D was followed with **30i** (19 mg, 0.9 mmol) to give the title compound as an oil (35 mg) which was used without further purification.

$^1\text{H NMR}$ (500 MHz, d_6 -DMSO) δ 12.58 (s, 1H, COOH), 4.04 (d, $J=5.3$ Hz, 2H, Hb), 3.73-3.65 (m, 4H, Hh and Hg), 3.60-3.52 (m, 8H, Hc-f). **Lab reference** PM121.

Data are in accordance with those reported in literature²⁴⁷.

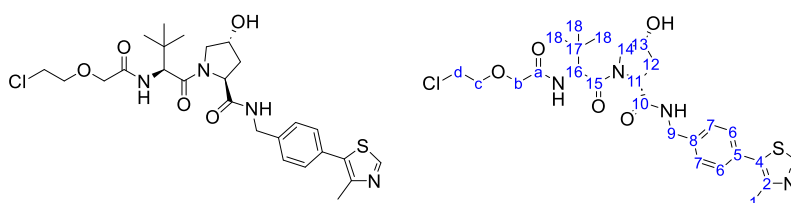
2-[2-[2-[2-[2-(2-chloroethoxy)ethoxy]ethoxy]ethoxy]ethoxy]ethoxy]acetic acid (31j)



General method D was followed with **30j** (118 mg, 0.4 mmol) to give the title compound as a pale yellow oil (47 mg) which was used without further purification.

$^1\text{H NMR}$ (500 MHz, d_6 -DMSO) δ 12.60 (s, 1H, COOH), 4.02 (d, $J=6.5$ Hz, 2H, Hb), 3.73-3.51 (m, 20H, Hc-l). **Lab reference** PM116 and PM198.

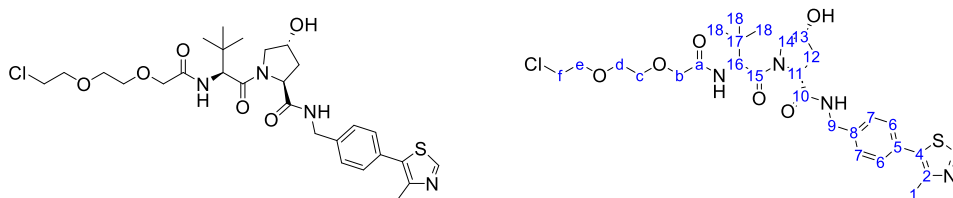
(2S,4R)-1-((S)-2-(2-(2-chloroethoxy)acetamido)-3,3-dimethylbutanoyl)-4-hydroxy-N-(4-(4-methylthiazol-5-yl)benzyl)pyrrolidine-2-carboxamide (32g)



General method B followed with VHL ligand **1** (150 mg, 0.28 mmol) and linker **31g**. The residue was then purified by automated column chromatography (C18 Gold, 5-95% MeCN in 1% CH₃COOH_(aq) over 40 CV) to give the title compound as a white solid (123 mg, 79%).

¹H NMR (500 MHz, d₆-DMSO) δ 8.98 (s, 1H, H3), 8.61 (t, *J*=6.0 Hz, 1H, 9-NH), 7.50 (d, *J*=9.6 Hz, 1H, 16-NH), 7.40 (m, 4H, H6 and H7), 5.15 (d, *J*=3.5 Hz, 1H, 13-OH), 4.57 (d, *J*=9.6 Hz, 1H, H16), 4.46-4.36 (m, 3H, H9 and H13), 4.24 (dd, *J*=15.8 and 5.5 Hz, 1H, H11), 4.03 (s, 2H, Hb), 3.81-3.74 (m, 4H, Hc and Hd), 3.64 (m, 2H, H14), 2.44 (s, 3H, H1), 2.08-2.04 and 1.93-1.88 (m, 2H, H12), 0.95 (s, 9H, H18). **¹³C NMR (125 MHz, d₆-DMSO)** δ 171.8 (C10), 169.1 (C15), 168.3 (Ca), 151.5 (C3), 147.7 (C2), 139.4 and 131.2 and 129.7 (C4, C5 and C8), 128.7 and 127.5 (C6 and C7), 70.9 (Cc), 67.3 (Cb), 68.9 and 58.8 (C9 and C13), 56.6 (C16), 43.6 (Cd), 41.6 (C11), 37.8 (C12), 35.8 (C17), 26.2 (C18), 15.9 (C1). **IR** (neat film, *v*_{max}, cm⁻¹) 3294 (br m, -OH), 2959 (m, C-H aromatic), 2861 (w, C-H aliphatic), 1661 (m, C=O), 1625 (s, C=O), 849 (s, C-Cl). **HRMS (ESI)** *m/z* calcd for C₂₆H₃₅ClN₄O₅S [M+H]⁺: 551.2089; found 501.2088. **Lab reference** PM99.

(2*S*,4*R*)-1-((*S*)-2-(2-(2-(2-chloroethoxy)ethoxy)acetamido)-3,3-dimethylbutanoyl)-4-hydroxy-*N*-(4-(4-methylthiazol-5-yl)benzyl)pyrrolidine-2-carboxamide (32h**)**

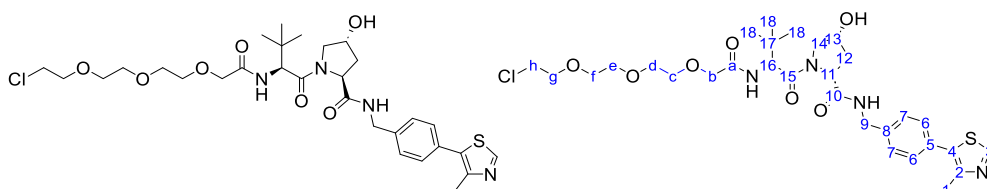


General method B followed with VHL ligand **1** (150 mg, 0.28 mmol) and linker **31h**. The residue was then purified by automated column chromatography (C18 Gold, 5-95% MeCN in 1% CH₃COOH_(aq) over 40 CV) to give the title compound as a white solid (113 mg, 67%).

¹H NMR (400 MHz, d₆-DMSO) δ 8.98 (s, 1H, H3), 8.59 (t, *J*=5.9 Hz, 1H, 9-NH), 7.42 (m, 1H, 16-NH), 7.40 (m, 4H, H6 and H7), 5.15 (br s, 1H, 13-OH), 4.57 (d, *J*=9.6 Hz, 1H, H16), 4.46-4.36 (m, 3H, H9 and H13), 4.24 (dd, *J*=15.8 and 5.6 Hz, 1H, H11), 3.98 (s, 2H, Hb), 3.79-3.60 (m, 10H, Hc-f and H14), 2.44 (s, 3H, H1), 2.08-2.03 and 1.93-1.87 (m, 2H, H12), 0.95 (s, 9H, H18). **¹³C NMR (101 MHz, d₆-DMSO)** δ 171.8 (C10), 169.1 (C15), 168.6 (Ca), 151.4 (C3), 147.7 (C2), 139.4 and 131.1 and 129.7 (C4, C5 and C8), 128.7 and 127.4 (C6 and C7), 70.6-69.4 (Cb-e), 68.9 and 58.7 (C9 and C13), 56.6 (C14), 55.7 (C16), 43.4 (Cf), 41.7 (C11), 37.9 (C12), 35.7 (C17), 26.1 (C18), 15.9 (C1). **IR** (neat film, *v*_{max}, cm⁻¹) 3295 (br m, -OH), 2919 (m, C-H aromatic), 2861 (w, C-H aliphatic), 1659 (m, C=O), 1626 (s, C=O), 849 (s, C-

Cl). **HRMS (ESI)** m/z calcd for $C_{28}H_{39}ClN_4O_5S$ $[M+H]^+$: 595.2352; found 595.2384. **Lab reference** PM128.

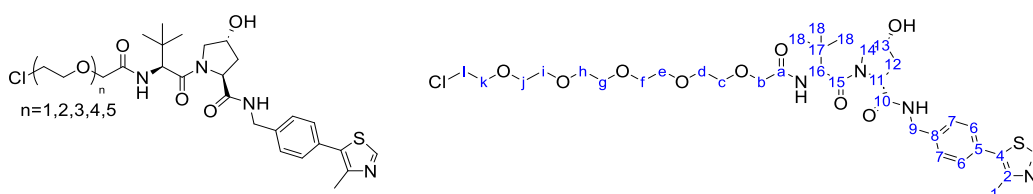
(2*S*,4*R*)-1-((*S*)-2-(*tert*-butyl)-14-chloro-4-oxo-6,9,12-trioxa-3-azatetradecanoyl)-4-hydroxy-*N*-(4-(4-methylthiazol-5-yl)benzyl)pyrrolidine-2-carboxamide (32i**)**



General method B followed with VHL ligand **1** (83 mg, 0.16 mmol) and linker **32i**. The residue was then purified by automated column chromatography (C18 Gold, 5-95% MeCN in 1% $CH_3COOH_{(aq)}$ over 40 CV) to give the title compound as a white solid (56 mg, 53%).

1H NMR (500 MHz, d_6 -DMSO) δ 8.98 (s, 1H, H3), 8.61 (m, 1H, 9-NH), 7.40 (m, 5H, 16-NH and H6 and H7), 5.16 (br s, 1H, 13-OH), 4.57 (d, $J=9.6$ Hz, 1H, H16), 4.45-4.35 (m, 3H, H9 and H13), 4.24 (m, 1H, H11), 4.03 and 3.97 (m, 2H, Hb), 3.80-3.57 (m, 14H, Hc-Hh and H14), 2.44 (s, 3H, H1), 2.08-2.03 and 1.93-1.88 (m, 2H, H12), 0.94 (s, 9H, H18). **^{13}C NMR (125 MHz, d_6 -DMSO)** δ 171.5 (C10), 169.1 (C15), 168.6 (Ca), 151.5 (C3), 147.7 (C2), 139.4 and 131.1 and 129.6 (C4, C5 and C8), 128.7 and 127.5 (C6 and C7), 70.9-69.3 (Cb-g), 68.9 and 58.7 (C9 and C13), 56.6 (C14), 55.7 (C16), 43.6 (Ch), 41.7 (C11), 37.9 (C12), 35.7 (C17), 26.2 (C18), 15.9 (C1). **IR** (neat film, ν_{max} , cm^{-1}) 3295 (br m, -OH), 2968 (m, C-H aromatic), 2909 (w, C-H aliphatic), 1661 (m, C=O), 1626 (s, C=O), 849 (s, C-Cl). **HRMS (ESI)** m/z calcd for $C_{30}H_{43}ClN_4O_7S$ $[M+H]^+$: 639.2614; found: 639.2628. **Lab reference** PM123.

(2*S*,4*R*)-1-((*S*)-2-(*tert*-butyl)-20-chloro-4-oxo-6,9,12,15,18-pentaoxa-3-azaicosanoyl)-4-hydroxy-*N*-(4-(4-methylthiazol-5-yl)benzyl)pyrrolidine-2-carboxamide (32j**)**

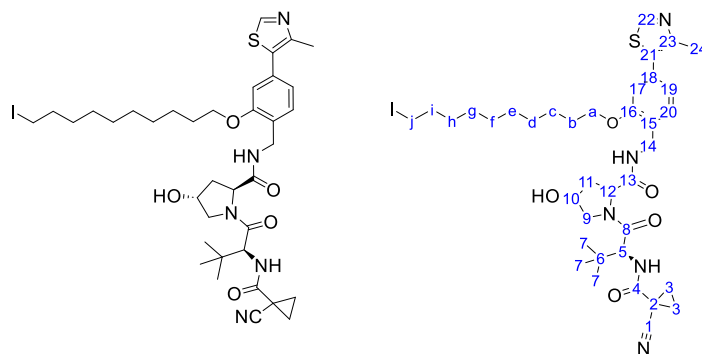


General method B followed with VHL ligand **1** (100 mg, 0.19 mmol) and linker **32j**. The residue was then purified by automated column chromatography (C18 Gold, 5-60% MeCN in 1% $CH_3COOH_{(aq)}$ over

40 CV) to give a white solid (65 mg) which was used without further purification (and likely contained a mixture of compounds).

¹H NMR (500 MHz, d₆-DMSO) δ 8.98 (s, 1H, H3), 8.61 (m, 1H, 9-NH), 7.46 (m, 1H, 16-NH), 7.40 (m, 4H, H6 and H7), 5.15 (d, *J*=3.4 Hz, 1H, 13-OH), 4.57 (d, *J*=9.6 Hz, 1H, H16), 4.46-4.36 (m, 3H, H9 and H13), 4.24 (dd, *J*=15.8 and 4.3 Hz, 1H, H11), 4.03, 3.98 and 3.97 (m, 2H, Hb), 3.38-3.57 (m, 9H, Hc-I and H14), 2.44 (s, 3H, H1), 2.07-2.04 and 1.92-1.90 (m, 2H, H12), 0.94 (s, 9H, H18). The Integrals for Hc-I do not add up to 20H likely due to a mixture of products. **HRMS (ESI)** *m/z* calcd for C₃₅H₅₁ClN₄O₉S [M+H]⁺: 727.3138; found: 727.3128. **Lab reference** PM105 and PM200.

(2*R*,4*R*)-1-((*S*)-2-(1-cyanocyclopropane-1-carboxamido)-3,3-dimethylbutanoyl)-4-hydroxy-*N*-(2-((10-iododecyl)oxy)-4-(4-methylthiazol-5-yl)benzyl)pyrrolidine-2-carboxamide (33)

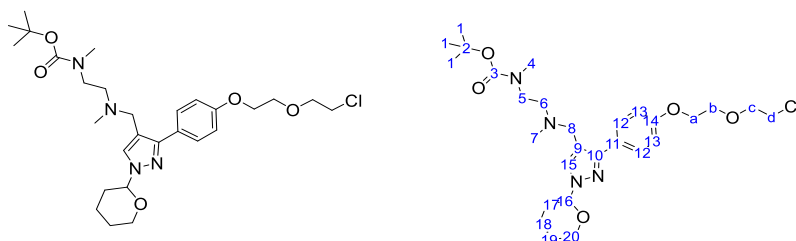


VHL ligand **2** (50 mg, 0.09 mmol, 1 eq) and Cs₂CO₃ (61 mg, 0.19 mmol, 2 eq) were dissolved in DMF (800 μL). 1,10-Diiododecane (330 mg, 0.28 mmol, 3 eq) in DMF (500 μL) was added and the reaction stirred overnight at room temperature. The crude reaction mixture was purified by automated column chromatography (C18 Gold, 5-95% MeCN in 0.1% HCOOH_(aq)) over 40 CV) to give the title compound as a colourless oil (40 mg, 53%).

¹H NMR (500 MHz, CDCl₃) δ 8.70 (s, 1H, H22), 7.33 (d, *J*=7.7 Hz, 1H, H20), 7.28 (m, 1H, 14-NH), 7.03 (d, *J*=8.4 Hz, 1H, 5-NH), 6.95 (dd, *J*=7.7 and 1.6 Hz, 1H, H19), 6.88 (d, *J*=1.5 Hz, 1H, H17), 4.74 (m, 1H, H12), 4.57 (m, 1H, H10), 4.55-4.52 and 4.44-4.40 (m, 2H, H14), 4.46 (d, *J*=8.5 Hz, 1H, H5), 4.02 (m, 2H, Ha), 3.91-3.90 and 3.65-3.62 (m, 2H, H9), 3.20 (m, 2H, Hj), 2.61-2.55 and 2.11-2.06 (m, 2H, H11), 2.54 (s, 3H, H24), 1.83 (m, 2H, Hi), 1.71-1.50 (m, 4H, H3), 1.41-1.31 (m, 14H, obs. 17H, Hb-Hh), 0.93 (s, 9H, H7). **¹³C NMR (125 MHz, CDCl₃)** δ 170.6 (C8), 170.4 (C13), 165.9 (C4), 157.0 (C16), 150.4 (C22), 148.5 (C23), 132.3 and 132.0 (C18 and C21), 129.4 (C20), 126.3 (C15), 121.5 (C19), 119.7 (C1), 112.2 (C17), 70.3 (C10), 68.3 (Ca), 58.50 and 58.48 (C5 and C12), 56.5 (C9), 38.9 (C14), 35.9 (C11), 33.6 (Ci), 30.6 (Ch), 29.6-29.3 (Cd, Ce, Cf, and Cg), 29.2 (Cb), 28.6 (C7), 26.3 (C6), 26.2 (Cc), 18.1 (C3), 16.2

(C24), 13.8 (C2), 7.5 (Cj). **IR** (neat film, ν_{\max} , cm^{-1}) 3393 (br m, NH amine), 3340 (br m, OH), 2925 (m, C-H aromatic), 2853 (m, C-H aliphatic), 2237 (2, C≡N nitrile), 1679 (s, C=O), 1627 (s, C=O), 593 (s, C-I). **HRMS (ESI)** m/z calcd for $\text{C}_{35}\text{H}_{52}\text{N}_5\text{O}_5\text{S}$ $[\text{M}+\text{H}]^+$: 806.2807; found 806.2812. **Lab reference** PM273.

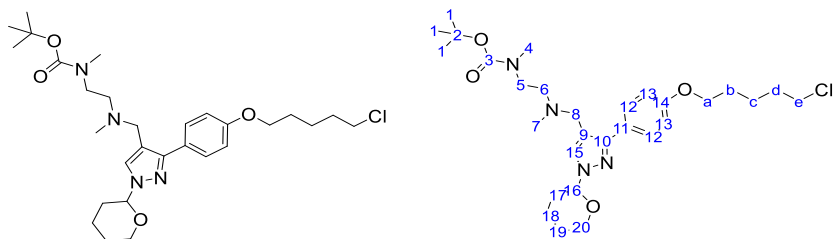
tert-butyl 2-(((3-(4-(2-(2-chloroethoxy)ethoxy)phenyl)-1-(tetrahydro-2H-pyran-2-yl)-1H-pyrazol-4-yl)methyl)(methyl)amino)ethyl)(methyl)carbamate (34)



General method E was followed with PRMT1 ligand **11** (100 mg, 0.23 mmol) and 2-(2-chloroethoxy)ethanol. The title compound was obtained as a white solid (67 mg, 54%).

^1H NMR (500 MHz, d_6 -DMSO) δ 7.81 (s, 1H, H15), 7.75 (d, $J=8.1$ Hz, 2H, H12), 6.98 (d, $J=8.8$ Hz, 2H, H13), 5.36 (dd, $J=9.8$ and 2.3 Hz, 1H, H16), 4.12 (m, 2H, Ha), 3.93 (m, 1H, H20), 3.81 (m, 2H, Hb), 3.75 (s, 4H, Hc and Hd), 3.63 (m, 1H, H20), 3.42 and 3.38 (s, 2H, H8), 3.29 (m, 2H, H5), 2.75 and 2.73 (s, 3H, H4), 2.51 (m, 2H, H6), 2.19 (s, 3H, H7), 2.12-2.05 (m, 1H, H17), 1.96-1.90 (m, 2H, H17 and H18), 1.66-1.63 (m, 1H, H18), 1.55-1.51 (m, 2H, H19), 1.37 and 1.34 (s, 9H, H1). Rotamers present. **^{13}C NMR (125 MHz, d_6 -DMSO)** δ 157.9 (C14), 154.8 (C3), 149.3 (C10), 130.7 (C15), 128.9 (C12), 126.3 (C11), 114.3 (C13), 86.7 (C16), 78.3 (C2), 70.7 (Cc), 68.8 (Cb), 67.1 (Ca), 66.8 (C20) 43.6 (Cd), 40.9 (C7), 34.1 (C4), 29.8 (C17), 28.0 (C1), 24.6 (C19), 22.1 (C18). Peaks indicated by HSQC δ 54.6 (C6), 52.2 (C8), 45.9 (C5). Peak indicated by HMBC δ 115.1 (C9). **IR** (neat film, ν_{\max} , cm^{-1}) 2939 (m, C-H aromatic), 2857 (w, C-H aliphatic), 1686 (s, C=O), 1612 (m, C=C), 1449 (C-H alkane), 1082 (m, C-O-C cyclic ether). **HRMS (ESI)** m/z calcd for $\text{C}_{28}\text{H}_{43}\text{ClN}_4\text{O}_5$ $[\text{M}+\text{H}]^+$: 551.2995; found 551.3007. **Lab Reference** PM135 (0.11 mmol, 43%), PM154 (0.11 mmol, 45%), PM158 (0.23 mmol, 54%).

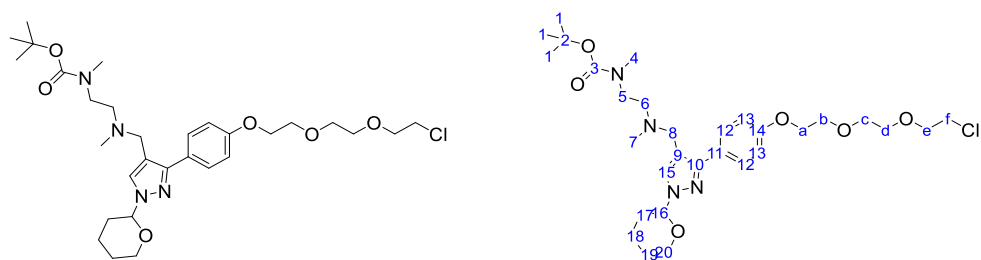
tert-butyl 2-(((3-(4-((5-chloropentyl)oxy)phenyl)-1-(tetrahydro-2H-pyran-2-yl)-1H-pyrazol-4-yl)methyl)(methyl)amino)ethyl)(methyl)carbamate (34 (n=5))



General method E was followed with PRMT1 ligand **11** (75 mg, 0.17 mmol) and 5-chloro-1-pentanol. The product was further purified by automated column chromatography (C18 Gold, 5-60% MeCN in 0.1 M NH₄OH_(aq)) over 45 CV) to give the title compound as a white solid (42 mg, 46%).

¹H NMR (500 MHz, d₆-DMSO) δ 7.78 and 7.74 (two s, 2H, H12 and H15), 6.96 (d, *J*=7.9 Hz, 2H, H13), 5.37 (m, 1H, H16), 4.00 (m, 2H, Ha), 3.93 (m, 1H, H20), 3.67 (m, 2H, He), 3.62 (m, 1H, H20), 3.33 and 3.26 (two s, 4H, H5 and H8), 2.75 and 2.73 (s, 3H, H4), 2.47 (s, 2H, H6), 2.17 (s, 3H, H7), 2.08 (m, 1H, H17), 1.95 (m, 2H, H17 and H18), 1.82-1.73 (m, 4H, Hb and Hd), 1.67 (m, 1H, H18), 1.58-1.52 (m, 4H, H19 and Hc), 1.37 and 1.34 (s, 9H, H1). Rotamers present. **¹³C NMR (125 MHz, d₆-DMSO)** δ 128.9 (C12), 114.3 (C13), 86.7 (C16), 67.2 (Ca), 66.8 (C20), 45.3 (Ce), 34.1 (C4), 31.8 (Cd), 29.8 (C17), 28.0 and 27.9 (Cb and C1), 24.6 (Cc), 23.0 (C19), 22.0 (C18). Peaks indicated by HSQC δ 130.6 (C15), 54.8 (C6), 52.4 and 46.0 (C5 and C8), 40.9 (C7). Peak indicated by HMBC δ 78.3 (C2). C3, C9, C10, C11 and C14 not identified. **IR** (neat film, *v*_{max}, cm⁻¹) 2939 (m, C-H aromatic), 2862 (w, C-H aliphatic), 1687 (s, C=O), 1612 (m, C=C), 1452 (m, C-H alkane), 1082 (m, C-O-C cyclic ether). **HRMS (ESI)** *m/z* calcd for C₂₉H₄₅ClN₄O₄ [M+H]⁺: 549.3202; found 549.3229. **Lab reference** PM167.

***tert*-butyl (2-(((3-(4-(2-(2-(2-chloroethoxy)ethoxy)ethoxy)phenyl)-1-(tetrahydro-2H-pyran-2-yl)-1H-pyrazol-4-yl)methyl)(methyl)amino)ethyl)(methyl)carbamate (**34** (m=2))**

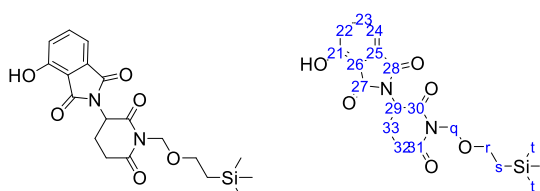


General method E was followed with PRMT1 ligand **11** (100 mg, 0.23 mmol) and 2-[2-(2-chloroethoxy)ethoxy]ethanol. The title compound was obtained as a white solid (94 mg, 70%).

¹H NMR (500 MHz, d₆-DMSO) δ 7.79 (s, 1H, H15), 7.76 (d, *J*=8.8 Hz, 2H, H12), 6.97 (d, *J*= 8.9 Hz, 2H, H13), 5.36 (dd, *J*=10.0 and 2.2 Hz, 1H, H16), 4.11 (m, 2H, Ha), 3.93 (m, 1H, H20), 3.77 (m, 2H, Hb), 3.72-3.67 (m, 4H, He and Hf), 3.64 (m, 1H, H20), 3.61 (m, 4H, Hc and Hd), 3.34 (s, 2H, H8), 3.27 (m,

2H, H5), 2.75 and 2.73 (s, 3H, H4), 2.47 (t, $J=6.2$ Hz, 2H, H6), 2.17 (s, 3H, H7), 2.13-2.06 (m, 1H, H17), 1.96-1.90 (m, 2H, H17 and H18), 1.72-1.62 (m, 1H, H18), 1.53 (m, 2H, H19), 1.36 and 1.34 (s, 9H, H1). Rotamers present. **^{13}C NMR (125 MHz, $\text{d}_6\text{-DMSO}$)** δ 157.8 (C14), 154.8 (C3), 149.2 (C10), 130.6 (C15), 128.7 (C12), 114.2 (C13), 86.7 (C16), 78.2 (C2), 70.6 (Ce), 69.9 and 69.7 (Cc and Cd), 69.0 (Cb), 67.0 (Ca), 66.8 (C20) 43.6 (Cf), 41.0 (C7), 34.0 (C4), 29.8 (C17), 28.0 (C1), 24.6 (C19), 22.1 (C18). Peaks indicated by HSQC δ 54.7 (C6), 52.3 (C8), 46.0 (C5). Peaks indicated by HMBC δ 126.7 (C11), 115.4 (C9). **IR** (neat film, ν_{max} , cm^{-1}) 2957 (m, C-H aromatic), 2873 (w, C-H aliphatic), 1622 (s, C=O), 1623 (s, C=O), 1536 (m, C=C), 1434 (m, C-H alkane), 1084 (m, C-O-C cyclic ether). **HRMS (ESI)** m/z calcd for $\text{C}_{30}\text{H}_{47}\text{ClN}_4\text{O}_6$ $[\text{M}+\text{H}]^+$: 595.3257; found 595.3255. **Lab reference** PM159 (0.11 mmol, 18%) PM163 (0.23 mmol, 70%).

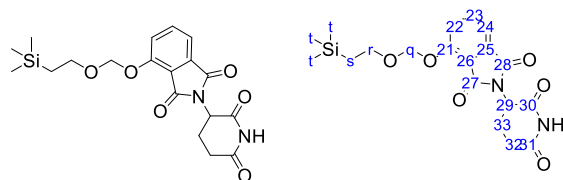
2-(2,6-dioxo-1-((2-(trimethylsilyl)ethoxy)methyl)piperidin-3-yl)-4-hydroxyisoindoline-1,3-dione (35)



A suspension of **38** (47 mg, 0.13 mmol, 1 eq) and 4-hydroxyisobenzofuran-1,3-dione (21 mg, 0.13 mmol, 1 eq) in trifluoroethanol (2 mL) was heated under microwave conditions for 2 hr at 150 °C. The solvent was removed *in vacuo* and the purified by automated column chromatography (C18 Gold, 5-95% MeCN in 0.1% $\text{HCOOH}_{(\text{aq})}$ over 45 CV) to give a purple solid (30 mg). Taking into account residual EtOAc in ^1H NMR spectra, the yield is 56%.

^1H NMR (500 MHz, CDCl_3) δ 11.22 (br s, 1H, 21-OH), 7.66 (dd, $J=8.3$ and 7.2 Hz, 1H, H23), 7.39 (d, $J=7.1$ Hz, 1H, H24), 7.25 (d, $J=8.4$ Hz, 1H, H22), 5.20 (dd, $J=13.1$ and 5.0 Hz, 1H, H29), 5.07 (s, 2H, Hq), 3.52 (m, ddd, $J=17.1$, 9.6 and 6.9 Hz, 2H, Hr), 3.02 and 2.78 (m, 2H, H32), 2.55 and 2.05 (m, 2H, H33), 0.84 (m, 2H, Hs), -0.02 (s, 9H, Ht). **^{13}C NMR (125 MHz, CDCl_3)** δ 171.7 and 170.0 (C30 and C31), 167.0 and 165.7 (C27 and 28), 155.6 (C21), 136.4 (C23), 133.1 (C26), 123.6 (C22), 114.3 (C25), 114.2 (C24), 68.3 (Cq), 66.0 (Cr), 49.2 (C29), 31.2 (C32), 21.0 (C33), 17.4 (Cs), -1.3 (Ct). **IR** (neat film, ν_{max} , cm^{-1}) 3324 (br w, O-H), 2953 (m, C-H aromatic), 2896 (w, C-H aliphatic), 1710 (s, C=O Imide), 1685 (s, C=O Imide), 1248 (m, Si-CH₃). **HRMS (ESI)** m/z calcd for $\text{C}_{19}\text{H}_{24}\text{N}_2\text{O}_6\text{Si}$ $[\text{M}+\text{Na}]^+$: 427.1296; found 427.1295. **Lab reference** PM223 (0.13 mmol, 56%) and PM245 (0.42 mmol, 30%).

2-(2,6-dioxopiperidin-3-yl)-4-((2-(trimethylsilyl)ethoxy)methoxy)isoindoline-1,3-dione (36)

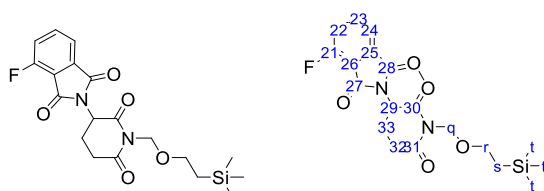


2-(2,6-Dioxopiperidin-3-yl)-4-hydroxyisoindoline-1,3-dione (73 mg, 0.27 mmol, 1 eq), K_2CO_3 (37 mg, 0.27 mmol, 1 eq), KI (9 mg, 0.05 mmol, 0.2 eq) were dissolved in DMSO (1 mL). SEMCl (50 μ L, 0.27 mmol, 1 eq) was added and the mixture heated at 80°C overnight. The mixture was diluted with water and extracted with EtOAc (x3). The combined organic layers were washed with water, dried with Na_2SO_4 and the solvent removed *in vacuo*. The residue was then purified by automated column chromatography (C18 Gold, 5-95% MeCN in 1% $CH_3COOH_{(aq)}$ over 40 CV) to give the title compound as an oil (12 mg, 11%).

Alternative conditions: General method F was followed with 2-(2,6-Dioxopiperidin-3-yl)-4-hydroxyisoindoline-1,3-dione {CAS: 5054-59-1} (51 mg, 0.19 mmol). The combined organic layers were then washed with water, dried with Na_2SO_4 and the solvent removed *in vacuo*. The residue was then purified by automated column chromatography (C18 Gold, 5-40% MeCN in 1% $CH_3COOH_{(aq)}$ over 40 CV) to give the title compound as an oil (43 mg, 58%).

1H NMR (500 MHz, d_6 -DMSO) δ 11.10 (s, 1H, 30-NH), 7.82 (dd, $J=8.5$ and 7.3 Hz, 1H, H23), 7.58 (d, $J=8.3$ Hz, 1H, H22), 7.51 (d, $J=7.1$ Hz, H24) 5.45 (m, 2H, Hq), 5.10 (dd, $J=12.9$ and 5.5 Hz, 1H, H29), 3.77 (m, 2H, Hr), 2.89 (m, 1H, H32), 2.61-2.47 (m, 2H, H32 and H33), 2.06-2.01 (m, 1H, H33), 0.89 (m, 2H, Hs), -0.04 (s, 9H, Ht). ^{13}C NMR (125 MHz, d_6 -DMSO) δ 172.8 and 169.9 (C30 and 31), 166.7 and 165.2 (C27 and C28), 154.2 (C21), 136.7 (C23), 133.2 (C26), 122.1 (C22), 117.3 (C25), 116.3 (C24), 93.1 (Cq), 66.3 (Cr), 48.8 (C29), 30.9 (C32), 22.0 (C33), 17.5 (Cs), -1.4 (Ct). IR (neat film, ν_{max} , cm^{-1}) 3219 (br w, N-H), 3109 (w, C-H aromatic), 2918 (w, C-H aliphatic), 1706 (s, C=O imide), 1252 (s, Si-CH₃), 1195 (m, C-O-C ether). HRMS (ESI) m/z calcd for $C_{19}H_{24}N_2O_6Si$ [M+Na]⁺: 427.1296; found 427.1317. Lab reference PM212 (0.27 mmol, 11%) and PM213 (0.19 mmol, 58%).

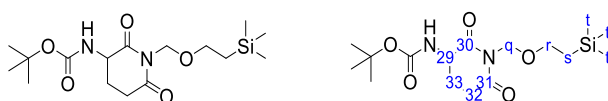
2-(2,6-dioxo-1-((2-(trimethylsilyl)ethoxy)methyl)piperidin-3-yl)-4-fluoroisoindoline-1,3-dione (37)



General method F was followed with 4-fluorothalidomide (210 mg, 0.68 mmol). The combined organic layers were washed with LiCl_(aq) (5%), washed with brine, dried with Na₂SO₄ and the solvent removed *in vacuo* to give the title compound as a yellow oil (312 mg, quantitative).

¹H NMR (500 MHz, d₆-DMSO) δ 7.96 (m, 1H, H23), 7.78 (d, *J*=7.2 Hz, 1H, H24), 7.74 (t, *J*=8.5 Hz, 1H, H22), 5.29 (dd, *J*=13.1 and 5.4 Hz, 1H, H29), 5.08 (s, 2H, Hq), 3.58-3.46 (m, 2H, Hr), 3.07-3.00 and 2.82-2.78 (m, 2H, H32), 2.59-2.50 and 2.12-2.07 (m, 1H, H33) 0.84 (m, 2H, Hs), -0.02 (s, 9H, Ht). **¹³C NMR (125 MHz, d₆-DMSO)** δ 171.6 and 169.7 (C30 and C31), 166.0 and 163.9 (C27 and 28), 156.8 (d, ¹*J*_{C-F}=262 Hz, C21), 138.1 (d, ³*J*_{C-F}=7.9 Hz, C23), 133.4 (C25), 123.0 (d, ²*J*_{C-F}=19.6 Hz, C22), 120.0 (d, ⁴*J*_{C-F}=3.0 Hz, C24), 117.0 (d, ²*J*_{C-F}=12.5 Hz, C26), 68.3 (Cq), 66.0 (Cr), 49.6 (C29), 31.1 (C32), 20.8 (C33), 17.4 (Cs), -1.4 (Ct). **IR** (neat film, *v*_{max}, cm⁻¹) 2952 (w, C-H aromatic), 2869 (C-H aliphatic), 1716 (s, C=O imide), 1686 (s, C=O imide), 1387 (s, C-F), 1249 (m, Si-CH₃), 1095 (m, C-O-C ether). **HRMS (ESI)** *m/z* calcd for C₁₉H₂₃FN₂O₅Si [M+Na]⁺: 429.1252; found 429.1258. **Lab reference** PM209 (0.33 mmol, 77%) and PM256 (0.68 mmol, quantitative).

***tert*-butyl (2,6-dioxo-1-((2-(trimethylsilyl)ethoxy)methyl)piperidin-3-yl)carbamate (38)**

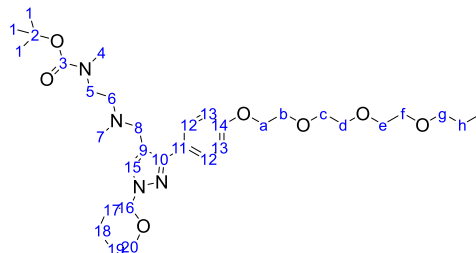
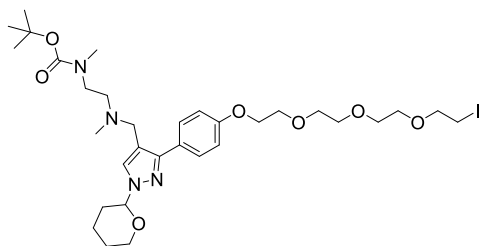


General method F was followed with *tert*-butyl(2,6-dioxopiperidin-3-yl)carbamate (500 mg, 2.2 mmol). The combined organic layers were washed with water, dried with Na₂SO₄ and the solvent removed *in vacuo* to give the title compound as a yellow oil (820 mg) which was used without further purification.

¹H NMR (500 MHz, d₆-DMSO) δ 7.27 (d, *J*=8.4 Hz, 1H, 29-NH), 5.02 (m, 2H, Hq), 4.32 (m, 1H, H29), 3.51 (m, 2H, Hr), 2.84 (m, 1H, H32 or H33), 2.67 (m, 1H, H32 or 33), 1.92 (m, 2H, H32 and 33), 1.40 (s, 9H, C(CH₃)₃), 0.82 (t, *J*=8.1 Hz, 2H, Hs), -0.02 (s, 9H, Ht). **Lab reference** PM221 (0.2 mmol, 98 mg) and PM233 (2.2 mmol, 820 mg).

Data are in accordance with those previously reported in the literature¹⁸⁷.

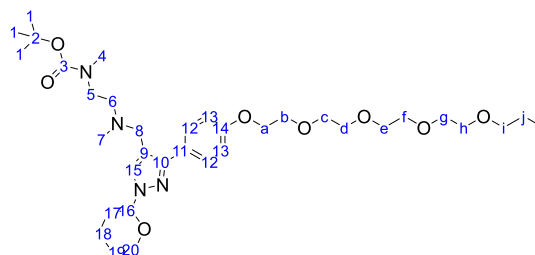
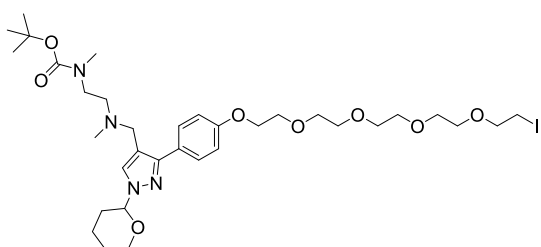
***tert*-butyl (2-(((3-(4-(2-(2-(2-(2-iodoethoxy)ethoxy)ethoxy)ethoxy)phenyl)-1-(tetrahydro-2H-pyran-2-yl)-1H-pyrazol-4-yl)methyl)(methyl)amino)ethyl)(methyl)carbamate (40I)**



General method G was followed with PRMT1 ligand **11** (39 mg, 0.09 mmol) and the linker **39I** (1-iodo-2-(2-(2-(2-iodoethoxy)ethoxy)ethoxy)ethoxy)ethane). The title compound was isolated as a yellow oil (41 mg, 65%).

¹H NMR (500 MHz, CDCl₃) δ 7.72-7.51 (m, 3H, H12 and H15), 6.97 (d, *J*=8.7 Hz, 2H, H13), 5.39 (dd, *J*=9.7 and 2.4 Hz, 1H, H16), 4.17 (m, 2H, Ha), 4.10 (m, 1H, H20), 3.98 (m, 1H, H8), 3.89 (m, 2H, Hb), 3.78-3.68 (m, 12H, H20 and H8 and Hc-g), 3.50 and 3.36 (m, 2H, H5), 3.27 (m, 2H, Hh), 2.82 (s, 3H, H4), 2.80 and 2.62 (m, 2H, H6), 2.33 (s, 3H, H7), 2.15-2.05 (m, 3H, H17 and H18), 1.73-1.68 (m, 2H, H18 and H19), 1.64-1.58 (m, 1H, H19), 1.45 (s, 9H, H1). Rotamers present. **¹³C NMR (125 MHz, CDCl₃)** δ 167.2 (C3), 158.7 (C14), 130.8 (C15), 129.7 (C12), 114.8 (C13), 87.9 (C16), 79.8 (d, C2), 72.0-70.3 (Cc-Cg), 69.8 (Cb), 68.0 (C20), 67.5 (Ca), 54.1 and 52.2 (C6), 51.8 and 49.8 (C8), 46.1 and 44.7 (C5), 40.5 (d, C7), 34.8 (d, C4), 30.6 (C17), 28.5 (C1), 25.0 (C19), 22.6 (C18), 3.1 (Ch). Rotamers present. C9, C10, C11 not identified. **IR** (neat film, *v*_{max}, cm⁻¹) 2927 (m, C-H aromatic), 2864 (m, C-H aliphatic), 1686 (s, C=O), 1082 (s, C-O-C cyclic ether). **HRMS (ESI)** *m/z* calcd for C₃₂H₅₁IN₄O₇ [M+H]⁺: 731.2875; found 731.2878. **Lab reference** PM229 (0.07 mmol, 51%), PM244 (0.09 mmol, 65%).

***tert*-butyl (2-(((3-(4-((14-iodo-3,6,9,12-tetraoxatetradecyl)oxy)phenyl)-1-(tetrahydro-2H-pyran-2-yl)-1H-pyrazol-4-yl)methyl)(methyl)amino)ethyl)(methyl)carbamate (40m)**

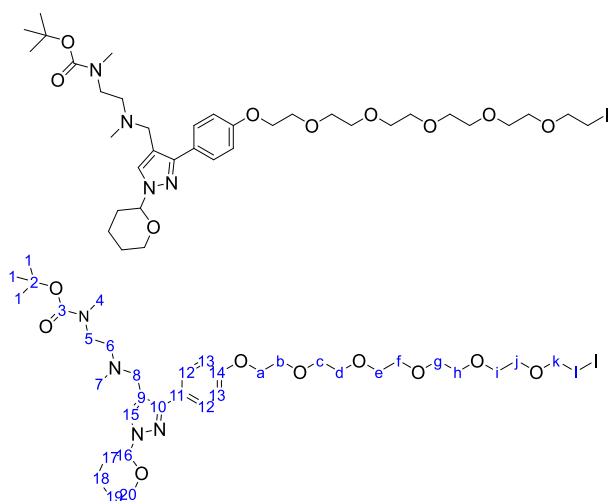


General method G was followed with PRMT1 ligand **11** (38 mg, 0.08 mmol) and linker **39m** (1,14-diiido-3,6,9,12-tetraoxatetradecane). The title compound was isolated as an orange oil (38 mg, 58%).

¹H NMR (500 MHz, CDCl₃) δ 7.87-7.56 (m, 3H, H12 and H15), 6.95 (d, *J*=8.8 Hz, 2H, H13), 5.37 (dd, *J*=9.6 and 2.7 Hz, 1H, H16), 4.15 (m, 2H, Ha), 4.07 (m, 1H, H20), 3.86 (m, 2H, Hb), 3.83 (m, 1H, H8),

3.75-3.65 (m, 15H, Hc-Hi and H20), 3.57 (m, 1H, H8), 3.45 and 3.33 (m, 2H, H5), 3.25 (m, 2H, Hj), 2.81 (s, 3H, H4), 2.75 and 2.55 (m, 2H, H6), 2.29 (m, 3H, H7), 2.16-2.03 (m, 3H, H17 and H18), 1.73-1.64 (m, 2H, H18 and H19), 1.62-1.58 (m, 1H, H19), 1.43 (s, 9H, H1). Rotamers present. **¹³C NMR (125 MHz, CDCl₃)** δ 158.7 (C14), 130.6 (C15), 129.7 (C12), 114.8 (C13), 88.0 (C16), 79.8 (d, C2), 72.1-70.3 (Cc-Ci), 69.9 (Cb), 68.1 (C20), 67.6 (Ca), 54.5 and 52.9 (C6), 52.3 and 50.5 (C8), 46.4 and 45.1 (C5), 40.9 (d, C7), 34.8 (d, C4), 30.6 (C17), 28.5 (C1), 25.1 (C19), 22.7 (C18), 3.1 (Cj). Rotamers present. C3, C9, C10, C11 not identified. **IR** (neat film, ν_{\max} , cm⁻¹) 2927 (m, C-H aromatic), 2865 (C-H aliphatic), 1687 (s, C=O), 1082 (s, C-O-C cyclic ether). **HRMS (ESI)** *m/z* calcd for C₃₄H₅₅IN₄O₈ [M+H]⁺: 775.3137; found 775.3169. **Lab reference** PM231 (0.07 mmol, 38%), PM247 (0.08 mmol, 58%).

***tert*-butyl (2-(((3-(4-((17-iodo-3,6,9,12,15-pentaoxaheptadecyl)oxy)phenyl)-1-(tetrahydro-2H-pyran-2-yl)-1H-pyrazol-4-yl)methyl)(methyl)amino)ethyl)(methyl)carbamate (40n)**

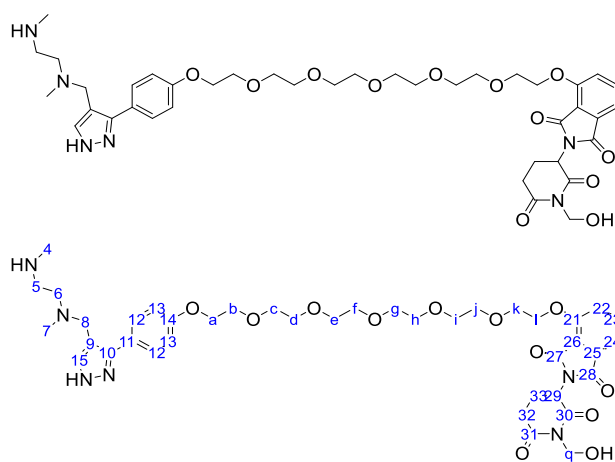


General method G was followed with PRMT1 ligand **11** (40 mg, 0.09 mmol) and linker **39n** (1,17-diiido-3,6,9,12,15-pentaoxaheptadecane). The title compound was isolated as a pale yellow oil (28 mg, 38%).

¹H NMR (700 MHz, CDCl₃) δ 7.72-7.57 (m, 3H, H12 and H15), 6.93 (d, *J*=8.7 Hz, 2H, H13), 5.36 (dd, *J*=9.9 and 2.5 Hz, 1H, H16), 4.14 (m, 2H, Ha), 4.07 (m, 1H, H20), 3.86 (m, 2H, Hb), 3.74-3.64 (m, 20H, Hc-k and H20 and H8), 3.47 (m, 1H, H8), 3.40 and 3.29 (m, 2H, H5), 3.24 (m, 2H, Hl), 2.80 (m, 3H, H4), 2.62 and 2.51 (m, 2H, H6), 2.26 and 2.24 (m, 3H, H7), 2.15-2.03 (m, 3H, H17 and H18), 1.71-1.65 (m, 2H, H18 and H19), 1.61-1.56 (m, 1H, H19), 1.42 and 1.41 (m, 9H, H1). Rotamers present. **¹³C NMR (176 MHz, CDCl₃)** δ 158.5 (C14), 151.1 (d, C10), 129.6 (C12), 129.2 (C15), 114.6 (C13), 87.9 (C16), 79.5 (d, C2), 72.1-70.3 (Cc-Ck), 69.9 (Cb), 68.0 (C20), 67.5 (Ca), 55.0 and 53.8 (C6), 52.7 and 51.7 (C8), 46.8 and 45.8 (C5), 41.6 (d, C7), 34.8 (d, C4), 30.7 (C17), 28.5 (C1), 25.1 (C19), 22.7 (C18), 3.1 (Cl).

Rotamers present. C3, C9, and C11 not identified. IR (neat film, ν_{\max} , cm^{-1}) 2928 (m, C-H aromatic), 2866 (m, C-H aliphatic), 1685 (s, C=O), 1083 (s, C-O-C cyclic ether). HRMS (ESI) m/z calcd for $\text{C}_{36}\text{H}_{59}\text{N}_4\text{O}_9$ $[\text{M}+\text{H}]^+$: 819.3399; found 819.3420. Lab reference PM232 (0.07 mmol, 17%), PM289 (0.09 mmol, 38%).

2-(1-(hydroxymethyl)-2,6-dioxopiperidin-3-yl)-4-((17-(4-(4-((methyl(2-(methylamino)ethyl)amino)methyl)-1H-pyrazol-3-yl)phenoxy)-3,6,9,12,15-pentaoxaheptadecyl)oxy)isoindoline-1,3-dione (42n)

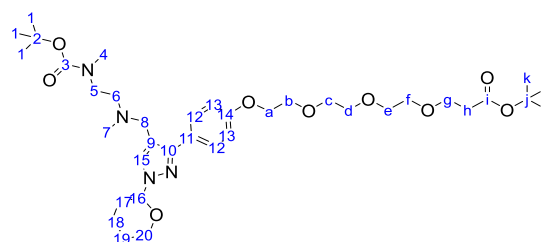
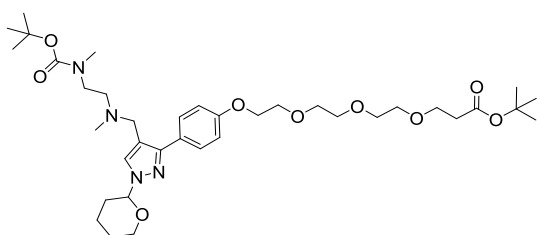


40n (9 mg, 0.01 mmol, 1 eq), CRBN ligand **35** (5 mg, 0.01 mmol, 1 eq) and Cs_2CO_3 (7 mg, 0.02 mmol, 2 eq) were dissolved in MeCN (1 mL) and heated at 80°C overnight to produce intermediate product **41n**. The solvent was removed *in vacuo* and the residue dissolved in DCM (1 mL) and TFA (1 mL) was added dropwise and the mixture stirred at room temperature for 1 hr. The solvent was removed *in vacuo* and the residue purified by preparative HPLC (5-40% MeCN (0.05% TFA) in H_2O (0.1% TFA) over 20 min) and lyophilised to give the title compound as a white solid (5 mg, 59%).

^1H NMR (700 MHz, d_6 -DMSO) δ 10.05 (br s, 15-NH), 8.71 (br s, 2H, 4-NH $_2^+$), 7.87 (s, 1H, H15), 7.81 (dd, $J=8.3$ and 7.5 Hz, 1H, H23), 7.54 (d, $J=8.6$ Hz, 1H, H22), 7.49 (d, $J=8.6$ Hz, 2H, H12), 7.46 (d, $J=7.2$ Hz, 1H, H24), 7.06 (d, $J=8.6$ Hz, 2H, H13), 5.18 (dd, $J=13.1$ and 5.4 Hz, 1H, H29), 5.05 (d, $J=3.7$ Hz, 2H, Hq), 4.36 (br s, 2H, H8), 4.34 (m, 2H, Hl), 4.13 (m, 2H, Ha), 3.80 (m, 2H, Hk), 3.76 (m, 2H, Hb), 3.64 (m, 2H, Hj), 3.58 (m, 2H, Hc), 3.53 (m, 4H, Hd and Hi), 3.50 (m, 8H, He-Hh), 3.23 and 3.16 (two br s, 4H, H5 and H6), 3.06-2.99 and 2.78-2.74 (m, 2H, H32), 2.63 (s, 3H, H4), 2.59-2.57 (m, 1H, H33), 2.55 (m, 3H, H7), 2.05-2.03 (m, 1H, H33). q-OH likely the broad peak at ~ 5.9 ppm. **^{13}C NMR (176 MHz, d_6 -DMSO)** δ 171.1 and 169.3 (C30 and C31), 166.8 and 165.3 (C27 and C28), 158.6 (C14), 158.1 (q, $^2J_{\text{C-F}}=34.8$ Hz, CF_3COO^-), 155.9 (C21), 137.0 (C23), 133.2 (C26), 129.5 (C12), 120.1 (C22), 116.3 (C25), 115.4 (C24), 114.8 (C13), 70.1 (Cj), 69.9 (Cc), 69.8-69.7 (Cd-Ci), 68.9 (Cb), 68.8 (Cl), 68.7 (Ck), 67.3

(Ca), 62.5 (Cq), 50.1 (C8), 49.4 (C29), 49.3 (C5 or C6), 42.5 (C5 or C6), ~39.4 (C4), 32.7 (C7), 31.3 (C32), 21.0 (C33). Peak indicated by HSQC δ 137.7 (C15). C9, C10, C11 not identified. **HPLC** (5-95% MeCN (0.05% TFA) in H₂O (0.05% TFA) over 15 min) R_t = 6.51 min. Purity= 85%. **HRMS (ESI)** m/z calcd for C₄₀H₅₄N₆O₁₂ [M+H]⁺: 811.3872; found 811.3857. **Lab reference** PM237.

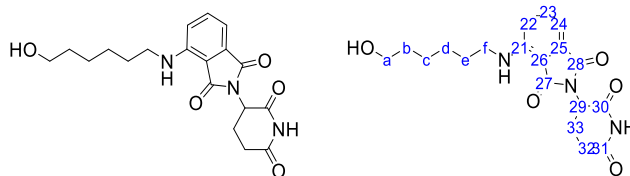
***tert*-butyl 3-(2-(2-(2-(4-(4-(((2-((*tert*-butoxycarbonyl)(methyl)amino)ethyl)(methyl)amino)methyl)-1-(tetrahydro-2*H*-pyran-2-yl)-1*H*-pyrazol-3-yl)phenoxy)ethoxy)ethoxy)ethoxy)propanoate (44)**



PRMT1 ligand **11** (50 mg, 0.11 mmol, 1 eq), *tert*-butyl 3-(2-(2-(2-iodoethoxy)ethoxy)ethoxy)propanoate (56 mg, 0.14 mmol, 1.2 eq), K₂CO₃ (31 mg, 0.23 mmol, 2 eq) were dissolved in MeCN (0.7 mL) and heated at 80°C for 8 hr. The solvent was removed *in vacuo* and the residue was purified by automated column chromatography (C18 Gold, 5-60% MeCN in 1% HCOOH_(aq)) over 60 CV) to give a pale orange oil (46 mg, 58%).

¹H NMR (500 MHz, CDCl₃) δ 7.67-7.51 (m, 3H, H12 and H15), 6.94 (d, J =8.8 Hz, 2H, H13), 5.37 (dd, J =9.5 and 2.3 Hz, 1H, H16), 4.14 (m, 2H, Ha), 4.07 (m, 1H, H20), 3.89 (m, 1H, H8), 3.68 (m, 2H, Hb), 3.73-3.59 (m, 12H, H20 and H8 and Hc-Hg), 3.45 and 3.32 (m, 2H, H5), 2.79 (s, 3H, H4), 2.75 and 2.58 (m, 2H, H6), 2.49 (m, 2H, Hh), 2.28 (s, 3H, H7), 2.16-2.03 (m, 3H, H17 and H18), 1.73-1.63 (m, 2H, H18 and H19), 1.61-1.56 (m, 1H, H19), 1.43 (s, 18H, H1 and Hk). Rotamers present. **¹³C NMR (125 MHz, CDCl₃)** δ 171.0 (Ci), 167.2 (C3), 158.8 (C14), 129.8 (C12), 114.9 (C13) 88.0 (C16), 80.6 (Cj and C2), 71.0-70.5 (Cc-Cf), 69.8 (Cb), 68.1 (C20), 67.5 (Ca). 67.0 (Cg), 54.1 and 52.2 (C6), 51.8 and 49.8 (C8), 46.1 and 44.9 (C5), 40.6 (d, C7), 36.4 (Ch), 34.8 (d, C4), 30.7 (C17), 28.5 and 28.2 (C1 and Ck), 25.0 (C19), 22.7 (C18). Rotamers present. C9, C10, C11 and C15 not identified. **IR** (neat film, ν_{\max} , cm⁻¹) 2932 (m, C-H aromatic), 2868 (w, C-H aliphatic), 1728 (m, C=O), 1691 (s, C=O), 1083 (m, C-O-C cyclic ether). **HRMS (ESI)** m/z calcd for C₃₇H₆₀N₄O₉ [M+H]⁺:705.4433; found 705.4449. **Lab reference** PM184.

2-(2,6-dioxopiperidin-3-yl)-4-((6-hydroxyhexyl)amino)isoindoline-1,3-dione (46)

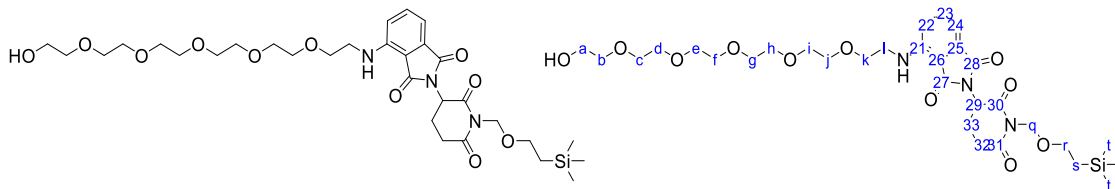


4-fluorothalidomide (55 mg, 0.20 mmol, 1 eq) and 6-amino-1-hexanol (26 mg, 0.22 mmol, 1.2 eq) were dissolved in DMSO (0.5 mL). DIPEA (100 μ L, 0.54 mmol, 3 eq) was added and the mixture heated at 130°C overnight. The mixture was purified by automated column chromatography (C18 Gold, 5-60% MeCN in 1% HCOOH_(aq)) over 40 CV) to give a yellow/green oil (42 mg, 62%).

¹H NMR (500 MHz, CDCl₃) δ 8.69 (s, 1H, 30-NH), 7.46 (dd, J =8.5 and 7.1 Hz, 1H, H23), 7.06 (d, J =7.0 Hz, 1H, H24), 6.86 (d, J =8.5 Hz, 1H, H22), 6.22 (br s, 1H, 21-NH), 4.90 (dd, J =12.3 and 5.4 Hz, 1H, H29), 3.62 (m, 2H, Ha), 3.25 (m, 2H, Hf), 2.87-2.68 and 2.12-2.08 (m, 4H, H32 and 33), 1.66 (m, 2H, He), 1.57 (m, 2H, Hb) 1.41 (m., 4H, Hc and Hd). a-OH not identified. **Lab reference** PM174.

Data are in accordance with those reported previously in literature²⁴⁸.

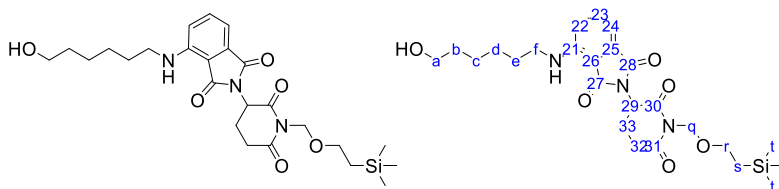
2-(2,6-dioxo-1-((2-(trimethylsilyl)ethoxy)methyl)piperidin-3-yl)-4-((17-hydroxy-3,6,9,12,15-pentaoxaheptadecyl)amino)isoindoline-1,3-dione (47o)



General method H was followed with CRBN ligand **37** (27 mg, 0.07 mmol) and linker {CAS: 39160-70-8} to give the title compound as a green oil (36 mg, 78%).

¹H NMR (500 MHz, CDCl₃) δ 7.46 (dd, J =8.5 and 7.5 Hz, 1H, H23), 7.06 (d, J =6.8 Hz, 1H, H24), 6.92 (d, J =8.5 Hz, 1H, H22), 6.44 (m, 1H, 21-NH), 5.24 (s, 2H, Hq), 4.92 (m, 1H, H29), 3.70-3.56 (m, 24H, Hr and Ha-k), 3.46 (m, 2H, Hl), 3.01-2.92 (m, 1H, H32), 2.80-2.71 (m, 2H, H32 and H33), 2.09-2.05 (m, 1H, H33), 0.92 (m, 2H, Hs), -0.02 (s, 9H, Ht). a-OH not identified. **¹³C NMR (125 MHz, CDCl₃)** δ 171.2 (C30 or C31), 169.4 (C27 or C28), 169.2 (C30 or C31), 167.8 (C27 or C28), 146.9 (C21), 136.1 (C23), 132.6 (C25), 116.9 (C22), 111.7 (C24), 110.4 (C26), 72.7-69.7 (Cb-Ck), 69.2 (Cq), 67.4 (Cr), 61.7 (Ca), 49.6 (C29), 42.5 (Cl), 32.1 (C32), 22.0 (C33), 18.1 (Cs), -1.3 (Ct). **IR** (neat film, ν_{\max} , cm⁻¹) 3450 (br w, OH), 3393 (m, NH secondary amine), 2949 (m, C-H, aliphatic), 2869 (w, C-H, aliphatic), 1689 (s, C=O). **HRMS (ESI)** m/z calcd for C₃₁H₄₉N₃O₁₁Si [M+H]⁺: 668.3209; found 668.3214. **Lab reference** PM214 (0.07 mmol, 78%), PM282 (0.13 mmol, 51%).

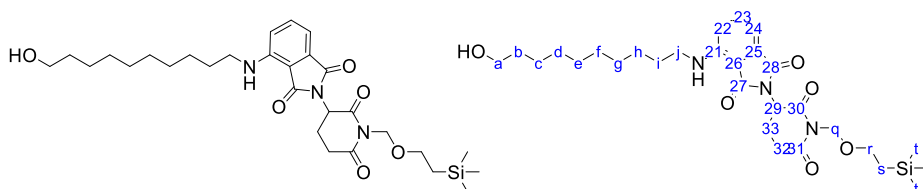
2-(2,6-dioxo-1-((2-(trimethylsilyl)ethoxy)methyl)piperidin-3-yl)-4-((6-hydroxyhexyl)amino)isoindoline-1,3-dione (47p)



General method H was followed with CRBN ligand **37** (49 mg, 0.12 mmol) and 6-amino-1-hexanol to give the title compound as a yellow/green solid (29 mg, 47%).

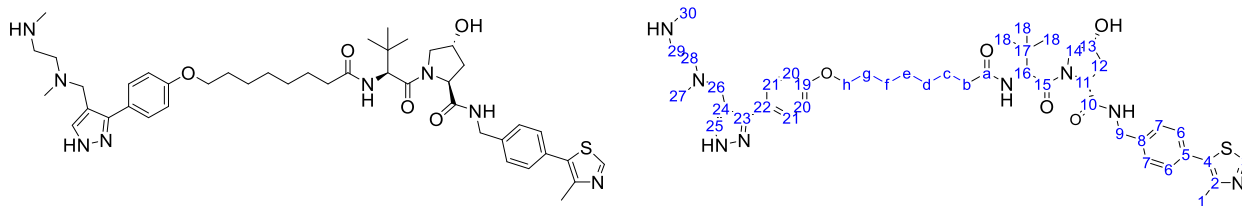
¹H NMR (500 MHz, CDCl₃) δ 7.47 (dd, *J*=8.5 and 7.2 Hz, 1H, H23), 7.07 (d, *J*=7.0 Hz, 1H, H24), 6.86 (d, *J*=8.5 Hz, 1H, H22), 6.21 (m, 1H, 21-NH), 5.26 (s, 2H, Hq), 4.92 (dd, *J*=12.6 and 5.3 Hz, 1H, H29), 3.67-3.56 (m, 4H, Ha and Hr), 3.26 (m, 2H, Hf), 3.02-2.94 (m, 1H, H32), 2.81-2.72 (m, 2H, H32 and H33), 2.13-2.05 (m, 1H, H33), 1.67 (m, 2H, He), 1.58 (m, 2H, Hb), 1.48-1.39 (m, 4H, Hc and Hd), 0.94 (m, 2H, Hs), -0.01 (s, 9H, Ht). a-OH not identified. **¹³C NMR (125 MHz, CDCl₃)** δ 171.2 (C30 or C31), 169.7 (C27 or C28), 169.3 (C30 or C31), 167.8 (C27 or C28), 147.1 (C21), 136.2 (C23), 132.7 (C25), 116.7 (C22), 111.5 (C24), 110.1 (C26), 69.3 (Cq), 67.5 (Cr), 62.9 (Ca), 49.7 (C29), 42.7 (Cf), 32.7 (Cb), 32.2 (C32), 29.3 and 26.7 and 25.6 (Cc, Cd and Ce), 22.1 (C33), 18.2 (Cs), -1.3 (Ct). **IR** (neat film, *v*_{max}, cm⁻¹) 3510 (br w, OH), 3398 (m, NH secondary amine), 2931 (m, C-H, aliphatic), 2869 (w, C-H, aliphatic), 1685 (s, C=O). **HRMS (ESI)** *m/z* calcd for C₂₅H₃₇N₃O₆Si [M+Na]⁺: 526.2344 ; found 526.2346. **Lab reference** PM281 (0.12 mmol, 47%), PM286 (0.15 mmol, 42%).

2-(2,6-dioxo-1-((2-(trimethylsilyl)ethoxy)methyl)piperidin-3-yl)-4-((10-hydroxydecyl)amino)isoindoline-1,3-dione (47q)



General method H was followed with CRBN ligand **37** (50 mg, 0.12 mmol) and 10-amino-1-decanol to give the title compound as a yellow/green oil (51 mg, 69%).

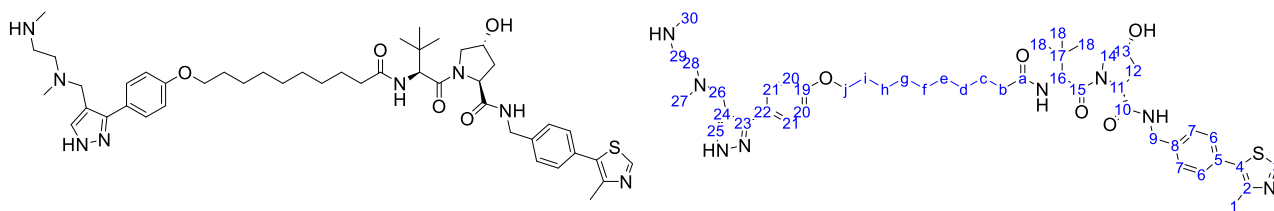
¹H NMR (400 MHz, CDCl₃) δ 7.46 (dd, *J*=8.4 and 7.3 Hz, 1H, H23), 7.05 (d, *J*=7.1 Hz, 1H, H24), 6.86 (d, *J*=8.5 Hz, 1H, H22), 6.20 (t, *J*=4.9 Hz, 1H, 21-NH), 5.25 (s, 2H, Hq), 4.92 (dd, *J*=12.5 and 4.9 Hz, 1H,



26c (40 mg, 0.06 mmol, 1 eq), PRMT1 ligand **11** (17 mg, 0.13, 2 eq), K_2CO_3 (17 mg, 0.13 mmol, 2 eq) and KI (2 mg, 0.01 mmol, 0.2 eq) were dissolved in MeCN (1 mL) and heated overnight at 80°C. The solvent was removed *in vacuo* and the residue purified by automated column chromatography (C18 Gold, 5-95% MeCN in 0.5% $HCOOH_{(aq)}$ over 45 CV). The product was then diluted with DCM, washed with water, dried with Na_2SO_4 and the solvent removed *in vacuo* to give a pale yellow solid (35 mg). The solid was dissolved in MeOH (0.5 mL) and $HCl_{(aq, 37\%)}$ (0.5 mL) was added dropwise and the mixture stirred at room temperature for 1 hr. The solvent was then removed *in vacuo* and the residue purified by preparative HPLC (5-70% MeCN (0.05% TFA) in H_2O (0.1% TFA) over 20 min) and lyophilised to give the title compound as a white solid (9 mg, 95%).

1H NMR (500 MHz, d_6 -DMSO) δ 10.11 (br s, 1H, 25-NH), 8.98 (s, 1H, H3), 8.76 (br s, 2H, 30-NH $_2^+$), 8.58 (t, $J=6.0$ Hz, 1H, 9-NH), 7.85 (d, $J=9.4$, 1H, 16-NH), 7.83 (br s, 1H, H25), 7.49 (d, $J=8.2$ Hz, 2H, H20), 7.40 (m, 4H, H6 and H7), 7.03 (d, $J=8.4$ Hz, 2H, H21), 4.55 (d, $J=9.4$ Hz, 1H, H16), 4.45-4.41 (m, 2H, H9), 4.35 (m, 1H, H13), 4.21 (dd, $J=15.9$ and 5.4 Hz, 1H, H11), 4.00 (t, $J=6.4$ Hz, 3H, Hh), 3.65 (m, 2H, H14), 3.21 and 3.13 (two br s, 4H, H28 and H29), 2.59 and 2.56 (two br s, 6H, H27 and H30), 2.44 (s, 3H, H1), 2.30-2.25 and 2.15-2.09 (m, 2H, Hb), 2.05-2.01 and 1.92-1.88 (m, 2H, H12), 1.71 (m, 2H, Hg), 1.55-1.38 (m, 4H, Cc and f) 1.36-1.26 (m, 4H, Cd and Ce), 0.94 (s, 9H, H18). H26 likely the broad peak at ~ 4.3 ppm. 13-OH likely broad peak at ~ 5.1 ppm. **^{13}C NMR (176 MHz, d_6 -DMSO)** δ 172.1 (Ca), 171.9 (C10), 169.7 (C15), 158.8 (C19), 158.1 (q, $^2J_{C-F}=33.4$ Hz, CF_3COO), 151.5 (C3), 147.7 (C2), 139.5 and 131.2 and 129.6 (C4, C5 and 8), 129.5 (C21), 128.6 and 127.4 (C6 and C7), 116.5 (q, $^1J_{C-F}=296.2$ Hz, CF_3COO^-), 114.8 (C20), 68.9 (C13), 67.5 (Ch), 58.7 (C9), 56.3 and 56.3 (C14 and C16), 41.6 (C11), ~ 40.3 (C27 or C30), 38.0 (C12), 35.2 (C17), 34.8 (Cb), 32.7 (C27 or C30), 28.6-28.5 (Cd, Ce and Cg), 26.4 (C18), 25.4 and 25.4 (Cc and Cf), 15.9 (C1). C22, C23, C24, C25, C26, C28 and C29 not identified. **HPLC** (5-95% MeCN (0.05% TFA) in H_2O (0.05% TFA) over 15 min) $R_t = 7.63$ min. Purity= 99%. **HRMS (ESI)** m/z calcd for $C_{54}H_{78}N_8O_8S$ $[M+H]^+$: 999.5736; found 999.5729. **Lab reference** PM89 and PM94.

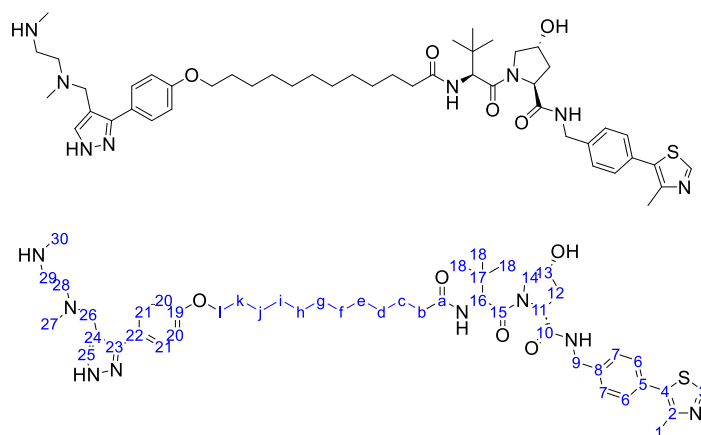
PROTAC D



General method I was followed with **26d** (42 mg, 0.06 mmol, 1 eq) and PRMT1 ligand **11** (28 mg, 0.06 mmol, 1 eq). The alkylation reaction was heated overnight at 80°C. Following deprotection, the residue was purified by preparative HPLC (5-60% MeCN (0.05% TFA) in H₂O (0.1% TFA) over 30 min) and lyophilised to give the title compound as a white solid (8 mg, 15%).

¹H NMR (700 MHz, d₆-DMSO) δ 10.08 (br s, 25-NH), 8.98 (s, 1H, H3), 8.75 (br s, 2H, 30-NH₂⁺), 8.56 (t, *J*=6.0 Hz, 1H, 9-NH), 7.84 (m, 2H, H25 and 16-NH), 7.48 (d, *J*=8.3 Hz, 2H, H21), 7.40 (m, 4H, H6 and H7), 7.04 (d, *J*=8.3 Hz, 2H, H20), 4.54 (d, *J*=9.4 Hz, H16), 4.43 (m, 2H, H9), 4.35 (m, 3H, H13 and H26), 4.22 (dd, *J*=15.8 and 5.4 Hz, 1H, H11), 4.00 (t, *J*=6.4 Hz, 2H, H_j), 3.65 (m, 2H, H14), 3.24 and 3.16 (two br s, 4H, H28 and H29), 2.63 and 2.55 (two br s, 6H, H27 and H30), 2.44 (s, 3H, H1), 2.29-2.24 and 2.12-2.08 (m, 2H, H_b), 2.04-2.02 and 1.92-1.88 (m, 2H, H12), 1.72 (m, 2H, H_i), 1.52-1.50 (m, 2H, H_c), 1.43-1.38 (m, 2H, H_h), 1.32-1.24 (m, 8H, C_d-C_g), 0.93 (s, 9H, H18). 13-OH not identified. **¹³C NMR (176 MHz, d₆-DMSO)** δ 172.1 (C_a), 171.9 (C10), 169.7 (C15), 158.6 (C19), 158.3 (q, ²*J*_{C-F}=34.6 Hz, C_{F3}C_{OO}), 151.5 (C3), 147.7 (C2), 139.5 and 131.2 and 129.6 (C4, C5 and C8), 129.5 (C21), 128.6 and 127.4 (C6 and C7), 116.3 (q, ¹*J*_{C-F}=288.8 Hz, C_{F3}C_{OO}), 114.8 (C20), 68.9 (C13), 67.6 (C_j), 58.7 (C9), 26.3 and 56.2 (C14 and C16), 50.2 (C26), 49.3 and 42.5 (C28 and C29), 41.6 (C11), ~39.7 (C27 or C30), 38.0 (C12), 25.2 (C_b), 33.7 (C17), 32.7 (C27 or C30), 28.9-28.5 (C_i and C_d-C_g), 26.4 (C18), 25.5 and 25.4 (C_c and C_h), 15.9 (C1). Peak indicated by HSQC δ 137.4 (C25). C22, C23 and C24 not identified. **HPLC** (5-95% MeCN (0.05% TFA) in H₂O (0.05% TFA) over 15 min) R_t = 8.32 min. Purity= 89%. **HRMS (ESI)** *m/z* calcd for C₄₆H₆₆N₈O₅S [M+H]⁺: 843.4950; found 843.4943. **Lab reference** PM230.

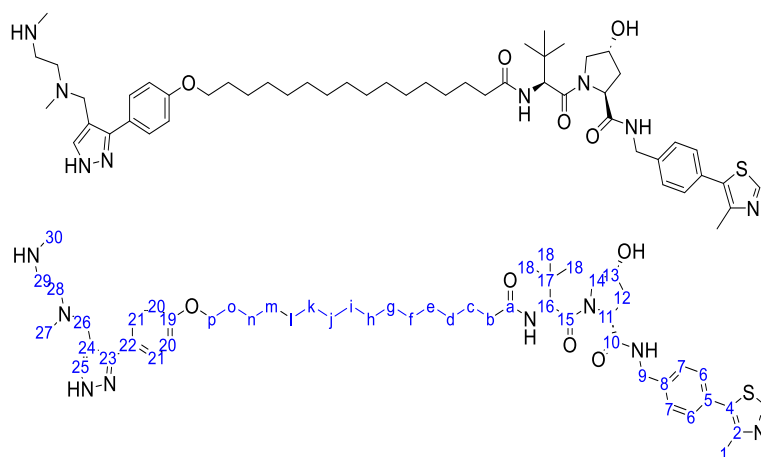
PROTAC E



General method I was followed with **26e** (27 mg, 0.04 mmol, 1 eq) and PRMT1 ligand **11** (17 mg, 0.04 mmol, 1 eq). The alkylation reaction was heated overnight at 80°C. Following deprotection, the residue was purified using automated column chromatography (C18 Gold, 5-95% MeCN in 1% CH₃COOH_(aq) over 45 CV), followed by preparative HPLC (5-95% MeCN (0.05% TFA) in H₂O (0.1% TFA) over 20 min) and lyophilised to give the title compound as a white solid (8 mg, 24%).

¹H NMR (700 MHz, d₆-DMSO) δ 10.11 (br s, 1H, 25-NH), 8.98 (s, 1H, H3), 8.74 (br s, 2H, 30-NH₂⁺), 8.56 (t, *J*=6.1 Hz, 1H, 9-NH), 7.84 (m, 2H, H25 and 16-NH), 7.50 (d, *J*=8.2 Hz, 2H, H21), 7.40 (m, 4H, H6 and H7), 7.03 (d, *J*=8.5 Hz, 2H, H20), 5.20 (br s, 1H, 13-OH), 4.54 (d, *J*=9.4 Hz, 1H, H16), 4.42 (m, 2H, H9), 4.35 (m, 1H, H13), 4.21 (dd, *J*=15.9 and 6.0 Hz, 1H, H11), 4.00 (t, *J*=6.5 Hz, 2H, H1), 3.65 (m, 2H, H14), 3.21 and 3.11 (two br s, 4H, H28 and H29), 2.58-2.54 (m, 6H, H27 and H30), 2.44 (s, 3H, H1), 2.28-2.34 and 2.17-2.08 (m, 2H, Hb), 2.04-2.02 and 1.92-1.89 (m, 2H, H12), 1.72 (m, 2H, Hk), 1.53-1.40 (m, 4H, Hc and Hj), 1.32-1.24 (m, 12H, Hd-Hi), 0.93 (s, 9H, H18). H26 likely the broad peak at ~4.2 ppm. **¹³C NMR (176 MHz, d₆-DMSO)** δ 172.1 (Ca), 172.0 (C10), 169.7 (C15), 158.7 (q, ²*J*_{C-F}=34.7 Hz, CF₃COO), 158.2 (C19), 151.9 (C3), 147.7 (C2), 139.5 and 131.2 and 129.6 (C4, C5 and C8), 129.4 (C21), 128.7 and 127.4 (C6 and C7), 114.7 (C20), 68.9 (C13), 67.6 (Cl), 58.7 (C9), 56.3 and 56.3 (C14 and C16), 41.7 (C11), 38.0 (C12), 35.2 (C17), 34.9 (Cb), 32.7 (C27 or C30), 29.0-28.7 (Cd-i and Ck), 26.4 (C18), 25.6 and 25.5 (Cc and Cj), 16.0 (C1). C22, C23, C24, C25, C26, C28, C29 and C27 or C30 not identified. **HPLC** (5-95% MeCN (0.05% TFA) in H₂O (0.05% TFA) over 15 min) R_t = 9.01 min. Purity= 96%. **HRMS (ESI)** *m/z* calcd for C₄₈H₇₀N₈O₅S[M+H]⁺: 871.5263; found 871.5320. **Lab reference** PM277.

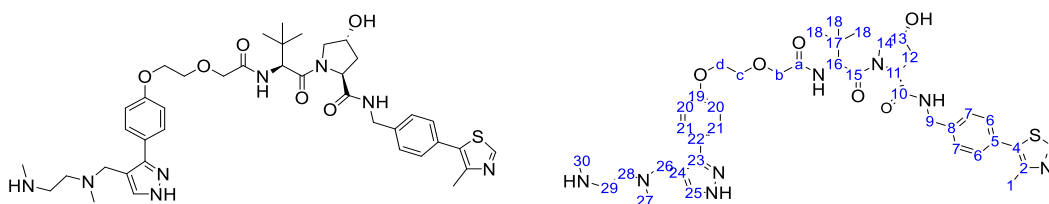
PROTAC F



General method I was followed with **26f** (53 mg, 0.07 mmol, 1 eq) and PRMT1 ligand **11** (31 mg, 0.07 mmol, 1 eq). The alkylation reaction was heated overnight at 80°C. Following deprotection, the residue was purified by preparative HPLC (5-95% MeCN (0.05% TFA) in H₂O (0.1% TFA) over 20 min) and lyophilised to give the title compound as a white solid (7 mg, 10%).

¹H NMR (700 MHz, d₆-DMSO) δ 10.17 (br s, 1H, 25-NH), 8.98 (s, 1H, H3), 8.76 (br s, 2H, 30-NH₂⁺), 8.56 (t, *J*=6.1 Hz, 1H, 9-NH), 7.88 (s, 1H, H25), 7.83 (d, *J*=9.4 Hz, 1H, 16-NH), 7.48 (d, *J*=8.5 Hz, 2H, H21), 7.40 (m, 4H, H6 and H7), 7.063 (d, *J*=8.5 Hz, 2H, H20), 4.54 (d, *J*=9.4 Hz, 1H, H16), 4.43 (m, 2H, H9), 4.33 (m, 3H, H13 and H26), 4.21 (dd, *J*=15.8 and 5.5 Hz, 1H, H11), 4.00 (t, *J*=6.4 Hz, 2H, H_p), 4.65 (m, 2H, H14), 3.24 and 3.16 (two br s, 4H, H28 and H29), 2.62 and 2.55 (two br s, 6H, H27 and H30), 2.44 (s, 3H, H1), 2.28-2.24 and 2.11-2.07 (m, 2H, H_b), 2.07-2.01 and 1.92-1.88 (m, 2H, H12), 1.72 (m, 2H, H_o), 1.53-1.39 (m, 4H, H_c and H_n), 1.32-1.23 (m, 20H, H_d-H_m), 0.93 (s, 9H, H18). 13-OH likely broad peak at ~5.2 ppm. **¹³C NMR (176 MHz, d₆-DMSO)** δ 172.1 (Ca), 172.0 (C10), 170.0 (C15), 158.8 (C19), 158.3 (q, ²*J*_{C-F}=34.7 Hz, CF₃COO⁻), 151.5 (C3), 147.7 (C2), 139.5 (C4, C5 or C8), 131.2 (C4, C5 or C8), 129.6 and 129.5 (C21 and C4, C5, or C8), 128.6 and 127.4 (C6 and C7), 116.1 (q, ¹*J*_{C-F}=294.1 Hz, CF₃COO⁻), 114.8 (C20), 68.9 (C13), 67.6 (C_p), 58.7 (C9), 56.3 and 56.3 (C14 and C16), 50.1 and 49.4 (C26 and C28 or C29), 42.5 (C28 or 29), 41.6 (C11), ~39.4 (C27 or C30), 38.0 (C12), 35.2 and 34.9 (C_b and C17), 32.6 (C27 or C30), 29.1-28.6 (C_d-m and C_o), 26.4 (C18), 25.5 and 25.4 (C_c and C_n), 15.9 (C1). Peak indicated by HSQC δ 137.7 (C25). C22, C23 and C24 not identified. **HPLC** (5-95% MeCN (0.05% TFA) in H₂O (0.05% TFA) over 15 min) *R*_t = 10.61 min. Purity= 93%. **HRMS (ESI)** *m/z* calcd for C₅₂H₇₈N₈O₅S [M+H]⁺: 927.5889; found 927.5893. **Lab reference** PM262.

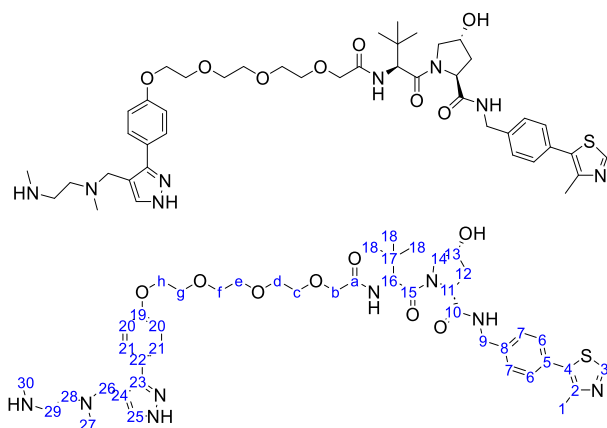
PROTAC G



General method I was followed with **32g** (33 mg, 0.06 mmol, 1 eq) and PRMT1 ligand **11** (29 mg, 0.06 mmol, 1.1 eq). The alkylation reaction was heated at 80°C for 4 days. Following deprotection, the residue was purified by automated column chromatography (C18 Gold, 5-60% MeCN in 1% HCOOH_(aq) over 45 CV), followed by preparative HPLC (5-60% MeCN (0.05% TFA) in H₂O (0.1% TFA) over 20 min) and lyophilised to give the title compound as a white solid (10 mg, 19%).

¹H NMR (500 MHz, d₆-DMSO) δ 10.08 (br s, 1H, 25-NH), 8.96 (s, 1H, H3), 8.72 (m, 2H, 30-NH₂⁺), 5.58 (t, *J*=6.0 Hz, 1H, 9-NH), 7.85 (s, 1H, 16-NH), 7.50 (m, 3H, H21 and H25), 7.39 (m, 4H, H6 and H7), 7.10 (d, *J*=8.8 Hz, 2H, H20), 4.60 (d, *J*=9.6 Hz, 1H, H16), 4.43 (m, 1H, H13), 4.34 (m, 2H, H9), 4.28 (dd, *J*=15.7 and 5.8 Hz, 1H, H11), 4.20 (s, 2H, Hd), 4.07 (m, 2H, Hb), 3.87 (m, 2H, Hc), 3.65 (m, 2H, H14), 3.22 and 3.15 (two br s, 4H, H28 and H29), 4.26 and 4.55 (two br s, 6H, H27 and H30), 2.42 (s, 3H, H1), 2.09-2.05 and 1.93-1.88 (m, 2H, H12), 0.96 (s, 9H, H18). H26 likely the broad peak at ~4.3 ppm. 13-OH likely broad peak at ~5.2 ppm. **¹³C NMR (125 MHz, d₆-DMSO)** δ 171.7 (C10), 169.2 (C15) 168.5 (Ca), 158.3 (C19), 158.1 (q, ²*J*_{C-F}=34.6 Hz, CF₃COO⁻), 151.5 (C3), 147.7 (C2), 139.4 and 131.1 and 129.7 (C4, C5 and C8), 129.5 (C21), 128.7 and 127.6 (C6 and C7), 116.2 (q, ¹*J*_{C-F}= 294.5 Hz, CF₃COO⁻), 114.9 (C20), 69.6 and 69.5 (Cb and Cc), 68.8 (C13), 67.1 (Cd), 58.7 (C9), 56.6 (C14), 55.7 (C16), 41.7 (C11), ~39.6 (C27 or C30), 38.0 (C12), 35.7 (C17), 32.7 (C27 or C30), 26.2 (C18), 15.9 (C1). C22, C23, C24, C25, C26, C28 and C29 not identified. **HPLC** (5-95% MeCN (0.05% TFA) in H₂O (0.05% TFA) over 15 min) R_t = 6.66 min. Purity= 97%. **HRMS (ESI)** *m/z* calcd for C₄₀H₅₄N₈O₆S [M+H]⁺: 775.3960; found 775.3969. **Lab reference** PM125 and PM131.

PROTAC H

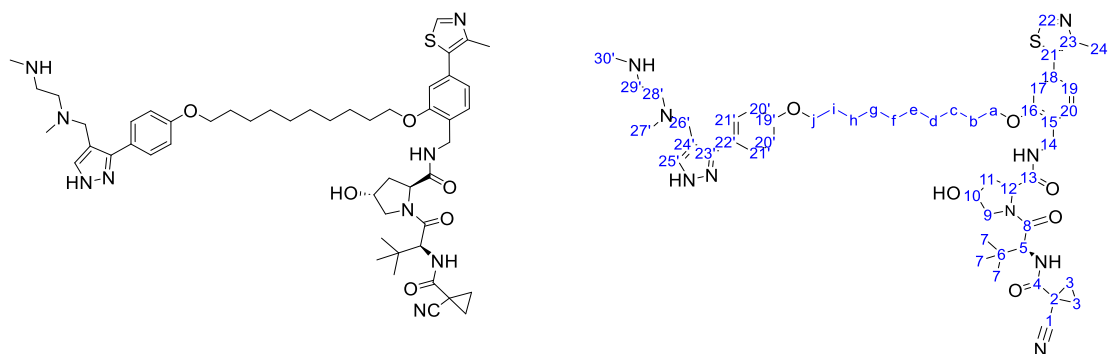


General method I was followed with **32i** (45 mg, 0.07 mmol, 1 eq) and PRMT1 ligand **11** (44 mg, 0.08 mmol, 1.1 eq). The alkylation reaction was heated at 80°C for 4 days. Following deprotection, the residue was purified by automated column chromatography (C18 Gold, 5-60% MeCN in 1% HCOOH_(aq) over 45 CV), followed by preparative HPLC (5-60% MeCN (0.05% TFA) in H₂O (0.1% TFA) over 20 min) and lyophilised to give the title compound as a white solid (6 mg, 10%).

¹H NMR (700 MHz, d₆-DMSO) δ 9.98 (br, s, 1H, 25-NH), 8.98 (s, 1H, H3), 8.67 (m, 2H, 30-NH₂⁺), 8.59 (t, *J*=6.0 Hz, 1H, 9-NH), 7.85 (br s, 1H, 16-NH), 7.50 (d, *J*=8.1 Hz, 2H, H21), 7.40 (m, 4H, H6 and H7), 7.05 (d, *J*=8.4 Hz, 2H, H20), 5.12 (br s, 1H, 13-OH), 4.57 (d, *J*=9.6 Hz, 1H, H16), 4.39 (dd, *J*=15.7 and 6.4 Hz, 1H, H13), 4.40 (m, 4H, H9 and H26), 4.25 (dd, *J*=15.7 and 5.6 Hz, 1H, H11), 4.11 (m, 2H, Hh), 3.97 (m, 2H, Hb), 3.74 (m, 2H, Hg), 3.67 (dd, *J*=10.7 and 4.0 Hz, 2H, H14), 3.60 (m, 8H, Hc-f), 3.21 and 3.14 (two br s, 4H, H28 and H29), 2.61 and 2.55 (two br s, 6H, H27 and H30), 2.44 (s, 3H, H1), 2.08-2.05 and 1.92-1.88 (m, 2H, H12), 0.95 (s, 9H, H18). H25 not identified. **¹³C NMR (176 MHz, d₆-DMSO)** δ 171.8 (C10), 169.1 (C15) 168.6 (Ca), 158.6 (C19), 158.3 (q, ²*J*_{C-F}=33.5 Hz, CF₃COO⁻), 151.5 (C3), 147.7 (C2), 139.5 and 131.1 and 129.7 (C4, C5 and C8), 129.5 (C21), 128.7 and 127.5 (C6 and C7), 116.5 (q, ¹*J*_{C-F}= 296.6 Hz, CF₃COO⁻), 114.8 (C20), 70.4-69.6 (Cb-g), 68.9 (C13), 67.2 (Ch), 58.8 (C9), 56.6 (C14), 55.7 (C16), 49.8 and 42.4 (C28 and C29), 41.7 (C11), ~39.7 (C27 or C30), 37.9 (C12), 35.7 (C17), 32.7 (C27 or C30), 26.2 (C18), 16.0 (C1). C22, C23, C24, C25 and C26 not identified. **HPLC** (5-95% MeCN (0.05% TFA) in H₂O (0.05% TFA) over 15 min) *R*_t = 6.61 min. Purity= 86%. The major impurity at 6.51 min is **PROTAC H** (12%). **HRMS (ESI)** *m/z* calcd for C₄₄H₆₂N₈O₆S [M+H]⁺: 863.4490 ; found 863.4476.

Lab reference PM130.

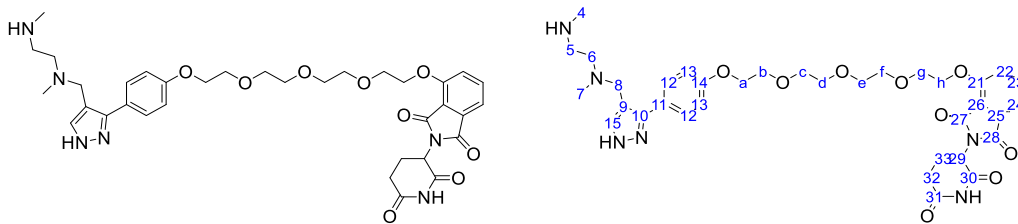
PROTAC K



33 (40 mg, 0.05 mmol, 1 eq), PRMT1 ligand **11** (24 mg, 0.06 mmol, 1.1 eq) and K_2CO_3 (14 mg, 0.1 mmol, 1 eq) were dissolved in MeCN (1 mL) and heated overnight at 50°C. The solvent was removed *in vacuo* and the residue dissolved in MeOH (2 mL). $HCl_{(aq, 37\%)}$ (1 mL) was added dropwise and the mixture stirred for 1 hr at room temperature. The solvent was removed *in vacuo* and the residue purified by automated column chromatography (C18 Gold, 5-95% MeCN in 1% $CHOOH_{(aq)}$ over 45 CV) to give an orange oil (12 mg, 26%).

1H NMR (500 MHz, d_6 -DMSO) δ 8.98 (s, 1H, H22) 8.50 (t, $J=5.9$ Hz, 1H, 14-NH), 7.62 (s, 1H, H25'), 7.59 (d, $J=8.5$ Hz, 2H, H21'), 7.39 (m, 2H, H19 or H20 and 5-NH) 7.00 (m, 3H, H20' and H17), 6.93 (dd, $J=7.8$ and 1.4 Hz, 1H, H19 or H20), 5.18 (br s, 1H, 10-OH), 4.52 (m, 2H, H5 and H12), 4.34 (m, 1H, H10), 4.24 (m, 2H, H14), 4.04 (m, 2H, Ha or Hj), 3.98 (m, 2H, Ha or Hj), 3.60 (m, 2H, H9), 3.41 (m, 2H, H26'), 2.96 (t, $J=6.3$ Hz, 2H, H29'), 2.53 (t, $J=6.3$ Hz, 2H, H28'), 2.47 (s, 3H, H30'), 2.45 (s, 3H, H24), 2.14 (s, 3H, H27'), 2.11-2.07 and 1.94-1.90 (m, 2H, H11), 1.74 (m, 4H, Hb and Hi), 1.62 and 1.50 (m, 4H, H3), 1.47-1.40 (m, 12H, Hc-Hh), 0.94 (s, 9H, H7). 25'-NH and 30'-NH not identified. **^{13}C NMR (125 MHz, d_6 -DMSO)** δ 172.8 (d, C13), 168.7 (d, C8), 164.4 (d, C4), 158.2 and 155.9 (C19' and C16), 151.4 (C22), 147.9 (C23), 131.3 and 130.9 (C18 and C21), 128.8 (C21'), 127.7 (C19 or C20), 126.9 (C15), 120.6 (C19 or 20), 120.1 (C1), 114.5 (C20'), 111.6 (C17), 68.9 (C10), 67.7 and 67.5 (Ca and Cj), 58.8 ad 57.3 (two d, C5 and C12), 56.7 (C9), 52.0 and 51.8 (C26' and C28'), 45.8 (C29'), 41.2 (C27'), 37.9 (C11), 37.2 (d, C14), 36.2 (C6), 32.9 (C30'), 29.0-28.7 (Cb-Ci), 26.1 (C7), 25.6-25.6 (Cb-Ci), 16.7 (d, C3), 16.0 (C24), 13.7 (d, C2). Doublets occur due to the exchange N-H protons with deuterium. C22', C23', C24', C25' not identified. **HPLC** (5-95% MeCN (0.05% TFA) in H_2O (0.05% TFA) over 15 min) R_t = 14.20 min. Purity= 96%. **HRMS** m/z calcd for $C_{51}H_{71}N_9O_6S$ [$M+Na^+$]: 960.5140; found 960.5131. **Lab reference** PM275.

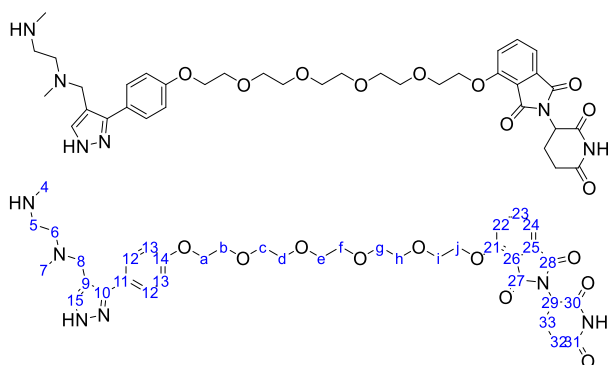
PROTAC L



40I (31 mg, 0.04 mmol, 1 eq), CRBN ligand **35** (26 mg, 0.06 mmol, 1.5 eq) and Cs_2CO_3 (28 mg, 0.09 mmol, 2 eq) were dissolved in MeCN (1 mL) and heated at 60°C overnight. The solvent was removed *in vacuo* and the residue dissolved in DCM (500 μL) and TFA (500 μL) was added dropwise and the mixture stirred at room temperature for 1 hr. The solvent was removed *in vacuo* and the residue purified by automated column chromatography (C18 Gold, 5-40% MeCN in 1% $\text{HCOOH}_{(\text{aq})}$ over 45 CV). The product was then dissolved in MeCN (200 μL) and $\text{NH}_4\text{OH}_{(\text{aq}, 35\%)}$ (50 μL) was added and the reaction stirred for 5 min. The mixture was re-acidified by the dropwise addition of $\text{HCl}_{(\text{aq}, 37\%)}$ until pH 1 was reached. The solvent was removed *in vacuo* and the residue purified by preparative HPLC (5-40% MeCN (0.05% TFA) in H_2O (0.1% TFA) over 20 min) and lyophilised to give the title compound as a colourless oil (2 mg, 7%).

^1H NMR (700 MHz, d_6 -DMSO) δ 11.10 (s, 1H, 30-NH), 10.0 (br s, 15-NH), 8.69 (br s, 2H, 4-NH₂⁺), 7.84 (br s, 1H, H15), 7.80 (dd, $J=8.4$ and 7.3 Hz, 1H, H23), 7.53 (d, $J=8.6$ Hz, 1H, H22), 7.50 (d, $J=8.0$ Hz, 2H, H12), 7.46 (d, $J=7.2$ Hz, 1H, H24), 7.05 (d, $J=8.5$ Hz, 2H, H13), 5.08 (dd, $J=12.9$ and 5.5 Hz, 1H, H29), 4.38 (br s, 2H, H8), 4.34 (m, 2H, Hh), 4.12 (m, 2H, Ha), 3.80 (m, 2H, Hg), 3.75 (m, 2H, Hb), 3.65 (m, 2H, Hf), 3.58 (m, 2H, Hc), 3.55 (m, 4H, Hd and He), 3.21 and 3.13 (two br s, 4H, H5 and H6), 2.90-2.85 (m, 1H, H32), 2.67-2.52 (m, 8H, H32 and H33 and H4 and H7), 2.04-2.00 (m, 1H, H33). **^{13}C NMR (176 MHz, d_6 -DMSO)** δ 172.8 and 169.9 (C30 and C31), 166.8 and 165.3 (C27 and C28), 158.6 (C14), 158.2 (q, $^2J_{\text{C-F}}=33.4$ Hz, CF_3COO^-), 155.8 (C21), 137.0 (C23), 133.2 (C26), 129.5 (C12), 120.0 (C22), 116.3 (C25), 115.4 (C24), 114.8 (C13), 70.2 (Cf), 69.9-69.8 (Cc-Ce), 68.9 (Cb and Ch), 68.7 (Cg), 67.2 (Ca), 48.7 (C29), ~40.0 and 32.7 (C4 and C7), 30.9 (C32), 22.0 (C33). C5, C6, C8, C9, C10, C11 and C15 not identified. **HPLC** (5-95% MeCN (0.05% TFA) in H_2O (0.05% TFA) over 15 min) $R_t=$ 6.25 min. Purity= 99%. **HRMS (ESI)** m/z calcd for $\text{C}_{35}\text{H}_{44}\text{N}_6\text{O}_9$ $[\text{M}+\text{H}]^+$: 693.3243; found 693.2247. **Lab reference** PM249 and PM252.

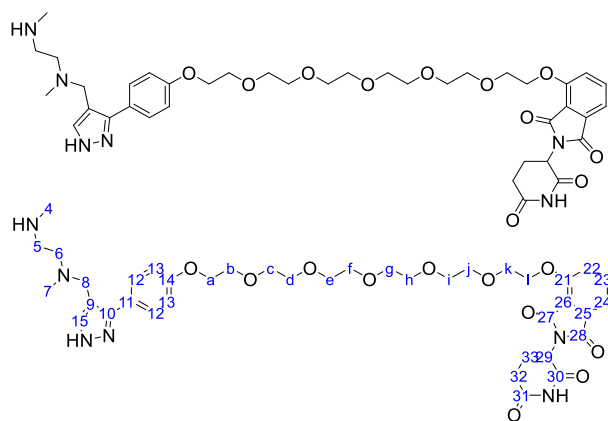
PROTAC M



40m (30 mg, 0.04 mmol, 1 eq), CRBN ligand **35** (23 mg, 0.06 mmol, 1.5 eq) and Cs_2CO_3 (25 mg, 0.08 mmol, 2 eq) were dissolved in MeCN (1 mL) and heated at 60°C overnight. The solvent was removed *in vacuo* and the residue dissolved in DCM (500 μL) and TFA (500 μL) was added dropwise and the mixture stirred at room temperature for 1 hr. The solvent was removed *in vacuo* and the residue purified by automated column chromatography (C18 Gold, 5-60% MeCN in H_2O over 60 CV). The product was then dissolved in MeCN (200 μL) and $\text{NH}_4\text{OH}_{(\text{aq}, 35\%)}$ (50 μL) was added and the reaction stirred for 5 min. The mixture was re-acidified by the dropwise addition of $\text{HCl}_{(\text{aq}, 37\%)}$ until pH 1 was reached. The solvent was removed *in vacuo* and the residue purified by preparative HPLC (5-35% MeCN (0.05% TFA) in H_2O (0.1% TFA) over 30 min) and lyophilised to give the title compound as a colourless oil (1 mg, 4%).

^1H NMR (700 MHz, d_6 -DMSO) δ 11.10 (s, 1H, 30-NH), 10.12 (br s, 15-NH), 8.70 (br s, 2H, 4-NH $_2^+$), 7.80 (dd, $J=8.5$ and 7.2 Hz, 1H, H23), 7.52 (m, 3H, H12 and H22), 7.46 (d, $J=7.2$ Hz, 1H, H24), 7.04 (m, 2H, H13), 5.08 (dd, $J=12.8$ and 5.4 Hz, 1H, H29), 4.38 (br s, 2H, H8), 4.34 (m, 2H, Hj), 4.12 (m, 2H, Ha), 3.80 (m, 2H, Hi), 3.75 (m, 2H, Hb), 3.64 (m, 2H, Hh), 3.58 (m, 2H, Hc), 3.53 (m, 4H, Hd and Hg), 3.51 (m, 4H, He and Hf), 3.20 (m, 4H, H5 and H6), 2.91-2.85 (m, 1H, H32), 2.67-2.52 (m, 8H, H32 and H33 and H4 and H7), 2.04-2.01 (m, 1H, H33). H15 not identified. **^{13}C NMR (176 MHz, d_6 -DMSO)** δ 172.8 and 169.9 (C30 and C31), 166.8 and 165.3 (C27 and C28), 158.0 (q, $^2J_{\text{C-F}}=31.2$ Hz, CF_3COO^-), 155.8 (C21), 137.0 (C23), 133.2 (C26), 129.4 (C12), 120.0 (C22), 116.3 (C25), 115.4 (C24), 114.7 (C13), 70.2 (Ch), 69.9 (Cc), 69.8 (Cd-Cg), 68.9-68.7 (Cb, Ci, Cj), 67.2 (Ca), 48.7 (C29), ~40.4 and 32.7 (C4 and C7), 30.9 (C32), 22.0 (C33). C5, C6, C8, C9, C10, C11, C14 and C15 not identified. **HPLC** (5-95% MeCN (0.05% TFA) in H_2O (0.05% TFA) over 15 min) $R_t=$ 6.41 min. Purity= 94%. **HRMS (ESI)** m/z calcd for $\text{C}_{37}\text{H}_{48}\text{N}_6\text{O}_{10}$ $[\text{M}+\text{H}]^+$: 737.3505; found 737.3455. **Lab reference** PM250, PM257.

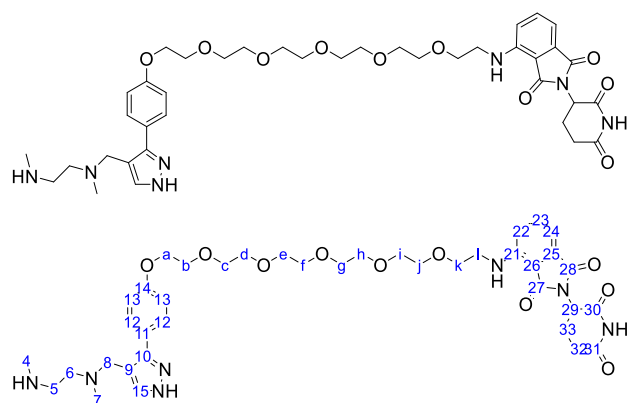
PROTAC N



42n (3 mg, 0.003 mmol, 1 eq) was then dissolved in MeCN (100 μ L) and $\text{NH}_4\text{OH}_{(\text{aq}, 35\%)}$ (20 μ L) was added and the reaction stirred for 5 min. The mixture was re-acidified by the dropwise addition of $\text{HCl}_{(\text{aq}, 37\%)}$ until pH 1 was reached. The solvent was then removed *in vacuo* and the residue purified by preparative HPLC (5-40% MeCN (0.05% TFA) in H_2O (0.1% TFA) over 20 min) and lyophilised to give the title compound as a colourless oil (1 mg, 43%).

$^1\text{H NMR}$ (700 MHz, d_6 -DMSO) δ 11.10 (s, 1H, 30-NH), 10.02 (br s, 15-NH), 8.67 (br s, 2H, 4-NH $_2^+$), 7.80 (dd, $J=8.3$ and 7.4 Hz, 1H, H23), 7.53 (d, $J=8.5$ Hz, 1H, H12), 7.51 (m, 1H, H22), 7.46 (d, $J=7.2$ Hz, 1H, H24), 7.05 (d, $J=8.1$ Hz, 2H, H13), 5.08 (dd, $J=13.0$ and 5.6 Hz, 1H, H29), 4.38 (br s, 2H, H8), 4.34 (m, 2H, Hl), 4.13 (m, 2H, Ha), 3.80 (m, 2H, Hk), 3.76 (m, 2H, Hb), 3.64 (m, 2H, Hj), 3.59 (m, 2H, Hc), 3.53 (m, 4H, Hd and Hi), 3.50 (m, 8H, He-Hh), 3.20 (m, 4H, H5 and H6), 2.91-2.85 (m, 1H, H32), 2.63-2.52 (m, 8H, H32 and H33 and H4 and H7), 2.03-2.01 (m, 1H, H33). H15 not identified. **$^{13}\text{C NMR}$ (176 MHz, d_6 -DMSO)** δ 172.8 and 169.9 (C30 and C31), 166.8 and 165.3 (C27 and C28), 155.8 (C21), 137.0 (C23), 133.2 (C26), 120.0 (C22), 116.3 (C25), 115.4 (C24), 114.7 (C13), 70.2 (Cj), 69.9 (Cc), 69.8-69.7 (Cd-Ci), 68.9 (Cb), 68.8 (Cl), 68.7 (Ck), 67.2 (Ca), 48.7 (C29), 40.4 (C4), 32.7 (C7), 30.9 (C32), 22.0 (C33). Peak indicated by HSQC δ 128.1 (C12), 50.6 (C8), 49.6 and 42.7 (C5 and C6). C9, C10, C11, C14 and C15 not identified. **HPLC** (5-95% MeCN (0.05% TFA) in H_2O (0.05% TFA) over 15 min) $R_t = 6.52$ min. Purity= 99%. **HRMS (ESI)** m/z calcd for $\text{C}_{39}\text{H}_{52}\text{N}_6\text{O}_{11}$ $[\text{M}+\text{H}]^+$: 781.3767; found 781.3748. **Lab reference** PM251.

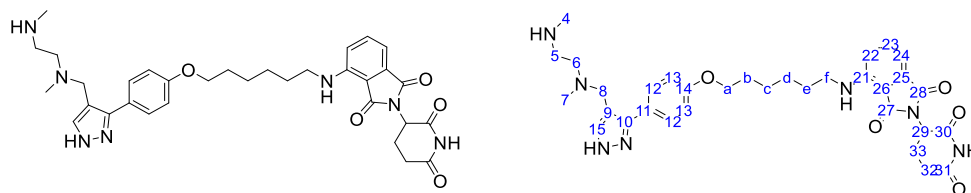
PROTAC O



General method J was followed with **47o** (18 mg, 0.03 mmol) to give a yellow oil (19 mg) that was used without further purification. The resulting yellow oil, PRMT1 ligand **11** (12 mg, 0.03 mmol, 1 eq) and Cs₂CO₃ (16 mg, 0.05 mmol, 2 eq) were dissolved in MeCN (3 mL) and stirred at room temperature overnight. The solvent was removed *in vacuo* and the residue dissolved in DCM (1 mL) and TFA (1 mL) was added dropwise and the mixture stirred at room temperature for 1 hr. The solvent was removed *in vacuo* and the residue dissolved in MeCN (600 μL) and NH₄OH_(aq, 35%) (200 μL) was added and the reaction stirred for 5 min. The mixture was re-acidified by the dropwise addition of HCl_(aq, 37%) until pH 1 was reached. The solvent was removed *in vacuo* and the residue purified by preparative HPLC (5-35% MeCN (0.05% TFA) in H₂O (0.1% TFA) over 20 min) and lyophilised to give the title compound as a green oil (7 mg, 38%).

¹H NMR (700 MHz, d₆-DMSO) δ 11.09 (s, 1H, 30-NH), 10.06 (br s, 1H, 15-NH), 8.70 (br s, 2H, 4-NH₂⁺), 7.85 (s, 1H, H15), 7.58 (dd, *J*=8.4 and 7.2 Hz, 1H, H23), 7.50 (d, *J*=8.5 Hz, 2H, H12), 7.14 (d, *J*=8.6 Hz, 1H, H22), 7.06 (d, *J*=8.6 Hz, 2H, H13), 7.07 (d, *J*=7.0 Hz, 1H, H24), 6.60 (m, 1H, 21-NH), 5.05 (dd, *J*=12.9 and 5.5 Hz, 1H, H29), 4.34 (br s, 2H, H8), 4.13 (m, 2H, Ha), 3.76 (m, 2H, Hb), 3.61 (m, 2H, Hk), 3.59-3.48 (m, 16H, Hc-Hj), 3.46 (m, 1H, Hl), 3.22 and 3.14 (two br s, 4H, H5 and H6), 2.89 (m, 1H, H32), 2.66-2.50 (m, 8H, H4 and H7 and H32 and H33), 2.02 (m, 1H, H33). **¹³C NMR (176 MHz, d₆-DMSO)** δ 172.8 and 170.1 (C30 and C31), 168.9 and 167.3 (C27 and C28), 158.6 (C14), 158.3 (q, ²*J*_{C-F}=33.8 Hz, CF₃COO⁻), 146.4 (C21), 136.2 (C23), 132.1 (C25), 129.5 (C12), 117.5 (C22), 116.3 (q, ¹*J*_{C-F}=295.2 Hz, CF₃COO⁻), 114.8 (C13), 110.7 (C24), 109.2 (C26), 69.9-69.9 (Cc-Cj), 68.9 (Cb and Ck), 67.2 (Ca), 50.2 (C8), 49.4 (C5 or C6), 48.6 (C29), 42.5 (C5 or C6), 41.7 (Cl), ~39.3 and 32.7 (C4 and C7), 31.0 (C32), 22.1 (C33). Peak indicated by HSQC δ 137.1 (C15). C9, C10 and C11 not identified. **HPLC** (5-95% MeCN (0.05% TFA) in H₂O (0.05% TFA) over 15 min) R_t = 6.95 min. Purity= 99%. **HRMS (ESI)** *m/z* calcd for C₃₉H₅₃N₇O₁₀ [M+H]⁺: 780.3927; found 780.3923. **Lab reference** PM254 and PM258

PROTAC P



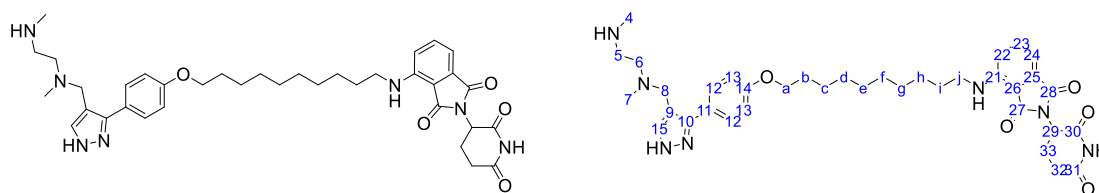
Route 1 General method E was followed with PRMT1 ligand **11** (54 mg, 0.13 mmol) and 6-amino-1-hexanol. The product was further purified by automated column chromatography (C18 Gold, 5-40% MeCN in 1% HCOOH_(aq) over 45 CV) to give a give intermediate product **45** as pale orange solid (18 mg, 0.03 mmol) which was used without further purification. The solid (18 mg, 0.03 mmol, 1 eq) and 4-fluorothalidomide (10 mg, 0.04 mmol, 1.1 eq) were dissolved in DMSO (10 mL/mmol) and DIPEA (20 μ L, 0.10 mmol, 3 eq) was added. The mixture was heated at 130°C overnight and then purified by automated column chromatography (C18 Gold, 5-95% MeCN in 1% HCOOH_(aq) over 60 CV). The product was dissolved in MeOH (0.5 mL) and HCl_(aq, 37%) (0.5 mL) was added dropwise and the mixture stirred at room temperature for 1 hr. The solvent was then removed *in vacuo* and the residue purified by preparative HPLC (5-60% MeCN (0.05% TFA) in H₂O (0.1% TFA) over 30 min) and lyophilised to give the title compound as a yellow oil (2 mg, 3%).

Route 2 General method J was followed with **47p** (32 mg, 0.06 mmol) to give a yellow oil (80 mg) that was used without further purification. The resulting yellow oil, PRMT1 ligand **11** (28 mg, 0.06 mmol, 1 eq), Cs₂CO₃ (42 mg, 0.12 mmol, 2 eq) and NaI (9 mg, 0.06 mmol, 1 eq) were dissolved in MeCN (3 mL) and heated at 60°C overnight. The solvent was removed *in vacuo* and the residue dissolved in DCM (1 mL) and HCl_(aq, 37%) (1 mL) was added dropwise and the mixture stirred at room temperature for 1 hr. The solvent was removed *in vacuo* and the residue dissolved in MeCN (600 μ L) and NH₄OH_(aq, 35%) (200 μ L) was added and the reaction stirred for 5 min. The mixture was re-acidified by the dropwise addition of HCl_(aq, 37%) until pH 1 was reached. The mixture was then diluted with water and washed with DCM. The solvent was removed from the aqueous layer under a stream of compressed air. The residue was then purified by preparative HPLC (5-60% MeCN (0.05% TFA) in H₂O (0.1% TFA) over 30 min) and lyophilised to give the title compound as a green oil (10 mg, 27%).

¹H NMR (700 MHz, d₆-DMSO) δ 11.09 (s, 1H, 30-NH), 10.23 (br s, 1H, 15-NH), 8.82 (br s, 2H, 4-NH₂⁺), 7.87 (s, 1H, H15), 7.58 (dd, *J*=8.5 and 7.1 Hz, 1H, H23), 7.48 (d, *J*=8.7 Hz, 2H, H12), 7.10 (d, *J*=8.6 Hz, 1H, H22), 7.03 (m, 3H, H13 and H24), 6.55 (br s, 1H, 21-NH), 5.05 (dd, *J*=12.9 and 5.5 Hz, 1H, H29), 4.34 (br s, 2H, H8), 4.01 (m, 2H, Ha), 3.32 (m, 2H, Hf), 3.25 and 3.18 (two br s, 4H, H5 and H6), 2.88 (m, 1H, H32), 2.62-2.51 (m, 8H, H4 and H7 and H32 and H33), 2.02 (m, 1H, H33), 1.75 (m, 2H, Hb), 1.62 (m, 2H, He), 1.48 (m, 2H, Hc), 1.43 (m, 2H, Hd). **¹³C NMR (176 MHz, d₆-DMSO)** δ 172.8 and 170.1 (C30 and C31), 169.0 and 167.3 (C27 and C28), 158.8 (C14), 158.4 (q, ²*J*_{C-F}=34.8 Hz, CF₃COO⁻), 146.4

(C21), 136.3 (C23), 132.2 (C25), 129.5 (C12), 117.2 (C22), 114.8 (C13), 110.4 (C24), 109.0 (C26), 67.5 (Ca), 50.1 (C8), 49.4 (C5 or C6), 48.5 (C29), 42.5 (C5 or C6), 41.8 (Cf), ~39.2 and 32.7 (C4 and C7), 31.0 (C32), 28.7 (Ce), 28.6 (Cb), 26.1 (Cd), 25.3 (Cc), 22.2 (C33). C9, C10, C11 and C15 not identified. **HPLC** (5-95% MeCN (0.05% TFA) in H₂O (0.05% TFA) over 15 min) R_t = 7.97 min. Purity= 99%. **HRMS (ESI)** *m/z* calcd for C₃₃H₄₁N₇O₅ [M+H]⁺: 616.3242; found 616.3237. **Lab reference** Route 1: PM173 and PM178. Route 2: PM288 and PM291.

PROTAC Q

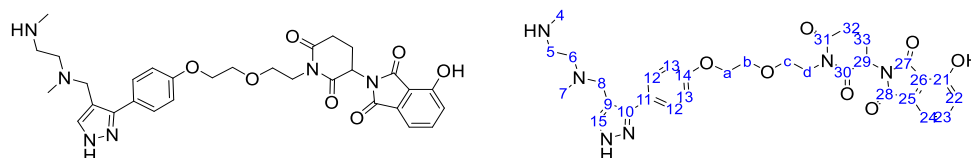


General method J was followed with **47q** (51 mg, 0.09 mmol, 1 eq) to give a yellow oil (90 mg) that was used without further purification. The resulting yellow oil, PRMT1 ligand **11** (38 mg, 0.09mmol, 1 eq), Cs₂CO₃ (59 mg, 0.18 mmol, 2 eq) and NaI (14 mg, 0.09 mmol, 1 eq) were dissolved in MeCN (3 mL) and heated at 60°C overnight. The solvent was removed *in vacuo* and the residue dissolved in DCM (1 mL) and TFA (1 mL) was added dropwise and the mixture stirred at room temperature for 1 hr. The solvent was removed *in vacuo* and the residue dissolved in MeCN (600 μL) and NH₄OH_(aq, 35%) (200 μL) was added and the reaction stirred for 5 min. The mixture was re-acidified by the dropwise addition of HCl_(aq, 37%) until pH 1 was reached. The mixture was then diluted with water and extracted with DCM. The organic layer was concentrated *in vacuo* and purified by preparative HPLC (5-60% MeCN (0.05% TFA) in H₂O (0.1% TFA) over 30 min) and lyophilised to give the title compound as a green oil (3 mg, 5%).

¹H NMR (500 MHz, d₆-DMSO) δ 11.09 (s, 1H, 30-NH), 10.26 (br s, 1H, 15-NH), 8.83 (br s, 2H, 4-NH₂⁺), 7.88 (s, 1H, H15), 7.58 (dd, *J*=8.5 and 7.1 Hz, 1H, H23), 7.48 (d, *J*=8.7 Hz, 2H, H12), 7.09 (d, *J*=8.7 Hz, 1H, H22), 7.02 (m, 3H, H13 and H24), 6.52 (br s, 1H, 21-NH), 5.04 (dd, *J*=12.8 and 5.5 Hz, 1H, H29), 4.33 (br s, 2H, H8), 3.99 (m, 2H, Ha), 3.29 (m, 2H, Hj), 3.25 and 3.20 (two br s, 4H, H5 and H6), 2.88 (m, 1H, H32), 2.64-2.52 (m, 8H, H4 and H7 and H32 and H33), 2.02 (m, 1H, H33), 1.72 (m, 2H, Hb), 1.57 (m, 2H, Hi), 1.41 (m, 2H, Hc), 1.31 (m, 10H, Hd-h). **¹³C NMR (125 MHz, d₆-DMSO)** δ 172.9 and 170.1 (C30 and C31), 169.0 and 167.3 (C27 and C28), 158.9 (C14), 158.3 (q, ²*J*_{C-F}=33.9 Hz, CF₃COO⁻), 146.5 (C21), 136.3 (C23), 132.2 (C25), 129.6 (C12), 117.2 (C22), 116.2 (q, ¹*J*_{C-F}=274.4 Hz, CF₃COO⁻), 114.8 (C13), 110.4 (C24), 109.0 (C26), 67.6 (Ca), 50.2 (C8), 49.4 (C5 or C6), 48.6 (C29), 42.6 (C5 or C6), 41.9 (Cj), ~39.5 and 32.7 (C4 and C7), 31.0 (C32), 29.0-28.8 (Ce-Ch), 28.7 (Ci and Cb), 26.1 (Cd), 25.3

(Cc), 22.2 (C33). Peak indicated by HSQC δ 137.7 (C15). C9, C10 and C11 not identified. **HPLC** (5-95% MeCN (0.05% TFA) in H₂O (0.0.5% TFA) over 15 min) R_t = 9.67 min. Purity= 95%. **HRMS (ESI)** m/z calcd for C₃₇H₄₉N₇O₅ [M+H]⁺: 671.3790; found 671.3757. **Lab reference** PM274 and PM276.

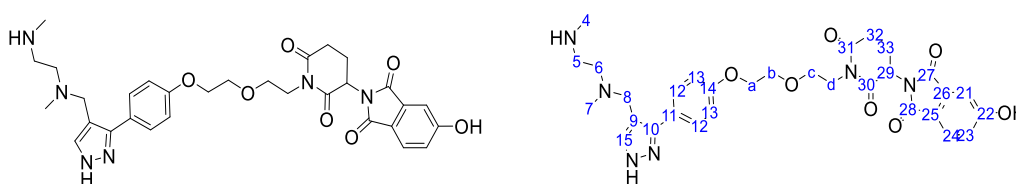
HBM1



General method K was followed with **34** (27 mg, 0.05 mmol, 1 eq) and 2-(2,6-Dioxopiperidin-3-yl)-4-hydroxyisoindoline-1,3-dione {CAS: 5054-59-1}. Following deprotection, the residue was purified by preparative HPLC (5-40% MeCN (0.05% TFA) in H₂O (0.1% TFA) over 20 min) and lyophilised to give the title compound a pale yellow solid (11 mg, 34%).

¹H NMR (500 MHz, d₆-DMSO) δ 11.35 (br s, 1H, 21-OH), 10.22 (br s, 1H, 15-NH), 8.80 (br s, 2H, 4-NH₂⁺), 7.86 (s, 1H, H15), 7.66 (dd, J =8.4 and 7.2 Hz, 1H, H23), 7.49 (d, J =8.7 Hz, 2H, H12), 7.32 (d, J =7.2 Hz, 1H, H24), 7.28 (d, J =8.4 Hz, 1H, H22), 7.07 (d, J =8.8 Hz, 2H, H13), 5.17 (dd, J =13.0 and 5.4 Hz, H29), 4.33 (m, 2H, H8), 4.12 (m, 2H, Ha), 3.94-3.81 (m, 2H, Hd), 3.76 (m, 2H, Hb), 3.52 (m, 2H, Hc), 3.23 and 3.17 (two br s, 4H, H5 and H6), 3.01-2.94 and 2.78-2.73 (m, 2H, H32), 2.61 and 2.55 (two br s, 6H, H4 and H7), 2.54 and 2.07-2.03 (m, 2H, H33). **¹³C NMR (125 MHz, d₆-DMSO)** δ 171.6 and 169.6 (C30 and C31), 167.0 and 165.8 (C27 and C28), 158.4 (q, $^2J_{C-F}$ =33.5 Hz, CF₃COO⁻), 155.6 (C21), 136.4 (C23), 133.1 (C15), 129.6 (C12), 123.6 (C22), 114.9 (C13), 114.3 (C24), 68.7 (Cb), 67.2 (Ca), 66.9 (Cc), 49.3 (C29), 38.6 (Cd), 31.2 (C32), 21.3 (C33). Peaks indicated by HSQC δ 50.5 (C8), 49.7 and 42.9 (C5 and C6), 39.3 and 33.1 (C4 and C7). C9, C10, C11, C14, C25 and C26 not detected. **HPLC** (5-95% MeCN (0.05% TFA) in H₂O (0.0.5% TFA) over 15 min) R_t = 6.18 min. Purity= 99%. **HRMS (ESI)** m/z calcd for C₃₁H₃₆N₆O₇ [M+H]⁺: 605.2718; found 605.2719. **Lab reference** PM141 (0.05 mmol, 6%) and PM155 (0.05 mmol, 34%).

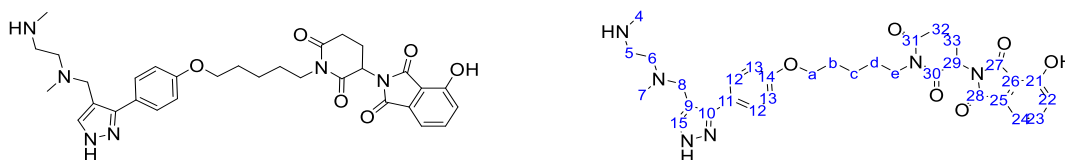
HBM2



General method K was followed with **34** (36 mg, 0.07 mmol, 1 eq) and 2-(2,6-Dioxopiperidin-3-yl)-5-hydroxyisoindoline-1,3-dione {CAS: 64567-60-8}. Following deprotection, the residue was purified by preparative HPLC (20-40% MeCN (0.05% TFA) in H₂O (0.1% TFA) over 20 min) and lyophilised to give the title compound a colourless oil (5 mg, 14%).

¹H NMR (500 MHz, d₆-DMSO) δ 11.11 (br s, 1H, 22-OH), 10.24 (br s, 15-NH), 8.78 (br s, 2H, 4-NH₂⁺), 7.89 (s, 1H, H15), 7.74 (d, *J*=8.1 Hz, H21), 7.49 (d, *J*=8.8 Hz, 2H, H12), 7.18 (m, 2H, H23 and H24), 7.06 (d, *J*=8.8 Hz, 2H, H13), 5.18 (dd, *J*=13.1 and 5.4 Hz, H29), 4.35 (m, 2H, H8), 4.12 (m, 2H, Ha), 3.94-3.80 (m, 2H, Hd), 3.76 (m, 2H, Hb), 3.51 (m, 2H, Hc), 3.23 and 3.17 (two br s, 4H, H5 and H6), 3.01-2.94 and 2.78-2.73 (m, 2H, H32), 2.62 and 2.54 (two br s, 6H, H4 and H7), 2.53 and 2.05-2.03 (m, 2H, H33). **¹³C NMR (125 MHz, d₆-DMSO)** δ 169.6 and 167.0 (C30 and C31), 166.9 and 163.7 (C27 and C28), 158.7 (C14), 158.3 (q, ²*J*_{C-F}=35.0 Hz, CF₃COO⁻), 134.1 (C22), 129.6 (C12), 125.7 (C21), 120.8 (C23 or C24), 116.1 (q, ¹*J*_{C-F}=294.3 Hz, CF₃COO⁻), 114.8 (C13), 110.0 (C23 or C24), 68.6 (Cb and C8), 67.2 (Ca), 66.9 (Cc), 49.5 and 49.4 (C29 and C5 or C6), 42.5 (C5 or C6), ~39.5 (C4 or C7), 38.7 (Cd), 32.6 (C4 or C7), 31.2 (C32), 21.3 (C33). Peak indicated by HSQC δ 137.4 (C15). C9, C10, C11, C25 and C26 not identified. **HPLC** (5-95% MeCN (0.05% TFA) in H₂O (0.05% TFA) over 15 min) R_t = 6.28 min. Purity= 99%. **HRMS (ESI)** *m/z* calcd for C₃₁H₃₆N₆O₇. [M+H]⁺: 605.2718; found 605.2724. **Lab reference** PM164.

HBM3

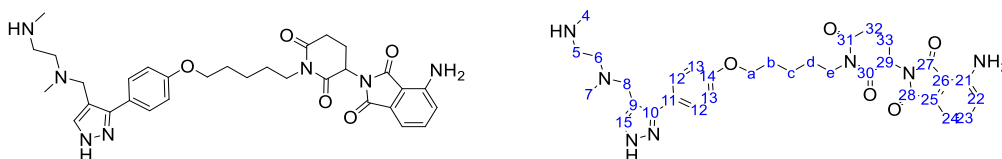


General method K was followed with **34**(*n*=5) (22 mg, 0.04 mmol, 1 eq) and 2-(2,6-Dioxopiperidin-3-yl)-4-hydroxyisoindoline-1,3-dione {CAS: 5054-59-1}. Following deprotection, the residue was purified by preparative HPLC (5-60% MeCN (0.05% TFA) in H₂O (0.1% TFA) over 30 min) and lyophilised to give the title compound a yellow oil (18 mg, 75%).

¹H NMR (500 MHz, d₆-DMSO) δ 11.34 (br s, 21-OH), 10.17 (br s, 1H, 15-NH), 8.79 (br s, 2H, 4-NH₂⁺), 7.84 (s, 1H, H15), 7.65 (dd, *J*=8.4 and 7.2 Hz, 1H, H23), 7.48 (d, *J*=8.6 Hz, 2H, H12), 7.31 (d, *J*=7.1 Hz, 1H, H24), 7.27 (d, *J*=8.4 Hz, 1H, H22), 7.04 (d, *J*=8.8 Hz, 2H, H13), 5.16 (dd, *J*=13.0 and 5.5 Hz, 1H, H29), 4.32 (m, 2H, H8), 4.00 (t, *J*=6.4 Hz, 2H, Ha), 3.68 (m, 2H, He), 3.22 and 3.17 (two br s, 4H, H5 and H6), 3.01-2.94 and 2.77-2.72 (m 2H, H32), 2.60 and 2.55 (two br s, 6H, H4 and H7), 2.52 and 2.06-2.03 (m, 2H, H33), 1.75 (m, 2H, Hb), 1.51 (m, 2H, Hd), 1.42 (m, 2H, Hc). **¹³C NMR (125 MHz, d₆-DMSO)** δ 171.7 and 169.6 (C30 and C31), 167.0 and 165.8 (C27 and C28), 158.8 (C14), 158.3 (q, ²*J*_{C-}

$\nu_{\text{C-F}}=35.2$ Hz, CF_3COO^-), 155.6 (C21), 136.4 (C23), 133.1 (C26), 129.5 (C12), 123.6 (C22), 114.8 (C13), 114.3 and 114.2 (C24 and C25), 67.4 (Ca), 50.2 (C8), 49.4 (C5 or C6), 49.2 (C29), 42.6 (C5 or C6), ~ 39.9 (Ce), ~ 39.3 (C4 or C7), 32.7 (C4 or C7), 31.2 (C32), 28.3 (Cb), 27.1 (Cd), 22.8 (Cc), 21.3 (C33). Peak indicated by HSQC δ 137.1 (C15). C9, C10, C11 not identified. **HPLC** (5-95% MeCN (0.05% TFA) in H_2O (0.0.5% TFA) over 15 min) R_t = 6.95 min. Purity= 99%. **HRMS (ESI)** m/z calcd for $\text{C}_{32}\text{H}_{38}\text{N}_6\text{O}_6$. $[\text{M}+\text{H}]^+$: 603.2926; found 603.2962. **Lab reference** PM168.

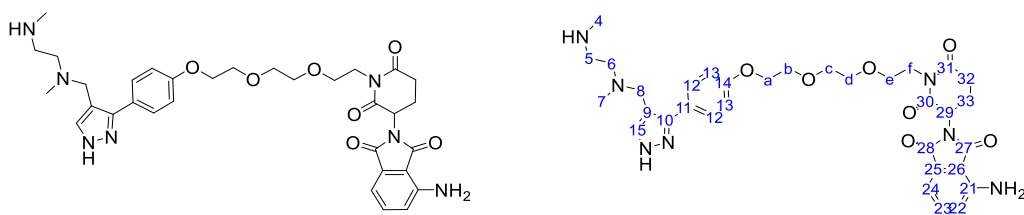
HBM4



General method K was followed with **34(n=5)** (20 mg, 0.04 mmol, 1 eq) and pomalidomide. Following deprotection, the residue was purified by preparative HPLC (5-40% MeCN (0.05% TFA) in H_2O (0.1% TFA) over 30 min) and lyophilised to give the title compound a yellow oil (18 mg, 37%).

$^1\text{H NMR}$ (500 MHz, $\text{d}_6\text{-DMSO}$) δ 10.31 (br s, 1H, 15-NH), 8.84 (br s, 2H, 4-NH $_2^+$), 7.89 (s, 1H, H15), 7.47 (m, 3H, H12 and H23), 7.02 (m, 4H, H13 and H22 and H24), 6.66 (br s, 2H, 21-NH $_2$), 5.14 (dd, $J=13.0$ and 5.4 Hz, 1H, H29), 4.35 (s, 2H, H8), 4.00 (m, 2H, Ha), 3.68 (m, 2H, He), 3.26 and 3.18 (two br s, 4H, H5 and H6), 3.02-2.94 and 2.77-2.72 (m, 2H, H32), 2.63 and 2.55 (two br s, 6H, H4 and H7), 2.53 and 2.06-2.03 (m, 12, H33), 1.75 (m, 2H, Hb), 1.51 (m, 2H, Hd), 1.42 (m, 2H, Hc). **$^{13}\text{C NMR}$ (125 MHz, $\text{d}_6\text{-DMSO}$)** δ 171.7 and 169.7 (C30 and C31), 168.6 and 167.4 (C27 and C28), 158.8 (C14), 158.4 (q, $\nu_{\text{C-F}}=35.2$ Hz, CF_3COO^-), 146.8 (C21), 135.5 (C23), 132.0 (C26), 129.6 (C12), 121.8 (C22), 115.0 (C25), 114.8 (C13), 111.0 (C24), 67.4 (Ca), 50.1 (C8), 49.4 (C5 or C6), 49.1 (C29), 42.5 (C5 or C6), ~ 39.4 (Ce), ~ 39.2 (C4 or C7), 32.6 (C4 or C7), 31.2 (C32), 28.3 (Cb), 27.1 (Cd), 22.8 (Cc), 21.5 (C33). Peak indicated by HSQC δ 137.7 (C15). C9, C10, C11 not identified. **HPLC** (5-95% MeCN (0.05% TFA) in H_2O (0.0.5% TFA) over 15 min) R_t = 9.68 min. Purity= 99%. **HRMS (ESI)** m/z calcd for $\text{C}_{32}\text{H}_{39}\text{N}_7\text{O}_5$ $[\text{M}+\text{H}]^+$: 602.3085; found 602.3077. **Lab reference** PM169.

HBM5



34(m=2) (54 mg, 0.09 mmol, 1 eq) and NaI (27 mg, 0.18 mmol, 2 eq) were dissolved in acetone (2 mL) and heated at 60°C for 4 hr. The solvent was removed *in vacuo*. The residue and pomalidomide (25 mg, 0.09 mmol, 1 eq) were dissolved in MeCN (2 mL) and DIPEA (40 μ L (0.23 mmol, 2 eq) was added and the reaction heated at 80°C overnight. The reaction was analysed by LC/MS and starting material **34(m=2)** remained. To the reaction, NMP (1 mL) and DIPEA (100 μ L) was added and the reaction heated at 110°C for 4 hr. The reaction was quenched with solid NaHCO₃ and the solvent removed *in vacuo*. The residue was purified by automated column chromatography (C18 Gold, 5-95% MeCN in 1% HCOOH_(aq) over 60 CV). The product was dissolved in MeOH (1 mL) and HCl_(aq, 37%) (0.5 mL) was added dropwise and the mixture stirred at room temperature for 1 hr. The solvent was then removed *in vacuo* and the residue purified by preparative HPLC (5-40% MeCN (0.05% TFA) in H₂O (0.1% TFA) over 20 min) and lyophilised to give the title compound as a yellow oil (4 mg, 7%).

¹H NMR (700 MHz, d₆-DMSO) δ 10.02 (br s, 1H, 15-NH), 8.68 (br s, 2H, 4-NH₂⁺), 7.85 (s, 1H, H15), 7.48 (m, 3H, H12 and H23), 7.06 (d, $J=8.5$ Hz, 2H, H13), 7.02 (d, $J=8.5$ Hz, 1H, H22), 7.00 (d, $J=6.9$ Hz, 1H, H24), 6.59 (br s, 2H, 21-NH₂), 5.15 (dd, $J=13.0$ and 5.3 Hz, 1H, H29), 4.35 (s, 2H, H8), 4.14 (m, 2H, Ha), 3.91-3.79 (m, 2H, Hf), 3.77 (m, 2H, Hb), 3.58-3.55 (m, 2H, Hc and Hd), 3.44 (m, 2H, He), 3.22 and 3.14 (two br s, 4H, H5 and H6), 2.99-2.94 and 2.77-2.74 (m, 2H, H32), 2.62 and 2.55 (two br s, 6H, H4 and H7), 2.54-2.52 and 2.05-2.03 (m, 12, H33). **¹³C NMR (176 MHz, d₆-DMSO)** δ 171.6 and 169.7 (C30 and C31), 168.5 and 167.3 (C27 and C28), 158.7 (C14), 158.3 (q, $^2J_{C-F}=35.0$ Hz, CF₃COO⁻), 146.8 (C21), 135.5 (C23), 132.0 (C26), 129.5 (C12), 121.8 (C22), 115.3 (C25), 114.8 (C13), 111.0 (C24), 69.8 and 69.6 (Cc and Cd), 68.9 (Cb), 67.3 (Ca), 66.7 (Ce), 50.2 (C8), 49.3 (C5 or C6), 49.1 (C29), 42.5 (C5 or C6), ~39.5 (C4 or C7), 38.6 (Cf), 32.7 (C4 or C7), 31.2 (C32), 21.4 (C33). C9, C10, C11 and C15 not identified. **HPLC** (5-95% MeCN (0.05% TFA) in H₂O (0.05% TFA) over 15 min) R_t = 6.25 min. Purity= 89%. **HRMS (ESI)** m/z calcd for C₃₃H₄₁N₇O₇ [M+H]⁺: 648.3140; found 648.3131. **Lab reference** PM172.

9.3 Stability Studies

MCF-7 cell media (DMEM supplemented with 10% FBS), Caffeine (400 μ M in DMSO) and PROTAC (400 μ M in DMSO) was incubated at 37°C in an ambient atmosphere. A 10-50 μ L aliquot of the mixture was taken at the indicated time point and an equal volume of ice-cold MeCN was immediately added. The sample was subjected to vortex mixing for 10 seconds and then centrifugation for 3 minutes at 13 G. The supernatants were analysed by analytical HPLC (5-60% or 5-40% MeCN (0.05% TFA) in H₂O (0.05% TFA) over 15 min). The same method was followed for stability studies in human serum (Sigma Aldrich, #H4522) and PBS pH 7.4 (in-house). 'Compound remaining, %' was determined by the integral of the respective peak for caffeine and PROTAC in the UV-HPLC chromatogram (λ = 254 nm). The integral for the PROTAC peak was divided by that of the caffeine peak and the ratio normalised to 0 hr incubation. Data was processed using GraphPad Prism Version 10.0.3.

9.4 Cell Culture

All *in vitro* experiments were undertaken at Cancer Research UK Cambridge Institute, University of Cambridge.

Cell Lines The MCF-7 and HPAF-II cell lines were obtained from the American Type Culture Collection (ATCC). The KP-3 cell line was obtained from the Japanese Cell Repository.

Cell Culture MCF-7 cells were cultured in Dulbecco's Modified Eagle Medium (DMEM) (gibco, 41966-029) supplemented with 10% Fetal Bovine Serum (FBS) (gibco, A3840402). HPAF-II cells cultured in Minimum Essential Medium (MEM) (gibco, 11095-080) supplemented with 1% sodium pyruvate (Thermo Scientific, 11360-039) and 10% FBS. KP-3 cells cultured in Roswell Park Memorial Institute (RPMI) 1640 Medium (Gibco, 21875-034) supplemented with 1% sodium pyruvate and 10% FBS. Cells were maintained for no more than 50 passages at 37°C with 5% CO₂.

Treatment with a probe compound Cells were counted using the Vi-CELL XR cell viability analyser, as per manufactures instructions, and the desired number of cells seeded in full media in individual 10 cm plates (Corning, #430167) or multiple well plate (96 well plate (Corning, #3610), 12 well plate (Corning, #3513), 6 well plate (Corning, #3516)) and the cells were allowed to adhere overnight. The cells were then treated with the probe compound. For 10 cm plates, the probe compound in DMSO was added directly to the cell culture media and the final DMSO concentration was 0.01%. For 96 well plates, the probe compound was diluted in Opti-MEM reduced serum media (Gibco, #31985070). Following treatment, the cells were incubated at 37°C in 5% CO₂.

Probe compound	Source	Catalogue #	Dilution
GSK3368715	MCE	#HY-128717A	10 μ M in DMSO (in house)
MG132	MCE	#HY-13259	50 μ M in DMSO (in house)
Cycloheximide	TOKU-E	#C084	10% in DMSO
		#C001	100 μ g mL ⁻¹ DMSO (in house)

siRNA MCF-7 cells were plated in a 10 cm plate (for Western blot) or a 96 well plate (for viability assay) and grown to 50-60% confluence. Cells were transfected with siRNA targeting PRMT1 or negative control siRNA (Horizon Discovery) at a final concentration of 20 nM in the presence of Lipofectamine RNAi MAX transfection Reagent (Invitrogen, #13778-150).

HaloPROTAC 3 The plasmid pH6HTC_PRMT1-Halo was a gift from Claudia Kutter (addgene plasmid # 175334; <http://n2t.net/addgene:175334> ; RRID:Addgene_175334). The bacteria stab was streaked into single colonies and a single colony inoculated as per the guidelines published by 'addgene'²⁴⁹. The plasmid was isolated and purified by the QIAfilter Plasmid Maxi Kit (Qiagen, #12263) as per manufacturer's instructions and analysed by NanoDrop ND-1000 Spectrophotometer. MCF-7 cells were transfected with the DNA plasmid with Lipofectamine 2000 (Invitrogen, 116680919) in a 1 μ g DNA:2.5 μ L Lipofectamine ratio in Opti-MEM reduced serum media (Gibco, #31985070). After 24 hr, the media was replaced with fresh media and after a further 24 hr, the cells were harvested and analysed by Western blot.

9.5 SDS-PAGE followed by Western Blot

Lysate preparation Upon removal from the incubator, the plates containing the cells were placed on ice. The media was aspirated and the plates washed with twice with ice cold PBS. RIPA buffer containing protease and phosphatase inhibitor was added and the cells were detached from the surface with a cell scraper. After centrifugation (8000 rpm for 3 min at 4°C), the supernatant was discarded and the pellet flash frozen and stored at -80°C or taken forward for lysis. The pellet was resuspended in RIPA buffer containing protease and phosphatase inhibitor and incubated at 4°C for 10 minutes with rotation. The sample was sonicated for 3 min (30 seconds on, 30 seconds off) and subjected to centrifugation (21,000 x g for 10 min at 4°C). The supernatant was transferred and the protein concentration quantified by the Direct Detect Spectrometer as per manufacturer's instructions.

SDS-PAGE 30 μ g of protein was denatured by heating at 80°C for 10 min in NuPAGE LDS sample buffer (4X), NuPAGE Sample Reducing Agent (10x) and made up to 25 μ L with RIPA buffer (multiplied

up as required). The samples were loaded onto a 4-12% Bis-Tris 1.0 mm pre-cast polyacrylamide gel (12 μ L loaded onto 12 well, 10 μ L loaded onto 15 well) with a molecular weight ladder. With the MOPS running buffer, voltage was applied with at 60 V for 30 minutes followed by 120 V. The voltage was stopped once the dye front reached the bottom of the gel (~90 minutes).

Western Blot The proteins were transferred from the gel to a PVDF membrane using an iBlot2 gel transfer device using the pre-programmed P0 method. Following transfer, the membrane was washed sequentially in methanol, H₂O and TBS-T (0.1% Tween-20 in TBS). The membrane was blocked with 5% milk in TBS for 1 hr at room temperature and then incubated with primary antibody in 1% milk in TBS-T overnight at 4 °C. The membrane was then washed three times for 5 min with TBS-T and incubated with secondary antibody in 1% milk in TBS-T for 1 hr at room temperature. The membrane was washed three times for 5 min with TBS-T washed once with TBS for 5 minutes and then imaged using the LiCor CLx or LiCor Odyssey. Protein quantification was performed by densitometry using Image Studio analysis software (LI-COR Biosciences).

Antibodies	Source	Catalogue #	Dilution
Rabbit anti-PRMT1	Cell Signaling	2449S	1:1000
Rabbit anti-PRMT1	abcam	EPR3292	1:1000
Rabbit anti-PRMT6	Cell Signaling	14641S	1:1000
Rabbit anti-PRMT5	Active Motif	31001	1:1000
Rabbit anti-asymmetric dimethyl arginine (ADMA)	Cell Signaling	13522S	1:1000
Rabbit anti-mono-methyl arginine (MMA)	Cell Signaling	8711S	1:1000
Rabbit anti-symmetric dimethyl arginine (SDMA)	Cell Signaling	13222S	1:1000
Mouse anti-FOXA1	Merck	Clone-2F83	1:1000
Mouse anti-6xHis	QIAGEN	34650	1:1000
Rabbit anti-Vinculin	Cell Signaling	E1E9V	1:1000
Mouse anti- β -Tubulin	Cell Signaling	86298S	1:1000
IRDye 800CW donkey anti-rabbit	LiCor	926-32213	1:5000
IRDye 680RD goat anti-mouse	LiCor	926-68070	1:7500
Reagents			
RIPA-Buffer (Pierce)	Thermo Scientific	89900	-
Protease Inhibitor (Pierce cOmplete EDTA-free protease inhibitor tablets)	Roche	11873580001	100x
Phosphatase Inhibitor (HALT Phosphatase inhibitor cocktail)	Thermo Scientific	78427	100x

NuPAGE LDS sample buffer	Invitrogen	NP0007	4x
NuPAGE sample reducing agent	Invitrogen		10x
Molecular weight ladder (Precision plus protein dual colour standard)	Bio-Rad	1610374	-
4-12% Bis-Tris 1.0 mm gel (12 well)	NuPAGE	NP0322	-
4-12% Bis-Tris 1.0 mm gel (15 well)	NuPAGE	NP0323	-
MOPS running buffer	NuPAGE	NP0001	20x
iBlot 2 gel transfer device	Invitrogen	NP0004	-
PVDF membrane (iBlot 2 transfer stacks, PVDF)	Invitrogen	IB24001	-
TBS	In-house	-	-
Tween-20 (10% Tween 20)	Bio-Rad	1610781	100x
Milk (skimmed milk powder)	Marvel Original	-	-

9.6 *in vitro* Assays

Colony Formation Assay MCF-7 cells were seeded into a 12-well plate (Corning, #3513) at a density of 200-250 cells/well for 24 hr at 37°C with 5% CO₂. Three replicate wells were treated with the DMSO stock of the desired compound. The media was replaced after 7 days and the cells allowed to adhere for 12-24 hr before retreatment with compound. To count the colonies, the plates were washed with PBS, and the cells fixed with ice-cold methanol (1 mL) for 30 minutes. The methanol was removed and 0.6 mL crystal violet solution was added (0.5 g Crystal Violet powder, 80 mL deionised H₂O and 20 mL methanol) and left for 15 minutes at room temperature. The plate was washed with H₂O (x2) and di-H₂O and left to air dry overnight. The plates were imaged using the GelCount mammalian-cell colony, spheroid and organoid counter.

Cell Viability Assay Cells were seeded in 96-well plates for 24 hr at 37°C with 5% CO₂. Treatment was added in Opti-MEM reduced serum media (Gibco, #31985070) and incubated at 37°C with 5% CO₂ for the defined period. Cell viability was determined using the CellTiter-Glo Luminescent Cell Viability assay (Promega, #G7571) as per manufacturer's instructions. A white back seal was added to the plate and luminescence was measured using the PHERAstar FS microplate reader. Cell viability was plotted as a percentage of the DMSO-treated cells. Data was processed using GraphPad Prism Version 10.0.3.

CRBN NanoBRET Target Engagement Assay The CRBN NanoBRET TE assay for live-cells was performed according to the manufacture's instruction (Promega, #N2910) with some modifications. MCF-7 cells were transiently transfected with the NanoLuc-CRBN fusion vector (Promega) and

Lipofectamine 2000 (Invitrogen, 116680919). 24 hr after transfection, the cells were resuspended in DMEM without phenol red (Gibco, 31053-028) at a density of 2×10^5 cells per mL and were plated into 96-well plates (Corning, #3474). The cells were incubated with 0.5 μ M CRBN NanoBRET tracer (Promega) and the probe compound for 2 hr at 37 °C with 5% CO₂. After 2 hr incubation, the samples were transferred to a 96 well plate (Corning, #3610) with a white back seal. 3X Nano-Glo substrate (Promega) with NanoLuc extracellular inhibitor (Promega) were added to cells. After 3 minutes at room temperature, BRET was measured using a CLARIOstar PLUS microplate reader equipped with a 450-80 nm band pass filter for donor emission and a 605/30-nm band pass filter for acceptor emission. The BRET ratio was calculated with the equation and the BRET was plotted as a percentage of the DMSO-treated cells.

$$BRET = \left[\frac{Acceptor_{sample}}{Donor_{sample}} - \frac{Acceptor_{no\ tracer\ control}}{Donor_{no\ tracer\ control}} \right]$$

Data was processed using GraphPad Prism Version 10.0.3 and the best-fit IC₅₀ values of each compound were calculated using the [inhibitor] vs response (variable slope) (four parameters) function.

References

- 1 F. Hermann, P. Pably, C. Eckerich, M. T. Bedford and F. O. Fackelmayer, *J. Cell Sci.*, 2008, **122**, 667–677.
- 2 J. Fuhrmann, K. W. Clancy and P. R. Thompson, *Chem. Rev.*, 2015, **115**, 5413–5461.
- 3 E. Guccione and S. Richard, *Nat. Rev. Mol. Cell Biol.*, 2019, **20**, 642–657.
- 4 H. W. Liao, J. M. Hsu, W. Xia, H. L. Wang, Y. N. Wang, W. C. Chang, S. T. Arold, C. K. Chou, P. H. Tsou, H. Yamaguchi, Y. F. Fang, H. J. Lee, H. H. Lee, S. K. Tai, M. H. Yang, M. P. Morelli, M. Sen, J. E. Ladbury, C. H. Chen, J. R. Grandis, S. Kopetz and M. C. Hung, *J. Clin. Invest.*, 2015, **125**, 4529–4543.
- 5 Y. Wang and M. T. Bedford, *Biochem. Soc. Trans.*, 2023, **51**, 725–734.
- 6 O. F. Sarmiento, L. C. Digilio, Y. Wang, J. Perlin, J. C. Herr, C. D. Allis and S. A. Coonrod, *J. Cell Sci.*, 2004, **117**, 4449–4459.
- 7 M. Le Romancer, I. Treilleux, N. Leconte, Y. Robin-Lespinasse, S. Sentis, K. Bouchekioua-Bouzaghrou, S. Goddard, S. Gobert-Gosse and L. Corbo, *Mol. Cell*, 2008, **31**, 212–221.
- 8 M. Saiful Islam, M. A. McDonough, R. Chowdhury, J. Gault, A. Khan, E. Pires and C. J. Schofield, *J. Biol. Chem.*, 2019, **294**, 11637–11652.
- 9 C. J. Webby, A. Wolf, N. Gromak, M. Dreger, H. Kramer, B. Kessler, M. L. Nielsen, C. Schmitz, D. S. Butler, J. R. Y. Iii, C. M. Delahunty, P. Hahn, A. Lengeling, M. Mann, N. J. Proudfoot, C. J. Schofield and A. Böttger, *Science*, 2009, **325**, 90–93.
- 10 L. J. Walport, R. J. Hopkinson, R. Chowdhury, R. Schiller, W. Ge, A. Kawamura and C. J. Schofield, *Nat. Commun.*, 2016, **7**, 11974.
- 11 B. Chang, Y. Chen, Y. Zhai and R. K. Bruick, *Science*, 2007, **318**, 444–447.
- 12 M. R. Pawlak, C. A. Scherer, J. Chen, M. J. Roshon and H. E. Ruley, *Mol. Cell. Biol.*, 2000, **20**, 4859–4869.
- 13 A. Fedoriw, S. R. Rajapurkar, S. O’Brien, S. V. Gerhart, L. H. Mitchell, N. D. Adams, N. Rioux, T. Lingaraj, S. A. Ribich, M. B. Pappalardi, N. Shah, J. Laraio, Y. Liu, M. Butticello, C. L. Carpenter, C. Creasy, S. Korenchuk, M. T. McCabe, C. F. McHugh, R. Nagarajan, C. Wagner, F. Zappacosta, R. Annan, N. O. Concha, R. A. Thomas, T. K. Hart, J. J. Smith, R. A. Copeland, M. P. Moyer, J. Campbell, K. Stickland, J. Mills, S. Jacques-O’Hagan, C. Allain, D. Johnston, A. Raimondi, M.

- Porter Scott, N. Waters, K. Swinger, A. Boriack-Sjodin, T. Riera, G. Shapiro, R. Chesworth, R. K. Prinjha, R. G. Kruger, O. Barbash and H. P. Mohammad, *Cancer Cell*, 2019, **36**, 100–114.
- 14 S. Hahn, *Nat. Struct. Mol. Biol.*, 2004, **11**, 394–403.
- 15 S. L. Klemm, Z. Shipony and W. J. Greenleaf, *Nat. Rev. Genet.*, 2019, **20**, 207–220.
- 16 T. Philips, *Nat. Educ.*, 2008, **1**, 199.
- 17 H. Q. H. Pham, X. Tao and Y. Yang, *Front. Epigenetics Epigenomics*, 2023, **1**, 1–20.
- 18 I. Guendel, L. Carpio, C. Pedati, A. Schwartz, C. Teal, F. Kashanchi and K. Kehn-Hall, *PLoS One*, 2010, **5**, e11379.
- 19 M. F. Montenegro, R. González-Guerrero, L. Sánchez-del-Campo, A. Piñero-Madrona, J. Cabezas-Herrera and J. N. Rodríguez-López, *Sci. Rep.*, 2020, **10**, 1–14.
- 20 S. V. Rao, L. Young, D. Cheeseman, S. Mack, J. Temple, C. S. R. Chilamakuri, E. Papachristou, C. Pelicano, A. Smith, D.-L. Couturier, M. Gill, D. Jodrell, A. Russell, I. Chernukhin and J. Carroll, *Cancer Res.*, 2024, **84**, 2_Supplement: C076.
- 21 Y. Yang and M. T. Bedford, *Nat. Rev. Cancer*, 2013, **13**, 37–50.
- 22 S. Caul and J. Broggio, Cancer Registration Statistics, England: 2017, <https://www.ons.gov.uk/peoplepopulationandcommunity/healthandsocialcare/conditionsanddiseases/bulletins/cancerregistrationstatisticsengland/2017>, (accessed 18 December 2023).
- 23 C. M. Perou, T. Sorlie, M. B. Eisen, M. Van De Rijn, S. S. Jeffrey, C. A. Rees, J. R. Pollack, D. T. Ross, H. Johnsen, L. A. Aksten, I. Fluge, A. Pergamenschikov, C. Williams, S. X. Zhu, P. E. Lønning, P. O. Brown, D. Botstein, S. Grant and H. Con, *Nature*, 2000, **533**, 747–752.
- 24 K. T. Hwang, J. Kim, J. Jung, J. H. Chang, Y. J. Chai, S. W. Oh, S. Oh, Y. A. Kim, S. B. Park and K. R. Hwang, *Clin. Cancer Res.*, 2019, **25**, 1970–1979.
- 25 M. Orth, P. Metzger, S. Gerum, J. Mayerle, G. Schneider, C. Belka, M. Schnurr and K. Lauber, *Radiat. Oncol.*, 2019, **14**, 141.
- 26 P. E. Oberstein and K. P. Olive, *Therap. Adv. Gastroenterol.*, 2013, **6**, 321–337.
- 27 L. Malbeteau, C. Poulard, C. Languilaire, I. Mikaelian, F. Flamant, M. Le Romancer and L. Corbo, *iScience*, 2020, **23**, 101236.
- 28 K. Mathioudaki, A. Scorilas, A. Ardavanis, P. Lymberi, E. Tsiambas, M. Devetzi, A. Apostolaki and M. Talieri, *Tumor Biol.*, 2011, **32**, 575–582.

- 29 L. M. Liu, W. Z. Sun, X. Z. Fan, Y. L. Xu, M. Bin Cheng and Y. Zhang, *Cancer Res.*, 2019, **79**, 2865–2877.
- 30 C. Song, T. Chen, L. He, N. Ma, J. ang Li, Y. F. Rong, Y. Fang, M. Liu, D. Xie and W. Lou, *Cell. Oncol.*, 2020, **43**, 51–62.
- 31 L. Wang, Z. Jia, D. Xie, T. Zhao, Z. Tan, S. Zhang, F. Kong, D. Wei and K. Xie, *Cancer Res.*, 2021, **80**, 4500–4513.
- 32 S. Suresh, S. Huard, A. Brisson, F. Némati, R. Dakroub, C. Poulard, M. Ye, E. Martel, C. Reyes, D. C. Silvestre, D. Meseure, A. Nicolas, D. Gentien, H. Fayyad-Kazan, M. Le Romancer, D. Decaudin, S. Roman-Roman and T. Dubois, *Cancers (Basel)*., 2022, **14**, 306.
- 33 Y. Gao, Y. Zhao, J. Zhang, Y. Lu, X. Liu, P. Geng, B. Huang, Y. Zhang and J. Lu, *Sci. Rep.*, 2016, **6**, 19874.
- 34 V. Giuliani, M. A. Miller, C. Y. Liu, S. R. Hartono, C. A. Class, C. A. Bristow, E. Suzuki, L. A. Sanz, G. Gao, J. P. Gay, N. Feng, J. L. Rose, H. Tomihara, J. R. Daniele, M. D. Peoples, J. P. Bardenhagen, M. K. Geck Do, Q. E. Chang, B. Vangamudi, C. Vellano, H. Ying, A. K. Deem, K. A. Do, G. Genovese, J. R. Marszalek, J. J. Kovacs, M. Kim, J. B. Fleming, E. Guccione, A. Viale, A. Maitra, M. Emilia Di Francesco, T. A. Yap, P. Jones, G. Draetta, A. Carugo, F. Chedin and T. P. Heffernan, *Nat. Commun.*, 2021, **12**, 4626.
- 35 J. W. Hwang, Y. Cho, G. U. Bae, S. N. Kim and Y. K. Kim, *Exp. Mol. Med.*, 2021, **53**, 788–808.
- 36 T. M. Djajawi, L. Pijpers, A. Srivaths, S. J. Vervoort, R. W. Johnstone, C. J. Kearney, T. M. Djajawi, L. Pijpers, A. Srivaths, D. Chisanga, K. F. Chan and S. J. Hogg, *CellReports*, 2024, **43**, 113831.
- 37 K. Nakai, W. Xia, H. W. Liao, M. Saito, M. C. Hung and H. Yamaguchi, *Breast Cancer*, 2018, **25**, 74–80.
- 38 G. Gao, L. Zhang, O. D. Villarreal, W. He, D. Su, E. Bedford, P. Moh, J. Shen, X. Shi, M. T. Bedford and H. Xu, *Nucleic Acids Res.*, 2019, **47**, 5038–5048.
- 39 K. S. You, Y. W. Yi, J. Cho, J. S. Park and Y. S. Seong, *Pharmaceuticals*, 2021, **14**, 1–76.
- 40 D. Cheng, N. Yadav, R. W. King, M. S. Swanson, E. J. Weinstein and M. T. Bedford, *J. Biol. Chem.*, 2004, **279**, 23892–23899.
- 41 M. S. Eram, Y. Shen, M. M. Szewczyk, H. Wu, G. Senisterra, F. Li, K. V. Butler, H. Ü. Kaniskan, B. A. Speed, C. Dela Seña, A. Dong, H. Zeng, M. Schapira, P. J. Brown, C. H. Arrowsmith, D.

- Barsyte-Lovejoy, J. Liu, M. Vedadi and J. Jin, *ACS Chem. Biol.*, 2016, **11**, 772–781.
- 42 R. Ferreira de Freitas, D. Ivanochko and M. Schapira, *Molecules*, 2019, **24**, 4492.
- 43 J. I. Brown, T. Koopmans, J. van Strien, N. I. Martin and A. Frankel, *ChemBioChem*, 2018, **19**, 85–99.
- 44 Q. Wu, D. Y. Nie, W. Ba-alawi, Y. S. Ji, Z. W. Zhang, J. Cruickshank, J. Haight, F. E. Ciamponi, J. Chen, S. Duan, Y. Shen, J. Liu, S. A. Marhon, P. Mehdipour, M. M. Szewczyk, N. Dogan-Artun, W. J. Chen, L. X. Zhang, G. Deblois, P. Prinos, K. B. Massirer, D. Barsyte-Lovejoy, J. Jin, D. D. De Carvalho, B. Haibe-Kains, X. J. Wang, D. W. Cescon, M. Lupien and C. H. Arrowsmith, *Nat. Chem. Biol.*, 2022, **18**, 821–830.
- 45 A. B. El-khoueiry, J. Clarke, T. Neff, T. Crossman, N. Ratia, C. Rathi, P. Noto, A. Tarkar, I. Garrido-laguna, E. Calvo, J. Rodón, B. Tran, P. J. O. Dwyer, A. Cuker and A. R. A. Razak, *Br. J. Cancer*, 2023, **129**, 309–317.
- 46 M. Maneiro, E. De Vita, D. Conole, C. S. Kounde, Q. Zhang and E. W. Tate, in *Progress in Medicinal Chemistry*, Elsevier B.V., 2021, vol. 60, pp. 67–190.
- 47 A. Hersko and A. Ciechanover, *Annu. Re. Biochem.*, 1998, **67**, 425–473.
- 48 X. Huang and V. M. Dixit, *Cell Res.*, 2016, **26**, 484–498.
- 49 Q. Yang, J. Zhao, D. Chen and Y. Wang, *Mol. Biomed.*, 2021, **2**, 23.
- 50 I. Dikic, S. Wakatsuki and K. J. Walters, *Nat. Rev. Mol. Cell Biol.*, 2009, **10**, 659–671.
- 51 K. N. Swatek and D. Komander, *Cell Res.*, 2016, **26**, 399–422.
- 52 K. E. Wickliffe, A. Williamson, H.-J. Meyer, A. Kelly and M. Rae, *Trends Cell Biol.*, 2012, **21**, 656–663.
- 53 K. M. Sakamoto, K. B. Kim, A. Kumagai, F. Mercurio, C. M. Crews and R. J. Deshaies, *Proc. Natl. Acad. Sci. U. S. A.*, 2001, **98**, 8554–8559.
- 54 A. R. Schneekloth, M. Pucheault, H. S. Tae and C. M. Crews, *Bioorganic Med. Chem. Lett.*, 2008, **18**, 5904–5908.
- 55 A. Lopez-Girona, D. Mendy, T. Ito, K. Miller, A. K. Gandhi, J. Kang, S. Karasawa, G. Carmel, P. Jackson, M. Abbasian, A. Mahmoudi, B. Cathers, E. Rychak, S. Gaidarova, R. Chen, P. H. Schafer, H. Handa, T. O. Daniel, J. F. Evans and R. Chopra, *Leukemia*, 2012, **26**, 2326–2335.
- 56 C. Galdeano, M. S. Gadd, P. Soares, S. Scaffidi, I. Van Molle, I. Birced, S. Hewitt, D. M. Dias and

- A. Ciulli, *J. Med. Chem.*, 2014, **57**, 8657–8663.
- 57 M. Zengerle, K. H. Chan and A. Ciulli, *ACS Chem. Biol.*, 2015, **10**, 1770–1777.
- 58 M. S. Gadd, A. Testa, X. Lucas, K. H. Chan, W. Chen, D. J. Lamont, M. Zengerle and A. Ciulli, *Nat. Chem. Biol.*, 2017, **13**, 514–521.
- 59 Arvinas, *ARV-471: Phase 2 VERITAC Trial Results*, San Antonio Breast Cancer Symposium, 2022.
- 60 D. P. Bondeson, A. Mares, I. E. D. Smith, E. Ko, S. Campos, A. H. Miah, K. E. Mulholland, N. Routly, D. L. Buckley, J. L. Gustafson, N. Zinn, P. Grandi, S. Shimamura, G. Bergamini, M. Faelth-Savitski, M. Bantscheff, C. Cox, D. A. Gordon, R. R. Willard, J. J. Flanagan, L. N. Casillas, B. J. Votta, W. Den Besten, K. Famm, L. Kruidenier, P. S. Carter, J. D. Harling, I. Churcher and C. M. Crews, *Nat. Chem. Biol.*, 2015, **11**, 611–617.
- 61 J. Sterling, J. R. Baker, A. McCluskey and L. Munoz, *Nat. Commun.*, 2023, **14**, 3228.
- 62 J. Flanagan, Y. Qian, S. Gough, M. Andreoli, M. Bookbinder, G. Cadelina, J. Bradley, E. Rousseau, R. Willard, J. Pizzano, C. Crews, A. Crew, I. Taylor and J. Houston, Abstract P5-04-18: ARV-471, an oral estrogen receptor PROTAC degrader for breast cancer, https://s3.us-east-1.amazonaws.com/arvinas-assets.investeddigital.com/scientific-publications/2018-SABCS-poster_final_v3.pdf, (accessed 23 October 2023).
- 63 X. Luo, I. Archibeque, K. Dellamaggiore, K. Smither, O. Homann, J. R. Lipford and D. Mohl, *iScience*, 2022, **25**, 103985.
- 64 P. M. Cromm and C. M. Crews, *Cell Chem. Biol.*, 2017, **24**, 1181–1190.
- 65 A. A. Adjei, *J. Clin. Oncol.*, 2006, **24**, 4054–4055.
- 66 W. R. Parulekar and E. A. Eisenhauer, *J. Natl. Cancer Inst.*, 2004, **96**, 990–997.
- 67 A. Lin, C. J. Giuliano, A. Palladino, K. M. John, C. Abramowicz, M. Lou Yuan, E. L. Sausville, D. A. Lukow, L. Liu, A. R. Chait, Z. C. Galluzzo, C. Tucker and J. M. Sheltzer, *Sci. Transl. Med.*, 2019, **11**, eaaw8412.
- 68 K. Moreau, M. Coen, A. X. Zhang, F. Pachl, M. P. Castaldi, G. Dahl, H. Boyd, C. Scott and P. Newham, *Br. J. Pharmacol.*, 2020, **177**, 1709–1718.
- 69 A. Gopalsamy, *J. Med. Chem.*, 2022, **65**, 8113–8126.
- 70 Ciulli Laboratory, Our paper reporting the first ternary crystal structure of a PROTAC bound to

- to its E3 ligase VHL and Brd4 target is now published in Nature Chemical Biology!, <https://www.lifesci.dundee.ac.uk/groups/alessio-ciulli//news/our-paper-reporting-first-ternary-crystal-structure-protac-bound-its-e3-ligase-vhl-and-brd4>, (accessed 5 December 2023).
- 71 D. P. Bondeson, B. E. Smith, G. M. Burslem, A. D. Buhimschi, J. Hines, S. Jaime-Figueroa, J. Wang, B. D. Hamman, A. Ishchenko and C. M. Crews, *Cell Chem. Biol.*, 2018, **25**, 78–87.
- 72 N. Z. Lei, X. Y. Zhang, H. Z. Chen, Y. Wang, Y. Y. Zhan, Z. H. Zheng, Y. M. Shen and Q. Wu, *Nucleic Acids Res.*, 2009, **37**, 832–848.
- 73 T. B. Nicholson, T. Chen and S. Richard, *Pharmacol. Res.*, 2009, **60**, 466–474.
- 74 O. M. Price, A. Thakur, A. Ortolano, A. Towne, C. Velez, O. Acevedo and J. M. Hevel, *J. Biol. Chem.*, 2021, **297**, 101336.
- 75 S. Tang, V. Sethunath, N. Y. Metaferia, M. F. Nogueira, D. S. Gallant, E. R. Garner, L. A. Lairson, C. M. Penney, J. Li, M. K. Gelbard, S. A. Alaiwi, J. H. Seo, J. H. Hwang, C. A. Strathdee, S. C. Baca, S. AbuHammad, X. Zhang, J. G. Doench, W. C. Hahn, D. Y. Takeda, M. L. Freedman, P. S. Choi and S. R. Viswanathan, *Cell Rep.*, 2022, **38**, 110417.
- 76 J. Filipović, M. Bosić, S. Čirović, M. Životić, D. Dunderović, D. Dordevic, S. Živković-Perišić, A. Lipkovski and J. Marković-Lipkovski, *Diagn. Pathol.*, 2019, **14**, 120.
- 77 A. Repenning, D. Happel, C. Bouchard, M. Meixner, Y. Verel-Yilmaz, H. Raifer, L. Holembowski, E. Krause, E. Kremmer, R. Feederle, C. U. Keber, M. Lohoff, E. P. Slater, D. K. Bartsch and U. Bauer, *EMBO J.*, 2021, **40**, e106777.
- 78 S. V. Sharma, D. A. Haber and J. Settleman, *Nat. Rev. Cancer*, 2010, **10**, 241–253.
- 79 T. Acheampong, R. D. Kehm, M. B. Terry, E. L. Argov and P. Tehranifar, *JAMA Netw. open*, 2020, **3**, e2013226.
- 80 C. Poulard, I. Treilleux, E. Lavergne, K. Bouchekioua-Bouzaghrou, S. Goddard-Léon, S. Chabaud, O. Trédan, L. Corbo and M. Le Romancer, *EMBO Mol. Med.*, 2012, **4**, 1200–1213.
- 81 A. V. Lee, S. Oesterreich and N. E. Davidson, *J. Natl. Cancer Inst.*, 2015, **107**, djv073.
- 82 A. M. Waters and C. J. Der, *Cold Spring Harb. Perspect. Med.*, 2018, **8**, a031435.
- 83 R. Sinha, A. Luna, N. Schultz and C. Sander, *Cell Reports Methods*, 2021, **1**, 100039.
- 84 E. J. Hanan, J. Liang, X. Wang, R. A. Blake, N. Blaquiére and S. T. Staben, *J. Med. Chem.*, 2020,

- 63**, 11330–11361.
- 85 A. A. McDonough, L. C. Veiras, J. N. Minas and D. L. Ralph, *Am. J. Physiol. - Cell Physiol.*, 2015, **308**, C426–C433.
- 86 D. L. Daniels, K. M. Riching and M. Urh, *Drug Discov. Today Technol.*, 2019, **31**, 61–68.
- 87 H. Dana, G. M. Chalbatani, H. Mahmoodzadeh, E. Gharagouzlo, R. Karimloo, O. Rezaiean, A. Moradzadeh, A. Mazraeh, V. Marmari, M. M. Rashno, N. Mehmandoost, F. Moazzen, M. Ebrahimi and S. J. Abadi, *Int. J. Biomed. Sci.*, 2017, **13**, 48–57.
- 88 S. Dhar, V. Vemulapalli, A. N. Patananan, G. L. Huang, A. Di Lorenzo, S. Richard, M. J. Comb, A. Guo, S. G. Clarke and M. T. Bedford, *Sci. Rep.*, 2013, **3**, 1311.
- 89 E. Shishkova, H. Zeng, F. Liu, N. W. Kwiecien, A. S. Hebert, J. J. Coon and W. Xu, *Nat. Commun.*, 2017, **8**, 1–13.
- 90 D. Cheng, G. Gao, A. Di Lorenzo, S. Jayne, M. O. Hottiger, S. Richard and M. T. Bedford, *J. Biol. Chem.*, 2020, **295**, 17060–17070.
- 91 M. Schneider, C. J. Radoux, A. Hercules, D. Ochoa, I. Dunham, L. P. Zalmas, G. Hessler, S. Ruf, V. Shanmugasundaram, M. M. Hann, P. J. Thomas, M. A. Queisser, A. B. Benowitz, K. Brown and A. R. Leach, *Nat. Rev. Drug Discov.*, 2021, **20**, 789–797.
- 92 F. Herrmann and F. O. Fackelmayer, *Genes to Cells*, 2009, **14**, 309–317.
- 93 L. M. Simpson, L. Glennie, A. Brewer, J.-F. Zhao, J. Crooks, N. Shpiro and G. P. Sapkota, *Cell Chem. Biol.*, 2022, **29**, 1482–1504.
- 94 P. V. Hornbeck, J. M. Kornhauser, S. Tkachev, B. Zhang, E. Skrzypek, B. Murray, V. Latham and M. Sullivan, *Nucleic Acids Res.*, 2012, **40**, 261–270.
- 95 T. Chen, T. Zhou, B. He, H. Yu, X. Guo, X. Song and J. Sha, *PLoS One*, 2014, **9**, e85744.
- 96 W. Kim, E. J. Bennett, E. L. Huttlin, A. Guo, J. Li, A. Possemato, M. E. Sowa, R. Rad, J. Rush, M. J. Comb, J. W. Harper and S. P. Gygi, *Mol. Cell*, 2011, **44**, 325–340.
- 97 K. Bhuripanyo, Y. Wang, X. Liu, L. Zhou, R. Liu, D. Duong, B. Zhao, Y. Bi, H. Zhou, G. Chen, N. T. Seyfried, W. J. Chazin, H. Kiyokawa and J. Yin, *Sci. Adv.*, 2018, **4**, e1701393.
- 98 Y. Lai, J. Li, X. Li and C. Zou, *J. Cell Sci.*, 2017, **130**, 3578–3587.
- 99 Y. Ma, S. Liu, H. Jun, J. Wang, X. Fan, G. Li, L. Yin, L. Rui, S. A. Weinman, J. Gong and J. Wu, *FASEB J.*, 2020, **34**, 14863–14877.

- 100 M. Békés, D. R. Langley and C. M. Crews, *Nat. Rev. Drug Discov.*, 2022, **21**, 181–200.
- 101 R. T. U. Haid and A. Reichel, *Pharmaceutics*, 2023, **15**, 195.
- 102 A. X. Zhang, K. Cassidy, G. Dahl, K. Moreau, F. Pachi and A. M. Zuhl, *SLAS Discov.*, 2021, **26**, 518–523.
- 103 I. Churcher, *J. Med. Chem.*, 2018, **61**, 444–452.
- 104 T. Mathieson, H. Franken, J. Kosinski, N. Kurzawa, N. Zinn, G. Sweetman, D. Poeckel, V. S. Ratnu, M. Schramm, I. Becher, M. Steidel, K. M. Noh, G. Bergamini, M. Beck, M. Bantscheff and M. M. Savitski, *Nat. Commun.*, 2018, **9**, 689.
- 105 M. W. Hetzer and B. H. Toyama, *Nat. Rev. Mol. Cell Biol.*, 2013, **14**, 55–61.
- 106 A. Mares, A. H. Miah, I. E. D. Smith, M. Rackham, A. R. Thawani, J. Cryan, P. A. Haile, B. J. Votta, A. M. Beal, C. Capriotti, M. A. Reilly, D. T. Fisher, N. Zinn, M. Bantscheff, T. T. MacDonald, A. Vossenkamper, P. Dace, I. Churcher, A. B. Benowitz, G. Watt, J. Denyer, P. Scott-Stevens and J. D. Harling, *Commun. Biol.*, 2020, **3**, 1–13.
- 107 J. Li, Z. Cai, L. P. Vaites, N. Shen, D. C. Mitchell, E. L. Huttlin, J. A. Paulo, B. L. Harry and S. P. Gygi, *Mol. Cell*, 2021, **81**, 4722–4735.
- 108 S. P. Davies, MRes Thesis, University of Birmingham, 2014.
- 109 S. B. Cambridge, F. Gnad, C. Nguyen, J. L. Bermejo, M. Krüger and M. Mann, *J. Proteome Res.*, 2011, **10**, 5275–5284.
- 110 A. Geier, R. Beery, M. Haimshon, R. Hemi and B. Lunenfeld, *Vitr. Cell. Dev. Biol. - Anim.*, 1992, **28A**, 415–418.
- 111 A. S. Potter, A. J. Casa and A. V. Lee, *J. Cell. Biochem.*, 2012, **113**, 110–121.
- 112 Y. Liu, K. Yu, X. Kong, K. Zhang, L. Wang, N. Zhang, Q. Chen, M. Niu, W. Li, X. Zhong, S. Wu, J. Zhang and Y. Liu, *Sci. Adv.*, 2023, **9**, eadg7112.
- 113 Y. Park, Y. Koga, C. Su, A. L. Waterbury, C. L. Johnny and B. B. Liao, *Angew. Chemie - Int. Ed.*, 2019, **58**, 5387–5391.
- 114 S. E. Dmitriev, D. O. Vladimirov and K. A. Lashkevich, *Biochem.*, 2020, **85**, 1389–1421.
- 115 A. Bricelj, C. Steinebach, R. Kuchta, M. Gütschow and I. Sosič, *Front. Chem.*, 2021, **9**, 707317.
- 116 Y. Shen, G. Gao, X. Yu, H. Kim, L. Wang, L. Xie, M. Schwarz, X. Chen, E. Guccione, J. Liu, M. T.

- Bedford and J. Jin, *J. Med. Chem.*, 2020, **63**, 9977–9989.
- 117 H. Chen, F. Chen, S. Pei and S. Gou, *Bioorg. Chem.*, 2019, **87**, 191–199.
- 118 A. C. Lai, M. Toure, D. Hellerschmied, J. Salami, S. Jaime-Figueroa, E. Ko, J. Hines and C. M. Crews, *Angew. Chemie - Int. Ed.*, 2016, **55**, 807–810.
- 119 B. E. Smith, S. L. Wang, S. Jaime-Figueroa, A. Harbin, J. Wang, B. D. Hamman and C. M. Crews, *Nat. Commun.*, 2019, **10**, 131.
- 120 J. Krieger, F. J. Sorrell, A. A. Wegener, B. Leuthner, F. Machrouhi-Porcher, M. Hecht, E. M. Leibrock, J. E. Müller, J. Eisert, I. V. Hartung and S. Schlesiger, *ChemMedChem*, 2023, **18**, e202200615.
- 121 D. Sehnal, S. Bittrich, M. Deshpande, R. Svobodová, K. Berka, V. Bazgier, S. Velankar, S. K. Burley, J. Koča and A. S. Rose, *Nucleic Acids Res.*, 2021, **49**, W431–W437.
- 122 D. L. Buckley, J. L. Gustafson, I. Van-Molle, A. G. Roth, H. S. Tae, P. C. Gareiss, W. L. Jorgensen, A. Ciulli and C. M. Crews, *Angew. Chemie - Int. Ed.*, 2012, **51**, 11463–11467.
- 123 C. Steinebach, S. A. Voell, L. P. Vu, A. Bricelj, I. Sosič, G. Schnakenburg and M. Gütschow, *Synth.*, 2020, **52**, 2521–2527.
- 124 A. I. Minchinton and I. F. Tannock, *Nat. Rev. Cancer*, 2006, **6**, 583–592.
- 125 X. Jiang, J. Yu, Z. Zhou, J. Kongsted, Y. Song, C. Pannecouque, E. De Clercq, D. Kang, V. Poongavanam, X. Liu and P. Zhan, *Med. Res. Rev.*, 2019, **39**, 2194–2238.
- 126 L. H. Mitchell, A. E. Drew, S. A. Ribich, N. Rioux, K. K. Swinger, S. L. Jacques, T. Lingaraj, P. A. Boriack-Sjodin, N. J. Waters, T. J. Wigle, O. Moradei, L. Jin, T. Riera, M. Porter-Scott, M. P. Moyer, J. J. Smith, R. Chesworth and R. A. Copeland, *ACS Med. Chem. Lett.*, 2015, **6**, 655–659.
- 127 K. A. Scott, N. Ropek, B. Melillo, S. L. Schreiber, B. F. Cravatt and E. V. Vinogradova, *Curr. Res. Chem. Biol.*, 2022, **2**, 100028.
- 128 US2014/029160, 2014.
- 129 N. T. Ross, R. Deane, S. Perry and B. L. Miller, *Tetrahedron*, 2013, **69**, 7653–7658.
- 130 L. Liu, Y. Zhang and B. Xin, *J. Org. Chem.*, 2006, **71**, 3994–3997.
- 131 R. G. Bryant, *J. Chem. Educ.*, 1983, **60**, 933–935.
- 132 J. M. Joo, B. B. Touré and D. Sames, *J. Org. Chem.*, 2010, **75**, 4911–4920.

- 133 R. M. Claramunt, C. Lopez, M. D. Santa Maria, D. Sanz and J. Elguero, *Prog. Nucl. Magn. Reson. Spectrosc.*, 2006, **49**, 169–206.
- 134 J. J. Drysdale and W. D. Phillips, *J. Am. Chem. Soc.*, 1957, **79**, 319–322.
- 135 D. Dimitrijevic, E. Fabian, B. Nicol, D. Funk-Weyer and R. Landsiedel, *Chem. Res. Toxicol.*, 2022, **35**, 1962–1973.
- 136 J. Tang, J. D. Gary, S. Clarke and H. R. Herschman, *J. Biol. Chem.*, 1998, **273**, 16935–16945.
- 137 J. E. Gestwicki, *Cell Chem. Biol.*, 2022, **29**, 713–715.
- 138 T. Charlène, L. Eve, C. Poulard and M. Le Romancer, *Life*, 2021, **11**, 1147.
- 139 A. G. Schwaid and I. Cornella-Taracido, *J. Med. Chem.*, 2018, **61**, 1767–1773.
- 140 US2014/029583, 2014.
- 141 T. A. Bemis, J. J. La Clair and M. D. Burkart, *J. Med. Chem.*, 2021, **64**, 8042–8052.
- 142 N. Bai, K. M. Riching, A. Makaju, H. Wu, T. M. Acker, S. C. Ou, Y. Zhang, X. Shen, D. N. Bulloch, H. Rui, B. W. Gibson, D. L. Daniels, M. Urh, B. M. Rock and S. C. Humphreys, *J. Biol. Chem.*, 2022, **298**, 101653.
- 143 R. I. Troup, C. Fallan and M. G. J. Baud, *Explor. Target. Anti-tumor Ther.*, 2020, **1**, 273–312.
- 144 J. A. Ward, C. Perez-Lopez and C. Mayor-Ruiz, *ChemBioChem*, 2023, **24**, e202300163.
- 145 Imaging PROTAC Mediated Degradation Complexes with Cryo-EM, <https://www.nanoimagingervices.com/blog/imaging-protac-mediated-degradation-complexes-with-cryo-em>, (accessed 17 December 2023).
- 146 K. Haubrich, V. A. Spiteri, W. Farnaby, F. Sobott and A. Ciulli, *Curr. Opin. Struct. Biol.*, 2023, **79**, 102534.
- 147 C. A. Lipinski, F. Lombardo, B. W. Dominy and P. J. Feeney, *Adv. Drug Deliv. Rev.*, 1997, **23**, 3–25.
- 148 D. F. Veber, S. R. Johnson, H.-Y. Cheng, B. R. Smith, K. W. Ward and K. D. Kopple, *J. Med. Chem.*, 2002, **45**, 2615–2623.
- 149 S. D. Edmondson, B. Yang and C. Fallan, *Bioorganic Med. Chem. Lett.*, 2019, **29**, 1555–1564.
- 150 B. Homayun, X. Lin and H. J. Choi, *Pharmaceutics*, 2019, **11**, 129.

- 151 V. Poongavanam, Y. Atilaw, S. Siegel, A. Giese, L. Lehmann, D. Meibom, M. Erdelyi and J. Kihlberg, *J. Med. Chem.*, 2022, **65**, 13029–13040.
- 152 Y. Atilaw, V. Poongavanam, C. Svensson Nilsson, D. Nguyen, A. Giese, D. Meibom, M. Erdelyi and J. Kihlberg, *ACS Med. Chem. Lett.*, 2021, **12**, 107–114.
- 153 L. Goracci, J. Desantis, A. Valeri, B. Castellani, M. Eleuteri and G. Cruciani, *J. Med. Chem.*, 2020, **63**, 11615–11638.
- 154 H. J. Maple, N. Clayden, A. Baron, C. Stacey and R. Felix, *Medchemcomm*, 2019, **10**, 1755–1764.
- 155 N. A. Zografou-Barredo, A. J. Hallatt, J. Goujon-Ricci and C. Cano, *Bioorganic Med. Chem.*, 2023, **88–89**, 117334.
- 156 J. Desantis, A. Mammoli, M. Eleuteri, A. Coletti, F. Croci, A. Macchiarulo and L. Goracci, *RSC Adv.*, 2022, **12**, 21968–21977.
- 157 X. Han, C. Wang, C. Qin, W. Xiang, E. Fernandez-Salas, C. Y. Yang, M. Wang, L. Zhao, T. Xu, K. Chinnaswamy, J. Delproposito, J. Stuckey and S. Wang, *J. Med. Chem.*, 2019, **62**, 941–964.
- 158 J. Lee and M. Schapira, *ACS Chem. Biol.*, 2021, **16**, 579–585.
- 159 T. A. Soucy, P. G. Smith, M. A. Milhollen, A. J. Berger, J. M. Gavin, S. Adhikari, J. E. Brownell, K. E. Burke, D. P. Cardin, S. Critchley, C. A. Cullis, A. Doucette, J. J. Garnsey, J. L. Gaulin, R. E. Gershman, A. R. Lublinsky, A. McDonald, H. Mizutani, U. Narayanan, E. J. Olhava, S. Peluso, M. Rezaei, M. D. Sintchak, T. Talreja, M. P. Thomas, T. Traore, S. Vyskocil, G. S. Weatherhead, J. Yu, J. Zhang, L. R. Dick, C. F. Claiborne, M. Rolfe, J. B. Bolen and S. P. Langston, *Nature*, 2009, **458**, 732–736.
- 160 Z. Wang, S. Shaabani, X. Gao, Y. L. D. Ng, V. Sapozhnikova, P. Mertins, J. Krönke and A. Dömling, *Nat. Commun.*, 2023, **14**, 8437.
- 161 H. Prinz, S. G. Bott and J. L. Atwood, *J. Am. Chem. Soc.*, 1986, **108**, 2113–2114.
- 162 P. I. Abronina, A. I. Zinin, A. V. Orlova, S. L. Sedinkin and L. O. Kononov, *Tetrahedron Lett.*, 2013, **54**, 4533–4535.
- 163 J. Clayden, N. Greeves and S. Warren, *Organic Chemistry*, Oxford University Press, Oxford, 2nd edn., 2012.
- 164 S. Kachbi-Khelfallah, M. Monteil, M. Cortes-Clerget, E. Migianu-Griffoni, J. L. Pirat, O. Gager, J.

- Deschamp and M. Lecouvey, *Beilstein J. Org. Chem.*, 2016, **12**, 1366–1370.
- 165 K. C. Waterman, W. B. Arikpo, M. B. Fergione, T. W. Graul, B. A. Johnson, B. C. Macdonald, M. C. Roy and R. J. Timpano, *J. Pharm. Sci.*, 2008, **97**, 1499–1507.
- 166 J. N. Hemenway, T. C. Carvalho, V. M. Rao, Y. Wu, J. K. Levons, A. S. Narang, S. R. Paruchuri, H. J. Stamato and S. A. Varia, *J. Pharm. Sci.*, 2012, **101**, 3305–3318.
- 167 K. C. Waterman, R. C. Adami, K. M. Alsante, J. Hong, M. S. Landis, F. Lombardo and C. J. Roberts, *Pharm. Dev. Technol.*, 2002, **7**, 1–32.
- 168 A. Guillou, D. F. Earley, S. Klingler, E. Nisli, L. J. Nüesch, R. Fay and J. P. Holland, *Bioconjug. Chem.*, 2021, **32**, 1263–1275.
- 169 S. P. Mcmanus, R. M. Karaman, M. R. Sedaghat-Herati, T. G. Shannon, T. W. Hovatter and J. M. Harris, *J. Polym. Sci. Part A Polym. Chem.*, 1990, **28**, 3337–3346.
- 170 M. J. Little, N. Aubry, M. E. Beaudoin, N. Goudreau and S. R. LaPlante, *J. Pharm. Biomed. Anal.*, 2007, **43**, 1324–1330.
- 171 H. A. Naqi, T. J. Woodman, S. M. Husbands and I. S. Blagbrough, *Anal. Methods*, 2019, **11**, 3090–3100.
- 172 J. Cornish, K. E. Callon, C. Q. X. Lin, C. L. Xiao, T. B. Mulvey, G. J. S. Cooper and I. R. Reid, *Am. J. Physiol. - Endocrinol. Metab.*, 1999, **277**, 779–783.
- 173 K. Sikora, D. Neubauer, M. Jaśkiewicz and W. Kamysz, *Int. J. Pept. Res. Ther.*, 2018, **24**, 265–270.
- 174 S. R. D. O. Melo, M. Homem-De-Mello, D. Silveira and L. A. Simeoni, *PDA J. Pharm. Sci. Technol.*, 2014, **68**, 221–238.
- 175 C. W. Chung, H. Dai, E. Fernandez, C. P. Tinworth, I. Churcher, J. Cryan, J. Denyer, J. D. Harling, A. Konopacka, M. A. Queisser, C. J. Tame, G. Watt, F. Jiang, D. Qian and A. B. Benowitz, *ACS Chem. Biol.*, 2020, **15**, 2316–2323.
- 176 S. Rana, M. Bendjennat, S. Kour, H. M. King, S. Kizhake, M. Zahid and A. Natarajan, *Biorg Med Chem Lett.*, 2019, **29**, 1375–1379.
- 177 P. H. Gross, K. J. Sheets, N. A. Warren, S. Ghosh, R. E. Varghese, K. E. Wass (KWass) and K. Kadimisetty, *Biochem. Biophys. Res. Commun.*, 2022, **628**, 68–75.
- 178 D. L. Buckley, K. Raina, N. Darricarrere, J. Hines, J. L. Gustafson, I. E. Smith, A. H. Miah, J. D.

- Harling and C. M. Crews, *ACS Chem. Biol.*, 2015, **10**, 1831–1837.
- 179 G. V Los, L. P. Encell, M. G. Mcdougall, D. D. Hartzell, N. Karassina, D. Simpson, J. Mendez, K. Zimmerman, P. Otto, G. Vidugiris, J. Zhu, A. Darzins, D. H. Klaubert, F. Bulleit, Robert and K. V. Wood, *ACS Chem. Biol.*, 2008, **3**, 373–382.
- 180 E. A. Caine, S. D. Mahan, R. L. Johnson, A. N. Nieman, N. Lam, C. R. Warren, K. M. Riching, M. Urh and D. L. Daniels, *Curr. Protoc. Pharmacol.*, 2020, **91**, e81.
- 181 K. Morgan and M. Juchheim, Plasmids 101: The Promoter Region – Let’s Go!, <https://blog.addgene.org/plasmids-101-the-promoter-region>, (accessed 24 November 2023).
- 182 V. G. Klein, C. E. Townsend, A. Testa, M. Zengerle, C. Maniaci, S. J. Hughes, K. H. Chan, A. Ciulli and R. S. Lokey, *ACS Med. Chem. Lett.*, 2020, **11**, 1732–1738.
- 183 E. A. Gunnell, A. Al-Noori, U. Muhsen, C. C. Davies, J. Dowden and I. Dreveny, *Biochem. J.*, 2020, **477**, 787–800.
- 184 X. Pan, H. Wang, C. Li, J. Z. H. Zhang and C. Ji, *J. Chem. Inf. Model.*, 2021, **61**, 3159–3165.
- 185 E. S. Fischer, K. Böhm, J. R. Lydeard, H. Yang, M. B. Stadler, S. Cavadini, J. Nagel, F. Serluca, V. Acker, G. M. Lingaraju, R. B. Tichkule, M. Schebesta, W. C. Forrester, M. Schirle, U. Hassiepen, J. Ottl, M. Hild, R. E. J. Beckwith, J. W. Harper, J. L. Jenkins and N. H. Thomä, *Nature*, 2014, **512**, 49–53.
- 186 S. Jaime-Figueroa, A. D. Buhimschi, M. Toure, J. Hines and C. M. Crews, *Bioorganic Med. Chem. Lett.*, 2020, **30**, 126877.
- 187 G. M. Burslem, P. Ottis, S. Jaime-Figueroa, A. Morgan, P. M. Cromm, M. Toure and C. M. Crews, *ChemMedChem*, 2018, **13**, 1508–1512.
- 188 J. Choy, S. Jaime-Figueroa, L. Jiang and P. Wagner, *Synth. Commun.*, 2008, **38**, 3840–3853.
- 189 T. W. Greene, *Greene’s Protective Groups in Organic Synthesis*, John Wiley & Sons, Hoboken, 2007.
- 190 T. Chandra, W. E. Broderick and J. B. Broderick, *Nucleosides, Nucleotides and Nucleic Acids*, 2010, **29**, 132–143.
- 191 C. Figliola, S. M. Greening, C. Lamont, B. R. Groves and A. Thompson, *Can. J. Chem.*, 2018, **96**, 534–542.
- 192 N. Y. Meredith, S. Borsley, I. V. Smolyar, G. S. Nichol, C. M. Baker, K. B. Ling and S. L. Cockroft,

- Angew. Chemie - Int. Ed.*, 2022, **61**, e202206604.
- 193 M. Konstantinidou, A. Oun, P. Pathak, B. Zhang, Z. Wang, F. ter Brake, A. M. Dolga, A. Kortholt and A. Dömling, *ChemMedChem*, 2021, **16**, 959–965.
- 194 United States, US 2020/001746 A1, 2020.
- 195 A. Vakalopoulos and H. M. R. Hoffmann, *Org. Lett.*, 2000, **2**, 1447–1450.
- 196 EP2022/050702, 2022.
- 197 B. Huang, X. Liu, Y. Tian, D. Kang, Z. Zhou, D. Daelemans, E. De Clercq, C. Pannecouque, P. Zhan and X. Liu, *Bioorganic Med. Chem. Lett.*, 2018, **28**, 1348–1351.
- 198 L. Tan, Z. Zhang, D. Gao, J. Luo, Z. C. Tu, Z. Li, L. Peng, X. Ren and K. Ding, *J. Med. Chem.*, 2016, **59**, 6807–6825.
- 199 H. Schumacher, R. L. Smith and R. T. Williams, *Brit. J. Pharmacol.*, 1965, **25**, 324–337.
- 200 M. Reist, P. A. Carrupt, E. Francotte and B. Testa, *Chem. Res. Toxicol.*, 1998, **11**, 1521–1528.
- 201 T. Nakamura, T. Noguchi, H. Miyachi and Y. Hashimoto, *Chem. Pharm. Bull.*, 2007, **55**, 651–654.
- 202 D. Bhangare, N. Rajput, T. Jadav, A. K. Sahu, R. K. Tekade and P. Sengupta, *J. Anal. Sci. Technol.*, 2022, **13**, 7.
- 203 J. Xu, D. Duran and B. Mao, *J. Liq. Chromatogr. Relat. Technol.*, 2006, **29**, 2795–2806.
- 204 A. Bricelj, Y. L. Dora Ng, D. Ferber, R. Kuchta, S. Müller, M. Monschke, K. G. Wagner, J. Krönke, I. Sosič, M. Gütschow and C. Steinebach, *ACS Med. Chem. Lett.*, 2021, **12**, 1733–1738.
- 205 E. Marcantoni, M. Massaccesi and E. Torregiani, *J. Org. Chem.*, 2001, **66**, 4430–4432.
- 206 Y. Q. Wu, D. C. Limburg, D. E. Wilkinson, M. J. Vaal and G. S. Hamilton, *Tetrahedron Lett.*, 2000, **41**, 2847–2849.
- 207 C. Mayato, R. L. Dorta and J. T. Vázquez, *Tetrahedron Lett.*, 2008, **49**, 1396–1398.
- 208 R. Kaul, Y. Brouillette, Z. Sajjadi, K. A. Hansford and W. D. Lubell, *J. Org. Chem.*, 2004, **69**, 6131–6133.
- 209 D. K. Brownsey, B. C. Rowley, E. Gorobets, B. S. Gelfand and D. J. Derksen, *Chem. Sci.*, 2021, **12**, 4519–4525.

- 210 T. Machleidt, C. C. Woodroffe, M. K. Schwinn, J. Méndez, M. B. Robers, K. Zimmerman, P. Otto, D. L. Daniels, T. A. Kirkland and K. V. Wood, *ACS Chem. Biol.*, 2015, **10**, 1797–1804.
- 211 K. M. Riching, S. Mahan, C. R. Corona, M. McDougall, J. D. Vasta, M. B. Robers, M. Urh and D. L. Daniels, *ACS Chem. Biol.*, 2018, **13**, 2758–2770.
- 212 D. B. Kitchen, H. Decornez, J. R. Furr and J. Bajorath, *Nat. Rev. Drug Discov.*, 2004, **3**, 935–949.
- 213 J. Min, A. Mayasundari, F. Keramatnia, B. Jonchere, S. W. Yang, J. Jarusiewicz, M. Actis, S. Das, B. Young, J. Slavish, L. Yang, Y. Li, X. Fu, S. H. Garrett, M. Yun, Z. Li, S. Nithianantham, S. Chai, T. Chen, A. Shelat, R. E. Lee, G. Nishiguchi, S. W. White, M. F. Roussel, P. R. Potts, M. Fischer and Z. Rankovic, 2021, **38105**, 26663–26670.
- 214 J. A. Jarusiewicz, S. Yoshimura, A. Mayasundari, M. Actis, A. Aggarwal, K. MCGowan, L. Yang, Y. Li, X. Fu, V. Mishra, R. Heath, S. Narina, S. M. Pruett-miller, G. Nishiguchi, J. J. Yang and Z. Rankovic, *ACS Med. Chem. Lett.*, 2023, **14**, 141–145.
- 215 H. Xie, C. Li, H. Tang, I. Tandon, J. Liao, B. L. Roberts, Y. Zhao and W. Tang, *J. Med. Chem.*, 2023, **66**, 2904–2917.
- 216 B. Jeffries, Z. Wang, J. Graton, S. D. Holland, T. Brind, R. D. R. Greenwood, J. Y. Le Questel, J. S. Scott, E. Chiarparin and B. Linclau, *J. Med. Chem.*, 2018, **61**, 10602–10618.
- 217 R. W. Carlson, *Clin. Breast Cancer*, 2005, **6**, S5–S8.
- 218 Y. Ishii, L. Papa, U. Bahadur, Z. Yue, J. Aguirre-Ghiso, T. Shioda, S. Waxman and D. Germain, *Clin. Cancer Res.*, 2011, **17**, 2292–2300.
- 219 L. M. Wodicka, P. Ciceri, M. I. Davis, J. P. Hunt, M. Floyd, S. Salerno, X. H. Hua, J. M. Ford, R. C. Armstrong, P. P. Zarrinkar and D. K. Treiber, *Chem. Biol.*, 2010, **17**, 1241–1249.
- 220 C. N. Pace, B. A. Shirley, M. McNutt and K. Gajiwala, *FASEB J.*, 1996, **10**, 75–83.
- 221 M. P. Jackson and E. W. Hewitt, *Essays Biochem.*, 2016, **60**, 173–180.
- 222 A. Ma, E. Stratikopoulos, K. Park, J. Wei, T. C. Martin, X. Yang, M. Schwarz, V. Leshchenko, A. Rialdi, B. Dale, A. Lagana, E. Guccione, S. Parekh, R. Parsons and J. Jin, *Nat. Chem. Biol.*, 2020, **16**, 214–222.
- 223 P. Ayaz, A. Lyczek, Y. T. Paung, V. R. Mingione, R. E. Iacob, P. W. de Waal, J. R. Engen, M. A. Seeliger, Y. Shan and D. E. Shaw, *Nat. Commun.*, 2023, **14**, 1885.
- 224 T. R. Stachowski and M. Fischer, *J. Med. Chem.*, 2022, **65**, 13692–13704.

- 225 R. Jafari, H. Almqvist, H. Axelsson, M. Ignatushchenko, T. Lundbäck, P. Nordlund and D. M. Molina, *Nat. Protoc.*, 2014, **9**, 2100–2122.
- 226 E. Szegezdi, S. E. Logue, A. M. Gorman and A. Samali, *EMBO Rep.*, 2006, **7**, 880–885.
- 227 J. Cantley, X. Ye, E. Rousseau, T. Januario, B. D. Hamman, C. M. Rose, T. K. Cheung, T. Hinkle, L. Soto, C. Quinn, A. Harbin, E. Bortolon, X. Chen, R. Haskell, E. Lin, S. F. Yu, G. Del Rosario, E. Chan, D. Dunlap, H. Koeppen, S. Martin, M. Merchant, M. Grimmer, F. Broccatelli, J. Wang, J. Pizzano, P. S. Dragovich, M. Berlin and R. L. Yauch, *Nat. Commun.*, 2022, **13**, 6814.
- 228 C. Kofink, N. Trainor, B. Mair, S. Wöhrle, M. Wurm, N. Mischerikow, M. J. Roy, G. Bader, P. Greb, G. Garavel, E. Diers, R. McLennan, C. Whitworth, V. Vetma, K. Rumpel, M. Scharnweber, J. E. Fuchs, T. Gerstberger, Y. Cui, G. Gremel, P. Chetta, S. Hopf, N. Budano, J. Rinnenthal, G. Gmaschitz, M. Mayer, M. Koegl, A. Ciulli, H. Weinstabl and W. Farnaby, *Nat. Commun.*, 2022, **13**, 1–15.
- 229 B. Jiang, E. S. Wang, K. A. Donovan, Y. Liang, E. S. Fischer, T. Zhang and N. S. Gray, *Angew. Chemie - Int. Ed.*, 2019, **58**, 6321–6326.
- 230 J. Krönke, C. Steinebach, Y. L. D. Ng, I. Sosič, C. S. Lee, S. Chen, S. Lindner, L. P. Vu, A. Bricelj, R. Haschemi, M. Monschke, E. Steinwarz, K. G. Wagner, G. Bendas, J. Luo and M. Gütschow, *Chem. Sci.*, 2020, **11**, 3474–3486.
- 231 G. Iannelli, C. Milite, N. Marechal, V. Cura, L. Bonnefond, N. Troffer-Charlier, A. Feoli, D. Rescigno, Y. Wang, A. Cipriano, M. Viviano, M. T. Bedford, J. Cavarelli, S. Castellano and G. Sbardella, *J. Med. Chem.*, 2022, **65**, 11574–11606.
- 232 M. Schapira and R. Ferreira De Freitas, *Medchemcomm*, 2014, **5**, 1779–1788.
- 233 Y. Shen, F. Li, M. M. Szewczyk, L. Halabelian, I. Chau, M. S. Eram, C. Dela Seña, K. S. Park, F. Meng, H. Chen, H. Zeng, A. Dong, H. Wu, V. V. Trush, D. Mcleod, C. A. Zepeda-Velázquez, R. M. Campbell, M. M. Mader, B. M. Watson, M. Schapira, C. H. Arrowsmith, R. Al-Awar, D. Barsyte-Lovejoy, H. Ü. Kaniskan, P. J. Brown, M. Vedadi and J. Jin, *J. Med. Chem.*, 2021, **64**, 3697–3706.
- 234 M. Schapira, M. F. Calabrese, A. N. Bullock and C. M. Crews, *Nat. Rev. Drug Discov.*, 2019, **18**, 949–963.
- 235 M. D. Stewart, T. Ritterhoff, R. E. Klevit and P. S. Brzovic, *Cell Res.*, 2016, **26**, 423–440.
- 236 N. Forte, D. Dovala, M. J. Hesse, J. M. McKenna, J. A. Tallarico, M. Schirle and D. K. Nomura,

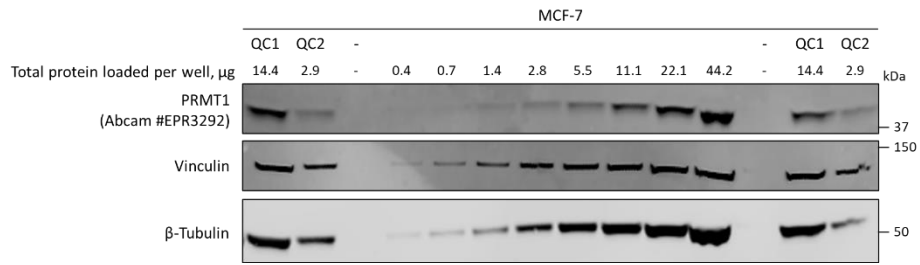
- ACS Chem. Biol.*, 2023, **18**, 897–904.
- 237 C. Bashore, S. Prakash, M. C. Johnson, R. J. Conrad, I. A. Kekessie, S. J. Scales, N. Ishisoko, T. Kleinheinz, P. S. Liu, N. Popovych, A. T. Weckler, L. Zhou, C. Tam, I. Zilberleyb, R. Srinivasan, R. A. Blake, A. Song, S. T. Staben, Y. Zhang, D. Arnott, W. J. Fairbrother, S. A. Foster, I. E. Wertz, C. Ciferri and E. C. Dueber, *Nat. Chem. Biol.*, 2023, **19**, 55–63.
- 238 W. C. Still, M. Kahn and A. Mitra, *J. Org. Chem.*, 1978, **43**, 2923–2925.
- 239 J. Coates, in *Encyclopedia of Analytical Chemistry*, ed. R. A. Meyers, John Wiley & Sons Ltd., Chichester, 2000, pp. 1–23.
- 240 J. Roger, F. Pozgan and H. Doucet, *J. Org. Chem.*, 2009, **74**, 1179–1186.
- 241 US2021/030928, 2021.
- 242 JP2016/073184, 2016.
- 243 H. Yang, Y. Ouyang, H. Ma, H. Cong, C. Zhuang, W. T. Lok, Z. Wang, X. Zhu, Y. Sun, W. Hong and H. Wang, *Bioorganic Med. Chem. Lett.*, 2017, **27**, 4635–4642.
- 244 N. D. Bogdan, M. Matache, V. M. Meier, C. Dobrotă, I. Dumitru, G. D. Roiban and D. P. Funeriu, *Chem. - A Eur. J.*, 2010, **16**, 2170–2180.
- 245 C. E. Schroeder, S. A. Neuenswander, T. Yao, J. Aubé and J. E. Golden, *Org. Biomol. Chem.*, 2016, **14**, 3950–3955.
- 246 US2016/0346400, 2016.
- 247 CN2020/103988, 2020.
- 248 X. Zhang, D. Thummuri, X. Liu, W. Hu, P. Zhang, S. Khan, Y. Yuan, D. Zhou and G. Zheng, *Eur. J. Med. Chem.*, 2020, **192**, 112186.
- 249 addgene.org, Addgene Plasmid Instructions, <https://www.addgene.org/recipient-instructions/myplasmid/>, (accessed 17 December 2023).
- 250 F. Carnevale Neto, T. N. Clark, N. P. Lopes and R. G. Linington, *J. Nat. Prod.*, 2022, **85**, 519–529.
- 251 Addgene_pH6HTC_PRMT1-Halo, <https://www.addgene.org/175334/>, (accessed 14 December 2023).
- 252 Y. Li, Y. Xu, L. Liu, X. Wang, M. Palmisano and S. Zhou, *J. Clin. Pharmacol.*, 2015, **55**, 563–572.

253 Clinical Pharmacology Review: Pomalidomide. Application number: 204026Orig1s000, https://www.accessdata.fda.gov/drugsatfda_docs/nda/2013/204026Orig1s000ClinPharmR.pdf, (accessed 23 November 2023).

Appendix 1 Supplementary Figures

Appendix 1A

A



B

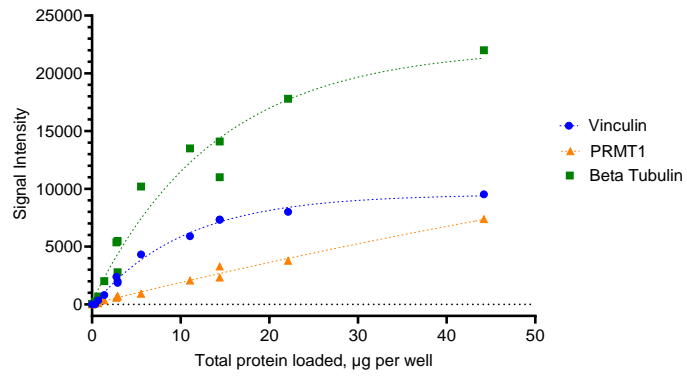
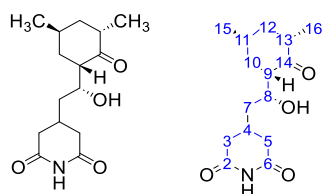


Figure 1 *The relationship between PRMT1 and total protein with an alternative anti-PRMT1 antibody (Abcam #EPR3292).* A) A dilution series of the cell-lysate derived from MCF-7 cells was analysed by Western blot. B) The protein bands were quantified with Image Studio analysis software and plotted against the amount of total protein loaded to the well.

Appendix 1B

Cycloheximide. Purchased from TOKU-E, Batch C001-46-2



^1H NMR (700 MHz, d_6 -DMSO) δ 10.64 (s, 1H, 2-NH), 4.38 (d, $J=6.2$ Hz, 1H, 8-OH), 38.3 (m, 1H, H8), 2.62 (m, 1H, H13), 2.57 (m, 1H, H3 or H5), 2.49 (m, 1H, H3 or H5), 2.46 (m, 1H, H9), 2.26 (m, 2H, H3 and H5), 2.21 (m, 1H, H4), 2.08 (m, 1H, H11), 1.96 (m, 1H, C10), 1.80 (m, 1H, C12), 1.63 (m, 1H, C10), 1.49 (m, 1H, C12), 1.31 (m, 2H, H7), 1.18 (d, $J=7.1$ Hz, 3H, C15), 0.86 (d, $J=6.4$ Hz, 3H, C16). **^{13}C NMR (176 MHz, d_6 -DMSO)** δ 213.6 (C14), 173.5 and 173.3 (C2 and C6), 65.0 (C8), 50.6 (C9), 42.3 (C12), 40.1 (C7), 39.8 (C13), 38.3 (C3 or C5), 36.8 (C3 or C5), 35.0 (C10), 26.9 (C4), 26.5 (C11), 18.2 (C15), 14.5 (C16). **LRMS (ESI)** m/z calcd for $\text{C}_{15}\text{H}_{23}\text{NO}_4$ $[\text{M}+\text{H}]^+$: 282.4; found 282.3. **HPLC** (5-60% MeCN (0.05% TFA) in H_2O (0.05% TFA) over 15 min) R_t = 10.46 min. Purity= 61%. **Lab reference** PM296.

Data are in accordance with those reported previously in literature²⁵⁰.

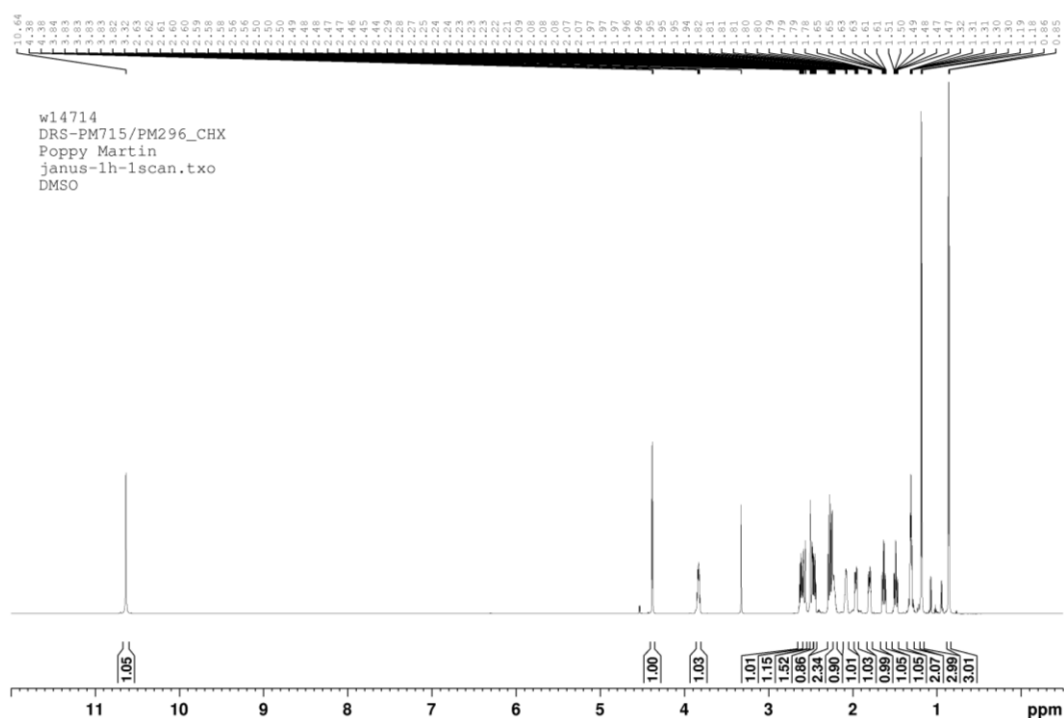


Figure 2 ^1H NMR (700 MHz, d_6 -DMSO) spectrum of cycloheximide.

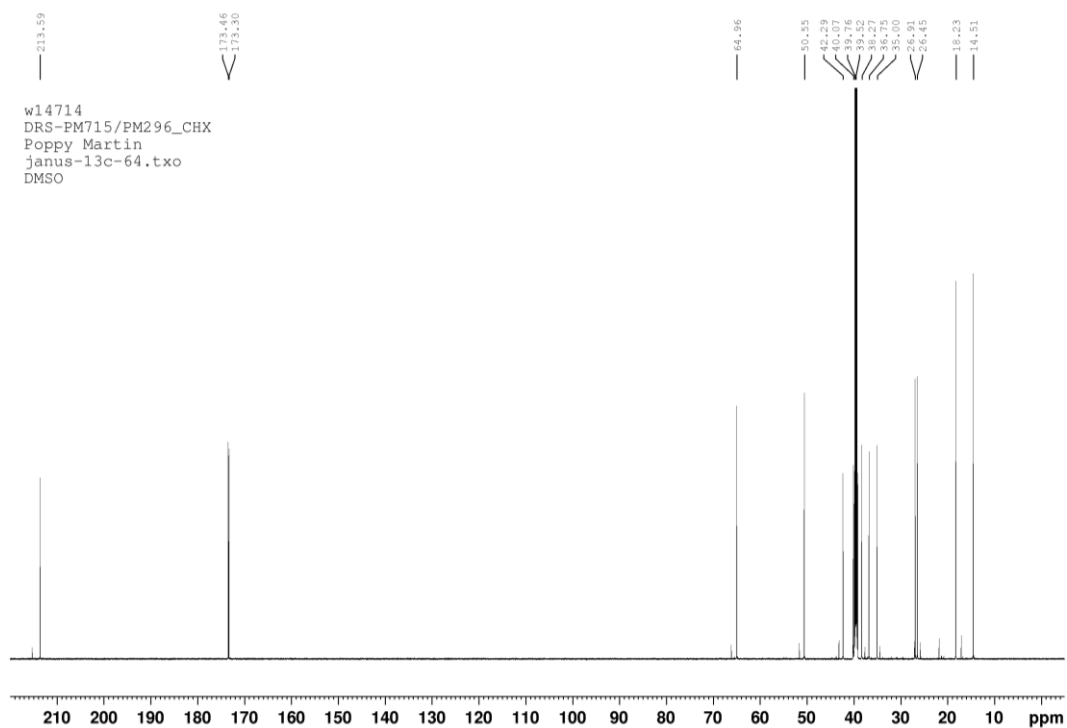


Figure 3 ^{13}C NMR (176 MHz, d_6 -DMSO) spectrum of cycloheximide.

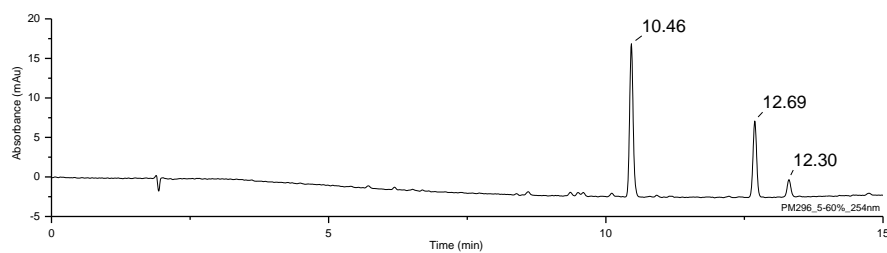
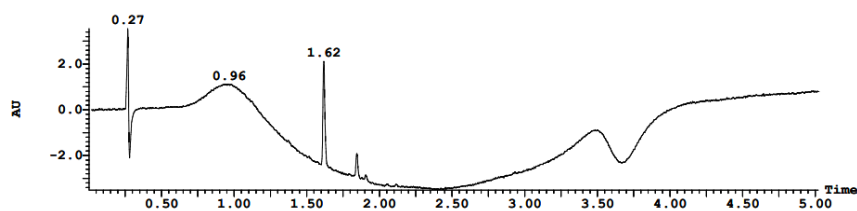


Figure 4 UV-HPLC chromatogram of cycloheximide. Absorbance recorded at $\lambda = 254$ nm.

A



B

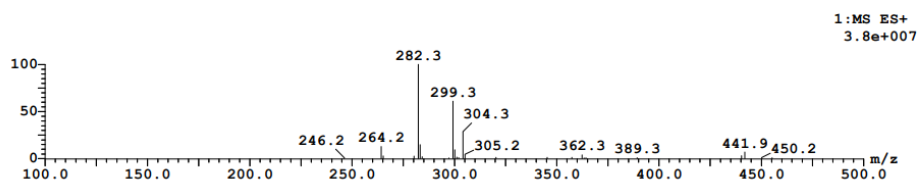


Figure 5 LC/MS analysis of cycloheximide. A) UV-HPLC chromatogram. Absorbance recorded at $\lambda = 254$ nm. B) ESI^+ spectrum for the peak at 1.62 min. The molecular weight of CHX is 281.2.

Appendix 1C

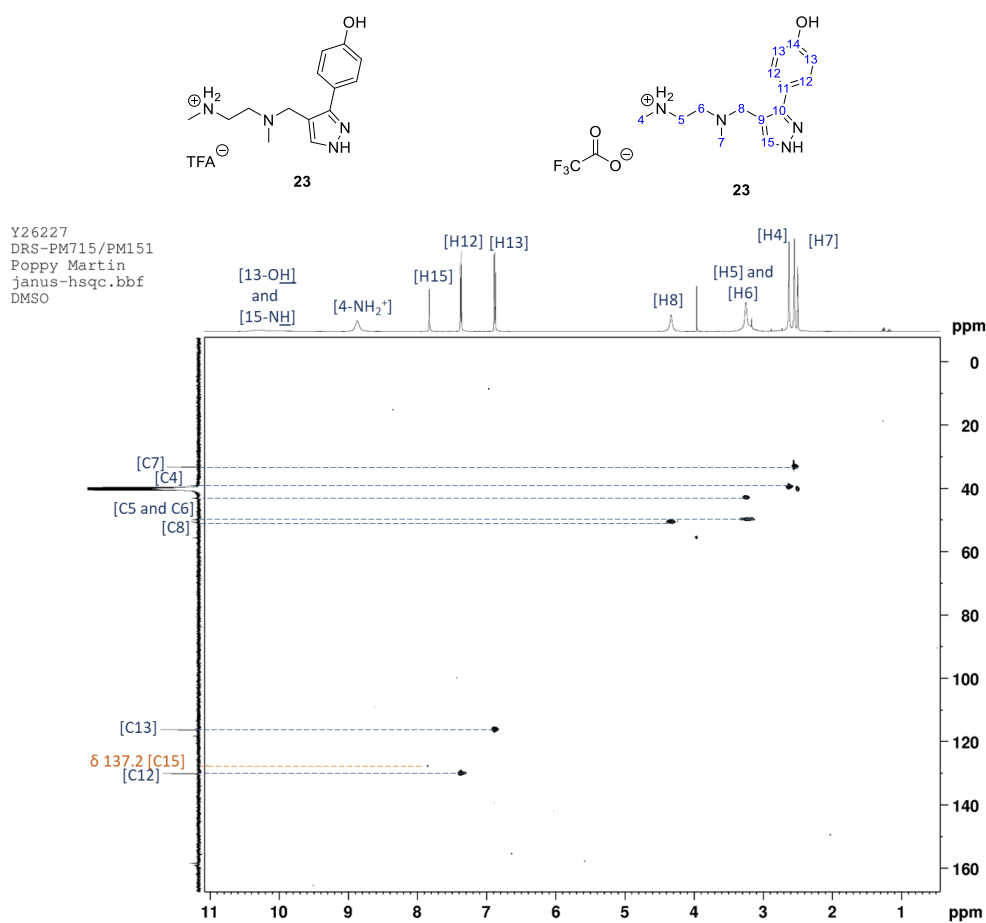


Figure 6 HSQC NMR spectrum of **23**. Peaks indicated in orange do not appear in the ^{13}C spectra.

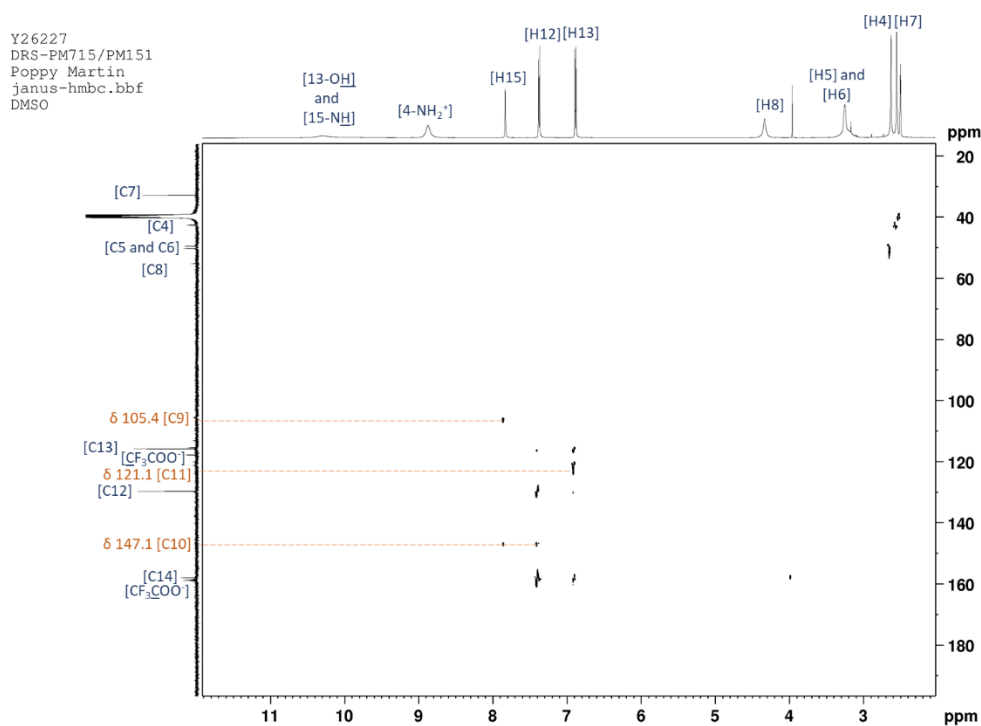
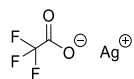


Figure 7 HMBC NMR spectrum of **23**. Peaks indicated in orange do not appear in the ^{13}C spectra.

Silver Trifluoroacetate. Obtained from commercial supplier.



^1H NMR (700 MHz, d_6 -DMSO) δ No peaks (DMSO and H₂O only). ^{13}C NMR (176 MHz, d_6 -DMSO) δ 159.3 (q, $^2J_{\text{C-F}}=32.7$ Hz, $\text{CF}_3\text{C}\underline{\text{O}}\text{O}^-$), 117.5 (q, $^1J_{\text{C-F}}=295.7$ Hz, $\underline{\text{C}}\text{F}_3\text{C}\text{O}\text{O}^-$). Lab reference PM294

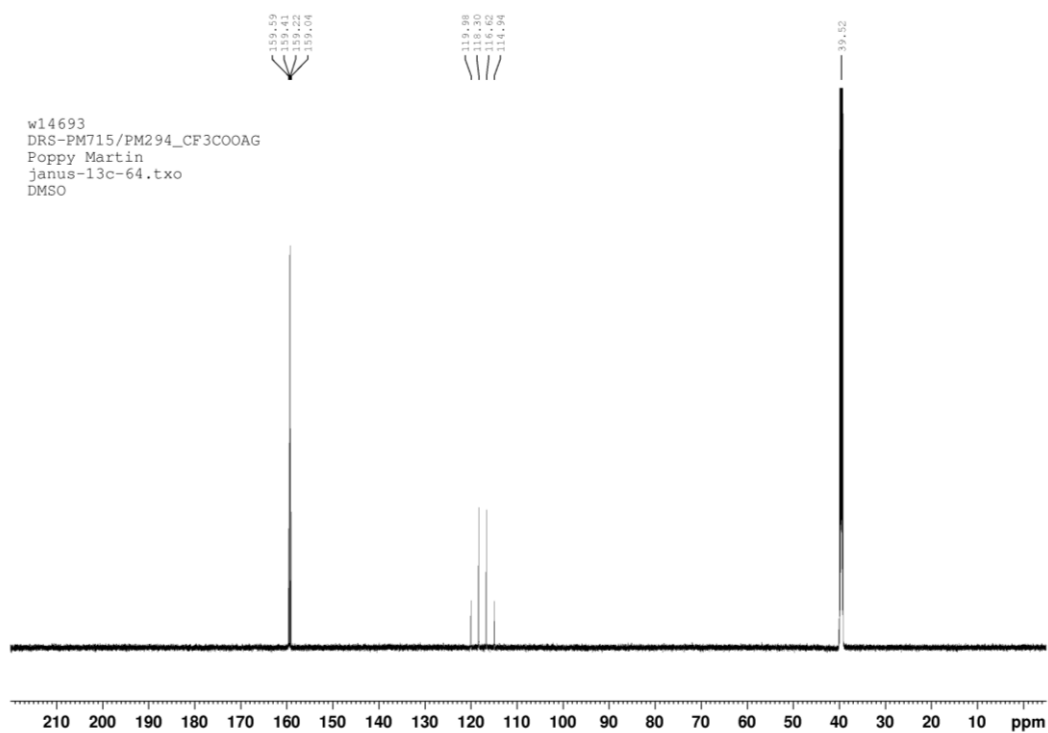


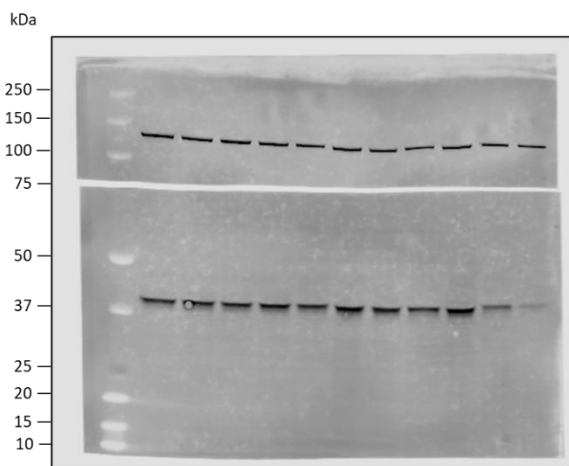
Figure 8 ^{13}C (176 MHz, d_6 -DMSO) NMR spectrum of silver trifluoroacetate.

Appendix 1D

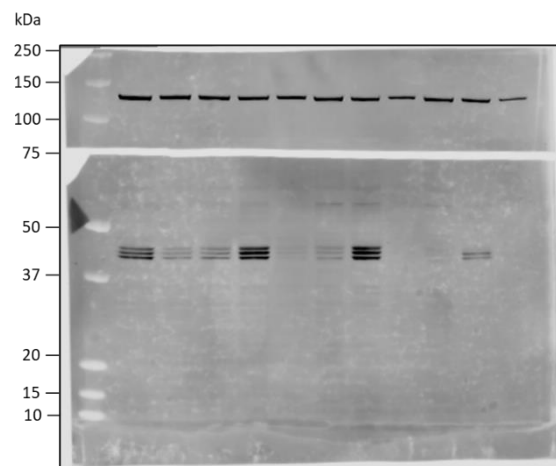
A

Lane (left to right)	1	2	3	4	5	6	7	8	9	10	11	12
hr	M _w ladder	24	24	24	48	48	48	72	72	72	X	X
GSK3368715 (10 μM)	X	-	+	-	-	+	-	-	+	-	X	X
23 (10 μM)	X	-	-	+	-	-	+	-	-	+	X	X

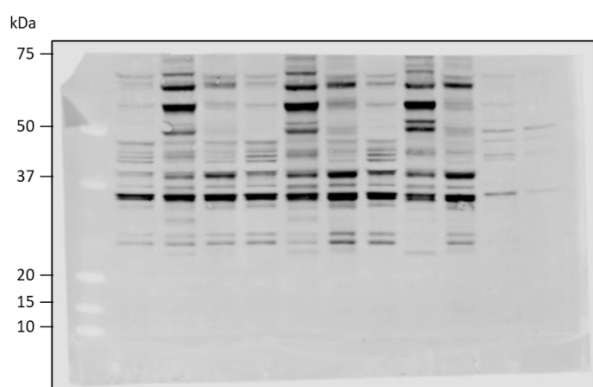
B



C



D



E

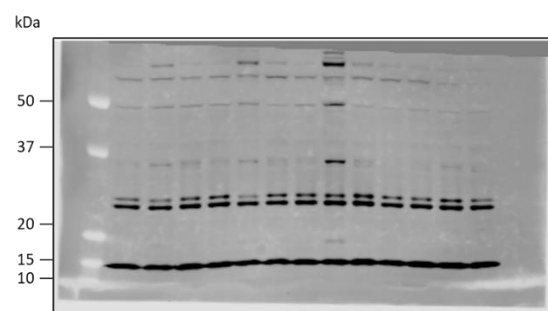


Figure 9 Full uncropped Western blots for Figure 4.19. A) Identity of the protein lysates loaded on each lane. B) Membrane cut at 75 kDa and the top section probed for vinculin. The bottom section probed for PRMT1. C) Membrane cut at 75 kDa and the top section probed for vinculin. The bottom section probed for ADMA. D) Membrane probed for MMA. E) Membrane probed for SDMA.

Appendix 1E

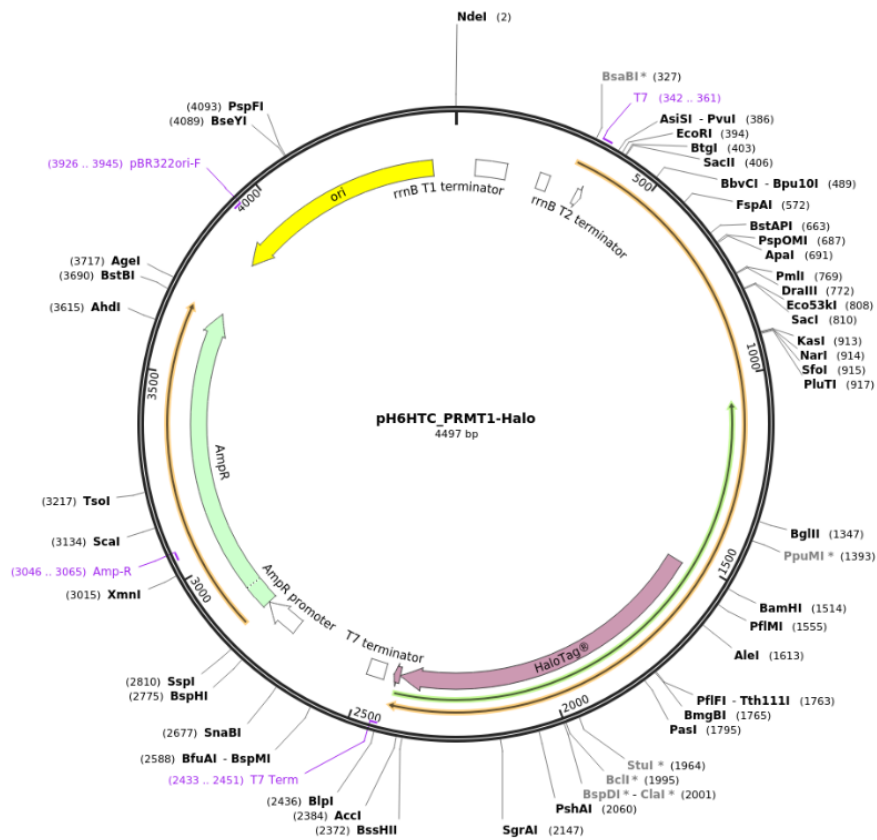


Figure 10 Plasmid map of the PRMT1-HaloTag-6xHis fusion protein. Figure reprinted from ²⁵¹.

Appendix 1F

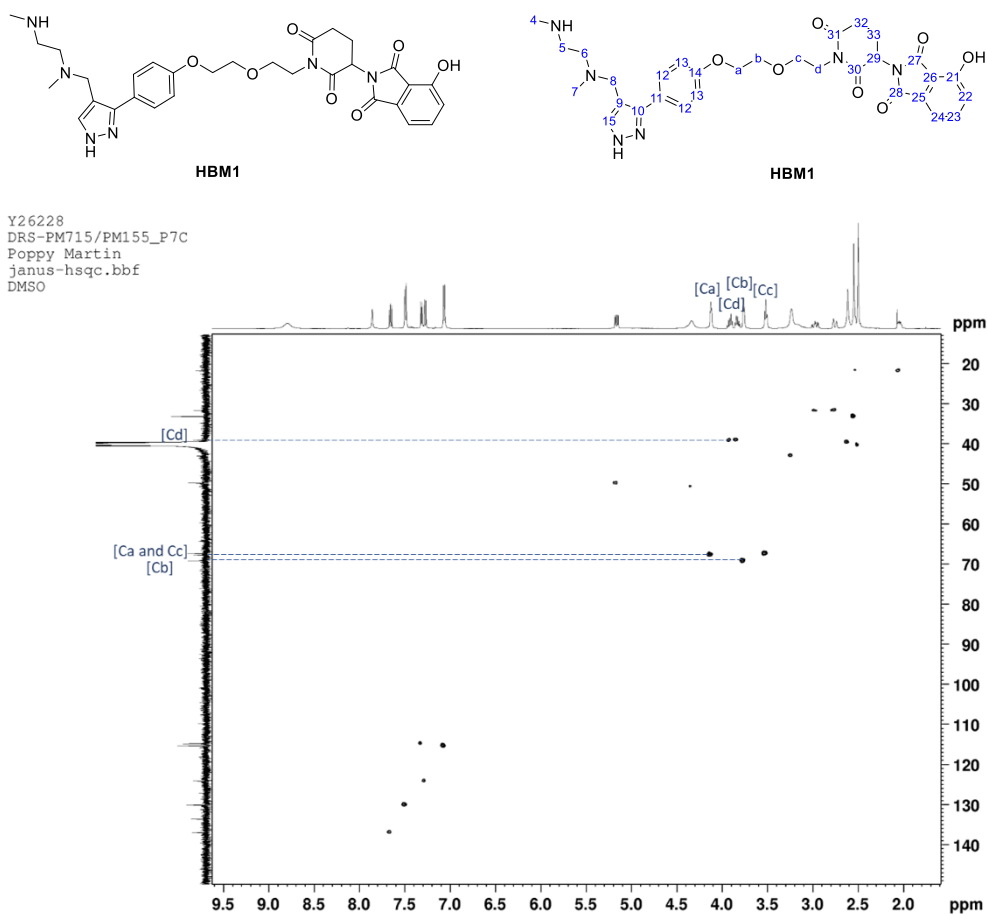


Figure 11 HSQC NMR spectrum of HBM1

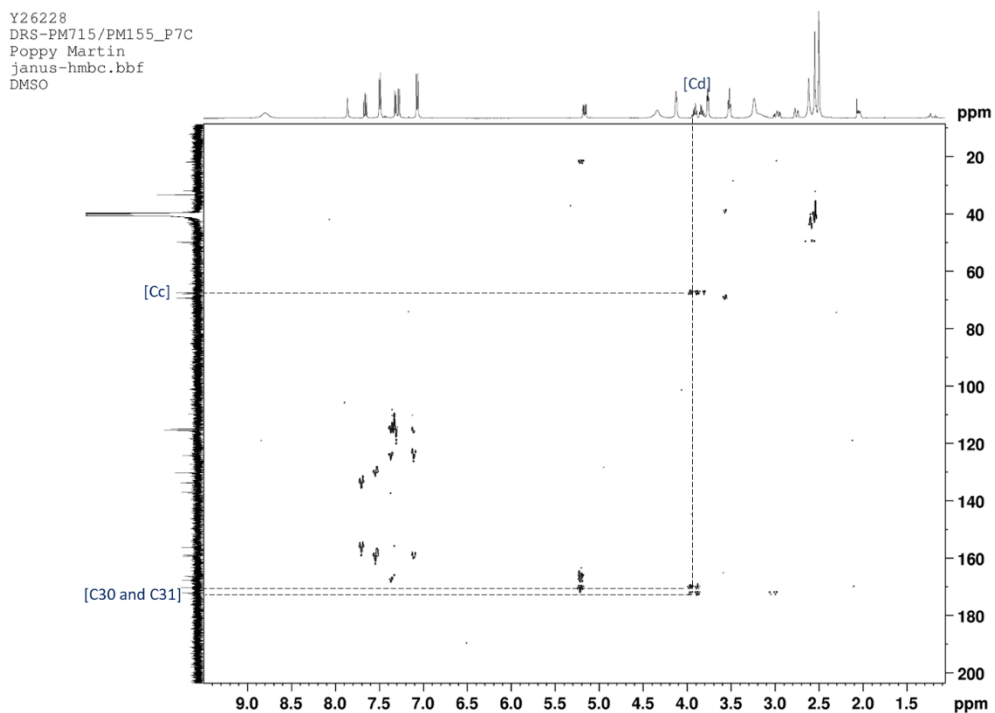


Figure 12 HMBC NMR spectrum of HBM1

Appendix 1G

The stability of pomalidomide was analysed using conditions identical to those used to determine PROTAC stability and the results compared to literature values. The half-life of pomalidomide was empirically determined in MCF-7 cell culture media, human serum and PBS (pH 7.4) (Figure 13). Unfortunately, due to an absence of reported half-lives and inaccurate empirical results, this experiment did not allow any conclusions on the validity of the assay to be made.

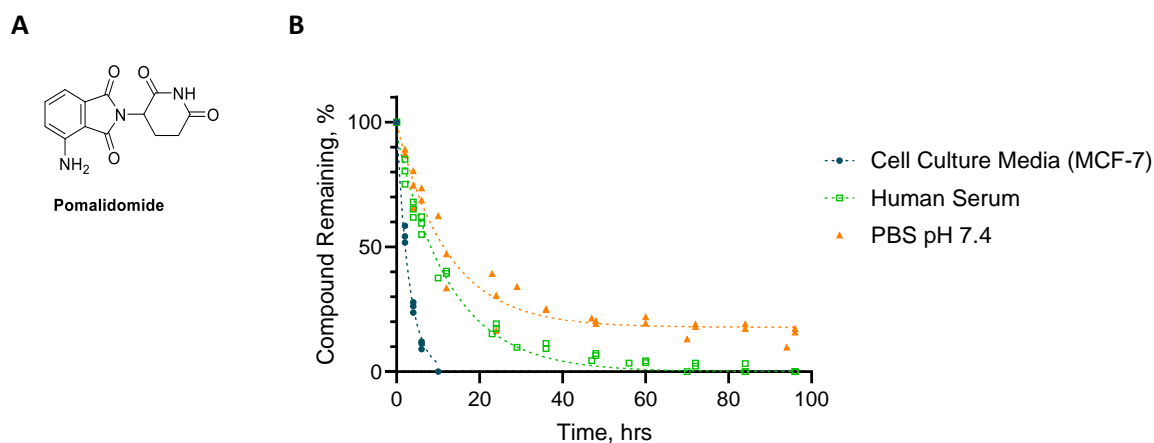


Figure 13 Pomalidomide Stability in cell culture medium, human serum and PBS. A) Structure of pomalidomide B) 400 μ M pomalidomide and 400 μ M caffeine was incubated at 37°C in an ambient atmosphere for 96 hr. Cell culture media is DMEM supplemented with 10% FBS. The Y-axis is the percentage of pomalidomide remaining compared to the peak area ratio of pomalidomide-to-caffeine at 0 hr. All data points from three independent experiments are shown. For cell culture media and human serum, the data was fitted with an exponential decay function with the plateau constrained to zero. The results for PBS do not fit this model and no constraints were used.

The data for PBS was considered inaccurate due to a plateau occurring at a non-zero value. This is likely from the coelution of a hydrolysis product with caffeine or pomalidomide. The samples were also analysed using a different mobile phase gradient and on a different HPLC instrument but they all yielded the same result. A single half-life for pomalidomide in PBS (pH 7.4) is reported in the literature of 32.5 hr²¹³.

The empirically determined half-life for pomalidomide in human serum is 8.9 hr. Due to data availability, this has been compared to half-life data for pomalidomides *in vivo* plasma stability. The empirically determined value agrees with these reported values (Table 1). This is promising, yet inconclusive.

Table 1 The half-life of pomalidomide in human serum.

	Pomalidomide half-life, hr	Reference
Incubation in human serum	8.9	Empirical observation
<i>in vivo</i>	7.5	252
<i>in vivo</i>	6-10	253

For the half-life in cell culture medium, an identical cell culture medium was not used and therefore the empirically derived half-life values cannot be compared to the reported values (Table 2). The stability of pomalidomide will be dependent on the composition of the cell media, including its pH and the concentration of different amino acids^{199,200}.

Table 2 The half-life of pomalidomide in cell culture media.

Cell line	Cell culture media composition	Pomalidomide half-life, hr	Reference
MCF-7	DMEM+10% FBS	2.1	Empirical observation
MV4-11	IMDM+ 10% FBS	12.5	213
HD-MB03	Neural basal medium containing Peni-Strep, L-glutamine, B27, heparin, bFGF, and EGF.	5.5	213

Appendix 1H

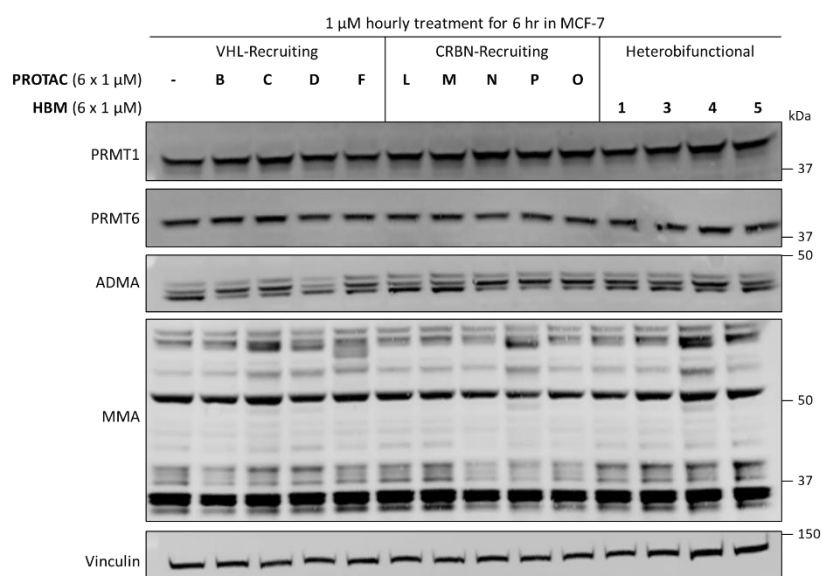


Figure 14 Western blot of selected VHL-recruiting PROTACs, selected CRBN-recruiting PROTACs and HBM1-5 in the MCF-7 cell line. 1 μ M of PROTAC was added hourly for six hours MCF-7 cells were treated with 1 μ M of the indicated compound and one-hour later an additional 1 μ M of the indicated compound was added. This was repeated 4 further times (the total concentration added was 6 μ M, and the total incubation time was 6 hr). The cells were then harvested for analysis by Western blot.

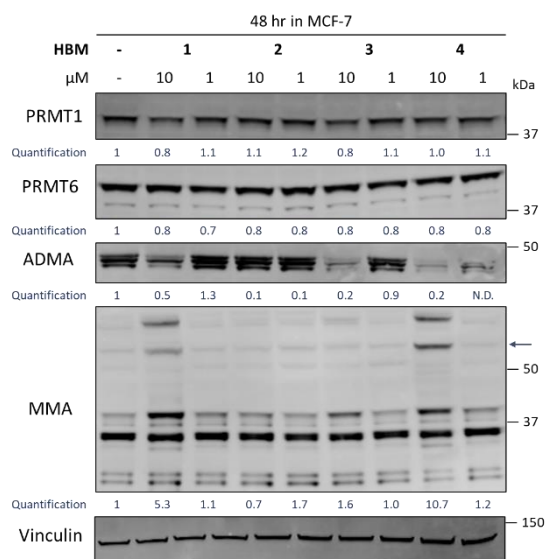


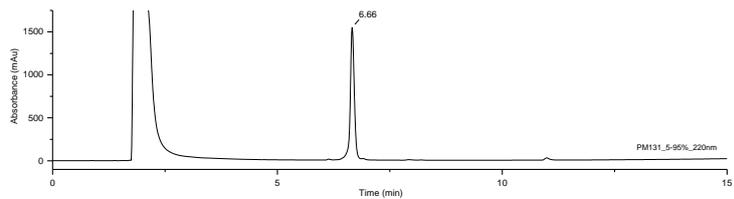
Figure 15 Western blot of HBM1-4 in the MCF-7 cell line for 48 hr. At 10 μ M, HBM1 and HBM3 induced the degradation of PRMT1 but not PRMT6. MCF-7 cells were treated with HBM1-5 at either 10 μ M or 1 μ M for 48 hr and then harvested for analysis by Western blot. The arrow (\leftarrow) indicates the band quantified for MMA.

Appendix 2 UV-HPLC Chromatograms of PROTAC A-Q and
HBM1-5

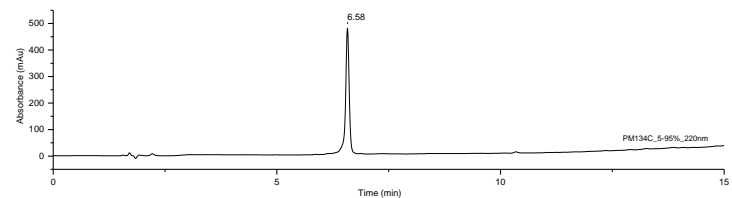
Table 1 Purity of PROTAC A-Q and HBM1-5 as determined by HPLC. The HPLC method was 5-95% MeCN (0.05% TFA) in H₂O (0.0.5% TFA) over 15 min and the UV chromatogram was recorded at $\lambda = 220$ nm. The DMSO stock solution of certain molecules was analysed and the large tailing peak at ~ 2 min can be attributed to DMSO. The solvent front has not been integrated in purity determination.

	Purity, %	UV-HPLC chromatogram
PROTAC A	97	
PROTAC B	99	
PROTAC C	99	
PROTAC D	89	
PROTAC E	96	
PROTAC F	93	

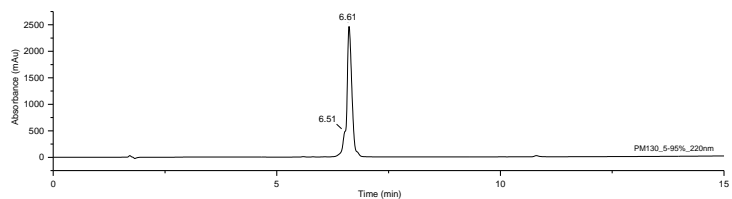
PROTAC G 97



PROTAC H 99

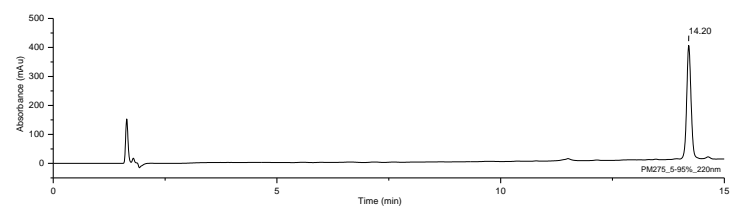


PROTAC I 86*

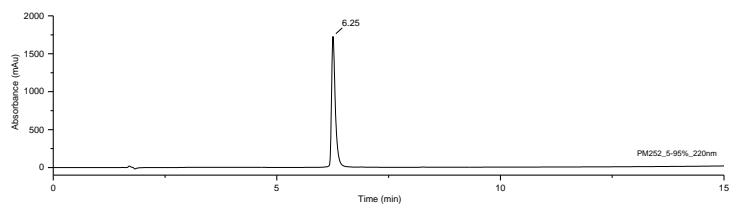


*The shoulder peak at 6.51 minutes is PROTAC H.

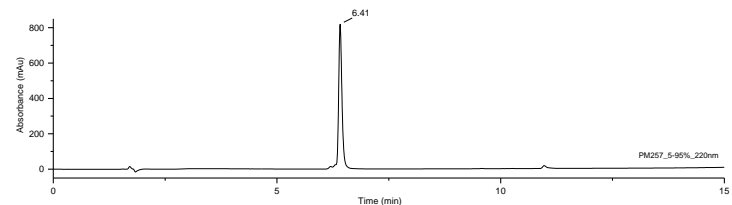
PROTAC K 96



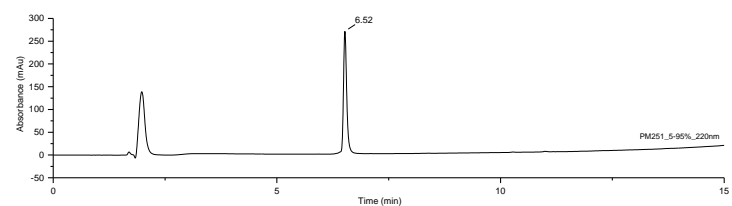
PROTAC L 99



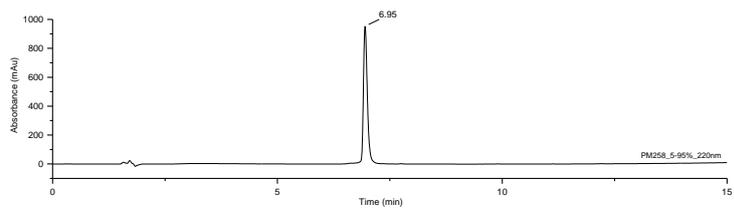
PROTAC M 94



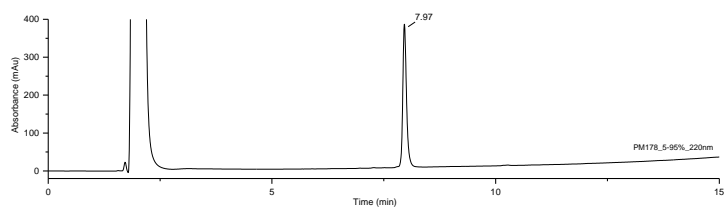
PROTAC N 99



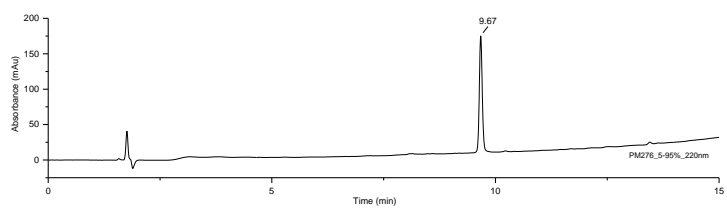
PROTAC O 99



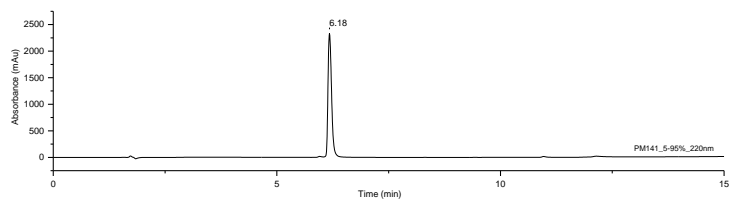
PROTAC P 99



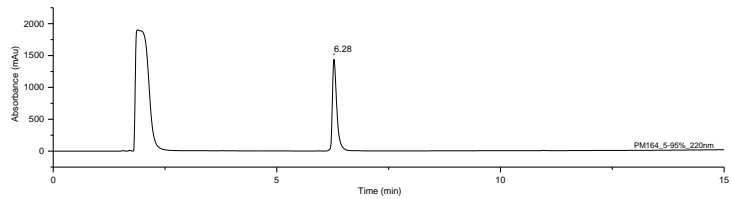
PROTAC Q 95



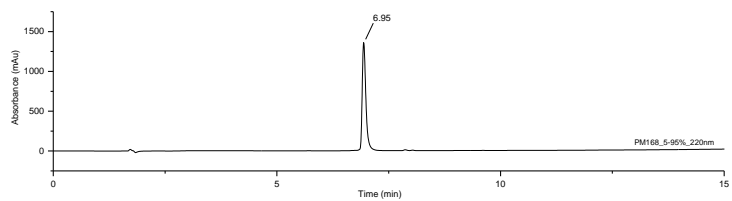
HBM1 99



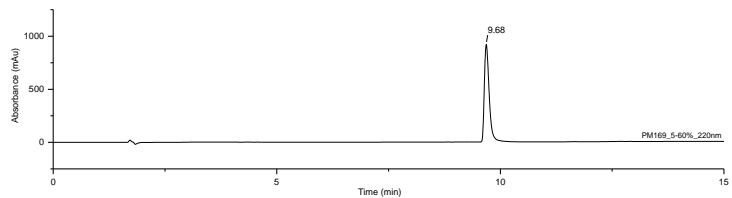
HBM2 99



HBM3 99

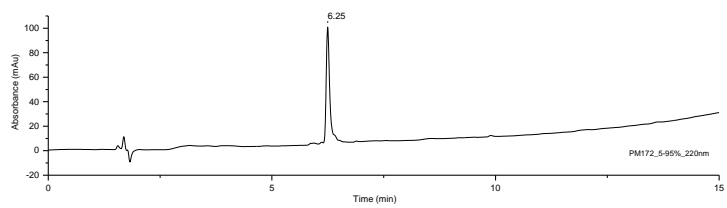


HBM4 99



HBM5

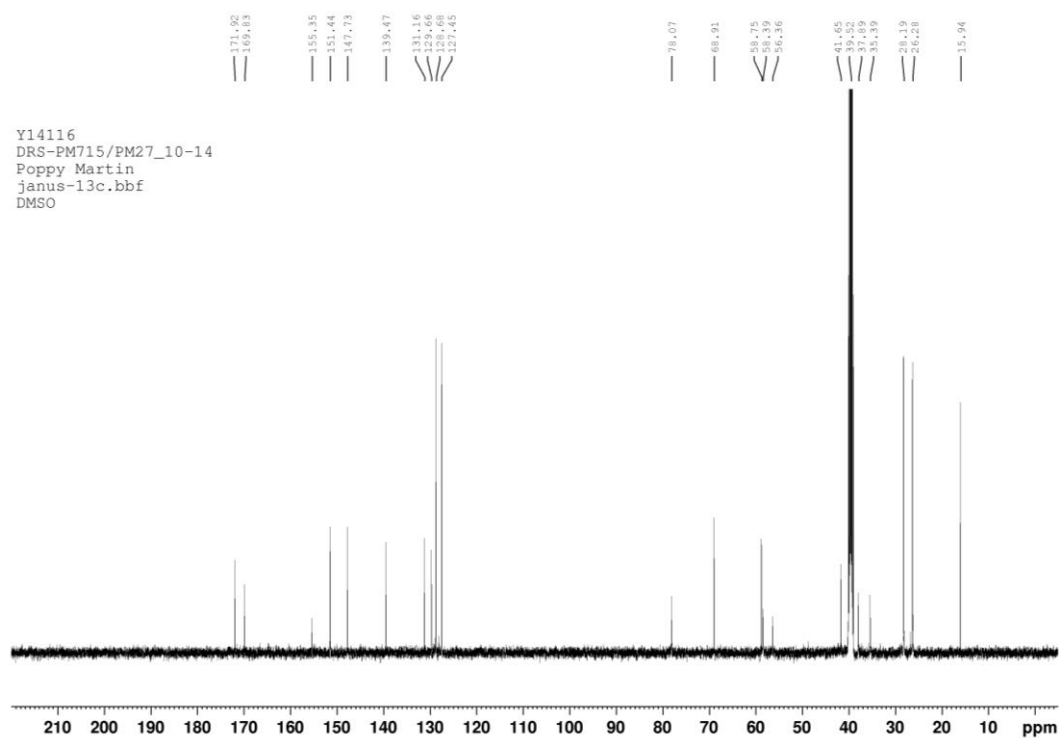
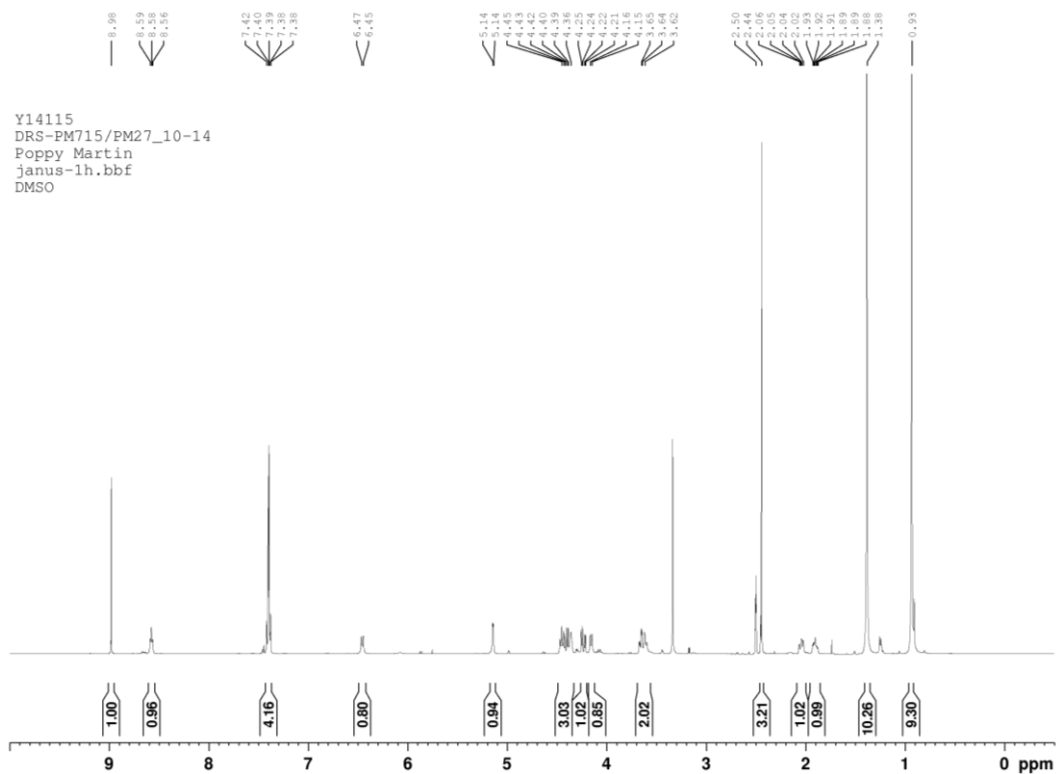
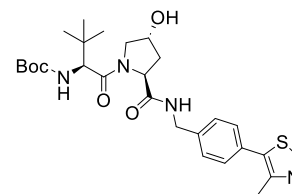
89



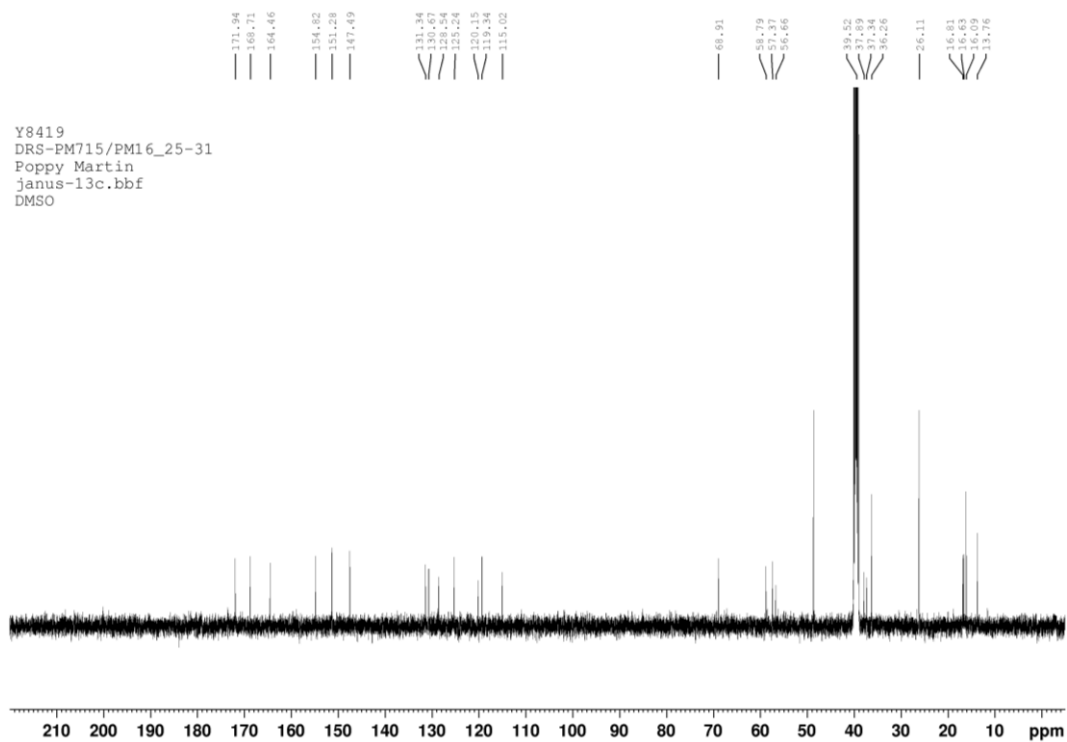
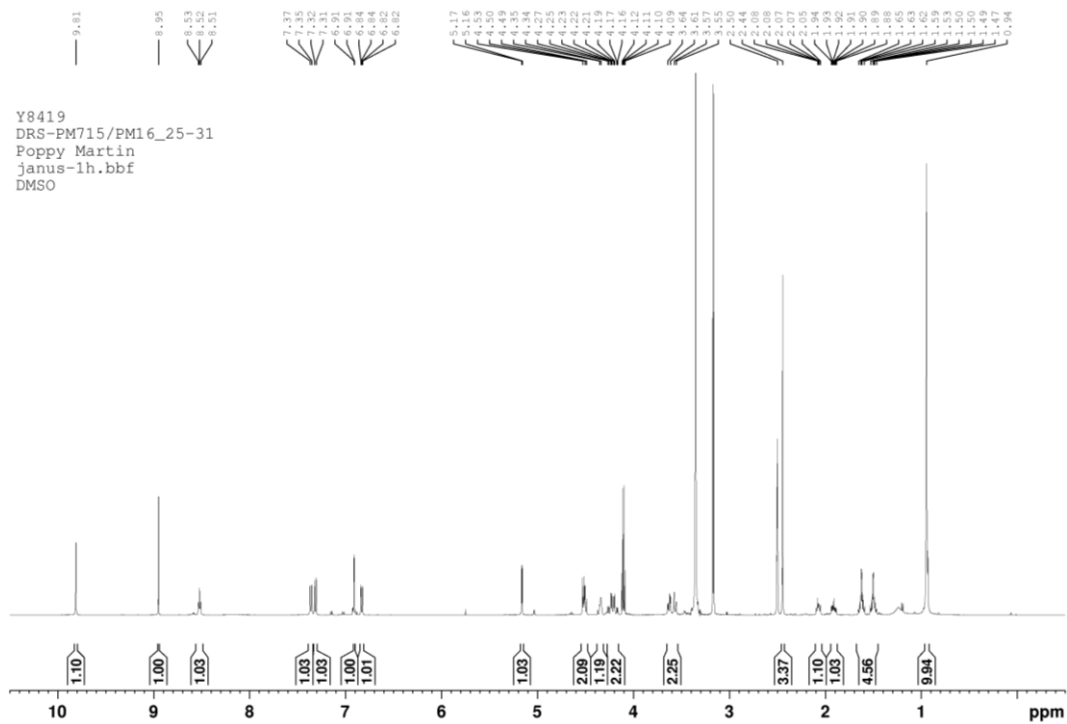
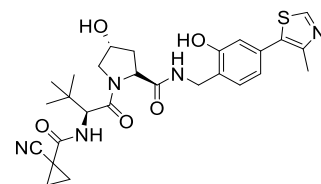
Appendix 3 NMR Spectra

Compound 1-47 followed by PROTAC A-Q and HBM1-5

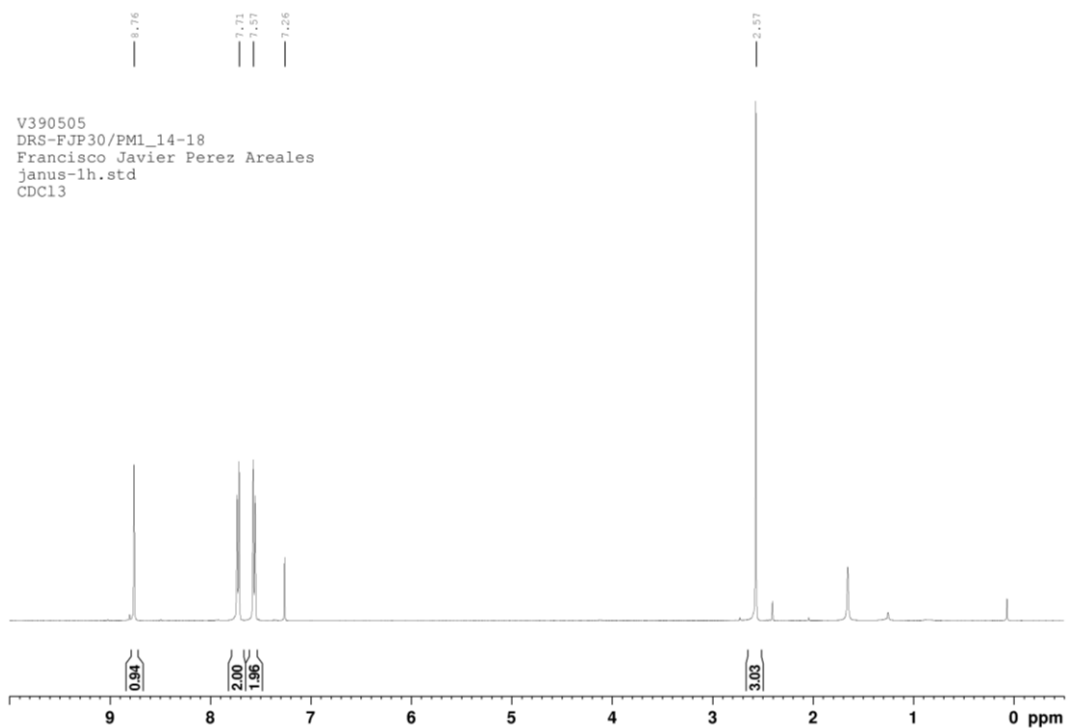
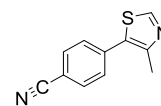
(1)



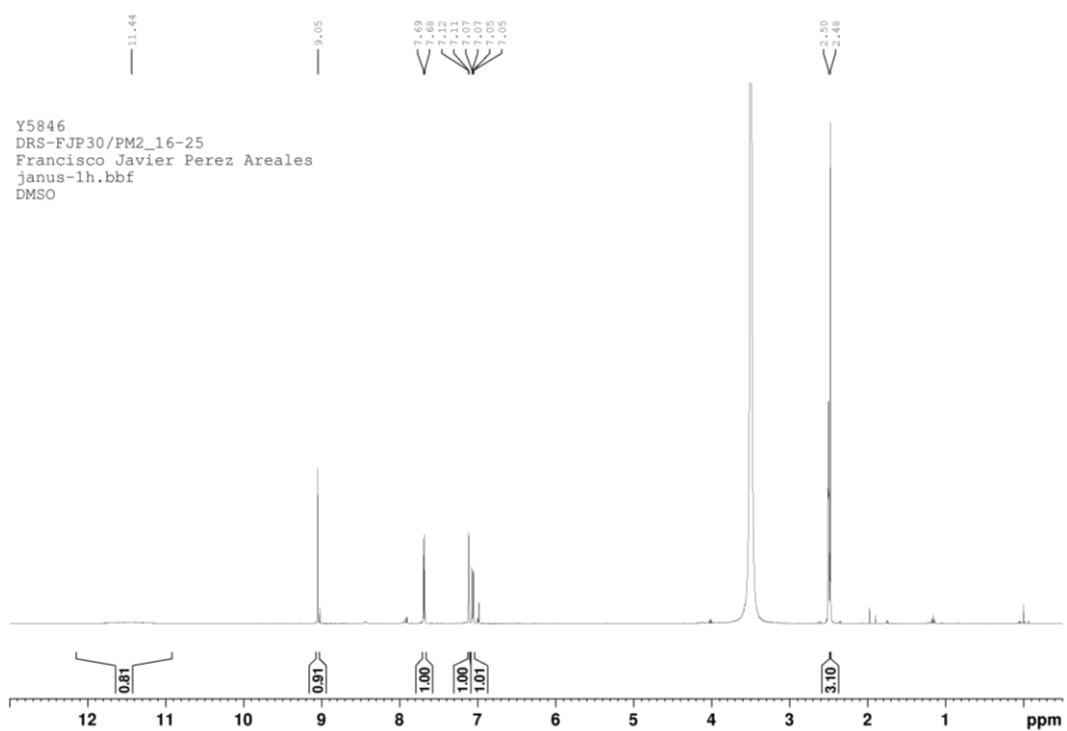
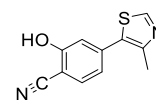
(2)



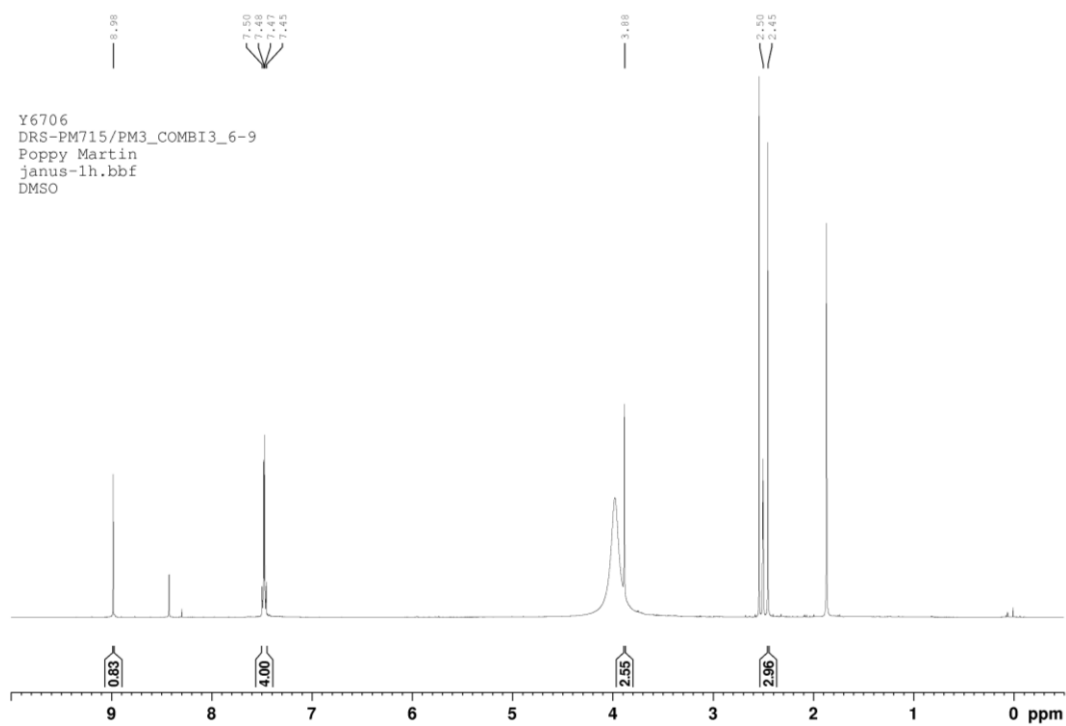
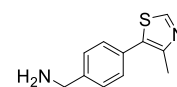
(4a)



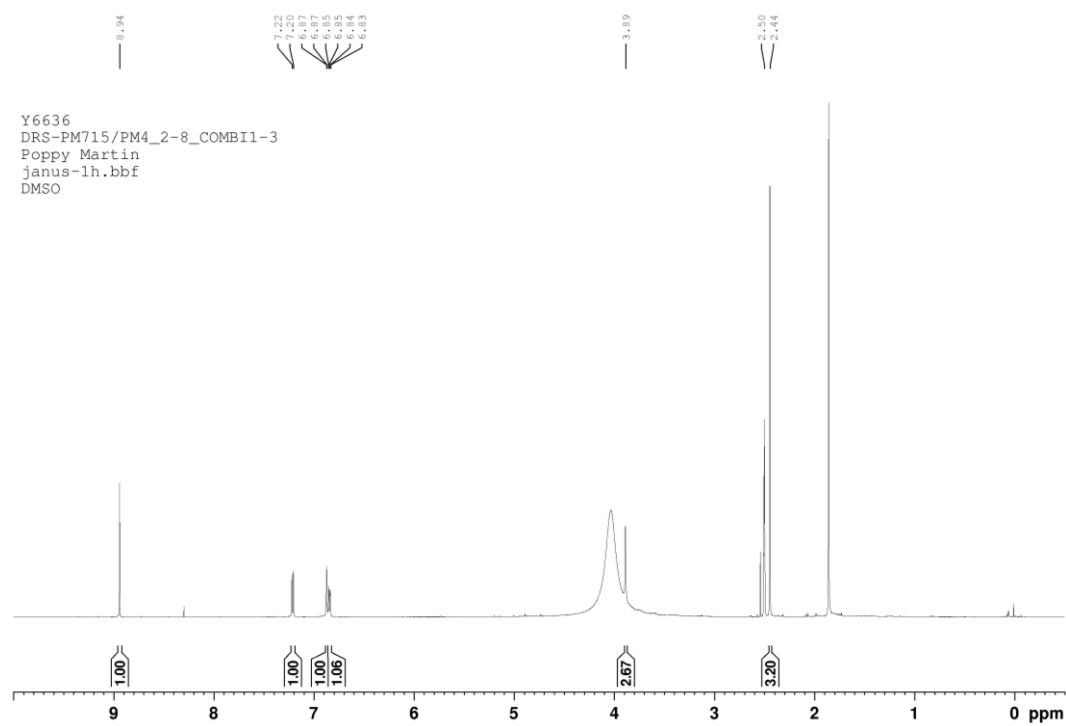
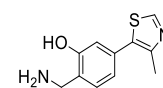
(4b)



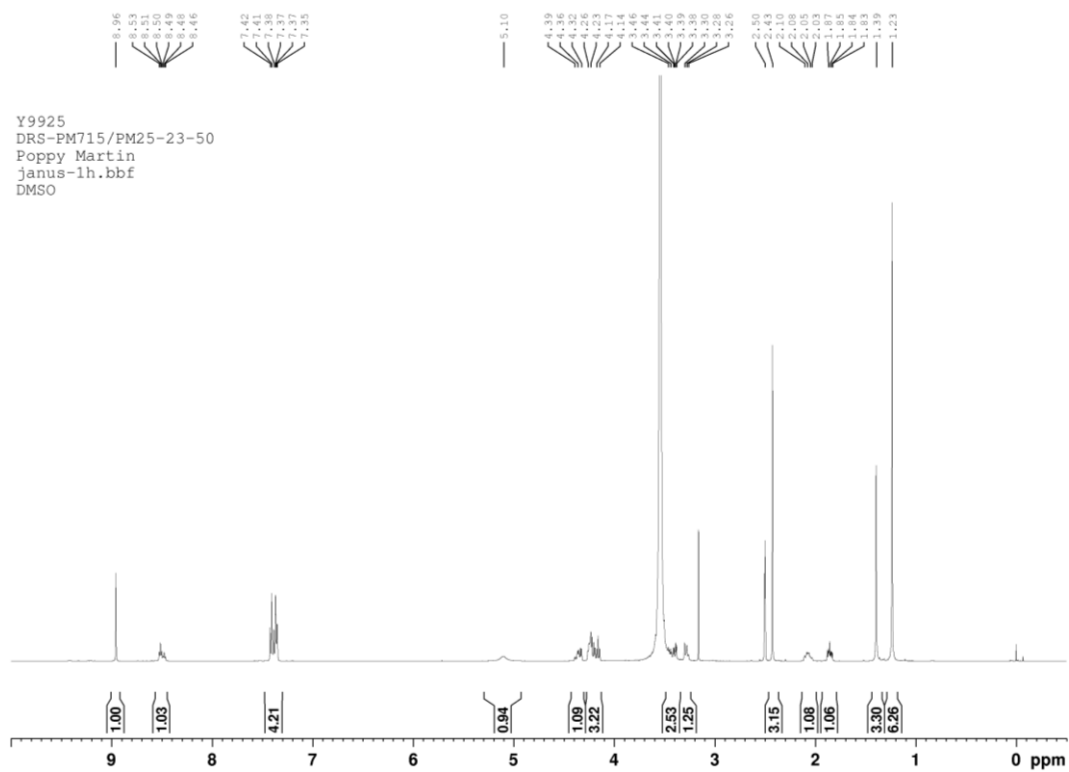
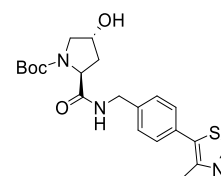
(5a)



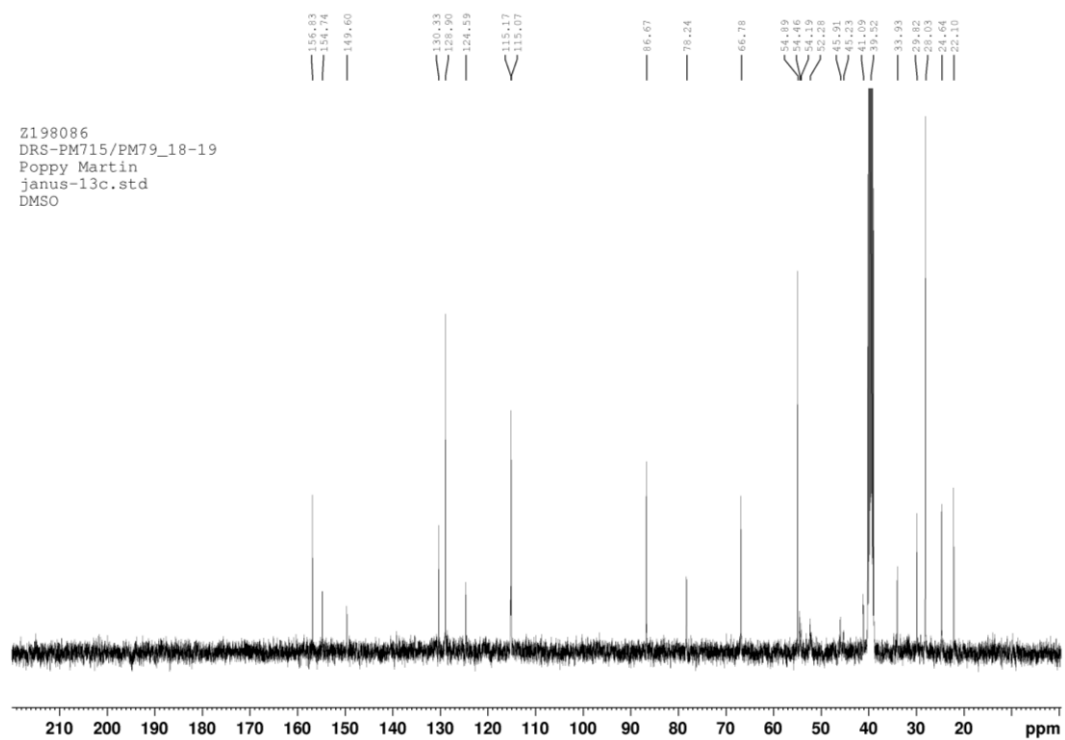
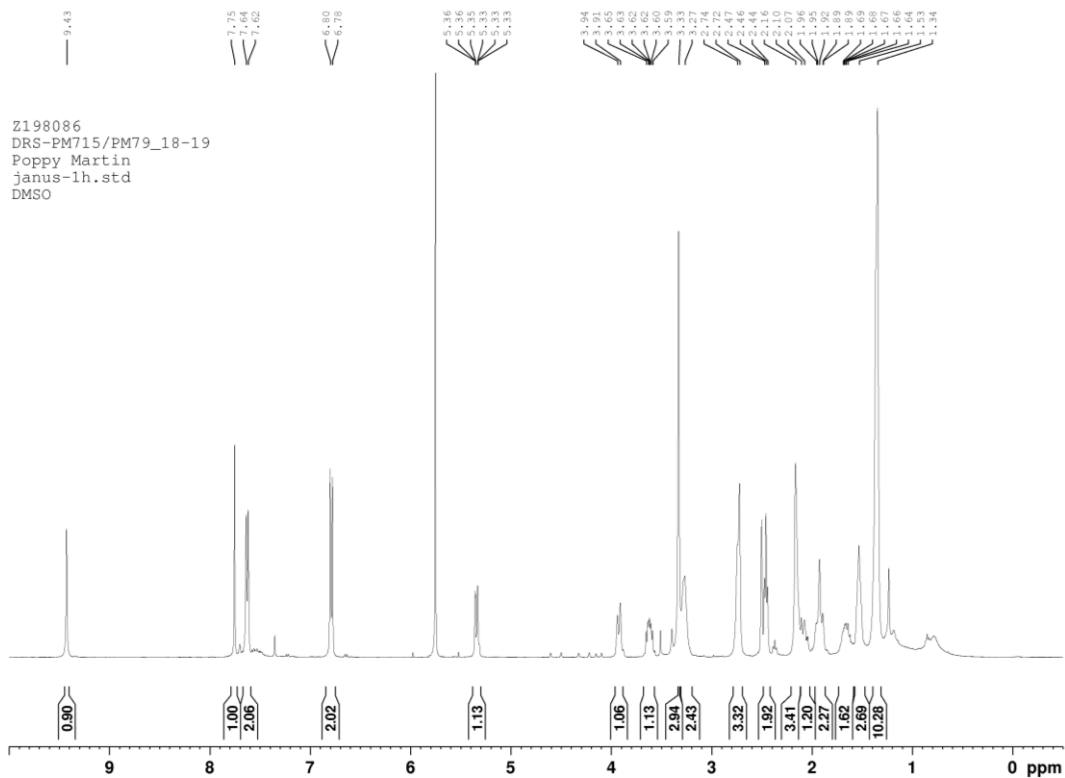
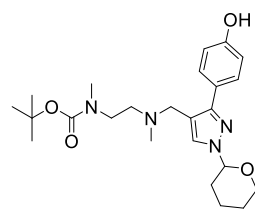
(5b)



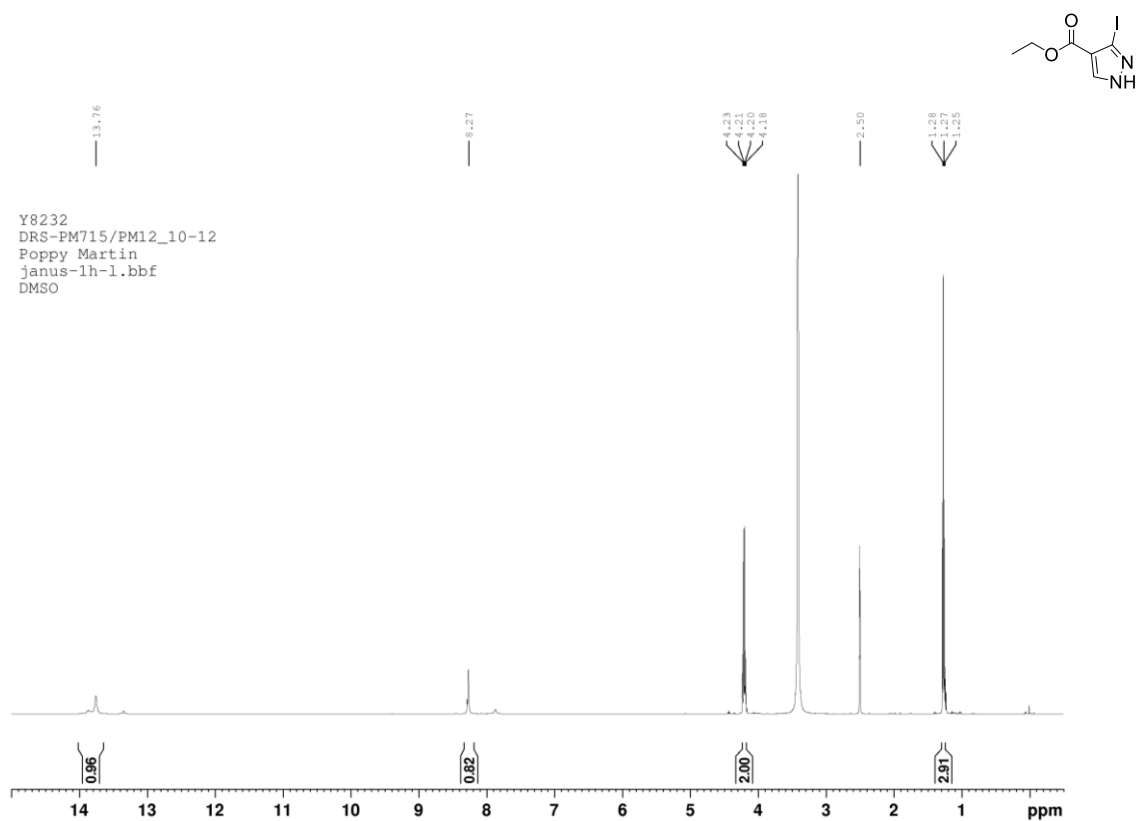
(10)



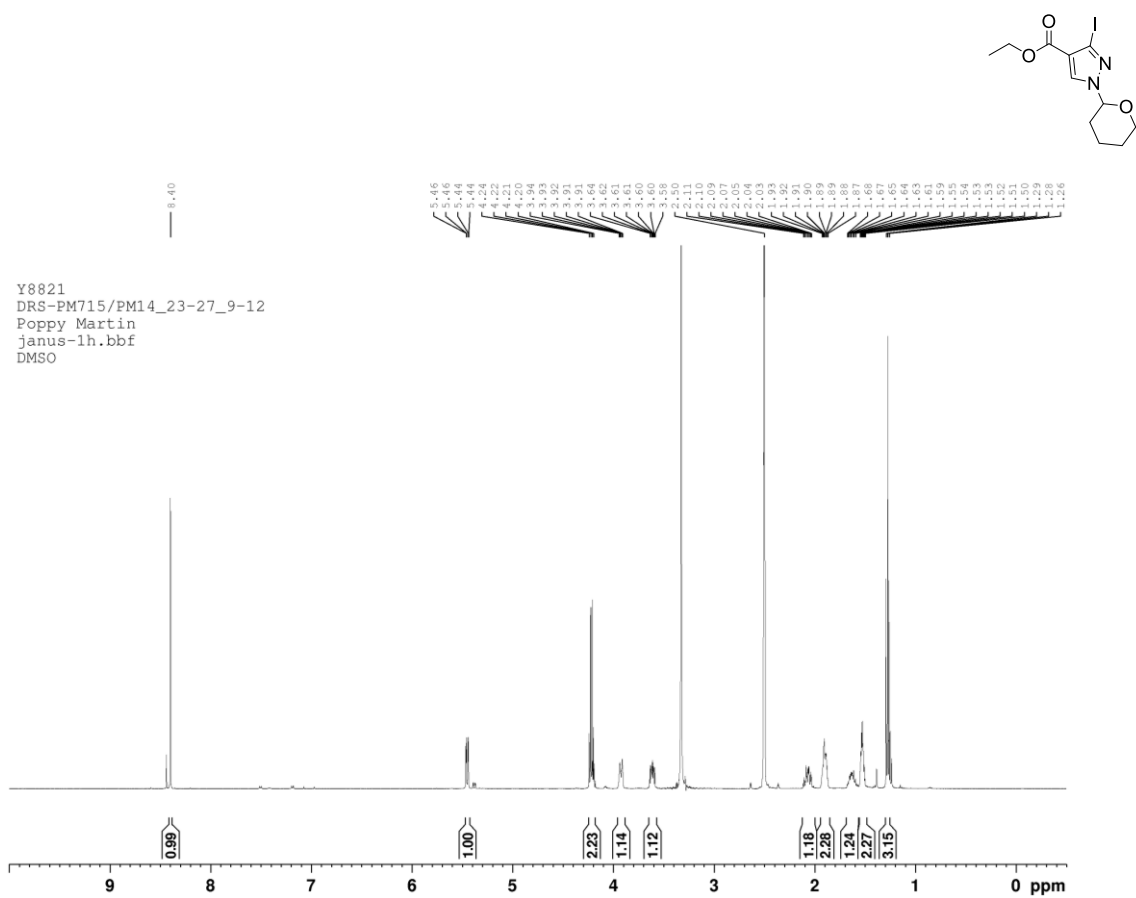
(11)



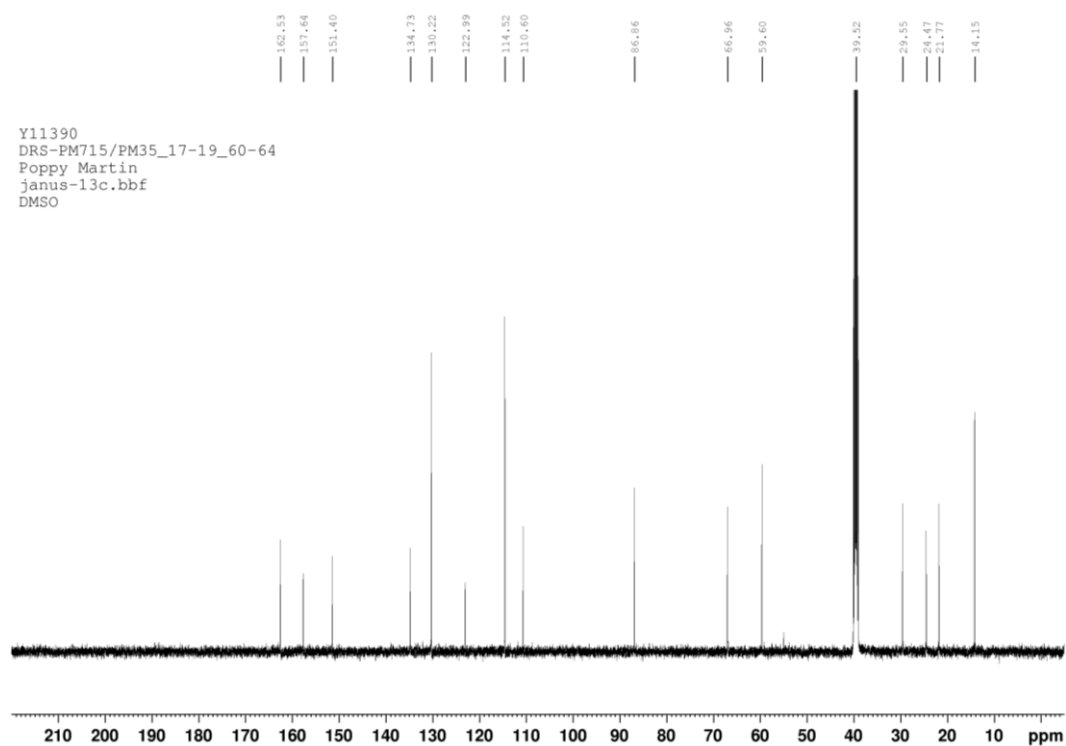
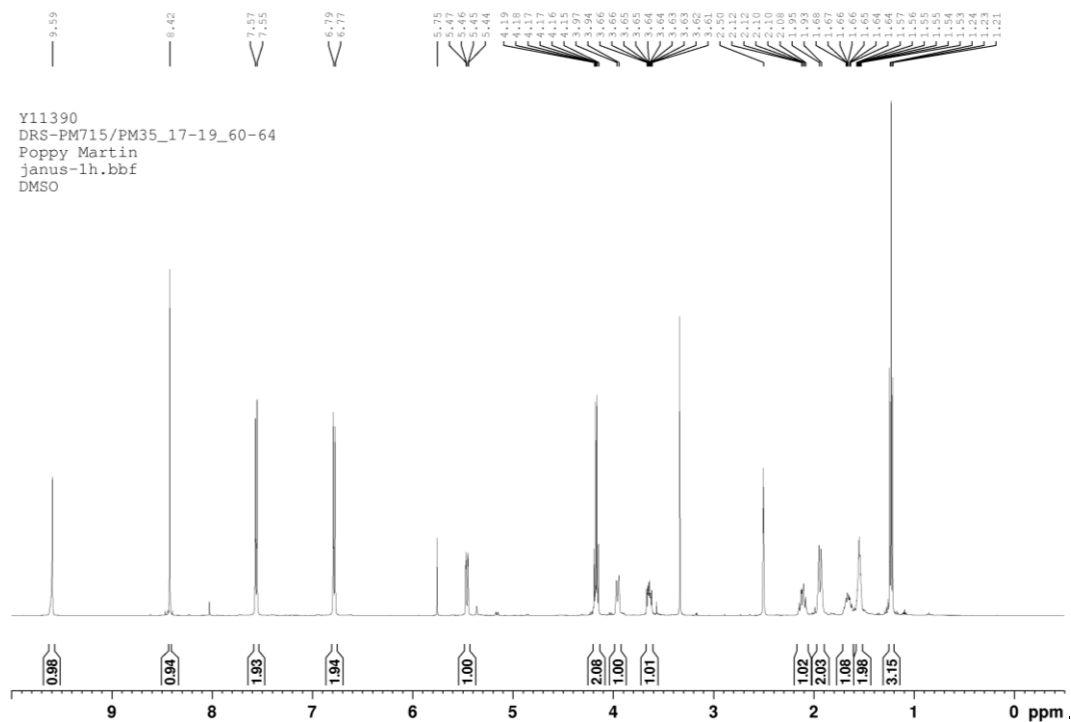
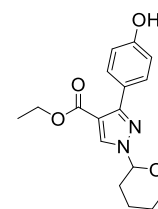
(12)



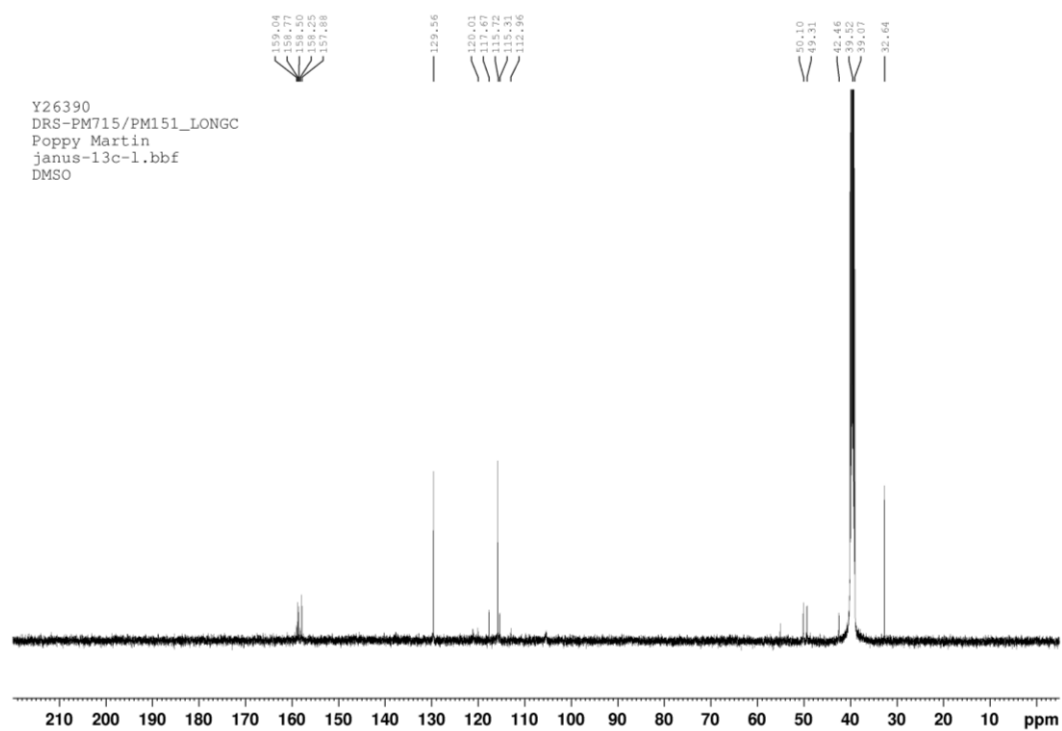
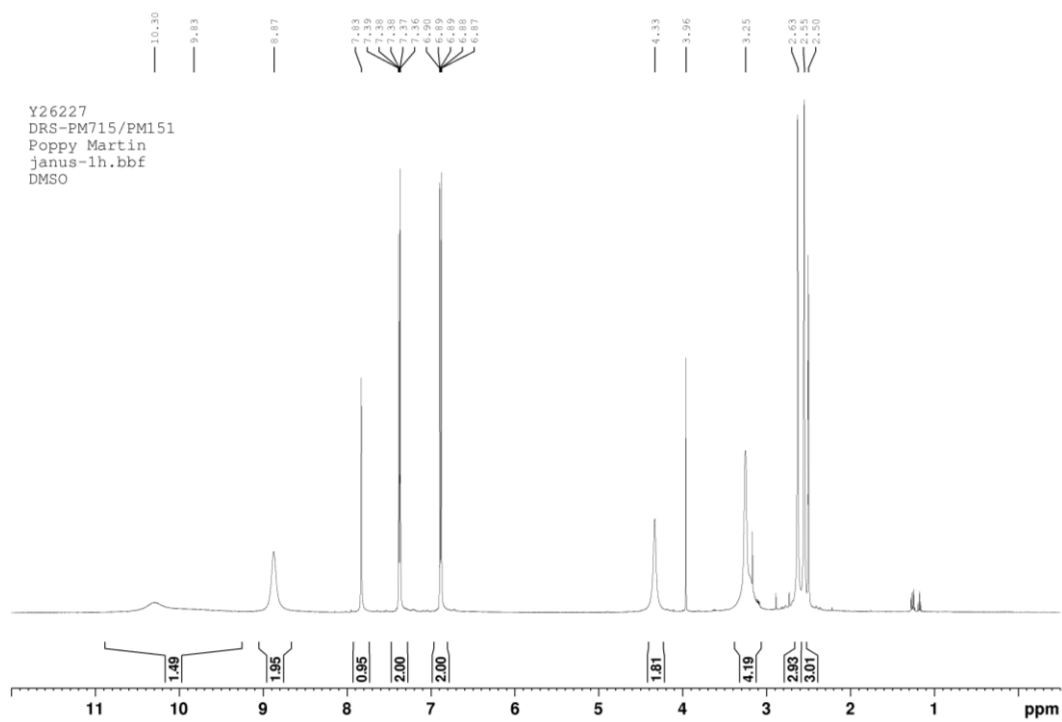
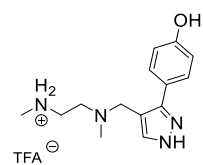
(13)



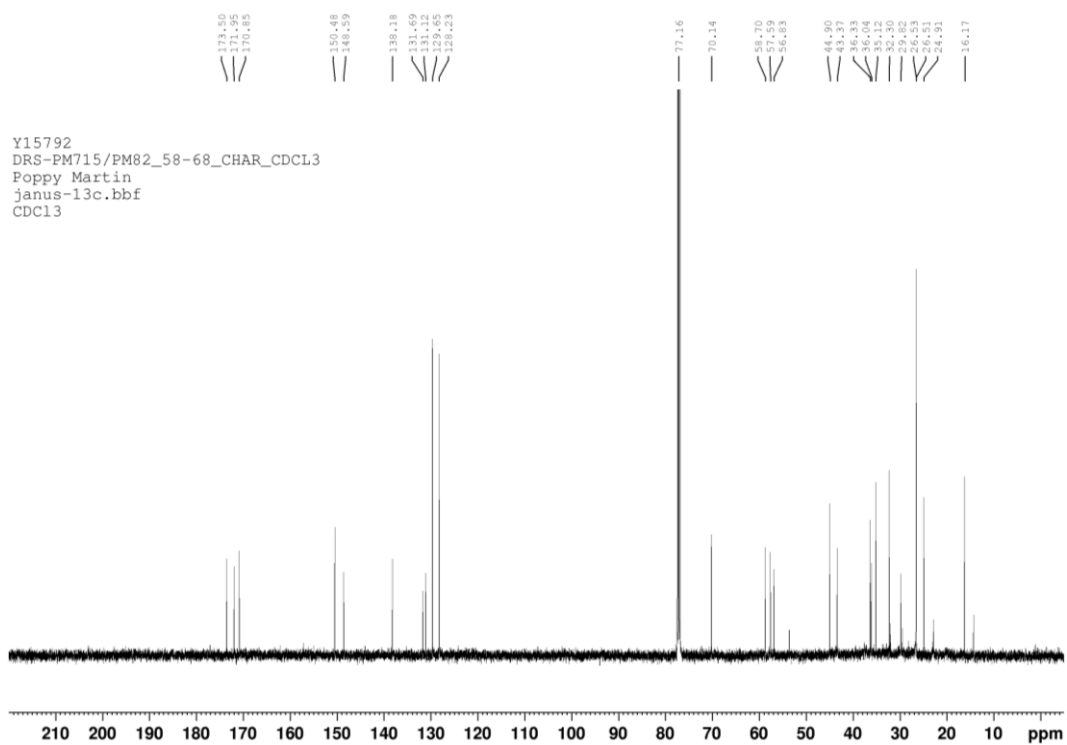
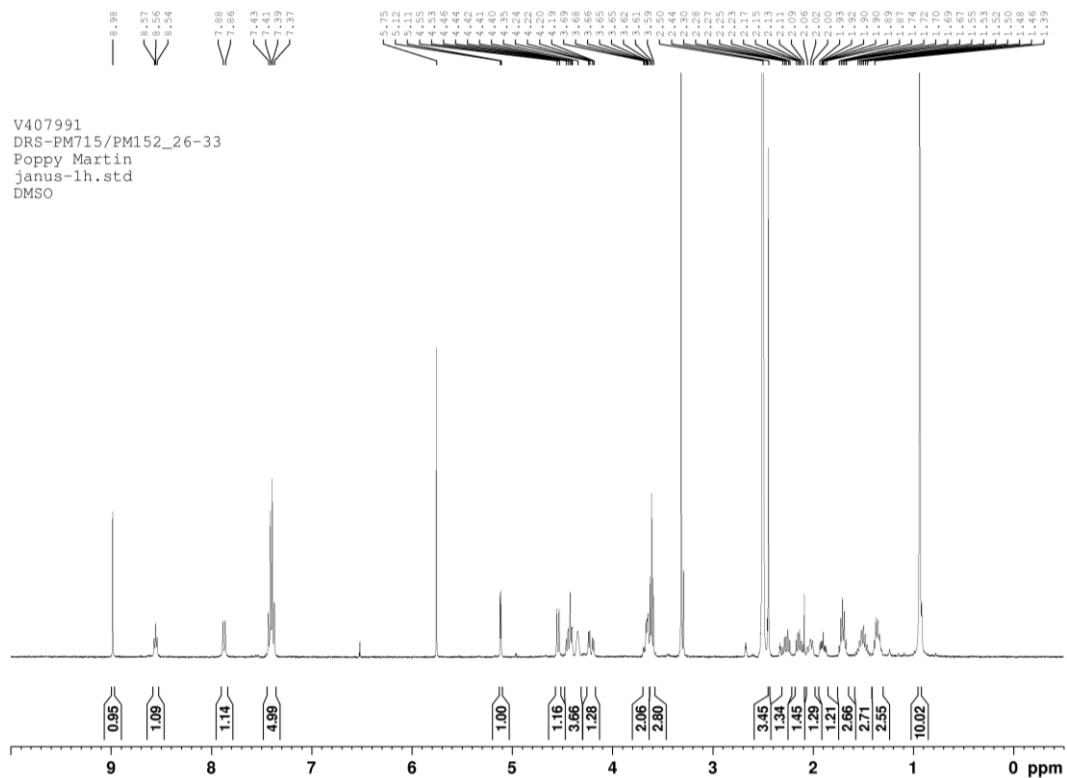
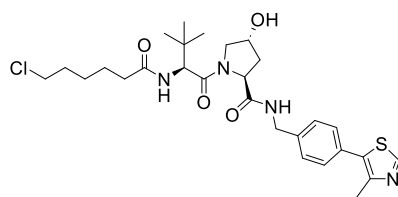
(22)



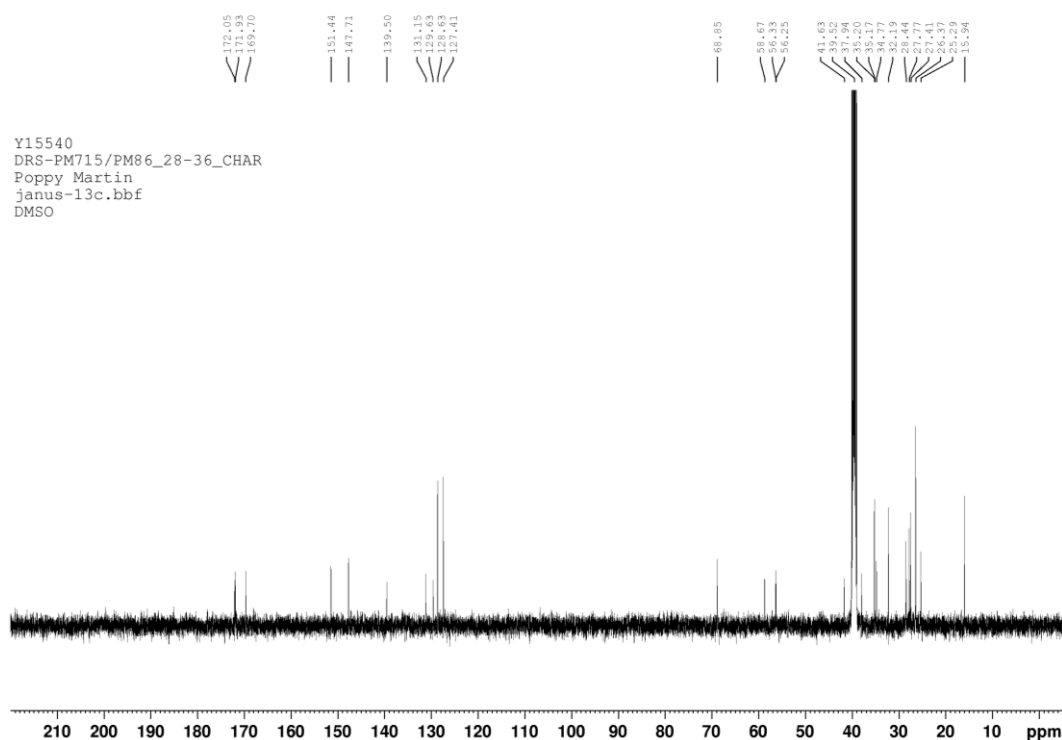
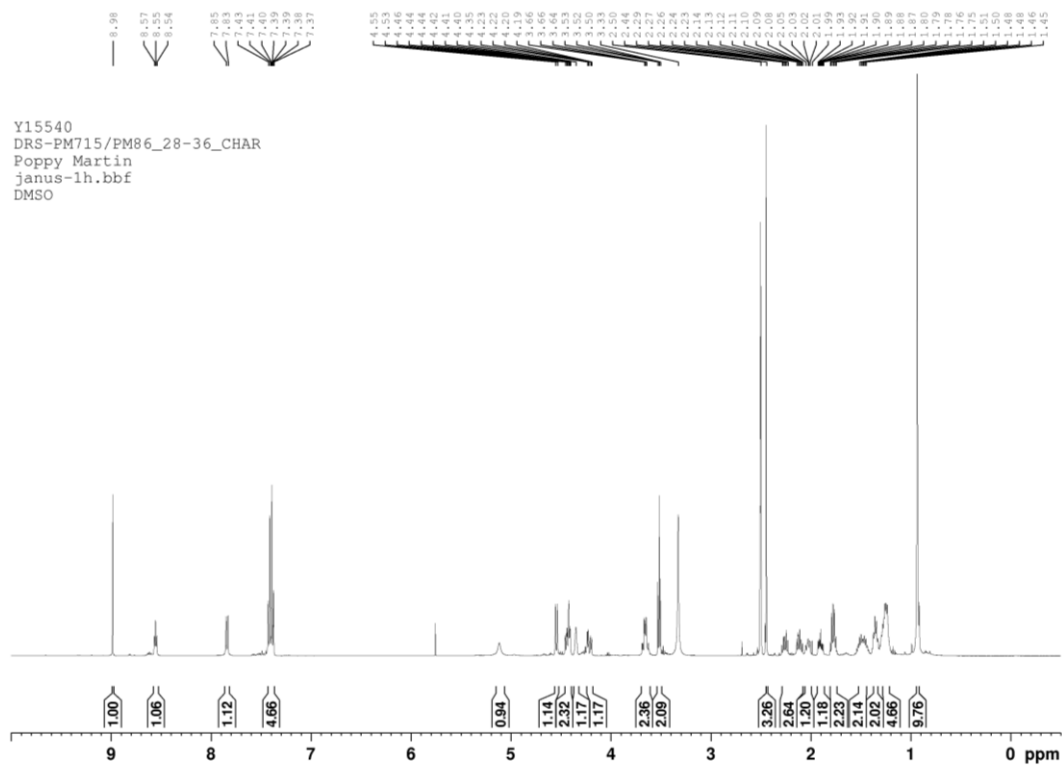
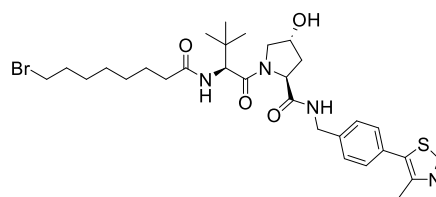
(23)



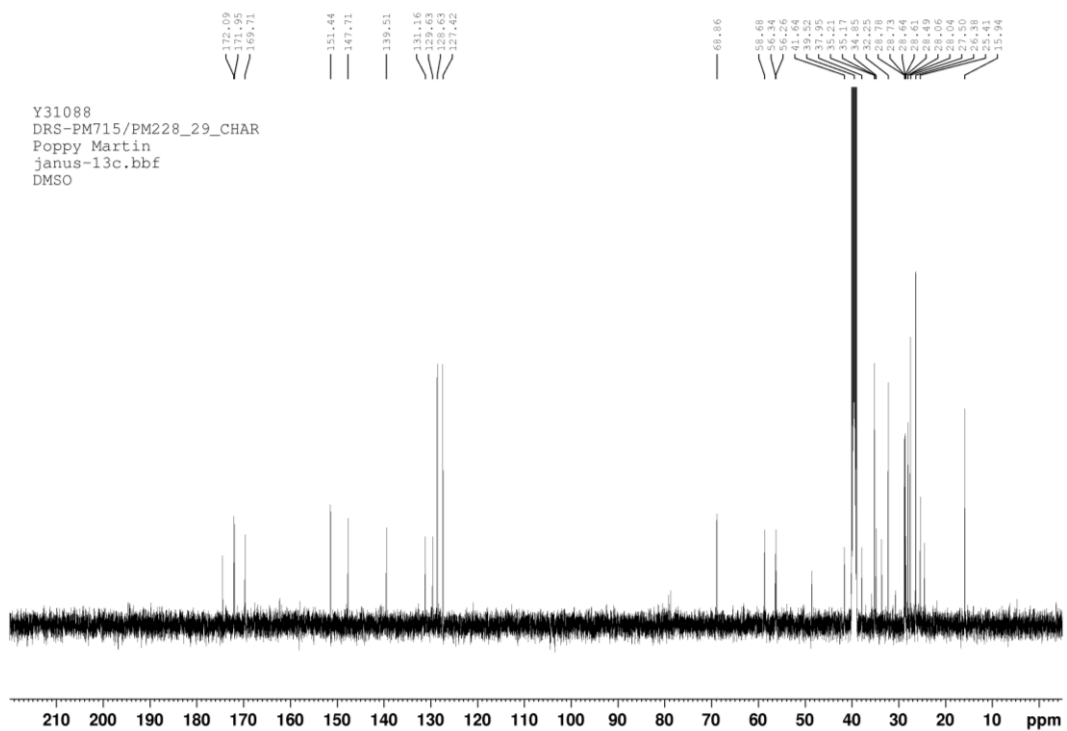
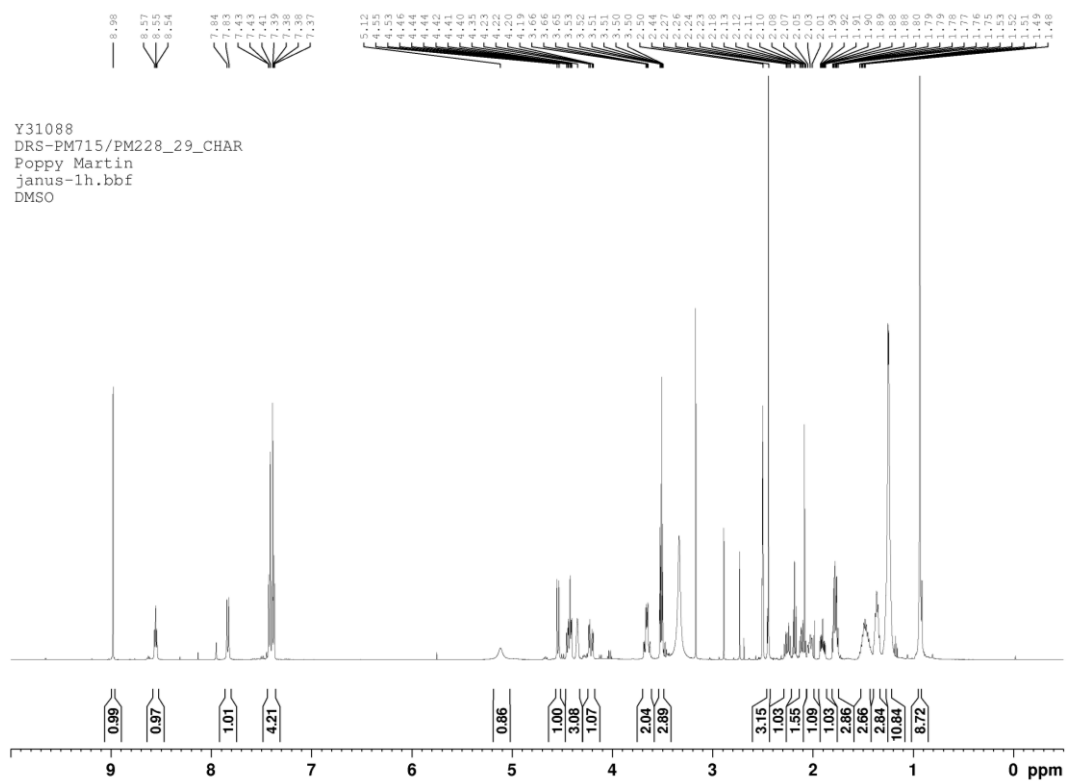
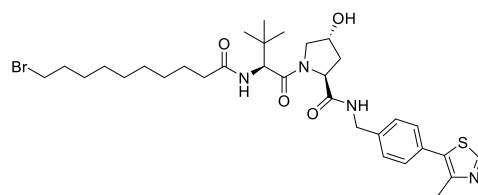
(24)



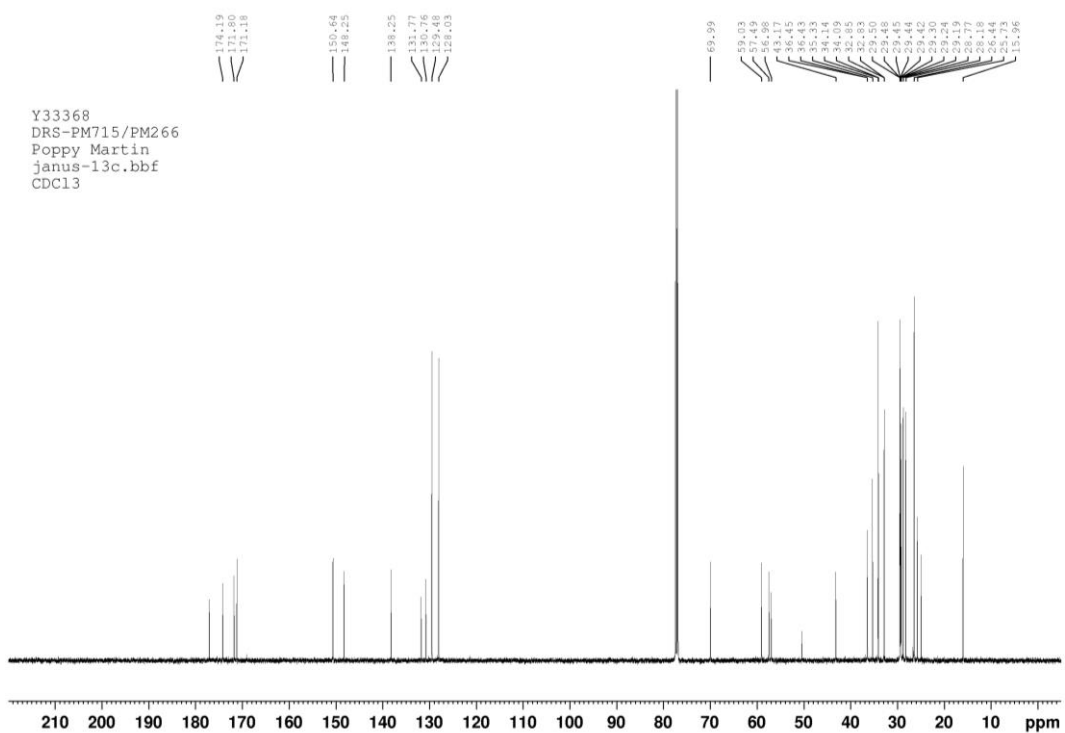
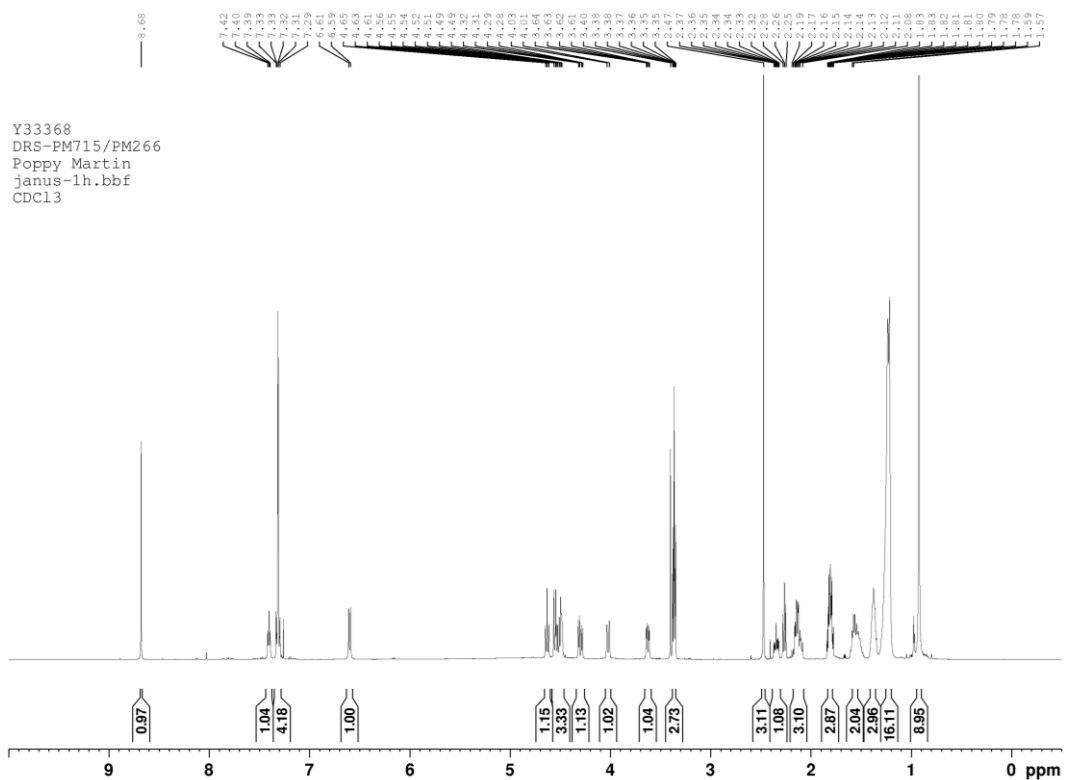
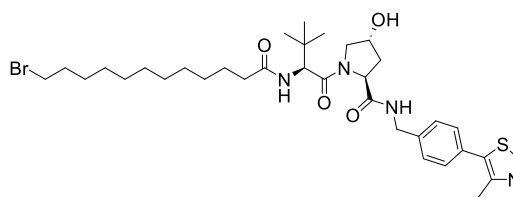
(26c)



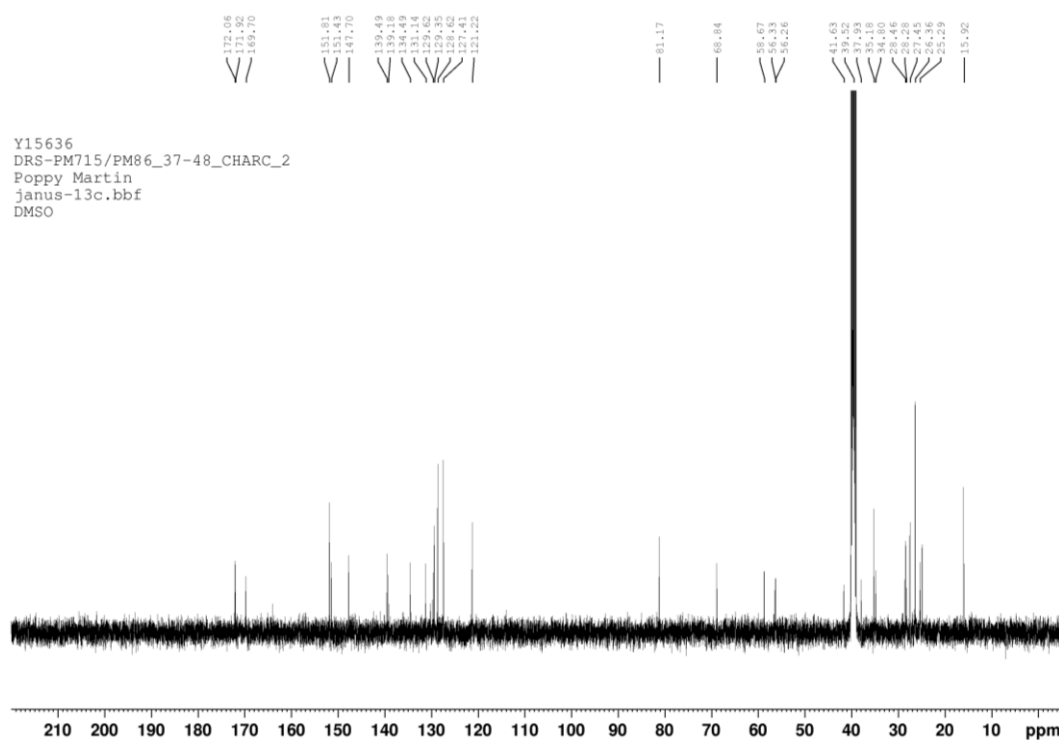
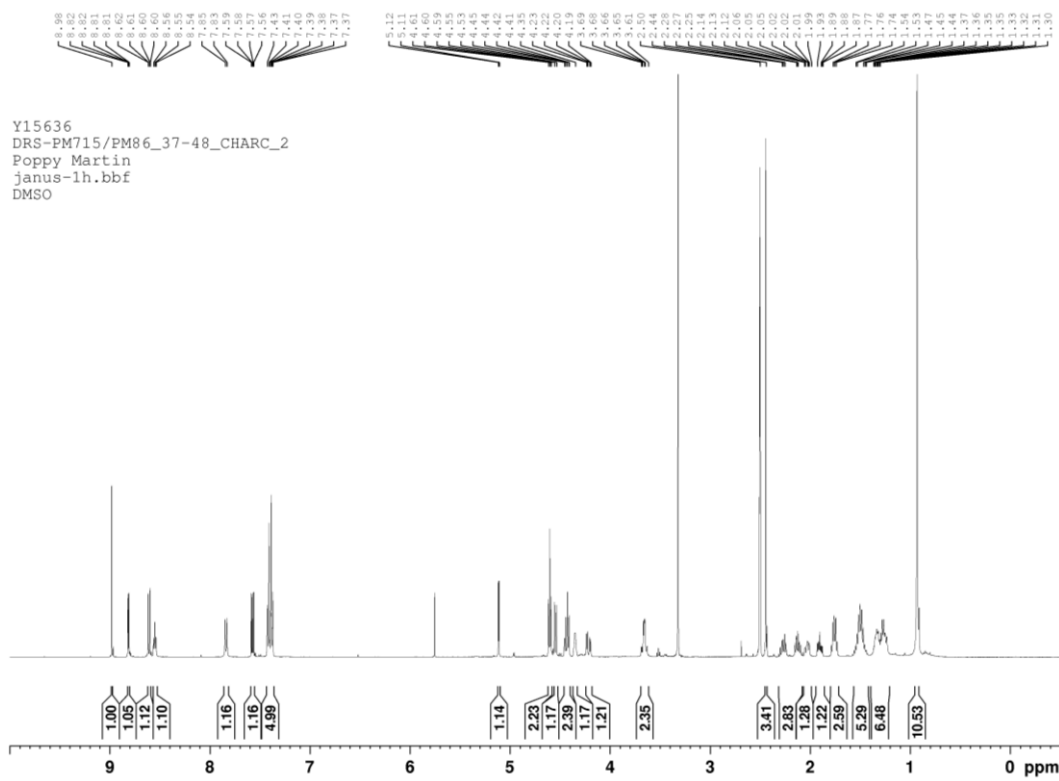
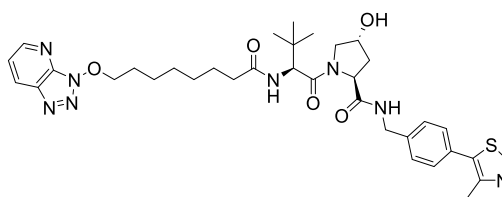
(26d)



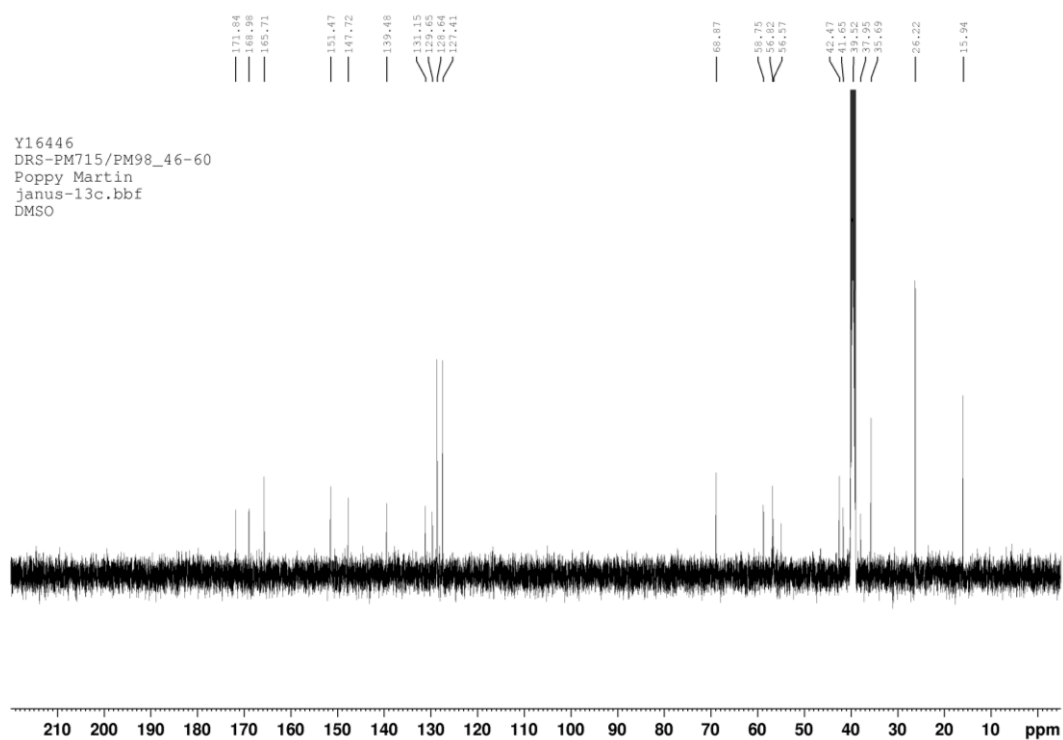
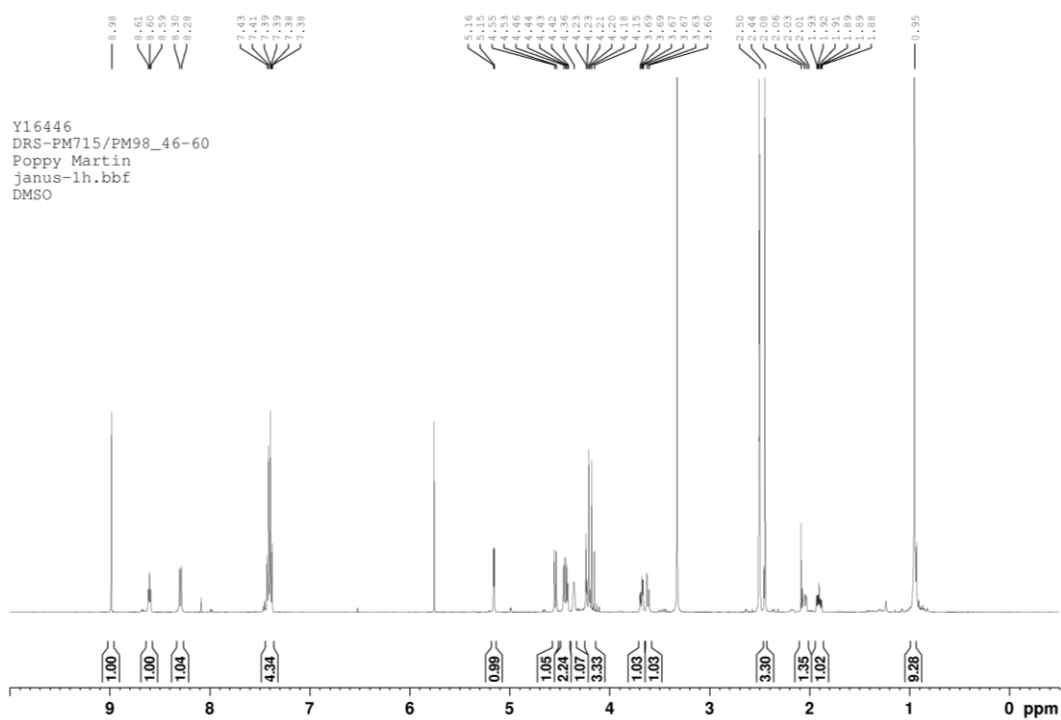
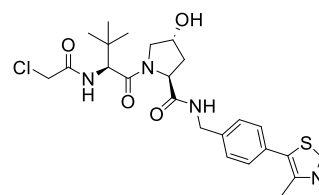
(26e)



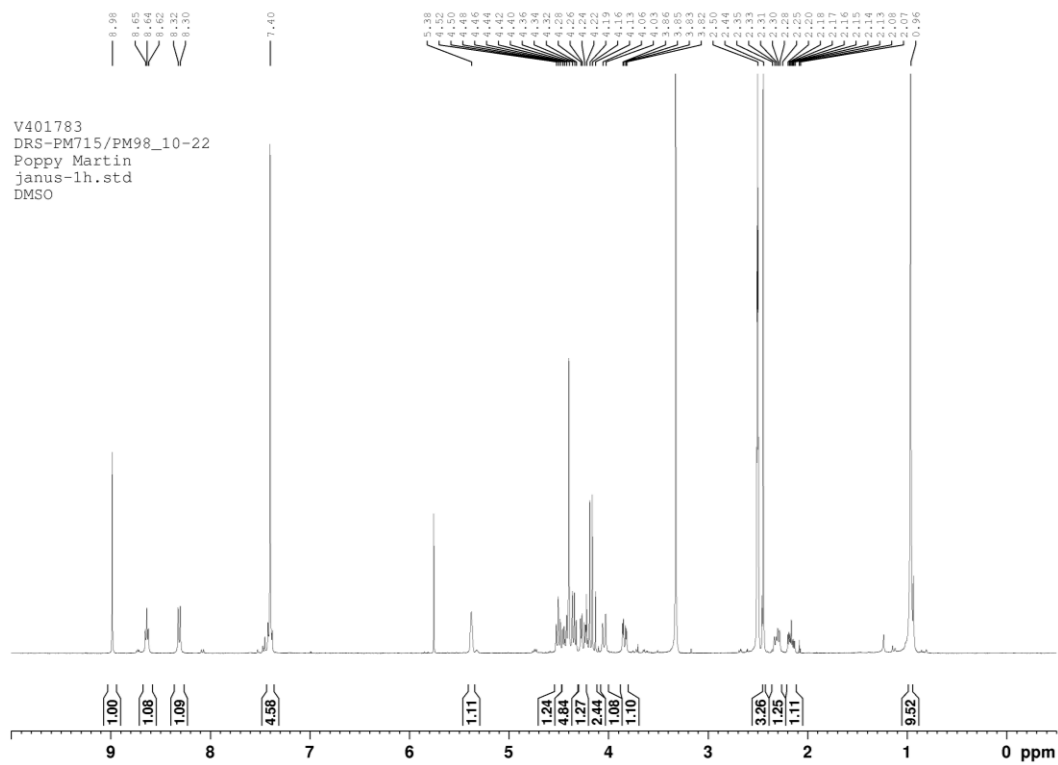
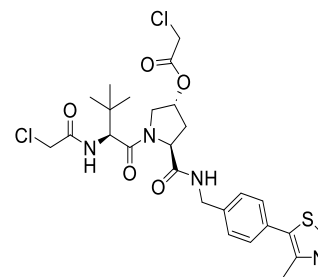
(27c)



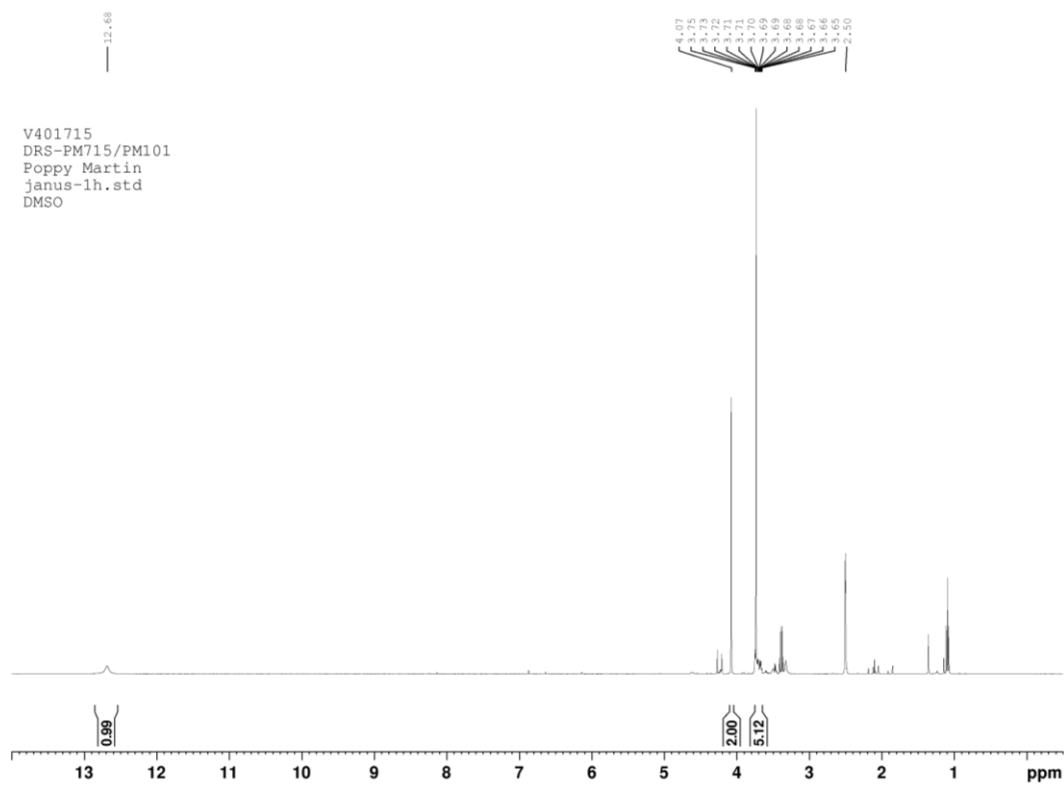
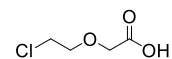
(28)



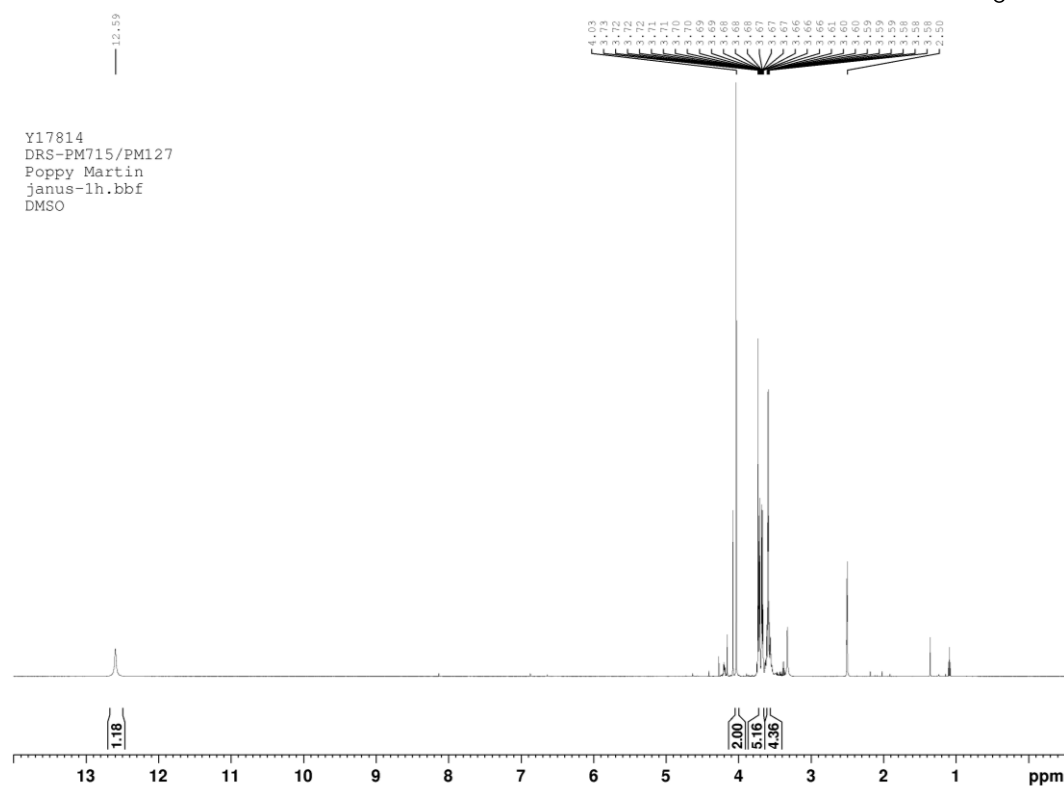
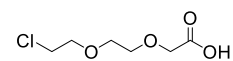
(29)



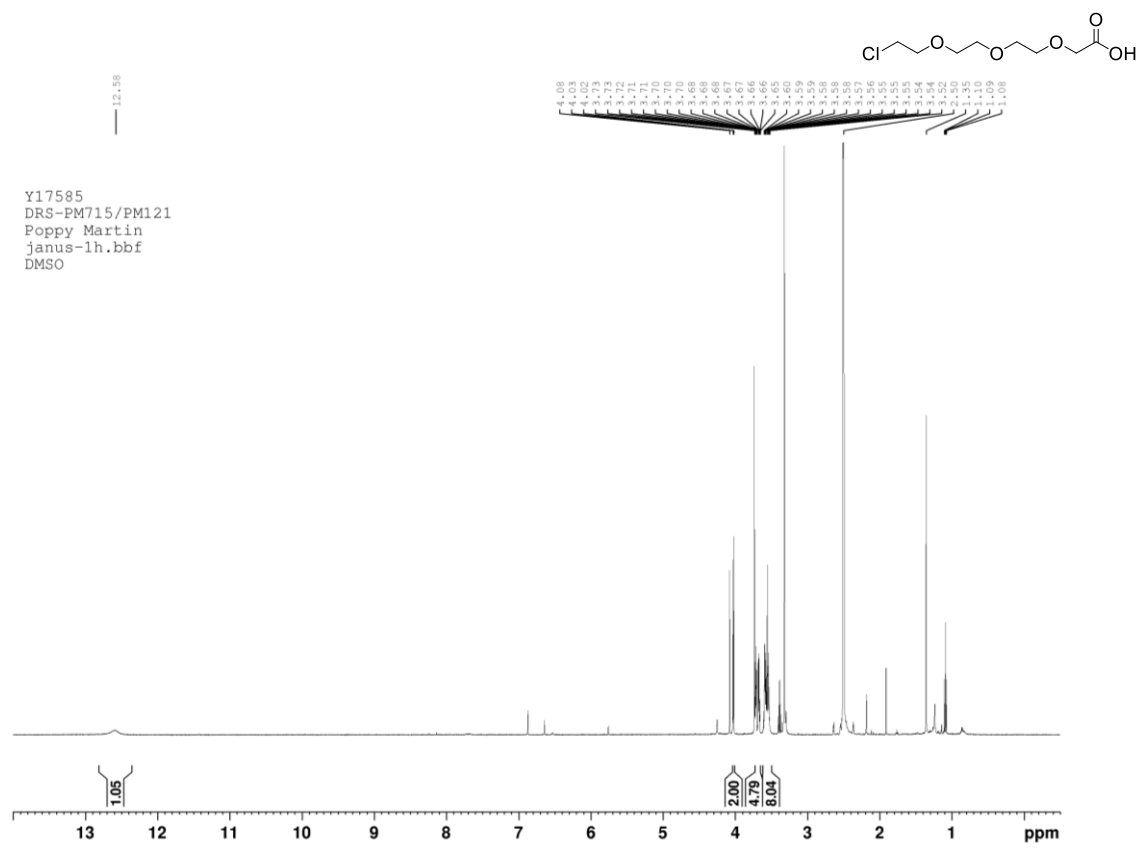
(31g)



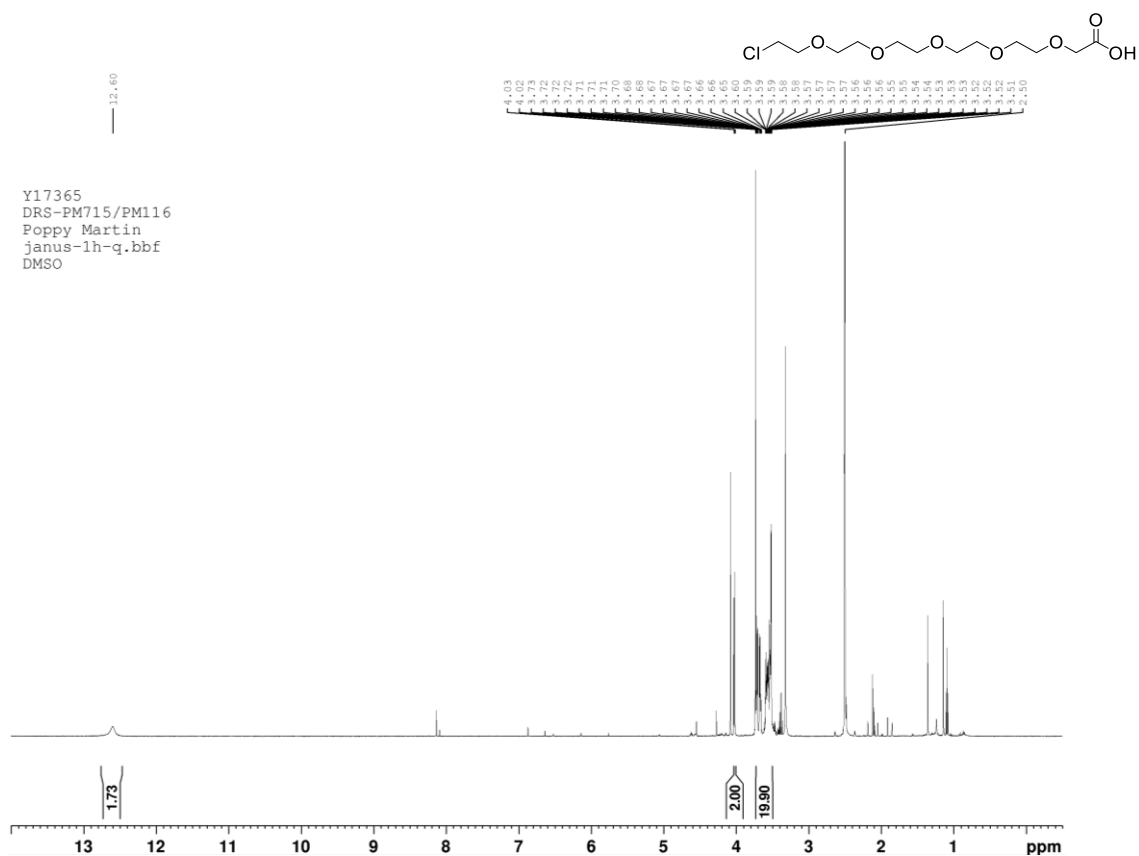
(31h)



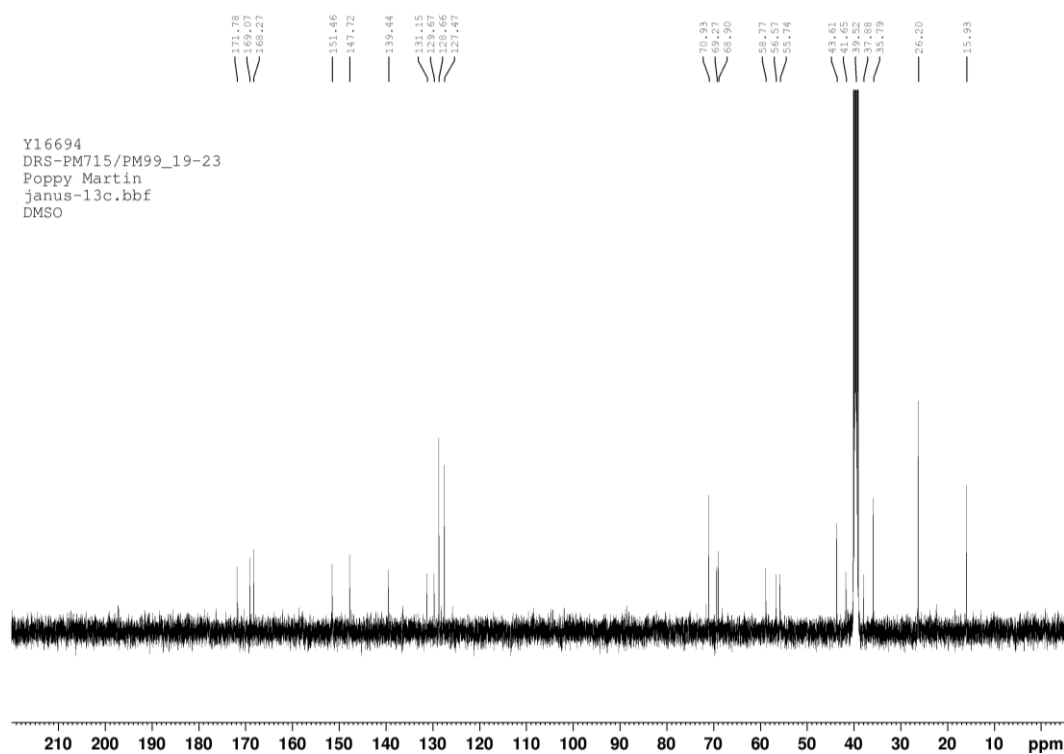
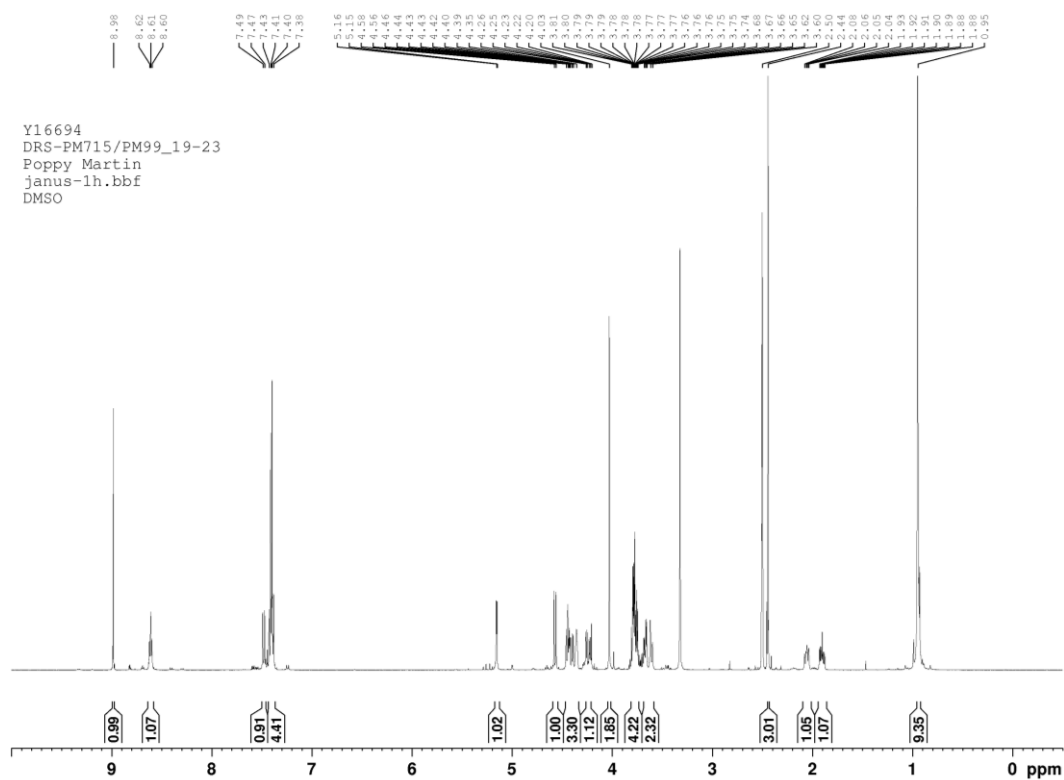
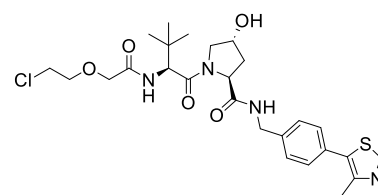
(31i)



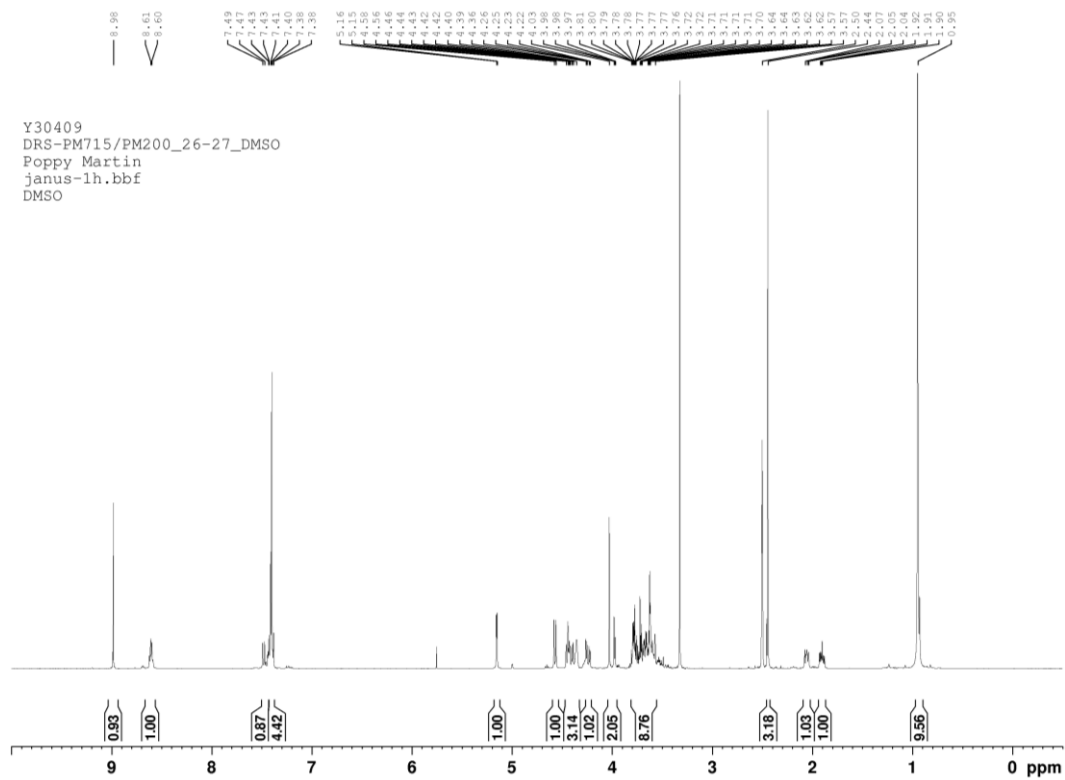
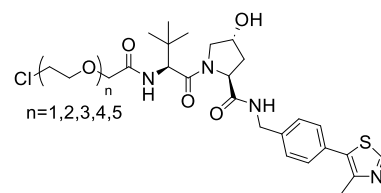
(31j)



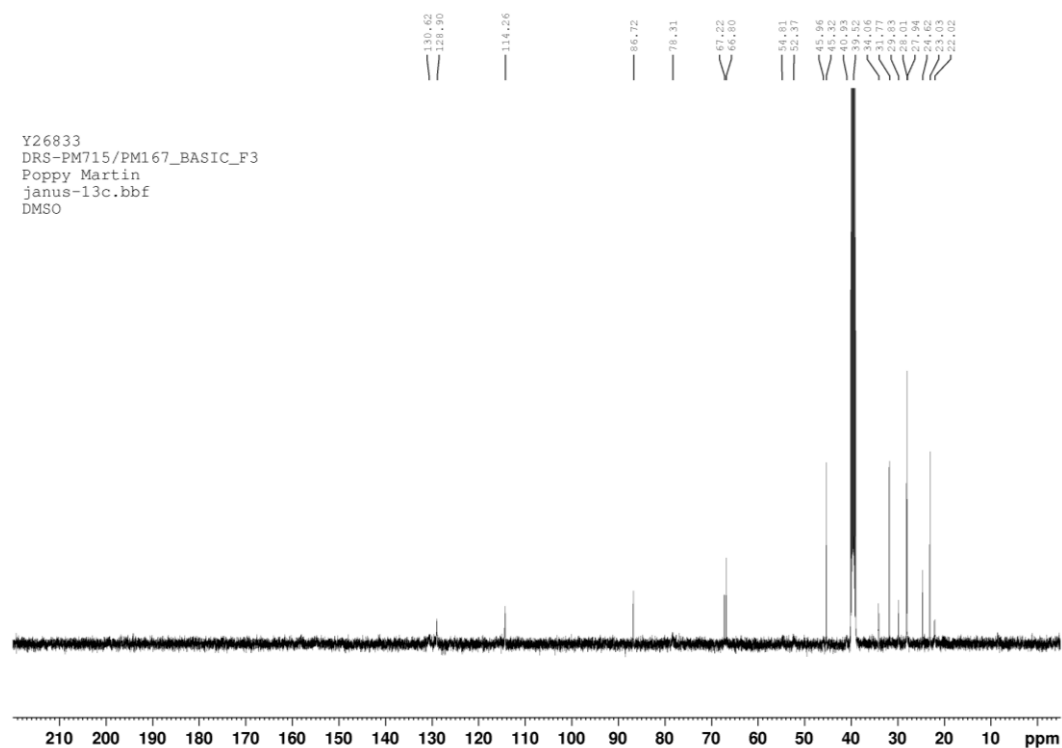
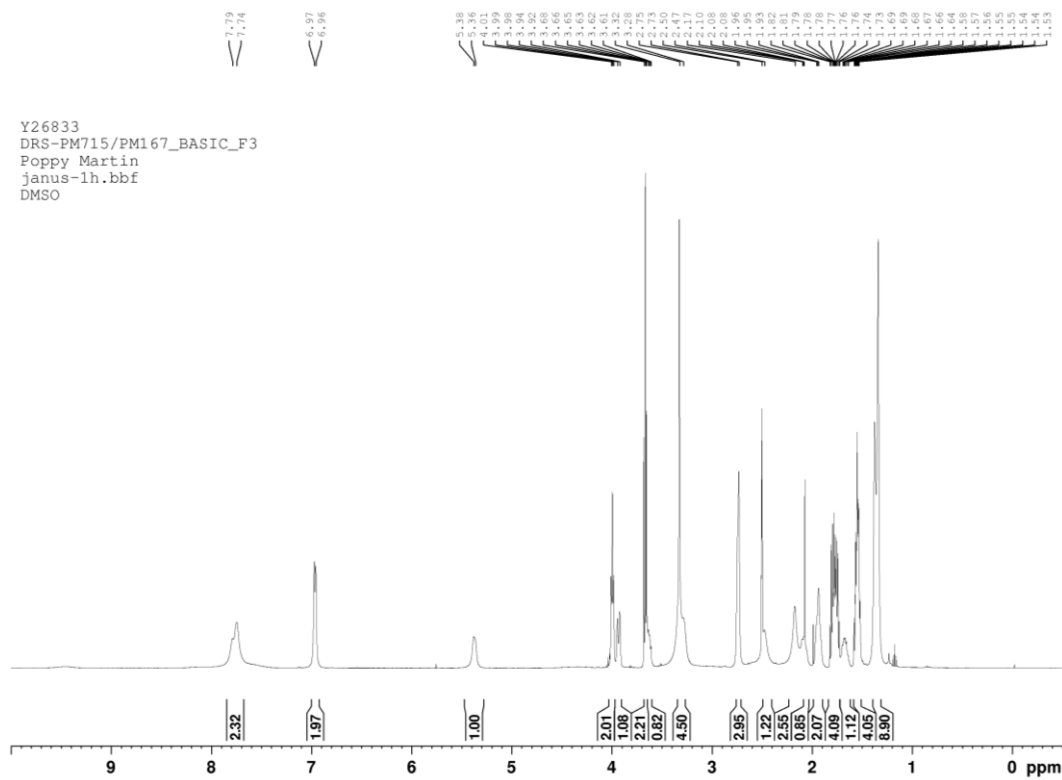
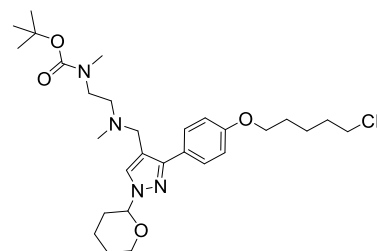
(32g)



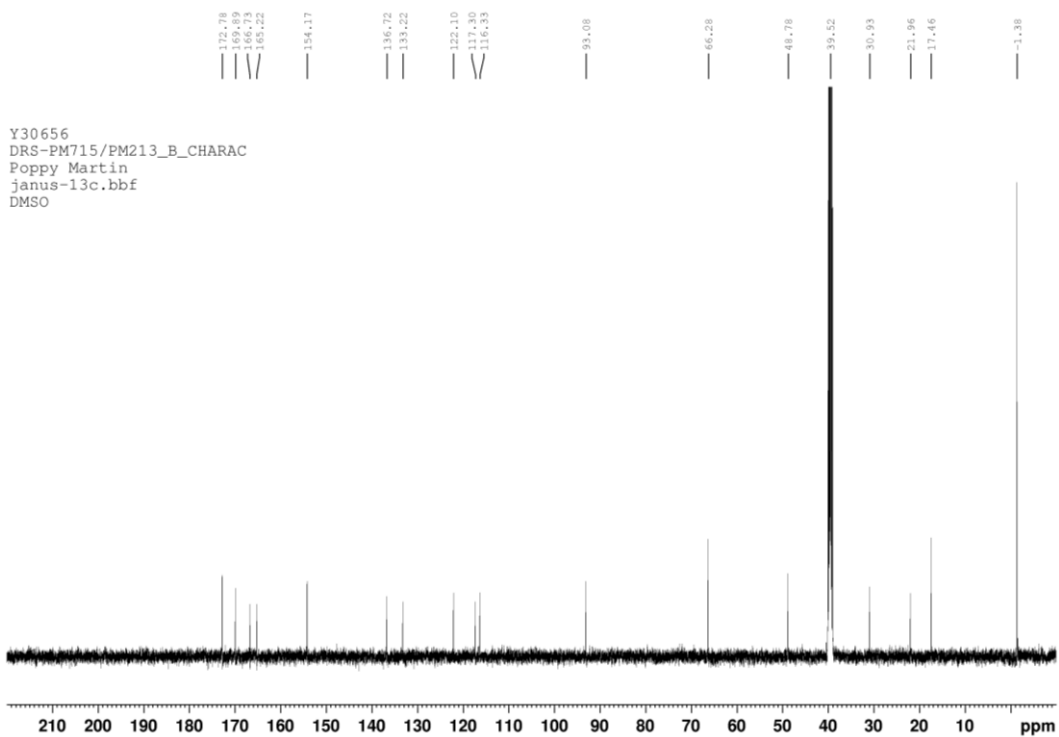
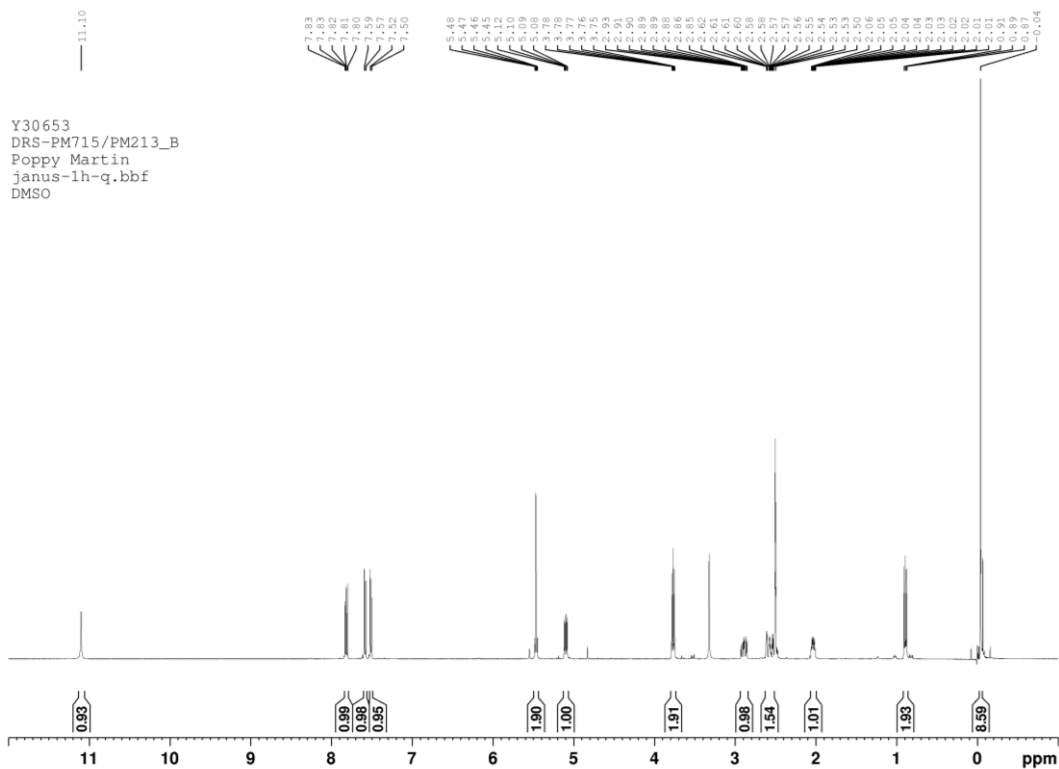
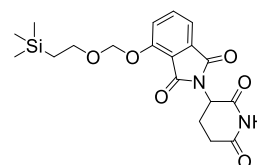
(32j)



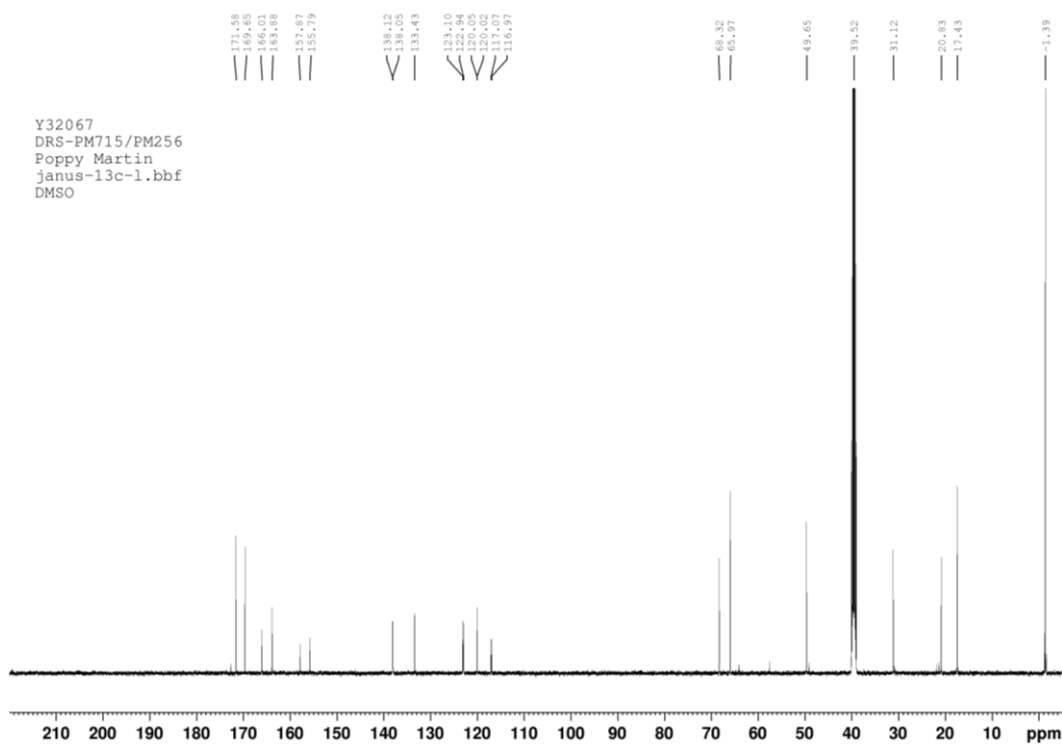
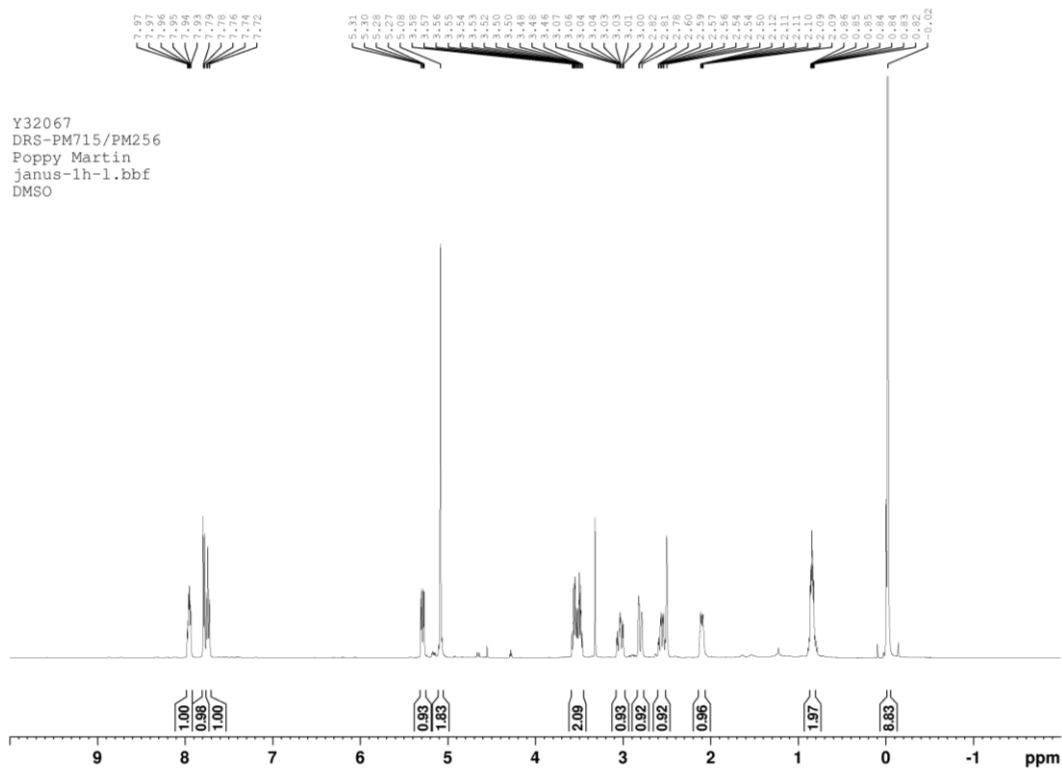
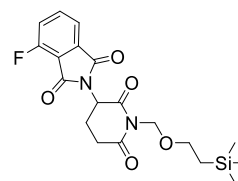
(34 (n=5))



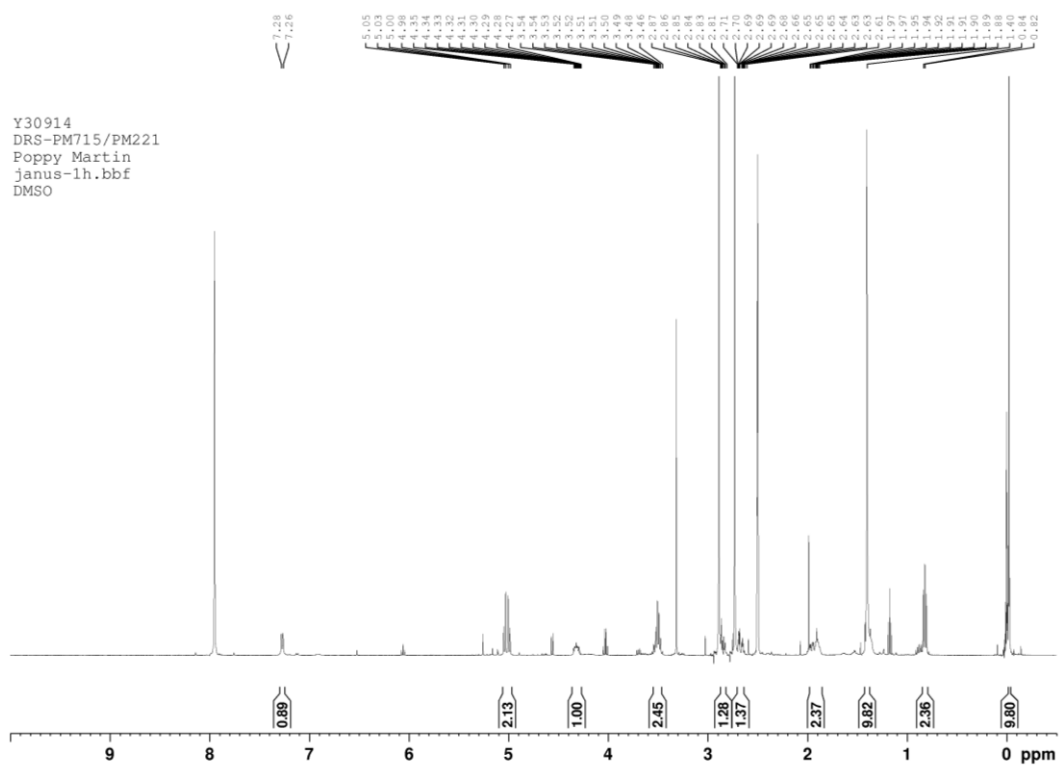
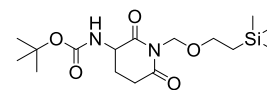
(36)



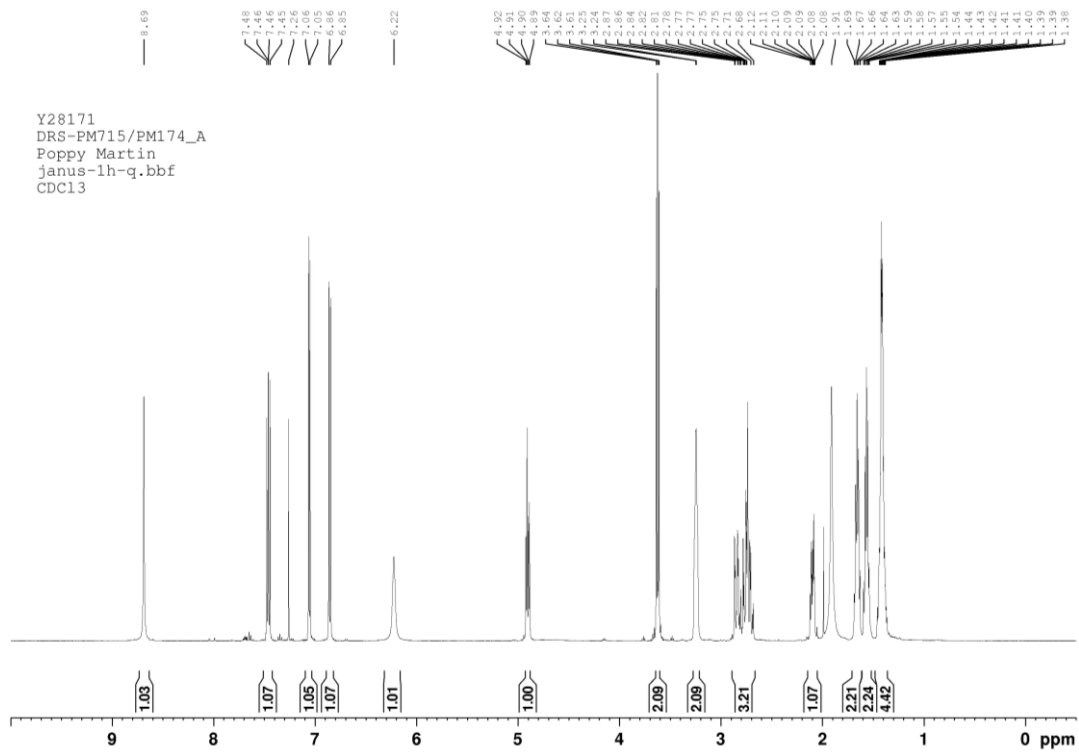
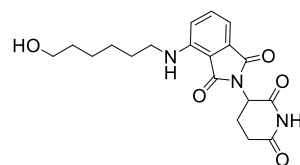
(37)



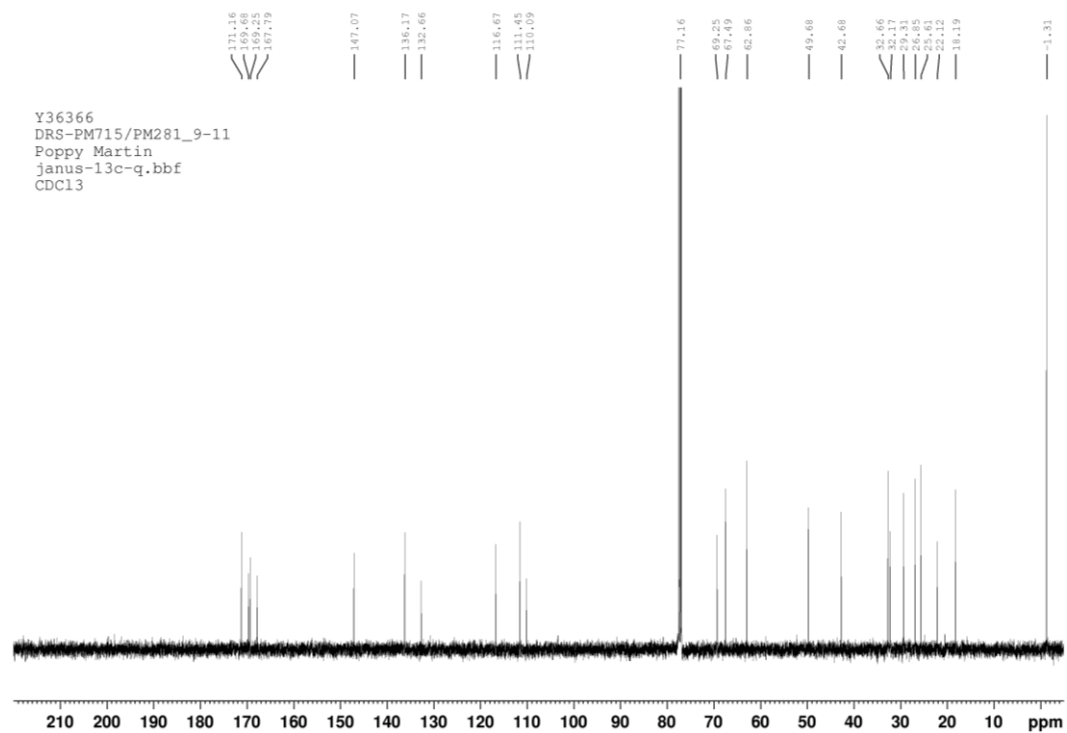
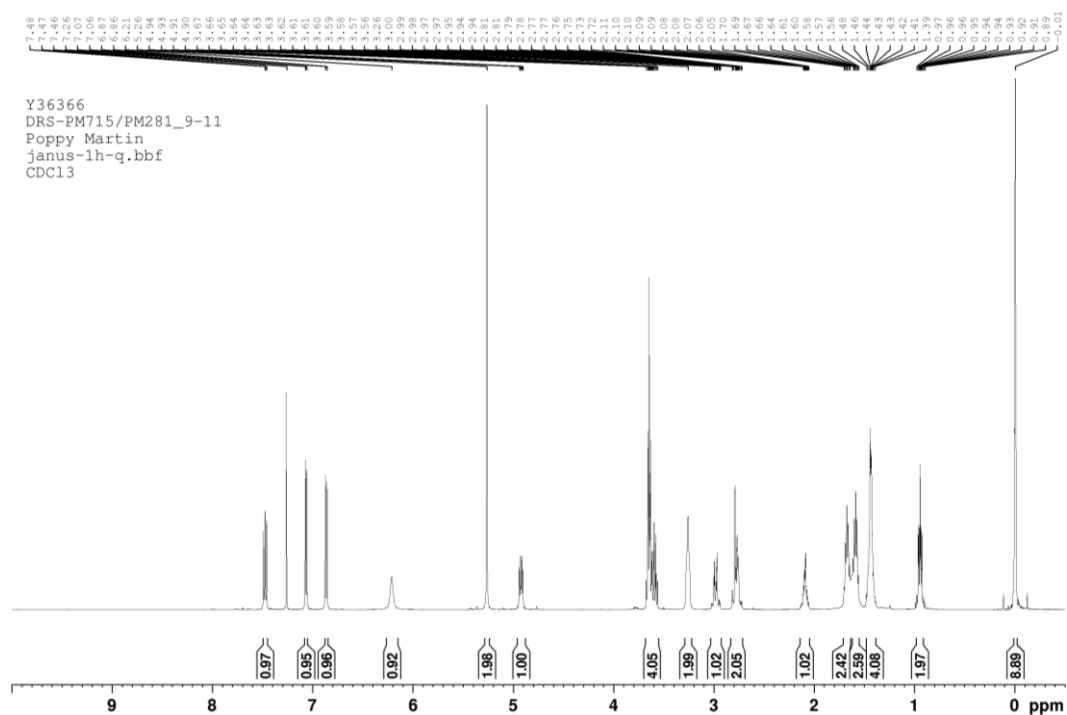
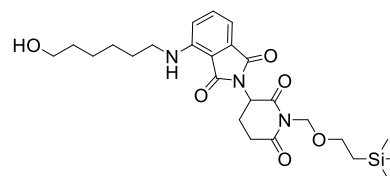
(38)



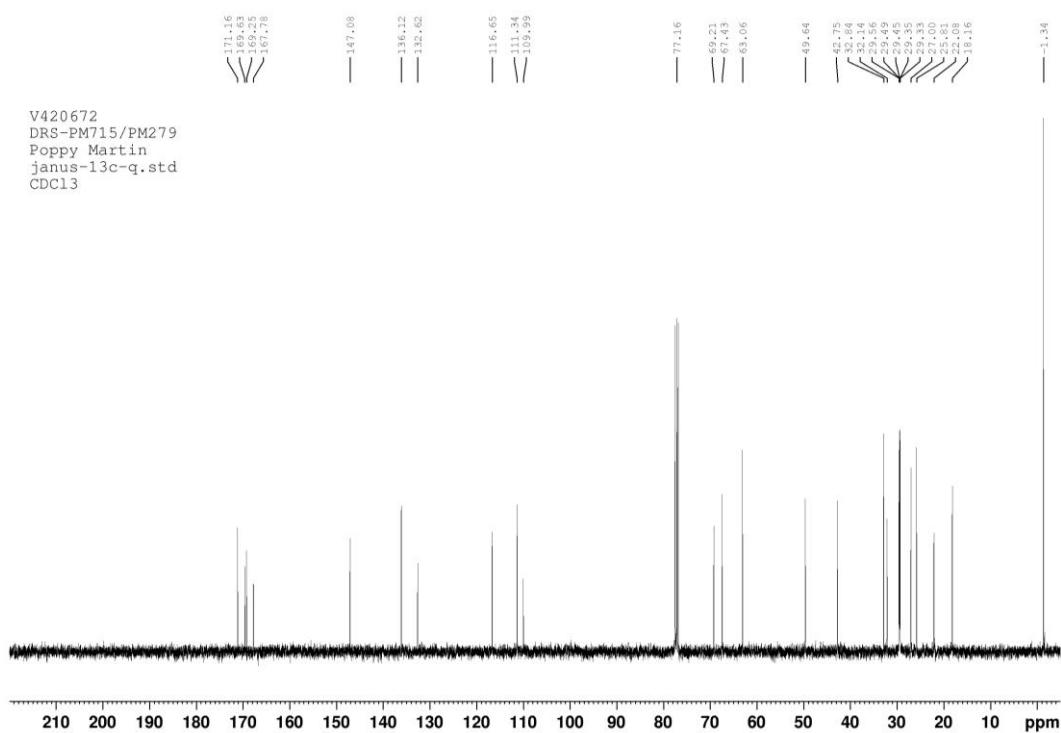
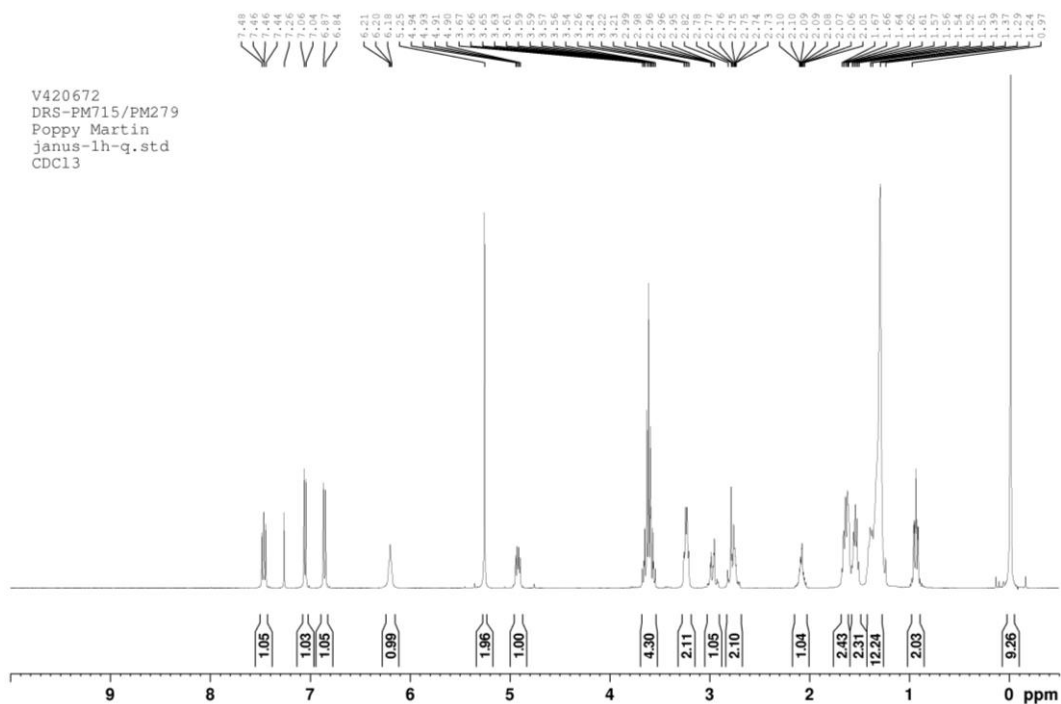
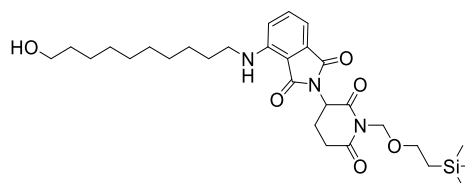
(46)



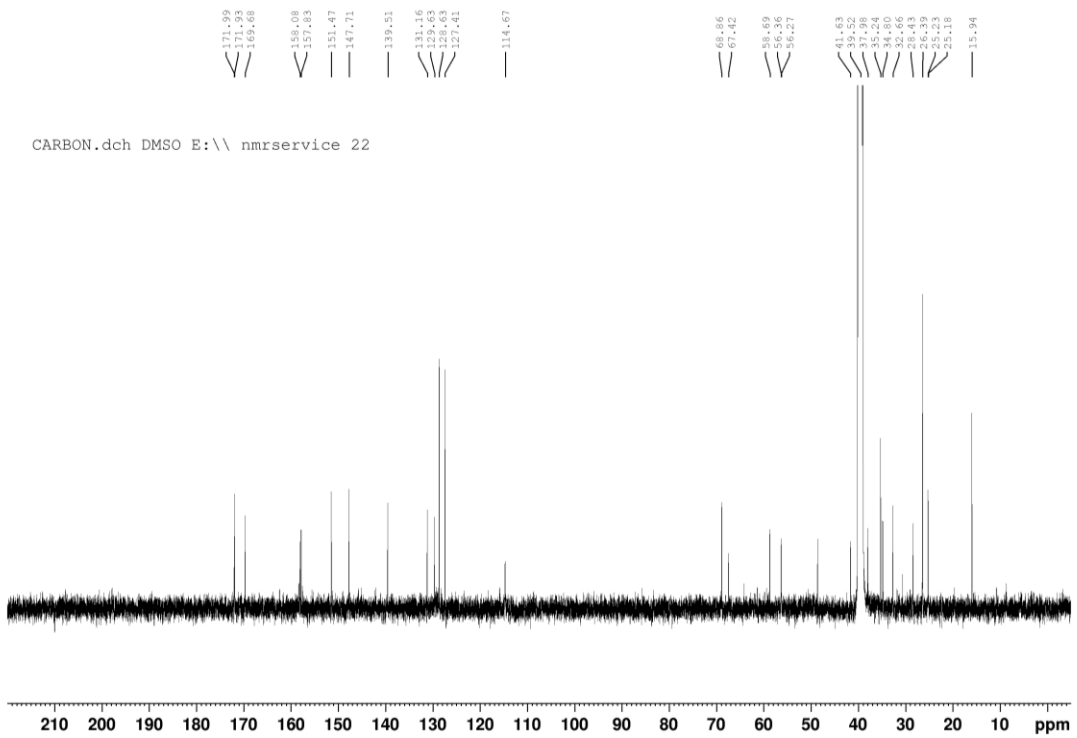
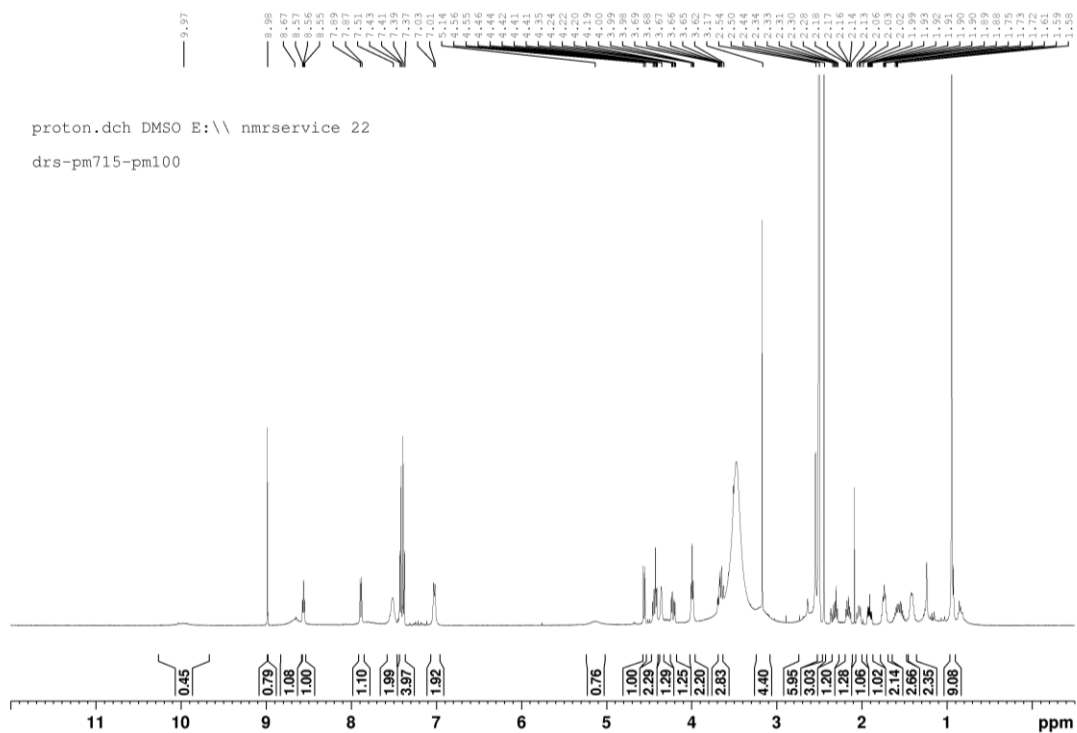
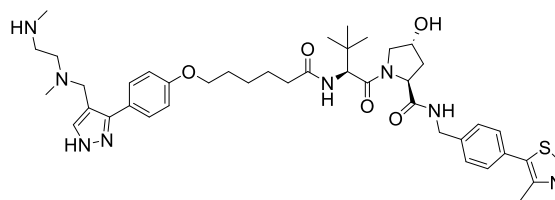
(47p)



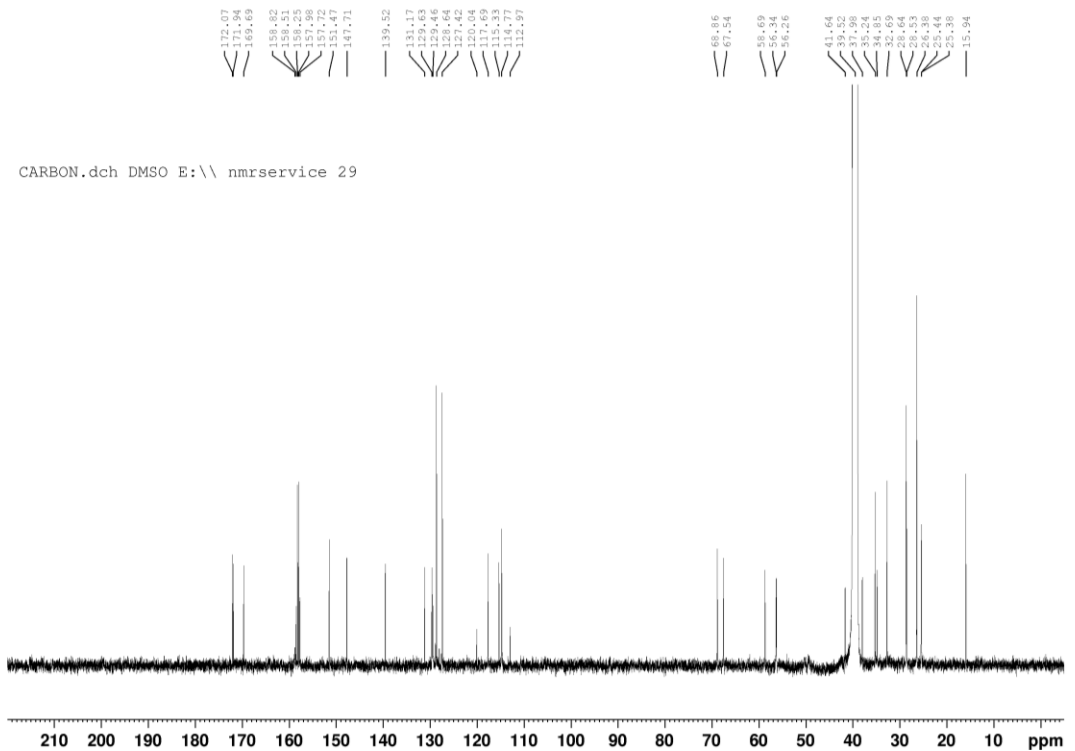
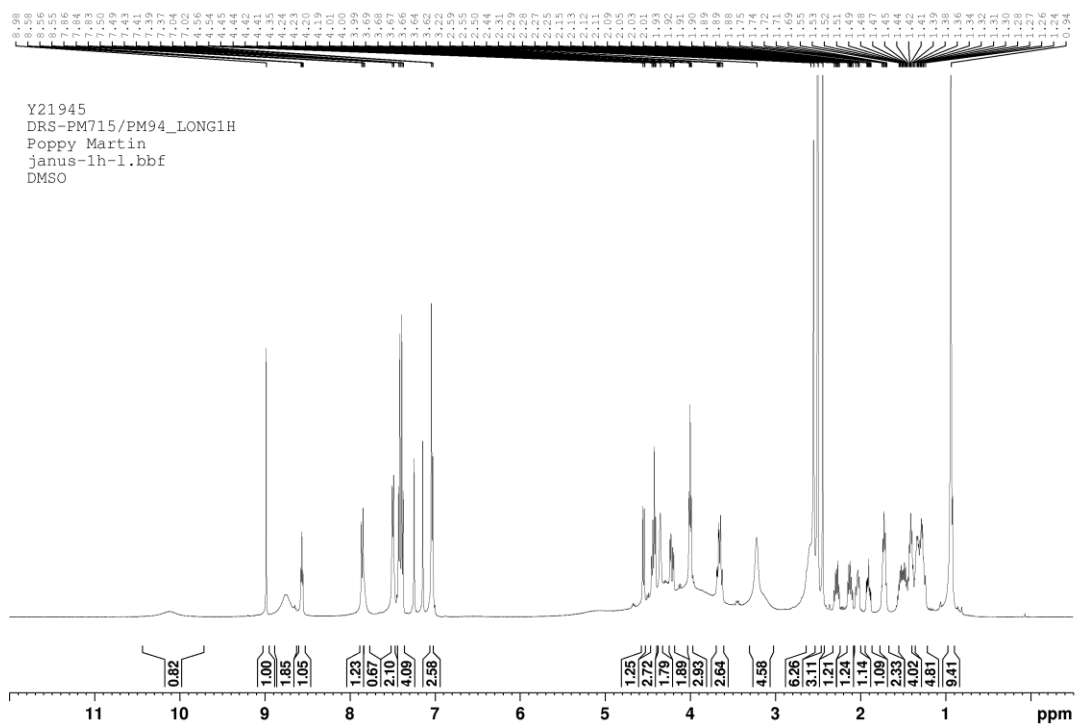
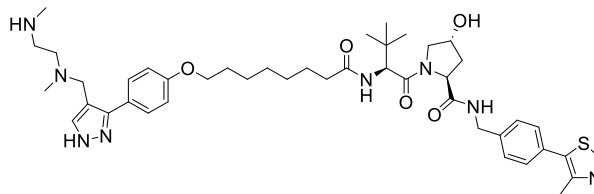
(47q)



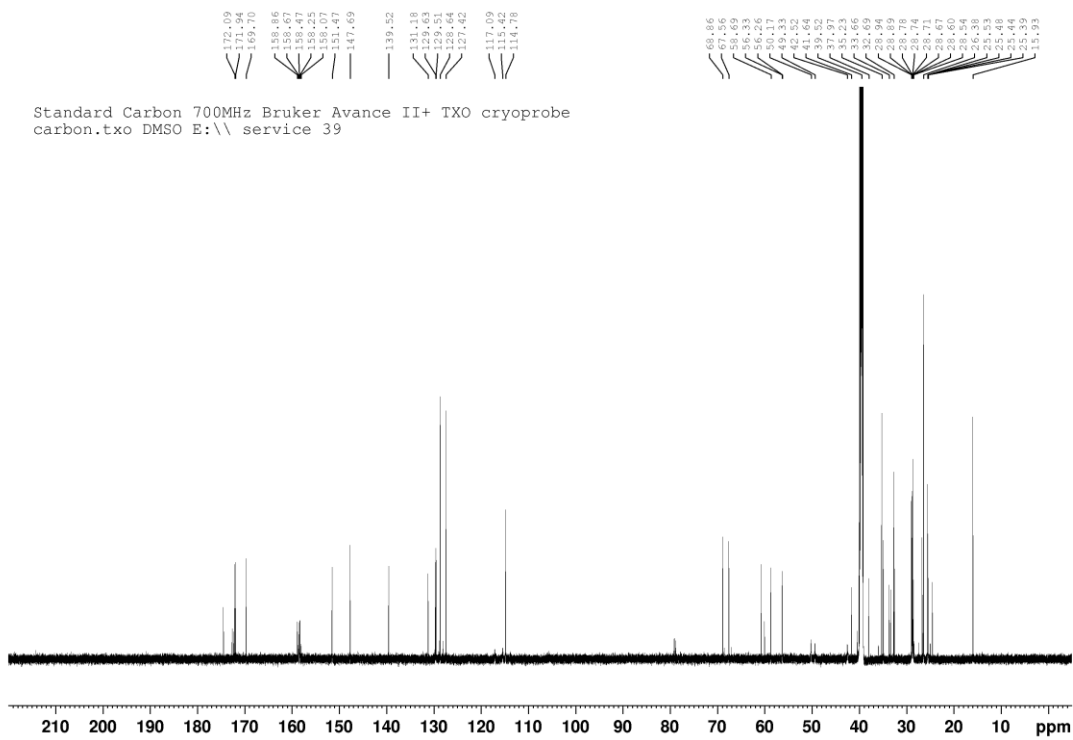
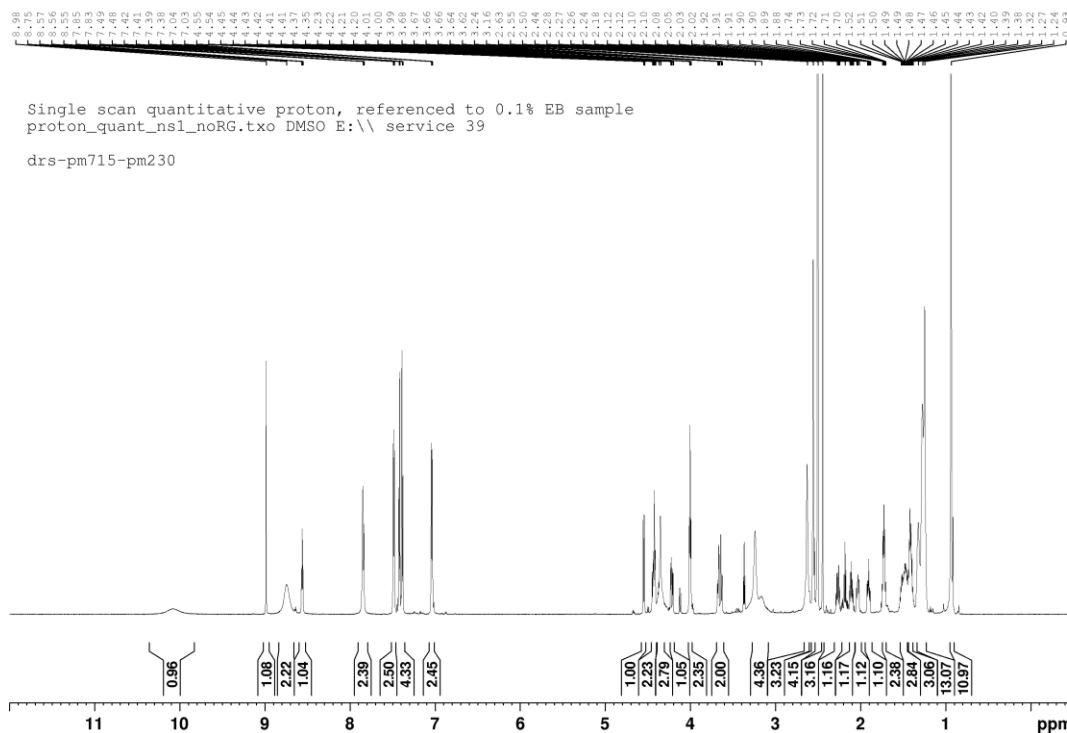
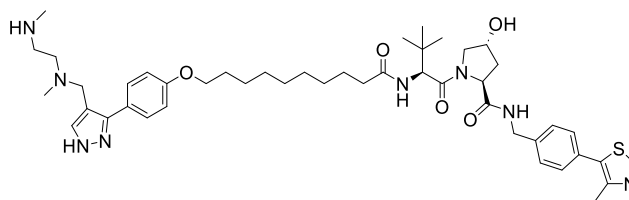
PROTAC B



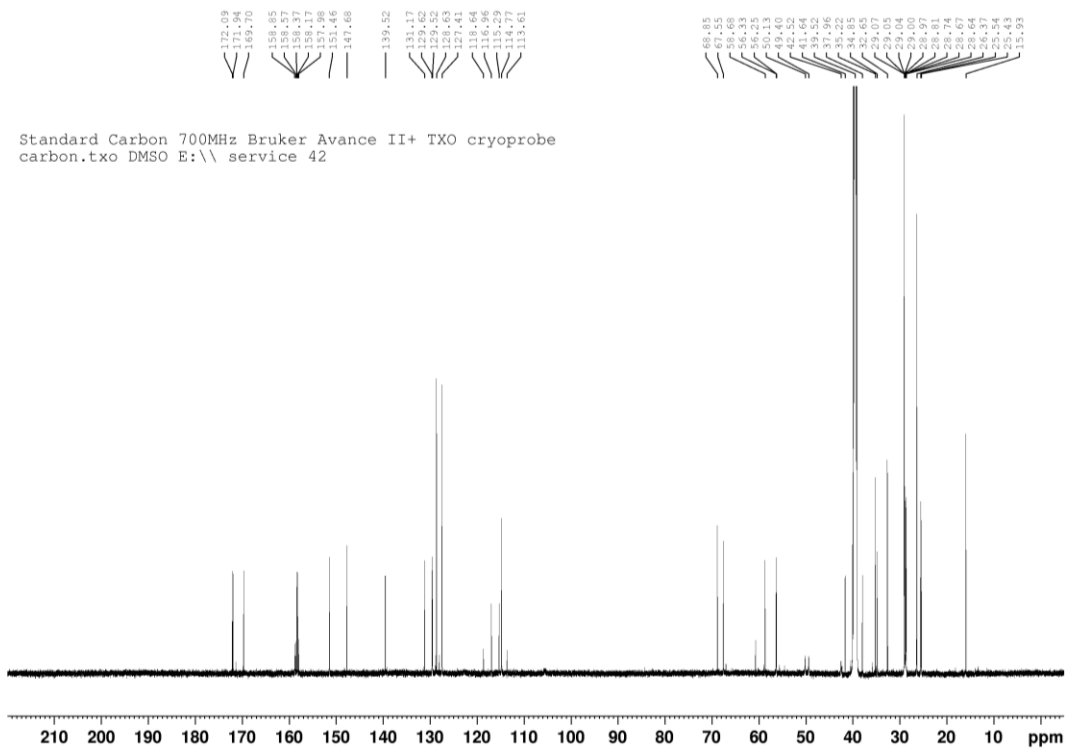
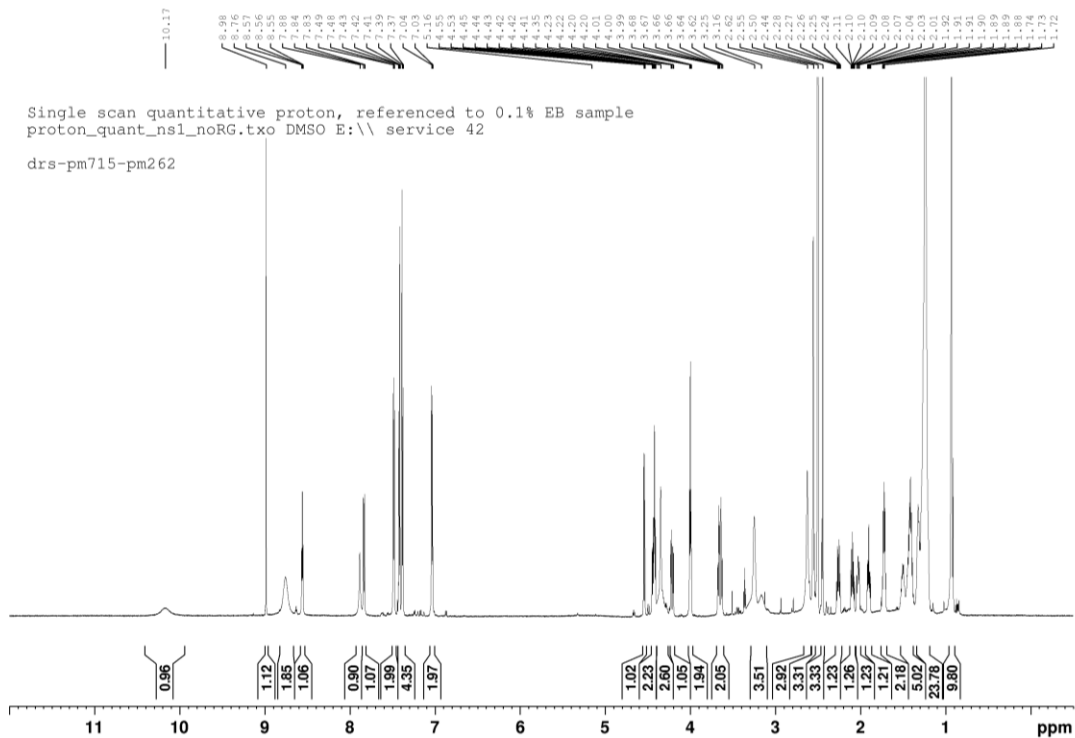
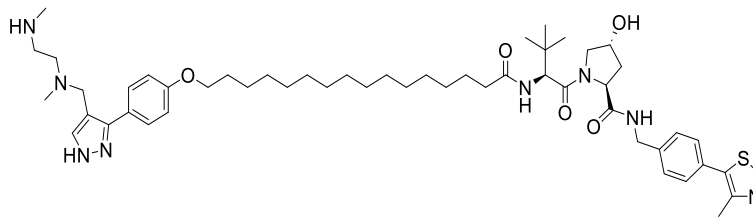
PROTAC C



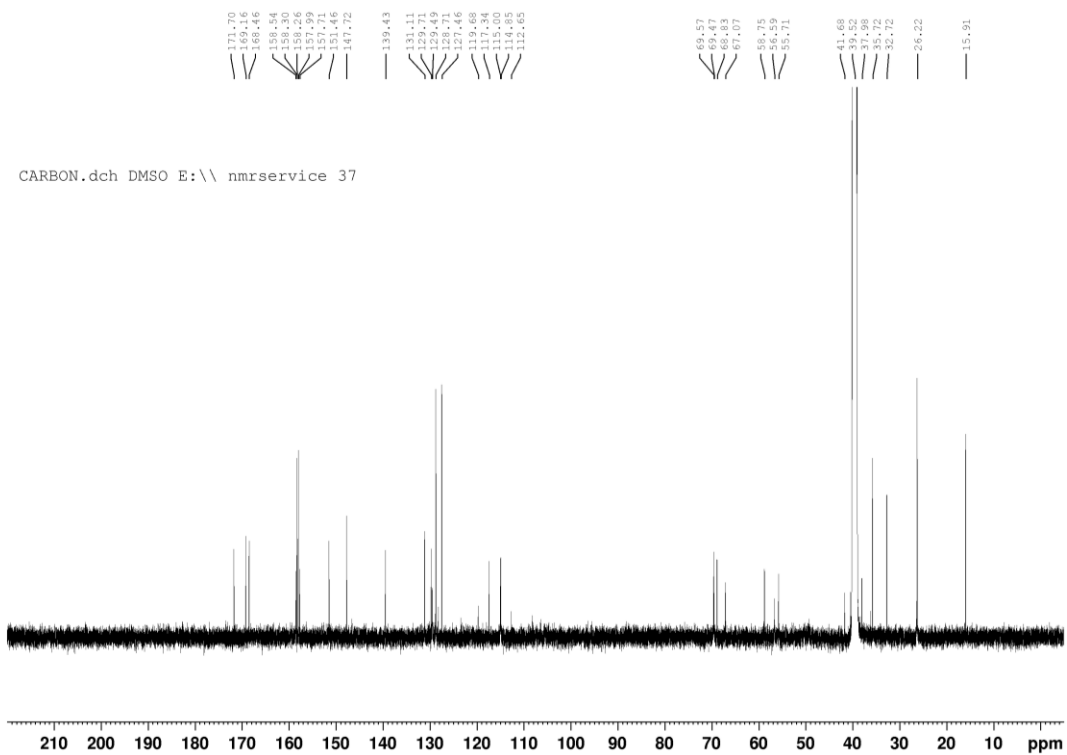
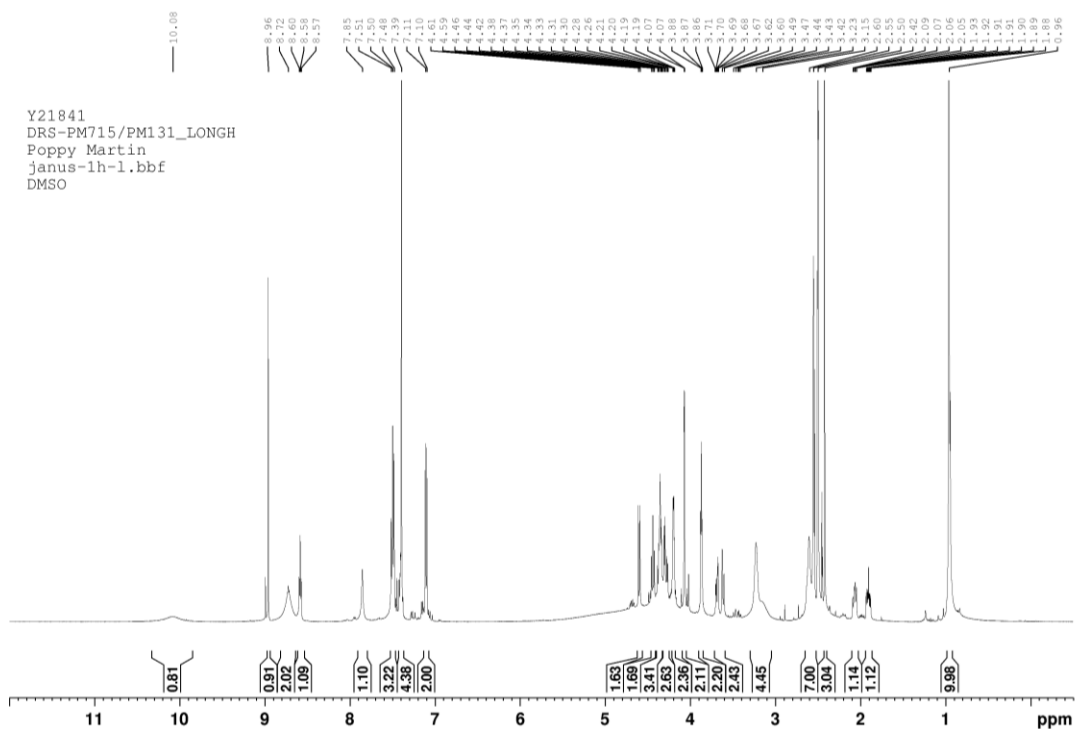
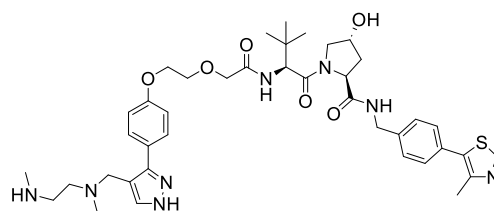
PROTAC D



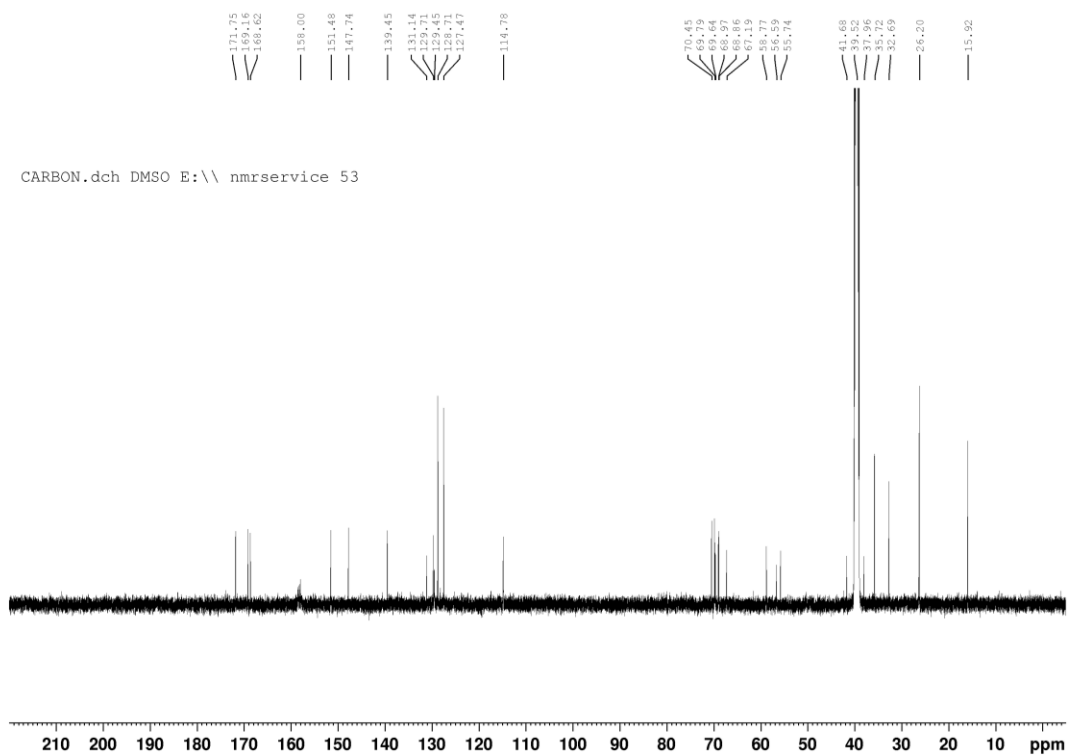
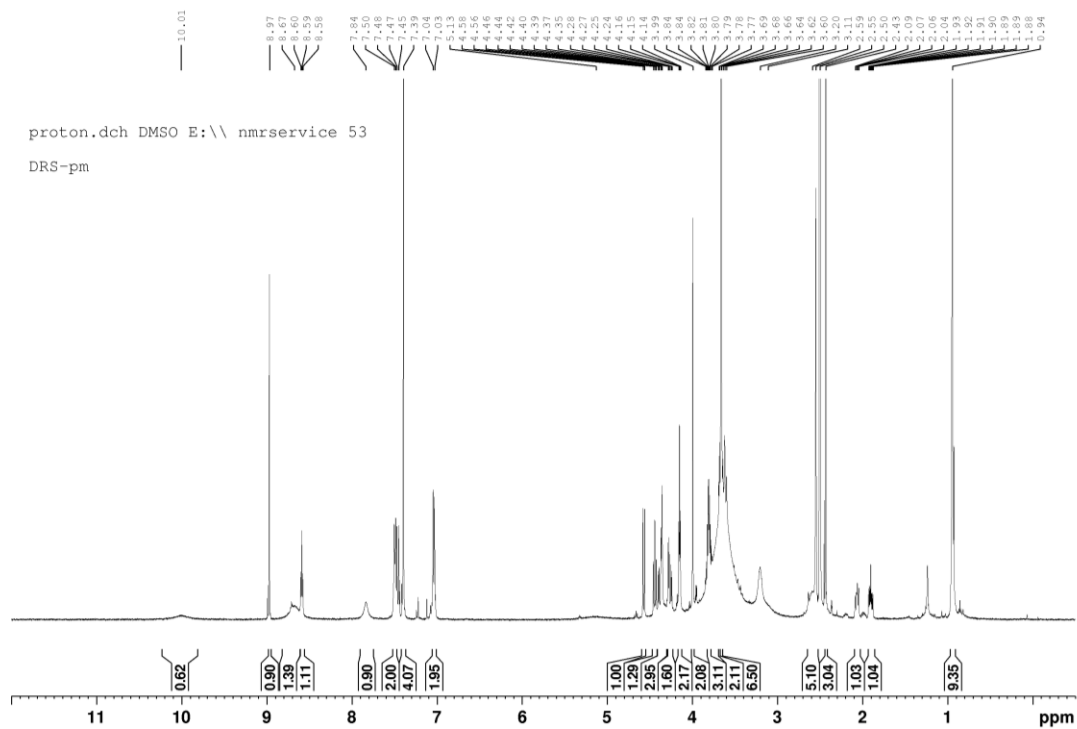
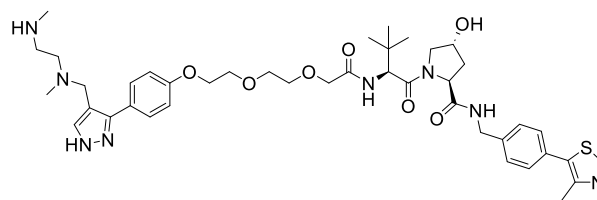
PROTAC F



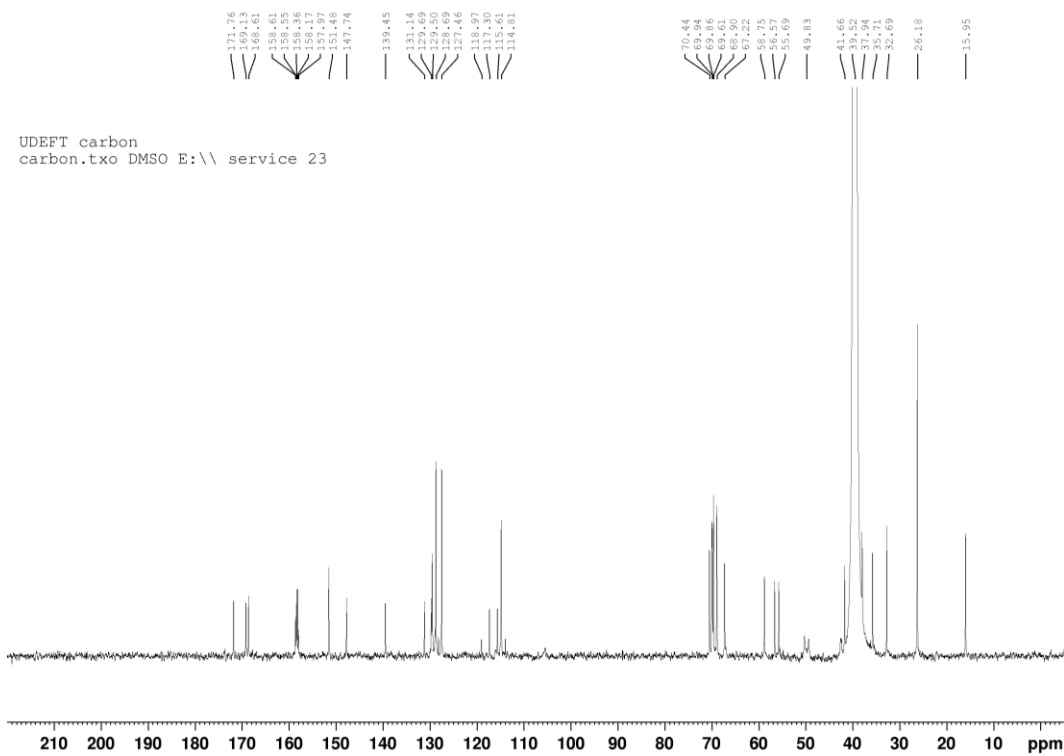
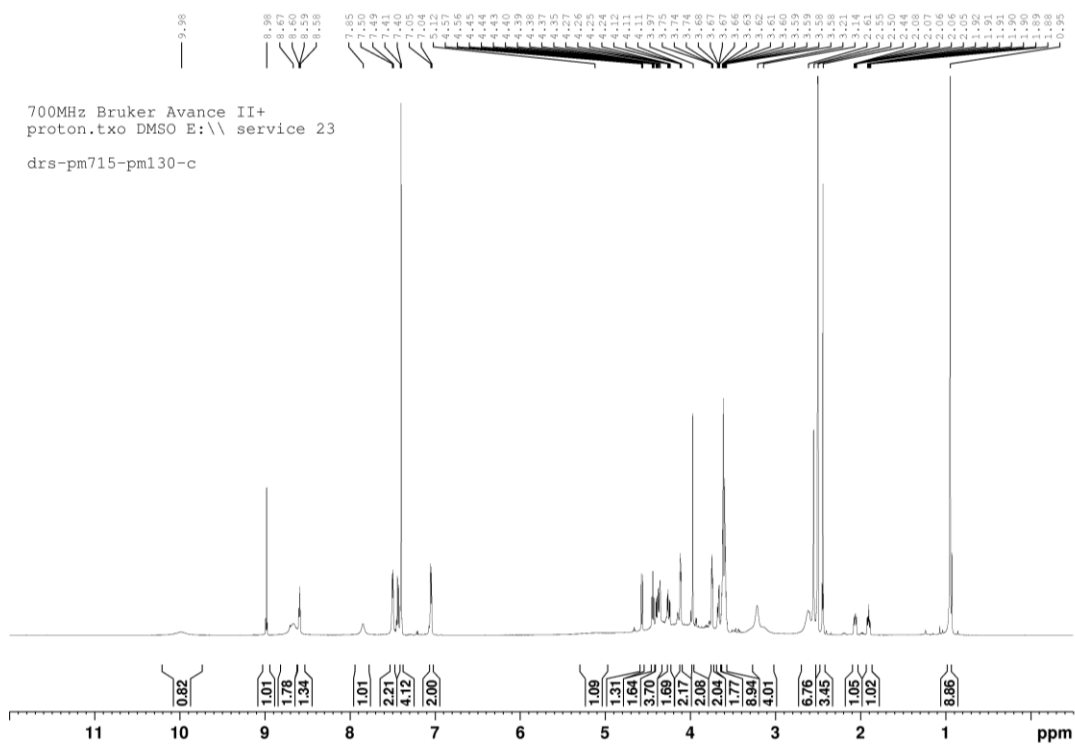
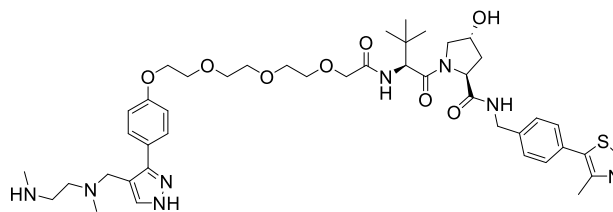
PROTAC G



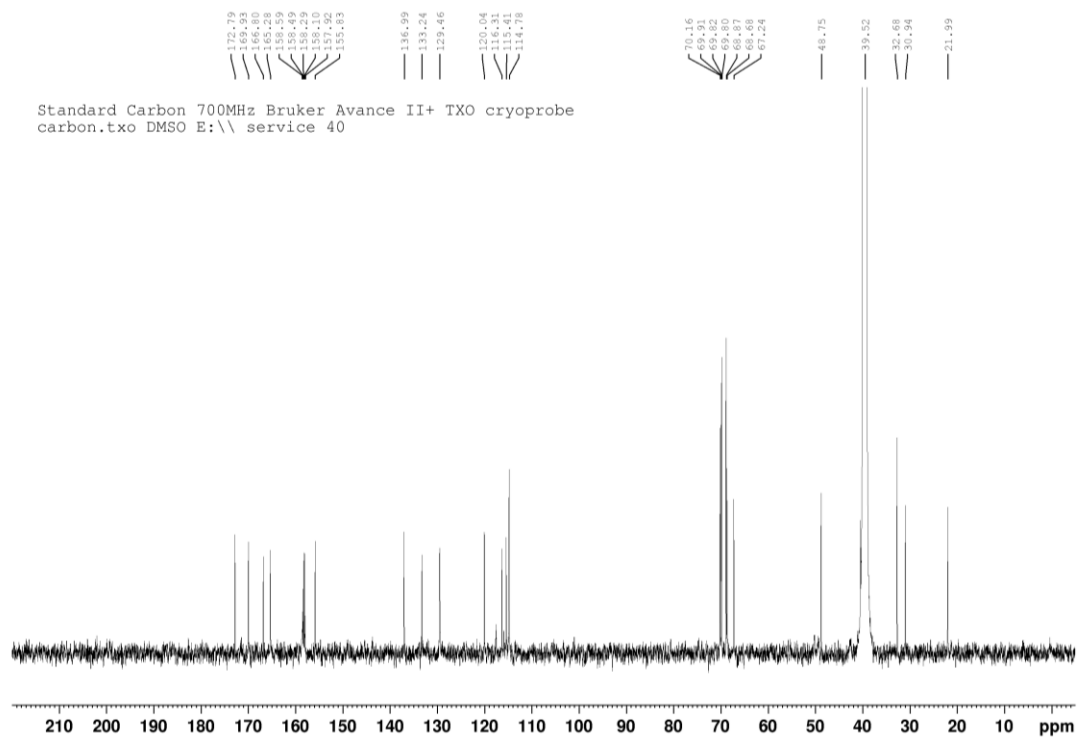
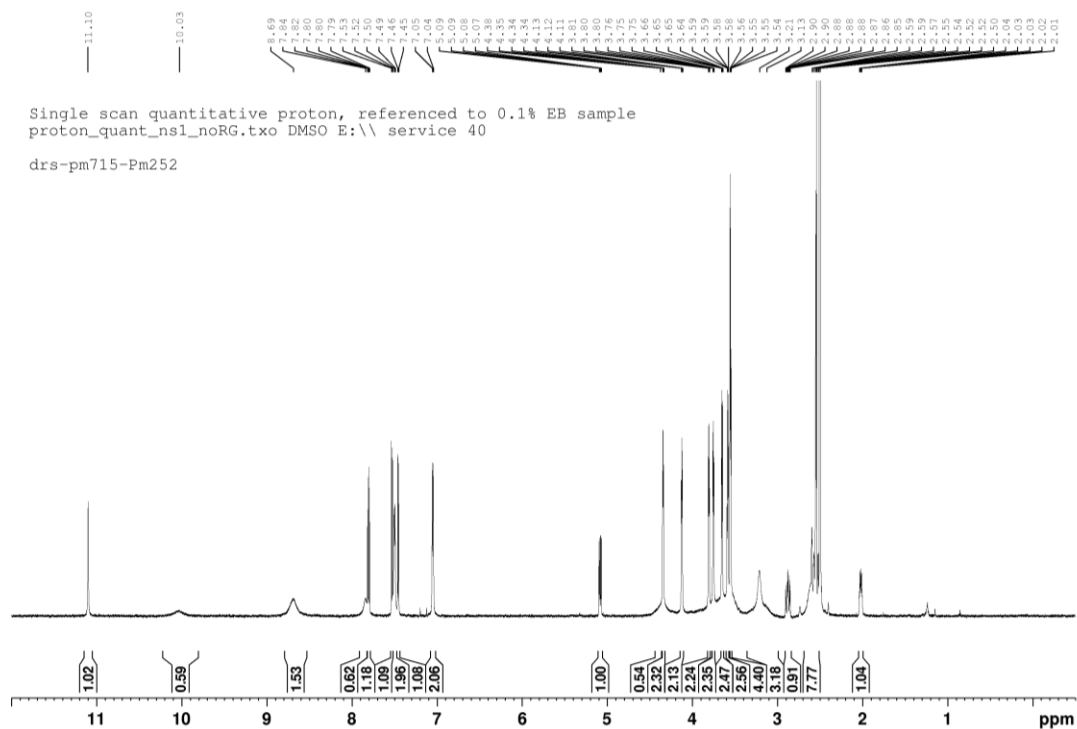
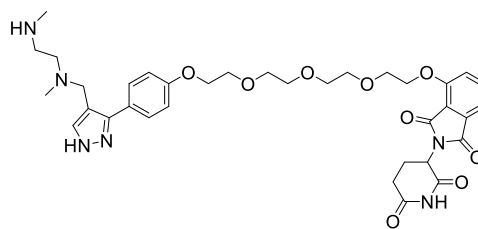
PROTAC H



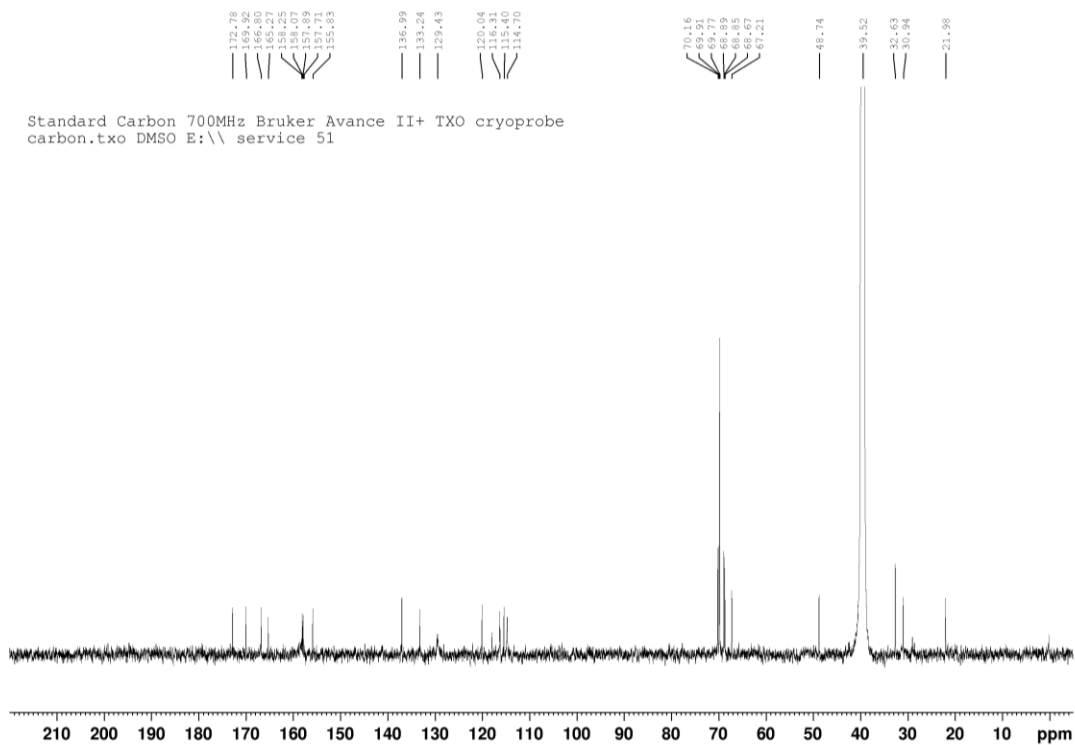
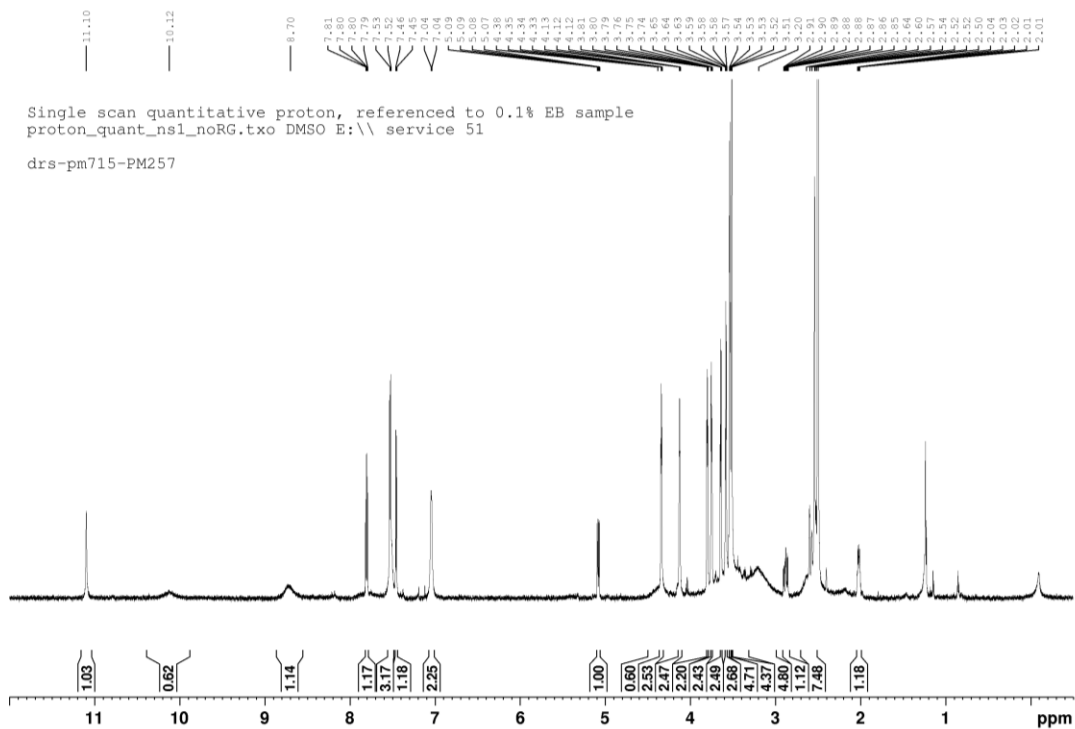
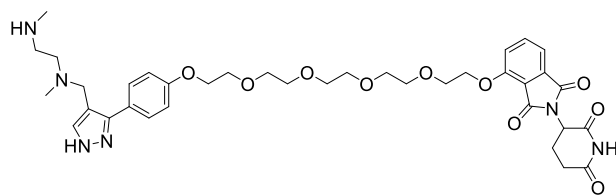
PROTAC I



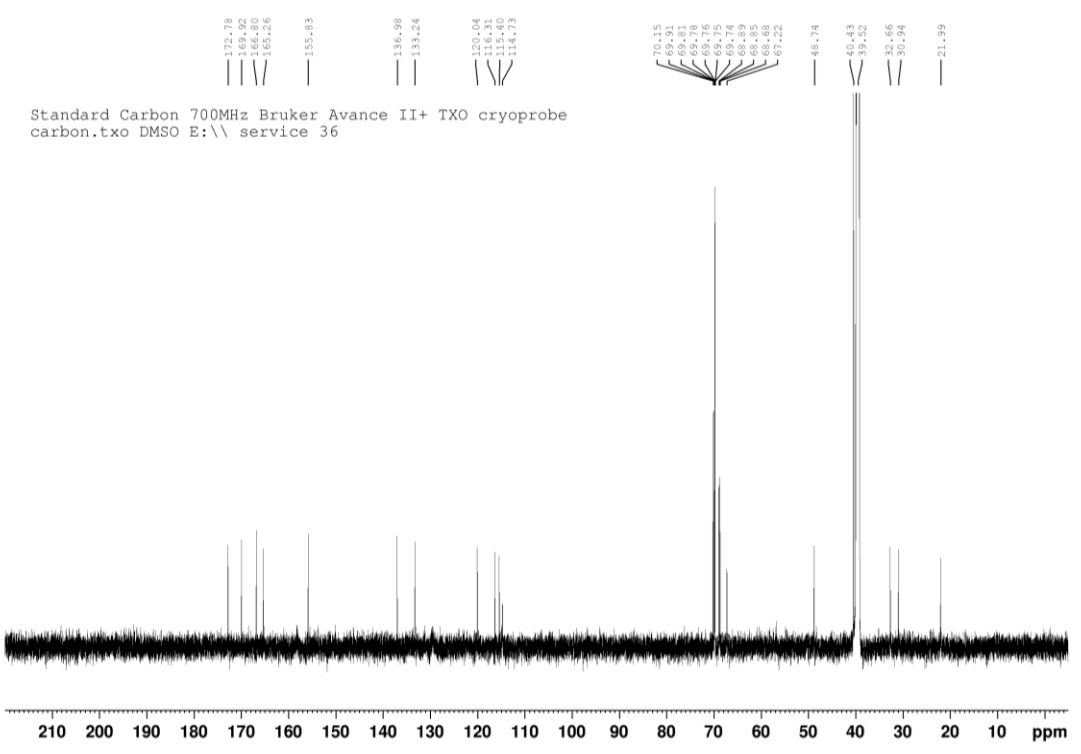
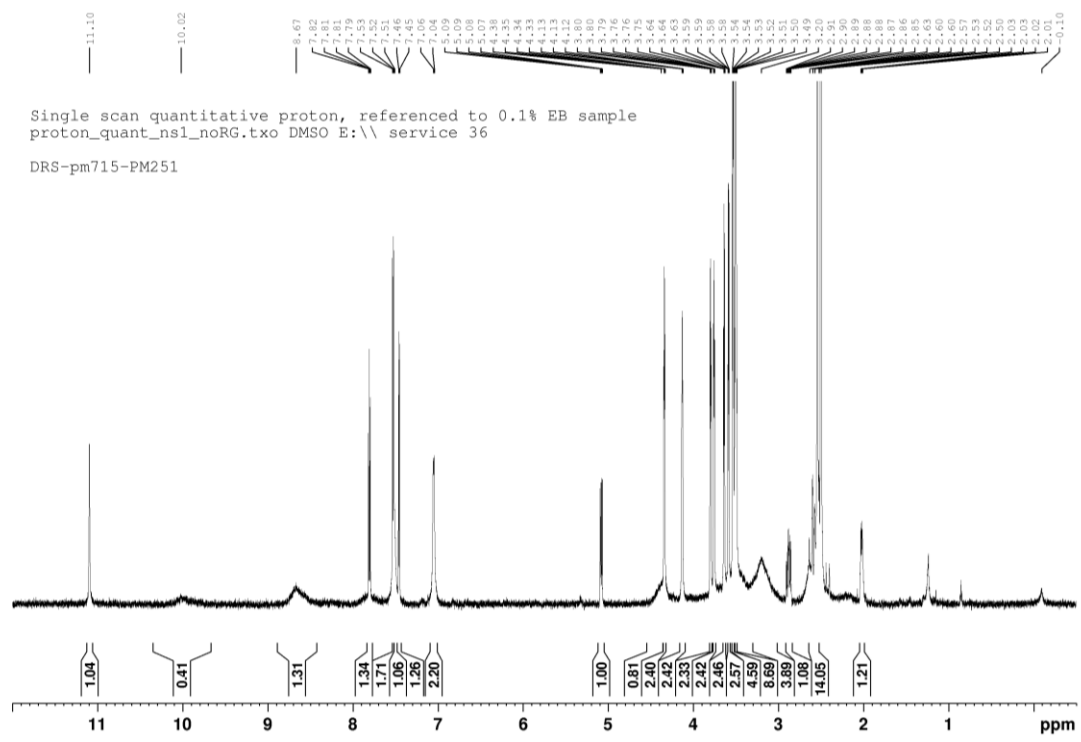
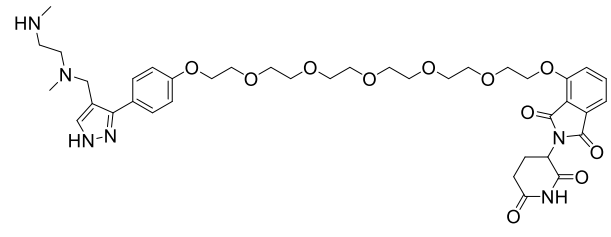
PROTAC L



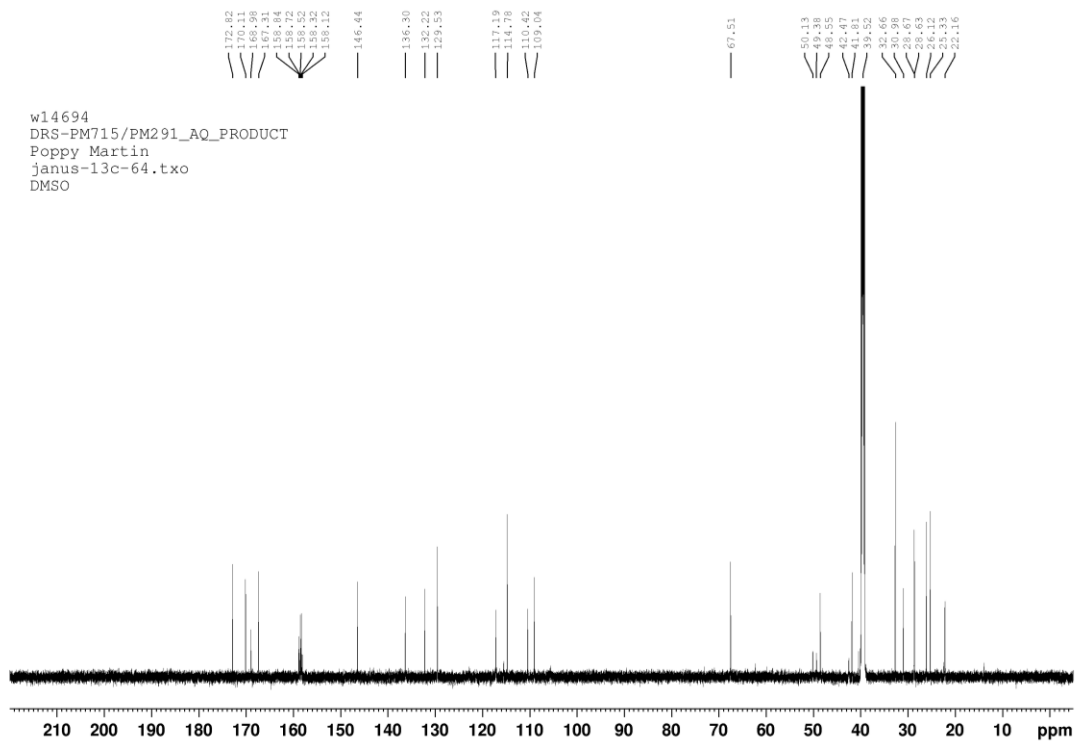
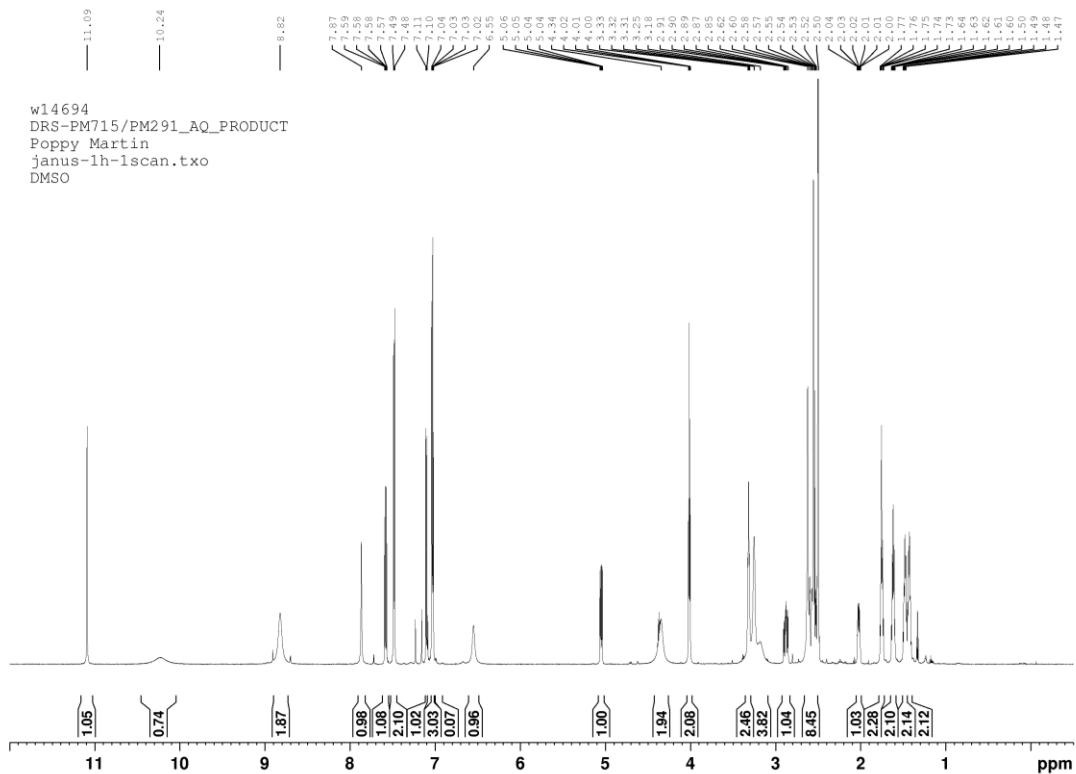
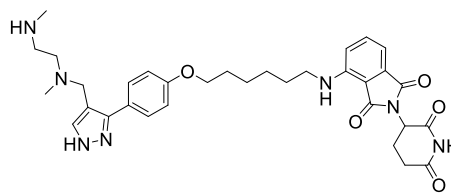
PROTAC M



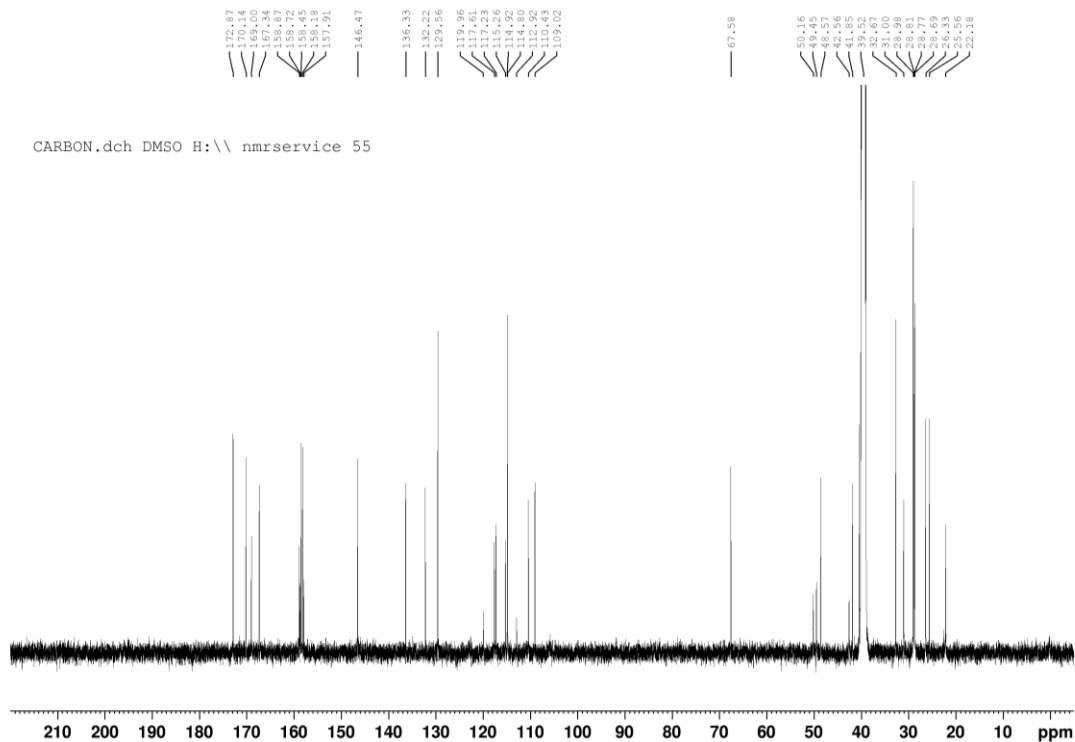
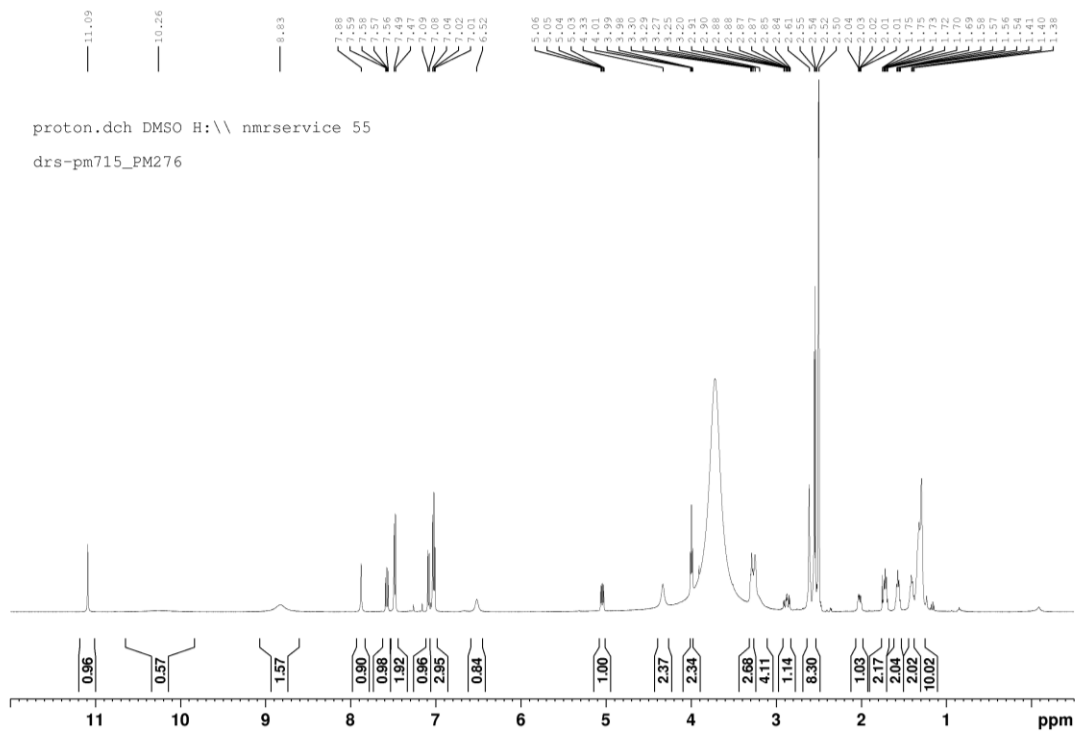
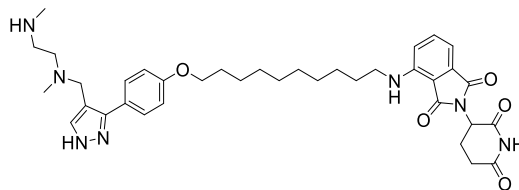
PROTAC N



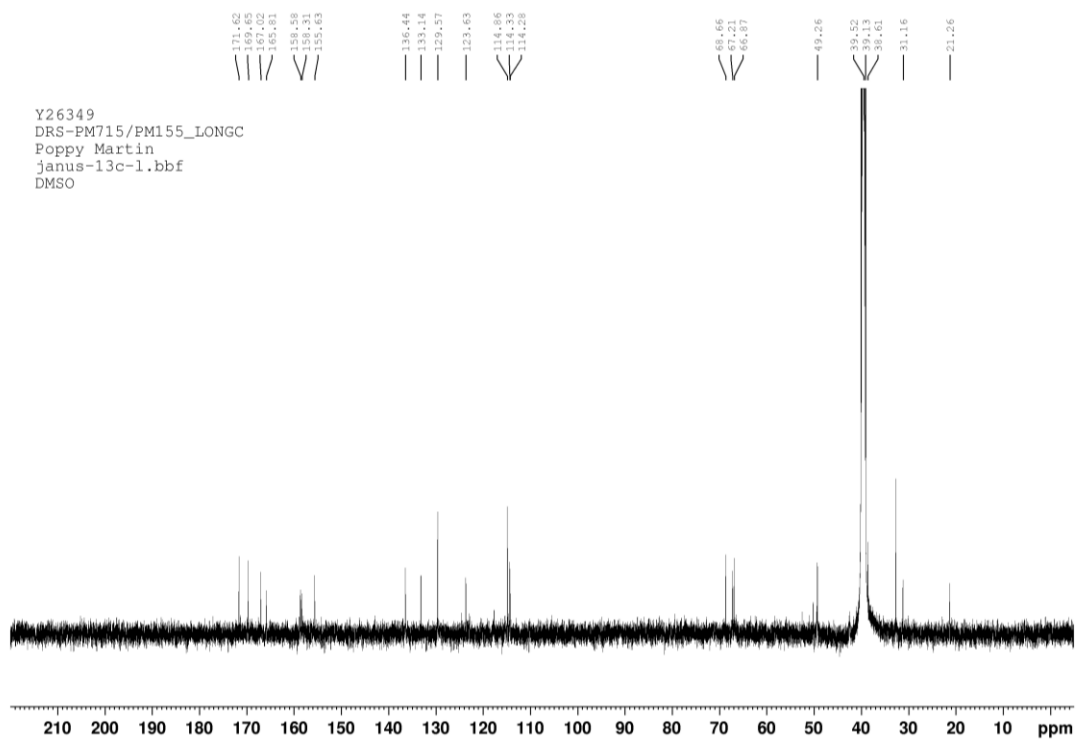
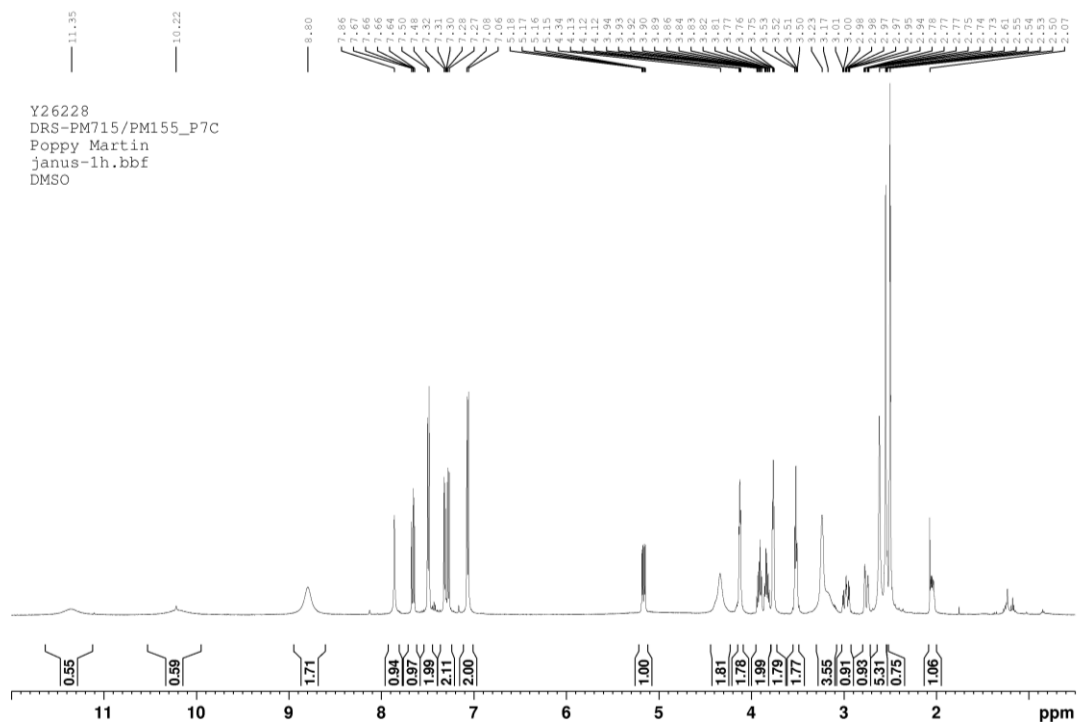
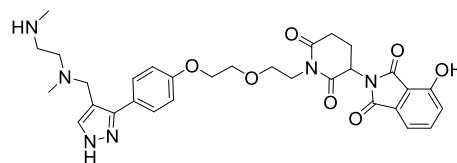
PROTAC P



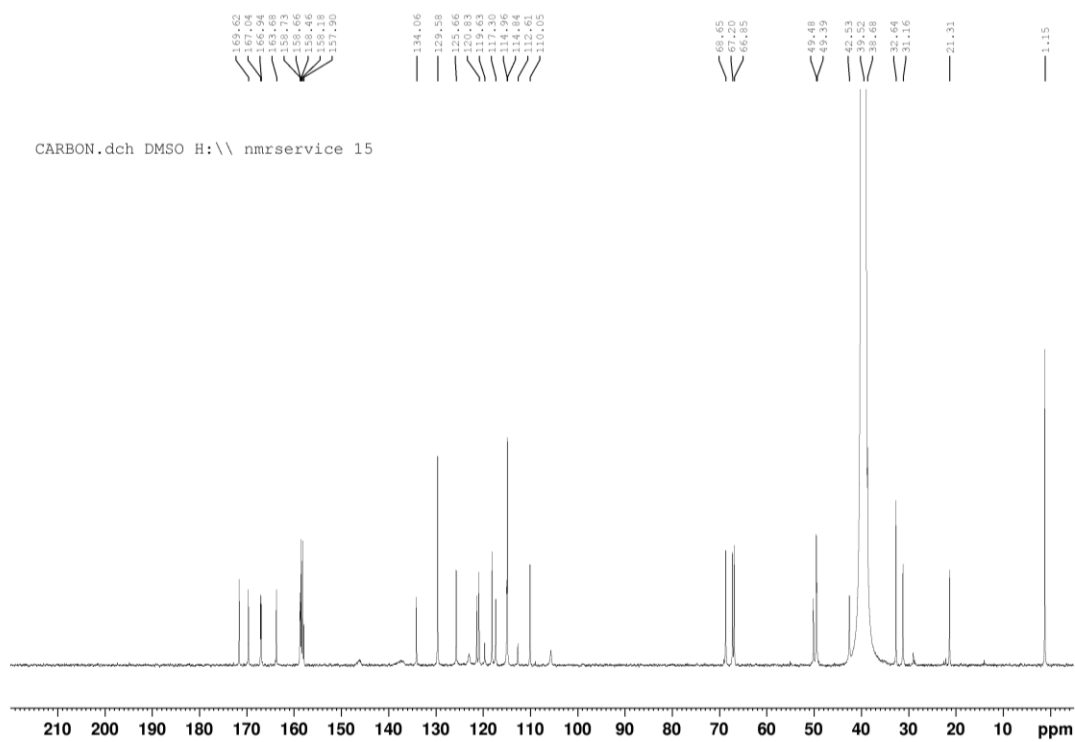
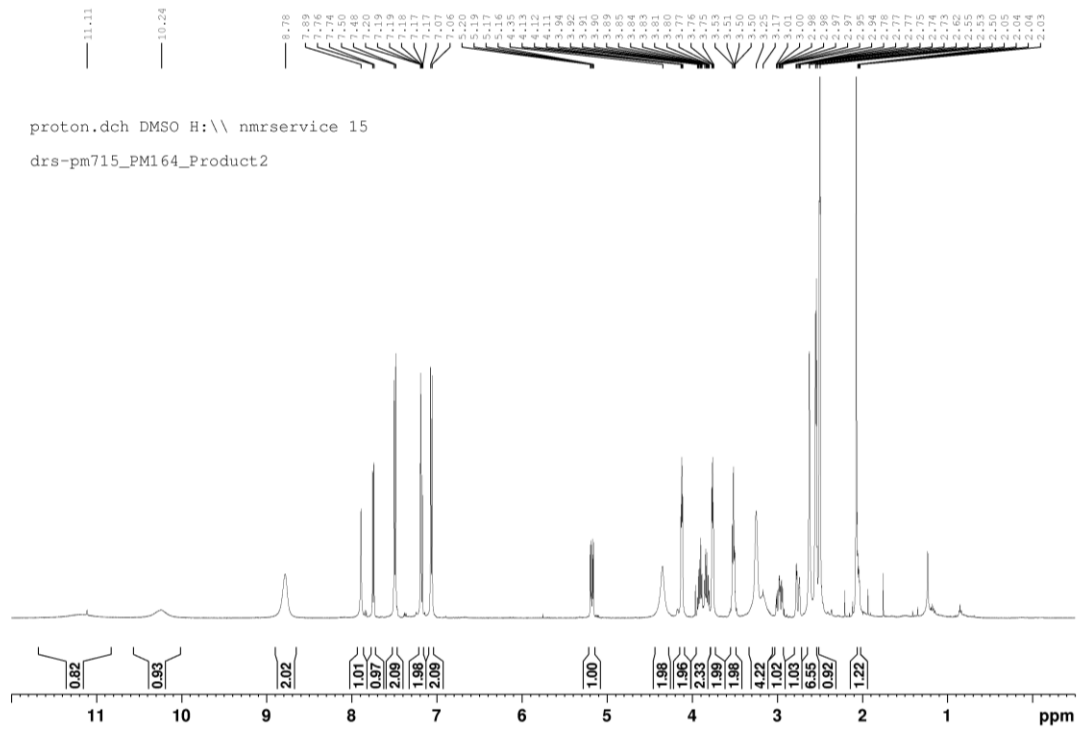
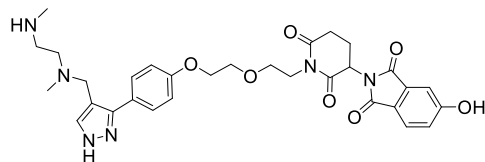
PROTAC Q



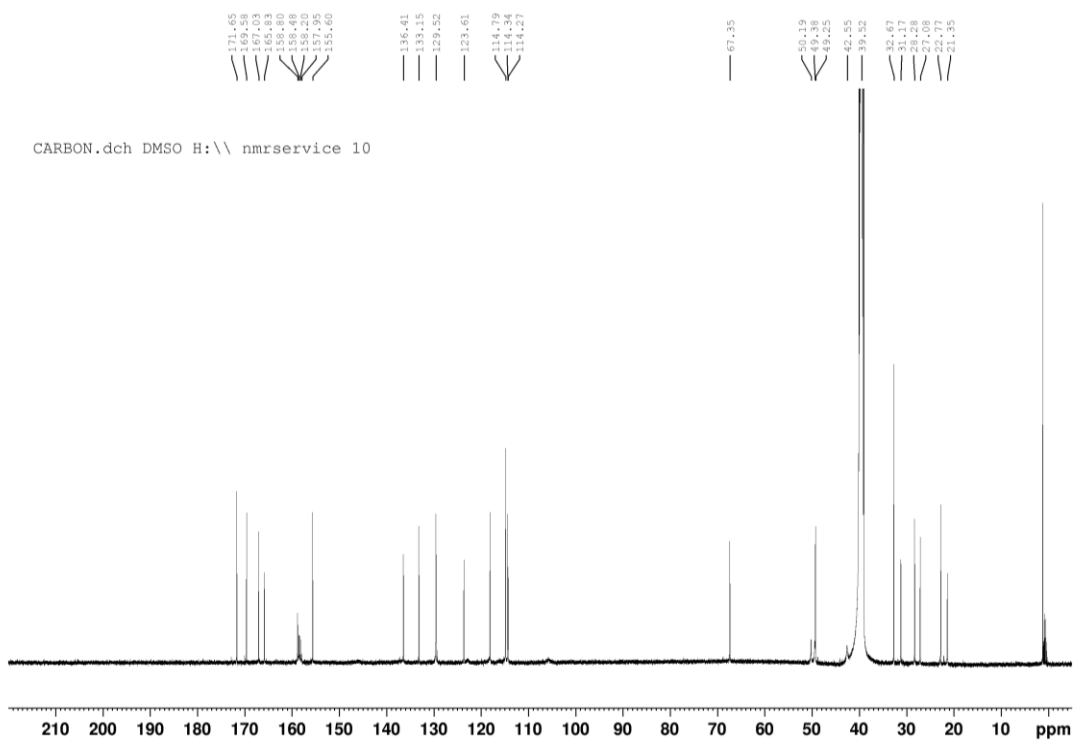
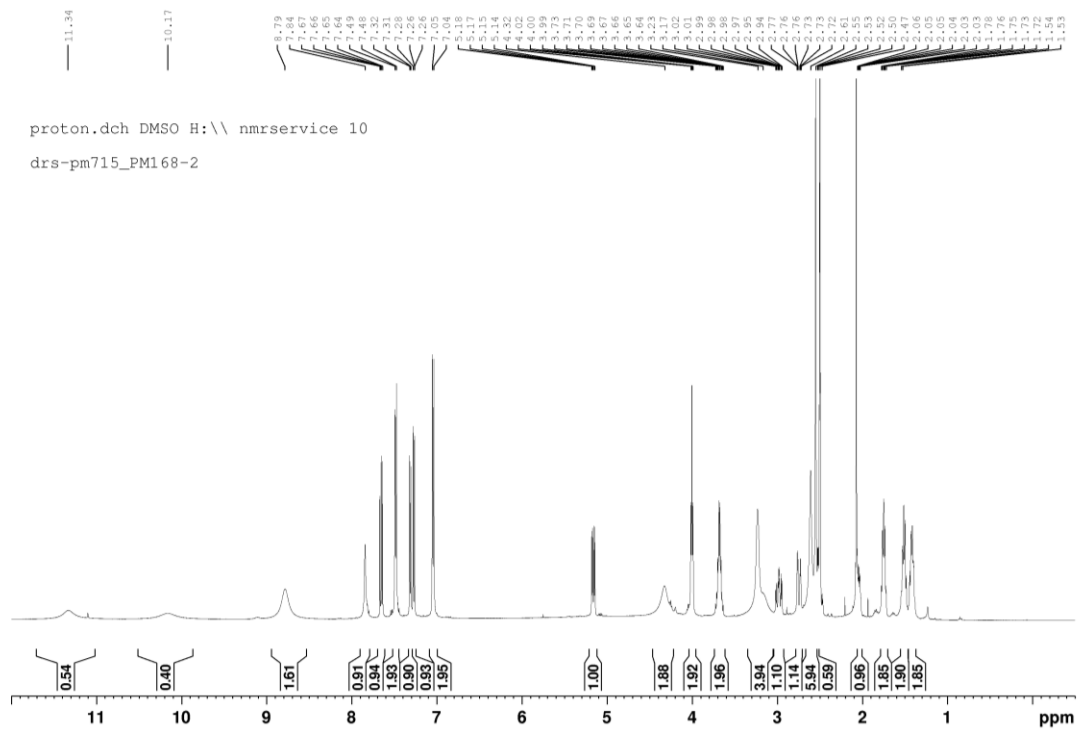
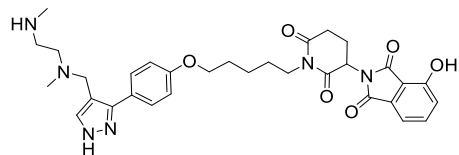
HBM1



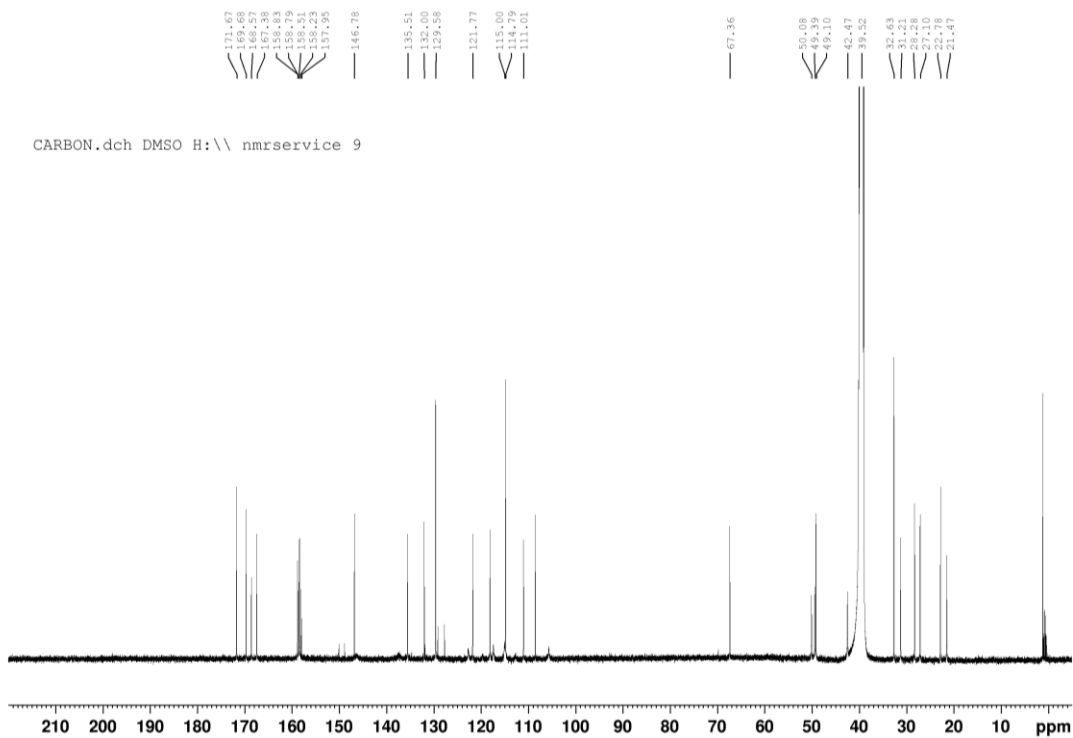
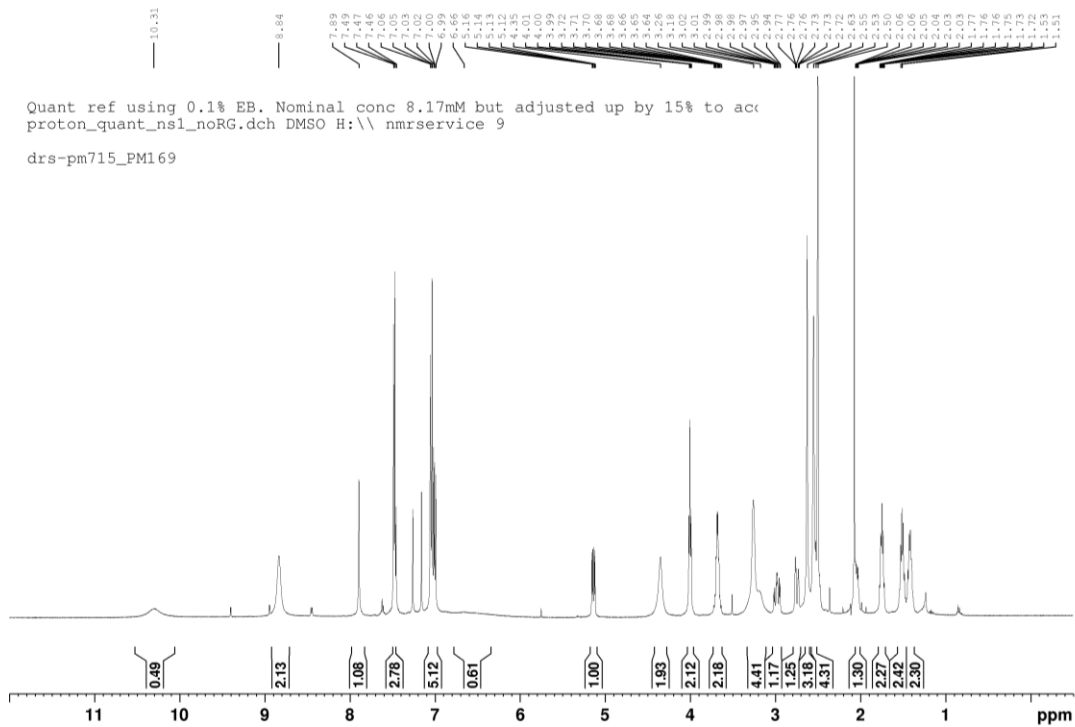
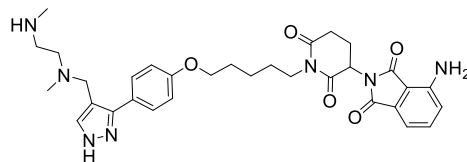
HBM2



HBM3



HBM4



HBM5

